Design, Synthesis and Characterisation of π-Extended Viologen-Based Molecular and Supramolecular Complexes with Cucurbit[n]urils

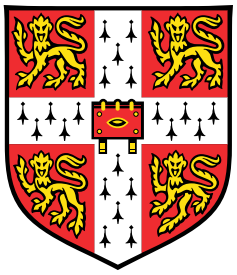

Magdalena Olesińska

Department of Chemistry
University of Cambridge

This dissertation is submitted for the degree of
Doctor of Philosophy

Jesus College

February 2019

Declaration

I hereby declare that except where specific reference is made to the work of others, the contents of this dissertation are original and have not been submitted in whole or in part for consideration for any other degree or qualification in this, or any other university. This dissertation is my own work and contains nothing which is the outcome of work done in collaboration with others, except as specified in the text and Acknowledgements. This dissertation contains fewer than 65,000 words including appendices, bibliography, footnotes, tables and equations and has fewer than 150 figures.

Magdalena Olesińska
February 2019

Acknowledgements

At this point I would like to acknowledge those who helped me in various ways to shape this thesis into what it is but also help me grown as a scientist and become a better person.

First and foremost I would like to thank my supervisor Professor Oren A. Scherman for giving me the opportunity to join his group and work on this project. After my CPGS viva, at the end of the first year, Oren told me that the only thing I needed to succeed is a huge injection of confidence. I am pretty sure I still need some more shots of confidence, nevertheless, I am grateful for motivation, encouragement and many lessons I received from Oren during my time in Melville Lab. Thanks to him I was part of the SASSYPOL ITN project that allowed me to meet incredible people, and I had fantastic opportunities to travel and work for a few months at both at Freiburg University and Eindhoven University. Thank you for plenty of freedom and trust.

I was very fortunate to spend some time at Northwestern Univeristy working with Natalia Powers-Riggs and Dr Ryan Young from Prof. Wasielewski's group. They introduced me to the world of advanced spectroscopy and I had great time exploring Evanston and Chicago.

I would like to say thank you to Dr Silvia Gomez-Coca and Dr Istvan Szabo from King's College London for their hard work and engagement in theoretical calculations of the extended viologen systems.

My gratitude goes to Dr Qianqi Lin, whose help and patience made it possible for me to refresh my undergraduate knowledge of electrochemistry and truly discover how powerful it is. I am also grateful for all the warm and encouraging words I have received from Ivana.

Junyang Huang thank you for our Raman spectroscopy collaboration, and also for many music and literature discoveries I made thanks to you.

Daniel Anton-Garcia, thank you for your help with fluorescence measurements. Our Wednesday "experiment sessions" were a truly great time for me, a time to get a different perspective.

I would like to say thank you to Dr Sean Ryan, who helped me a lot during my first year in the group. Sean, you are the messiest chemist I know but you inspired me a lot, helped me get started with my research in the Melville and I have learned so many things from you.

Dr David Clark, it was a pleasure to work with you on the peptide project. Thank you for your optimism, and help fixing the HPLC. I think our mutual love for Radiohead music and constant pang of conscience regarding more eco-friendly lifestyle sealed our friendship. However, I am still waiting for the Bjork tickets you promised ...

I would like to thank Dr Kamil Sokolowski not only for his great friendship but also as a postdoc in this group he motivated me, encouraged, listened to my complaints and self-doubts while teaching me a lot about chemistry. Kamil's brutal comments about posters, papers, thesis chapters were great lessons on how to write and present my work conceptually but also how to control my "hot bloodiness". I want to thank you Kamil for answering a lot of panic calls from America regrading EPR measurements and quick on-line refreshers and training on how to use the broken wet box in Prof. Fraser Stoddart's lab.

Dr Yuchao Wu deserves a big thank you from me. My first collaborator in the lab, and my neighbour for a good amount of time, first in the office and later in the lab. Yuchao tought me a lot about Chinese culture and Chinese bad words. My PhD experience wouldn't be the same without our chats about work, experiments, projects and how important it was for my reputation to hide the fact that I like some Korean movies.

I would like to say thank you to Dr Guanglu Wu, who introduced me to the wonders of precise NMR and ITC characterisation.

I was happy to meet Dr Aniello Palma and Dr Stefan Mommer and learn a lot from their refreshed and critical approaches to organic chemistry.

I would like to say thank you to Dr Dominique Hoogland and Dr Alex Groombridge with whom I started my PhD. Our 12 o'clock lunch and coffee breaks were truly stress relieving times. Thank you for so many inspiring chats and support during my PhD.

Thank you Dr Jade A. McCune. I moved 10 times in Cambridge and at least half of my moves were done with her help. I also hope I didn't completely destroy Jade with the countless experimental and Polish movies I forced her to watch.

I would also like to say a big thank you to everybody in the Melville Lab, who made my PhD an incredible experience.

Here, I would like to thank several people who took some time to proofread this thesis: Dominique, David, Setu, Tobias, Kamil, Ivana and Stefan. Thank you!

I want to say thank you to my parents and sisters. The love and support I received from my family and friends kept me going and I was continuing with what I decided to do so far away from home.

Finally, I want to thank Tobias for his encouragement as he kept pushing me to submit my thesis. Thank you Tobi for being a hero fixing horrible latex errors, managing my panic attacks, surviving all these years and keeping up with all my crazy ideas.

Abstract

Viologens, 4,4'-bipyridinium dications (V^{2+}), have attracted much attention as electron mediators in a variety of photochemical, electrochemical and chemical processes ranging from catalysis, electrochromic devices to solar energy conversion and storage systems. The different applications of viologens are related primarily to their facile one electron reduction of dicationic species, V^{2+}, to radical monocations, $V^{+\bullet}$. Moreover, the dynamic interactions of V^{2+} derivatives with cucurbit[n]uril (CB[n], for n=7 or 8) macrocycles, the dimerisation of $V^{+\bullet}$ radical cations inside the CB[8] molecular cavity as well as redox controlled stoichiometry of V^{2+} based inclusion complexes make these systems highly attractive for supramolecular chemistry and dynamic nanosystems, *i.e.* molecular machines. This doctoral thesis focuses on design, synthesis and characterisation of π-extended viologen-based molecular and supramolecular systems. Integral to the project was to study assembly processes that involve extended viologen derivatives and CB[n] macrocycles as well as characterisation of the physicochemical properties of resulting host-guest systems. A brief overview of viologen and cucurbit[n]uril chemistry as well as fundamentals regarding self-assembly processes and how can they influence the optoelectronic properties of materials are discussed in Chapter 1.

Chapter 2 describes the synthesis and characterisation of extended methyl viologen (EV[X]MV) derivatives with an aromatic extension between the pyridinium rings ([X]= phenylene, naphthalene, pyrene, chrysene, thiophene and dithiophene), their interactions with CB[7] and CB[8] macrocycles as well as physicochemical properties of the resultant host-guest systems are studied. Methyl viologen (MV^{2+}) is a well-known guest for both CB[7] and CB[8] macrocycles. On account of the different binding modes with CB[n], the optical as well as redox properties of MV^{2+} can be modulated. Here, the effect of the aromatic extension ([X]) on EV[X]MVs before and upon complexation with CB[7] and CB[8] is investigated using nuclear magnetic resonance (NMR), steady-state UV – Vis and photoluminescence (PL) spectroscopies as well as isothermal titration calorimetry (ITC) and cyclic voltammetry (CV). Interestingly, dimerisation of selected extended methyl viologens with CB[8] and the charge accumulative properties of the resultant complexes were observed.

In Chapter 3, synthesis and characterisation of a family of extended viologens with aromatic substituents (EV[X]R, further denoted as extended aryl viologens), their interactions with CB[8] macrocycles as well as physiochemical properties of the resultant host-guest systems are studied. The design and synthesis of these new class of π-conjugated viologen derivatives are elaborated involving different aromatic bridging units, as well as rigid aromatic peripheral functionalisation with electron donating and electron withdrawing groups on the pyridinium rings. Upon mixing with CB[8], the extended aryl viologen derivatives functionalised with electron donating groups self-assemble into 2:2 complexes. Moreover, the extended work on EV[X]R molecules functionalised with different aromatic substituents, which are simultaneously encapsulated within CB[8] to form heteroquarternery complexes is discussed. The nature and dynamics of the resulting $CB[8]_2 \cdot (EV[X]R)_2$ homo- and hetero-complexes are studied both in the ground as well as exited states upon interaction with light utilising NMR, steady-state and time-resolved spectroscopies as well as ITC experiments.

Finally, in Chapter 4 the synthetic approach towards asymmetric aryl viologen (AV) and extended aryl viologen (EV[X]RR', where [X]= naphthalene) is presented. Firstly, synthetic pathways based on the Zinke reaction for asymmetric aryl substitution of AV and EV are discussed. Secondly, the supramolecular binding of the obtained asymmetric EV[Np]RR' with CB[8] is investigated along with the effect of supramolecular dimer formation on the optical properties. Finally, the application of asymmetric aryl viologens in the formation of a bio-inspired nanofibers is presented.

Table of contents

List of figures

List of tables

Abbreviations

Asp	Aspartic acid
ADA	1-adamantanamine hydrochloride
CB[n]	Cucurbit[*n*]uril
CB[5]	Cucurbit[5]uril
CB[6]	Cucurbit[6]uril
CB[7]	Cucurbit[7]uril
CB[8]	Cucurbit[8]uril
CB[10]	Cucurbit[10]uril
CD	Cyclodextrins
CT	Charge Transfer
CV	Cyclic Voltammetry
D	Diffusion coefficient
D_{G}	Diffusion coefficient of guest molecule
$D_{\mathrm{G:CB[8]}}$	Diffusion coefficient of CB[8]:guest 2:2 complex
$D_{\mathrm{G:CB[7]}}$	Diffusion coefficient of CB[7]:guest 2:1 complex
DMF	Dimethylformamide
DMSO	Dimethyl Sulfoxide
DNB	2,4-dinitrochlorobenzene
DOSY	Diffusion-Ordered Spectroscopy
DPV	Differential Pulse Voltammetry

D_2O	Deuterated water
EDG	Electron Donating Group
ΔH	Entalphy
ΔS	Entropy
EPR	Electron Paramagnetic Resonance
EtOH	Ethanol
EV	Extended viologen
EV[X]R	Extended aryl viologen
EV[CH]	6,12-di(pyridin-4-yl)chrysene
EV[CH]DNB	4,4'-(chrysene-6,12-diyl)bis(1-(2,4-dinitrophenyl)pyridin-1-ium)
EV[CH]MV	4,4'-(chrysene-6,12-diyl)bis(1-methylpyridin-1-ium) iodide
EV[CH]H	4,4'-(chrysene-6,12-diyl)bis(1-phenylpyridin-1-ium)
EV[CH]Me	4,4'-(chrysene-6,12-diyl)bis(1-(p-tolyl)pyridin-1-ium)
EV[X]MV	Extended methyl viologens
EV[DTh]	5,5'-di(pyridin-4-yl)-2,2'-bithiophene
EV[DTh]DNB	4,4'-([2,2'-bithiophene]-5,5'-diyl)bis(1-(2,4-dinitrophenyl)pyridin-1-ium)
EV[DTh]MV	4,4'-([2,2'-bithiophene]-5,5'-diyl)bis(1-methylpyridin-1-ium) iodide
EV[DTh]Me	4,4'-([2,2'-bithiophene]-5,5'-diyl)bis(1-(p-tolyl)pyridin-1-ium)
EV[Np]	1,4-di(pyridin-4-yl)naphthalene
EV[Np]Br	4,4'-(naphthalene-1,4-diyl)bis(1-(4-bromophenyl)pyridin-1-ium)
EV[Np]CF_3	4,4'-(naphthalene-1,4-diyl)bis(1-(4-(trifluoromethyl)phenyl)pyridin-1-ium)
EV[Np]DNB	4,4'-(naphthalene-1,4-diyl)bis(1-(2,4-dinitrophenyl)pyridin-1-ium)
EV[Np]DNB_{asym}	1-(2,4-dinitrophenyl)-4-(4-(pyridin-4-yl)naphthalen-1-yl)pyridin-1-ium
EV[Np]MV	4,4'-(naphthalene-1,4-diyl)bis(1-methylpyridin-1-ium)
EV[Np]Me	4,4'-(naphthalene-1,4-diyl)bis(1-(p-tolyl)pyridin-1-ium)

EV[Np]H 4,4'-(naphthalene-1,4-diyl)bis(1-phenylpyridin-1-ium)

EV[Np]NH_2 4,4'-(naphthalene-1,4-diyl)bis(1-(4-aminophenyl)pyridin-1-ium)

EV[Np]NMe_2 4,4'-(naphthalene-1,4-diyl)bis(1-(4-(dimethylamino)phenyl)pyridin-1-ium)

EV[Np]OMe 4,4'-(naphthalene-1,4-diyl)bis(1-(4-methoxyphenyl)pyridin-1-ium)

EV[Np](OMe)(EtCOOH) 1-(4-(2-carboxyethyl)phenyl)-4-(4-(1-(4-methoxyphenyl)pyridin-1-ium-4-yl)naphthalen-1-yl)pyridin-1-ium

EV[Np]SMe 4,4'-(naphthalene-1,4-diyl)bis(1-(4-(methylthio)phenyl)pyridin-1-ium)

EV[$Pyr_{1,6}$] 1,6-di(pyridin-4-yl)pyrene

EV[$Pyr_{1,6}$]DNB 4,4'-(pyrene-1,6-diyl)bis(1-(2,4-dinitrophenyl)pyridin-1-ium)

EV[$Pyr_{1,6}$]MV 4,4'-(pyrene-1,6-diyl)bis(1-methylpyridin-1-ium) iodide

EV[$Pyr_{1,6}$]Me 4,4'-(pyrene-1,6-diyl)bis(1-(p-tolyl)pyridin-1-ium)

EV[$Pyr_{2,7}$] 2,7-di(pyridin-4-yl)pyrene

EV[$Pyr_{2,7}$]DNB 4,4'-(pyrene-2,7-diyl)bis(1-(2,4-dinitrophenyl)pyridin-1-ium)

EV[$Pyr_{2,7}$]MV 4,4'-(pyrene-2,7-diyl)bis(1-methylpyridin-1-ium) iodide

EV[$Pyr_{2,7}$]Me 4,4'-(pyrene-2,7-diyl)bis(1-(p-tolyl)pyridin-1-ium)

EV[Ph] 1,4-di(pyridin-4-yl)benzene

EV[Ph]DNB 4,4'-(1,4-phenylene)bis(1-(2,4-dinitrophenyl)pyridin-1-ium)

EV[Ph]MV 4,4'-(1,4-phenylene)bis(1-methylpyridin-1-ium)

EV[Ph]Me 4,4'-(1,4-phenylene)bis(1-(p-tolyl)pyridin-1-ium)

EV[Th] 2,5-di(pyridin-4-yl)thiophene)

EV[Th]DNB 4,4'-(pthiophene-2,5-diyl)bis(1-(2,4-dinitrophenyl)pyridin-1-ium)

EV[Th]MV 4,4'-(thiophene-2,5-diyl)bis(1-methylpyridin-1-ium) iodide

EV[Th]Me 4,4'-(thiophene-2,5-diyl)bis(1-(p-tolyl)pyridin-1-ium)

Φ_{PL} Photoluminescence quantum yield

k_{rad} Fluorescence radiative rate

k_{nrad}	Fluorescence non-radiative rate
fsTA	Femtosecond Transient Absorption Spectroscopy
ΔG	Gibbs free energy
GSB	Ground State Bleaching
HPLC	High Performance Liquid Chromatography
Ile	Isoleucine
ITC	Isothermal Titration Calorimetry
K	Binding constant
Keq	Equilibrium binding constant
$\mathbf{MV^{\bullet+}}$	Methylviologen radical
m	Atomic mass
NIR	Near-infrared
NMP	N-Methyl-2-Pyrrolidone
NMR	Nuclear Magnetic Resonance
nsTA	Nanosecond Transient Absorption Spectroscopy
PA	Photoinduced Absorption
PET	Photoinduced Electron Transfer
PL	Photoluminescence
SE	Stimulated Emission
T	Temperature
TA	Transient Absorption Spectroscopy
TCSPC	Time-Correlated Single Photon Counting
TFA	Trifluoroacetic Acid
THF	Tetrahydrofuran
UV – Vis	Ultraviolet-visible
z	Charge number

λ_{em}^{max}	Maximum emission wavelength
λ_{abs}^{max}	Maximum absorption wavelength
λ	Wavelength
τ	Fluorescent life time
τ_1	Fluorescent lifetime (decay constant 1)
τ_2	Fluorescent lifetime (decay constant 2)
τ_3	Fluorescent lifetime (decay constant 3)
τ_4	Fluorescent lifetime (decay constant 4)

List of Publications

G. Wu*, **M. Olesińska***, Y. Wu, D. Matak-Vinkovic, and O. A. Scherman, Mining 2:2 Complexes from 1:1 Stoichiometry: Formation of Cucurbit[8]uril-Diarylviologen Quaternary Complexes Favored by Electron-Donating Substituents, *J. Am. Chem. Soc., 139*, **2017**, Pages 3202–3208

J. A. McCune, S. Kunz, **M. Olesińska**, and O. A. Scherman, DESolution of CD and CB Macrocycles, *Chem. Eur. J., 23*, **2017**, Pages 8601–8604

A. S. Groombridge, **M. Olesińska**, G. Wu, and O. A. Scherman, Multivalent Intramolecular Complexes with Cucurbit[n]urils:Versatile Control in Complex Mixtures, under review.

D. E. Clarke*, **M. Olesińska***, T. Mönch, and O. A. Scherman, Aryl-Viologen Pentapeptide Self-Assembled Conductive Nanofibers, under review.

M. Olesińska, G. Wu, S. Gomez-Coca, D. Anton-Garcia, I. Szabo, E. Rosta and O. A. Scherman, Modular supramolecular dimerization of optically-tunable extended aryl viologens, submitted.

M. Olesińska, N. Powers-Riggs, R. M. Young, M. R. Wasielewski and O. A. Scherman, manuscript in preparation.

M. Olesińska, L. Qianqi, J. Huang, K. Sokołowski, J. Baumberg and O. A. Scherman, manuscript in preparation.

*Denotes joint first authorship

Chapter 1

Introduction

This chapter discusses the fundamentals necessary to understand the work presented in the thesis. Chapter 1 is divided into three sections. Section 1.1 gives a brief introduction of self-assembly processes based on molecular recognition and describes molecular H- and J-aggregates as well as aggregates of electronically excited entities. Section 1.2 introduces self-assembly processes based on host-guest interactions focusing on CB[n] macrocycles. Finally, in section 1.3 the chemistry of viologens is discussed, along with its typical spectroscopic properties and their utilisation in supramolecular chemistry.

1.1 Self-assembly Based on Molecular Recognition

Supramolecular chemistry describes and studies systems where molecules non-covalently interact with each other and self-assemble to form more advanced structures. It is a powerful tool in producing novel, complex and dynamic materials as one can control intra- and intermolecular interactions. Although non-covalent intermolecular forces are weaker than covalent bonds, they introduce a new level of molecular organisation.[1] Non-covalent interactions such as electrostatic interactions (ion-ion interaction), hydrogen bonding, van der Waals forces and π-effects are briefly described below.

Ion-ion interaction is a type of electrostatic interaction between oppositely charged molecules. The strength of this interaction is proportional to $1/r^2$, where r is the distance between two charges.[2]

Hydrogen bonding is a type of bond between a hydrogen atom with partial positive charge and another atom with a lone pair of electrons (specifically a nitrogen, oxygen, or fluorine). Typically, the functional group of a molecule that provides a proton to a hydrogen bond is called the hydrogen bond donor. The part of a molecule that provides

an lone pair of electrons (*i.e.* an oxygen or nitrogen centre) is called a hydrogen bond acceptor.[2]

van der Waals interactions are dipole-dipole or induced dipoles interaction. As a result from the constantly shifting electron density in both molecules, they mutually attract each other. The average of these interactions gives the attractive force between dipoles which is proportional to $1/r^6$, where r is the distance between two dipoles.[2]

π interactions occur between molecules such as benzene, which are characterised by partial negative charge on account of their π-cloud.[2] The $\pi - \pi$ interactions involve neighbouring molecular π systems, that interact in three different ways, *i.e.* as face-to-face, face-to-edge or slip stacks. The electrostatic repulsion of the electrons in the π cloud determines the stability of their ring arrangement and configurations of molecules. Cation-π interaction occurs between the conjugated, negatively charged system and a cation.[2] In the most stable arrangement, the cation is cantered directly over the π-system and is in direct van der Waals contact distance with it. Small ions with high charge density form stronger cation-π complexes than larger ions. Electron withdrawing groups on the ring system weaken cation interactions, while electron donating groups strengthen them. Anion-π interactions occur when an anion sits on top of an electron-poor π-system, usually provided by the incorporation of electron-withdrawing substituents to a conjugated molecule.[3]

Non-covalent interactions involving π-systems are one of the most studied because of their role in a variety of fields in chemistry, biology and materials science.[3, 4] The intermolecular interactions control the assembly processes of molecular systems. The photophysical properties of those molecular systems can be explained by their intermolecular interactions and overall morphology.[2, 5–8] The brief description of one of the most fundamental type of molecular organisation, especially important for the interpretation of the data in this thesis, *i.e.* J- and H- type of aggregation as well as the formation of excimer-like dimers are described in following section 1.1.1 and section 1.1.2. The spectroscopic signatures of these processes, as well as observed optoelectronic properties of the resultant materials are discussed.

1.1.1 J- and H- Aggregates

Self-assembly of highly-conjugated chromophores in different types of aggregates affects the optoelectronic properties of a system.[9, 10] There are three major types of arrangement:

H (head-to-head), **J** (head-to-tail) and **oblique** (a mix of both H- and J-aggregates) (Figure 1.1). Each type of aggregate shows its signature in UV – Vis spectrum, *i.e.* a blue or red shift of the absorption maximum in comparison to the absorption of the monomeric species.

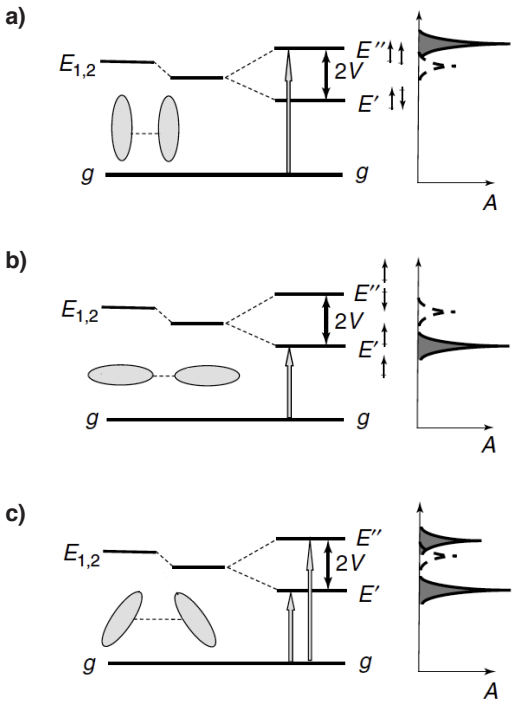

Fig. 1.1 Schematic representation of the relationship between chromophore arrangement and spectral shift based on the molecular exciton theory. a) Energy diagram and schematic absorption spectrum for H-dimer. b) Energy diagram and schematic absorption spectrum for J-dimer. c) Energy diagram and schematic absorption spectrum for oblique dipoles. Light gray shapes show the molecular arrangement.The small arrows represent dipole orientation. The dark gray area peak is the new dimer absorption (*A*), dashed line represents the original monomer transition. Schematic taken from ref. [11].

Molecules with an angle between their centroids (angle of slippage) larger than 32° have J-type of aggregation.[5, 11, 12] This results in sharp, red (bathochromic) shifted absorption bands. Aggregates with a small slippage angle, smaller than 32°, show blue (hypsochromic) shifts that are distinctive features of H-type arrangements.[5, 11, 12] Many J-aggregates show fluorescence with high quantum yields in contrast to H-aggregates, which are reported to be non-fluorescent.[5] Based on exciton theory, molecules in aggregates can be regarded as dipoles.[11] Upon excitation, their excitonic states split into two states (in-phase and out-of-phase dipoles).[11] The transition to the upper state in head-to-head aggregates with parallel transition moments gives a blue-shifted absorption spectra as depicted in Figure 1.1.

In addition, according to the Kasha rule, the higher lying states are essentially non-emitting, due to fast relaxation to lower states, while the lower states are dipole forbidden, so no emission is expected from the H-aggregate configuration.[5] The transition to the lower state in head-to-tail aggregates results in red-shifted absorption and red-shifted emission spectra (see Figure 1.1).
Control over the formation of H- or J-aggregates allows for the manipulation of observed optical properties of materials.[13] Studies by Gosh *et al.* show that aggregation can be controlled through appropriate design of the molecule. For example by introducing side chains with steric hindrance at specific points in the molecule, the formation of H-aggregates is prevented. Similar observations were made by Cai *et al.*, who also reported the effect of temperature and solvent on reversible formation of H- or J- aggregates.[9]

1.1.2 Excimers

Excimers (E*) are defined as dimers of two identical molecules, one in excited state (M*) and one in ground state (M), that are formed due to molecular photo-association.[14] Many aromatic hydrocarbons and their derivatives exhibit fluorescence of excimers, which is characteristic for π-stacking systems with close contacts (<0.4 nm).

In the 1950s', Förster and Kasper made the first observations and studies on excimers of pyrene in solution.[15, 16] They observed a quenching of the fluorescence in a concentrated pyrene solution. Aggregation-quenched emission is often observed for aromatic hydrocarbons like pyrene and perylene that form so called "sandwich shaped excimers". However, there are examples of excimer-like structures of high luminescence.[17–22] Different literature reports suggest that the emissive properties of excimers mainly originate from the packing structure.[23] Typically, loosely packed excimers result in low emission, whereas highly packed excimers with distinct $\pi - \pi$ interactions are often characterised by strong emission.[23]

At the moment, contradicting theories exist about the role of the excimer state in singlet fission, which has resulted in more detailed studies of excimers (see Figure 1.2d).[24] Therefore, it is of great interest to understand the nature of excimers and how their formation can be controlled. The formation and decay processes of excimers can be studied by observing the characteristic spectroscopic features of large Stokes shifts (approximately 5000 cm^{-1} or more) and excimer fluorescence, which is red-shifted, broad and structureless compared to the monomeric species. The original definition of excimers precludes the existence of stable ground state for excimer-like dimers.[14, 25] By this convention, no changes in the absorption spectrum can be observed. However, there are several reports on sandwich dimers (head-to-head oriented dimers) and associated dimers observed in polymers, in crystals or

molecules measured in liquids under high-pressure, that are stable in their ground state and emit like excimers (see Figure 1.2a-c).[26–30]

Two processes are involved in excimer formation, namely the exciton-resonance and charge-transfer interactions. The type of dominant interaction depends vastly on the class of molecules forming the dimer, their structural arrangement, the chemical environment and external factors such as applied pressure. Typically, excited charge-transfer (CT) complexes

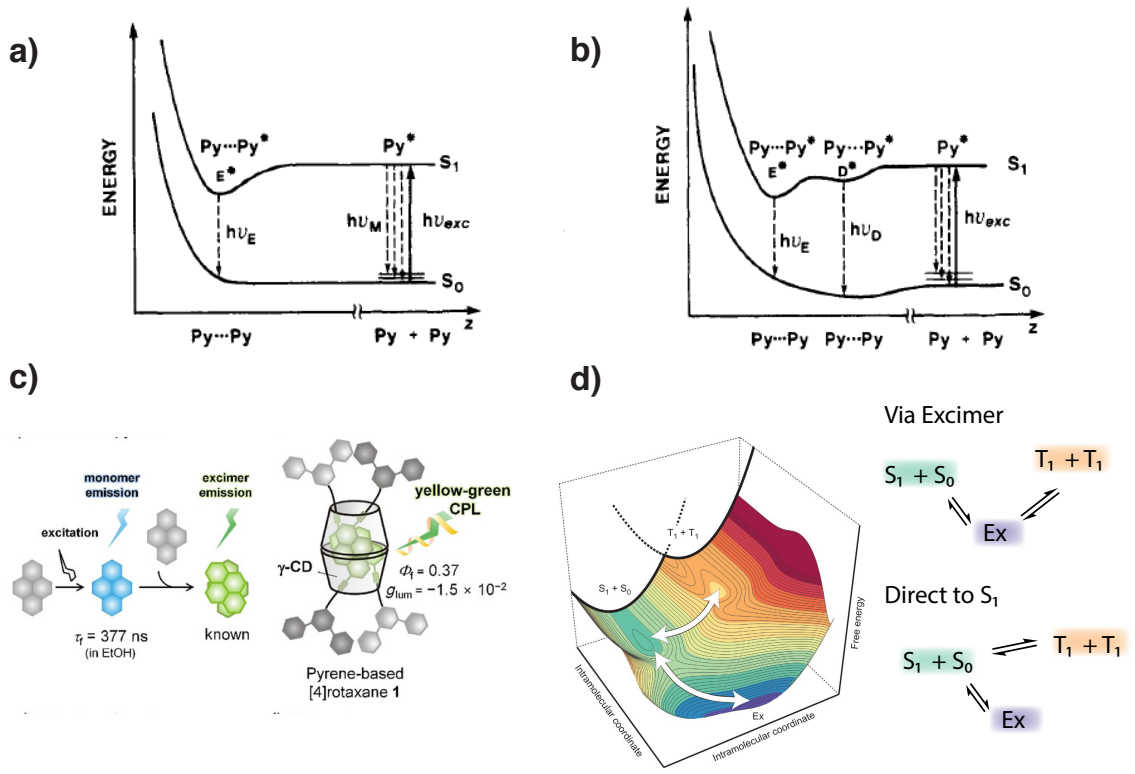

Fig. 1.2 Formation of the excimer-like state of molecules. a) Schematic potential energy diagrams for pyrene excimer formation in the absence of ground-state association. Graph reprinted with permission from ref. [31]. b) The potencial energy diagram for pyrene excimer with the ground state association. Graph reprinted with permission from [31]. c) Pyrene-based [4]rotaxane. Graph reprinted with permission from ref. [32]. d) The intermolecular coordinate of the distance and disposition of the two chromophores. The intramolecular coordinate interconverts singlet and triplet chromophore geometries. In this model, the tightly bound excimer state (Ex) may have triplet-triplet T_1 - T_1 character, yet the route to free T_1 - T_1 is *via* S_1+S_0. Graph reprinted with permission from ref. [24].

are formed in benzene-like molecular complexes, whereas in systems with increased aromatic conjugation, the excition-resonance interaction is more dominant.[33] Several reports have highlighted the need to reformulate the excimer definition and the necessity to use new, more

accurate terms like: "kinetic excimer", "spectroscopic excimer", "singlet excimer" or "triplet excimer".[12, 34]

A kinetic excimer is formed due to a collision between the excited state (lowest singlet) and ground state molecules. This describes mostly the event of formation of excimers in solutions with a particular molecular arrangement.

On the other hand, a spectroscopic excimer focuses on the optical properties that arise from the formation of an excited dimer or excimer-like structures.[34]

A singlet excimer is characterised by a broad, red-shifted and structureless emission spectrum with respect to the monomer fluorescence spectrum. This type of excimer is stabilised by both CT and exciton-resonance interactions.

A triplet excimer is stabilised only by CT interactions.[33] They are considered to be less stable, and formed for dimers of non-sandwich orientations.[35, 36]

A special type of excimers are exciplexes. Exciplexes are formed between donor and acceptor molecules, and are thus stabilised by CT interactions only.[37] Exciplexes occur in molecular blends and dimers are formed by the interaction of an excited molecule with a ground state counterpart of a different molecule.

1.2 Self-assembly Based on Host-Guest Chemistry of Cucurbit[n]uils

The host-guest chemistry of macrocyclic compounds is based on identification of complementary units.[38] Besides cyclodextrins and calixarenes, a very promising self-assembly motif in aqueous media is based on the barrel-shaped cyclic oligomer of cucurbit[n]uril (CB[n]) (see Figure 1.3). Cucurbit[n]urils are a family of water-soluble host macrocycles often used in synthetic and material sciences on account of their capability to complex different types of guest molecules.[38, 39] These highly symmetrical molecules include CB[5], CB[6], CB[7], CB[8] and CB[10] homologues. They differ in the number of glycouril units (n = 5, 6, 7, 8, 10) linked by methylene bridges, and have two identical carbonyl-laced portals (See Figure 1.3).

The first reported cucurbituril, CB[6], was synthesised by Behrend in 1905, and fully characterised by Mock in 1980.[40, 41] Mock proposed the name "Cucurbituril" based on the X-ray structure of a molecule he isolated that resembled a pumpkin (latin *Cucurbitaceae*).[42] Since the 1980s, the original synthetic protocol of acid-catalysed condensation of glycouril with an excess of formaldehyde has been modified to yield a mixture of CB[n]

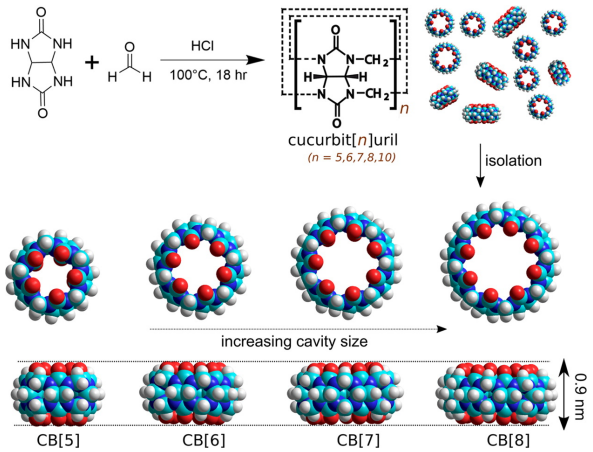

Fig. 1.3 X-Ray structures of cucurbit[n]urils. Adapted from [38].

homologues.[43, 44] The purification and separation of each component is based on their solubility in water, water/methanol and diluted hydrochloric acid solutions.[43–45]

Cucurbit[n]urils attract much attention due to the varying cavity diameter (4.4 Å to 8.8 Å) between homologues, which tunes their interactions with different molecules (see Table 1.1). For CB[5] to CB[8], the hydrophobic cavity volume ranges between 82 $Å^3$ to 479 $Å^3$, their hydrophilic carbonyl portals have a diameter between 2.4 Å to 6.9 Å, while the depth of the homologues is uniform throughout the CB[n] series (9.1 Å).[38] The ability to encapsulate a variety of molecules is one of the most exploited properties of the cucurbit[n]uril family. Furthermore, among other supramolecular macrocycles, cucurbit[n]urils show high binding constants of up to Keq=1×10^{15} M^{-1}.[46]

Table 1.1 Dimensions of cucurbit[n]uril homologues.

CBn	5	6	7	8
Portal (Å)	2.4	3.9	5.4	6.9
Cavity (Å)	4.4	5.8	7.3	8.8
Cavity Volume ($Å^3$)	82	164	279	479

The smaller cucurbit[n]urils *i.e.* CB[5], CB[6] can accommodate one guest.[47, 48] Typically CB[5] encapsulates gas molecules such as Kr, Xe, N_2, O_2, Ar, N_2O, NO, CO, CO_2, and CH_4 or solvents like methanol and acetonitrile. [49] Moreover, CB[5] can bind two cations, for example Pb^{2+}, NH_4^+, as well as alkali metals, alkaline earth metals, transitions metals etc., through interaction with its carbonyl portals. CB[6], due to its bigger cavity, can readily accommodate positively charged organic molecules such as protonated aminoalkanes,

amino alcohols or amino acids.[50, 51] CB[7] can form strong complexes in a 1:1 or 2:1 (host:guest) ratio, with positively charged aromatic compounds including adamantanes, naphthalene, stilbene, viologen, and ferrocene, molecules that are too big for CB[5] and CB[6] cavities.[52–54] High solubility of CB[7] in water, up to 30 mM, together with high association constants with guest molecules makes this macrocycle attractive for drug encapsulation. CB[8], due to its large cavity size, has the ability to encapsulate up to two aromatic guests.[55] CB[8] based hetero-ternary complexes, involving two different molecules, and homo-ternary complexes, involving two of the same molecules have been reported (Figure 1.4).[44, 56] Simultaneous encapsulation of two guests along with their high complexation binding made CB[8] based system attractive for many applications including supramolecular hydrogels, drug delivery systems and sensors.[57–61] The performance of those systems or functional materials is often based on efficiency of host-guest binding. Thus, this is extremely important to understand what is the driving force and mechanism of complexation.

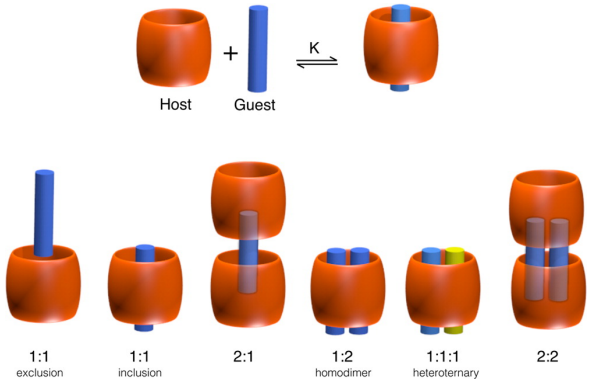

Fig. 1.4 The type of CB[n]-based complexes. Reprinted with permission from [38].

1.2.1 Mechanism of CB[n] Host-Guest Complexation

There are several non-covalent intermolecular interactions and supramolecular effects between hosts and guests, which explain their affinity to each other and the binding process itself.

Firstly, the size complementarity. As described before, the cavity diameter determines the type of molecules that can be encapsulated in each homologue.

Secondly, the dipolar interactions.[62] These interactions involve either the coordination between a metal ion or a polar molecule and polar carbonyl groups of the CB[n] portals.[63] One of the structural properties of the CB[n] family is the high electron density at the carbonyl oxygens and their hydrophobic cavity.[64] This high electonegativity allows CB[n]s

to strongly bind positively charged species via the ion-dipole effect. The electrostatic attraction due to changes in the electron-density distribution, can increase the attraction between the host and guest molecules.[45]

Finally, the non-classical hydrophobic effect, which can be described as an enthalpic gain from the "high-energy" water release upon binding the non-polar molecule, changing the interactions inside the cavity.[65, 66] Inside the hydrophobic cavity of macrocycle there are water molecules (around 8 and 13 for CB[7] and CB[8], respectively). [67] These water molecules, connected together through hydrogen bonds, are energetically frustrated due to the size constrains of the cavity. The smaller the cavity, the greater the restriction in the number of possible hydrogen binding configurations the water molecules may adopt. Release of high energy water from the host molecule, and formation of stable hydrogen-bonded network makes the binding of the guest an enthalpy-driven process. It was reported that stable hydrogen-bonded networks of water are formed inside cavities of at least 1 nm size in diameter.[67] Following this, the non-classical hydrophobic effect of binding, *i.e.* the enthalpic loss upon release of water, should be bigger for CB[7] then for CB[8] host molecule. However, CB[8] can accommodate a larger guest or simultaneously more then one guest, thus upon complexation, more cavity water can be displaced, which adds to the value of ΔH. Thermodynamic parameters not only can help in determination if the binding occurs, but also can give information about type of host-guest complexation. Recent publication by Wu *et al.* summarised thermodynamic data reported in literature for CB[8] complexes with different guests.[68] Different complexes were characterised with appropriate values of the overall binding enthalpies and the temperature entropy product (see Figure 1.5). Enthalpy values were found to be around $-40\,\mathrm{kJ\,mol^{-1}}$ or lower. Complexes involving encapsulation of two guest had enthalpies values ranging from $-50\,\mathrm{kJ\,mol^{-1}}$ to $80\,\mathrm{kJ\,mol^{-1}}$

1.2.2 Cucurbit[n]uril Complexation of Fluorescent Guests

Over the past years, the effect of encapsulation of various small molecules in different supramolecular macrocycles has been studied. The main driving force of this research is their potential application in detection, imaging, and stimuli-responsive materials. For example various analytes (such as 1-anilinonaphthalene-8-sulfonate (1,8-ANS)) were detected through their enhanced luminescence via host—guest inclusion complexes.[59, 69–71]

The encapsulation of water-soluble fluorescent molecules is particularly interesting because of their sensitivity to changes to micro environmental parameters such as viscosity, solvent polarity *etc*.[71, 72] This allows for their use as sensors in biological and environmental systems.[73–75]

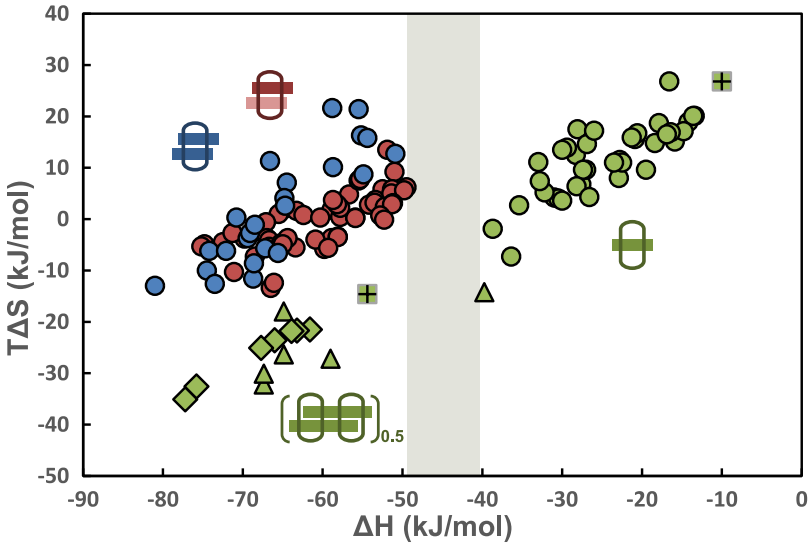

Fig. 1.5 Thermodynamic data for CB[8]-mediated host-guest complexation determined by ITC in buffered aqueous solution. Enthalpy and Entropy data for 2:1 homoternary complexes (blue), 1:1:1 heteroternary complexes (red), and complexes with 1:1 binding stoichiometry (green). Reprinted with permission from [68].

There are already reports on the complexation of fluorescent dyes in supramolecular macrocycles including cyclodextrins, crown-ethers and CB[n]s, for labelling and detection of biological molecules.[65, 76, 77] Such complexes possess higher thermo- and photostabilities, show longer excited state lifetimes, enhancement of the fluorescence quantum yields and resistance towards the fluorescence quenchers such as oxygen, compared to the uncomplexed fluorescent molecule.[77–79] There are several factors behind these effects. The inclusion of a fluorophore into the cavity of a host, separates and protects it from solvent-induced quenching and possible quenching by oxygen or other components present in the system (mechanical protection, Figure 1.6a).[71] Moreover, the geometrical confinement and reduced rotational and vibrational freedom of the fluorophore in a host cavity limits the nonradiative decay pathways of fluorescent deactivation(Figure 1.6b). The encapsulation may also cause deaggregation of guest molecules and thereby enhance their fluorescence, prevent self-quenching.[80]

The cucurbit[n]uril family provides an opportunity to study encapsulation of different fluorophores on account of differences in the inner cavity volume of different CB[n] homologues. So far, complexation with CB[7] has been the most utilised system due to its high water solubility.[81] There are reports on fluorophore inclusion in the CB[7] cavity, changing or tuning the optical properties of the enclosed molecule.[82] Nau *et al.* reported studies where the fluorescence lifetime of 2,3-diazabicyclo[2.2.2]oct-2-ene (DBO) encapsu-

lated in the CB[7] increased (from 325 ns to 690 ns) in aerated aqueous solution. However, no changes in fluorescence occurred when a degassed solution was used (indicating that oxygen is incapable of quenching the encapsulated chromophore).[83] The same system in deuterated water showed fluorescence lifetime of 970 ns due to less efficient quenching. However, photoproduct formation from guests in the cavity of the host can also occur and may cause a decrease in florescence. An example of such photocatalysis is the formation of the non-fluorscent [4+4] photodimerised antracenes in CB[8] cavity, studied by Biedermann and Carvalho.[84, 85] Manipulation of the optical properties of the molecule is one of the interesting effects that can occur upon complexation of CB[8] with fluorescent dyes. This phenomenon can be used to design new types of sensors, and self-diagnostic polymeric structures.

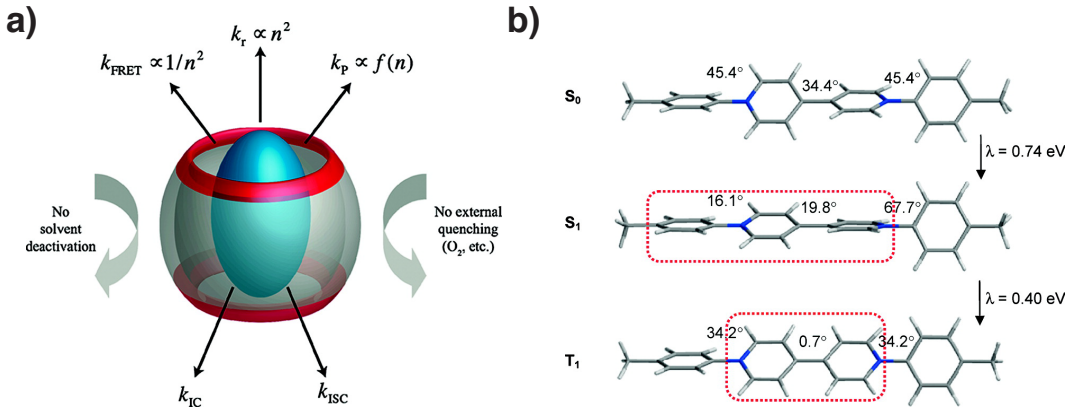

Fig. 1.6 The effect of the fluorescent guest encapsulation in cucurbit[n]uril. a) Illustration of the mechanical protection of a fluorophore inside CB and the effect on photophysical decay pathways for excited-state dyes upon inclusion. Reprinted with permission from [86]. b) Demonstration of the rigidochromic effect of guest encapsulation within CB cavity. Reprinted with permission from [87].

1.3 Viologens

Viologens is a *trivial name* for the family of N-substituted 4,4'-bipyridines. An example generic structure of viologen is depicted in Figure 1.7. These compounds are known for their reversible redox reactions and were originally used as redox indicators, herbicides and "electron mediators" in many photochemical processes.[88] Recently, viologens have attracted much attention mostly for their optoelectronic properties. On account of their

stable coloured radicals there are many examples of using viologens in electrochromic display devices.[89–93] Viologens are also widely used in organic batteries like redox flow batteries or radical batteries.[94, 95] The ease of synthetic modifications of viologens and thus, possibility to tune their properties, has made these molecules an attractive building block for more complex supramolecular systems. Through the use of host-guest structural arrangements, such as catenanes and rotaxanes, it is possible to achieve more stable viologen radicals.[96–98] This allows the creation of systems comprising molecular machines and molecular switches, examples of which are further discussed in Chapter 2. The dynamic interactions of $MV^{\bullet+}$ derivatives with supramolecular macrocycles (such as CB[n]), as well as redox controlled stoichiometry of $MV^{\bullet+}$ based inclusion complexes make these systems a powerful trigger in supramolecular chemistry and dynamic nanosystems.

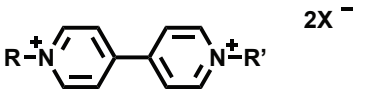

Fig. 1.7 The generic structure of viologens.

1.3.1 Synthetic Modifications of Viologen

This subsection discusses the most popular synthetic methods to obtain and chemically modify viologens.

In principle, there are two well established in the literature strategies that enable access to a wide variety of viologen derivatives. The first approach is based on coupling reactions. The commonly used reactions are:

- Winters coupling which is a reaction on 1-substituted pyridines coupled in the presence of cyanide ions (see Figure 1.8a).[99]
- Suzuki coupling which is an aryl-aryl C-C bond cross-coupling that allows for the formation of viologen and extended viologen derivatives (see Figure 1.8b). This approach will be described in more details in Chapter 2 and Chapter 4.

The second method for viologen structure modification is based on N-substitution on 4,4'-bipyridine:

- Anderson reaction or Menshutkin reaction it is the quaternisation reaction on pyridines with an excess of alkyl halide (see Figure 1.8c).[100]
- Mitsunobu reaction which is the preparation of pyridinium salts with N-alkylate functionalisation using pyridinium salts as acidic nucleophiles.(see Figure 1.8d).[101]

• Zinke reaction proposed in 1903 by Theodor Zincke a reaction where, through forming a quaternary pyridinium salt and its further reaction with aniline, it was possible to obtain the N-aryl pyridinium compound (see Figure 1.8e and Figure 1.9).[102–104] This method and its application for synthesis of asymmetric viologens is described in more details in Chapter 3 and Chapter 4.

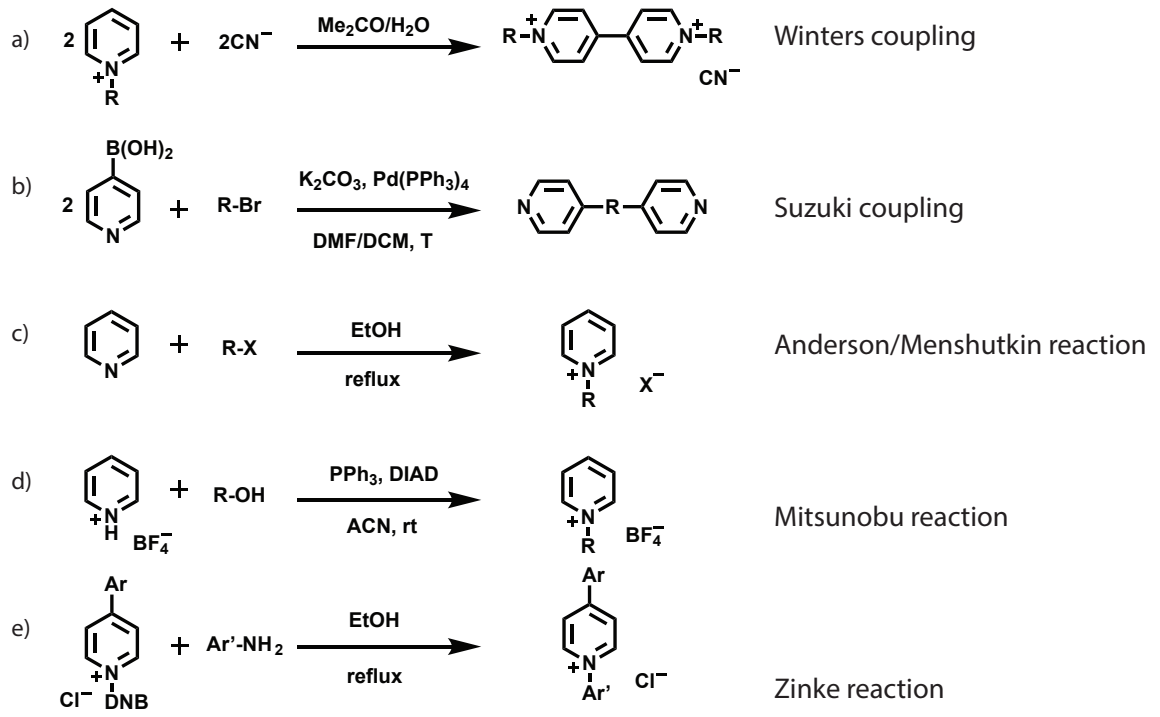

Fig. 1.8 Typical reactions for viologen modifications: a) Winters coupling b) Suzuki coupling also for extended bipyridines c) the Anderson/Menshutkin reaction d) Mitsunobu reaction e) Zinke reaction. Side products have been omitted for clarity.

1.3.2 Physicochemical Properties of Viologen

This subsection discusses selected methods, which are useful in the characterisation of viologen based systems presented in this thesis, namely cyclic voltammetry (CV), UV – Vis and electron paramagnetic resonance (EPR) spectroscopy.

As mentioned before, viologens are well known for their redox properties. Methyl viologen (MV^{2+}) can undergo a one electron reduction forming radical cations ($MV^{+\cdot}$) followed by a second electron reduction yielding a doubly reduced viologen (MV^{0}).[106, 107] A CV graph depicted in Figure 1.10 shows those two reactions as two reversible single-electron waves. The first reduction potential, at around -0.7 V, leads to the formation

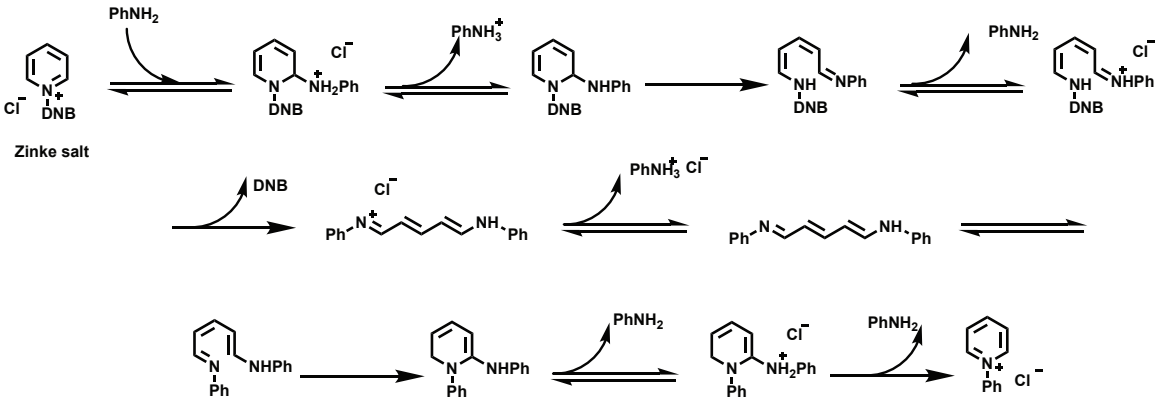

Fig. 1.9 Proposed mechanism of Zinke reaction adapted from [105]. The Zincke reaction is an ANROC mechanism type reaction *i.e.* **N**ucleophilic **A**ddition of an amine to the carbon in a second position of the pyridinium salt, followed by an reaction with amine and 2,4-dinitrobenzene elimination of the **R**ing **O**penning to the dianiline salts in a *cis* and *trans* conformation, and finally the 6π -electrocyclic ring **C**losure step. Side products have been omitted for clarity. Abbreviation used in the figure: DNB- 2,4-Dinitrobenzene; Ph- Phenyl.

of the radical cation, while the second reduction potential, at around -1 V, results in the fully reduced, neutral methyl viologen.[108] The shape of the cyclic voltammogram for viologen derivatives in water depends on the type of viologen and its solubility in the electrolyte.[109] There are examples of CV performed on asymmetric alkylated viologens, where precipitation of the molecule on the electrode causes sharp oxidative peaks and results in a non-reversible cycle.[109, 110] In general, change of the N-substitution on viologen affects the recorded reduction potential.[106, 108, 109, 111, 112] Aromatic viologens tend to have higher reduction potential in comparison to alkylated viologens.[109, 111] Such properties of viologen has led to their application as redox mediators and as electron acceptors in charge-transfer complexes for electrical and ionic conductors.[106, 107] Additionally, electrodes modified with viologen based polymer species have been of increasing interest due to their electric, optical and magnetic performance.[107, 113]

The radicals of viologens are coloured, as a result of a single, free electron in the radical.[108] The $MV^{+\cdot}$ water solution has an intensive blue colour, and its UV – Vis spectrum has characteristic absorption peak at 600 nm. Upon increasing the concentration of the methyl viologen radical cation, the colour of the solution changes to violet.[114] This is attributed to the formation of methyl viologen radical cations dimers (see Figure 1.11). The colour of the solution *i.e* the switch between monomeric and dimeric species, can be controlled with temperature.[115] With the decrease of temperature the blue solution turns violet, and upon increasing the temperature the violet solution becomes blue.[115, 116] Figure 1.11 shows the UV – Vis spectra recorded for mono reduced alkylated viologen $(1)^{+\cdot}$ and its dimer $[(2)^{2+}]_{dim}$.

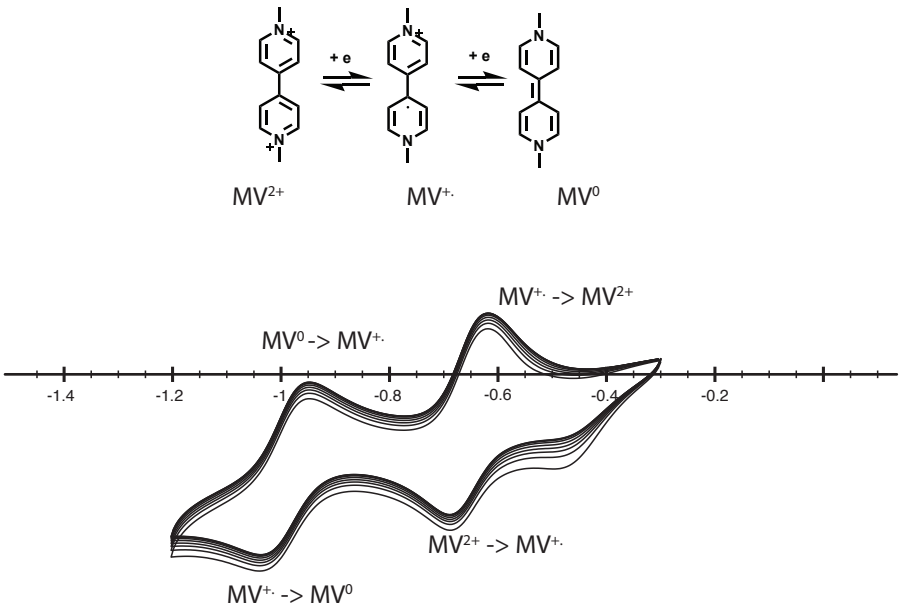

Fig. 1.10 Three redox states of methyl viologen and its cyclic voltammogram in KCl aqueous solution.

The absorption spectrum peak at 400 nm for the viologen radical dimer is blue-shifted in comparison to the absorption spectrum of the monomer as a result of face-to-face interactions of dipole moments of two molecules in close proximity (see also Figure 1.1a).[117, 118] The characteristic new absorption band around 850 nm is typical for radical dimers of viologen. The absorption band in the NIR region suggests an allowed electronic transition from a filled bonding molecular orbital to an anti-bonding orbital within the diamagnetic viologen dimer.

Paramagnetic radicals of viologens and the process of their dimerisation can be studied with EPR.[109, 115, 119, 120] On account of singlet state electronic configuration, the diamagnetic dimerised viologens are characterised by silent EPR signal.[119] As previously mentioned, the reversible process of dimerisation can be controlled with a temperature change.[115] By making use of this, the EPR profile of the paramagnetic radical and the diamagnetic dimerised radical can be characterised and the equilibrium of dimerisation measured.[115, 119] The dimerisation of viologens is observed in concentrated solutions (1 M).[116] The process of dimerisation is enhanced with addition of CB[8], that can bind and stabilised within its molecular cavity two methyl viologen radicals (K_{eq}=2×10^7 M^{-1}).[121] Upon chemical or electrochemical reduction of methyl viologen in presence of CB[8], the characteristic violet colour of dimerised radicals can be observed, indicating homoternary complexation.[121, 122] The reversible dimerisation of methyl viologen radicals within

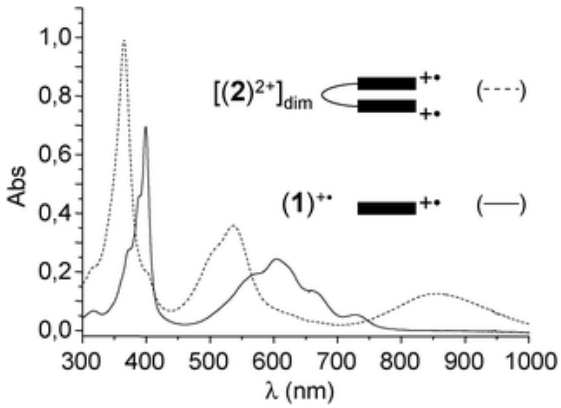

Fig. 1.11 UV – Vis spectra recorded after exhaustive one-electron reduction per viologen in alkylated viologen derivatives. Figure reprinted with an permission from ref. [117].

CB[8] cavity via changes of temperature or competing guests encapsulation, is a powerful switch widely utilised in material science.[122, 123]

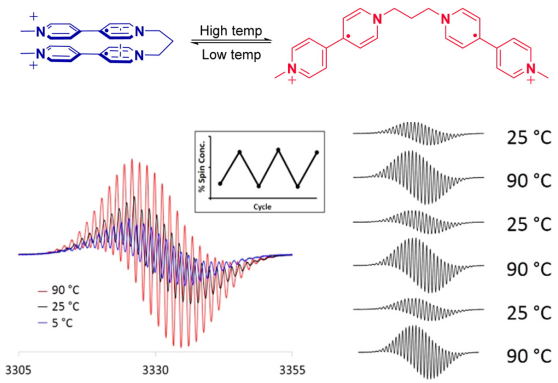

Fig. 1.12 a) Scheme of diamagnetic dication pimer and its reversible thermomagnetic switch to paramagnetic diradical dication. b) EPR spectrum of 2 mM aqueous solution of diamagnetic diradical dication pimer in buffer at different temperatures. Figure reprinted with an permission from ref. [115]

1.4 Aim and Scope

This doctoral thesis focuses on design, synthesis and characterisation of π-extended viologen-based molecular and supramolecular systems. The aim is to expand the knowledge on assembly processes that involve extended viologen derivatives and CB[n] macrocycles as this can help to understand the physicochemical properties of resulting host-guest systems and eventually improve design and efficiency of optoelectronic devices and materials.

In Chapter 2 the synthesis and characterisation of a series of extended methyl viologen (EV[X]MV) derivatives with an aromatic extension between the pyridinium rings, their interactions with CB[7] and CB[8] macrocycles as well as physicochemical properties of the resultant host-guest systems are studied. Methyl viologen (MV^{2+}) is a well-known guest for both CB[7] and CB[8] macrocycles. On account of the different binding modes with CB[n], the optical as well as redox properties of MV^{2+} can be modulated. Here, the effect of the aromatic extension ([X]) on EV[X]MVs before and upon complexation with CB[7] and CB[8] is investigated using nuclear magnetic resonance (NMR), steady-state UV – Vis and photoluminescence (PL) spectroscopies as well as isothermal titration calorimetry (ITC) and cyclic voltammetry (CV).

Chapter 3 provides study on a family of extended viologens with aromatic substituents (EV[X]R, further denoted as extended aryl viologens), their interactions with CB[8] macrocycles as well as physiochemical properties of the resultant host-guest systems are studied. The design and synthesis of these new class of π-conjugated viologen derivatives are elaborated involving different aromatic bridging units, as well as rigid aromatic peripheral functionalisation with electron donating and electron withdrawing groups on the pyridinium rings. The nature and dynamics of the resulting $CB[8]_2 \cdot (EV[X]R)_2$ homo- and hetero-complexes are studied both in the ground as well as exited states upon interaction with light utilising NMR, steady-state and time-resolved spectroscopies as well as ITC experiments.

Finally, in Chapter 4 the synthetic approach towards asymmetric aryl viologen (AV) and extended aryl viologen (EV[X]RR') is presented. The application of asymmetric aryl viologens in the formation of a bio-inspired nanofibers is discussed.

Chapter 2

Synthesis and Characterisation of Extended Methyl Viologens

This work has been compiled into a manuscript in preparation for submission for publication:

Olesińska, M., Qianqi L., Huang J., Sokołowski K., Baumberg, J.R., Scherman, O.A.*, manuscript in preparation.

In this chapter, the focus is on studies on design and synthesis of π-extended methyl viologen (EV[X]MV) molecules. Firstly, EV[X]MV molecules with [X] different types of bridging units between the two pyridins were synthesised. Secondly, the interaction of EV[X]MVs with CB[7] and CB[8] was studied using nuclear magnetic resonance (NMR) and isothermal titration calorimetry (ITC). Subsequently, the effect of encapsulation of selected EV[X]MVs within the macrocycles on their optoelectronic properties is measured and analysed with steady state spectroscopy and cyclic voltammetry (CV).

2.1 Introduction

The nature of inter- and intramolecular interactions amongst molecules is significant in the rational design of new supramolecular systems. Control over assembly processes of molecular systems allows to direct the physiochemical properties of materials.[124–127]

In colloidal systems, properties of a suspension can be manipulated by modulation of attractive and repulsive forces between constituent particles, which overall balance ensure stability of the mixture. By weakening the repulsive forces one can initiate aggregation processes, which usually leads to microscopic solid products.[2] The intense research on the structure of solid state matter, has produced extremely useful insights into intermolecular

forces that govern assembly processes, *i.e.* dipol-dipol and van der Waals interactions, hydrogen and halogen bonding, hydrophobic effect, as well as $\pi - \pi$ interactions (previously described in Chapter 1). These structural insights have laid the foundations for the design principles of donor-acceptor systems based on organic molecules. In these systems, molecules are held together by electrostatic forces between electron-poor acceptor and electron-rich donor molecules. When molecules are characterised by a highly conjugated π-system, it is possible that they will assemble in stacks due to $\pi - \pi$ interactions. There are examples in literature where this interaction is so dominant that it over-rules the repulsive electrostatic interactions between the ions, leading to aggregate formation.[128] Therefore, π-conjugated systems have been attracting much attention due to their promising applications in many technologies, involving organic electronic devices such as organic light-emitting diodes, field effect transistors and solar cells.[129, 130] Interestingly, the $\pi - \pi$ stacking pattern can result in π-homodimerisation among conjugated radical anions or cations. It has been demonstrated that the stacking of conjugated radical cations, particularly those formed by bipyridinium or tetrathiafulvalene, can be enhanced remarkably when they are incorporated into rationally designed, preorganised frameworks or entrapped into a confined space.[131, 132] Considering the importance of radical cations and dications of π-conjugated systems in charge transfer and charge separation processes, many underlying phenomena still have to be studied. Amongst these are the distributions of charges and spins as well as the relationships between the molecular structures of the system components and their electronic, optical and magnetic properties.

On account of their redox properties, viologens and their derivatives are one of the most important molecules used in molecular machine systems, electrochromic devices and hybrid organic batteries.[94] It is due to properties such as the ease of reduction, reversible electron-transfer reactions, stable redox states, and redox photochromism that viologens have been present in the scientific literature since the 1930s.[88] The radical cation of methyl viologen is relatively stable, however, the existence of oxygen in the system accelerates reverse electron transfer. To achieve higher stability of the radical cation, many structural alterations in viologen have previously been made (see Figure 2.1). One of the most popular approaches to change the optoelectronic properties of viologens, is through the nitrogen substituents. Another is by changing the bridging unit between the two pyridines, through π-extension of the ethylene bond or insertion of an (hetero)aromatic ring [133, 134]. In 1992 Fukuyo *et al.* reported on the extension of viologen by means of aromatic phenylene and five-membered heteroaromatics as thiophene and fullerene.[135] The electrochemical, as well as photophysical characterisation revealed that one electron reduction of heteroaromatic extended viologens resulted in stable cation radicals. Polydienylene extensions turned out

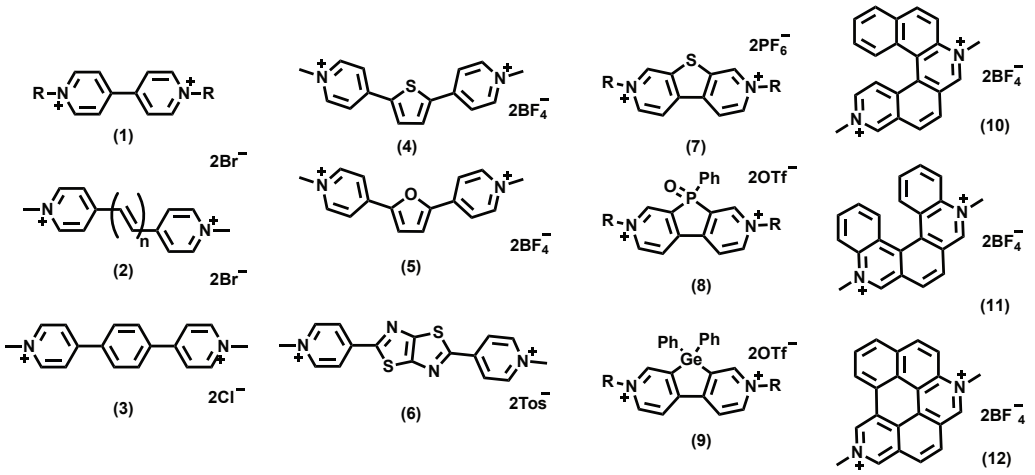

Fig. 2.1 Selected viologen derivatives. (1) Methyl viologen, symmetric and asymmetric alkylated N-substituents [110, 119], (2) polyene linked extended viologen [143], (3) phenylene extended viologen [133], (4) thiophene-bridged viologen [135, 143], (5) furan-bridged viologen [135], (6) thiazolothiazole extended viologen [134], (7) sulfur-bridged viologen [144], (8) phosphole-bridged viologens [145–147], (9) germanium-bridged viologen [148] and (10-12) [5]-heli-viologens. [149]

to form less stable radical cations. The result was explained by the presence of a double bond between pyridinium rings reducing the electron withdrawing character against each other.[133] Evans *et al.* were the first to suggest that better overlap between $\pi - \pi$ orbitals could be the reason for higher delocalization of unpaired electron density over the molecule, leading to a higher stability of the radical cation.[136]

Stabilised radicals of viologen can also be achieved by dispersion in aprotic matrices, polymers and viscous solvents, as well as by inclusion in host molecules like cucurbit[n]uril.[120–122, 133, 137, 138] Additionally, stable viologen based radicals can be obtained by multi-stage redox systems.[96–98, 139] The molecular system of homo[2]catenane (HC), asymmetric[2]catenane (AC) and symmetric[2]catenane (SC) based on bipyridine or 2,7-diazapyrenium units showed up to seven different redox states that can be chemically or electrochemically switched between each other in a reversible manner (see Figure 2.2). The stability of those radicals is based on mechanically interlocked molecules and the geometry fixed by radical-pairing interactions as well as $\pi - \pi$ stacking. Such inclusion complexes allow for facile electron transfer as well as the electron trapping within the catenane. Organic molecules or systems that feature multiple stable redox-states or mixed-valence states offer various applications in energy storage, spintronics, solar energy devices and electrochromic devices. [110, 140–142]

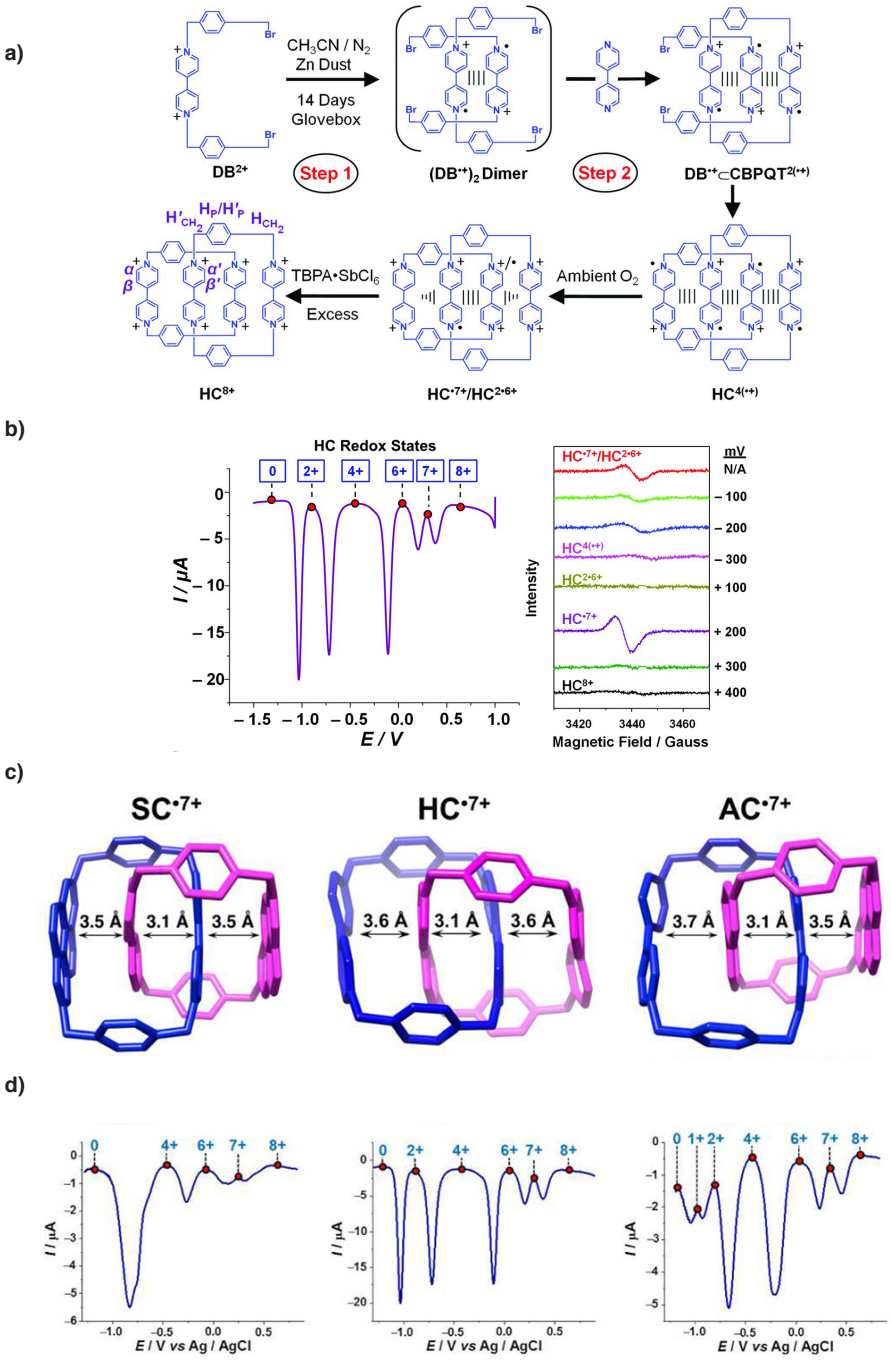

Fig. 2.2 The interlocked, multi-stage redox viologen based systems. a) The synthetic route from 2+ to 8+ charged species. Adapted from ref. [96]. b) The differential pulse voltammetry (DPV) of the six redox states of system depicted in a) together with its EPR signal performance showing the dia- and paramagnetic properties. Adapted from ref. [96]. c) and d) Analogous viologen multi-stage redox based systems, exhibiting through the differential pulse voltammetry five, six and seven different stable redox states. Adapted from ref. [98].

2.2 Results and Discussion

2.2.1 Synthesis of EV[X]MVs

Extended bipyridines with various conjugated cores *i.e.* phenylene, naphthalene, 1,6-pyrene, 2,7-pyrene, chrysene, thiophene and dithiophene were synthesised using Suzuki coupling of pyridine 4-boronic acid and corresponding dibromo species, as depicted in Figure 2.3. The synthesis was adapted from literature procedure by Barnes *et al.*[150] An acid-base purification was used to purify and separate all EV[X]s. Next, each bipyridin was reacted with iodomethane, yielding charged extended methyl viologens (EV[X]MV, where X=Ph (Phenylene), Np (naphthalene), $Pyr_{1,6}$ (Pyrene-1,6), $Pyr_{2,7}$ (Pyrene-2,7), CH (Chrysene), Th (Thiophene) and DTh (Dithiophene)) with I^- as the counterion. Molecules where isolated via ether precipitation and recrystallisation from absolute ethanol or methanol. It is important to note that synthesis and isolation of EV[Np]MV, EV[CH]MV, EV[$Pyr_{1,6}$]MV and EV[$Pyr_{2,7}$]MV molecules are reported for the first time. Synthetic details can be found in experimental section 2.4.

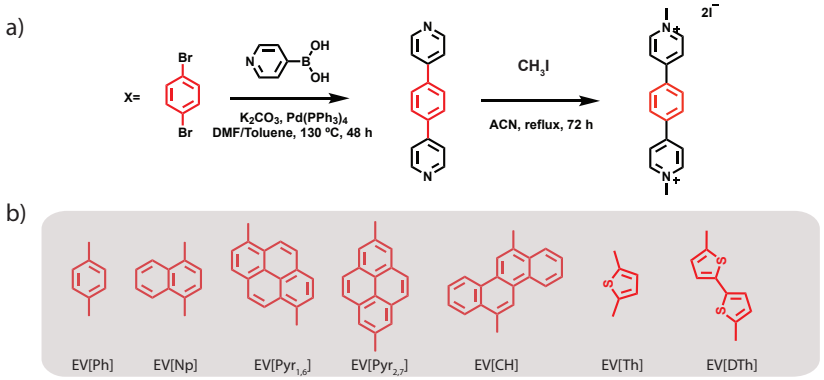

Fig. 2.3 Schematic representation of the EV[X]MVs a) The synthesis of EV[X]MVs. b) Chemical structure of EV[X]MVs core extension.

2.2.2 Interactions of EV[X]MVs with CB[8] and CB[7]

Interaction between EV[X]MV and CB[8] and CB[7] were studied with ^{1}H NMR experiments. Typically, binding of a guest with the hydrophobic CB[8] or CB[7] cavity results in an upfield shift of the encapsulated protons and downfield shift of protons in close proximity to the CB[n] portals. Strong and less dynamic bindings are characterised by sharp, well resolved NMR spectrum, whereas dynamic complexation often results in broadening of the signals.

EV[Ph]MV ^{1}H NMR spectrum of 1:1 ratio mixture of EV[Ph]MV and CB[8] shows a weak 0.02 ppm downfield shift of H_d and 0.08 ppm upfield shift of H_a protons (see Figure 2.4). There are strong upfield shifts of H_b and H_c with 0.42 ppm and 0.81 ppm for the 2:1 host-guest complex, which shifts further to 0.48 ppm and 0.93 ppm, then 0.55 ppm and 1.11 ppm respectively for 1:1 and 1:2 complex (see Figure 2.4, and Figure A.27). The bigger shift for H_c and H_b suggests that these protons are most affected by the presence of the CB[8] cavity. Hence, the host molecule probably assembles in the middle of the guest molecule, on the phenylene core. Peaks for the 1:1 and 2:1 complexes with CB[8] are very broad. This is typical for dynamic complexes or elongated structures. Peaks for the 1:2 host-guest complex are sharp and there is no sign of free, uncomplexed guest. Such a spectrum suggest that two EV[Ph]MV molecules bind with CB[8], with the macrocycle binding to the core of the molecule.

Upon addition of CB[7], EV[Ph]MV exhibits a 0.06 ppm upfield shift of the methyl proton (Figure 2.4 and Figure A.26). This small shift suggests that this part of the molecule is outside the cavity of the macrocycle and just slightly affected by the carbonyl rim. All the aromatic protons of EV[Ph]MV are shifted upfield. Peak H_a, H_b and H_c are shifted upfield with about 0.08, 0.33 and 0.95 ppm respectively. Shifts of about 1 ppm upfield are typically indicative of a strong effect of CB[7] presence. Sharp peaks suggest strong and slow complexation on the NMR time scale. The comparison of the NMR spectra for EV[Ph]MV mixed in 1:2 ratio with CB[8] and 1:1 ratio with CB[7] suggest a binding mode where both macrocycles are bound around the phenylene core of EV[Ph]MV. Thus, CB[7] encapsulates a single molecule, whereas CB[8] can bind two molecules on account of its larger cavity.

EV[Np]MV Naphthalene extended methyl viologen, upon adding to CB[8] in 1:1 ratio, exhibits marginal (ca. 0.07 ppm) downfield shifts of the methyl proton (see Figure 2.5 and Figure A.28). Such a shift suggests that this part of the molecule is outside the cavity of the macrocycle, and is slightly affected by the carbonyl rims of CB[8]. In the 1:1 mixture of EV[Np]MV and CB[8], all the aromatic protons of the guest are shifted upfield. Here, peak H_a is shifted downfield with only about 0.08 ppm, similar to H_f. Peak H_b is shifted 0.41 ppm downfield. Peaks on the aromatic naphthalene core H_d, H_c and H_e, are shifted downfield with 0.86 ppm, 0.55 ppm and 0.74 ppm respectively. Such high shifts suggest complete inclusion inside the CB[8] cavity. Calculated concentrations and integration of CB[8] and guest signals suggest 1:1 binding for EV[Np]MV with the host encapsulating the naphthalene core. Sharp, well resolved peaks indicate that on the NMR time scale, the complex is non-dynamic.

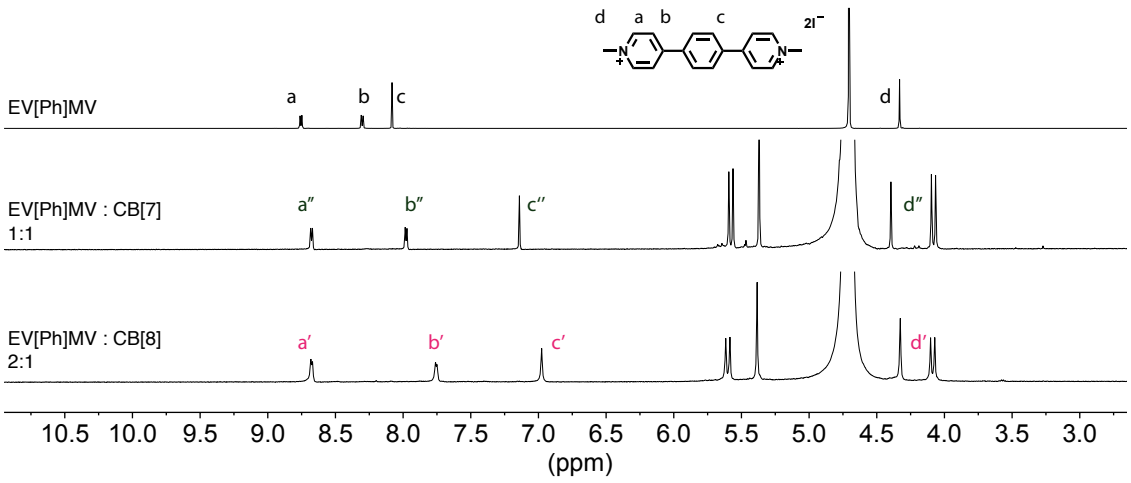

Fig. 2.4 ^{1}H NMR of 1:2 complexes of EV[Ph]MV with CB[8] and 1:1 complex with CB[7]. Measurements performed in D_2O with I^- as counterions.

In contrast to that, EV[Np]MV complexed with CB[7] is characterised by broad peaks (see Figure 2.5 and Figure A.29). Peaks H_f and H_a are upfield shifted with approximately 0.35 ppm and 0.56 ppm, fairly affected by presence of the CB[7]. However, peaks H_b, H_c, H_d and H_e show small upfield (of maximum 0.05 ppm), or small downfield (of maximum 0.02 ppm) shifts that suggest no effect of the CB[7] cavity. Based on these results, EV[Np]MV molecule binds 1:1 with CB[8] where the macrocycle completely encapsulates the naphthalene core. The EV[Np]MV complexation mode with CB[7] is 1:1 or 2:1 (host:guest ratio), where host molecules encapsulate only the charged pyridinium part.

EV[Pyr$_{1,6}$]MV ^{1}H NMR spectra of EV[Pyr$_{1,6}$]MV mixed with CB[8] in a 1:1 ratio show small downfield shifts of H_g and H_b protons, and upfield shift of H_a protons (see Figure 2.6 and Figure A.32). Protons of aromatic 1,6-pyrene core are all upfield shifted with approximately 0.38 ppm for H_c, 0.65 ppm for H_d, 0.23 ppm for H_e and 0.40 ppm for H_f. Such shifting behaviour suggests 1:1 binding with the CB[8] macrocycle bound to the aromatic core of the guest molecule. This is unexpected taking into account the size of the aromatic core and the asymmetrical connection to the pyridinium moieties. However, the distances between H_f and H_c (6.9 Å) and between H_e and H_c (ca. 5.9 Å) are small enough to fit the CB[8] portal and cavity.[1] Moreover, it has previously been reported that CB[n]s are capable to slightly distort their structure upon guest encapsulation.[151]

[1]The geometry of EV[Pyr$_{1,6}$]MV molecule was optimised with Avogadro software, with additional assumption of Van der Waals hydrogen atom radius.

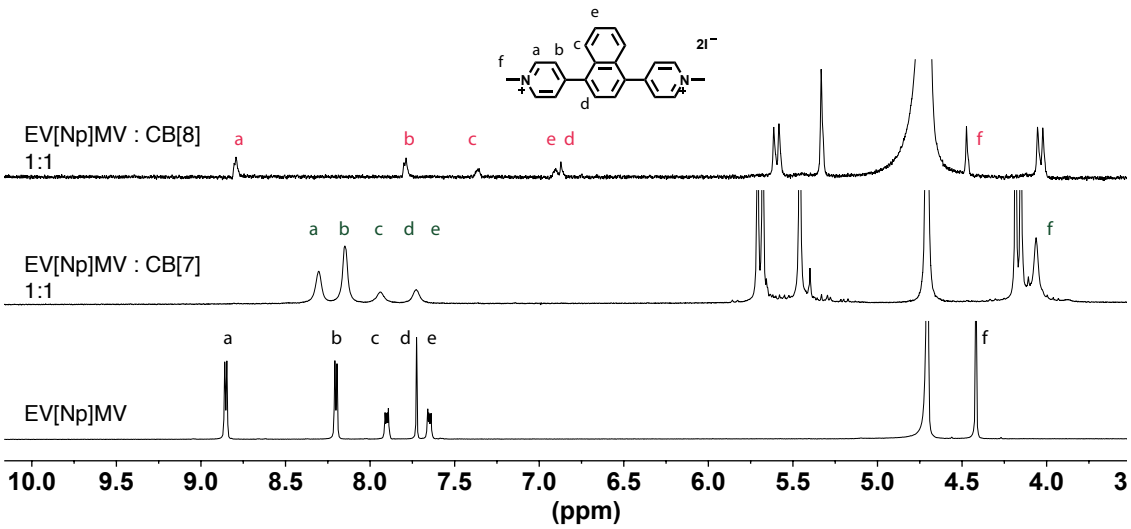

Fig. 2.5 ^{1}H NMR spectra of 1:1 complex of EV[Np]MV with CB[8] and CB[7]. Measurements performed in D_2O with I^- as counterions.

EV[$Pyr_{1,6}$]MV interaction with CB[7] is highly dynamic on the NMR time scale (see Figure 2.6 and Figure A.33). In a 1:1 mixture, all the peaks are broad and not well resolved. Only the NMR spectrum of a 3:1 ratio mixture of CB[7] and EV[$Pyr_{1,6}$]MV reveals 0.17 ppm, 0.20 ppm and 0.03 ppm upfield shifts for H_g, H_a and H_b respectively (see Figure A.33). Based on peak integration, there is a 2:1 host-guest complexation of EV[$Pyr_{1,6}$]MV with CB[7], where the host molecule is bound to the charged pyridinium moiety.

Unfortunately, the ^{1}H NMR spectra of EV[$Pyr_{2,7}$]MV titrated to CB[7] and CB[8] solution show only extremely broad peaks, making them difficult to analyse. That is on account of the low solubility of the guest molecule in water and strong π-π stacking.

EV[CH]MV The ^{1}H NMR spectrum for EV[CH]MV interaction with CB[8] in 1:1 ratio is shown in Figure 2.7 (see Figure A.30 for the spectrum corresponding to the 1:2 mixture). All proton peaks, for both, the guest and host molecules are broad. Such spectrum suggests dynamic complexation. By increasing the ratio of the macrocycle, the resolution of CB[8] peaks improves. This could indicate formation of a more stable complex. Moreover, a 0.66 ppm upfield shift of H_h protons was observed. This suggest inclusion of these protons inside the cavity of the macrocycle. A small 0.05 ppm upfield shift of H_a suggest either marginal effect of CB[8] on this part of the molecule, or partial inclusion and partial exclusion by the cavity and hence appearance of an average signal. Peaks H_d, H_b, H_c are all downfield shifted. These observations can be indicative of a binding mode between EV[CH]MV and CB[8] similar to that with CB[7], namely at the pyridinium moieties. However, proton shifts

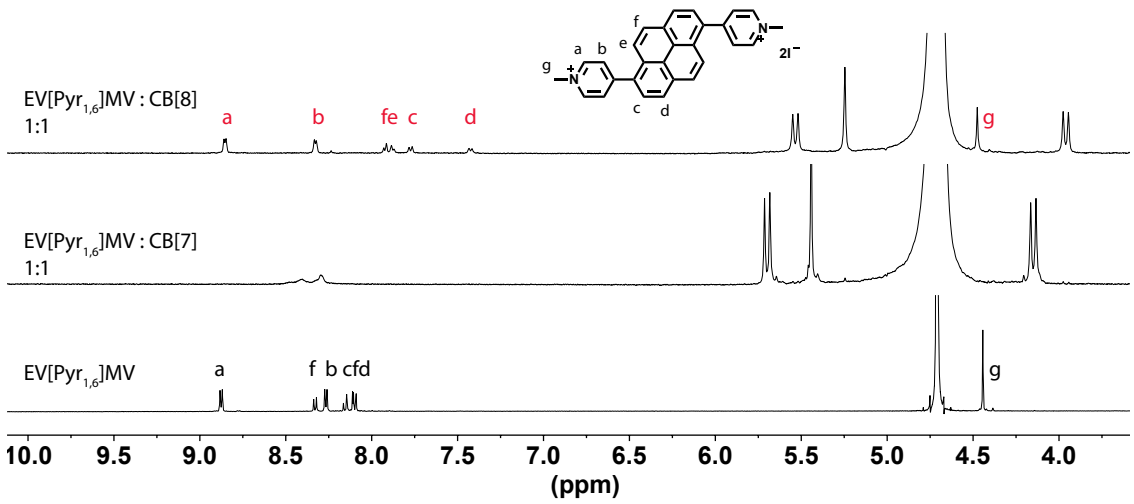

Fig. 2.6 ^{1}H NMR spectra of 1:1 complex of EV[Np]MV with CB[8] and CB[7]. Measurements performed in D_2O with I^- as counterions.

caused by the presence of CB[8] for these particular protons are not that strong. Moreover, upfield shifts of peaks H_f and H_g could arise from π-π stacking interaction. The consequence of stacking of those protons should have deshielding effect ($+\delta$ dispersion interactions *i.e.* downfield shift). Another possible reason for upfield shifts of these protons could be the magnetic anisotropic effect from the ring current of the chrysene rings. Since the anisotropy effects cause shielding of protons placed above the ring, and deshielding effects for protons to the side of it, it is possible that observed shifts for EV[CH]MV molecule are a result of both effects.

Chrysene extended methyl viologen upon addition to CB[7] solution, shows 0.18 ppm and 0.26 ppm upfield shifts of the methyl proton in 1:1 and 2:1 binding mixtures respectively (see Figure 2.7, and Figure A.31). Proton H_a is also shifted upfield with 0.20 ppm for 1:1 and 0.32 ppm for 2:1 ratio host-guest complexes. Peaks H_b and H_c have the biggest downfield shifts (up to 0.5 ppm) for 2:1 complex CB[7] with EV[CH]MV. Peaks H_d and H_e are also shifted downfield with ca. 0.16 ppm and 0.20 ppm respectively. The smallest downfield shifts are observed for H_f and H_g. Protons most affected by the presence of the macrocycle are H_h and H_a. They are characterised by upfield shifts, which means that they are encapsulated in the cavity of CB[7]. Protons H_b and H_c, H_d and H_e show downfield shifts that are a consequence of interaction with CB[7] portal. Protons H_f and H_g are almost not affected by the presence of CB[7]. Based on these shifts, it is suggested that CB[7] binds around the pyridinium moieties of the molecule. The NMR spectrum for EV[CH]MV shows as well that the 1:2 complex causes much stronger shifts, however, broadening of peaks seems to be

more pronounced (see Figure A.31). This could be the effect of increasing dynamics of the complex.

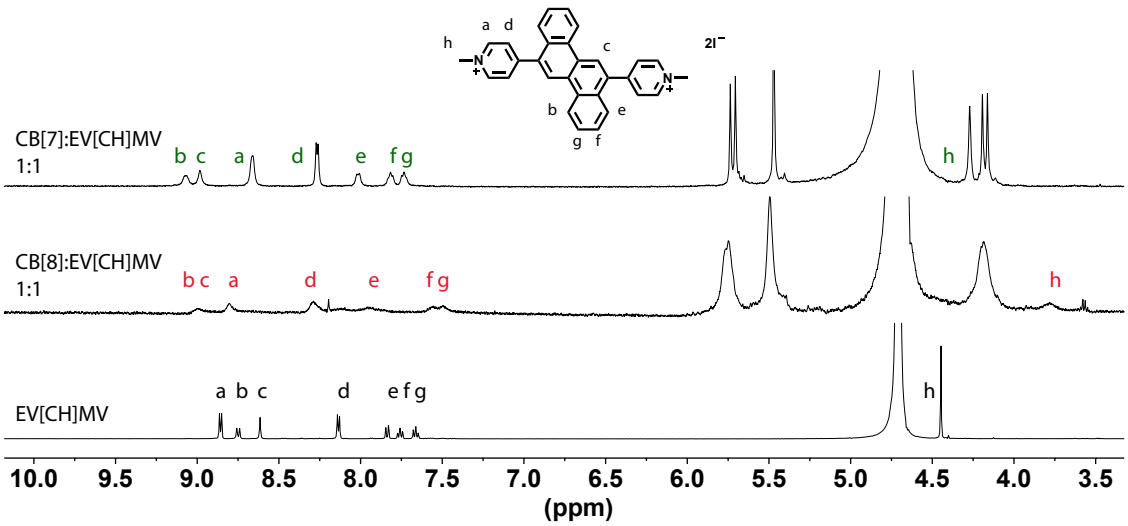

Fig. 2.7 ^{1}H NMR spectra of 1:1 complex of EV[CH]MV with CB[8] and CB[7]. Measurements performed in D_2O with I^- as counterions.

EV[Th]MV Thiophene extended methyl viologen upon addition to CB[8], exhibits a 0.01 ppm upfield shift of methyl proton. This suggests that methyl part of the molecule is minimally or not affected by the presence of the macrocyle (see Figure 2.8 and Figure A.34). When CB[8] and EV[Th]MV are in 1:1 ratio, proton H_a is shifted upfield with about 0.05 ppm, only slightly affected by presence of CB[8] rims. Peaks H_b and H_c are shifted upfield by 0.72 ppm and 0.91 ppm, respectively. Shifts of about 1 ppm are typically for protons that are affected the most by the presence of CB[n]s. In 1:2 ratio mixture of CB[8] and EV[Th]MV peaks do not exhibit shifts. However, they appear sharper, when compared to the 1:1 host-guest mix. There are no peaks from free guest molecule visible, however, new peaks next to $H_{c'}$ and $H_{d'}$ arise. Based on these observations and NMR integration, EV[Th]MV binds with CB[8] in 1:2 manner, with the thiophene core inside the host cavity. Presumably, due to steric hindrance, there is dynamic shuffling between two guest molecules inside the host cavity, thus the splitting of peaks occurs.

Complexation with CB[7] results in similar shifts as observed for CB[8]:EV[Th]MV (see Figure 2.8 and Figure A.35). There is a 0.08 ppm downfield shift of H_d proton, suggesting that this proton is slightly outside the CB[7] cavity. Protons H_a, H_b and H_c have 0.05 ppm, 0.58 ppm and 0.88 ppm shifts respectively, indicating that the thiophene core is

mostly affected by the shielding presence of CB[7]. The peaks are sharp and well resolved, suggesting that this complex is stable and non-dynamic.

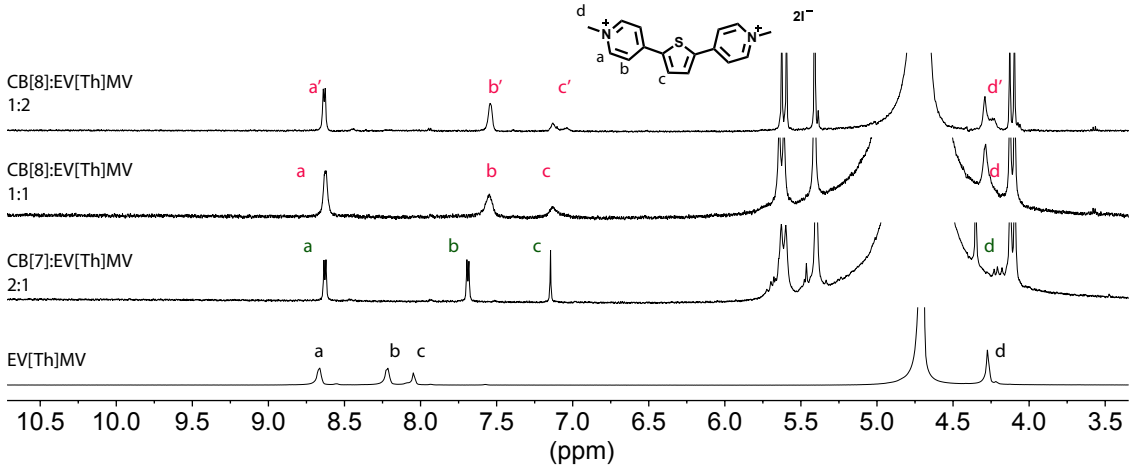

Fig. 2.8 ^{1}H NMR titrations of EV[Th]MV to CB[8] and CB[7]. Measurements performed in D_2O with I^- as counterions.

EV[DTh]MV EV[DTh]MV upon mixing with CB[8] in 2:1 host-guest ratio, exhibits 0.75 ppm and 0.79 ppm upfield shifts of H_a and H_b protons (see Figure 2.9 and Figure A.34). Peaks for these protons show 0.62 ppm and 0.73 ppm upfield shifts in 1:1 mixture. The H_f proton exhibits a 0.50 ppm and 0.44 ppm upfield shift in the 2:1 and 1:1 mixtures respectively. Protons on dithiophene rings H_c and H_d show 0.45 ppm and 0.19 ppm upfield shifts in 2:1 ratio. Then, in 1:1 mixture there are small further upfield shifts to 0.47 ppm and 0.28 ppm. The NMR spectra for these titrations are broad and not well resolved. And peaks are getting broader for the 1:1 ratio. The shifting behaviour suggests that in a solution with excess of CB[8], EV[DTh]MV binds with the macrocycle with its pyridinium moiety. However, the complexation mode appears to change upon further addition of the guest. As a result the host molecule shifts further onto the dithiophene core of EV[DTh]MV. At the same time, the complex that is formed is more dynamic.

^{1}H NMR titrations of EV[DTh]MV into CB[7] reveals weak 0.05 ppm downfield shift of H_e proton (see Figure 2.9 and Figure A.37). There are strong 0.59 ppm and 0.41 ppm upfield shifts of H_d and H_c protons, respectively. And weak 0.14 ppm upfield shifts for H_a and H_b. Titration of EV[DTh]MV into CB[7] solution suggests that CB[7] binds mostly the thiophene core. Sharp and well resolved peaks indicate that the host-guest complex that is formed is non-dynamic on the NMR time scale.

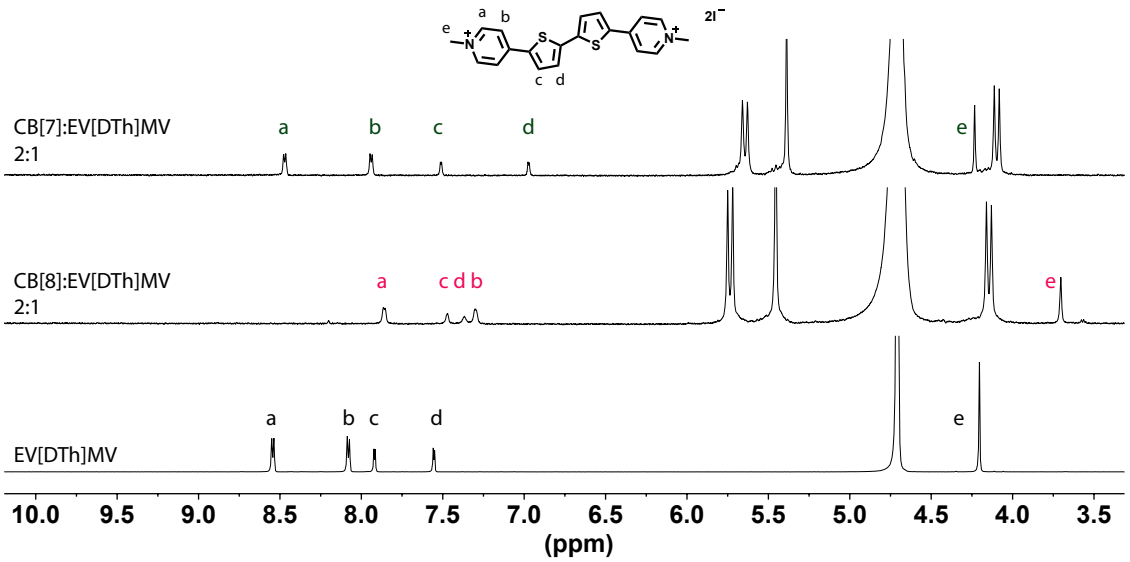

Fig. 2.9 ^{1}H NMR titrations of EV[DTh]MV to CB[8] and CB[7]. Measurements performed in D_2O with I^- as counterions.

2.2.3 Thermodynamics of Binding with CB[8] and CB[7]

To further evaluate supramolecular interaction of extended methyl viologens with CB[8] and CB[7], the binding was subsequently studied with ITC.

In an ITC experiment small aliquots of guest solution are titrated into a sample cell containing a host solution. Upon binding (exothermic or endothermic reaction) the resulting heat differences between sample cell and reference cell are measured and plotted as a function of the subsequent injections. The thermodynamic parameters obtained from these titrations *i.e.* changes in enthalpies (ΔH), binding constants (K), Gibbs free energy (ΔG) and entropy changes (ΔS) are important indicators of complexation type. As described in Chapter 1, CB[8] can encapsulate one or two guests typically in 1:1, 1:1:1 or 2:1 manner. CB[7] can typically encapsulate one guest in 1:1 manner. Each type of binding has its signature in the thermodynamic data obtained from ITC.[152]

The thermodynamic data obtained for methyl viologen (MV) together with selected EV[X]MVs and their binding with CB[8] or CB[7] are shown in Table 2.1 and Table 2.2 respectively. All the EV[X]MV:CB[8] encapsulations are energetically favourable and enthalpically driven. Upon binding with CB[8] the entropy temperature product ($T\Delta S$) and enthalpy (ΔH) data for EV[Np]MV and EV[$Pyr_{1,6}$]MV suggests typical 1:1 complexation (see Figure A.40 and Figure A.42).[68] Titration isotherms for EV[Ph]MV and EV[Th]MV with CB[8] suggest sequential binding (in Table 2.1 EV[Ph]MV* and EV[Th]MV* denote that values presented in a table are for the first stage of binding, for the second stage see

Table 2.1 Thermodynamic data of EV[X]MVs binding with CB[8] (T=298 K, 50mM sodium acetate buffer (pH = 4.75)).

	ΔG ($kJ\,mol^{-1}$)	ΔH ($kJ\,mol^{-1}$)	$T\Delta S$ ($kJ\,mol^{-1}$)	K (M^{-1})
MV	-33.99	-27.15	6.84	8.99×10^5
EV[Ph]MV*	-36.81	-42.25	-5.44	2.81×10^6
EV[Np]MV	-40.09	-41.84	-1.75	1.05×10^7
EV[$Pyr_{1,6}$]MV	-38.25	-41.84	-3.59	5.04×10^6
EV[Th]MV*	-46.5	-91.24	-44.71	1.42×10^8
EV[DTh]MV	-38.09	-96.00	-57.91	4.72×10^6

Figure A.38 and Figure A.43). This could be explained by the fact that phenylene and thiophene extended viologen according to NMR titration (see previous section), bind with CB[8] in a 1:2 manner. Such a pattern could also be explained by the phenylene core being small enough for the CB[8] macrocycle to thread along the guest molecule. This potentially allows for two stage binding of the molecule to the host. Enthalpy and entropy values for EV[Th]MV and EV[DTh]MV suggest more complex binding with the macrocycle (see Table 2.1 and Figure A.43 and Figure A.45). High values of enthalpy for EV[Th]MV could be explained by dynamic complexation, causing the change in solvation of the molecule and the release of a larger amount of high energy water from the CB[8] cavity. This explanation is in accordance with results from the NMR titration.

Additionally, the binding constants K for the EV[X]MVs and CB[8] complexes were found to be within $8.9 \times 10^5\ M^{-1}$ to $1.4 \times 10^8\ M^{-1}$, indicating strong host-guest binding.

Binding with CB[7] is energetically favourable and enthalpically driven for all EV[X]MVs molecules (Table 2.2). The entropy and enthalpy data for EV[Ph]MV, EV[Th]MV and EV[DTh]MV encapsulation with CB[7] suggests a typical 1:1 binding mode. The isotherm for EV[Np]MV titration to CB[7] shows typical dynamic binding between guest and host (see Figure A.41). Hence, thermodynamic values reported are low on account of a less ordered system (low $T\Delta S = -56.51\,kJ\,mol^{-1}$)) and frequent release of high energy water from the cavity of CB[7]. The binding constant (K) for EV[Np]MV:CB[7] is significantly lower ($9.25 \times 10^3\ M^{-1}$) in comparison to other complexes (see Table 2.2). This observation is supported by ^{1}H NMR experiments. Interestingly, EV[Th]MV and EV[DTh]MV show similar enthalpy change, but slightly different values for their entropy upon complexation with CB[7]. Encapsulation of EV[DTh]MV is characterised by lower value of $T\Delta S$, in comparison to EV[Th]MV, suggesting that EV[DTh]MV:CB[7] it is less ordered system. This could be explained with more complicated structure of the molecule and higher number of degrees of freedom.

Table 2.2 Thermodynamic data of EV[X]MVs binding with CB[7] (T= 298 K, 50mM sodium acetate buffer (pH = 4.75)).

	ΔG (kJ mol^{-1})	ΔH (kJ mol^{-1})	$T\Delta S$ (kJ mol^{-1})	K (M^{-1})
MV	-38.62	-24.70	13.92	5.83×10^6
EV[Ph]MV	-43.48	-29.50	13.98	5.69×10^7
EV[Np]MV	-22.64	-79.15	-56.51	9.25×10^3
EV[Th]MV	-44.07	-41.84	2.23	5.25×10^7
EV[DTh]MV	-40.32	-41.84	-1.51	1.16×10^7

2.2.4 Steady State Spectroscopic Characterisation

After investigation of the complexation of EV[X]MVs with CB[8] and CB[7] using NMR and ITC techniques, their photophysical properties were studied.

Steady-state electronic absorption and photoluminescence (PL) emission as well as their photophysical properties were measured and are summarised in Table 2.3. Absorption and emission spectra of EV[X]MVs in water for different guest molecules and their complexes with CB[7] or CB[8] are presented in Figures 2.10 to 2.16.

The electronic absorption maxima show significant red shifts of 20 nm to 30 nm with increasing conjugation of the aromatic core between EV[Ph]MV, EV[Np]MV, EV[CH]MV and EV[Pyr$_{1,6}$]MV . The introduction of asymmetry in case of EV[Pyr$_{2,7}$]MV results in a 90 nm hypsochromic shift in comparison to EV[Pyr$_{1,6}$]MV. A red shift of 60 nm in absorption upon extending the thiophene conjugation can be observed for EV[Th]MV and EV[DTh]MV.

The emission maxima for the series of EV[X]MVs exhibit a similar trend. These observations are in accordance with the Woodward–Fieser rules.[153, 154] In analogy to the results for absorption, π-expansion leads to a smaller HOMO-LUMO gap and smaller photoexcitation energies. The common feature for extended methyl viologens is main 0-0 absorption band, except for EV[DTh]MV which also has 0-1 transition visible as a shoulder peak (Figure 2.16). Interestingly, emission spectra for pyrene extended viologens are featureless. On account of large Stokes shifts observed for these monomers (for EV[Pyr$_{1,6}$]MV there is a 110 nm Stokes shift, for EV[Pyr$_{2,7}$]MV it is 215 nm), this could suggest formation of aggregates, presumably excimer-like species or systems featuring the aggregation induced emission.

The host-guest complexes for EV[X]MVs were formed by mixing previously calibrated stock solutions of a molecule and CBs. Upon complexation with a macrocycle, hypsochromic or bathochromic shifts are observed on account of the change in local environment but also

on account of encapsulation in more confined space *i.e.* CB[n] cavity.[75] The monomeric species of EV[X]MVs are mostly highly emissive with Φ_{PL} as high as 0.96 for EV[Np]MV. Upon complexation with CB[7] the PL quantum yield is increasing due to deaggregation effect, but also on account of the mechanical protection of the dye by CB[7] (described previously in Chapter 1).

Interestingly, Φ_{PL} for 1:2 host guest complexes of CB[8] and EV[Ph]MV, EV[Th]MV and EV[DTh]MV is significantly lower. Such fluorescence emission quenching could be explained by static quenching upon formation of a dimer inside the cavity of a macrocycle. The time-resolved fluorescence measurements of EV[X]MVs and their complexes with CB[8] and CB[7] indicate that the major decay mechanism for them is via fluorescence (see Figures A.47 to A.53). For most of the molecules studied here the biexponential fitting yields major emissive components decay with a time constant of up to 6 ns. The only exception can be observed for EV[$Pyr_{2,7}$]MV, where triexponential fitting yields in approximately 88 % of the fluorescence decay with 21 ns time constant, 10 % with 57 ns, and the remaining 2 % shows a fluorescence decay of 2 ns (see Figure A.51). Such a long-lived emission of the host-guest complex, together with high Stokes shift (11 866 cm^{-1}) and low fluorescence quantum yield, suggest the existence of a stable excited state, the excimer-like species. [23, 36]

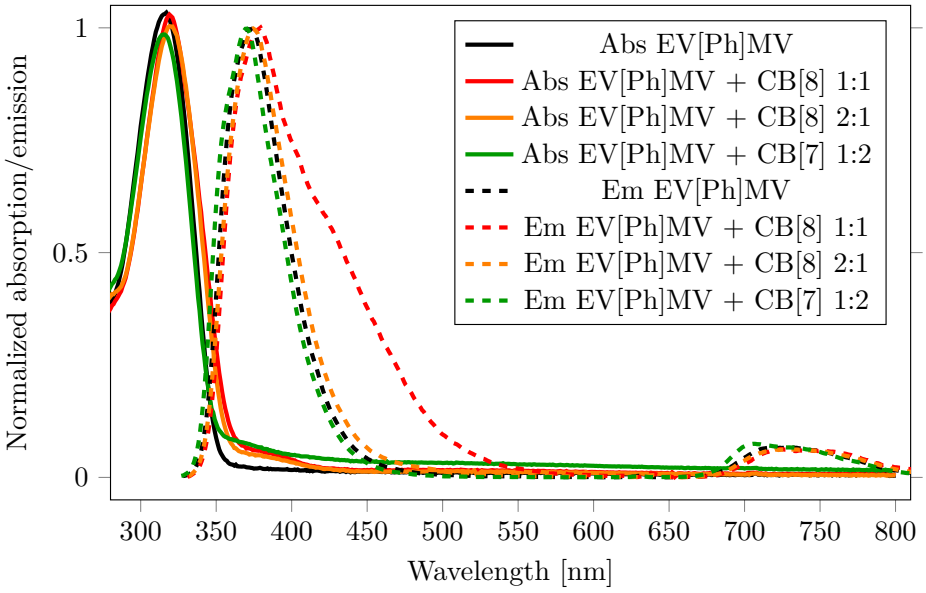

Fig. 2.10 Normalised absorption (solid lines) and emission (dashed lines) spectra of EV[Ph]MV and its complexes with 1 eq of CB[8], 0.5 eq of CB[8] and 2 eq of CB[7].

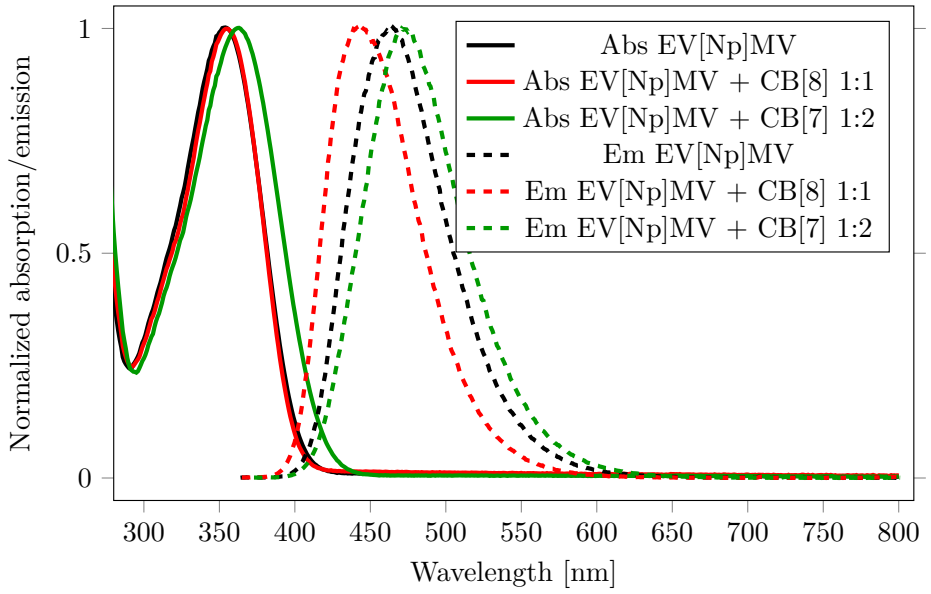

Fig. 2.11 Normalised absorption (solid lines) and emission (dashed lines) spectra of EV[Np]MV and its complexes with 1 eq of CB[8] and 2 eq of CB[7].

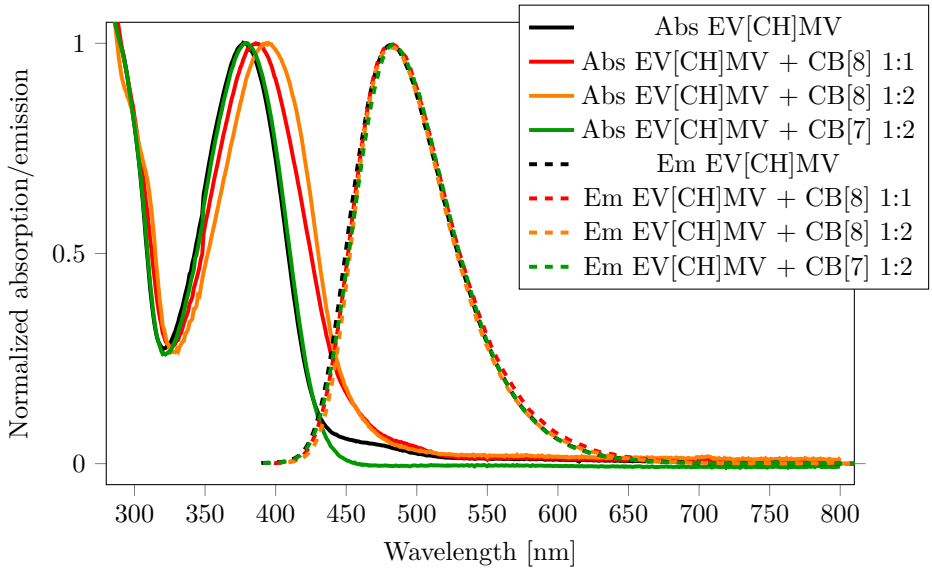

Fig. 2.12 Normalised absorption (solid lines) and emission (dashed lines) spectra of EV[CH]MV and its complexes with 1 eq of CB[8], 2 eq of CB[8] and 2 eq of CB[7].

Table 2.3 Steady-state spectral data of EV[X]MVs in water.

Host	Guest	Host:Guest	λ_{abs}^{max} (nm)	$\varepsilon*$ [$M^{-1}cm^{-1}$]	λ_{em}^{max} (nm)	Stokes shift [nm] ([cm^{-1}])	Φ_{PL}	τ_1 (ns)	τ_2 (ns)
EV[Ph]MV	-	-	317	18611	372	55 (4664)	0.78	1.40	-
EV[Ph]MV	CB[8]	1:2	320	23080	379	59 (4864)	0.33	1.60 (84 %)	25 (16 %)
EV[Ph]MV	CB[7]	2:1	314	28580	369	55 (4747)	0.88	0.2 (64 %)	1.7 (36 %)
EV[Np]MV	-	-	355	11070	463	108 (6570)	0.96	5.7	-
EV[Np]MV	CB[8]	1:1	355	10080	444	90 (5726)	0.91	6.4	-
EV[Np]MV	CB[7]	2:1	361	13080	473	112 (6559)	0.98	6.8	-
EV[CH]MV	-	-	378	21500	480	102 (5622)	0.67	5.2	-
EV[CH]MV	CB[8]	1:1	386	12927	480	94 (5073)	-	5.3	-
EV[CH]MV	CB[8]	2:1	395	11740	482	87 (4570)	0.37	5.4	-
EV[CH]MV	CB[7]	2:1	380	18250	482	102 (5569)	0.58	5.3	-
EV[$Pyr_{1,6}$]MV	-	-	408	27130	518	110 (5205)	0.38	4.6	-
EV[$Pyr_{1,6}$]MV	CB[8]	1:1	427	24130	508	81 (3734)	0.66	6.0	-
EV[$Pyr_{1,6}$]MV	CB[8]	1:2	427	24130	508	82 (3734)	-	6.0	-
EV[$Pyr_{1,6}$]MV	CB[7]	2:1	410	27290	518	108 (5085)	0.50	4.6 (93 %)	8.0 (7 %)
EV[$Pyr_{2,7}$]MV	-	-	318	28340	533	215 (12685)	<0.01	-	-
EV[$Pyr_{2,7}$]MV	CB[8]	1:1	325	31510	529	204 (11866)	0.07	2.4 (2 %)	21 (88 %) 57 (9 %)
EV[$Pyr_{2,7}$]MV	CB[7]	2:1	326	24200	545	219 (12326)	0.03	1.4 (46 %)	20 (54 %)
EV[Th]MV	-		370	74626	423	53 (3386)	0.74	1.9	-
EV[Th]MV	CB[8]	1:2	374	59490	416	42 (2699)	0.49	2.5	-
EV[Th]MV	CB[7]	2:1	368	70830	422	54 (3477)	0.78	2.6	-
EV[DTh]MV	-		432	9007	503	71 (3267)	0.08	1.9 (83 %)	8.7 (17 %)
EV[DTh]MV	CB[8]	1:1	444	12390	501	57 (2562)	0.06	2.1 (40 %)	6.2 (60 %)
EV[DTh]MV	CB[8]	1:2	452	22715	501	49 (2164)	0.10	1.8 (86 %)	5.2 (14 %)
EV[DTh]MV	CB[7]	2:1	444	42103	497	53 (2402)	0.53	1.5 (86 %)	3.1 (14 %)

* For not normalised absorption data see Figures A.73 to A.79.

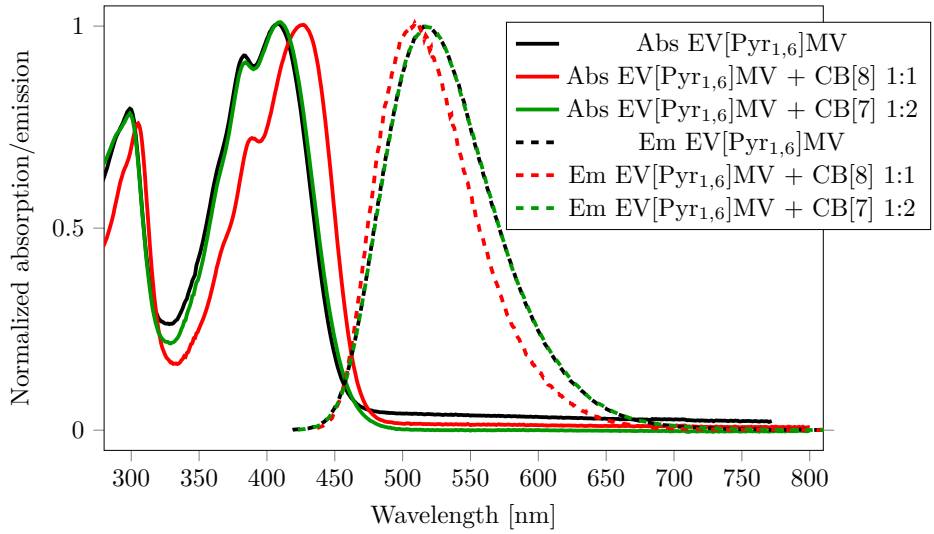

Fig. 2.13 Normalised absorption (solid lines) and emission (dashed lines) spectra of EV[Pyr$_{1,6}$]MV and its complexes with 1 eq of CB[8] and 2 eq of CB[7].

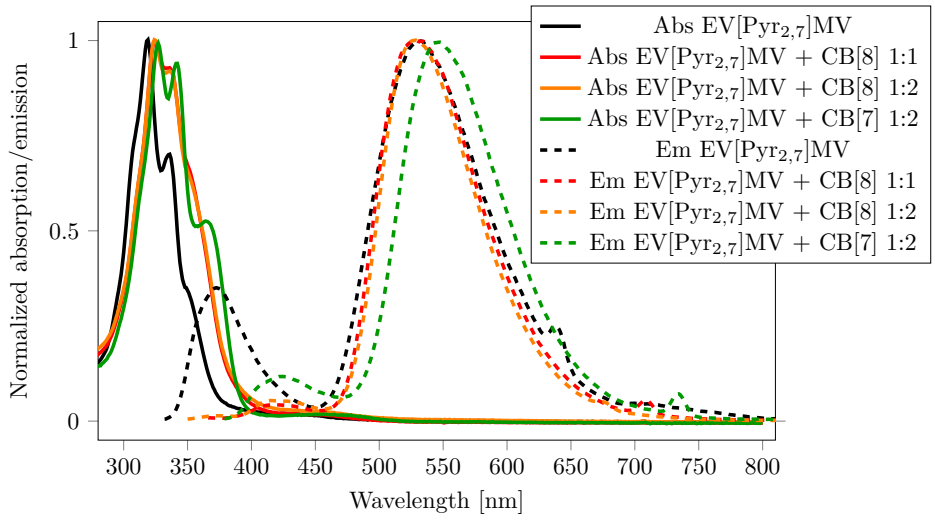

Fig. 2.14 Normalised absorption (solid lines) and emission (dashed lines) spectra of EV[Pyr$_{2,7}$]MV and their complexes with 1 eq of CB[8], 2 eq of CB[8] and 2 eq of CB[7].

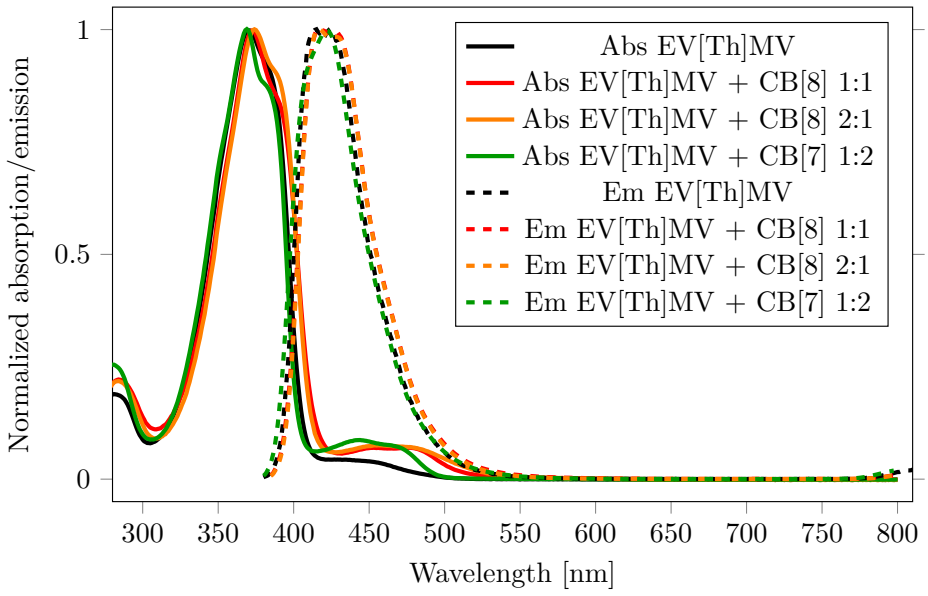

Fig. 2.15 Normalised absorption (solid lines) and emission (dashed lines) spectra of EV[Th]MV and their complexes with 1 eq of CB[8], 0.5 eq of CB[8] and 2 eq of CB[7].

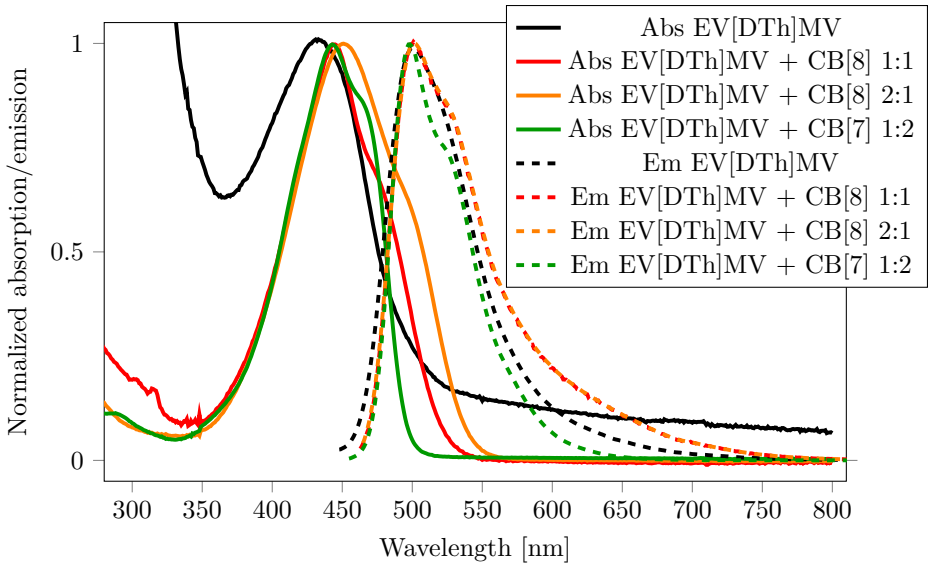

Fig. 2.16 Normalised absorption (solid lines) and emission (dashed lines) spectra of EV[DTh]MV and their complexes with 1 eq of CB[8], 0.5 eq of CB[8] and 2 eq of CB[7].

2.2.5 Electrochemical Characterisation

Cyclic Voltammetry (CV) of selected EV[X]MVs were recorded in a nitrogen saturated 0.1 M KCl aqueous solution. The three-electrode configuration was used: the glassy carbon as a working electrode, a platinum wire as the counter electrode and Ag/AgCl as a reference electrode. CV was performed at variable scan rates ranging from 25 mV s^{-1} to 400 mV s^{-1}, for different concentrations of molecules, EV[X]MV saturated with CB[8], and 1:2 ratio EV[X]MV:CB[7] mixed solutions. The scans were run from 1 V to −1.5 V. All redox potentials for EV[Ph]MV, EV[Np]MV and EV[Th]MV and their complexes with CB[8] and CB[7] are summarised in Table 2.4 and denoted in Figure 2.18, Figure 2.24 and Figure 2.22.

Table 2.4 Electrochemical redox potentials of EV[X]MVs in aqueous solution.

	E_{i} [V]	E_{ii} [V]	E_{iii} [V]	E_{iv} [V]
MV	-	-	-0.702	-1.055
MV:CB[8]	-	-	-0.738	-
MV:CB[7]	-	-	-0.707	-1.012
EV[Ph]MV	0.662	0.422	-0.979	-1.238
EV[Ph]MV:CB[8]	0.648	0.4	-0.978	-1.237
EV[Ph]MV:CB[7]	-	-	-	-
EV[Np]MV	-	0.4	-1.060	-
EV[Np]MV:CB[8]	0.706	0.413	-1.050	-
EV[Np]MV:CB[7]	-	0.405	-1.026	-
EV[Th]MV	0.648	0.335	-0.819	-1.0
EV[Th]MV:CB[8]	0.709	0.416	-0.743	-0.945
EV[Th]MV:CB[7]	0.675	0.412	-1.036	-

Here, all extended methyl viologens have more negative reduction potential than methyl viologen. This originates from the more extended aromatic ring system, and thus more electron-rich character of the molecule. The reduction of molecule *i.e.* addition of electron into the system, becomes thermodynamically more difficult. Thus, from selected extended methyl viologens, EV[Np]MV possesses the most negative reduction potential. Multiple electron transfer redox waves were observed for all three compounds and their complexes with CB[8] or CB[7] macrocycle (Figure 2.18, Figure 2.24, Figure 2.22).

Cyclic voltammograms of EV[Ph]MV are depicted in Figure 2.18. There, characteristic for methyl viologen, two one-electron reduction peaks shifted to more negative potential by 300 mV were observed. The separation between first reduction potential (E_{iii}) and second reduction potential (E_{iv}) is ca. 50 mV higher in comparison to methyl viologen indicating that EV[Ph]MV$^{\bullet+}$ radical is slightly more stable. Concentration studies on EV[Ph]MV

revealed that with increasing concentration two reduction peaks appear at the positive potential. Viologen radical cations on account of the radical-pairing interaction tend to form dimers in solid state and in highly concentrated solutions.[116, 155, 156] By increasing the π-surface in extended methyl viologens, the self-association of those viologens will be stronger. Interestingly, two reduction peaks at positive potential are also observed for EV[Ph]MV molecule mixed with CB[8] macrocycle (see Figure 2.18). Based on NMR results, EV[Ph]MV binds in 1:2 manner (Section 2.2.1). Enhanced by electron-rich phenylene core, EV[Ph]MV has already strong enough $\pi - \pi$ interaction, which can compensate or compete with the Coulombic repulsion. Moreover, the association constant of $2.81 \times 10^6\ \mathrm{M}^{-1}$ for EV[Ph]MV and CB[8] measured by ITC suggests that this 1:2 host-guest complex is strong (Table 2.1).

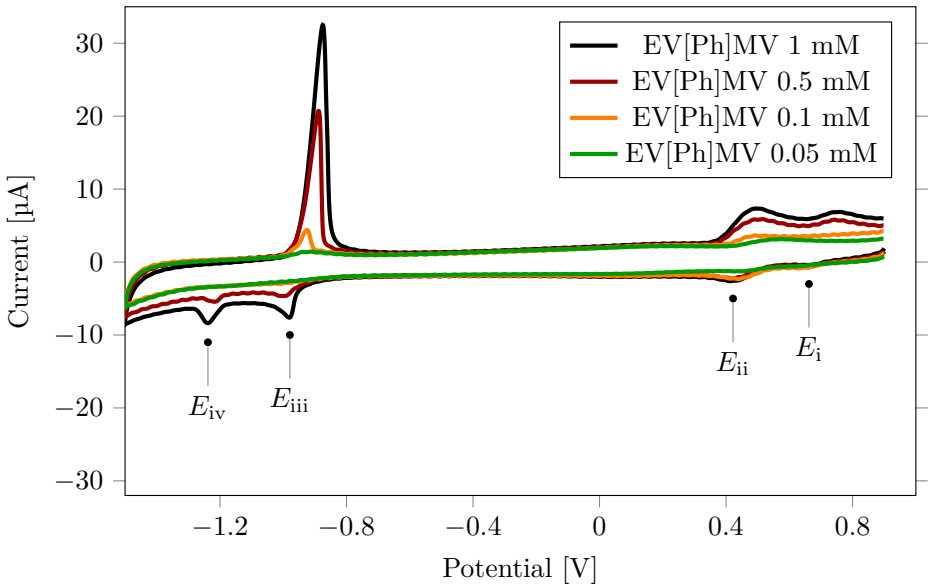

Fig. 2.17 Cyclic voltammograms of EV[Ph]MV in varying concentrations: 0.05 mM, 0.1 mM, 0.5 mM, 1 mM. Measurement was done with scan rate of $100\,\mathrm{mV\,s^{-1}}$ in 0.1 M KCl solution vs Ag/AgCl, at T=298 K.

Evidence from the dimerisation of EV[Ph]MV and observed reduction potentials E_{i}, E_{ii}, E_{iii}, and E_{iv} can be now attributed to the following reactions:

$$E_{\mathrm{i}}\text{: } (\mathrm{EV[Ph]MV})_2^{4+} \overset{\mathrm{e^-}}{\rightleftharpoons} (\mathrm{EV[Ph]MV^{\bullet+}})(\mathrm{EV[Ph]MV^{2+}})$$

First reduction potential observed for this system, comes from reduction on dimerised species to $\mathrm{EV[Ph]MV^{\bullet+}}$ and $\mathrm{EV[Ph]MV^{2+}}$ mixed valence complex (see Figure 2.18). Upon further reduction diradical species is formed, with total 2+ charge:

$$E_{\mathrm{ii}}\text{: } (\mathrm{EV[Ph]MV^{\bullet+}})(\mathrm{EV[Ph]MV^{2+}}) \overset{\mathrm{e^-}}{\rightleftharpoons} (\mathrm{EV[Ph]MV^{\bullet+}})_2$$

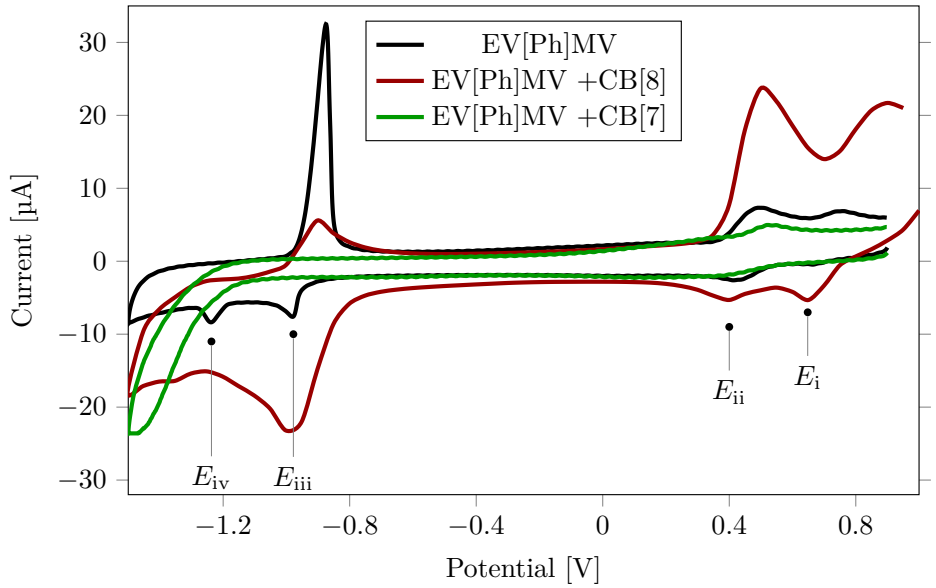

Fig. 2.18 Cyclic voltammograms of 1 mM EV[Ph]MV (black curve), upon mixing with 1 eq CB[8] (red curve) and with 2 eq CB[7] (green curve). Measurement was done with scan rate of 100 mV s^{-1} in 0.1 M KCl solution vs Ag/AgCl, at T=298 K.

The third reduction to EV[Ph]MV$^{\bullet+}$ and EV[Ph]MV^{0} mixed valence complex with total charge 1+ occurs at −0.978 V:

$$E_{iii}\text{: } (\text{EV[Ph]MV}^{\bullet+})_2 \overset{e^-}{\rightleftharpoons} (\text{EV[Ph]MV}^{\bullet+})(\text{EV[Ph]MV}^{0})$$

And the final reduction to EV[Ph]MV^{0} happens at −1.369 V:

$$E_{iv}\text{: } (\text{EV[Ph]MV}^{\bullet+})(\text{EV[Ph]MV}^{0}) \overset{e^-}{\rightleftharpoons} (\text{EV[Ph]MV}^{0})_2$$

It has been reported that the neutral species are not that strongly bound by CB[n].[138] Thus, the reaction E_{iii} probably happens with the dissociation of the complex. At higher scan rate for EV[Ph]MV mixed with CB[8], E_i is shifted towards more negative values (see Figure A.60). Moreover, the distance between E_i and E_{ii} is getting smaller with increased scan rate. This could indicate that the EV[Ph]MV^{4+} dimer in CB[8] exist primarily. When the scan rate is slow, the dissociation of the dimer can be observed, and the two separate reduction waves corresponding to reaction E_i and E_{ii} are visible. Once the scan rate becomes faster than the dissociation rate, the reduction of EV[Ph]MV^{4+} is observed to occur as a single reduction wave. As a control, cyclic voltammograms of the EV[Ph]MV mixed with CB[8], and then after addition of 1-adamantanamine hydrochlorid (ADA) were measured (Figure 2.20). ADA is a stronger binding guest to CB[8] compared to EV[Ph]MV, hence it replaces EV[Ph]MV in the host-guest complex.[38] Upon addition of ADA, redox peaks at positive region disappear. This control experiment confirmed that redox peaks at positive

potential correspond to the electrochemical reactions of a dimer. Redox peaks in negative region are better defined. The third reduction peak appeared at -0.978 V and the fourth at -1.234 V, which is similar to first and second redox potential for free EV[Ph]MV (E_{iii} and E_{iv} in Table 2.4).

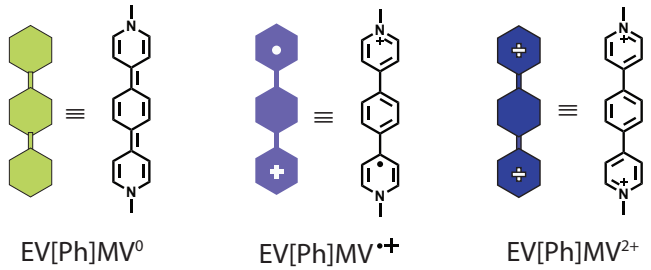

Fig. 2.19 The three redox states of the EV[Ph]MV.

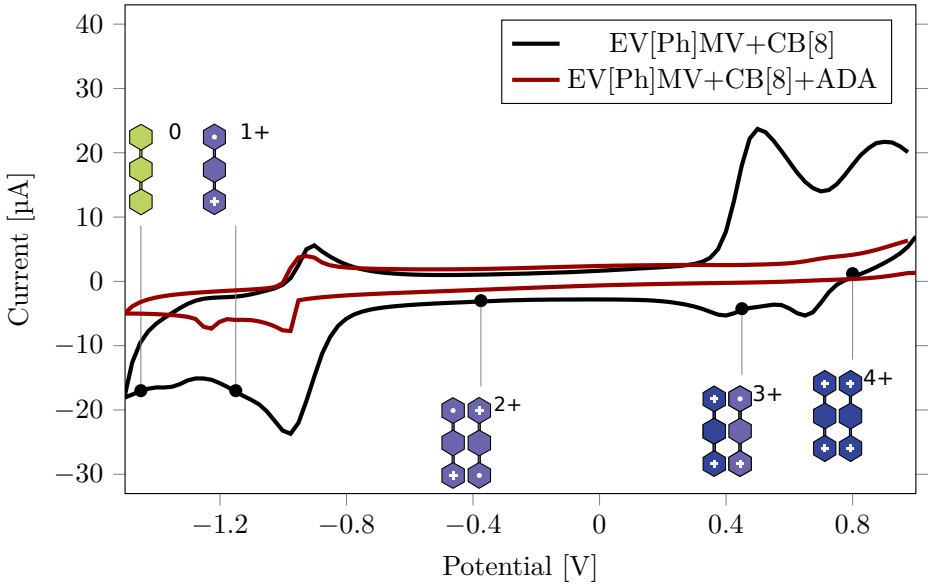

Fig. 2.20 The cyclic voltammogram of 1 mM EV[Ph]MV mixed with CB[8] (black curve), and after addition of an excess of ADA (red curve). Measurement was done with scan rate of 100 mV s^{-1} in 0.1 M KCl solution vs Ag/AgCl, at T=298 K.

Furthermore, EV[Ph]MV mixed with CB[7] in 1:2 ratio does not show any characteristic peaks. Since CB[7] binds only with one guest, the positive region is not showing any radical reactions that occur on the dimerised species. The lack of any redox peaks in negative region, is due to CB[7] binding. The macrocycle inhibits the electron transfer between the molecules and the electrode, by blocking the electrode surface due to its steric hindrance.

The cyclic voltammogram for EV[Th]MV is similar to that of EV[Ph]MV, as EV[Th]MV also binds in 1:2 manner to CB[8] (Figure 2.22), and it has analogous redox reactions. A comparison of CVs for EV[Th]MV, EV[Th]MV mixed with CB[7] and mixed with CB[8] (Figure 2.22), shows that CB[8] enhances the intensity of reduction peaks in positive potential region, again indicating that CB[8] facilitates the dimeristion of viologens.

The cyclic voltammograms for EV[Np]MV show as well dimer behaviour (Figure 2.24 and Figure 2.23). In high concentration two reduction peaks can be observed, upon dilution three peaks, presumably on account of equilibrium between dimeric and monomeric species. However, based on the oxidation pattern, this process involves four electron transfers in total. Upon mixing with a CB[8] weak first reduction potential E_{i} can be observed. This could suggest that the 1 mM solution of EV[Np]MV strongly dimerise, whereas, mixing with CB[8] facilitates the formation of $(\mathrm{EV[Np]MV^{\bullet+}})(\mathrm{EV[Np]MV^{2+}})$, a total 3+ species.

It can be concluded that, in addition to radical-pairing interactions, the EV[Ph]MV, EV[Th]MV and EV[Np]MV dimers are most likely stabilised by additional $\pi-\pi$ interactions between their aromatic surfaces. Additionally, upon formation a supramolecular complex with CB[8] their dimerisation is facilitated and their electron storage is doubled.

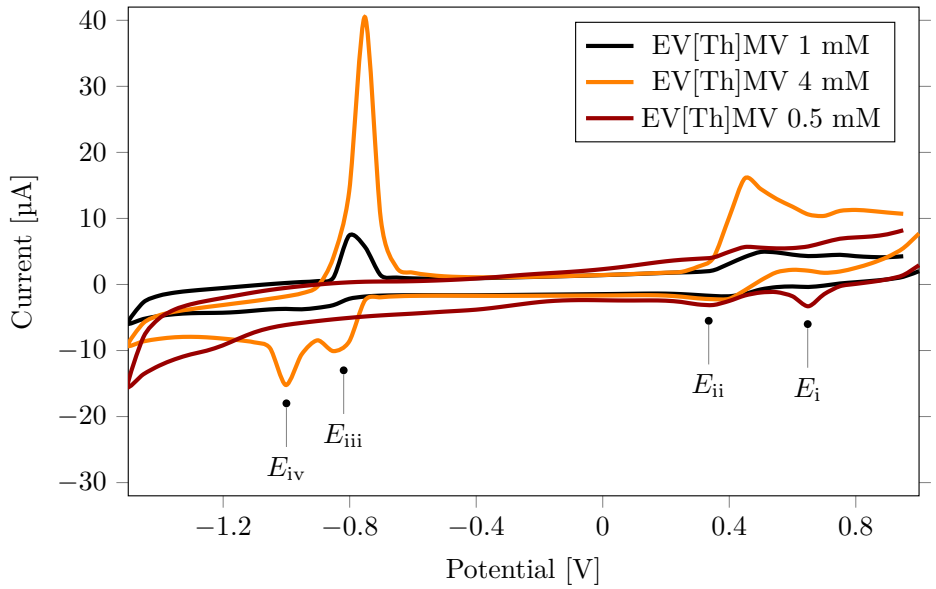

Fig. 2.21 Cyclic voltammograms of 1 mM EV[Th]MV (black curve), upon mixing with 1 eq CB[8] (red curve) and with 2 eq CB[7] (green curve). Measurement was done with scan rate of 100 mV s^{-1} in 0.1 M KCl solution vs Ag/AgCl, at T=298 K.

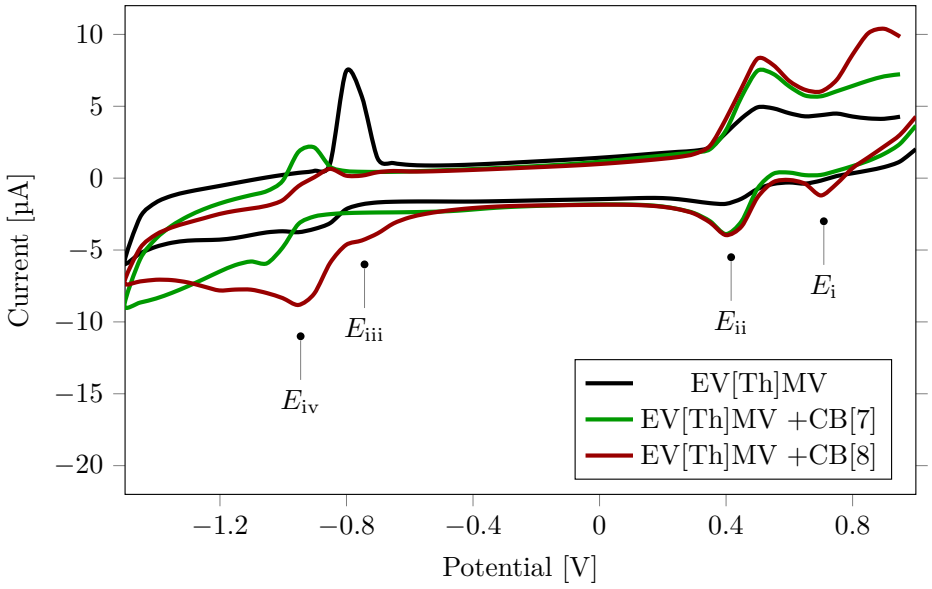

Fig. 2.22 Cyclic voltammograms of EV[Th]MV in varying concentrations 0.1 mM, 0.5 mM, 1 mM. Measurement was done with scan rate of 100 mV s^{-1} in 0.1 M KCl solution vs Ag/AgCl, at T=298 K.

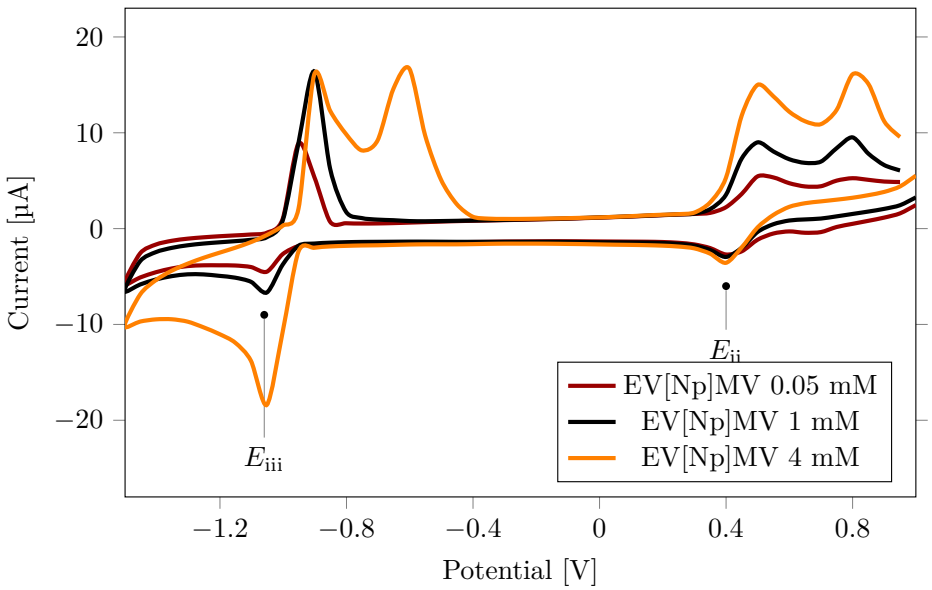

Fig. 2.23 Cyclic voltammograms of EV[Np]MV in varying concentrations 0.1 mM, 0.5 mM, 1 mM. Measurement was done with scan rate of 100 mV s^{-1} in 0.1 M KCl solution vs Ag/AgCl, at T=298 K.

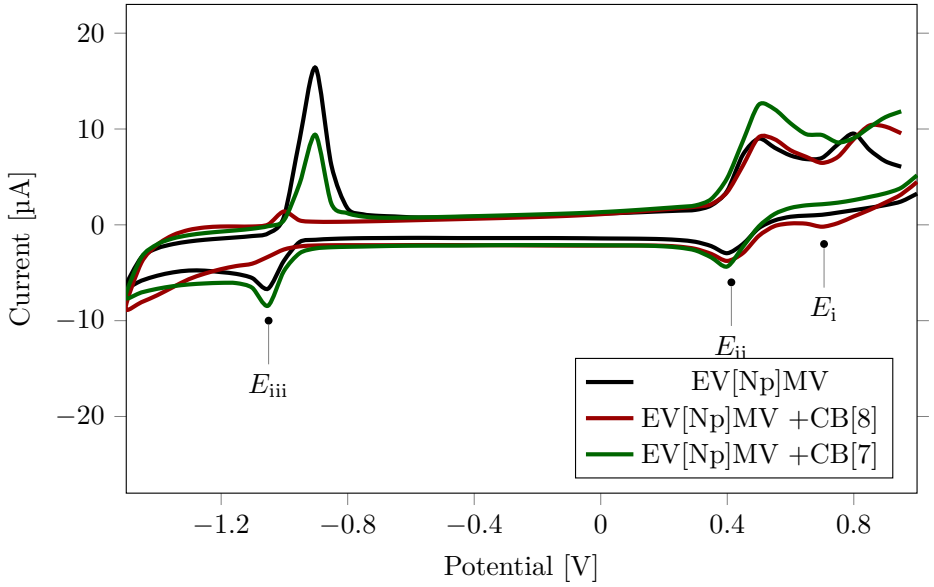

Fig. 2.24 Cyclic voltammograms of 1 mM EV[Np]MV (black curve), upon mixing with 1 eq CB[8] (red curve) and with 2 eq CB[7] (green curve). Measurement was done with scan rate of 100 mV s^{-1} in 0.1 M KCl solution vs Ag/AgCl, at T=298 K.

2.3 Conclusions

New extended methyl viologens have been synthesised and their properties on molecular and supramolecular level have been characterised. A variety of techniques including NMR, steady state spectroscopy and cyclic voltammetry were used to study the monomeric molecules and their supramolecular complexes with CB[8] and CB[7] macrocycles. It was presented that by changing the molecular structure of methyl viologen (a non-fluorescent molecule) new, highly emissive molecules were obtained. Furthermore, modulation of the bridging unit in extended methyl viologens results in tunability of optical properties. The emission colours of the newly synthesised molecules ranged from bright blue and green to yellow. The emission maximum and its intensity was successfully altered through encapsulation with CB[8] or CB[7] macrocycle. This paves the way for a new family of supramolecular, non-covalent water soluble dyes with various applications including labelling.

Moreover, an unexpected doubling in electron storage emerging from a higher $\pi - \pi$ surface and 1:2 host guest complexation of EV[X]MVs was described. Electrochemical characterisation showed that $(EV[Ph]MV)_2$:CB[8], $(EV[Th]MV)_2$:CB[8] and $(EV[Np]MV)_2$:CB[8] undergo a four-electron reduction mechanism. The recognition of these extended viologens is based on their $\pi - \pi$ stacking and the radical-pairing interaction but also highly enhanced by encapsulation in CB[8] cavity. Such systems build from molecules with wide range of redox states, triggered by external electric field, have a great potential for electro-conductive materials.[139] Ability to control the aggregation patterns of those molecules, here EV[X]MVs with CB[8] and CB[7], is beneficial for control of optoelectronic performance of the future novel materials.

2.4 Experimental

2.4.1 Instrumentation and Materials

Materials All the materials as following were purchased from commercial suppliers and used without further purification: 4-Pyridinylboronic acid (97 %, Fisher Scientific), 1,6-Dibromopyrene (95 %, Fluorochem), 2,7-Dibromopyrene (95 %, Fluorochem), 1,4-Dibromonaphthalene (>98 %, Acros Organics), 1,4-Dibromobenzene (>98 %, Alfa Aesar), 2,5-Dibromothiophene (96 %, Alfa Aesar), 5,5'-Dibromo1,2'-bithiophene (99 %, Alfa Aesar), 6,12-Dibromochrysene (95 %, Fluorochem), Iodomethane (99 %, Sigma-Aldrich, Tetrakis(triphenylphosphine) palladium(0) (99.8 % (metals basis), Pd 9 % min, Alfa Aesar), 1-adamantanamine hydrochloride (>97 %, Sigma-Aldrich), potassium hydrogen carbonate (anhydrous, Fisher Scientific), N,N-Dimethylformamide (anhydrous, Sigma-Aldrich),

toluene (Fisher Scientific), ethanol (absolute, Fisher Scientific) and diethyl ether (>99 %, Aldrich). Milli-Q water (18.2 MΩ cm) was used for preparation of all non-deuterated aqueous solutions, CB[8] was synthesized according to the published procedure.[43]

Nuclear Magnetic Resonance Spectroscopy ^{1}H NMR spectra were acquired at 298 K, and recorded on a Bruker AVANCE 500 with TCI Cryoprobe Spectrometer (500 MHz) being controlled by TopSpin2. ^{13}C NMR (126 MHz) spectra were recorded on a Bruker AVANCE III QNP Cryoprobe with external reference TMS set to 0 ppm. Titrations were performed by using stock solutions of host and guest solutions calibrated against the concentrated solution of 3-(Trimethylsilyl)-1-propanesulfonic acid sodium salt.

Isothermal Titration Calorimetry (ITC) All ITC experiments were carried out on a Microcal ITC200 at 298.15 K in 50 mM sodium acetate buffer (pH = 4.75). In a typical ITC experiment, the host molecule (CB[8]) was in the sample cell, and guest molecule was in the injection syringe with a concentration of about ten times concentration of host. The concentration of CB[8] was calibrated by the titration with a standard solution of 1-adamantanamine. All raw data of ITC were integrated by NITPIC (v.1.2.0), fitted in Sedphat (v.12.1b), and visualized through GUSSI (v.1.1.0). The resulted thermograms show the integrated heats of injections, with the error bars representing estimated errors for these values according to [157].

UV – Vis Spectroscopy UV – Vis spectra were recorded on a Varian Cary 400 UV – Vis spectrophotometer using a Suprasil Quartz (QS) cuvette with 1 cm path length at 298 K. EV[X]MV, EV[X]MV:CB[8] or EV[X]MV:CB[7] aqueous solutions were tested in the concentration of 0.01 mM.

Fluorescence Spectroscopy Fluorescence spectroscopy was recorded on an Agilent Cary Eclipse fluorescence spectrophotometer using a Suprasil Quartz (QS) cuvette with 1 cm path length at 298 K.

Time-Correlated Single Photon Counting TCSPC was recorded using a FS5 Spectrofluorometer, Edinburgh Instrument. A TCSPC laser (360 nm) was used for fluorescence lifetime measurements at peak emission wavelength for measured molecules and complexes. A Suprasil Quartz (QS) cuvette with 1 cm path length was used for all measurements. The data was fit with the exponential reconvolution function and the non-linear least square method.

Fluorescence Quantum Yield Measurements The absolute fluorescence quantum yield was determined using an Edinburgh Instruments Integrating Sphere Module (SC-30) on a spectrofluorometer. Fluorescence spectra analysis software Fluoracle and Quantum Yield Wizard were used to obtain quantum yields. For fluorescence quantum yield measurements the optical density for all EV[X]MV, EV[X]MV:CB[8] or EV[X]MV:CB[7] aqueous solutions was in a range of 0.1 to 0.06.

Cyclic voltammetry Cyclic Voltammetry experiments were carried out at 25 °C in nitrogen purged 0.1 M KCl aqueous solutions with Metrohm Eco Chemie Autolab PGSTAT12 Potentiostat, working on GPES 4.9 software. The three-electrode configuration was used: the 3 mm glassy carbon as a working electrode, a platinum wire as the counter electrode and RE-5B Ag/AgCl BASI as a reference electrode. The glassy carbon electrode was polished before each measurement with i) 1 µm ii) 0.3 µm, and iii) 0.05 µm alumina-H_2O slurry. CV was performed at variable scan rates ranging from 25 mV s^{-1} to 400 mV s^{-1}, for different concentrations of molecules, for EV[X]MV saturated with CB[8], and for 1:2 ratio EV[X]MV:CB[7] mixed solutions. The scans were run from 1 V to −1.5 V.

2.4.2 Synthetic protocols

The extended viologen EV[Ph] was synthesised using a modified literature procedure.[150] EV[Np], EV[$Pyr_{1,6}$], EV[$Pyr_{2,7}$], EV[CH], EV[Th], EV[DTh] were obtained using the same general method with appropriate 1,4-dibromonapthyl, 1,6-dibromopyrene, 2,7-dibromopyrene, 6,12-Dibromochrysene, 2,5-Dibromothiophene and 5,5'-Dibromo1,2'-bithiophene, respectively.

1,4-Di(pyridin-4-yl)benzene - EV[Ph]

4-Pyridinylboronic acid (1.25 g, 10 mmol), 1,4-dibromobenzene (1 g, 4.2 mmol) and K_2CO_3 (2.8 g, 20.4 mmol) were added to a 1:1 mixture of dry, degassed toluene and DMF (300 ml). Next, $Pd(PPh_3)_4$ (0.39 g, 0.34 mmol) was added to the reaction mixture and the solution heated to 130 °C under N_2 for 72 h. Thereafter, the reaction mixture was cooled to room temperature and filtered. The organic phase was concentrated under vacuum and the residue dissolved in CH_3Cl and washed three times with water. The collected organic phase was concentrated under vacuum and the residue dissolved in acetone. Concentrated HCl was then added dropwise to the solution, resulting in precipitation of the product. The precipitate was collected by filtration and then dissolved in H_2O. Finally, aqueous NaOH (10 M) was added dropwise to the H_2O layer until the pH was ca. 8-9, resulting in the precipitation of white

powder of EV[Ph] (0.8 g, 82 %).
^{1}H NMR (500 MHz, $CDCl_3$) δ (ppm): 8.70 (dd, J = 4.75; 1.51 Hz, 4H), 7.77 (s, 4H), 7.56 (dd, J = 4.55 Hz; 1.61 Hz, 4H). **^{13}C NMR** (125 MHz, $CDCl_3$) δ (ppm): 150.30, 147.52, 138.82, 127.79, 121.57 **MS** ESI-MS: m/z [M+H]+ calc for $C_{16}H_{12}N_2H$: 233.1073, found: 233.1074

1,4-Di(pyridin-4-yl)naphthalene - EV[Np]

^{1}H NMR (500 MHz, $CDCl_3$) δ (ppm): 8.77 (dd, J = 4.45 Hz; 1.53 Hz, 4H), 7.90 (m, 2H), 7.51 (m, J = 4.55; 8H). **^{13}C NMR** (125 MHz, $CDCl_3$ δ (ppm): 149.38, 148.96, 138.09, 131.10, 127.03, 126.36, 125.80, 125.17. **MS** ESI-MS: m/z [M+H]+ calc for $C_{20}H_{14}N_2H$: 283.1230, found: 283.1229

1,6-Di(pyridin-4-yl)pyrene - EV[Pyr$_{1,6}$]

^{1}H NMR (500 MHz, $CDCl_3$) δ (ppm): 8.83 (d, J = 6.0 Hz, 4H), 8.29 (d, J = 7.8 Hz, 2H), 8.18 (d, J = 9.2 Hz, 2H), 8.12 (d, J = 9.3 Hz, 2H), 8.00 (d, J = 7.8 Hz, 2H), 7.62 (d, J = 6.0 Hz, 4H). **^{13}C NMR** (125 MHz, $CDCl_3$) δ (ppm): 147.12, 146.81, 132.50, 128.59, 125.92, 125.68, 124.92, 123.08, 122.61, 122.49, 122.44 **MS** ESI-MS: m/z [M+H]+ calc for $C_{26}H_{16}N_2H$: 357.1386, found: 357.1389

2,7-Di(pyridin-4-yl)pyrene - EV[Pyr$_{2,7}$]

^{1}H NMR (500 MHz, $CDCl_3$) δ (ppm): 8.82 (d, J = 6.0 Hz, 4H), 8.49 (s, 4H), 8.24 (s, 4H), 7.85 (d, J = 5.2 Hz, 4H). **MS** ESI-MS: m/z [M+H]+ calc for $C_{26}H_{16}N_2H$: 357.1386, found: 357.1386

6,12-Di(pyridin-4-yl)chrysene - EV[CH]

^{1}H NMR (500 MHz, $CDCl_3$) δ (ppm): 8.87 (dd, J = 10.7 Hz, 7.2 Hz, 6H), 8.69 (s, 2H), 7.99 (d, J = 8.0 Hz, 2H), 7.78 (t, J = 7.6 Hz, 2H), 7.64 (dd, J = 19.4 Hz, 6.9 Hz, 6H). **MS** ESI-MS: m/z [M+H]+ calc for $C_{28}H_{18}N_2H$: 383.1543, found: 383.1542

2,5-Di(pyridin-4-yl)thiophene - EV[Th]

^{1}H NMR (500 MHz, $CDCl_3$) δ (ppm): 8.64 (d, J = 6.3 Hz, 4H), 7.55 (s, 2H), 7.53 – 7.50 (m, 4H). **^{13}C NMR** (125 MHz, $CDCl_3$) δ (ppm): 150.38, 142.61, 140.85, 126.64, 119.79. **MS** ESI-MS: m/z [M+H]+ calc for $C_{14}H_{10}N_2SH$: 239.0637, found: 239.0637

5,5'-Di(pyridin-4-yl)-2,2'-bithiophene - EV[DTh]

^{1}H NMR (500 MHz, DMSO) δ (ppm): 7.85 (d, J = 6.5 Hz, 4H), 7.18 (d, J = 4.0 Hz, 2H), 7.06 (d, J = 5.8 Hz, 4H), 6.81 (d, J = 4.0 Hz, 2H). **MS** ESI-MS: m/z [M+H]+ calc for $C_{18}H_{12}N_2S_2H$: 321.0515, found: 321.0516

4,4'-(1,4-Phenylene)bis(1-methylpyridin-1-ium) iodide - EV[Ph]MV

1,4-di(pyridin-4-yl)benzene (EV[Ph]) (1 g, 4.3 mmol) and 4 eq of methyl iodide (0.61 g, 270 µl, 17.2 mmol) were dissolved in methanol (50 ml). The solution was heated to 56 °C overnight. Thereafter, the reaction mixture was cooled to room temperature and 80% of solution evaporated under reduced pressure. Highly concentrated residue was then added dropwise to diethyl ether resulting in precipitation of the product. The precipitate was collected by filtration and then recrystallised from methanol yielding yellow coloured EV[Ph]MV (76 %). **^{1}H NMR** (500 MHz, D_2O) δ (ppm): 8.75 (d, J = 6.8 Hz, 4H), 8.30 (d, J = 6.9 Hz, 4H), 8.08 (s, 4H), 4.33 (s, 6H) **^{13}C NMR** (125 MHz, D_2O) δ (ppm): 154.98, 145.15, 136.99, 129.04, 125.21, 47.44 **MS** ESI-MS: m/z [M]2+ calc for $C_{18}H_{18}N_2$: 131.0730, found: 131.0725

This general procedure was applied for all other EV[X]MV molecules.

4,4'-(Naphthalene-1,4-diyl)bis(1-methylpyridin-1-ium) iodide - EV[Np]MV

^{1}H NMR (500 MHz, D_2O) δ (ppm): 8.85 (d, J = 6.3 Hz, 4H), 8.20 (d, J = 6.3 Hz, 4H), 7.94 – 7.87 (m, 2H), 7.72 (d, J = 0.9 Hz, 2H), 7.65 (dd, J = 6.4 Hz, 3.3 Hz, 2H), 4.42 (s, 6H). **^{13}C NMR** (125 MHz, D_2O) δ (ppm): 156.70, 144.96, 136.34, 130.06, 128.88, 128.29, 127.41, 125.10, 47.77. **MS** ESI-MS: m/z [M-Cl]2+ calc for $C_{22}H_{20}N_2$: 156.0808, found: 158.0804

4,4'-(Pyrene-1,6-diyl)bis(1-methylpyridin-1-ium) iodide - EV[Pyr$_{1,6}$]MV

^{1}H NMR (500 MHz, D_2O) δ (ppm): 8.88 (d, J = 6.3 Hz, 4H), 8.38 (d, J = 8.0 Hz, 2H), 8.29 (d, J = 6.4 Hz, 4H), 8.22 (d, J = 9.3 Hz, 2H), 8.14 (dd, J = 11.2 Hz, 8.5 Hz, 4H), 4.44 (s, 6H). **^{13}C NMR** (125 MHz, D_2O) δ (ppm): 157.36, 144.76, 131.93, 131.58, 129.17, 129.12, 128.00, 127.86, 125.99, 124.58, 123.88, 48.83, 47.65. **MS** ESI-MS: m/z [M]2+ calc for $C_{268}H_{22}N_2$: 193.0886, found: 193.0884

4,4'-(Pyrene-2,7-diyl)bis(1-methylpyridin-1-ium) iodide - EV[Pyr$_{2,7}$]MV

^{1}H NMR (500 MHz, D_2O) δ (ppm): 8.67 (d, J = 6.2 Hz, 4H), 8.55 (s, 4H), 8.36 (d, J = 7.4 Hz, 4H), 8.20 (s, 4H), 4.23 (s, 6H). **MS** ESI-MS: m/z [M]2+ calc for $C_{28}H_{22}N_2$: 193.0888, found: 193.0884

4,4'-(Chrysene-6,12-diyl)bis(1-methylpyridin-1-ium) iodide - EV[CH]MV

^{1}H NMR (500 MHz, D_2O) δ (ppm): 8.86 (d, J = 6.6 Hz, 4H), 8.75 (d, J = 8.5 Hz, 2H), 8.62 (s, 2H), 8.16 – 8.12 (m, 4H), 7.84 (dd, J = 8.4 Hz, 1.3 Hz, 2H), 7.79 – 7.73 (m, 2H), 7.66 (ddd, J = 8.1 Hz, 6.9 Hz, 1.1 Hz, 2H), 4.45 (s, 6H). **^{13}C NMR** (125 MHz, D_2O) δ (ppm): 156.81, 144.83, 134.17, 130.34, 128.78, 128.17, 128.16, 128.15, 128.07, 127.73, 125.11, 123.79, 123.57, 47.75. **MS** ESI-MS: m/z [M]2+ calc for $C_{30}H_{24}N_2$: 206.0964, found: 206.0964

4,4'-(Thiophene-2,5-diyl)bis(1-methylpyridin-1-ium) iodide - EV[Th]MV

^{1}H NMR (500 MHz, D_2O) δ (ppm): 8.64 (d, J = 7.1 Hz, 4H), 8.19 (d, J = 7.0 Hz, 4H), 8.02 (s, 2H), 4.25 (s, 6H). **^{13}C NMR** (125 MHz, D_2O) δ (ppm): 147.76, 145.20, 142.55, 132.62, 123.24, 47.37. **MS** ESI-MS: m/z [M]2+ calc for $C_{16}H_{16}N_2S$: 134.0512, found: 134.0508

4,4'-([2,2'-Bithiophene]-5,5'-diyl)bis(1-methylpyridin-1-ium) iodide - EV[DTh]MV

^{1}H NMR (500 MHz, D_2O) δ (ppm): 8.54 (d, J = 6.9 Hz, 4H), 8.08 (d, J = 7.0 Hz, 4H), 7.92 (d, J = 4.1 Hz, 2H), 7.55 (d, J = 4.1 Hz, 2H), 4.20 (s, 6H) **^{13}C NMR** (125 MHz, D_2O) δ (ppm): 148.13, 144.73, 142.48, 137.06, 132.62, 128.06, 122.22, 46.99. **MS** ESI-MS: m/z [M]2+ calc for $C_{20}H_{18}N_2S_2$: 175.0450, found: 175.0558

2.5 Acknowledgements

Dr. Qianqi Lin, Department of Physics, the Cavendish Laboratory helped in designing, conducting and analysing of cyclic voltammetry measurements.

Chapter 3

Supramolecular CB[8]-Based Dimerisation of Optically-tunable Extended Aryl Viologens

Part of this work has been compiled into a manuscript in preparation for submission for publication:

Olesińska M., Wu G., Gomez-Coca S., Anton-Garcia, D., Szabo I., Rosta E. and, Scherman, O.A. 'Modular supramolecular dimerisation of optically tunable highly emissive extended aryl viologens', submitted.

Olesińska, M., Powers-Riggs, N., Ryan, Y. M., Wasielewski, M.R. and Scherman, O.A., manuscript in preparation.

This chapter is focused on the extent of interchromophoric interactions, in both the ground and excited states, based on the 2:2 complexes steady-state electronic transitions and fluorescence lifetimes as a function of their binding with CB[8]. Here, the synthesis and characterisation of the family of extended aryl viologens (EV[X]R) is presented. The type of complexation of these molecules with CB[8] and CB[7] are probed with ITC and NMR experiments. For this family of compounds and their supramolecular complexes, steady-state and transient absorption spectroscopies are used to investigate the observed optical properties.

3.1 Introduction

Achieving precise control over the spatial arrangement of organic photoemissive molecules on surfaces and in solutions is of interest in the area of photovoltaic device construction,

light-emitting diodes, sensing and bio-imaging.[127, 158] Both covalent and non-covalent interactions between luminescent molecules have been used to control their spatial distance in order to optimise their optical properties. Recently, a number of examples have been reported in the literature demonstrating detailed control over the photo-emissive states of discrete organic molecules or complexes. These include the luminescence of molecular rotors based on aggregation induced emission[159], generation of excimers with modifications in covalently-bound chromophores[152, 160, 161] and H/J-aggregate formation on account of encapsulation within supramolecular macrocycles or self-assembled cages.[26–30, 162–166] Nevertheless, these systems are challenging to synthesise chemically and do not provide a modular approach for tuning optoelectronic properties.

Cucurbit[n]urils are a family of macrocyclic host molecules often used in synthetic and material sciences due to their variety of sizes and capability to complex different types of guest molecules in an aqueous environment (see Section 1.2).[38] In particular, CB[8] is of interest because of its ability to host two guest moieties simultaneously. As previously reported by Wu *et al.*, CB[8] with symmetric diaryl viologens bearing electron-donating groups binds in a 2:2 manner.[68] The formation of such 2:2 complexes originates from both the favourable Coulombic interactions as well as $\pi - \pi$ stacking, which leads to interesting observations of their optical properties. A uniform red-shift in the absorption of the 2:2 complexes relative to their monomeric UV – Vis spectra was observed, and in a few specific cases an intense fluorescence emission typical for J-aggregates.[68]

In order to take advantage of the strict 2:2 complex formation through the CB[8] binding motif, an extended π-bridging unit between the two pyridyl groups in extended aryl viologens (EV[X]R) as shown in Figure 3.1 is introduced in this chapter. This directs the CB[8] macrocycle to bind around the aryl pyridyl groups and facilitates $\pi - \pi$ stacking of the linker units, which provides control over the spatial arrangement of the EV[X]R monomers. The donor-acceptor character of molecules coupled in the close proximity imposed by CB[8] macrocycles leads to positive or negative Coulombic interaction.[167] This results in competition between a favourable electrostatic interaction as well as $\pi - \pi$ stacking that has a strong effect on photophysical performance of the formed dimers.

Here, the hypothesis that the emissive excited state properties of the dimeric complexes of CB[8] and extended aryl viologens ($(\mathrm{CB[8]})_2 : (\mathrm{EV[X]R})_2$) would not only be influenced by the host-guest interactions in their ground state but also in their excited state as an excimer-like complex was studied. Similar to the observations for molecular packing of naphthalene, anthracene and phenanthrene under pressure or in the solid state with energies of their electronic transitions shifted towards the red (lower energy), and their broadened and featureless spectral bands.[22] In the system presented here, the complexation of guests

inside the confined space of the CB[8] macrocycle results in distinct $\pi - \pi$-stacking in solution.

It was recently shown by Wu *et al.* that the distance between molecules can affect charge transfer interactions, excimer formation and excimer efficiency.[152] However, this recent report and many other publications are focused mostly on covalent dimers, where molecules are not free to rotate or rearrange.[127, 152, 168–170] Given that the supramolecular dimeric systems reported here are dynamic, it can be reason that upon excitation, the two guest molecules are still able to rearrange in their excited states within the complex and reach their most stable excited state geometry.

3.2 Results and Discussion

3.2.1 Synthesis of Extended Aryl Viologens

Symmetric extended aryl viologen (EV[X]R) derivatives with various bridging units *i.e.* [X]= phenylene, naphthalene, 1,6-pyrene, 2,7-pyrene, chrysene, thiophene and dithiophene were synthesised in a three-step procedure, as depicted in Figure 3.1. Bipyridine derivatives were made through Suzuki coupling of pyridine-4-boronic acid and the corresponding dibromo species (1,4-dibromobenzene, 1,4-dibromonapthyl, 1,6-dibromopyrene, 2,7-dibromopyrene, 6,12-dibromochrysene, 2,5-dibromothiophene and 5,5'-dibromo1,2'-bithiophene) as previously described in Chapter 2. These bipyridine derivatives then underwent a two-step Zinke reaction with first formation of the Zinke salts. The symmetric and asymmetric Zinke salts were separated using HPLC with gradient of water/acetontitrile (0.1% TFA) solution. Subsequent reaction of the symmetric Zinke salt with appropriate para R substituted aniline yielded various extended aryl viologens, EV[Ph]R, EV[Np]R, EV[$Pyr_{1,6}$]R, EV[$Pyr_{2,7}$]R, EV[CH]R, EV[Th]R and EV[DTh]R (where R=Me; for EV[Np]R R=Me, OMe, H, NH_2, NMe_2, SMe, Br, CF_3, Cl). All molecules were characterised with increased extended conjugate π-systems. The effect on optical properties as well as binding properties of the functional group on each derivative was analysed.

3.2.2 NMR Characterisation of Homoquaternary 2:2 Complex Formation

The interaction between CB[8] and CB[7] and the series of EV[Ph]Me, EV[Np]R (R=Me, OMe, SMe, CF_3, Br), EV[$Pyr_{1,6}$]Me, EV[$Pyr_{2,7}$]Me, EV[CH]H , EV[Th]Me and EV[DTh]Me was studied by ^{1}H NMR experiments. Guest complexation with the hydrophobic cavity

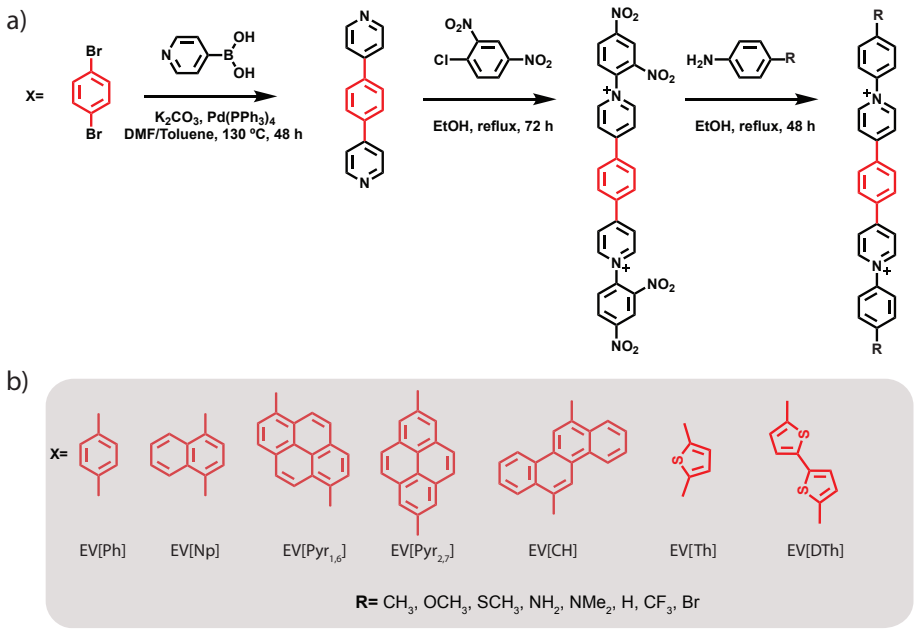

Fig. 3.1 a) The scheme of the EV[X]R synthesis, b) Chemical structures of EV[X]R bridging unit. Cl^- counterions have been removed for clarity.

of CB[8] or CB[7] typically results in an upfield shift of the encapsulated protons and a downfield shift of protons in close proximity to the carbonyl portals. Through the utilisation of precise NMR measurements and precalibrated mixed solutions, and the combination of signals shifts and spectrum integration, information about binding manner of host and guest can be derived.

EV[Ph]Me

Mixing EV[Ph]Me and CB[8] in a 1:1 stoichiometric ratio, results in 0.40 ppm, 0.84 ppm, 0.71 ppm, 0.26 ppm, 0.18 ppm and 0.36 ppm upfield shift of proton H_a, H_b, H_c, H_d, H_e and H_f respectively (see Figure 3.2 for proton assignments). The upfield shifts are typically indicative of encapsulation or partial encapsulation inside the cavity of CB[8]. In the top spectrum in Figure 3.2 the broad NMR peaks can be attributed to the unencumbered aromatic linker unit. In this case, the phenylene ring, which is small enough to enter the hydrophobic cavity as the CB[8] macrocycles can shuttle back and forth in a complex. Additionally, weak upfield shift for H_a, H_d, H_e and H_f indicates that these protons are affected by dynamic shuffling of CB[8], meaning that the observed shifts are likely to be an average between encapsulated or partially encapsulated tolyl group of a monomer. Moreover, splitting of peaks corresponding to the methine protons located at the CB[8] portals can be observed. Such splitting is indicative of an asymmetric environment around CB[8]. Based on the

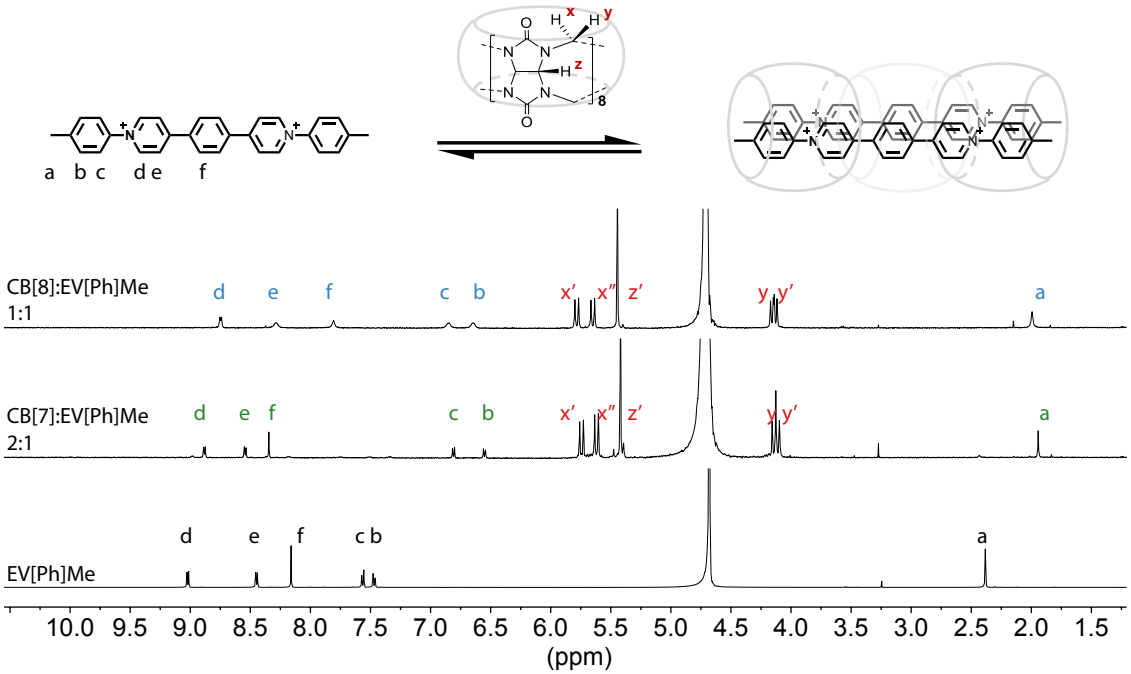

Fig. 3.2 ^{1}H NMR complexes of EV[Ph]Me with 1 eq of CB[8] and 2 eq of CB[7]. Measurements performed in D_2O with Cl^- as counterions.

observed shifts of these protons and the integration of the spectrum, it can be concluded that EV[Ph]Me forms a 2:2 dynamic host-guest complex with CB[8].

The titration of the EV[Ph]Me molecule into CB[7] until a 2:1 host-guest ratio is reached, results in 0.44 ppm, 0.92 ppm, 0.76 ppm and 0.12 ppm upfield shift of proton H_a, H_b, H_c and H_d respectively (see Figure 3.2 and Figure B.43). Such shifting behaviour suggests encapsulation of those protons inside the cavity of CB[7]. Protons H_e and H_f are shifted downfield, indicating that these protons are outside the cavity of the macrocyle. Splitting of the CB[7] rim protons has been previously observed with 2:1 ratio mixtures for aryl viologens.[87] Again, it is indicative of an asymmetric environment around CB[7]. The peaks for this host-guest mixture are sharp and well resolved, suggesting that this complex is stable and non-dynamic. Based on the integration of the spectrum and described shifts, a 2:1 complex of CB[7] and EV[Ph]Me can be proposed where the macrocycle is bound around the tolyl groups.

EV[Np]R

Augmenting the bridging unit from Ph to Np results in a less dynamic complex, as the bulkier Np retards the rate of CB[8] shuttling (Figure 3.3). Upon addition of EV[Np]Me into CB[8]

to reach the 1:1 stoichiometric ratio, 0.43 ppm, 1.05 ppm, 0.85 ppm and 0.29 ppm upfield shifts of proton H_a, H_b, H_c and H_d respectively, was observed. As seen in example above, these upfield shifts are indicative of encapsulation or partial encapsulation inside the cavity of CB[8]. Shifts of protons H_b, H_c and H_d are the result of magnetic shielding by the

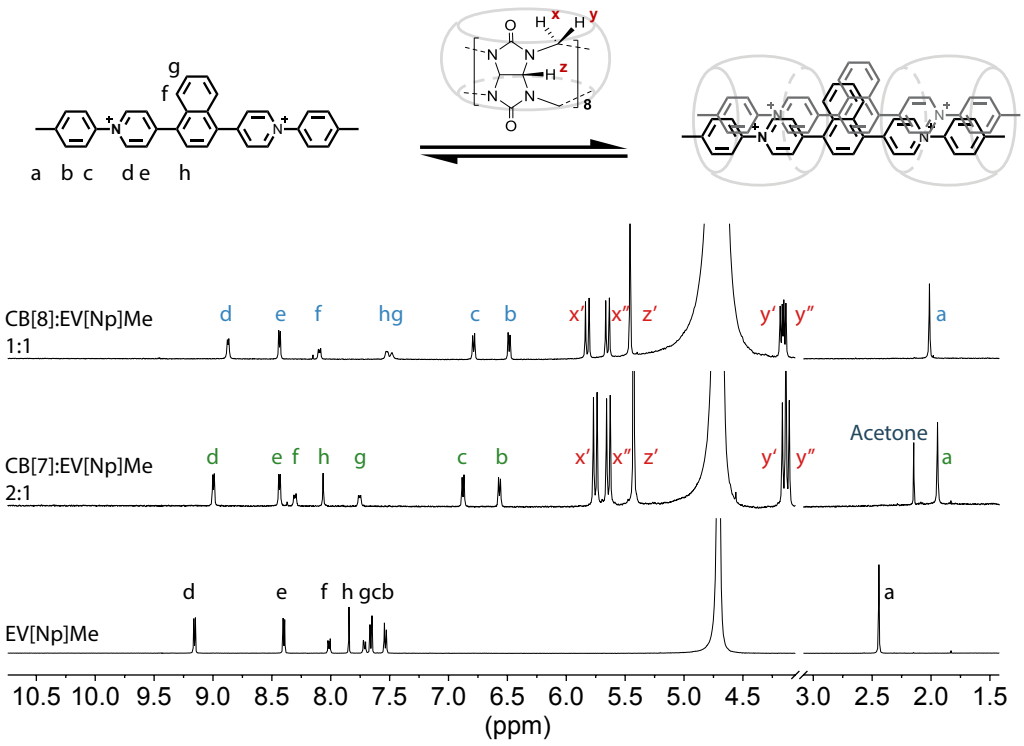

Fig. 3.3 ^{1}H NMR complexes of EV[Np]Me with 1 eq of CB[8] and 2 eq of CB[7]. Measurements performed in D_2O with Cl^- as counterions.

CB[8] cavity. Proton H_e shifts slightly downfield as a result of interactions with the CB[8] portal. Protons on the aromatic Np bridging moiety, H_g and H_h, are broadened relative to the rest of the guest protons and exhibit an upfield shift of 0.2 ppm, which likely originates from ring current effects. Moreover, splitting of peaks corresponding to the methine protons located at the CB[8] portals can be observed. A similar shifting behaviour and corresponding binding mode with CB[8] was observed for all Np based molecules N-functionalised with electron-donating groups (for more examples see Figures B.44 to B.49). Interestingly, functionalisation with electron-withdrawing groups do not demonstrate 2:2 binding features (Figure 3.4 and Figure B.49). The ^{1}H NMR spectrum for EV[Np]CF_3 interaction with 1 eq of CB[8] reveals a typical 1:1 binding, with the macrocycle bound around the bridging Np unit (Figure 3.4).

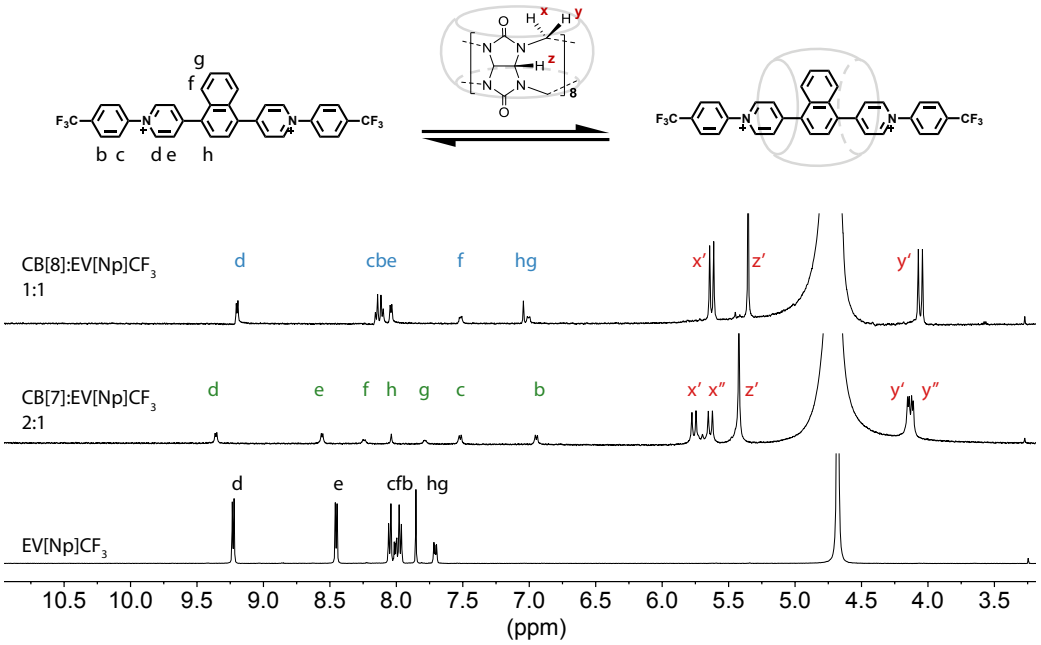

Fig. 3.4 ^{1}H NMR complexes of EV[Np]CF_3 with 1 eq of CB[8] and 2 eq of CB[7]. Measurements performed in D_2O with Cl^- as counterions.

Upon addition of the EV[Np]Me or EV[Np]CF_3 molecule into 2 eq of CB[7] solution, sharp and well-resolved peaks can be observed (see Figure 3.3 and Figure 3.4). The upfield shifts of protons on p-(Trifluoromethyl)benzyl or tolyl groups suggest their encapsulation in CB[7] cavity. The splitting of CB[7] rim protons is also observed. Based on spectrum integration, and the shifting behaviour of guest and host protons, it can be inferred that CB[7] binds to EV[Np]R around the N-functionalised groups in 2:1 manner.

DOSY characterisation of supramolecular complexes

The formation of supramolecular assemblies of EV[Np]R with CB[8] and CB[7] were tested with diffusion-ordered spectroscopy (DOSY) NMR experiments. This method has been shown previously to probe well the CB-based supramolecular assembly. [171]

The measured diffusion coefficients (D) of monomeric EV[Np]R guests and their supramolecular complexes are listed in Table 3.1. The combined diffusion coefficients of EV[Np]R species complexed with CB[8] or CB[7] plotted as a function of D_G of monomeric EV[Np]R is shown in Figure 3.5.

DOSY results show clear differences in diffusion coefficients for monomeric and CB[7] and CB[8] complexed species. All the monomeric EV[Np]R with avarage molecular weight of 556 g mol^{-1}, diffuse with similar diffusion coefficient (see Table 3.1 and Figure 3.5, grey

Table 3.1 Diffusion coefficient (D) data of EV[Np]R guest molecules (G) and their complexes with CB[8] and CB[7] (T=298 K).

Guest	D_G (m^2/s)	$D_{G:CB[8]}$ (m^2/s)	$D_{G:CB[7]}$ (m^2/s)
EV[Np]H	4.05	2.06	2.24
EV[Np]Me	3.85	1.98	2.20
EV[Np]OMe	3.83	1.97	2.18
EV[Np]SMe	3.73	1.99	2.17
EV[Np]NH_2	3.91	2.02	2.26
EV[Np]NMe_2	3.53	2.00	2.15

points). The diffusion coefficients of the free EV[Np]R guests diffusing as single molecular species fall between D_G=3.53 $m^2\,s^{-1}$ and 4.05 $m^2\,s^{-1}$. Upon formation of 2:1 host-guest complex with CB[7], the average molecular weight increase to 2880 $g\,mol^{-1}$ and the decrease in D is observed (see Table 3.1 and Figure 3.5, green points). Here, CB[7] based complexes diffuse with $D_{G:CB[7]}$=2.15 $m^2\,s^{-1}$ to 2.26 $m^2\,s^{-1}$. With the formation of 2:2 homoquaternary complex with CB[8] there is further increase in average molecular weight 3768 $g\,mol^{-1}$, and greater decrease in D is observed (see Table 3.1 and Figure 3.5, red points). CB[8] based complexes diffuse with $D_{G:CB[8]}$=1.97 $m^2\,s^{-1}$ to 2.06 $m^2\,s^{-1}$. These results support the formation of distinct host:guest complexes of EV[Np]R with CB[8] and CB[7].

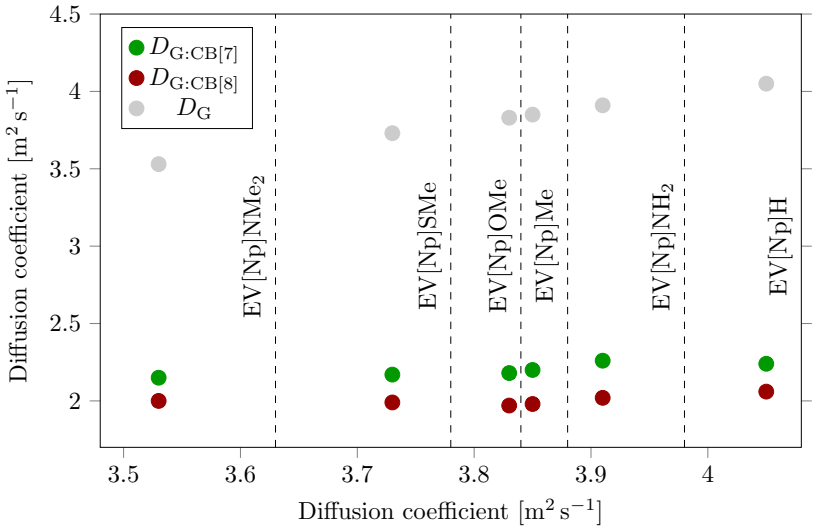

Fig. 3.5 Diffusion coefficient of EV[Np]R guest molecules (grey point) and their complexes with 1 eq of CB[8] (red points), 2eq of CB[7] (green points).

EV[CH]H

The ^{1}H NMR spectrum for EV[CH]H interaction with CB[8] at a 1:1 ratio mixture is shown in Figure 3.6. All proton peaks of the guest molecules are broad and are difficult to assign. The splitting of CB[8] macrocycle rim protons is indicative of 2:2 binding mode.[87, 172, 173] The calculations based on previously calibrated solutions, suggest that a 2:2 complex is formed. Such broad spectrum could suggest that this complex is dynamic. However, on account of the extended π-surface of EV[CH]H molecule and the higher degree of complexity, different conformations of this molecule inside the cavity of the macrocycle are possible, and need to be taken into consideration. The two different types of arrangements of chrysene based molecules are depicted in Figure 3.7. Due to the different spatial overlap of the molecular π-systems, the broad spectrum of this 2:2 complex could be explained with the magnetic anisotropic effect from the ring current of the chrysene rings.

Upon addition of CB[7] to the EV[CH]H solution, upfield shifts of proton H_b, H_c, H_a and H_d by 0.88 ppm, 0.99 ppm, 0.54 ppm and 0.38 ppm were observed. Therefore, the protons from N-functionalised side groups, are considered to be inside the cavity of macrocycle. Protons H_f and H_j, H_g and H_e show downfield shifts that are a consequence of interaction with CB[7] portals. Protons H_h and H_i are almost not affected by the presence of the host molecule. These features indicate that CB[7] can deaggregate the guest-molecule and binds in a 2:1 manner with EV[CH]H .

EV[Pyr$_{1,6}$]Me

1 eq of EV[Pyr$_{1,6}$]Me was added into a solution of 1 eq of CB[8] as depicted in Figure 3.9. In the NMR spectrum, strong upfield shifts of protons H_c, H_b and H_d can be observed, indicating that the macrocycle binds to the side moieties of the guest molecule. The 0.36 ppm upfield shift of H_a suggests that this part of a molecule is partially encapsulated in CB[8]. The upfield shifts of protons on Pyr$_{1,6}$ core can be explained by the magnetic anisotropic effect from the ring current of the highly extended π-surface of stacked pyrenes. On account of these anisotropic effects, the shielding effects for protons placed above the ring, and deshielding effects for protons to the side of it, the signals are shifted accordingly in the NMR spectrum. It is possible that these observed shifts for protons H_i, H_g, H_h and H_f result from both effects as well as the presence of the CB[8] portals. The splitting of the proton peaks originating from the macrocycle as well as integration of the spectrum suggest that this molecule binds with CB[8] in a 2:2 manner. Similarly to EV[CH]H, this molecule can exhibit different conformations inside the cavity (Figure 3.8). This could explain the

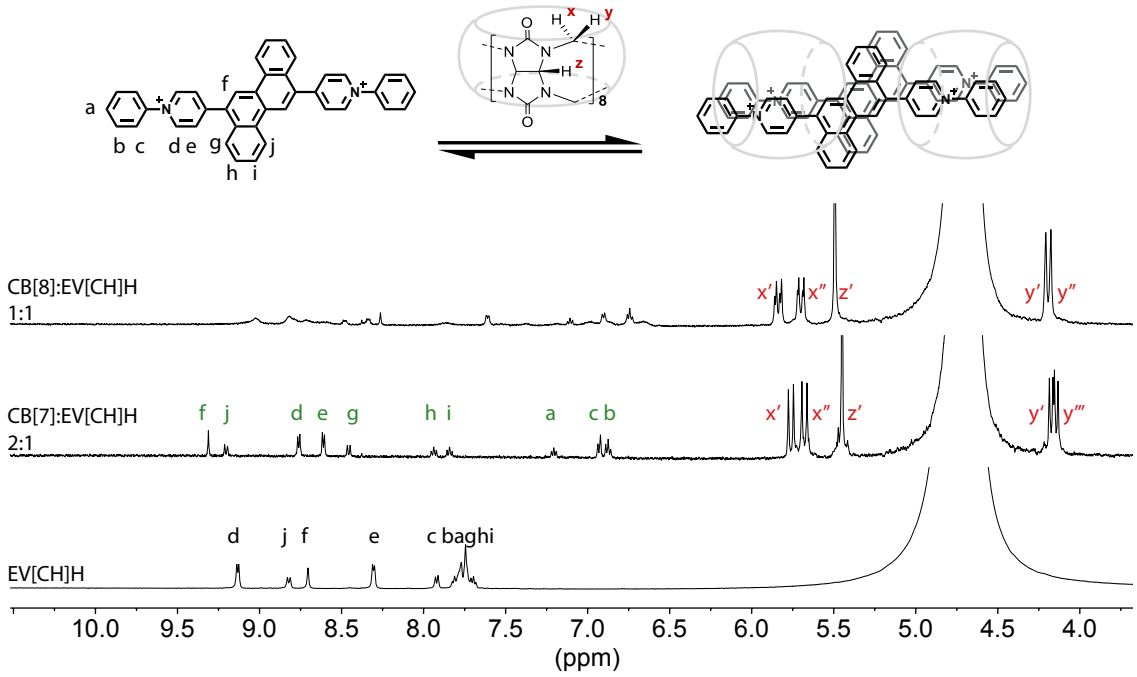

Fig. 3.6 ^{1}H NMR complexes of EV[CH]H with 1 eq of CB[8] and 2 eq of CB[7]. Measurements performed in D_2O with Cl^- as counterions.

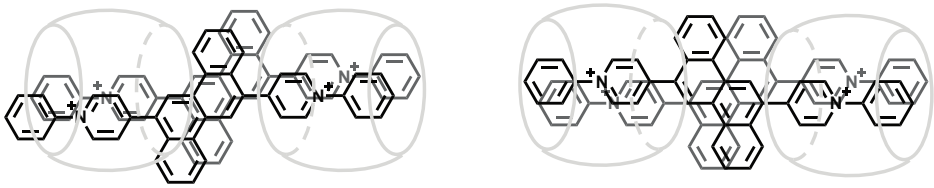

Fig. 3.7 Possible complex conformations of EV[CH]H with 1 eq of CB[8].

broadening of the H_c and H_b peaks, suggesting that one of the conformations is energetically less stable.

EV[$Pyr_{1,6}$]Me mixed with CB[7] in 2:1 host-guest ratio shows an upfield shift of the tolyl moiety of the molecule (Figure 3.9). Such shifting behaviour as well as the downfield shifts of the aromatic protons of the pyrene core suggest that the macrocycle binds around the N-functional group.

The titration studies of EV[$Pyr_{2,7}$]Me into CB[8] were not successful. The highly planar and rigid structure of the molecule, render them prone to parallel stacking as a product of their highly conjugated, aromatic structure. Furthermore, with its low solubility in the formed complex, the NMR spectrum resolution was too low to be conclusive.

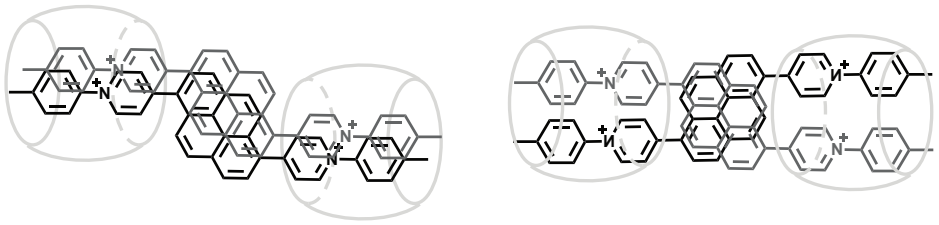

Fig. 3.8 Possible complex conformations of EV[$Pyr_{1,6}$]Me with 1 eq of CB[8].

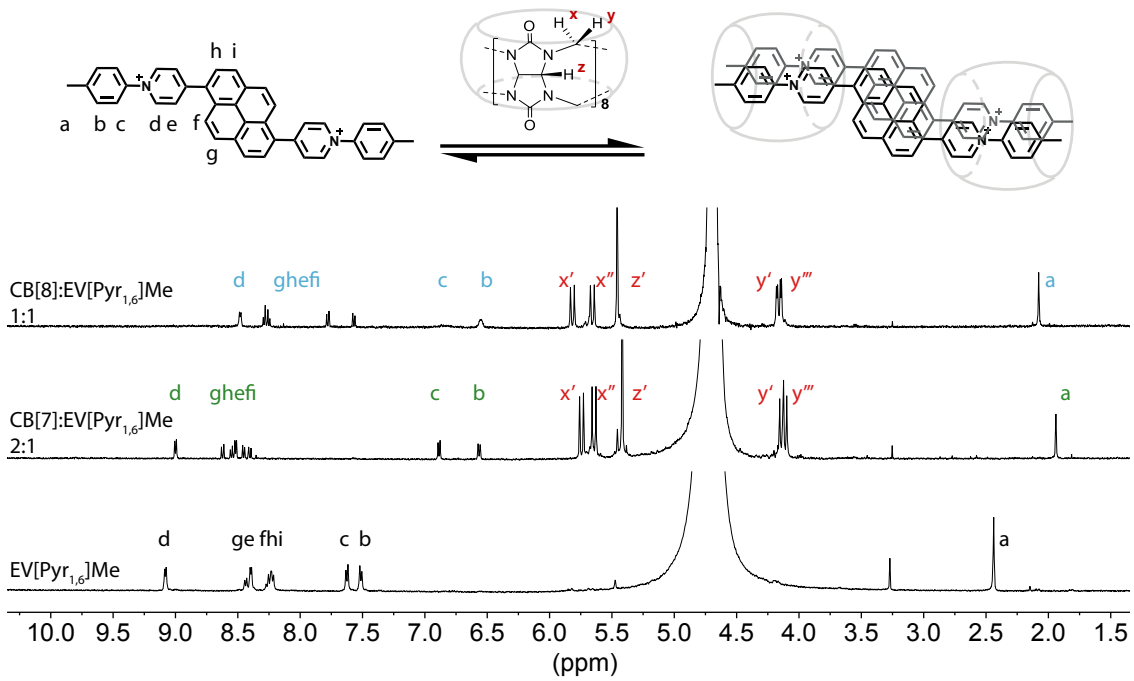

Fig. 3.9 ^{1}H NMR complexes of EV[$Pyr_{1,6}$]Me with 1 eq of CB[8] and 2 eq of CB[7]. Measurements performed in D_2O with Cl^- as counterions.

EV[Th]Me

Upon adding the thiophene extended viologen to CB[8], the NMR spectrum exhibits approximately 1 ppm upfield shifts for H_c, H_b and H_d protons. This suggests that these protons are located inside the cavity of CB[8] (see Figure 3.10 and Figure B.50). Peak H_a is shifted upfield by ca. 0.5 ppm. Such shifts can be observed for protons inside the cavity of the macrocycle, but it could also be a result of dynamic inclusion and exclusion from the cavity. When CB[8] and EV[Th]Me are mixed at a 1:1 ratio mixture, proton H_e shows a weak negative δ-shift of 0.06 ppm. This can be interpreted as a small effect of CB[8] portal interaction on the H_e proton. Here, proton H_f is only slightly affected by complexation with CB[8] and results in shift of 0.01 ppm. The acute angle between the pyridinium rings and the central thiophene unit explain the peak broadening in the CB[8]:EV[Th]Me complex. In this case, there is a greater steric hindrance between the molecules and consequently, a system with a more dynamic behaviour can be observed. Complexation with CB[7] results in

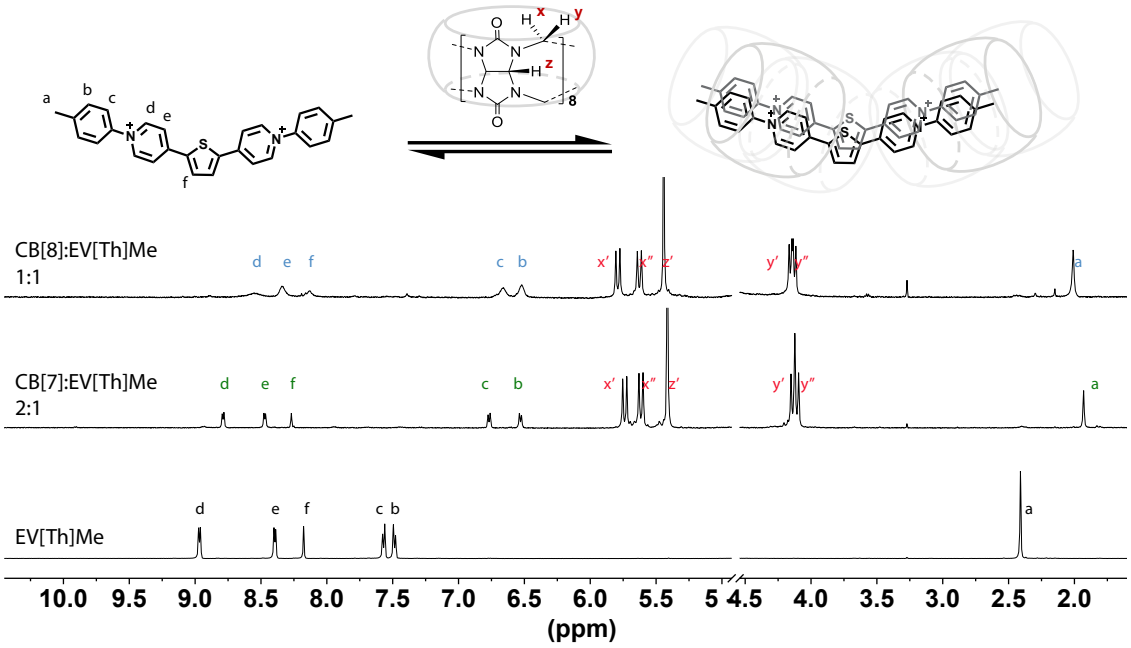

Fig. 3.10 ^{1}H NMR complexes of EV[Th]Me with 1 eq of CB[8] and 2 eq of CB[7]. Measurements performed in D_2O with Cl^- as counterions.

similar protons shifts as observed for the 2:2 CB[8]:EV[Th]Me mixture (see Figure 3.10 and Figure B.51). Protons H_a, H_b, H_c and H_d have 0.41 ppm, 0.99 ppm, 0.80 ppm and 0.18 ppm upfield shifts, respectively. This indicates that the toluidine side group is mostly affected by the shielding presence of the CB[7] macrocycle. A 0.07 ppm and 0.09 ppm downfield shift of H_e and H_f proton is observed. This suggest that these protons are outside of the CB[7]

cavity. The spectrum of CB[7]:EV[Th]Me in 2:1 ratio is characterised by sharp and well resolved peaks, indicating a non-dynamic complex.

EV[DTh]Me

The ^{1}H NMR spectrum of EV[DTh]Me mixed with 1 eq of CB[8] is shown in Figure 3.11. There are upfield shifts of H_a, H_b, H_c and H_d protons that can be identified as protons inside the CB[8] cavity. Protons H_f and H_g exhibit downfield shifts indicating weak interaction with the CB[8] portals. A splitting of H_e protons suggests asymmetric 2:2 binding with CB[8]. The binding mode can be confirmed by both the spectrum integration and the asymmetric splitting of CB[8] rim protons.

Upon mixing EV[DTh]Me with CB[7] peaks H_a, H_b and H_d are shifted upfield by 0.42 ppm, 0.89 ppm, 0.71 ppm and 0.11 ppm respectively. Such shifts suggest inclusion in macrocycle cavity. Peaks H_e, and H_f and H_g have small downfield shifts of around 0.10 ppm. Splitting of CB[7] rim protons can also be observed, which is mostly interpreted as an effect of the asymmetrical environment around the macrocycle. Based on the shifting behaviour of the guest and host protons coupled with the spectrum integration, CB[7] binds to the EV[DTh]Me molecule around the tolyl moieties in a 2:1 manner.

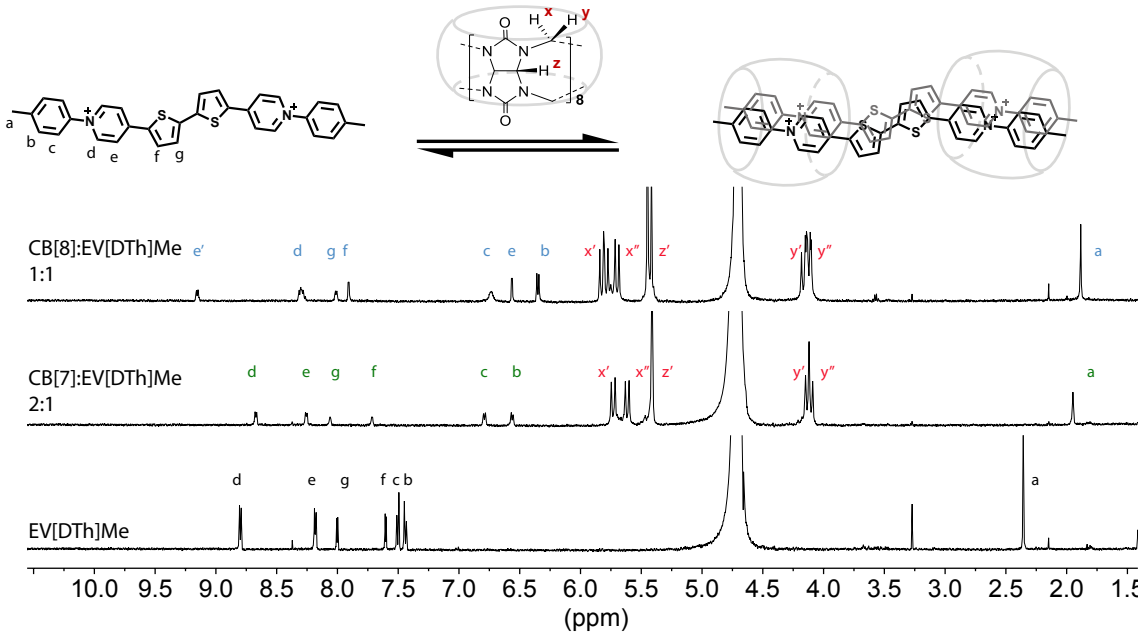

Fig. 3.11 ^{1}H NMR complexes of EV[DTh]Me with 1 eq of CB[8] and 2 eq of CB[7]. Measurements performed in D_2O with Cl^- as counterions.

3.2.3 Thermodynamics of Binding with CB[8] and CB[7]

Supramolecular interactions of extended viologens with CB[8] and CB[7] were evaluated with ITC. The thermodynamic data *i.e.* changes in enthalpy, binding constant, Gibbs energy and entropy are important indicators of complexation type. Typically, mixing stoichiometric quantities of host and guest leads to the formation of 1:1 host-guest complexes. However, by analysing thermodynamic values it was previously shown that it is possible to form 2:2 complexes for diarylviologens bearing electron-donating groups and CB[8].[68] The favoured formation of 2:2 over 1:1 complexes is characterised by the magnitude of the overall binding enthalpy (see Chapter 1). A special type of binding where two molecules are hosted by two CB[8]s is characterised by enthalpy values of approximately $-50\,\mathrm{kJ\,mol^{-1}}$ (or lower), and the entropy temperature product of approximately $-20\,\mathrm{kJ\,mol^{-1}}$ (or lower).[68] The complexation processes with CB[8] and CB[7] for all EV[X]Rs molecules are characterised by favourable values of Gibbs free energy and is characteristic for non-covalent aggregation. Moreover, all the complexations of EV[X]R with CB[8] are driven by favourable enthalpy.

Enthalpy and entropy values obtained for extended aryl viologens EV[Np]Me and EV[$Pyr_{1,6}$]Me, bearing both electron donating or electron withdrawing groups were found to suggest typical 2:2 binding with CB[8] (see Table 3.2 and for thermographs see Chapter B). Whereas for the EV[Ph]Me molecule, the thermodynamic data ($\Delta H = -95\,\mathrm{kJ\,mol^{-1}}$ and $T\Delta S = -56\,\mathrm{kJ\,mol^{-1}}$) are much higher, suggesting a more complicated encapsulation mode. Similarly, a high enthalpic gain of $-103\,\mathrm{kJ\,mol^{-1}}$ is observed for EV[DTh]Me. Those values can be explained by threading of CB[8] on to the core of the molecule, which causes the release of more cavity water and also influences the solvation state of guest molecule. The phenylene and dithiophene core is small enough to be encapsulated or partially encapsulated by the CB[8] macrocycle. In the case of EV[Np]Me and EV[$Pyr_{1,6}$]Me, the steric hindrance is too big and only pyridine moieties are complexed. The small values of ΔH and $T\Delta S$ for the 2:2 binding of EV[Th]Me with CB[8], can be explained by only partial encapsulation of a guest molecule.

Through comparing of the angles between the horizontal plane of the core units and the planes of pyridinium units *i.e.* 180° for EV[Ph]Me, 150° for EV[DTh]Me and 121° for EV[Th]Me, the differences in thermodynamic parameters could be explained.[1] In case of EV[Th]Me an acute angle of ca. 121° between the plane of a thiophene core and pyridines could prevent binding with CB[8] in a 2:2 manner. It is possible that the binding is more dy-

[1]The angles for EV[Th]Me and EV[DTh]Me molecules were calculated based on the BARLEM (Figure A.80) and COBDAA (Figure A.81 crystallographic data available in The Cambridge Crystallographic Data Centre (CCDC). The angles for EV[Ph]Me were calculated based on a geometry optimisation performed with Avogadro v.1.1.1. See Figure A.81.

Table 3.2 Thermodynamic data of EV[X]Rs binding with CB[8] (T=298 K, 50mM sodium acetate buffer (pH = 4.75)).

	ΔG (kJ mol^{-1})	ΔH (kJ mol^{-1})	$T\Delta S$ (kJ mol^{-1})	K (M^{-1})
EV[Ph]Me	-38.47	-95.18	-56.71	5.49×10^6
EV[Np]Me	-42.68	-67.57	-24.73	3.21×10^7
EV[Pyr$_{1,6}$]Me	-39.20	-62.80	-23.60	7.36×10^6
EV[Th]Me	-43.25	-53.65	-10.39	3.78×10^7
EV[DTh]Me	-52.49	-103.01	-50.51	1.57×10^9

namic, since the steric hindrance between two CB[8] macrocycles will cause their repulsion. The ^{1}H NMR titration for the EV[Th]Me molecule is in agreement with the ITC results (See previous section).

Interestingly, the ITC results for EV[Np]Br with CB[8] suggests that encapsulation is more in 2:1 host-guest complexation region (Figure B.80). This result along with previously conducted NMR experiments on extended aryl viologens bearing electron withdrawing groups suggest, that only extended aryl viologens with electron donating side groups can form 2:2 complexes.

The binding constants K for the EV[X]Me and CB[8] complexes were found to be within 5.5×10^6 M^{-1} to 1.7×10^9 M^{-1}, indicating strong host-guest binding.

As mentioned already in Chapter 1, when considering both the hydrophobic effect phenomena and the theory of energetically frustrated water inside the cavity, upon decreasing the size of the host cavity, the entropy contribution has a greater influence where less energetically frustrated water is released upon binding.[174] With this in mind, encapsulation of EV[X]Rs in CB[7] is also characterised by a favourable ΔG. The process is mostly enthalpically driven except for EV[Th]Me, which is considered to be entropically driven (Table 3.3). The high $T\Delta S$ value for CB[7]:EV[Th]Me could be explained by the combination of the acute molecular angle and dynamic binding with the macrocycle, increasing the overall entropy of system. Additionally, the binding constants K for the EV[X]Me and CB[7] complexes were found to be within 1.7×10^6 M^{-1} to 9.6×10^6 M^{-1}, indicating strong host-guest binding.

Table 3.3 Thermodynamic data of EV[X]Rs binding with CB[7] (T=298 K, 50mM sodium acetate buffer (pH = 4.75)).

	ΔG (kJ mol^{-1})	ΔH (kJ mol^{-1})	$T\Delta S$ (kJ mol^{-1})	K (M^{-1})
EV[Ph]Me	-35.49	-36.86	-1.38	1.65×10^6
EV[Np]Me	-38.45	-31.95	6.50	5.45×10^6
EV[Pyr$_{1,6}$]Me	-39.85	-35.08	4.77	9.59×10^6
EV[Th]Me	-36.73	-16.96	19.77	2.72×10^6
EV[DTh]Me	-36.48	-22.57	13.91	2.47×10^6

3.2.4 Steady-state Photophysical Characterisation of Homoquaternary 2:2 Dimers

Complexation inside the CB[8] cavity affects the local environment of extended viologens, which can in turn alter their optical properties. It has been reported that encapsulation in CB[8] can cause a red shift in the absorption and emission bands, an increase in both PL quantum yields (Φ_{PL}) and fluorescence lifetimes (τ) as well as an increase in the radiative k_{rad} and decrease in the non-radiative k_{nrad} decay rates.[75, 162, 165, 175] For the extended viologen family reported here, we expect the structural differences within this series (increasing the π-surface area, breaking the symmetry of the molecule and inclusion of a heteroatoms in the bridging unit) to augment both complexation with CB[8] as well as their respective electronic transition energies. Steady-state electronic absorption and fluorescence emissions of symmetric extended aryl viologens as well as their photophysical properties are summarised in Table 3.4.

The UV – Vis and emission spectra of extended viologens reveal pronounced conjugation effects upon the addition of extra aromatic groups. Through increasing the conjugation length, an approximate 30 nm red-shift in the maximum absorption and fluorescence emission peak can be observed (see Figures 3.12 to 3.14). Similarly, for higher heteroaromatic conjugation, the red shift in absorption and emission maximum can be observed (Figures 3.17 and 3.18). The change in symmetry of the molecule results in a blue shift in the absorption for EV[Pyr$_{2,7}$]Me, and probably on account of the higher degree of aggregation, no emission could be registered for this molecule in its monomeric state (Figures 3.15 and 3.16).

For all of the EV[X]R studied here, the 1:1 complexes of molecules with CB[8] exhibit bathochromic shifts in absorption and in emission.

The emission spectra of EV[Pyr$_{1,6}$]Me, EV[Pyr$_{2,7}$]Me, EV[Th]Me and EV[DTh]Me mixed with 1 eq of CB[8] are red shifted, broad and structureless.

The emission spectrum observed for EV[Th]Me is characteristic of the formation of an excimer state, where due to a 2:2 complex formation, two thiophene extended viologens are electronically coupled in the excited state. This observation is in agreement with the low PL quantum yield of Φ_{PL}=0.07 observed for this system. Correspondingly, monomeric EV[Th]Me and the non-aggregated 2:1 complexes with CB[7] have high PL quantum yield of 0.62 and 0.67, respectively (see Table 3.4).

The Stokes shift of 128 nm for the EV[Np]Me:CB[8], 233 nm for EV[$Pyr_{2,7}$]Me:CB[8] and 137 nm for the EV[Th]Me:CB[8] complex indicated that the dipole moments of the photoexcited states have been changed significantly and could suggest the formation of a intramolecular charge transfer state.

Bathochromic shifts of absorption spectra for all the CB[8]$_2$·(EV[X]R)$_2$ complexes are indicative of the J-dimer structural orientation for the guest molecules in this supramolecular complex. The broad, structureless red-shifts in emission for those 2:2 complexes could all be a product of the charge transfer transitions, which has been previously suggested by Wasielewski *et al.* and are also characteristic steady state parameters for excimers.[152] At the same time, complexes which contain CB[7] exhibit no shift or show hypsochromic shifts in their absorption or emission spectrum.

The time-correlated single photon counting measurements (TCSPC) of the extended viologen molecules as free guest and in the presence of 1 eq of CB[8] and 2 eq of CB[7] were carried out. These experiments were performed to gain further insight into the possible EV[X]R-EV[X]R interactions as well as their kinetics in the excited state. The extracted lifetime data for EV[X]R and their complexes are compiled in Table 3.4 (for the emission decay profiles see Figures B.87 to B.94).

Following the excitation of EV[Ph]Me at its λ_{em}^{max}, the major emissive component decays with the time constant of 1.5 ns. Upon encapsulation within the CB[8] cavity, long-lived fluorescence was observed with a decay time of 10.9 ns. Interestingly, with the increase of the π surface, longer fluorescence lifetimes can be observed. In light of this, CB[8] complexes with EV[Np]Me, EV[$Pyr_{1,6}$]Me and EV[$Pyr_{2,7}$]Me have a major emissive component decaying with a time constant of almost 17 ns, 19 ns and 24 ns respectively. Such long-lived emission of complexes indicate the existence of a stable excited state. Again, complexes with CB[7] do not exhibit any enhancement of fluorescence lifetime, they are rather similar to the monomeric species. This observation was also confirmed by NMR experiments, in complexation with 2 eq of CB[7] was found to deaggregate the molecule.

The radiative and non-radiative decay constants for EV[X]R molecules and their supramolecular complexes with CB[8] and CB[7] are summarised in Table 3.4. It has been reported that inclusion of dye molecules inside CBs leads to a decrease in k_{nrad} on account of the mechani-

cal protection from quenchers present in solution. [71, 75, 176] The $CB[8]_2 \cdot (EV[X]Me)_2$ complexes (where X= Ph, Np, $Pyr_{1,6}$, DTh), give rise to a notable decrease in both k_{rad} and k_{nrad} (see Table 3.4). The $CB[8]_2 \cdot (EV[CH]Me)_2$ complex shows decrease in radiative and increase in non-radiative decay rates in comparison to free guest (see Table 3.4). The $CB[8]_2 \cdot (EV[Th]Me)_2$ complex has lower radiative but higher non-radiative decay rates in comparison to free guests (see Table 3.4). Such observations for thiophene based molecule could be explained by a high non-radiative decay due to inter-system crossing or internal conversion within this complex. On the other hand the photophysical processes occurring within the 2:2 complex clearly depend on the core structure, molecular geometry and the way the stacking occurs withing the distinct dimeric complex.[5, 167] Values of radiative and non-radiative complexes can give the information about the arrangement of guest molecules within supramolecular complex. The presence of the charged pyridinium units and the extended aromatic cores that can interact provides competition between Coulombic repulsion and π-stacking. This can result in H- or J-type aggregation between the type of molecules in the CB[8]-mediated supramolecular dimers. With the head-to-tail arrangement of molecules due to negative Coulomb coupling one can observe the increase in k_{rad}.[167] In accordance to exciton theory, the values of the radiative decay rate scales as the transition dipole moment squared, meaning that the expected dimer decay rate should be twice that of the monomer (so called superradiance effect). [6] In the case of the head-to-head arrangement an increase in k_{nrad} is observed and the k_{rad} decay is suppressed. This phenomena is highly pronounced in case of EV[Th]Me when complexed with CB[8], which has low radiative but still maintains high non-radiative decay rates. Thiophene based molecules and polymers are known to have a stable triplet state.[177] The complexation of EV[Th]Me and EV[DTh]Me with CB[8] and CB[7] is enhancing the lifetime of a triplet state of the molecule (see Section 3.2.5) probably on account of the protection from the oxygen. However, the increase or stable value of k_{rad} for the EV[Th]Me and EV[DTh]Me 2:1 complexes with CB[7] can suggest that those molecules in their dimeric complex have H-type of aggregation.

To gain more insight into dynamic, static and spectroscopic properties of the EV[X]Me:CB[8] dimeric complexes, molecular dynamics simulations for selected molecules were performed, followed by quantum chemical calculations (See Figures B.124 to B.129 and Table B.2). The obtained optimised geometries suggest a stronger effect of $\pi - \pi$ interactions and a smaller Coulombic repulsion giving rise to final structures that stabilized head-to-head geometries compared with head-to-tail arrangements.

Increases in radiative decays for all EV[X]Me molecules and their complexes with CB[7] follow the literature reports for other encapsulated guests. Such results shows that those guest molecules are in 2:1 host:guest complex, where they are in deaggregated, truly monomeric

state. Inclusion in CB[7] cavities separates them from possible quenchers in the solution, and reduces their k_{nrad} on account of the rigidochromic effect (see Section 1.2.2).

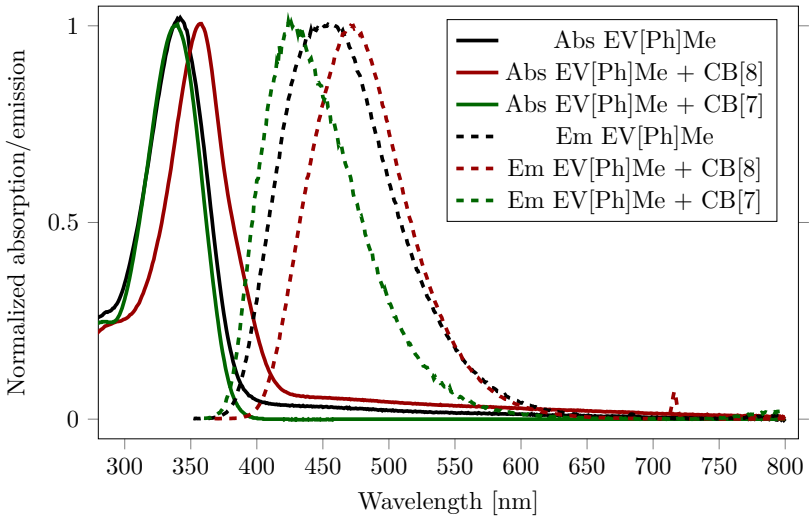

Fig. 3.12 Normalised absorption (solid lines) and emission (dashed lines) spectra of EV[Ph]Me and its complexes with 1 eq of CB[8], 2 eq of CB[7].

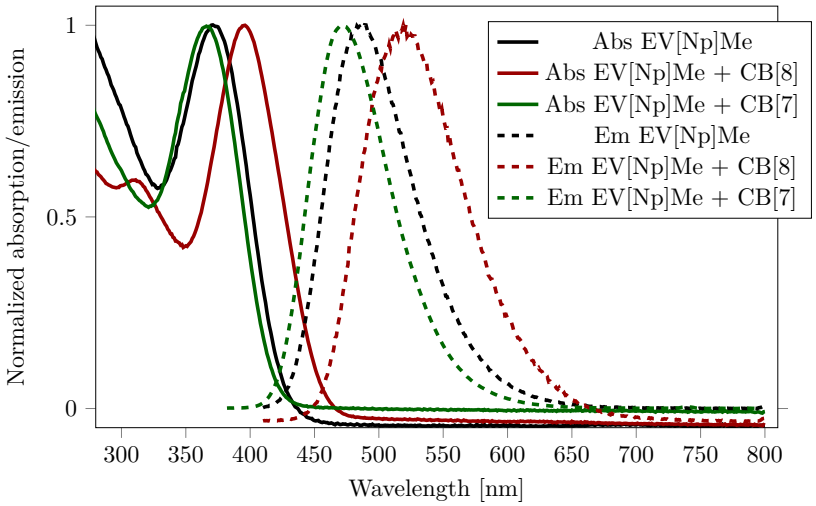

Fig. 3.13 Normalised absorption (solid lines) and emission (dashed lines) spectra of EV[Np]Me and its complexes with 1 eq of CB[8], 2 eq of CB[7].

Table 3.4 Steady-state spectral data of EV[X]Rs in water.

Guest	Host	Host:Guest	λ_{abs}^{max} [nm]	$\varepsilon*$ [$M^{-1}cm^{-1}$]	λ_{em}^{max} [nm]	Stokes shift [nm] ([cm^{-1}])	Φ_{PL}	τ_1 [ns]	τ_2 [ns]	k_{rad} [ns^{-1}]	k_{nrad} [ns^{-1}]
EV[Ph]Me	-	-	343	24400	456	113 (7225)	0.65	1.5	-	4.33	2.33
EV[Ph]Me	CB[8]	1:1	358	37200	472	114 (6747)	0.92	2.5 (23%)	10.9 (77%)	0.84	0.07
EV[Ph]Me	CB[7]	2:1	340	46427	420	80 (5602)	0.93	1.4	-	6.64	0.50
EV[Np]Me	-	-	370	15700	485	115 (6408)	0.68	4.2	-	1.62	0.76
EV[Np]Me	CB[8]	1:1	396	24900	518	122 (5947)	0.58	6.8 (31%)	17.1 (69%)	0.33	0.24
EV[Np]Me	CB[7]	2:1	366	21873	473	107 (6181)	0.89	3.2	-	2.78	0.34
EV[CH]Me	-	-	392	13645	515	123 (6093)	0.65	3.8 (97%)	10 (3%)	1.71	0.92
EV[CH]Me	CB[8]	1:1	428	11616	538	110 (4777)	0.74	3.9 (71%)	15 (29%)	1.89	0.66
EV[CH]Me	CB[7]	2:1	385	17526	509	124 (6327)	0.64	3.1	-	2.06	1.16
EV[$Pyr_{1,6}$]Me	-	-	424	44452	550	126 (5403)	0.20	2.3 (94%)	7.1 (5%)	0.87	3.47
EV[$Pyr_{1,6}$]Me	CB[8]	1:1	456	59466	570	114 (4386)	0.47	18.72	-	0.25	0.28
EV[$Pyr_{1,6}$]Me	CB[7]	2:1	427	82196	542	115 (4969)	0.30	2.1 (94%)	9.5 (6%)	1.43	3.33
EV[$Pyr_{2,7}$]Me	-	-	329	79947	-	-	-	-	-	-	-
EV[$Pyr_{2,7}$]Me	CB[8]	1:1	378	49521	611	233 (10088)	0.03	6.3 (7%)	24.4 (93%)	0.01	0.39
EV[$Pyr_{2,7}$]Me	CB[7]	2:1	338	68130	542	204 (11136)	0.04	5.5 (36%)	19.9 (64%)	0.02	0.48
EV[Th]Me	-		397	51740	453	56 (3114)	0.62	1.3	-	4.77	2.92
EV[Th]Me	CB[8]	1:1	407	77700	544	137 (6187)	0.07	2.7 (82%)	6.7 (18%)	0.26	3.44
EV[Th]Me	CB[7]	2:1	395	38353	456	61 (3386)	0.67	1.4	-	4.79	2.35
EV[DTh]Me	-		455	70713	525	70 (2930)	0.54	1.6	-	3.37	2.87
EV[DTh]Me	CB[8]	1:1	478	72876	552	74 (2805)	0.17	3.2	-	0.53	2.59
EV[DTh]Me	CB[7]	2:1	456	69535	527	71 (2954)	0.64	1.6	-	4.00	2.25

Fluorescence radiative rate estimated by the equation $k_{rad} = \Phi_{PL}/\tau_{S1}$; $k_{nrad} = (1/\tau_{S1})$ - k_{rad}

* For not normalised absorption data see Figures B.117 to B.123.

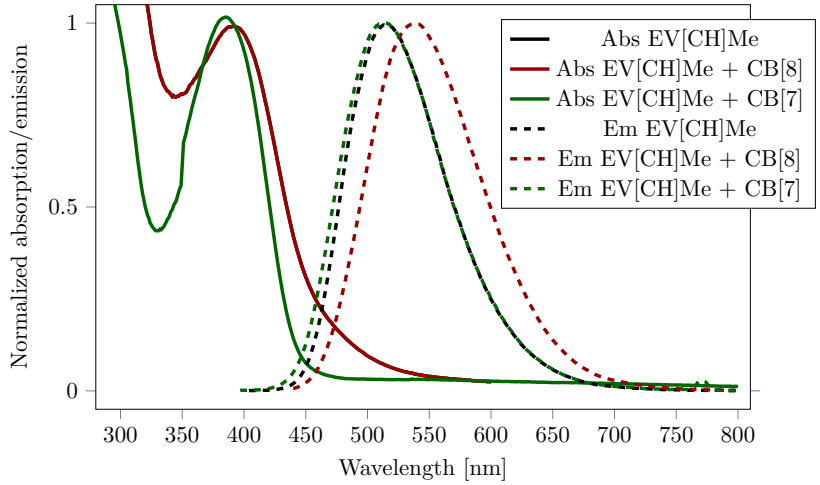

Fig. 3.14 Normalised absorption (solid lines) and emission (dashed lines) spectra of EV[CH]Me and its complexes with 1 eq of CB[8], 2 eq of CB[7].

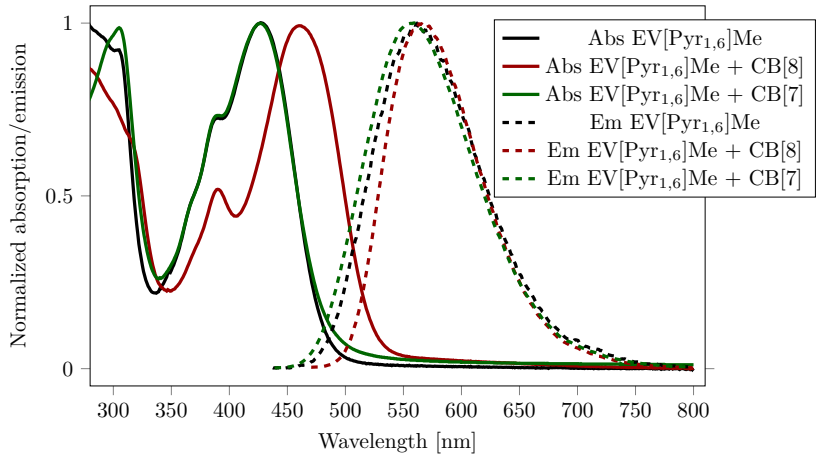

Fig. 3.15 Normalised absorption (solid lines) and emission (dashed lines) spectra of EV[$Pyr_{1,6}$]Me and its complexes with 1 eq of CB[8], 2 eq of CB[7].

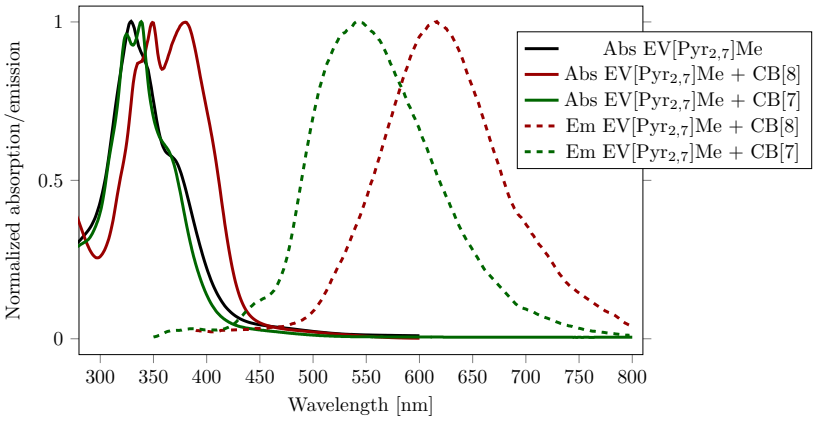

Fig. 3.16 Normalised absorption (solid lines) and emission (dashed lines) spectra of EV[$Pyr_{2,7}$]Me and its complexes with 1 eq of CB[8], 2 eq of CB[7].

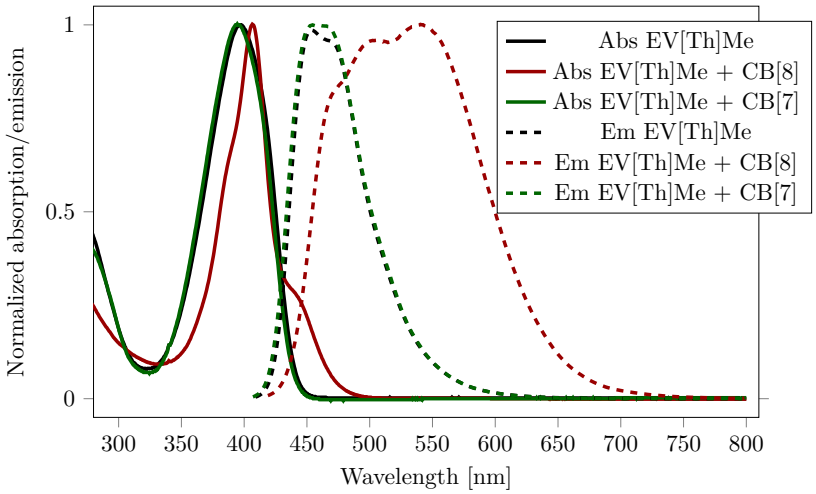

Fig. 3.17 Normalised absorption (solid lines) and emission (dashed lines) spectra of EV[Th]Me and its complexes with 1 eq of CB[8], 2 eq of CB[7].

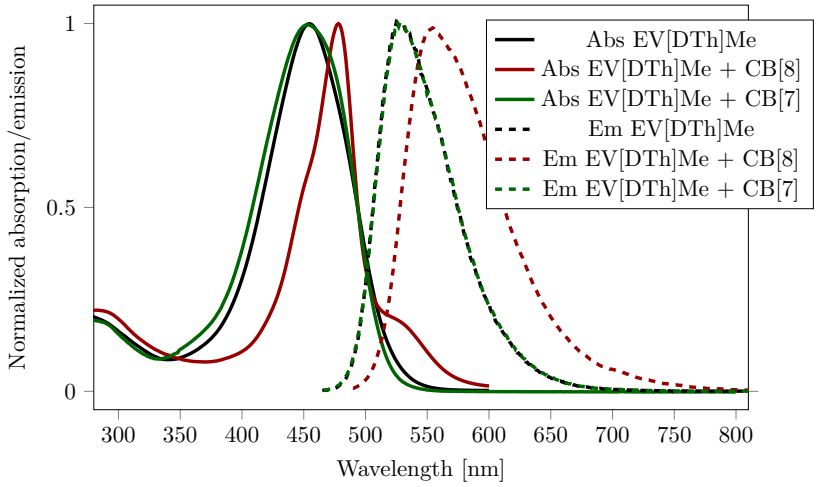

Fig. 3.18 Normalised absorption (solid lines) and emission (dashed lines) spectra of EV[DTh]Me and its complexes with 1 eq of CB[8], 2 eq of CB[7].

3.2.5 Time-resolved Photophysical Characterisation of Homoquaternary 2:2 Dimers

To understand in-depth the dynamics of the excited states of the guests within CB[8], time-resolved absorption measurements in aqueous solutions of the guests molecules and their 2:2 complexes at room temperature were performed.

In transient absorption spectroscopy techniques, a pump-probe experiment, light pulses are used to initiate electronic or vibrational transitions of a system, which are then measured by the probe-pulse in a time resolved manner.[11] Upon the pump-pulse, a molecule undergoes transitions to higher lying states and gives rise to photoinduced absorption bands (PA) that are subsequently followed by transitions to lower lying states identified by the stimulated emission bands (SE).

EV[Ph]Me

EV[Ph]Me in solution was excited with a 355 nm pump-pulse, promoting the compound to the ^{1}*EV[Ph]Me singlet excited state, as indicated from the 639 nm and 1215 nm excited state absorption features, as well as the ground state bleach and stimulated emission features at 380 nm and 440 nm, respectively (see Figure 3.19). Examination of the kinetics of the excited state absorption at short times (femtosecond transient spectroscopy fsTA) at 630 nm reveal an initial rapid (instrument limited) conversion, followed by a bi-exponential decay with time constants τ_1=0.3 ps and τ_2=1.78 ns. The initial τ_1 decay is assigned to a structural relaxation between the aromatic rings, as theorised by Wu *et al.*[152]. The second nanosecond decay is attributed to the return from the singlet excited state to the ground state. Examination of the photophysics at longer times (nanosecond transient spectroscopy nsTA) shows a bi-exponential decay with time constants of τ_1=1.80 $\pm$ 0.05 ns and τ_2=8.45 $\pm$ 2.74 µs. The first time constant τ_1 matches the decay constants for fluorescence measurements. Following the 1.8 ns decay, the small amount of remaining signal can be attributed to an excited triplet state. With the addition of CB[8], the excited state features broaden considerably (Figure 3.20). The NIR excited state absorption feature at 1214 nm remains unchanged, but three absorptive features now exist at 453 nm, 523 nm and 648 nm in the visible region, indicating 2:2 complex formation and its ability to access more higher energy states. Like the monomer, the (EV[Ph]Me)$_2$: CB[8]$_2$ complex undergoes an instrument limited conversion followed by a structural relaxation and a decay to the ground state in 13.9 ps and 2.35 ns, respectively. In the nanosecond spectra for supramolecular dimer, a peak at 630 nm decays tri-exponentially with time constants of τ_1=2.06 $\pm$ 0.13 ns, τ_2=11.10 $\pm$ 0.45 ns and τ_3=11.0 $\pm$ 1.2 µs.

The observation of bi-exponential decay for EV[Ph]Me$_2$:CB[8]$_2$ complex can be explained by its dynamic nature at the instrument timescale. The decay at a similar rate for monomer (ca. 2 ns) can be observed, while the later time corresponds to a dimeric system. At

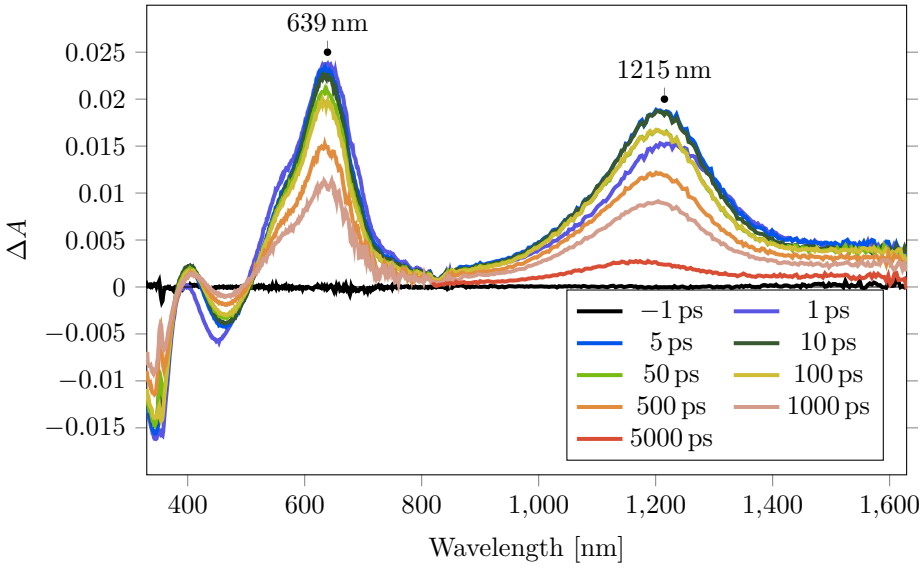

Fig. 3.19 Combined visible and near-infrared femtosecond transient absorption spectra of EV[Ph]Me (λ=355 nm, 600 nJ pulse^{-1}). All measurements were taken in deuterated water.

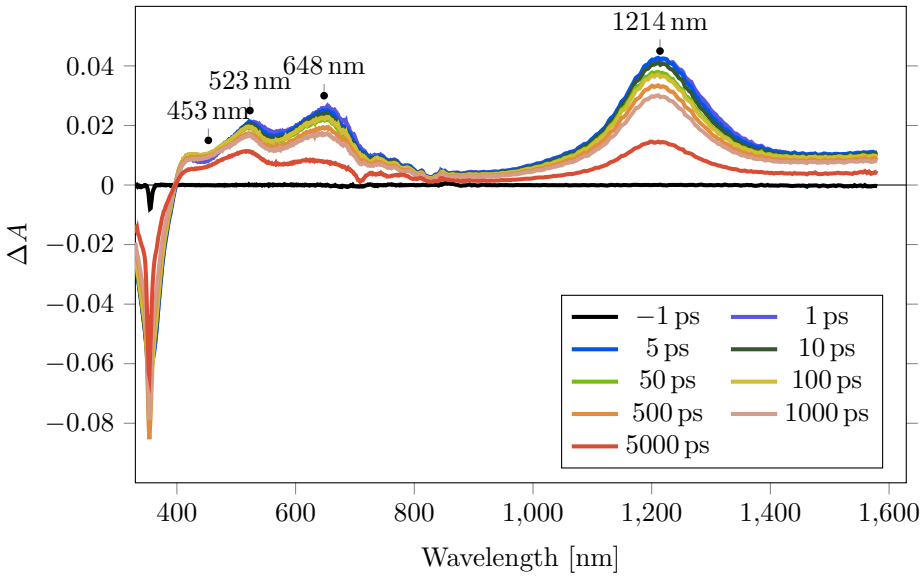

Fig. 3.20 Combined visible and near-infrared femtosecond transient absorption spectra of EV[Ph]Me with 1 eq of CB[8] (λ=355 nm, 600 nJ pulse^{-1}). All measurements were taken in deuterated water.

longer times, EV[Ph]Me_2 : CB[8]$_2$ dimer also exhibits a bi-exponential decay with lifetimes similar to those observed from fluorescence measurements, in addition to a long-lived triplet lifetime. Compared to the τ_2=8.45 ± 2.74 µs lifetime of the triplet in the monomer, the τ_3=11.0 ± 1.2 µs lifetime seen in dimer, along with a higher signal at longer times indicates that CB[8] encourages triplet formation.

EV[Np]Me

EV[Np]Me in solution was excited with a 365 nm pump-pulse, promoting the compound to the ^{1}*EV[Np]Me singlet excited state, as indicated from the 681 nm and 1505 nm excited state absorption features, as well as ground state bleach and stimulated emission features at 380 nm and 431 nm, respectively (Figure 3.21). From the femtosecond transient absorption experiment, the peak at 680 nm decays with a lifetime of τ_1=0.3 ps, τ_2=5.43 ± 0.26 ps, τ_3=555.7 ± 16.2 ps and τ_4=4.42 ± 0.68 ns. The τ_1, τ_2 and τ_3 can be assigned to the fast structural relaxation similarly to the EV[Ph]Me molecules. The τ_4 is a decay for the excited singlet state relaxation, and it is in good agreement with fluorescence lifetime measured by TCSPC (see section 3.2.4). Photo-excitation of the EV[Np]Me:CB[8] 2:2

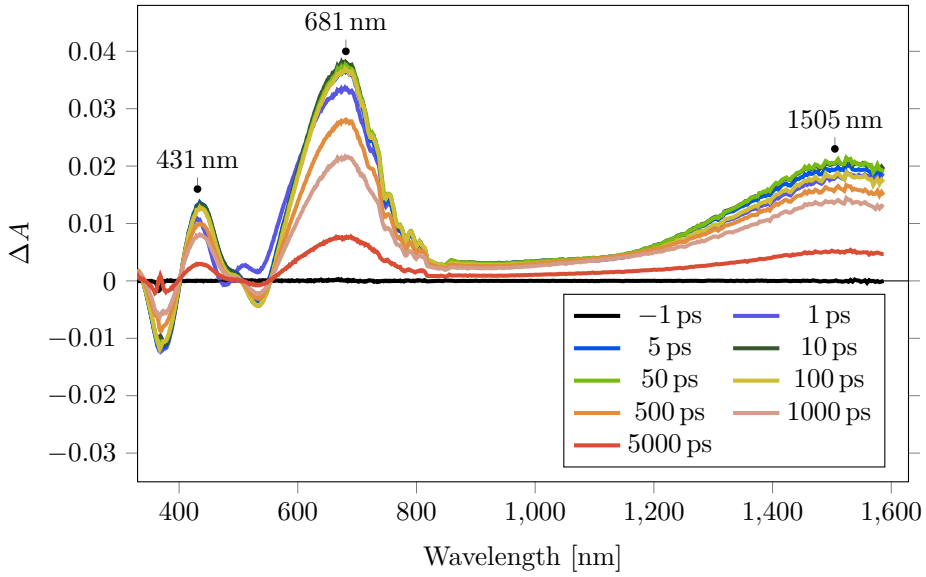

Fig. 3.21 Combined visible and near-infrared femtosecond transient absorption spectra of EV[Np]Me (λ=365 nm, 600 nJ pulse^{-1}). All measurements were taken in deuterated water.

complex produces two absorption peaks at 680 nm and 1500 nm (Figure 3.22). At 680 nm, the femtosecond spectrum contains, a tri-exponential decay with time-constants of τ_1= 0.17 ± 0.01 ps, τ_2=86.5 ± 3.6 ps and τ_3=2.56 ± 0.08 ns. For longer times, this signal decays with τ_1= 4.6 ± 0.7 ns, τ_2=16.5 ± 0.7 ns and τ_3=4.8 ± 0.3 µs. Interestingly, similar absorption features can be observed for the EV[Np]Me:CB[7] 1:2 complex (Figure 3.23). The

nanosecond transient absorption experiment for EV[Np]Me:CB[7] complex, shows features at 691 nm with decay constants τ_1= 3.9 ns and τ_2=9.1 ± 2.2 µs. The multi-exponential decays of the stimulated emissions for CB[7] and CB[8] complexes suggest that there are multiple configurations of EV[Np]Me within the complex. Short decays in a range of picoseconds are characteristic for fast structural relaxations. Results from fsTA and nsTA suggest a significant reorganisation of the molecules within the macrocycle upon photoexciation. This means that the guest molecules have multiple degrees of freedom in these dimeric complexes. However, the geometries of S0 and S1 for free and encapsulated guests are different. In both the monomeric and dimeric samples transition from S0 to S1 state, relaxation from S1 to S0 and then a PA transition to a triplet like state (the single broad PA at 500 nm to 700 nm) can be observed. Similarly, for both the CB[8] based dimer and the monomeric EV[Np]Me, the SE bands show a large blue shift over time. This can be attributed to a relaxation from the Franck-Condon region to S1. In the dimeric species this region is larger and faster, purely because the Franck-Condon region is different.

It is unlikely that any of the EV[Np]Me compounds form excimer in solution with or without CB[8]. Moreover, the spectrum for EV[Np]Me:CB[7]$_2$, a complex that would preclude a dimeric excimer-like structure, exhibits similar features to the monomeric species and the (EV[Np]Me)$_2$:CB[8]$_2$ complex. However, elongation of the triplet state of the EV[Np]Me upon encapsulation in the CB[8] and CB[7] macrocycles is strongly pronounced.

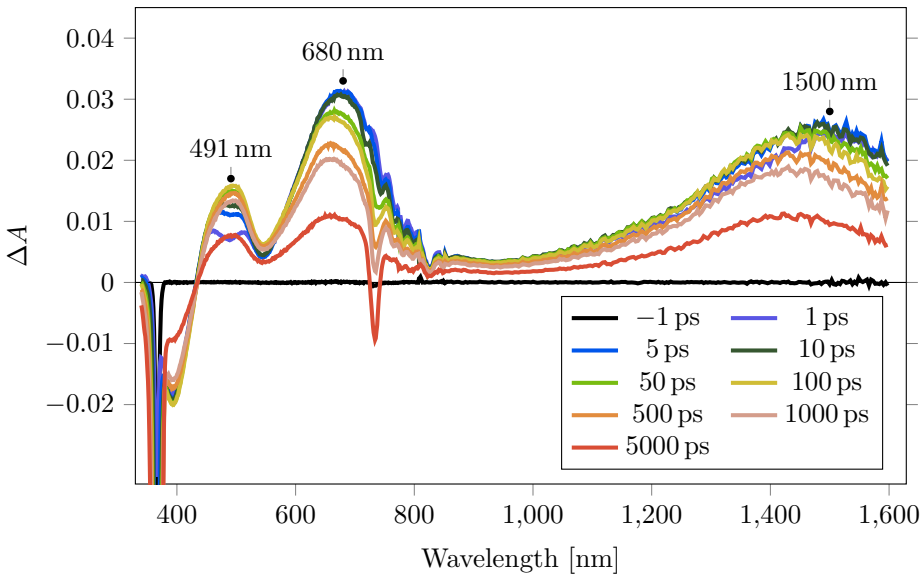

Fig. 3.22 Combined visible and near-infrared femtosecond transient absorption spectra of EV[Np]Me with 1 eq of CB[8] (λ=365 nm, 600 nJ pulse^{-1}). All measurements were taken in deuterated water.

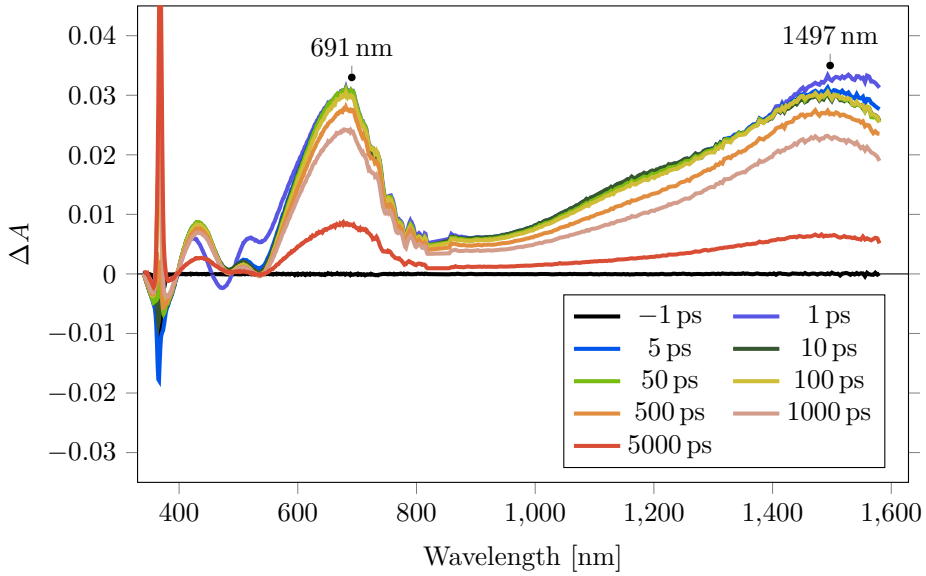

Fig. 3.23 Combined visible and near-infrared femtosecond transient absorption spectra of EV[Np]Me with 2 eq of CB[7] (λ=365 nm, 600 µJ pulse^{-1}). All measurements were taken in deuterated water.

EV[Th]Me

The photo-excitation of EV[Th]Me at 414 nm produced the lowest excited singlet state ^{1}*EV[Th]Me with an absorption peak at 683 nm (Figure 3.24). For the femtosecond TA spectra this absorption decays bi-exponentially with time constants of τ_1=2.40 ps and τ_2=1.24 $\pm$ 0.01 ns. For the nanosecond TA, the spectra demonstrates the long living kinetics of τ_1=1.57 $\pm$ 0.02 ns and τ_2=3.14 $\pm$ 0.57 µs. The maximum absorption for the monomeric EV[Th]Me is at 397 nm, which is also visible as a negative peak in Figure 3.21 as a GSB process (ground state bleaching peak), indicating the transition from S0 to S1. The peak at 465 nm overlaps with the emission spectrum, indicating a simulated emission. The first decay constant is assigned to an internal rotational relaxation of the phenylene group relative to the pyridinium groups, while the relaxed excited single state decays with the nanosecond time constant.[152]

The sample of EV[Th]Me mixed in 1:1 ratio with CB[8], shows three absorption peaks at 476 nm, 637 nm and 1122 nm (Figure 3.25). The peak at 1122 nm *i.e.* in low energy region, can suggest charge transfer complex, a spectral signature of triplet excimer.[178] The dimeric sample has a peak at 637 nm for the femtosecond spectra that decays bi-exponentially with time constants of τ_1=1.10 ps and τ_2=2.34 $\pm$ 0.02 ns. For the nsTA spectra the bi-exponential decay with time constants of τ_1=3.20 ns and τ_2=5.54 $\pm$ 0.06 µs is observed.

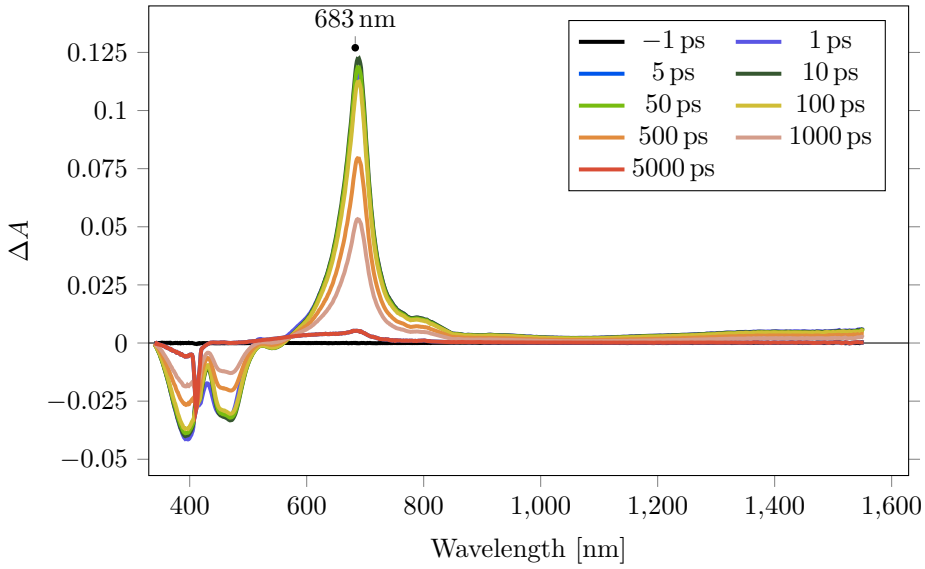

Fig. 3.24 Combined visible and near-infrared femtosecond transient absorption spectra of EV[Th]Me (λ=414 nm, 760 nJ pulse^{-1}). Measurements were taken in deuterated water.

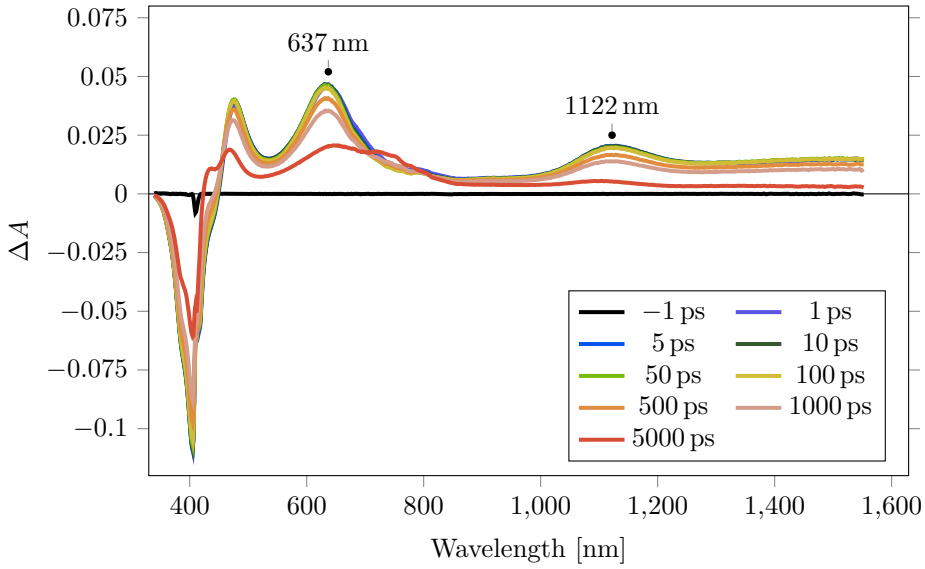

Fig. 3.25 Combined visible and near-infrared femtosecond transient absorption spectra of EV[Th]Me with 1 eq of CB[8] (λ=414 nm, 760 nJ pulse^{-1}). Measurements were taken in deuterated water.

EV[DTh]Me The photo-excitation of the EV[DTh]Me at λ=330 nm resolved in lowest excited singlet state with absorption peaks at λ=683 nm (Figure 3.24). Examination of the kinetics of the excited state absorption at 600 nm revealed an initial rapid (instrument limited) conversion, followed by a bi-exponential decay with time constants τ_1=194.9 $\pm$ 15.5 ps and

τ_2=2.13 ± 0.05 ns. The initial τ_1 decay is assigned to a structural relaxation between the aromatic rings, as theorised by Wu *et al.* [152] The second nanosecond decay is attributed to the return from the singlet excited state to the ground state. Examination of the photophysical features at longer times indicated a bi-exponential decay with time constants of τ_1=2.8 ns, τ_2=7.5 ± 0.1 ns. The nsTA measurements performed in air free conditions showed decay times of τ_1=2.26 ± 0.68 µs and τ_2=66.5 ± 0.6 µs.

Upon addition of CB[8], the excited state features broaden considerably (Figure 3.27). The NIR excited state absorption feature at 1570 nm has substantially increased. Like the monomer, the (EV[DTh]Me)$_2$:CB[8]$_2$ complex undergoes an instrument limited conversion followed by a structural relaxation and a decay to the ground state in 9.94 ps and 4.25 ns, respectively. The spectra obtained for the supramolecular dimer exhibits a peak at 599 nm for the nanosecond spectra which decays bi-exponentially with time constants of τ_1=4.7 ns and τ_2=89.2 ± 1.2 µs. For the nanosecond spectra and in oxygen free conditions, the (EV[DTh]Me)$_2$:CB[8]$_2$ dimer decays bi-exponentially with time constants of τ_1=4.9 ns and τ_2=183.9 ± 2.9 µs.

Signals in NIR TA are often considered to be indicative of excimer-like structures.[152, 178] Here, the presence of a peak at 1570 nm for the dimeric species and small intensities of this peak for the EV[DTh]Me:CB[7]$_2$ sample suggest that the 2:2 CB[8] dimer has the characteristics of a triplet excimer. At fsTA, the EV[DTh]Me:CB[7]$_2$ complex exhibits a decay with time-constant of τ_1=1.34 ns. At longer times, EV[DTh]Me:CB[7]$_2$ exhibits a tri-exponential decay with time-constants τ_1=1.9 ns, τ_2=3.1 µs and τ_3=56.7 µs. When comparing these values to the τ=7.5 µs lifetime of the triplet in the monomer, the τ=89.0 ± 1.2 µs lifetime attributed to the dimer coupled with a higher signals at longer times indicates that CB[8] is driving triplet formation.

In summary, for all time-resolved experiments of selected EV[X]Me with [X]=phenylene, naphthalene, thiophene and dithiophene, it was observed that upon CB[8] or CB[7] encapsulation the lifetime of the triplet state was substantially extended. In particular, for both of the thiophene based compounds, the difference between the monomer and dimeric complex with CB[8] was found to be the highly extended lifetime of the triplet state. For both the EV[Th]Me and EV[DTh]Me systems, with and without CB[8], the fsTA and nsTA data can be fitted to a bi-exponential decay, with a fast component, and a longer components in the nanosecond and microsecond range, respectively. The short time component (<10 ps) is likely due to structural planarization, because the excitation wavelength was found to be of lower energy than the absorption maximum. The ns time component corresponds to decay from the excited singlet state, and the microsecond component corresponds to the triplet

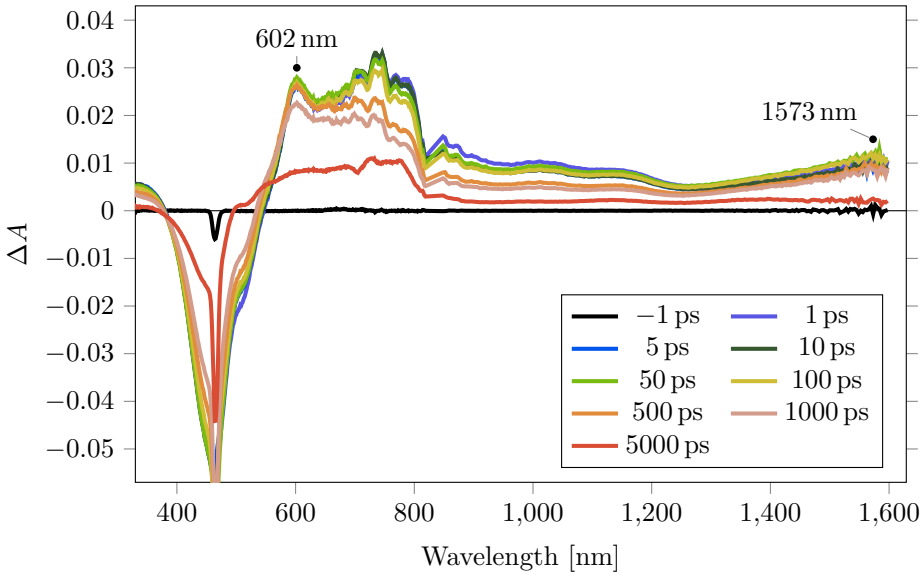

Fig. 3.26 Combined visible and near-infrared femtosecond transient absorption spectra of EV[DTh]Me (λ=465 nm, 760 nJ pulse^{-1}). Measurements were taken in deuterated water.

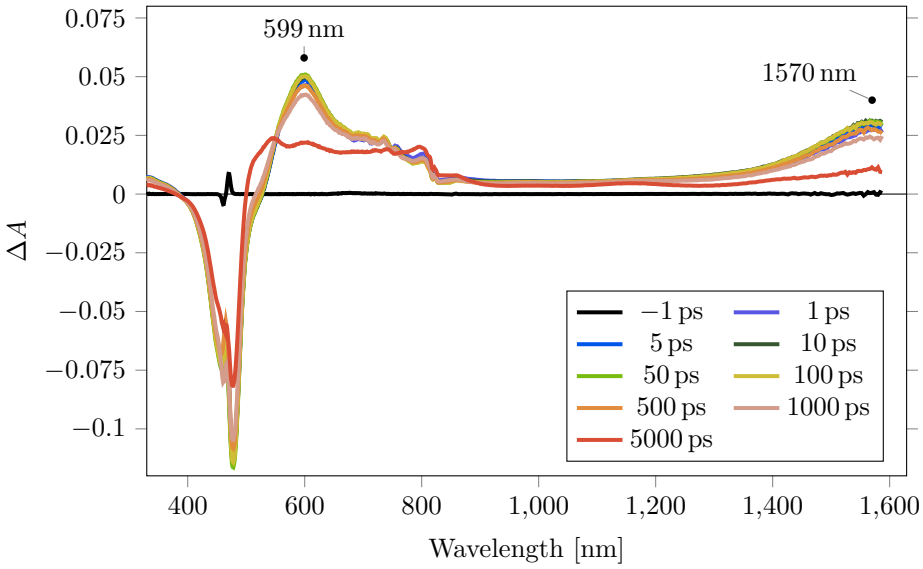

Fig. 3.27 Combined visible and near-infrared femtosecond transient absorption spectra of EV[DTh]Me with 1 eq of CB[8] (λ=465 nm, 760 nJ pulse^{-1}). Measurements were taken in deuterated water.

decay. This is further supported by the fact that the CB[8]:thiophene based systems in air free conditions yield substantially slower decay of the final state, since the absence of oxygen would extend the triplet decay. In addition, the absorption spectrum for the thiophene based

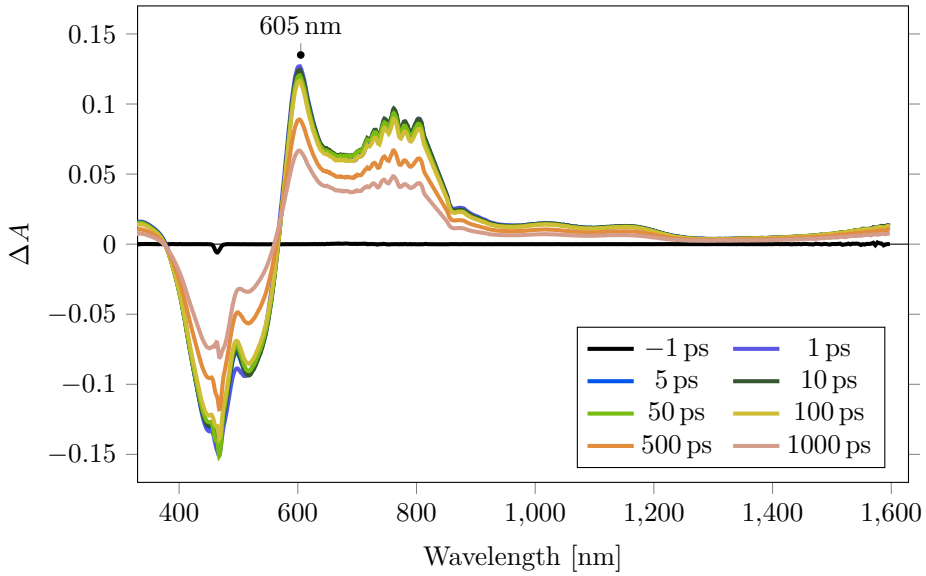

Fig. 3.28 Combined visible and near-infrared femtosecond transient absorption spectra of EV[DTh]Me with 2 eq of CB[7] (λ=465 nm, 760 nJ pulse^{-1}). Measurements were taken in deuterated water.

molecules suggest that dimeric structures of these molecules with CB[8] are triplet excimers, which are stabilised by CT interactions.

For the EV[Np]Me molecule and its supramolecular complexes with CB[8] and CB[7], the TA experiment suggests that the formation of dimeric complexes has access to higher energy levels, but there is no indication of excimer formation. For the EV[Ph]Me molecule, the difference in absorption features between EV[Ph]Me and EV[Ph]Me with CB[8] suggests that this could be a dimeric construct stabilised by CT or resonance making it a singlet excimer-like complex.

3.2.6 Controlled 2:2 Heteroquaternary Dimerisation of Extended Aryl Viologens with CB[8]

Following the previous studies on the homoquaternary complexes with CB[8], the possibility of heteroquaternary complexes formation was examined.

Previous literature examples of pair-selective encapsulation within supramolecular capsules typically have been reported for catalytic reactions including Diels-Alder or 1,3-dipolar cycloadditions.[179–183] Other examples are focused on dye encapsulation and the modulation of fluorophore optical properties with second guest co-encapsulation.[163, 184] Here, the possibility of selective co-encapsulation within CB[8] based 2:2 heteroquaternary complex of EV[Np]R molecules is explored. Since individual monomers of EV[Np]R form

Table 3.5 Thermodynamic data of EV[Np]R binding with CB[8] (T=298 K).

	ΔG (kJ mol^{-1})	ΔH (kJ mol^{-1})	$T\Delta S$ (kJ mol^{-1})	K (M^{-1})
EV[Np]H	-41.49	-56.08	-14.59	1.86×10^7
EV[Np]Me	-42.68	-67.57	-24.73	3.21×10^7
EV[Np]OMe	-42.66	-58.27	-15.61	2.97×10^7
EV[Np]SMe	-43.25	-68.26	-24.99	3.78×10^7
EV[Np]NMe_2	-42.49	-59.04	-16.55	2.77×10^7
EV[Np]NH_2	-40.65	-71.11	-30.47	1.32×10^7

homoquaternanry complexes, the real challenge in this work lies in the control over the statistical mixture, when all the components are combined.

Isothermal Titration Calorimetry

Thermodynamic parameters of binding are indicative of the binding mode, as previously described in both Chapter 1 and in section 3.2.3. ITC measurements for EV[Np]R, where R is an electron donating group, binding with CB[8] are summarised in Table 3.5 (see Chapter B for ITC thermographs). Those results together with the values presented in Table 3.2 have shown that all EV[Np]R molecules and EV[Ph]Me, EV[$Pyr_{1,6}$]Me are characterised by very similar ΔG and K. This observation suggests that those molecules have a similar binding manner to a host molecule and it means that they could form mixed complexes.

Structural Characterisation of Heteroquaternary Complexes

Several factors contribute to the binding between the CB[n] host and guest molecules. One is the desolvation effect of the host cavity and the guest, measured here with ITC. [185] Additionally, based on the results reported previously in this chapter, the electrostatic interactions between two monomers within the complex plays important role in quaternary assembly. Only EV[X]R with electron donating R-groups could form 2:2 complexes with CB[8]. Another factor that is affecting the attraction between the guest and host molecules is their size and shape complementarity. This aspect for the formation of EV[Np]R heteroquaternary complexes with CB[8] is studied with the proton NMR experiments.

^{1}H NMR of 2:2 homoquaternary complexes of EV[Np]NMe_2 and EV[Np]Me with CB[8], as well as a mix of EV[Np]NMe_2, EV[Np]Me molecules with CB[8] in 2:1:1 host:$guest_1$:$guest_2$ ratio are depicted in Figure 3.29. Splitting of peaks corresponding to the methine protons located at the CB[8] portals can be observed. This splitting is indicative of an asymmetric environment around CB[8] and based on previous experiments, can be con-

sidered to be a 2:2 complexes. The observed shifts of macrocycle protons and integration of the spectrum, confirms the 2:1:1 host:guest$_1$:guest$_2$ complex. The methyl signals of the pair-encapsulated EV[Np]NMe$_2$ and EV[Np]Me were desymmetrised and their shift of 0.04 ppm and 0.07 ppm, respectively, were observed. This EV[Np]NMe$_2$:EV[Np]Me:CB[8]$_2$ heteroquaternary complex is formed within a 88% yield.

^{1}H NMR of 2:2 homoquaternary complexes of EV[Np]NMe$_2$ and EV[Np]OMe with CB[8] as well as a mix of EV[Np]NMe$_2$, EV[Np]OMe molecules with CB[8] in 2:1:1 ratio are depicted in Figure 3.30. Similarly to the previous pair-mixed example, the CB[8] rim proton peak splitting can be observed, suggesting the formation of a 2:2 complex. The proton NMR spectrum for the pair-encapsulated EV[Np]NMe$_2$ and EV[Np]OMe shows that for both guests' methyl signals are shifted by 0.03 ppm. Based on the peaks integration and shifted signals of the guests the EV[Np]NMe$_2$:EV[Np]OMe:CB[8] heteroquaternary complex is formed with 80% yield.

^{1}H NMR of 2:2 homoquaternary complexes of EV[Np]NMe$_2$ and EV[Np]H with CB[8], as well as a mix of EV[Np]NMe$_2$, EV[Np]H molecules with CB[8] in 2:1:1 host:guest$_1$:guest$_2$ ratio are depicted in Figure 3.31. Proton NMR experiments for the EV[Np]NMe$_2$:EV[Np]H:CB[8]$_2$ mix reveals tight encapsulation of guest molecules in the cavity of the macrocycle. Characteristic methyl signals of the EV[Np]NMe$_2$ guest showed shifts of 0.07 ppm upon co-encapsulation with EV[Np]H. Peak integration for this heteroquaternary complex indicates 97% yield.

^{1}H NMR of 2:2 homoquaternary complexes of EV[Np]OMe and EV[Np]H with CB[8] as well as a mix of EV[Np]OMe, EV[Np]H molecules with CB[8] in 2:1:1 host:guest$_1$:guest$_2$ ratio are depicted in Figure 3.32. For this system the heteroquaternary complex is formed with 55% yield.

NMR experiments suggest that the heteroquaternary EV[Np]R:EV[Np]R':CB[8]$_2$ with the highest yield of 97% was achieved for the molecules with the bulkiest (R=NMe$_2$) and the smallest (R'=H) functional group. By mixing other molecules such as EV[Np]Me or EV[Np]OMe together with EV[Np]NMe$_2$ the purity of corresponding heteroquaternary complexes were obtained with 80-88% yield. In contrast, the pair-mixed complex for guest with both small functional group like EV[Np]OMe and EV[Np]H, showed only 55% hetero-complex purity. Those results suggest that EV[Np]NMe$_2$ on account of the steric effect of bulkier functional group could have higher energy barrier for the 2:2 complex formation. Thus, the formation of a co-encapsulated heteroquaternary complex with a guest of similar attraction to the macrocycles and with smaller functional group occurs with higher yield. This is confirmed with the experiment for mixing of EV[Np]Rs with R=OMe and R=H. The

results of NMR experiments suggest that size matching is the most crucial for EV[Np]R pair-encapsulation within the CB[8] macrocycle.

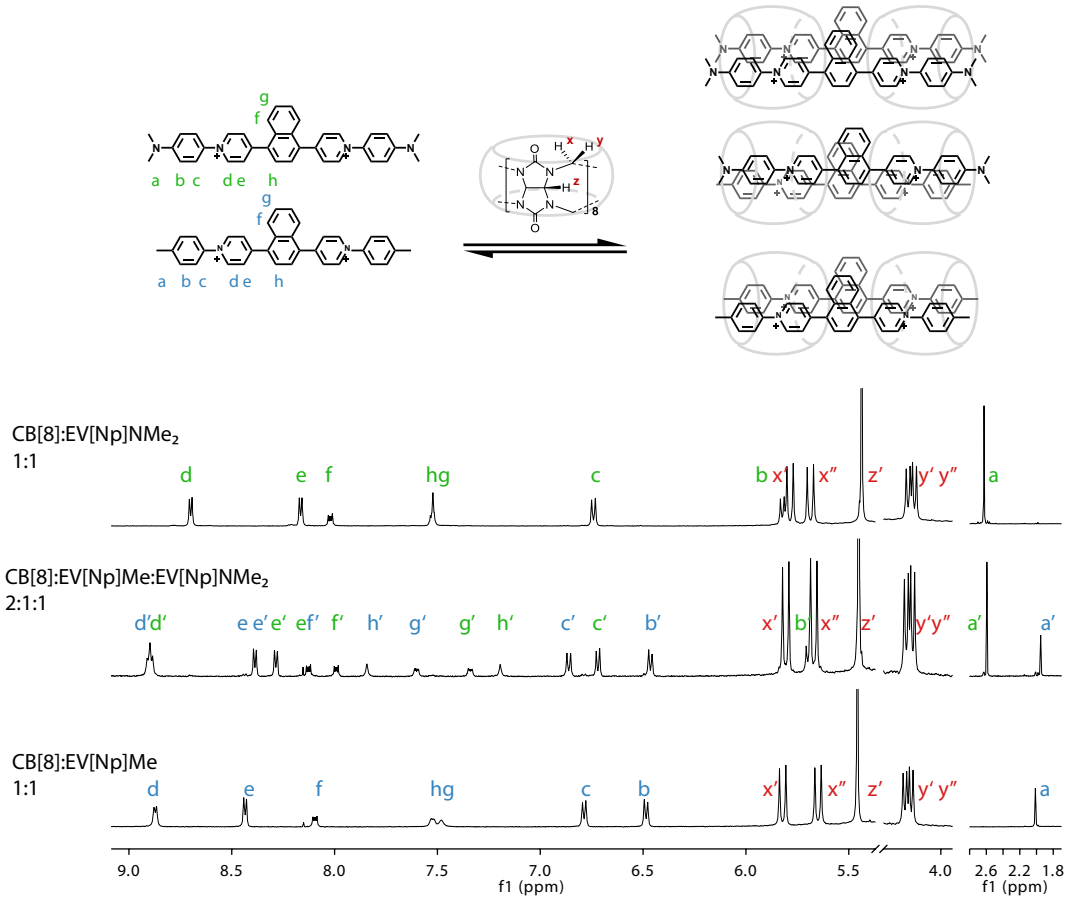

Fig. 3.29 ^{1}H NMR of EV[Np]NMe$_2$ and EV[Np]Me mixed in 2:1:1 ratio with CB[8]. Measurements performed in D_2O with Cl^- as counterions.

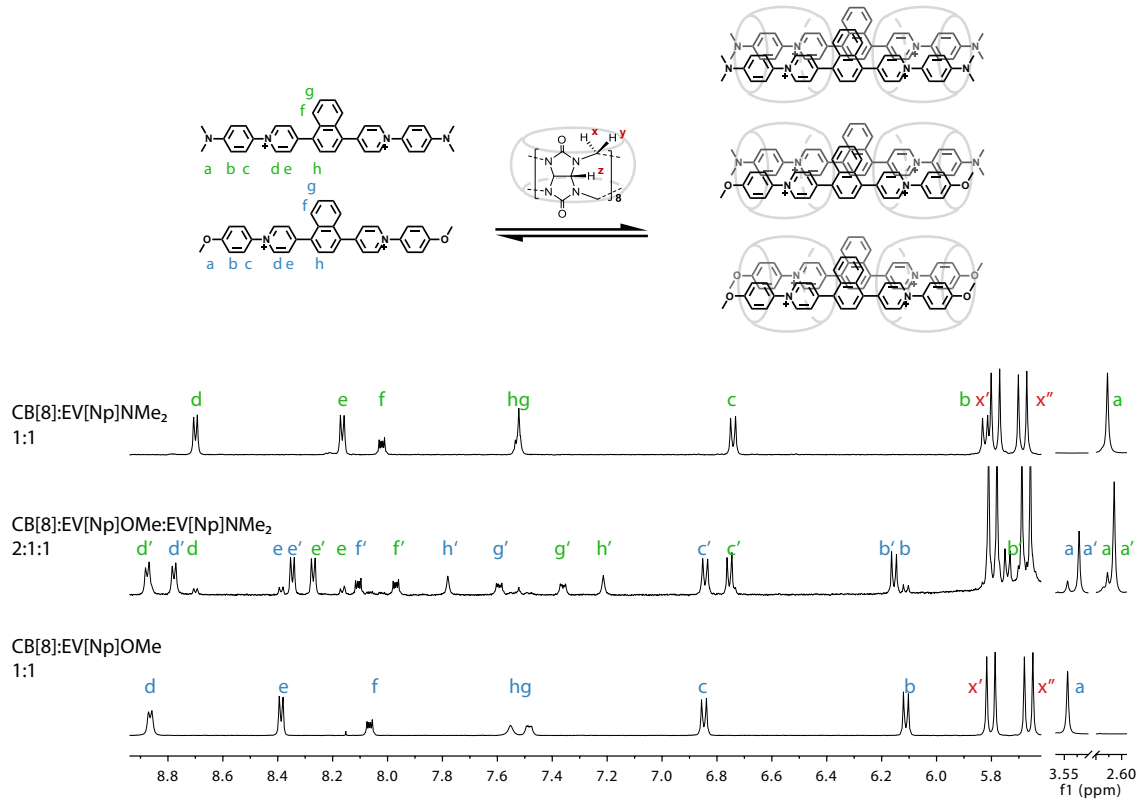

Fig. 3.30 ^{1}H NMR of EV[Np]NMe$_2$ and EV[Np]OMe mixed in 2:1:1 ratio with CB[8]. Measurements performed in D_2O with Cl^- as counterions

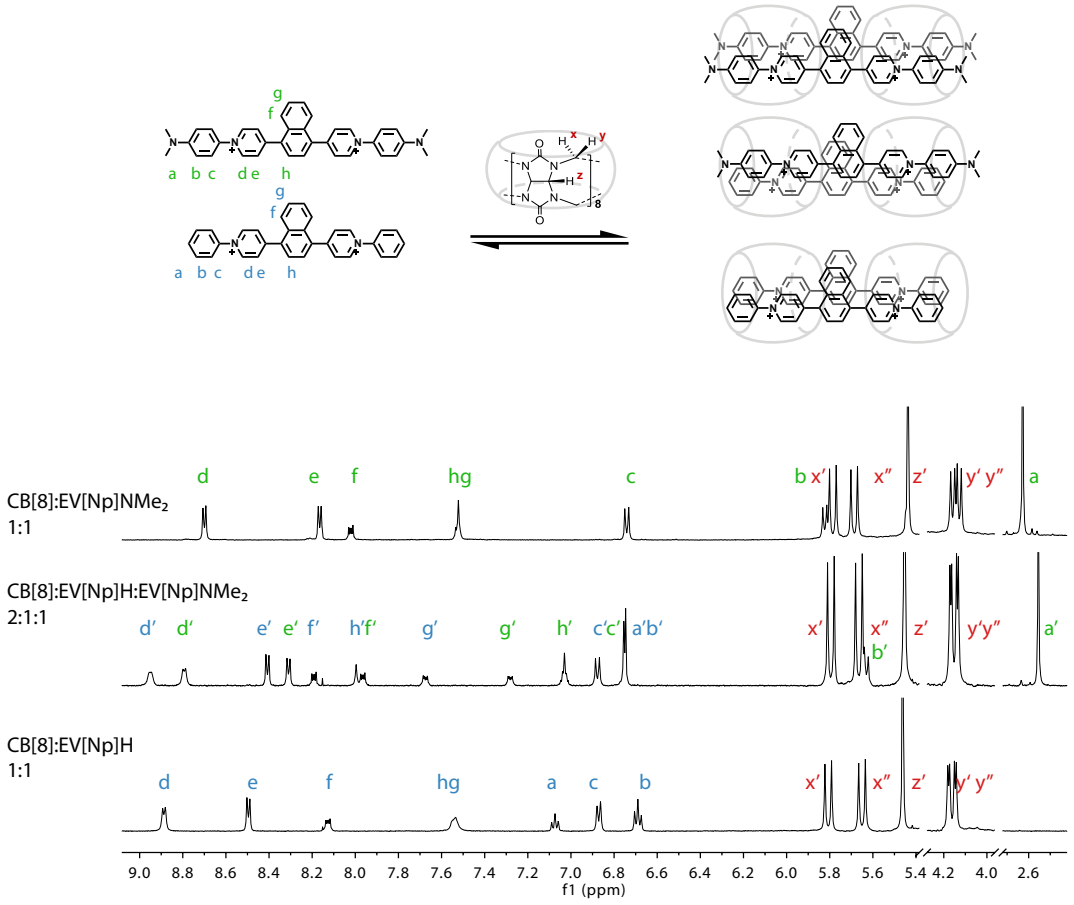

Fig. 3.31 ^{1}H NMR of EV[Np]NMe$_2$ and EV[Np]H mixed in 2:1:1 ratio with CB[8]. Measurements performed in D_2O with Cl^- as counterions

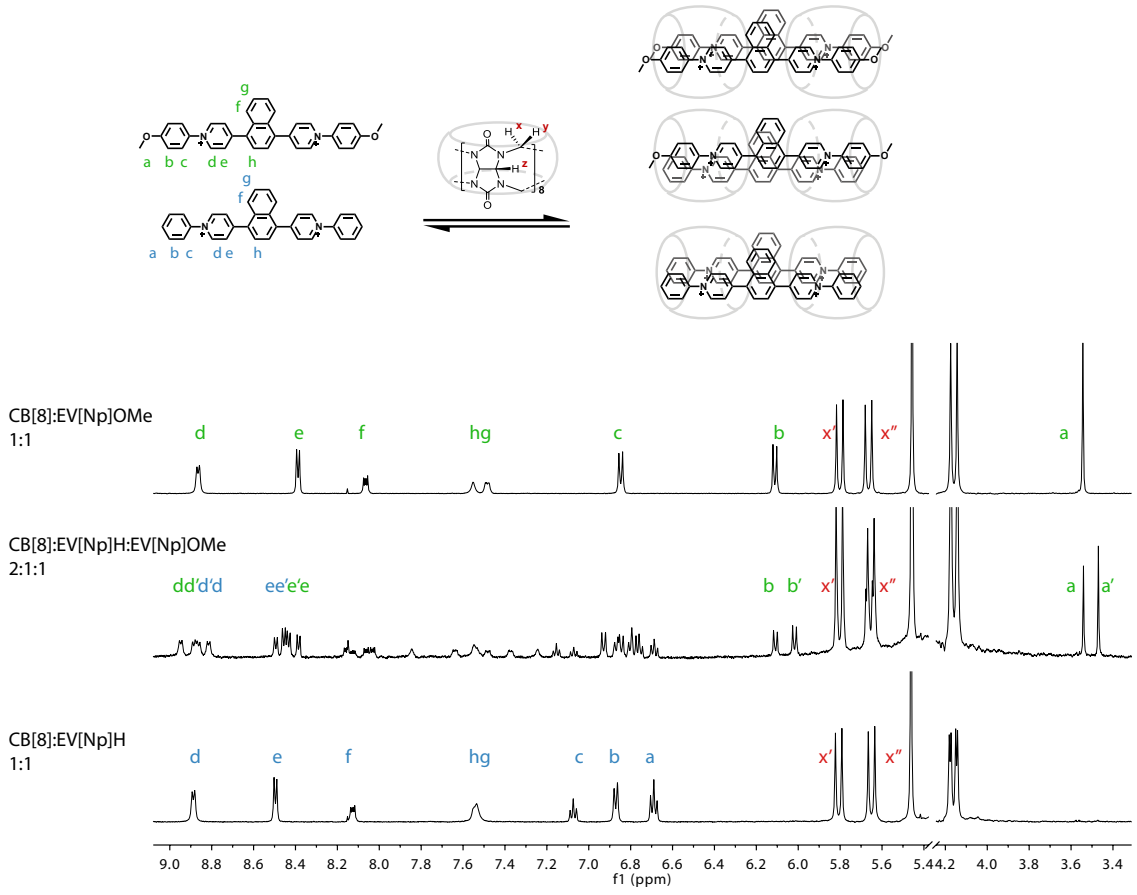

Fig. 3.32 ^{1}H NMR of EV[Np]OMe and EV[Np]H mixed in 2:1:1 ratio with CB[8]. Measurements performed in D_2O with Cl^- as counterions

Steady State Spectroscopic Characterisation

Finally, the effect on optical properties of molecules upon mixed pair-encapsulation within CB[8] macrocycles was studied. The UV – Vis spectroscopy for previously calibrated NMR samples of 2:2 homo- and heteroquaternary complexes were performed. Upon formation of quaternary mixed complexes, the colour of the solution did not change drastically. However, the UV – Vis for mixed complexes showed changes in their spectrum, that were not only simple overlaps of absorption features of homoquaternary complexes.

The aqueous solution of the 2:2 complex of CB[8] and the EV[Np]NMe_2 has an absorption maximum at 492 nm. The absorption maximum for 2:2 complex of CB[8] with EV[Np]Me is present at 395 nm. When 1 eq of EV[Np]NMe_2 is mixed with 1 eq of EV[Np]Me, according to NMR experiments a heteroquaternanry complex was formed with 88% yield. This complex has a broad absorption band around 501 nm, which is red shifted by around 10 nm when compared to the absorption maxium of the homoquaternary EV[Np]NMe_2 complex (Figure 3.33). There is also a 14 nm blue shift of the absorption band when compared to that of the homoquaternary EV[Np]Me complex.

The 2:2 heteroquaternary complex of EV[Np]NMe_2 mixed with EV[Np]OMe exhibits 11 nm blue shift of the absorption band from 493 nm (the λ_{abs}^{max} for homoquaternanry complex of EV[Np]NMe_2) to 484 nm (see Figure 3.34). One can also observe the red shift of absorption peak from 384 nm (the λ_{abs}^{max} for homoquaternanry complex of EV[Np]OMe) to 398 nm.

The UV – Vis spectrum of 2:1:1 ratio mixture of CB[8], EV[Np]NMe_2 and EV[Np]H, which from the proton NMR experiment has the highest exchange ratio of 97%, is shown in Figure 3.35. Interestingly, the absorption peak at 493 nm observed for homoguaternary complex of EV[Np]NMe_2 with CB[8], upon mixing with the homoquaternary complex of EV[Np]H with CB[8], is significantly broadened and no shifts can be observed. On the other hand the absorption maximum peak at 396 nm observed previously for 2:2 complex of EV[Np]H with CB[8], upon formation of the heteroquaternary complex, is ca. 10 nm blue shifted.

From these UV – Vis experiments no simple overlap of absorption spectra was observed. This suggests that the exchange of guests within CB[8] cavity has occurred. Both the small changes in spectra and little colour changes most probably stem from the lack of high diversity of the R groups in these EV[Np]R molecules. However, the principle of fine-tuning of optical properties of extended aryl viologen based dyes upon pairwise encapsulation within CB[8] macrocycle has been demonstrated through these experiments.

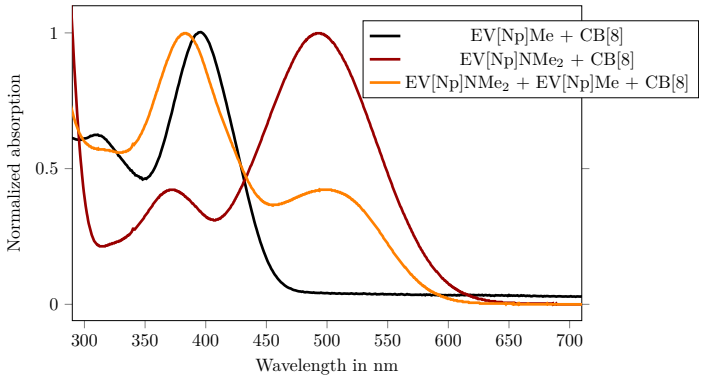

Fig. 3.33 Normalised absorption spectra of CB[8], EV[Np]NMe_2 and EV[Np]Me mixed in 2:1:1 ratio.

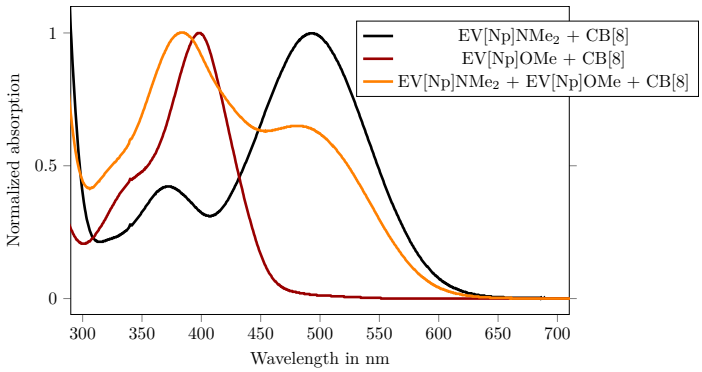

Fig. 3.34 Normalised absorption spectra of CB[8], EV[Np]NMe_2 and EV[Np]OMe mixed in 2:1:1 ratio.

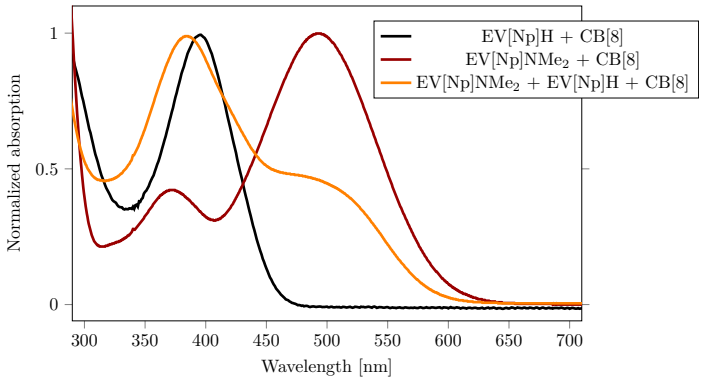

Fig. 3.35 Normalised absorption spectra of CB[8], EV[Np]NMe_2 and EV[Np]H mixed in 2:1:1 ratio.

3.2.7 Conclusions

This chapter has illustrated the design and synthesis of a new family of extended aryl viologens (EV[X]R). These new viologen derivatives consist of both molecular recognition units (R functionalised phenyl moieties) and optically tunable π-bridging units ([X]) between charged pyridiniums. It was shown that in aqueous solution EV[X]Rs with R of electron donating character readily undergo self-assembly with CB[8] macrocycles in a 2:2 manner forming dimeric complexes in which the two chromophores are stacked and locked into place. Thus, the results presented in this chapter suggest that the appropriate charge stabilisation and rigid functionalisation on pyridines of EV[X]R are critical in achieving a 2:2 complex formation. Moreover, the size of the aromatic core has an effect on the binding type. Smaller cores such as Ph can interact with CB[8] and lead to more dynamic host-guest complexes. On the other hand, bridging units with higher aromatic conjugation were found to stabilise the complex on account of their bulkier cores. The binding properties of these family of molecules towards CB[8] were assessed through ^{1}H NMR and ITC measurements.

Subsequently, the effect of encapsulation on EV[X]R spectroscopic properties was investigated. Steady-state spectroscopy, PL quantum yield, fluorescence lifetime measurements along with time-resolved spectroscopy were used to characterise the EV[X]R molecules as well as their corresponding complexes with the CB[7] and CB[8] macrocycles. The proximity of the stacked EV[X]Rs in CB[8] complexes results in an excimer-like excited state exhibiting red-shifted absorption and emission with elongated lifetime and substantial quantum yield change. Moreover, the optical properties of resultant dimeric complexes were found to be [X] unit dependent. Thus, by 'plugging in' different bridging units, it was possible to generate luminescence in a wide spectral range. Here, the new family of dyes based on EV[X]R molecules exhibited excitation wavelengths ranging from 343 nm up to 478 nm and emission wavelengths in the range of 420 nm to 611 nm. Upon mixing with CB[8], a difference of at least 20 nm in excitation wavelength was observed when compared to the monomeric species of the dimeric complex.

To gain more insight into the dynamics of the excited states of the homoquaternary complexes, transient absorption spectroscopy was performed for the selected EV[Ph]Me, EV[Np]Me, EV[Th]Me and EV[DTh]Me systems, as well as their supramolecular complexes with CB[8] and CB[7]. The nsTA experiments showed the effect of the CB[8] and CB[7] macrocycles on the formation and the lifetime of the triplet states. The thiophene CB[8] based complex exhibited a triplet state with a time constant of up to 184 µs in air free conditions. Moreover, the classical signatures of excimer-like structures were identified for the EV[Th]Me and EV[DTh]Me 2:2 complexes with CB[8]. These composites were found to form triplet state excimers which are stabilised by a CT interaction.

The EV[Ph]Me molecules, upon mixing with CB[8], were considered to form a singlet excimer and based on its transient absorption spectrum features was thought to be stabilised by a combination of CT and excition resonance. However, explicit evidence could not be obtained to ratify this hypothesis.

In the final part of Chapter 3, the pair-selective encapsulation of different substituted extended aryl viologens inside the CB[8] cavity was explored. Here, the CB[8] macrocycle was used as a supramolecular fastening for EV[Np]R and EV[Np]R' guests. The aspect of having control over the statistical mixture based on size complementarity was achieved for complexes involving the EV[Np]NMe_2 and EV[Np]H guests. The studies on modulation of the absorption properties of the formed mixed complexes were presented.

The evolution of homo- and heteroquaternary complexes is crucial for the fine-tuning of the optical properties of these emissive complexes. Having the ability to control the formation of the dimeric species provides the opportunity to study more detailed systems that exhibit excimer-like features or even singlet fission properties, which are important for the development of future functional materials. Moreover, on account of the interesting optical properties and high binding affinity of EV[X]Rs to CB[8] this system can be used in imaging applications.[161]

3.3 Experimental

3.3.1 Instrumentation and Materials

Materials

All the materials as following were purchased from commercial suppliers and used without further purification: Pyridin-4-ylboronic acid (97%, Fisher Scientific), 1,6-Dibromopyrene (95%, Fluorochem), 1,4-Dibromonaphthalene (>98%, Acros Organics), 1,4-Dibromobenzene, Tetrakis(triphenylphosphine)palladium(0) (99.8% (metals basis), Pd 9% min, Alfa Aesar), aniline (>99.5 %, Sigma-Aldrich), p-Toluidine (>99 %, Alfa Aesar), p-Anisidine (>99 %, Sigma-Aldrich), 4-(Methylthio)aniline (>98 %, Alfa Aesar), p-Phenylenediamine (>97 %, Alfa Aesar), N,N-Dimethyl-p-phenylenedia9mine (>97 %, Sigma-Aldrich), 4-(Trifluoromethyl) aniline (99 %, Sigma-Aldrich), 4-Bromoaniline (97 %, Sigma-Aldrich), 1-adamantanamine hydrochloride (>97%, Sigma), ethanol (absolute, Fisher Scientific), acetonitrile (REAG. PH EUR, Merck Millipore) and diethyl ether (>99%, Aldrich). Cucurbit[8]uril (CB[8]) was synthesized according to the published procedure.[43]

Nuclear Magnetic Resonance Spectroscopy

^{1}H NMR spectra were acquired in heavy water (D_2O) at 298 K, and recorded on a Bruker AVANCE 500 with TCI Cryoprobe Spectrometer (500 MHz) being controlled by TopSpin2. ^{13}C NMR (126 MHz) spectra were acquired in heavy water (D_2O), and recorded on a Bruker AVANCE III QNP Cryoprobe with external reference TMS set to 0 ppm. Titrations were performed by using stock solutionsof host and guest calibrated against the concentrated solution of 3-(Trimethylsilyl)-1-propanesulfonic acid sodium salt. Chemical Shifts are recorded in ppm (δ) in D_2O (internal reference set to δ 4.79 ppm). All spectra were recored at 298 K.

Isothermal Titration Calorimetry (ITC)

All ITC experiments were carried out on a Microcal ITC200 at 298.15 K in 50 mM sodium acetate buffer (pH = 4.75). In a typical ITC, the host molecule (CB[8]) was in the sample cell, and guest molecule was in the injection syringe with a concentration of about ten times concentration of host. The concentration of CB[8] was calibrated by the titration with a standard solution of 1-adamantanamine. All raw data (thermograms) of ITC were integrated by NITPIC (v.1.2.0), fitted in Sedphat (v.12.1b), and visualized through GUSSI (v.1.1.0). The resulted thermograms show the integrated heats of injections, with the error bars representing estimated errors for these values according to [157].

UV – Vis Spectroscopy

UV – Vis spectra were recorded on a Varian Cary 400 UV – Vis spectrophotometer using a Suprasil Quartz (QS) cuvette with 1 cm path length at 298 K. EV[X]R, EV[X]R:CB[8] and EV[X]R:CB[7] aqueous solutions were tested in the concentration of 0.01 mM.

Fluorescence Spectroscopy

Fluorescence spectroscopy was recorded on an Agilent Cary Eclipse fluorescence spectrophotometer using a Suprasil Quartz (QS) cuvette with 1 cm path length at 298 K.

Time-Correlated Single Photon Counting

Time-resolved fluorescence was recorded using a FS5 Spectrofluorometer, Edinburgh Instrument. A TCSPC laser (360 nm) was used for fluorescence lifetime measurements at peak emission wavelength for measured molecules and complexes. A Suprasil Quartz (QS) cuvette

with 1 cm path length was used for all measurements. The data was fit with the exponential reconvolution function and the non-linear least square method.

Fluorescence Quantum Yield Measurements

The absolute fluorescence quantum yield was determined using an Edinburgh Instruments Integrating Sphere Module (SC-30) on a spectrofluorometer. The fluorescence spectra analysis software Fluoracle and Quantum Yield Wizard were used to obtain quantum yields. For fluorescence quantum yield measurements the optical density for all EV[X]R, EV[X]R:CB[8] or EV[X]R:CB[7] aqueous solutions was in a range of 0.1 to 0.06.

Transient Absorption Spectroscopy

Femtosecond and Nanosecond Transient UV/VIS/NIR Absorption (fsTA/nsTA) spectroscopy was done using probe: 330 nm to 1600 nm, with 50 fs-400 ms window. This laser system is based on a regeneratively amplified Ti:sapphire laser system (Spitfire, Spectra-Physics; output: 828 nm, 1 W, 1 kHz, 110 fs) that drives a non-collinear optical parametric amplifier (TOPAS-White, Light-Conversion, LLC; output: 250 nm to 1000 nm, 20 fs), and a laboratory-constructed collinear narrow-band optical parametric amplifier (output: 480 nm to 800 nm, 150 fs) to generate excitation (pump) pulses. The probe was generated within a non-linear crystal inside a customised spectrometer (Helios, Ultrafast Systems, LLC) to probe the first 8 ns of the dynamics. Longer time-window measurements were performed using a digitally delayed supercontinuum probe (EOS, Ultrafast Systems, LLC) with a resolution of 600 ps, giving a seamless measurement of the dynamics from the femtosecond to microsecond windows. The kinetic analysis was based a global fit to selected single-wavelength kinetics. For the TA measurements the optical density of all EV[X]R, EV[X]R:CB[8] and EV[X]R:CB[7] samples was in a range of 0.4-0.6.

High Pressure Liquid Chromatography (HPLC) HPLC was performed on Varian HPLC - Agilent using a Phenomenex C18 Kinetic-Evo column with a 5 μm pore size, a 110 particle size and with the dimensions 150 x 21.2 mm. A gradient from 5% acetonitrile 95% water (with 0.1% TFA) to 100% acetonitrile was run.

HPLC-LCMS HPLC-LCMS was performed on Waters ZQ with Waters 2795, with 50 x 4.6 mm C18 column (Phenomenex Kinetix solid core column), using acetonitryle:water (1:1) as a mobile phase.

3.3.2 Synthetic Protocols

EV[Ph], EV[Np], EV[$Pyr_{1,6}$], EV[$Pyr_{2,7}$], EV[CH], EV[Th] and EV[DTh] were synthesised with the procedure described in Chapter 2. The symmetric Zinke salt for all EV[X]R was prepared using general procedure described below.

4,4'-(1,4-Phenylene)bis(1-(2,4-dinitrophenyl)pyridin-1-ium) - EV[Ph]DNB

The substrates 1,4-di(pyridin-4-yl)benzene (1 g, 4.3 mmol) and 1-chloro-2,4-dinitrobenzene (12.91 g, 2.6 mmol) were refluxed for 72 h in ethanol. After that, the reaction mixture was cooled down to room temperature and concentrated. The residue was precipitated with diethyl ether and dried. The precipitate was purify via reverse-phase HPLC with eluent gradient of H_2O/MeCN 0.1 % TFA. Collected fractions were concentrated in vacuum, dissolved in 2 mM aqueous HCl and then lyophilized. Pure yellow solid in 65 % yield was obtained. **^{1}H NMR** (500 MHz, D_2O) δ (ppm): 9.33 (d, J = 2.5 Hz, 2H), 9.15 – 9.08 (m, 4H), 8.87 (dd, J = 8.8 Hz and 2.5 Hz, 2H), 8.67 – 8.60 (m, 4H), 8.29 (s, 4H), 8.21 (d, J = 8.7 Hz, 2H). **^{13}C NMR** (125 MHz, D_2O) δ (ppm): 158.28, 149.58, 145.28, 143.03, 138.50, 137.28, 131.17, 130.56, 129.76, 125.58, 122.69 **MS** ESI-MS: *m/z* [M]2+ calc for $C_{28}H_{18}N_6O_8$: 283.0588, found: 283.0581

4,4'-(Naphthalene-1,4-diyl)bis(1-(2,4-dinitrophenyl)pyridin-1-ium) - EV[Np]DNB

^{1}H NMR (500 MHz, D_2O) δ (ppm): 9.34 (d, J = 2.5 Hz, 2H), 9.20 (dd, J = 5.0 Hz and 1.8 Hz, 4H), 8.88 (dd, J = 8.6 Hz and 2.5 Hz, 2H), 8.53 (dd, J = 5.1 Hz and 1.9 Hz, 4H), 8.25 (d, J = 8.7 Hz, 2H), 8.06 (dd, J = 6.5 Hz and 3.4 Hz, 2H), 7.92 (s, 2H), 7.74 (dd, J = 6.5 Hz and 3.2 Hz, 2H). **^{13}C NMR** (125 MHz, D_2O) δ (ppm): 160.28, 149.65, 145.16, 143.04, 138.58, 136.61, 131.24, 130.62, 130.07, 129.25, 128.84, 128.14, 125.12, 122.75. **MS** ESI-MS: m/z [M]2+ calc for $C_{32}H_{20}N_6O_8$: 308.0666, found: 308.0722

4,4'-(Pyrene-1,6-diyl)bis(1-(2,4-dinitrophenyl)pyridin-1-ium) - EV[$Pyr_{1,6}$]DNB

^{1}H NMR (500 MHz, D_2O) δ (ppm): 9.38 (d, J = 2.5 Hz, 1H), 9.23 (d, J = 6.6 Hz, 2H), 8.94 (dd, J = 8.6 Hz and 2.5 Hz, 1H), 8.59 (d, J = 6.6 Hz, 2H), 8.39 (d, J = 8.1 Hz, 1H), 8.31 (d, J = 8.6 Hz, 1H), 8.25 (d, J =7.9 Hz, 1H), 8.18 (q, J = 9.2 Hz, 3H). **^{13}C NMR** (125 MHz, D_2O) δ (ppm): 160.83, 149.64, 144.82, 143.09, 138.63, 132.64, 132.50, 131.28, 131.11, 130.69, 129.57, 129.41, 128.50, 128.06, 126.48, 123.80, 122.77. **MS** ESI-MS: m/z [M]2+ calc for $C_{38}H_{22}N_6O_8$: 345.0744, found: 345.0744

4,4'-(Pyrene-2,7-diyl)bis(1-(2,4-dinitrophenyl)pyridin-1-ium) - EV[Pyr$_{2,7}$]DNB

^{1}H NMR (500 MHz, D_2O) δ (ppm): 9.33 (d, J = 2.5 Hz, 2H), 9.11 (d, J = 6.5 Hz, 4H), 8.91 (dd, J = 8.6 Hz and 2.5 Hz, 2H), 8.75 (d, J = 5.7 Hz, 4H), 8.53 (s, 4H), 8.23 (d, J = 8.6 Hz, 2H), 8.11 (s, 4H). **MS** ESI-MS: m/z [M]2+ calc for $C_{38}H_{22}N_6O_8$: 345.0744, found: 345.0744

4,4'-(Chrysene-6,12-diyl)bis(1-(2,4-dinitrophenyl)pyridin-1-ium) - EV[CH]DNB

^{1}H NMR (500 MHz, DMSO) δ (ppm): 9.64 (d, J = 6.3 Hz, 2H), 9.43 – 9.35 (m, 2H), 9.24 (d, J = 2.5 Hz, 1H), 9.10 (dd, J =8.6 Hz and 2.6 Hz, 1H), 8.90 (d, J = 6.5 Hz, 2H), 8.55 (d, J = 8.6 Hz, 1H), 8.17 (d, J = 8.3 Hz, 1H), 8.01 (t, J = 7.6 Hz, 1H), 7.93 (t, J = 7.5 Hz, 1H). **MS** ESI-MS: m/z [M]2+ calc for $C_{40}H_{24}N_{608}$: 358.0822, found: 358.0822

4,4'-(Thiophene-2,5-diyl)bis(1-(2,4-dinitrophenyl)pyridin-1-ium) - EV[Th]DNB

^{1}H NMR (500 MHz, D_2O) δ (ppm): 9.32 (s, 2H), 9.02 (d, J = 6.1 Hz, 4H), 8.86 (d, J = 11.2 Hz, 2H), 8.54 (d, J = 4.8 Hz, 4H), 8.33 – 8.27 (m, 2H), 8.19 (d, J = 9.7 Hz, 2H) **^{13}C NMR** (125 MHz, D_2O) δ (ppm): 150.75, 149.54, 145.26, 143.85, 143.04, 138.46, 134.61, 131.16, 130.57, 123.54, 122.70, 117.47, 115.14. **MS** ESI-MS: m/z [M]2+ calc for $C_{26}H_{16}N_6O_8S$: 286.0370, found: 286.0372

4,4'-([2,2'-Bithiophene]-5,5'-diyl)bis(1-(2,4-dinitrophenyl)pyridin-1-ium) - EV[DTh]DNB

^{1}H NMR (500 MHz, D_2O) δ (ppm): 9.26 (d, J = 2.5 Hz, 1H), 8.85 – 8.77 (m, 3H), 8.33 – 8.27 (m, 2H), 8.17 – 8.08 (m, 2H), 7.69 (d, J = 4.2 Hz, 1H). **^{13}C NMR** (125 MHz, D_2O) δ (ppm): 151.14, 149.39, 144.67, 144.48, 143.11, 138.57, 137.30, 134.83, 131.19, 130.53, 129.21, 122.67, 122.17 **MS** ESI-MS: m/z [M]2+ calc for $C_{30}H_{18}N_6O_8S_2$: 327.0308, found: 327.0309

The substituted EV[X]R were synthesised with a general procedure starting from appropriate symmetric Zinke salt and functionalised amine.

4,4'-(1,4-Phenylene)bis(1-(p-tolyl)pyridin-1-ium) dichloride - EV[Ph]Me

4,4'-(1,4-phenylene)bis(1-(2,4-dinitrophenyl)pyridin-1-ium) (1 g, 1.6 mmol) and toluidine (0.5 g, 4.7 mmol) were refluxed for 24 h in 100 mL of ethanol. After that, the reaction mixture was cooled down to room temperature and concentrated. The residue precipitated in diethyl ether and dried.

^{1}H NMR (500 MHz, D_2O) δ (ppm): 9.03 (d, J = 6.8 Hz, 4H), 8.45 (d, J = 6.9 Hz, 4H), 8.16 (s, 4H), 7.58 (d, J = 8.5 Hz, 4H), 7.48 (d, J = 8.4 Hz, 4H), 2.39 (s, 6H). **^{13}C NMR** (125 MHz, D_2O) δ (ppm): 155.55, 144.09, 142.58, 139.87, 137.03, 130.92, 129.32, 125.32, 123.55, 20.26. **MS** ESI-MS: m/z [M]2+ calc for $C_{30}H_{26}N_2$: 207.1043, found: 207.1041

4,4'-(1,4-Phenylene)bis(1-phenylpyridin-1-ium) dichloride - EV[Ph]H

^{1}H NMR (500 MHz, D_2O) δ (ppm): 9.07 (dd, J = 5.3 Hz and 1.5 Hz, 4H), 8.49 (dd, J = 5.2 Hz and 1.2 Hz, 4H), 8.19 (s, 4H), 7.74 – 7.63 (m, 10H). **^{13}C NMR** (125 MHz, D_2O) δ (ppm): 162.84, 155.93, 144.28, 142.27, 137.09, 131.52, 130.52, 129.37, 125.39, 123.92. **MS** ESI-MS: m/z [M]2+ calc for $C_{28}H_{22}N_2$: 193.0886, found: 193.0882

4,4'-(1,4-Phenylene)bis(1-(4-methoxyphenyl)pyridin-1-ium) dichloride - EV[Ph]OMe

^{1}H NMR (500 MHz, D_2O) δ (ppm): 8.97 (d, J = 7.0 Hz, 4H), 8.39 (d, J = 7.0 Hz, 4H), 8.12 (s, 4H), 7.65 – 7.59 (m, 4H), 7.19 – 7.14 (m, 4H), 3.82 (s, 6H). **^{13}C NMR** (126 MHz, D_2O) δ (ppm): 161.23, 155.02, 143.91, 136.88, 135.40, 129.28, 125.24, 125.23, 115.57, 55.82. **MS** ESI-MS: m/z [M]2+ calc for $C_{30}H_{26}N_2O_2$: 223.0992, found: 223.0986

4,4'-(Naphthalene-1,4-diyl)bis(1-(p-tolyl)pyridin-1-ium) dichloride - EV[Np]Me

^{1}H NMR (500 MHz, D_2O) δ (ppm): 9.13 (dd, J = 5.0 Hz and 1.9 Hz, 4H), 8.37 (dd, J = 5.3 Hz and 1.6 Hz, 4H), 7.99 (dd, J = 6.5 Hz and 3.3 Hz, 2H), 7.82 (s, 2H), 7.70 (dd, J = 6.5 Hz and 3.3 Hz, 2H), 7.66 – 7.60 (m, 4H), 7.51 (d, J = 7.7 Hz, 4H), 2.42 (s, 6H). **^{13}C NMR** (125 MHz, D_2O) δ (ppm): 157.50, 143.95, 142.64, 140.06, 136.45, 130.95, 130.12, 129.03, 128.50, 127.69, 125.11, 123.69, 20.26. **MS** ESI-MS: m/z [M]2+ calc for $C_{34}H_{28}N_2$: 232.1121, found: 232.1118

4,4'-(Naphthalene-1,4-diyl)bis(1-phenylpyridin-1-ium) dichloride - EV[Np]H

^{1}H NMR (500 MHz, D_2O) δ (ppm): 9.18 (d, J = 6.7 Hz, 4H), 8.41 (d, J = 6.6 Hz, 4H), 8.01 (dd, J = 6.5 Hz and 3.3 Hz, 2H), 7.84 (s, 2H), 7.77 (dd, J = 7.0 Hz and 2.9 Hz, 4H), 7.74 – 7.67 (m, 8H). **MS** ESI-MS: m/z [M]2+ calc for $C_{32}H_{24}N_2$: 218.0964, found: 218.0965

4,4'-(Naphthalene-1,4-diyl)bis(1-(4-methoxyphenyl)pyridin-1-ium) dichloride - EV[Np]OMe

^{1}H NMR (500 MHz, D_2O) δ (ppm): 9.10 (dd, J = 5.3 Hz and 1.5 Hz, 4H), 8.35 (dd, J = 5.2 Hz and 1.3 Hz, 4H), 7.99 (dd, J = 6.5 Hz and 3.3 Hz, 2H), 7.81 (s, 2H), 7.73 – 7.68 (m,

6H), 7.22 (dd, J = 6.8 Hz and 2.4 Hz, 4H), 3.87 (s, 6H). **^{13}C NMR** (125 MHz, D_2O) δ (ppm): 161.27, 157.26, 143.96, 136.47, 135.76, 130.15, 129.03, 128.51, 127.70, 125.48, 125.13, 115.62, 55.87. **MS** ESI-MS: m/z [M]2+ calc for $C_{34}H_{28}N_2O_2$: 248.1070, found: 248.1070

4,4'-(Naphthalene-1,4-diyl)bis(1-(4-(dimethylamino)phenyl)pyridin-1-ium) dichloride - EV[Np]NMe$_2$

^{1}H NMR (500 MHz, D_2O) δ (ppm): 9.02 (d, J = 6.7 Hz, 2H), 8.27 (d, J = 6.6 Hz, 2H), 7.98 (dd, J = 6.5 Hz and 3.3 Hz, 1H), 7.78 (s, 1H), 7.69 (dd, J = 6.5 Hz and 3.3 Hz, 1H), 7.60 (d, J = 9.1 Hz, 2H), 7.01 (d, J = 9.0 Hz, 2H), 2.95 (s, 6H). **^{13}C NMR** (125 MHz, D_2O) δ (ppm): **MS** ESI-MS: m/z [M]2+ calc for $C_{36}H_{34}N_4$: 261.1386, found: 261.1390

4,4'-(Naphthalene-1,4-diyl)bis(1-(4-aminophenyl)pyridin-1-ium) dichloride - EV[Np]NH$_2$

^{1}H NMR (500 MHz, D_2O) δ (ppm): 9.13 – 9.02 (m, 4H), 8.40 – 8.29 (m, 4H), 8.00 (dd, J = 6.5, 3.3 Hz, 2H), 7.82 (s, 2H), 7.70 (dd, J = 6.5, 3.3 Hz, 2H), 7.61 – 7.47 (m, 4H), 7.07 – 6.95 (m, 4H), 6.66 (s, 1H). **MS** ESI-MS: m/z [M]2+ calc for $C_{36}H_{34}N_4$: 261.1386 , found: 261.1390

4,4'-(Naphthalene-1,4-diyl)bis(1-(4-(methylthio)phenyl)pyridin-1-ium) dichloride - EV[Np]SMe

^{1}H NMR (500 MHz, D_2O) δ (ppm): 9.17 – 9.15 (m, 2H), 8.45 – 8.36 (m, 2H), 8.01 (dd, J = 6.5, 3.3 Hz, 1H), 7.84 (s, 1H), 7.75 – 7.67 (m, 3H), 7.61 – 7.53 (m, 2H), 2.55 (s, 3H). **^{13}C NMR** (126 MHz, D_2O) δ (ppm): 143.86, 143.45, 136.48, 130.14, 129.11, 128.54, 127.75, 127.02, 126.45, 125.74, 125.14, 124.32, 14.12. **MS** ESI-MS: m/z [M]2+ calc for $C_{34}H_{28}N_2S_2$: 264.0841, found: 264.0838

4,4'-(Naphthalene-1,4-diyl)bis(1-(4-(trifluoromethyl)phenyl)pyridin-1-ium) dichloride - EV[Np]CF$_3$

^{1}H NMR (500 MHz, D_2O) δ (ppm): 9.32 (d, J = 6.9 Hz, 2H), 8.59 – 8.51 (m, 2H), 8.18 – 8.03 (m, 5H), 7.95 (s, 1H), 7.81 (dt, J = 6.6, 3.3 Hz, 1H). **MS** ESI-MS: m/z [M]2+ calc for $C_{34}H_{22}F_6N_2$: 286.0838 , found: 286.0840

4,4'-(Naphthalene-1,4-diyl)bis(1-(4-bromophenyl)pyridin-1-ium) dichloride - EV[Np]Br

^{1}H NMR (500 MHz, D_2O) δ (ppm): 9.22 – 9.15 (m, 2H), 8.46 – 8.40 (m, 2H), 8.01 (dd, J = 6.5, 3.3 Hz, 1H), 7.93 – 7.88 (m, 2H), 7.85 (s, 1H), 7.74 – 7.68 (m, 3H) **MS** ESI-MS: m/z [M]2+ calc for $C_{32}H_{22}Br_2N_2$: 297.0059, found: 297.0062

4,4'-(Pyrene-1,6-diyl)bis(1-phenylpyridin-1-ium) dichloride - EV[Pyr$_{1,6}$]H

^{1}H NMR (500 MHz, DMSO) δ (ppm): 9.15 (d, J = 5.8 Hz, 4H), 8.50 – 8.42 (m, 6H), 8.33 (d, J = 8.0 Hz, 4H), 8.27 (d, J = 7.8 Hz, 2H), 7.80 – 7.75 (m, 4H), 7.71 – 7.66 (m, 6H). **^{13}C NMR** (125 MHz, DMSO – d_6) δ (ppm): 143.97, 142.47, 131.84, 131.81, 130.84, 129.84, 129.50, 128.79, 126.66, 126.65, 126.64, 125.20, 124.23, 124.19, 120.46. **MS** ESI-MS: m/z [M]2+ calc for $C_{38}H_{26}N_2$: 255.1043, found: 255.1041

4,4'-(Pyrene-1,6-diyl)bis(1-(p-tolyl)pyridin-1-ium) dichloride - EV[Pyr$_{1,6}$]Me

^{1}H NMR (500 MHz, D_2O) δ (ppm): 9.09 (d, J = 6.5 Hz, 2H), 8.43 (dd, J = 14.9 Hz and 7.2 Hz, 3H), 8.24 (dd, J = 22.4 Hz and 7.3 Hz, 3H), 7.63 (d, J = 8.2 Hz, 2H), 7.50 (d, J = 8.1 Hz, 2H), 2.42 (s, 3H). **^{13}C NMR** (125 MHz, D_2O) δ (ppm): 167.97, 143.50, 139.88, 134.24, 132.32, 131.41, 131.02, 129.46, 129.30, 128.45, 128.04, 126.28, 124.02, 123.57, 48.83, 20.32 **MS** ESI-MS: m/z [M]2+ calc for $C_{40}H_{30}N_2$: 269.1199, found: 269.1199

4,4'-(Pyrene-2,7-diyl)bis(1-(p-tolyl)pyridin-1-ium) dichloride - EV[Pyr$_{2,7}$]Me

^{1}H NMR (500 MHz, D_2O) δ (ppm): broad spectrum 8.41, 7.99, 7.25 **MS** ESI-MS: m/z [M]2+ calc for $C_{40}H_{30}N_2$: 269.1199, found: 269.1201

4,4'-(Chrysene-6,12-diyl)bis(1-phenylpyridin-1-ium) dichloride - EV[CH]H

^{1}H NMR (500 MHz, D_2O) δ (ppm): 9.13 (d, J = 6.1 Hz, 2H), 8.82 (dd, J = 152.2 Hz and 8.4 Hz, 1H), 8.70 (s, 1H), 8.30 (d, J = 5.9 Hz, 2H), 7.92 (d, J = 8.1 Hz, 1H), 7.84 – 7.66 (m, 7H). **MS** ESI-MS: m/z [M]2+ calc for $C_{40}H_{28}N_2$: 268.1121 , found: 268.1124

4,4'-(Chrysene-6,12-diyl)bis(1-(p-tolyl)pyridin-1-ium) dichloride - EV[CH]Me

^{1}H NMR (500 MHz, D_2O) δ (ppm): 9.16 (d, J = 6.3 Hz, 4H), 8.94 (d, J = 8.4 Hz, 2H), 8.89 (s, 2H), 8.44 (d, J = 6.3 Hz, 4H), 7.98 (d, J = 8.5 Hz, 2H), 7.85 (d, J = 7.6 Hz, 2H), 7.73 (d, J = 7.7 Hz, 2H), 7.67 (d, J = 7.9 Hz, 4H), 7.53 (d, J = 8.1 Hz, 4H), 2.46 (s, 6H). **MS** ESI-MS: m/z [M]2+ calc for $C_{42}H_{32}N_2$: 282.1277, found: 282.1269

4,4'-(Thiophene-2,5-diyl)bis(1-(p-tolyl)pyridin-1-ium) dichloride - EV[Th]Me

^{1}H NMR (500 MHz, D_2O) δ (ppm):8.97 (d, J = 6.5 Hz, 2H), 8.39 (d, J = 6.5 Hz, 2H), 8.18 (s, 1H), 7.57 (d, J = 8.1 Hz, 2H), 7.49 (d, J = 8.1 Hz, 2H), 2.41 (s, 3H). **^{13}C NMR** (125 MHz, D_2O) δ (ppm): 148.36, 144.11, 143.09, 142.55, 139.87, 133.39, 130.91, 123.46, 123.39, 20.26. **MS** ESI-MS: m/z [M]2+ calc for $C_{28}H_{24}N_2S$: 210.0825, found: 210.0828

4,4'-([2,2'-Bithiophene]-5,5'-diyl)bis(1-(p-tolyl)pyridin-1-ium) dichloride - EV[DTh]Me

^{1}H NMR (500 MHz, D_2O) δ (ppm):8.80 (d, J = 6.9 Hz, 4H), 8.18 (d, J = 6.8 Hz, 4H), 8.00 (d, J = 4.1 Hz, 2H), 7.60 (d, J = 4.1 Hz, 2H), 7.50 (d, J = 8.4 Hz, 4H), 7.44 (d, J = 8.3 Hz, 4H), 2.36 (s, 6H). **^{13}C NMR** (125 MHz, D_2O) δ (ppm): 13C NMR (126 MHz, D_2O) δ 160.98, 147.88, 143.26, 142.72, 137.00, 134.81, 133.74, 128.81, 124.55, 122.11, 115.56, 55.73 **MS** ESI-MS: m/z [M]2+ calc for $C_{32}H_{26}N_2S_2$: 251.0763, found: 251.0759

3.4 Acknowledgements

Dr Guanglu Wu has measured and helped in analysis of selected 500 MHz NMR spectra of EV[Np] based molecules. Dr Guanglu Wu is also acknowledged for the conducting the DOSY experiments for EV[Np]R, CB[8]:EV[Np]R and CB[7]:EV[Np]R complexes. Daniel Anton Garcia helped in measurements of PL quantum yields and fluorescence lifetimes. Dr Silvia Gomez-Coca has performed theoretical calculations and help in analysis of the results. Natalia Powers-Riggs and Dr Ryan Young, Department of Chemistry, Northwestern University, have performed Transient Spectroscopy measurements and helped in analysis of the transient spectroscopy data.

Chapter 4

Asymmetrisation of Aryl and Extended Aryl Viologens

Part of this work has been complied into a manuscript:

Clark D.*, Olesińska M.*, Mönch T. and Scherman O.A., Aryl-Viologen Pentapeptide Self-Assembled Conductive Nanofibers, under review.

*These authors contributed equally to this work.

The focus of this chapter is to obtain asymmetric aryl and extended aryl viologens. Zinke reaction conditions to obtain asymmetric N-substitution on aryl viologen (AV) are discussed. Furthermore, the effect of aromatic extension between the two pyridines on the asymmetric N-substitution via Zinke reaction is reported. Subsequently, the binding properties of an asymmetric extended aryl viologen (EV[Np](OMe)(EtCOOH)) to CB[8] and CB[7], and the effect of this encapsulation on the optical properties of the molecule is measured via steady state spectroscopy techniques. Here, the conjugation of one of asymmetric aryl viologen to a pentapeptide, successive nano-fiber formation and its conductive properties are described. Such conductive nanofibers, with facile and controllable assembly in aqueous environments, have potential for future exploration in optoelectronic applications.

4.1 Introduction

Heterocyclic chemistry is the part of organic chemistry that deals with cyclic molecules (aromatic and non-aromatic) in which at least one ring atom is not a carbon. The most common heteroatoms are nitrogen, oxygen and sulphur. Synthetic heterocycles are of high importance due to their usage as herbicides, dyes, organic conductors, and pharmaceuticals

[186–190].
Pyridine, a simple benzene analogue with an sp^2 hybridised N-atom, is a member of the six-membered heterocycle family. Due to the lone electron pair on the electronegative nitrogen atom, the electron density on the remaining six π-electrons of the aromatic ring is substantially reduced. Such electron deficiency retards the pyridine ring reactivity towards electrophilic substitution. Instead, it favours nucleophilic attack (S_NAr), and therefore nucleophilic substitution of a suitable leaving group. Due to its moderately basic character, quaternisation is the most common functionalisation of pyridines. The aromatic substitution on pyridine or bipyridine can be obtained through the Zinke reaction, as mentioned in Chapter 1 and Chapter 3. Work presented in this thesis and several examples in the literature report on symmetric aromatic substituted bipyridines.[152, 191] Notably, there are only two reported methods for asymmetric functionalisation of bipyridines.[89, 192] However, a deeper understanding of these reactions and optimisation of their efficiency is needed to allow for a wider use of these molecules. Moreover, the asymmetric functionalisation of bipyridines can be used for the synthesis of so called "push-pull" molecules with electron donating and electron withdrawing substituents. Systems based on such molecules could be used in nonlinear optics or dye-sensitised solar cells.[193–195]

4.2 Results and Discussion

4.2.1 Synthesis of Asymmetric Aryl and Extended Aryl Viologens

N-Aryl asymmetric functionalisation of 4,4'-bipyridne was done via Zinke reaction. The double activation of 4,4'-bipyridine with 2,4-dinitrochlorobenzene (DNB) leads to the symmetric product **(1)**, so called Zinke salt as depicted in Figure 4.1. Further reaction of **(1)** with corresponding R-anilines (R and R') yields a mixture of symmetric and asymmetric functionalised products **(2)**, **(3)** and **(4)** (Figure 4.1). Due to small differences in polarity of these molecules their separation is difficult.

A more viable route for obtaining asymmetric bipyridines is through a mono-functional Zinke salt **(5)**. This product can be readily obtained through control of stoichiometry of the reactants and reaction time. The symmetric product is obtained in high yields (90%) when the reaction is carried out in ethanol for at least 48h with an excess of 2,4-dinitrochlorobenzene.[191] Changing the stoichiometry to be equimolar and stopping the reaction after 24 h yields the asymmetric product in 70% yield, with 30% of mixed unreacted bipyridne and symmetric product. The separation of those is based on their substantial difference in solubility in nonpolar solvents. Symmetric Zinke salt of aryl viologen is precipitated

from cold diethyl ether, whereas the asymmetric Zinke salt of aryl viologen precipitates from acetone or THF.

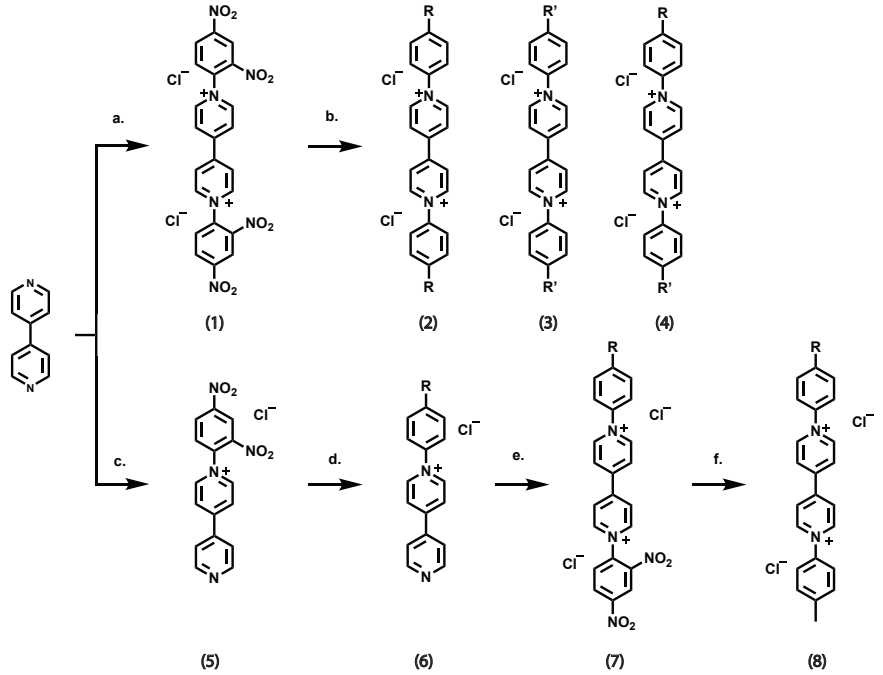

Fig. 4.1 Reaction scheme for synthesis of symmetric and asymmetric aryl-aryl' viologens. a. 2 eq 2,4-dinitrochlorobenzene, EtOH, 90 °C, 72 h b. R- and R'-aniline, EtOH, 90 °C, 24 h c. 1 eq 2,4-dinitrochlorobenzene, EtOH, 90 °C, 24 h to 48 h d. R-aniline, EtOH, 90 °C, 24 h to 48 h; e. reaction conditions listed in Table 4.1 f. R'-aniline, EtOH, 90 °C, 24 h to 48 h.

In order to obtain the asymmetric aryl-aryl' functionalisation of 4,4'-bipyridine, a two-step procedure was adapted.[89] First, the asymmetric Zinke salt **(5)** of bipyridine was synthesised (Figure 4.1). The general route for single activation of bipyridine proceeds via an aromatic substitution with an electrophile (here, stoichiometric 2,4-dinitrochlorobenzene) as mentioned before. The product was purified *via* precipitation as the chlorinated product is soluble in water and insoluble in organic solvents, resulting in 70 % yield. Subsequently, the obtained Zinke salt **(5)** was reacted in ethanol for 24 h with different anilines to yield the desired mono-substituted aryl viologens **(6)** in 60 % to 86 % yield (see Figure 4.1). The second activation of bipyridine was performed using a method developed by Walder *et al.*[89] However, using acetonitrile as solvent and 2,4-dinitrophenyl 4-methylbenzenesulfonate for the reaction depicted in Figure 4.1 was not successful, and no substitution occurred. To overcome the difficulties caused by the decrease in nucleophilicity of mono-substituted pyridine, the influence of various reaction conditions (solvent, counterion and leaving group

on reactant), was studied.[196–198] The studied conditions and their effect on the reaction are summarised in Table 4.1.

Table 4.1 Reaction conditions of aromatic substitution on asymmetric aryl viologen.

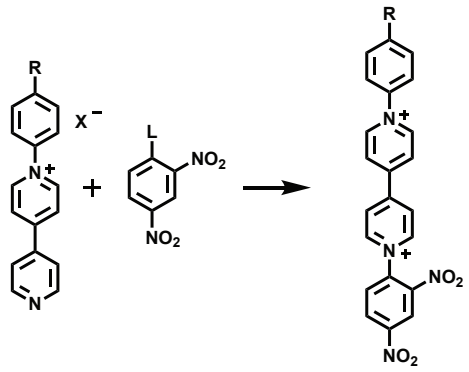

(6) (7)

Entry	R	L	Solvent	X^-	t [h]	Ratio **(6)**:**(7)**	Reaction conversion in %*
1	-Me	-Tos	DMF	Cl^-	120	1:5	85
2	-Me	-Cl	NMP	Cl^-	24	1:5	56
3	-Me	-Tos	NMP	Cl^-	48	1:5	10
4	-Me	-Tos	NMP	Cl^-	72	1:5	22
5	-Me	-Tos	NMP	Cl^-	96	1:5	28
6	-Me	-Cl	PC	Cl^-	72	1:5	nf
7	-Me	-Tos	PC	Cl^-	72	1:5	nf
8	-Me	-Cl	DMF/MeCN	Cl^-	72	1:5	nf
9	-Me	-Cl	DMSO	Cl^-	72	1:5	17
10	-Me	-Cl	DMSO	Cl^-	96	1:5	21
11	-Me	-Cl	MeCN	Cl^-	96	1:5	nf
12	-Me	-Tos	MeCN	Cl^-	96	1:5	nf
13	-H	-F	MeCN	Cl^-	72	1:1	nf
14	-Me	-F	MeCN	Cl^-	62	1:5	nf
15	-Me	-F	MeCN	Cl^-	62	1:2	nf
16	-Me	-F	EtOH	Cl^-	168	1:10	nf
17	-Me	-F	MeCN	Cl^-	168	1:10	nf
18	-H	-F	MeCN	PF_6^-	72	1:5	nf
19	-H	-Cl	EtOH	Cl^-	96	1:5	nf

All the reaction were conducten at T=90°C. Abbreviatios: nf- not found, Tos- tosylate, DMF-N,N-dimethylformamide, NMP- N-methyl-2-pyrrolidone, PC- propylene carbonate, MeCN-acetonitrile, EtOH- ethanol. *The reaction conversion of **(6)** to corresponding **(7)** estimated with HPLC LC-MS.

The results suggest that in aprotic polar solvents with high polarity index (such as DMF, NMP and DMSO), the reaction conversion is enhanced. A possible explanation is that in the presence of polar aprotic solvents the formation of a transition state occurs, whereas polar protic solvents promote formation of hydrogen bonding with ortho-NO_2 groups of the electrophile. Additionally, the effect of the leaving group was studied. For typical S_NAr reactions, the observed trend in reactivity among halide leaving groups is $F > Cl \approx Br > I$. However, an extensive study on different systems revealed high solvent dependency on the rate of displacement of the leaving group.[199, 200] One example is reported by Um *et al.* where the importance of the transition states caused by solvation effects is shown.[199] In a different study, Parker *et al.* show an increased reaction rate for chlorine over fluorine in polar aprotic solvent such as DMF and DMSO while no difference in rate is observed in methanol.[201] Here, in the case of asymmetric aryl viologens, only the reaction of **(6)** with R= Me in the presence of 2,4-dinitrophenyl 4-methylbenzenesulfonate in DMF shows good result (see Table 4.1). However, reactions conducted in NMP show a higher reaction conversion with 1-chloro-2,4-dinitrobenzene than with 2,4-dinitrophenyl 4-methylbenzenesulfonate. Thus, so far no influence of the substrate counter-ion on the reaction conversion was found. These results indicate that to form the Zincke salt from substituted bipyridine, polar aprotic solvents combined with 1-chloro-2,4-dinitrobenzene as a reactant should be used.

Publications by Ruhbaum and Katritzky show that if pyridine is substituted in position two and six with electron withdrawing groups, the Zincke salt is not formed or obtained in extremely low yields.[202, 203] Results presented in Table 4.1 confirm those reports. Here, it is found that formation of the Zinke salt on bipyridine is challenging since the charged pyridine has a strong deactivating character. A report by Greenwood *et al.* suggests the use of high molarity allow for this reaction to take place.[192]

To facilitate this reaction, the reactivity of the inactivated pyridine on the bipyridine has to be increased. Thus, an aromatic bridging unit between two pyridines was introduced as the electron donating extension (Figure 4.2). The 1,4-di(pyridin-4-yl)naphthalene (EV[Np]) was synthesised according to the procedure described in Chapter 2. Next, the Zinke reaction with 1 eq of 2,4-dinitrochlorobenzene was conducted as depicted in Figure 4.2(a). This reaction after 48 h yields 70 % of asymmetric product **(10)**, 20 % of symmetric product and 10 % of starting material. All species were separated via preparative HPLC. The subsequent exchange reaction of asymmetric Zinke salt **(10)** (reaction b in Figure 4.2) depends on the electron donating (EDG) or electron withdrawing (EWG) character of R group in the para position of the aniline. Reactions with electron donating anilines last 24 h, whereas for electron withdrawing aniline the reaction time has to be extended to at least 48 h. The resulting

asymmetric aryl extended viologens **(11)** are obtained in yields of 60 % for anilines with EWG, and up to 90% for anilines with EDG. Formation of the Zinke salt of the asymmetric extended viologen **(12)**, requires 5-10 eq excess of 2,4-dintirochlorobenzene (DNB), and the reaction times of 48 h to 72 h (depending on R functionality of the asymmetric EV **(11)**). The yield of the following replacement of DNB with R'-aniline also depends on the electron withdrawing or donating character of the R' group and varies from 60 to 80%.

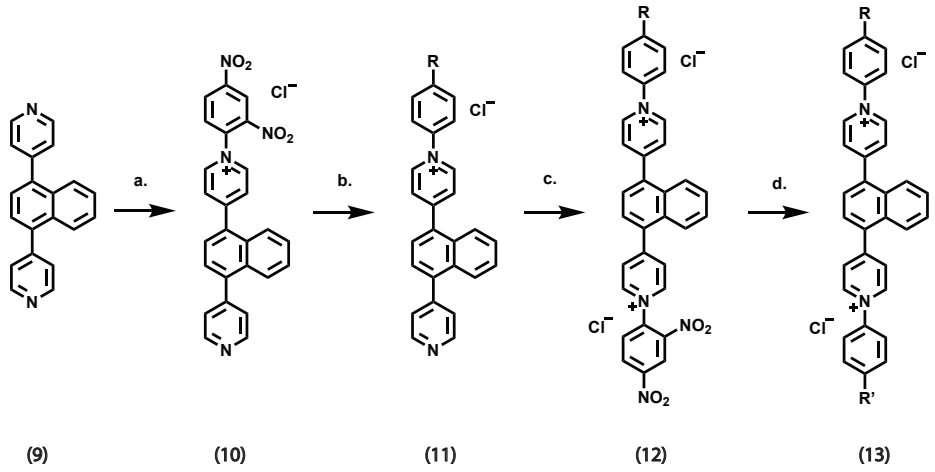

Fig. 4.2 Reaction scheme for synthesis of asymmetric aryl-aryl' extended viologen EV[Np]RR'; a. 1 eq 2,4-dinitrochlorobenzene, EtOH, 90 °C, 24 h; b. R-aniline (R= -CH_3,-OCH_3), EtOH, 90 °C, 24 h to 48 h; c. 10 eq 2,4-dinitrochlorobenzene, EtOH, 90 °C, 48 h to 72 h; d. R'-aniline(R'=-NO_2,-Ph$(CH_2)_2$COOH), EtOH, 90 °C, 24 h to 48 h.

4.2.2 ^{1}H NMR Characterisation of Supramolecular Complexes

The EV[Np](OMe)(EtCOOH) molecule was synthesised according to the method described in section 4.2. This molecule comprise a bipyridine **(9)** (Figure 4.2), functionalised in N - positions with carboxyethylphenyl and methoxyphenyl residues. The interaction between CB[8] or CB[7] and EV[Np](OMe)(EtCOOH) was investigated by ^{1}H NMR titration. The binding of the guest was manipulated by varying the pH of the solution through protonation and deprotonation of a carboxylic acid group.

^{1}H NMR spectra in Figure 4.3 show the binding between the guest molecule and CB[7]. EV[Np](OMe)(EtCOOH) mixed with CB[7] in 1:2 ratio exhibits upfield shifts for H_h, H_k and H_j protons (0.39, 0.24 and 0.1 ppm, respectively). Protons H_g, $H_{g'}$, H_f and $H_{f'}$ are shifted approximately 1 ppm upfield. Similarly, protons on pyridinium moieties H_e and $H_{e'}$ are shifted upfield with 0.30 and 0.97 ppm accordingly. In contrast, peaks H_d and $H_{d'}$ show no significant shift. These upfield shifts are indicative of encapsulation or partial encapsulation

of the guest inside the cavity of CB[7]. The extend of the shifts is used to estimate the position of CB[7] on the guest molecule. Consequently, the position of proton peaks suggest that the macrocyle binds around the methoxyphenyl moiety. Furthermore, the weak upfield shift of H_j might suggest the intramolecular bending of the side chain of carboxylic acid. Here, CB[7] has stronger effect on $H_{e'}$ proton. Such shifting behaviour suggests that if deprotonated, the bent carboxylic group is immersed in the macrocycle cavity and shows attractive interaction with the charged pyridine. The aromatic protons of the [Np] bridging unit H_a, $H_{a'}$, H_b, $H_{b'}$, H_c and $H_{c'}$ are all shifted downfield, indicating they are affected by the CB[7] carbonyl rims and the anisotropic $\pi - \pi$-stacking effect, confirming the position of the macrocycle on the methoxyphenyl group.

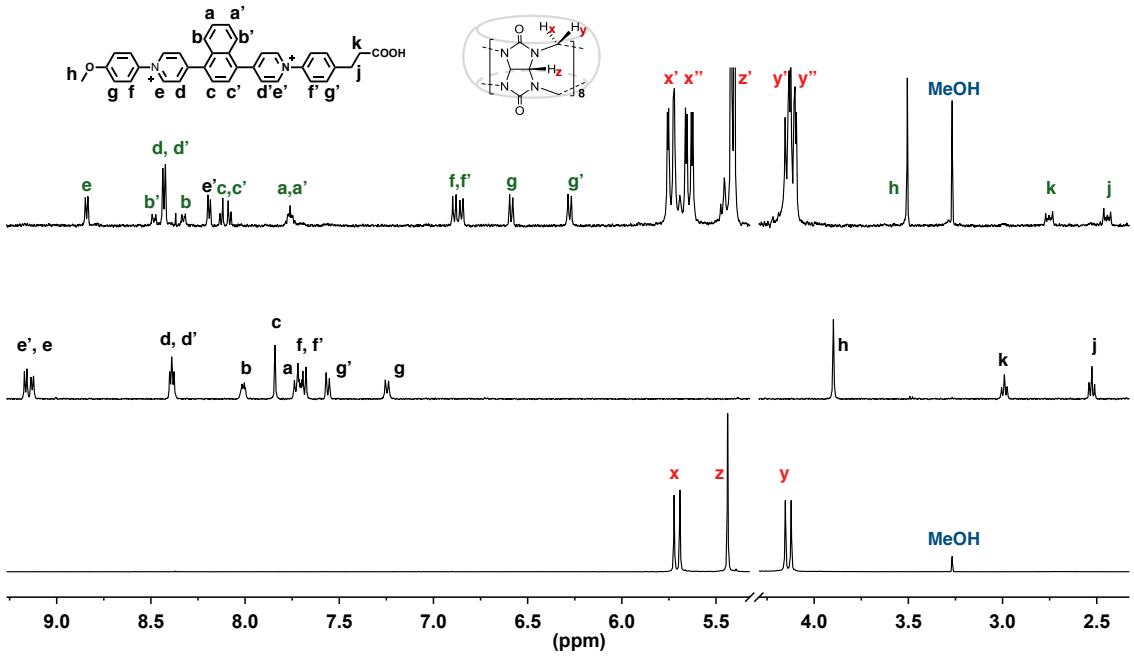

Fig. 4.3 ^{1}H NMR of 1 eq of EV[Np](OMe)(EtCOOH) mixed with 2 eq of CB[7] at pH = 9 in D_2O, with Cl^- as counterions.

^{1}H NMR spectra in Figure 4.4 show the binding relation between the guest molecule and CB[8] in acidic and neutral pH. EV[Np](OMe)(EtCOOH) mixed with CB[8] in 1:1 ratio at pH = 2 results in characteristic splitting of the methine protons of the macrocycle, indicating the 2:2 binding mode. The strong upfield shifts of H_g, $H_{g'}$, H_f, $H_{f'}$, H_h, H_k and H_j suggest encapsulation or partial encapsulation inside the cavity of CB[8]. However, since this molecule is of asymmetric nature, there are four different possible arrangements of the monomers in the 2:2 complex (Figure 4.5). Thus, protons on the aromatic naphthalene core,

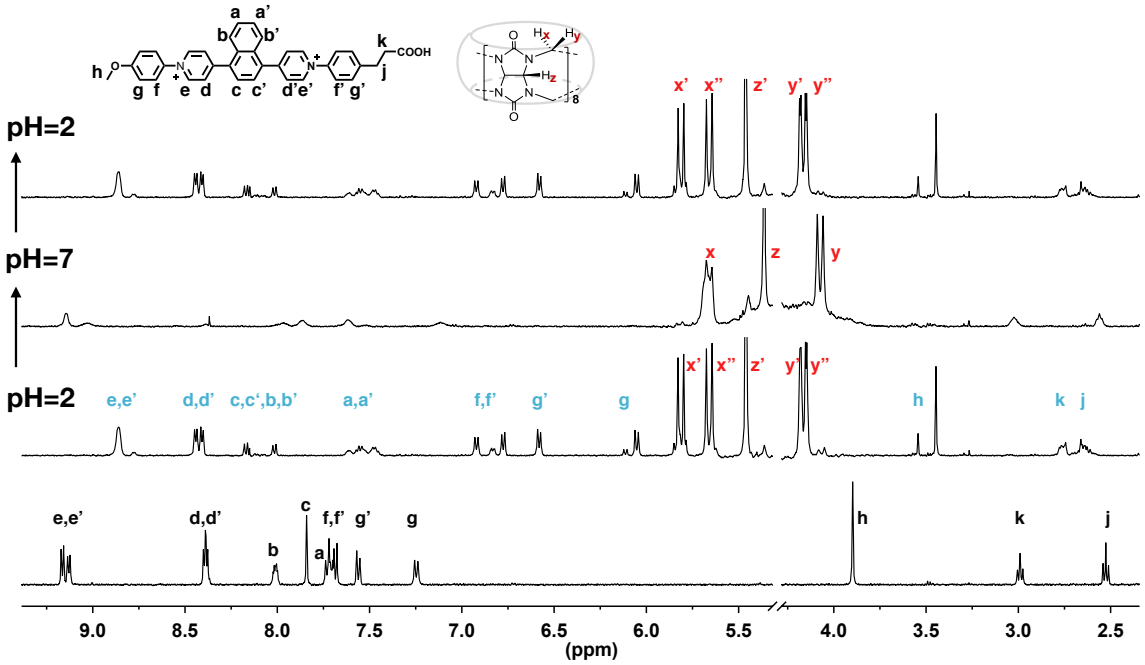

Fig. 4.4 ^{1}H NMR of EV[Np](OMe)(EtCOOH) mixed in 1:1 ration with CB[8] at different pH in D_2O, with Cl^- as counterions.

affected by different $\pi - \pi$ interaction points (head-head overlap, head-tail overlap) as well as the functional end groups, exhibit complicated shifts, splitting patterns and broadening.

Interestingly, the same host-guest mixture under basic conditions does not show 2:2 binding. Due to deprotonation of the carboxylic group, interaction with CB[8] is blocked. And no splitting of CB[8] peaks is observed. Moreover, only H_e and H_h protons exhibit shifts, suggesting an interaction between CB[8] and the methoxyphenyl moiety but not with other parts of the guest.

All peaks for guest and host are broad, suggesting dynamic complexation. Upon adjustment of pH back to pH = 2, the peaks of 2:2 complex could be observed once again (Figure 4.4). Furthermore, changes in luminescent properties of the sample can be observed upon changes in pH. Free EV[Np](OMe)(EtCOOH) has blue luminescence. Upon mixing with CB[8] in 1:1 ratio in pH = 2, the fluorescence changes from blue to green. A change in pH from acidic to basic results in blue emission. Subsequent change from basic pH back to acidic pH results in green fluorescence from 2:2 complex.

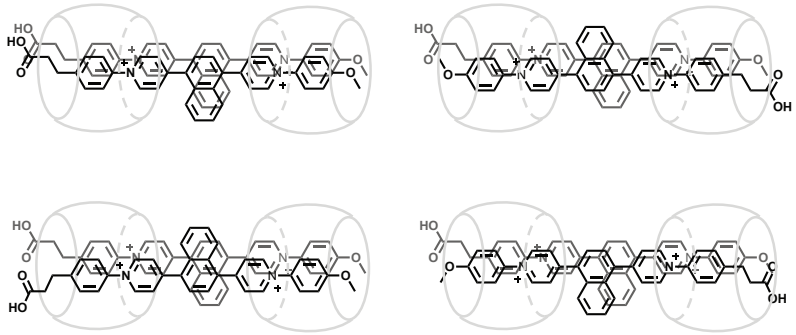

Fig. 4.5 Possible conformational orientations of EV[Np](OMe)(EtCOOH) mixed in 1:1 ration with CB[8]. Counterions have been omitted for clarity.

4.2.3 Photophysical Characterisation

The binding of EV[Np](OMe)(EtCOOH) with CB[8] and CB[7] was further investigated by UV – Vis and PL spectroscopy. The steady-state spectroscopy data are summarised in Table 4.2. As shown in Figure 4.6, the addition of CB[8] to EV[Np](OMe)(EtCOOH) in acidic conditions, resulted in a 20 nm red shift of the absorption peak and increase in molar absorption coefficient from $\varepsilon = 21\,159\,\mathrm{M}^{-1}\,\mathrm{cm}^{-1}$ for the monomeric molecule to $\varepsilon = 27\,173\,\mathrm{M}^{-1}\,\mathrm{cm}^{-1}$ for the supramolecular complex. The fluorescence maximum of the guest molecule upon mixing with CB[8] significantly red shifts (from 484 nm to 515 nm) and the quantum yield was determined to increase from 36% to 78% in the prescence of 1 eq of CB[8]. Time-resolved fluorescence measurements of this complex at the maximum of its emission exhibits the major emissive component (80%) decaying with a time constant of 13.9 ns. The long-lived emission of the EV[Np](OMe)(EtCOOH) with CB[8] indicates the existence of a stable excited state. In contrast, the host-guest complex with CB[7] results in no shift in absorption, but the complex has higher molar absorption coefficient $\varepsilon = 24\,168\,\mathrm{M}^{-1}\,\mathrm{cm}^{-1}$. The emission spectrum of EV[Np](OMe)(EtCOOH):CB[7]$_2$ complex shows a weak blue shift and the quantum yield is substantially increased from 36% to 86% on account of mechanical protection by the CB[7] cavity.

Table 4.2 Steady-state spectral data of EV[Np](OMe)(EtCOOH) in water.

System	λ_{abs}^{max} (nm)	λ_{em}^{max} (nm)	Stokes shift (nm)	Φ_{PL}	τ_1 (ns)	τ_2 (ns)
EV[Np](OMe)(EtCOOH)	371	484	113	0.36	1.6	-
(EV[Np](OMe)(EtCOOH))$_2$:(CB[8])$_2$	397	515	118	0.78	4.3	13.9
EV[Np](OMe)(EtCOOH):(CB[7])$_2$	371	482	111	0.86	-	-

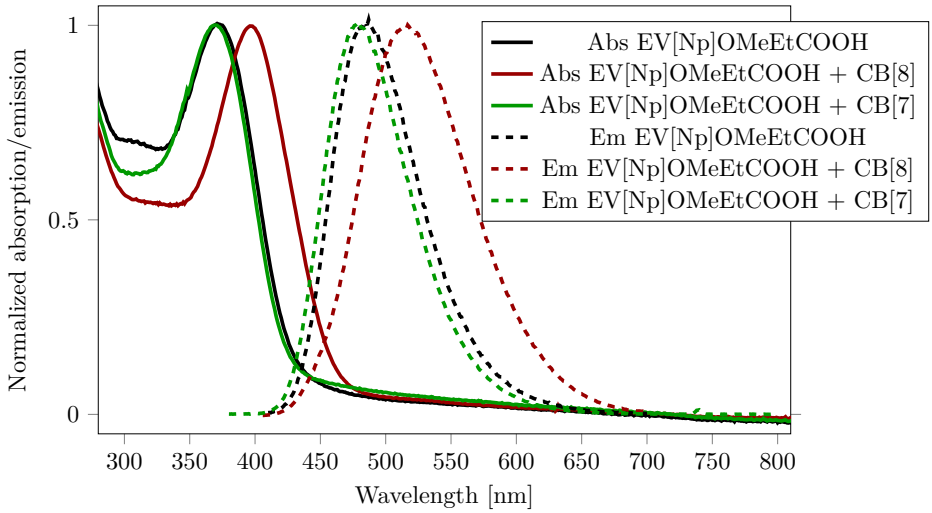

Fig. 4.6 Normalised absorption (solid lines) and emission (dashed line) spectra of EV[Np](OMe)(EtCOOH) and its complexes with 1 eq of CB[8] at pH = 2, and with 2 eq of CB[7] at pH = 9. All measurements were performed at a concentration of 10 µM.

4.2.4 Formation of Conductive Nanofibers

Asymmetric aryl viologens and extended viologens are an attractive class of materials for various applications, taking advantage of their unique optoelectronic properties. One of the potential application is the formation of molecular wires and electronic circuit, which are currently of great interest in nanoscience.[112, 204] Typical approaches to generate these molecular constructs have involved the development of polymers, which can transfer charge along their extended molecular structure.[112] More recently, supramolecular interactions such as π-π stacking and the oligopeptide self-assembly of aromatic species have been used to fabricate conductive nanomaterials including nanofibers and nanotubes.[204–206]

Oligopeptide β-sheet self-assembly can generate a variety of nanostructures in aqueous solutions.[207–211] In a few examples, certain peptide sequences have been able to form nanospheres,[212] fibrous and plate-like assemblies,[213], micelles and nanotubes.[214, 215] Through further functionalisation of peptides with aromatic and hydrophobic synthetic groups,[207, 216–218] additional $\pi - \pi$ stacking and hydrophobic interactions can be introduced to promote self-assembly.[209] In light of this, oligopeptides have been combined with aromatic semiconductive subunits such as perylene imide moieties in an attempt to control the assembly and enhance the semiconductivity of these subunits.[219, 220] Furthermore, β-sheet assemblies formed from aromatic phenylalanine-phenylalanine dipeptide sequences have been shown to generate quantum confined structures with underlying semiconductive properties.[204, 221, 222] Recently, Clarke *et al.* reported pentapeptide motifs that

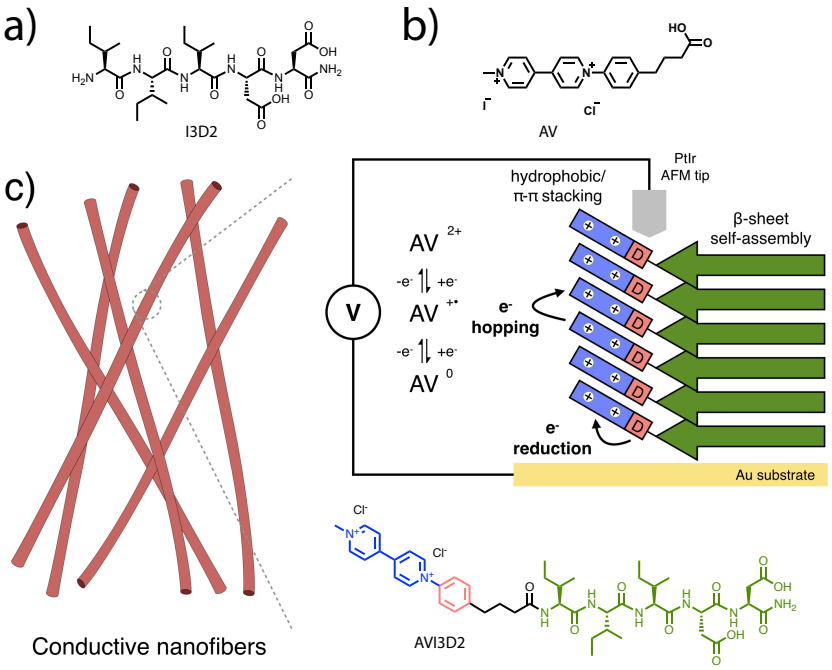

Fig. 4.7 Chemical structure of a) I3D2 peptide and b) asymmetric aryl viologen here denote as AV. c) Schematic representation of the chemical structure of the AVI3D2 conjugate and the proposed supramolecular stacking arrangement towards self-assembled conductive nanofibers.

contain three aliphatic isoleucine (Ile) residues, an amino acid with a high propensity to form β-sheets[223, 224], coupled with two aspartic acid (Asp) residues at the C-terminus which promote solubility (Figure 4.7a).[225] Upon protonation of the Asp residues, charge recognition/hydrogen bonding drives β-sheet self-assembly and in turn, the formation of nanofibers.[225]

Here, a viologen molecule (AV, Figure 4.7b) is conjugated to the I3D2 peptide through simple amide coupling to yield an AV labelled pentapeptide sequence (AVI3D2). By functionalising mono arylated methyl-viologen with the pentapeptide motif (I3D2), it is possible to utilise β-sheet self-assembly in aqueous media to drive the formation of nanofibers. The electrochemical properties of viologens, as described before in Chapter 1 and Chapter 2, enable the formation of nanofibers with conductive properties. Such conductive nanofibers, with facile and controllable assembly in aqueous environments, have potential for future exploration in optoelectronic applications.

Nanofibers formation and optical characterisation

To investigate the self-assembly of AVI3D2, stock solutions were prepared at both high (8 mM) and low (1 mM) concentrations in basic aqueous media through sonication. Small volumes of HCl were then added to achieve a final solution of pH 4, triggering the protonation of the Asp residues and consequently, the self-assembly of the peptide. Aqueous solutions of both AVI3D2 and AV show a photoluminescence with a maxima between 500 nm to 510 nm and a Stokes shift of 180 nm to 190 nm (Figure 4.8 and Figures C.20 to C.23). The emission peak intensity and wavelength for these molecules was found to be dependent on pH. At the concentrations of 1 mM and 8 mM, the AV molecule displayed an increase in emission in acidic conditions (see Figures C.20 and C.21). This phenomena can be produced by counter ion exchange, with an iodide being replaced with a second chloride, or due to solvation effects, driven by the protonation of the carboxylic acid group on the terminus.[226] At the lower concentration of 1 mM, AVI3D2 has very little change in emission spectrum at different pH, with only a slight decrease in intensity observed in acidic conditions (see Figure C.22). In contrast, the emission intensity of AVI3D2 (8 mM) is quenched by 40 % and has a blue shift of 10 nm at pH 4 (Figure 4.8). The emission of photoluminescent molecules is known to

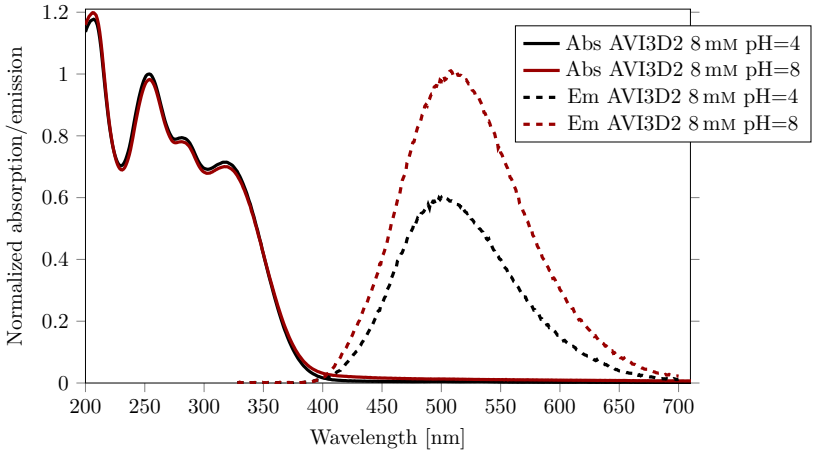

Fig. 4.8 Normalised steady-state photoluminescence spectra of AVI3D2 (8 mM) at different pH following excitation at 320 nm. Dotted lines represent absorbance of AVI3D2 (0.1 mM) at the corresponding pH.

be influenced by intermolecular stacking arrangements.[227] Photoinduced Electron Transfer (PET) can generate a quenching effect when donor and acceptor are in close proximity (on the sub-nanometer length scale) through hydrophobic and π-π stacking interactions.[227] Therefore, the emission spectra of AVI3D2 demonstrates that pH can be used to trigger the β-sheet assembly of the peptide and in turn invoke a hydrophobic/$\pi-\pi$ stacking of the AV portion of the molecule (Figure 4.7c).

To further investigate the supramolecular structure of the AVI3D2 molecule in its assembled state, spectroscopic techniques were utilised. In line with emission spectra, CD experiments confirmed the concentration and pH dependence of the self-assembly of AVI3D2 and the I3D2 peptide (Figures 4.9). At a concentration of 8 mM in acidic conditions, both AVI3D2 and the I3D2 peptide have spectra that resemble a β-sheet, with a minimum present at 216 nm to 220 nm (Figure 4.9 and Figure C.27). At 1 mM, both the AVI3D2 and I3D2 peptide have a CD signature of a typical random coil (Figures 4.9). This random coil to β-sheet transition can also be witnessed at the higher concentration of 8 mM through changes in pH. By simply altering the pH from 8 to 4, the CD spectra of both AVI3D2 and the I3D2 display a clear switch to a β-sheet signature (Figures 4.9). This highlights that the protonation of the Asp residues causes the β-sheet formation.

The CD spectra of β-sheets are known to have a greater variability than other peptide secondary structures.[228] β-Sheets have both significant intermolecular and intrastrand hydrogen bonding, and can form antiparallel, parallel, or mixed β-sheets.[228, 229] Interestingly, AVI3D2 and I3D2 have distinctly different β-sheet CD signals, with I3D2 having a 4 nm red-shift in minimum (220 nm) when compared to AVI3D2 (216 nm) (Figure C.27). Previous studies have suggested that a red-shift in the CD spectra of β-sheets is representative of more twisted and distorted arrangements.[225, 228, 230, 231] These observations suggest that the conjugation of the AV moiety at the N-terminus of the I3D2 peptide influences the β-sheet conformation and generates less twisted stacking arrangements, likely through additional hydrophobic/π-π interactions.

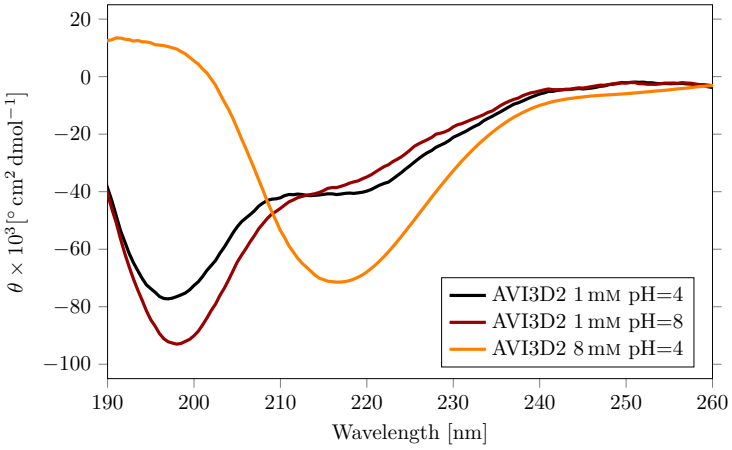

Fig. 4.9 Circular dichroism spectra of AVI3D2 at different pH and concentration.

This observation was further supported by the FTIR spectra showing a prominent peak at $\approx$1630 cm^{-1} known as vibration band of the amide I region (Figure 4.10), indicating a β-sheet conformation.[232, 233] Recently, it has been reported that Asp positioning can

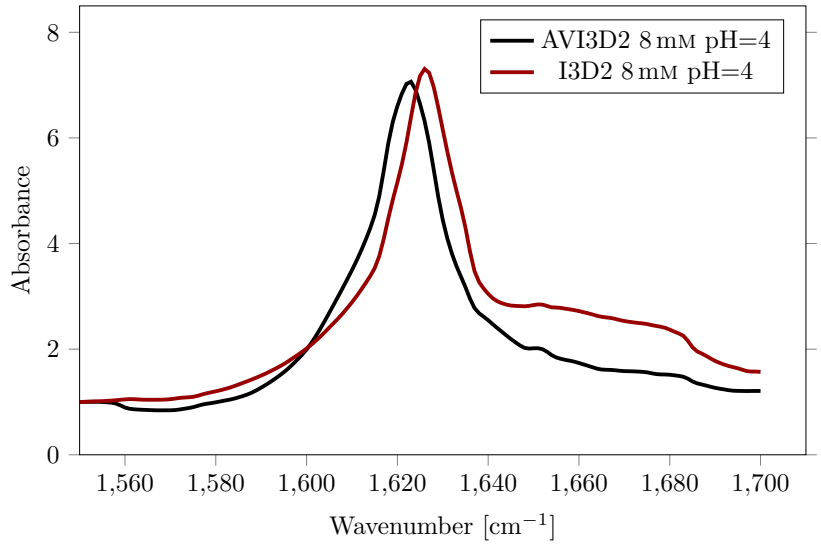

Fig. 4.10 FTIR spectra of AVI3D2 and I3D2 peptide at a concentration of 8 mM and pH 4.

influence the stacking orientation of tripeptide β-sheet structures, where Asp at the C-terminus was shown to generate a parallel β-sheet conformation.[234] Whilst it cannot be explicitly defined whether the AVI3D2 and I3D2 assemblies are in an antiparallel or a parallel orientation, the FTIR spectra for these sequences have no obvious antiparallel behavior, which is usually depicted by an amide I splitting between 1680 cm^{-1} to 1690 cm^{-1}.[233] Therefore, from the combination of PL and spectroscopic studies, it is concluded that both sequences form parallel β-sheets, where the planar AV region of the AVI3D2 sequence is stacked (Figure 4.7c).

Morphology and conductivity measurements

The morphology and conductive properties of the self-assembled AVI3D2 structures were characterised using conductive atomic force microscopy (c-AFM) operating in contact mode coupled with an ORCA^{TM} cantilever. At the higher concentration (8 mM), where spectroscopic studies indicated β-sheet formation, both AVI3D2 and the I3D2 peptide formed nanofibers (Figures 4.11a and 4.11b). However at 1 mM, the I3D2 peptide and AVI3D2 conjugate formed amorphous aggregates, likely driven by drying effects (see Figure C.29a).

Using the ORCA^{TM} module, the conductive properties of the different materials were probed. This technique allows for conductivity (IV) curve measurements to be taken at specific locations on the substrate. The AVI3D2 materials displayed a non-linear IV curve, typical for that of an organic semiconductor, whereas the I3D2 fibers and aggregates had no apparent conductivity (Figures 4.11c, 4.11d and Figure C.29c). Interestingly, the IV curves indicated an enhanced conductivity in the AVI3D2 nanofibers (8 mM) when compared to

the AVI3D2 amorphous aggregates (1 mM) (Figures 4.11c, 4.11d and Figure C.28c). This is further supported by the short-circuit current map of the AVI3D2 nanofibers (Figure 4.11a, ii) and the points corresponding to where the IV curves were taken (Figures 4.11c and 4.11d). Thicker fibers/denser regions appear to be of a darker contrast, suggesting an increased conductivity, and this also correlates with the IV curves taken at points 1 and 2. This, demonstrates that the β-sheet and supramolecular stacking in the nanofibers improved conductivity over the amorphous structures for the AVI3D2 materials.

Viologens in their neutral or radical cation state are considered to have a higher conductivity than their dication form.[106, 114] However, as a dication, charge transfer is permitted with a donor species (neutral or anionic) and consequently, conductivity is improved.[112, 235] The viologen's aryl-group functionalization is known to improve intramolecular electron transfer. It acts as an electron donor with the electron-poor viologen as an acceptor, generating an enhancement in single molecule conductivity.[111, 152] With the application of charge, the dication viologen species will be reduced to either a radical cation or a neutral species through electron donation from the donor-acceptor pair. This will produce a mixed valency/redox distribution throughout the assembly. In a solid state, mixed-valency viologen systems are known to have a high conductivity due to an electron hopping mechanism from viologen to viologen in different redox states.[236–238] The spectroscopic studies performed for this system suggest that the AV moieties are in close proximity and therefore, supposedly here a similar mechanism where electron transfer (hopping) from viologen to viologen can be permitted along the nanofiber's supramolecular stack. Similarly, previous studies of nanofibrillar structures demonstrated that $\pi - \pi$ stacking of conductive molecules can facilitate charge separation and allow for electron and hole transport through intermolecular π-electron delocalisation.[205, 206]

The directional organisation present in the assembled AVI3D2 nanofibers is likely to produce a variation in charge carrier mobility along the different axes of the nanofibers. As previously mentioned, the thicker fibers/denser regions appear to have an increased conductivity, for example at $-10\,\mathrm{V}$ point 2 is seven times larger than current at point 1 (Figures 4.11c and 4.11d). This could be a result of fiber orientation and charge carrier mobility, although this is difficult to determine from the AFM topography maps. It is also difficult to deduce the quality and orientation of contact between the fibers and substrate. With c-AFM being a contact-based measurement, differences in contact are likely to generate large variations in the conductivity curve measurements.

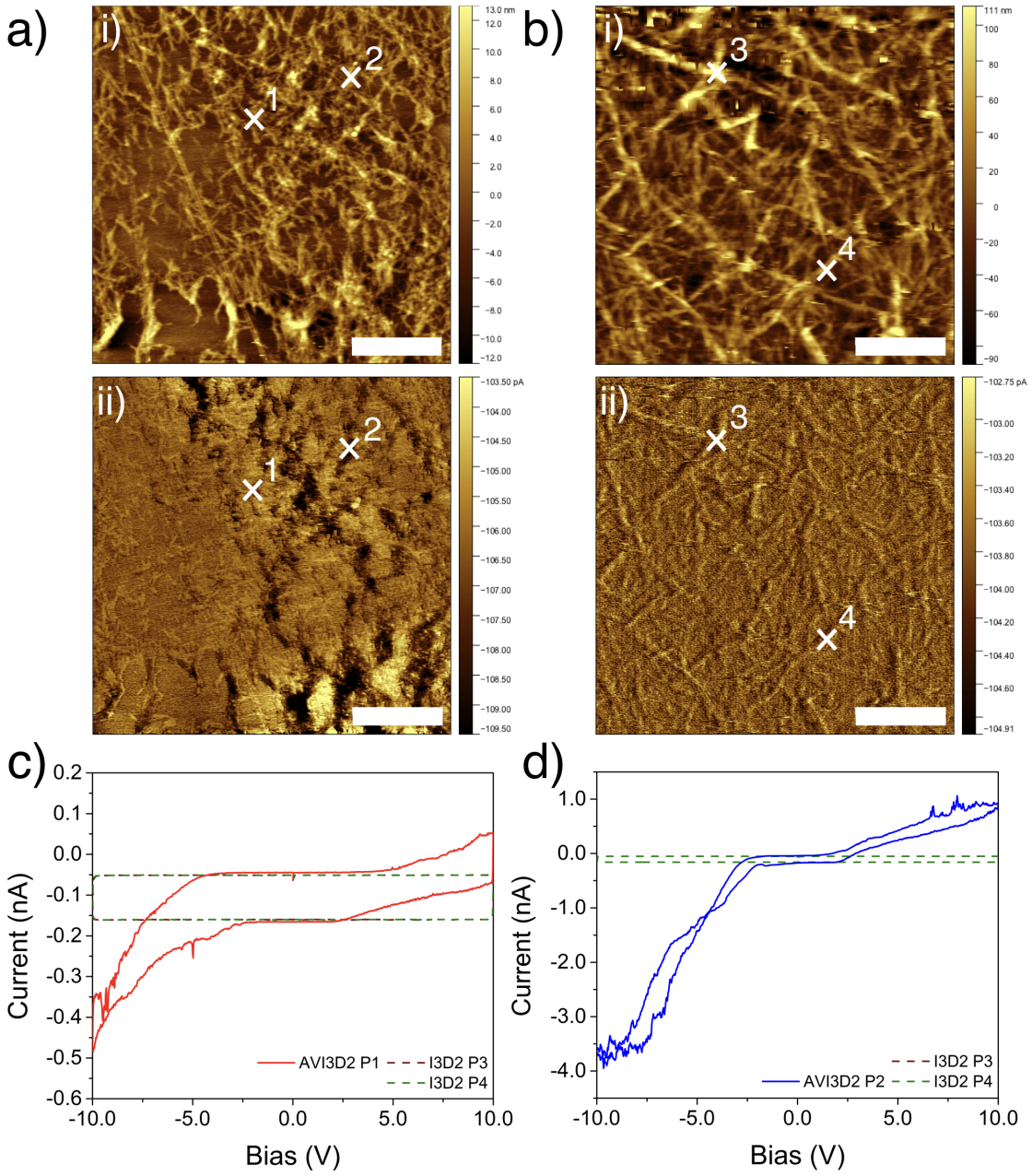

Fig. 4.11 c-AFM measurements of AVI3D2 and I3D2 at a concentration of 8 mM. a) Topography map (i) and short-circuit current map of AVI3D2 nanofibers (ii). b) Topography map (i) and short-circuit current map of I3D2 nanofibers (ii). Conductivity curves for AVI3D2 at point 1 (c) and point 2 (d), demonstrating conductive nature of the AVI3D2 nanofibers. Scale bar on all images is 5 µm.

4.2.5 Conclusion

In conclusion, this chapter demonstrated the synthesis of asymmetric aryl and extended aryl viologens *via* Zinke reaction. By changing the reactivity of single activated extended viologens, through incorporation of the bridging unit between the two pyridines, the second N-aromatic activation was achieved. It was shown that electron donating and electron withdrawing asymmetric N-aromatic functionalisation can be accessed following step-wise Zinke reaction. This work provides an accessible way to synthesise functional molecules, donor-acceptor, π-conjugated dyes whose optoelectronic properties are optimised through molecular modifications, external stimuli and supramolecular interaction.

Here, the ability to reversibly manipulate the complexation and optical performance of a EV[Np](OMe)(EtCOOH) dye to CB[8] by control of pH of the solution was studied. Investigation of the NMR features, revealed that regardless of a side functionality, the Np based asymmetric molecule still shows 2:2 complexation with CB[8] that provides red shifts in absorption, high molar absorption coefficient and strong emission with quantum yield of nearly 75 %. Such properties are promising for the development of a new generation of supramolecular dyes. The ability to incorporate anchoring groups (e.g carboxylic acid), makes it possible to use extended aryl viologen dyes as labels.[239]

Furthermore, in this chapter the AV labelled pentapeptide sequence, which can form conductive nanofibers through pH triggered β-sheet assembly was presented. C-AFM measurements identified the semi-conductive behaviour of the nanofibers and that the nanofiber morphology has an enhanced conductivity when compared to amorphous aggregates. The high conductivity of these nanofibers results from viologen reduction, followed by electron transport (hopping) between viologens along the supramolecular stack. These conductive nanofibers with facile and controllable assembly in aqueous environments have potential for future application in optoelectronics.

4.3 Experimental

4.3.1 Instrumentation and Materials

Materials All the materials as following were purchased from commercial suppliers and used without further purification: Pyridin-4-ylboronic acid (97%, Fisher Scientific), 1,4-Dibromonaphthalene (>98%, Acros Organics), Tetrakis(triphenylphosphine) palladium(0) (99.8% (metals basis), Pd 9% min, Alfa Aesar), ethanol (absolute, Fisher Scientific), acetonitrile (REAG. PH EUR, Merck Millipore), diethyl ether (>99%, Aldrich), 4,4-bipyridine, p-Toluidine (>99 %, Alfa Aesar), p-Anisidine (>99 %, Sigma-Aldrich), 1-chloro-2,4-dinitrobenzene

(≥99%, CAS: 97-00-7), 4-Nitroaniline (≥99%, Sigma Aldrich), 4-(4-Aminophenyl)butyric acid (95%), methyl iodide (≥99.0%). CB[8] was synthesised according to the published procedure.[43] All Fmoc-protected amino acids, solvents and rink amide 4-methyl-benzhydrylamine (MBHA) resin used for peptide synthesis were purchased from AGTC Bioproducts (UK).

Nuclear Magnetic Resonance Spectroscopy (NMR). ^{1}H NMR spectra were acquired in deuterium oxide (D_2O) at 298 K, and recorded on a Bruker AVANCE 500 with TCI Cryoprobe Spectrometer (500 MHz) being controlled by TopSpin2. ^{13}C NMR (126 MHz) spectra were acquired in deuterium oxide (D_2O), and recorded on a Bruker AVANCE III QNP Cryoprobe with external reference TMS set to 0 ppm. Titrations were performed by using stock solutions of host and guest calibrated against the concentrated solution of 3-(Trimethylsilyl)-1-propanesulfonic acid sodium salt. ^{1}H NMR, ^{13}C NMR and DOSY spectra of peptide based samples were acquired in either D_2O or D_2O doped with K_2CO_3 at 298 K.

UV – Vis Spectroscopy UV – Vis spectra were recorded on a Varian Cary 400 UV – Vis spectrophotometer using a Suprasil Quartz (QS) cuvette with 1 cm path length at 298 K. EV or EV-CB[8] aqueous solutions were tested in the concentration of 0.01 mM.

Fluorescence Spectroscopy Fluorescence spectroscopy of EV based molecules was recorded on an Agilent Varian Cary Eclipse fluorescence spectrophotometer using a Suprasil Quartz (QS) cuvette with 1 cm path length at 298 K. The fluorescence of the AVI3D2 conjugate was recorded using a 120 µL quartz three-window fluorescence cuvette. Peptide-based samples were excited at 320 nm with a 5 nm excitation/emission slit.

Time-Correlated Single Photon Counting Time-resolved fluorescence was recorded using a FS5 Spectrofluorometer, Edinburgh Instrument. A TCSPC laser (360 nm) was used for fluorescence lifetime measurements at peak emission wavelength for measured molecules and complexes. A Suprasil Quartz (QS) cuvette with 1 cm path length was used for all measurements. The data was fit with the exponential reconvolution function and the non-linear least square method.

Fluorescence Quantum Yield Measurements The absolute fluorescence quantum yield was determined using an Edinburgh Instruments Integrating Sphere Module (SC-30) on a spectrofluorometer. Fluorescence spectra analysis software Fluoracle and Quantum Yield Wizard were used to obtain quantum yields.

High Pressure Liquid Chromatography (HPLC) HPLC was performed on Varian HPLC - Agilent using a Phenomenex C18 Kinetic-Evo column with a 5 micron pore size, a 110 particle size and with the dimensions 150 x 21.2 mm. A gradient from 5% acetonitrile 95% water to 100% acetonitrile was applied.

HPLC-LCMS HPLC-LCMS was performed on Waters ZQ with Waters 2795, with 50 x 4.6 mm C18 column (Phenomenex Kinetix solid core column), using acetonitryle:water (1:1) as a mobile phase.

Circular Dichroism (CD) Circular Dichroism measurements were carried out in the far-UV on a Chirascan spectrometer (Applied Photophysics). All scans were performed at 295 KK from 180 nm to 260 nm at 0.5 nm intervals with an acquisition time of 1 s and using a 0.1 mm path length quartz plate cuvette. The spectra collected was averaged across two scans and corrected via background subtraction.

Fourier Transform Infrared Spectroscopy (FTIR) Fourier transform infra-red (FT-IR) spectroscopy was carried out using a Perkin-Elmer Spectrum 100 FT-IR Spectrometer in the amide I region (1550 cm^{-1} to 1700 cm^{-1}) at a resolution of 1 cm^{-1} and averaged from 16 consecutive scans. The solutions were lyophilized, and the resultant dried material used for analysis. All the spectra were normalized to the absorbance at 1550 cm^{-1}, which is assumed to be insensitive to peptide secondary structure.

Conductive Atomic Force Microscopy (c-AFM) Conductive Atomic Force Microscopy was utilised to investigate the morphology and conductive properties of the different materials. All samples were prepared by pipetting 5 µL of a stock solution onto a gold substrate and spread using a N_2 jet to obtain a thin layer. They were then left to dry overnight under vacuum. All measurements were carried out on a MFP-3D AFM System (Asylum/Oxford Instruments) operating in contact mode coupled with an ORCA^{TM} module and a PtIr coated SCM-PIC tip (Bruker) with nominal spring constant of 0.2 $N\,m^{-1}$. Images were produced using a gain of 5×10^8 $V\,A^{-1}$ and a -4.0 V bias. The system's NPS™ nano-positioning closed loop sensors and "pick a point" force curve interface was used to positioned the cantilever at a point of interest on the map. The bias voltage was then swept from -10.0 V to 10.0 V and the response current measured. The conductivity (IV) data was averaged across 4 scans.

4.3.2 Synthetic Protocols

EV[Np] was synthesised with the procedure described in Chapter 2.

1-(2,4-Dinitrophenyl)-4-(4-(pyridin-4-yl)naphthalen-1-yl)pyridin-1-ium) chloride EV[Np]DNB$_{asym}$

^{1}H NMR (500 MHz, D_2O) δ (ppm): 9.36 (d, J = 2.5 Hz, 1H), 9.20 (d, J = 6.8 Hz, 2H), 8.92 – 8.87 (m, 3H), 8.53 (d, J = 6.8 Hz, 2H), 8.29 – 8.24 (m, 3H), 8.06 (d, J = 8.8 Hz, 1H), 7.94 (d, J = 8.9 Hz, 1H), 7.89 (d, J = 7.4 Hz, 1H), 7.79 (d, J = 7.4 Hz, 1H), 7.75 – 7.66 (m, 2H). **^{13}C NMR** (126 MHz, D_2O) δ (ppm): 145.11, 144.03, 143.98, 131.24, 130.97, 130.61, 129.21, 129.08, 129.06, 128.73, 128.63, 128.52, 128.20, 127.72, 127.68, 125.24, 125.13, 125.00, 123.72, 122.74, 20.47, 20.30, 13.20. **MS** ESI-MS: m/z [M]+ calc for $C_{26}H_{17}N_4O_4$:449.1244, found: 449.1239

4-(4-(Pyridin-4-yl)naphthalen-1-yl)-1-(p-tolyl)pyridin-1-ium) chloride EV[Np]Me$_{asym}$

^{1}H NMR (500 MHz, D_2O) δ (ppm): 9.02 (d, J = 6.5 Hz, 2H), 8.58 (d, J = 5.3 Hz, 2H), 8.27 (d, J = 6.4 Hz, 2H), 8.03 – 7.88 (m, 2H), 7.79 – 7.35 (m, 10H), 2.42 (s, 3H). **MS** ESI-MS: m/z [M]+ calc for $C_{27}H_{21}N_2$: 373.1699, found: 373.1696

4,4'-(naphthalene-1,4-diyl)bis(1-phenylpyridin-1-ium) dichloride - EV[Np]OMeDNB

^{1}H NMR (500 MHz, D_2O) δ (ppm): 9.36 (d, J = 2.6 Hz, 1H), 9.21 (d, J = 6.5 Hz, 2H), 9.14 (d, J = 6.5 Hz, 2H), 8.91 (d, J = 8.5 Hz, 1H), 8.55 (d, J = 6.0 Hz, 2H), 8.39 (d, J = 6.5 Hz, 2H), 8.27 (d, J = 8.7 Hz, 1H), 8.05 (dd, J = 23.3, 8.8 Hz, 2H), 7.95 – 7.82 (m, 2H), 7.74 (d, J = 8.6 Hz, 4H), 7.25 (d, J = 8.8 Hz, 2H), 3.90 (s, 3H). **MS** ESI-MS: m/z [M]2+ calc for $C_{33}H_{24}N_4O_5$: 278.0868, found: 278.0865

1-(2,4-dinitrophenyl)-4-(4-(1-(p-tolyl)pyridin-1-ium-4-yl)naphthalen-1-yl)pyridin-1-ium) dichloride - EV[Np]MeDNB

^{1}H NMR (500 MHz, D_2O) δ (ppm): 9.34 (d, J = 2.5 Hz, 1H), 9.21 – 9.10 (m, 4H), 8.88 (dd, J = 8.7, 2.5 Hz, 1H), 8.56 – 8.49 (m, 2H), 8.41 – 8.34 (m, 2H), 8.24 (d, J = 8.7 Hz, 1H), 8.09 – 8.03 (m, 1H), 7.99 (ddd, J = 6.3, 4.4, 2.6 Hz, 1H), 7.89 (d, J = 7.4 Hz, 1H), 7.84 (d, J = 7.4 Hz, 1H), 7.74 – 7.68 (m, 2H), 7.66 – 7.59 (m, 2H), 7.54 – 7.48 (m, 2H), 2.42 (s,

3H). **^{13}C NMR** (126 MHz, D_2O) δ (ppm): 163.10, 162.82, 160.38, 157.43, 149.64, 145.11, 144.03, 143.98, 143.04, 142.68, 140.09, 138.58, 137.04, 136.06, 131.24, 130.97, 130.61, 130.21, 130.01, 129.21, 129.08, 128.73, 128.63, 128.20, 127.68, 125.24, 125.00, 123.72, 122.74, 119.78, 117.46, 115.14, 112.82, 61.69, 20.47, 20.30, **MS** ESI-MS: m/z [M]2+ calc for $C_{33}H_{24}N_4O_4$: 270.0893, found: 270.0891

1-(4-nitrophenyl)-4-(4-(1-(p-tolyl)pyridin-1-ium-4-yl)naphthalen-1-yl)pyridin-1-ium) dichloride - EV[Np]MeNO$_2$

^{1}H NMR (500 MHz, D_2O) δ (ppm): 9.29 (d, J = 6.8 Hz, 2H), 9.17 (d, J = 6.7 Hz, 2H), 8.65 – 8.39 (m, 6H), 8.15 – 7.97 (m, 4H), 7.94 – 7.84 (m, 2H), 7.81 – 7.64 (m, 4H), 7.55 (d, J = 8.2 Hz, 2H), 2.45 (s, 3H). **MS** ESI-MS: m/z [M]2+ calc for $C_{33}H_{25}N_3O_2$: 247.5968, found: 247.5968

4,4'-(Naphthalene-1,4-diyl)bis(1-phenylpyridin-1-ium) dichloride - EV[Np]OMe(CH$_2$)$_2$COOH

^{1}H NMR (500 MHz, D_2O) δ (ppm): 9.15 (dd, J = 17.5, 6.5 Hz, 4H), 8.39 (dd, J = 6.7, 5.0 Hz, 4H), 8.06 – 7.96 (m, 2H), 7.84 (s, 2H), 7.78 – 7.65 (m, 6H), 7.56 (d, J = 8.3 Hz, 2H), 7.25 (d, J = 8.6 Hz, 2H), 3.90 (s, 3H), 2.99 (t, J = 7.4 Hz, 2H), 2.53 (t, J = 7.4 Hz, 2H) **MS** ESI-MS: m/z [M-H]+ calc for $C_{36}H_{30}N_2O_3$: 537.2184, found: 537.2186

1-(2,4-Dinitrophenyl)-[4,4'-bipyridin]-1-ium) chloride

4,4-Bipyridine (10 g, 64 mmol) and 1-chloro-2,4-dinitrobenzene (13 g, 64 mmol) were refluxed in ethanol (250 mL) for 24 h under the protection of N_2 gas. After cooling to room temperature, the mixture was concentrated to ca. 30 mL and precipitated by adding diethyl ether (6050 mL). After standing for 1 h, the precipitate was collected by suction filtration and washed with diethyl ether. After being dried in a vacuum-oven at 60 °C, a yellow solid of (mg) was obtained in 80% yield.

^{1}H NMR (400 MHz, D_2O) δ (ppm): 9.33 (d, J = 2.4 Hz, 1H), 9.18 (d, J = 6.5 Hz, 2H), 8.91-8.86 (m, 1H), 8.77 (d, J = 5.7 Hz, 2H), 8.61 (d, J = 6.5 Hz, 2H), 8.20 (d, J =8.7 Hz, 1H)., 8.00-7.93 (m, 2H). **MS** ESI-MS: m/z [M]+ calcd for $C_{16}H_{11}N_4O_4$: 323.0775, found: 323.0775

1-(4-(4-Carboxybutyl)phenyl)-1'-methyl-[4,4'-bipyridine]-1,1'-diium

1-(2,4-dinitrophenyl)-[4,4'-bipyridin]-1-ium (2 g, 5.57 mmol), 4-(4-Aminophenyl)butyric acid (3 g, 16.72 mmol) and catalytic amount of trimethylamine were refluxed in ethanol (250 mL) overnight under the protection of N_2 gas. After cooling to room temperature, the mixture was concentrated to ca. 30 mL and precipitated by adding diethyl ether (600 mL). After standing for 1 h, the precipitate was collected by suction filtration and washed with diethyl ether. Obtained 1-(4-(3-carboxypropyl)phenyl)-[4,4'-bipyridin]-1-ium (1 g, 2.81 mmol) and methyl iodide (396 mg, 174 µL, 2.81 mmol) were refluxed in ethanol (100 mL) overnight under the protection of N_2 gas. After cooling to room temperature, the mixture was concentrated to ca. 30 mL and precipitated by adding diethyl ether, the precipitate was collected by suction filtration and washed with diethyl ether. After being dried in a vacuum-oven at 60 °C, a brown solid of 1-(4-(4-carboxybutyl)phenyl)-1'-methyl-[4,4'-bipyridine]-1,1'-dium 700 mg) was obtained in 49.8% yield.

^{1}H NMR (400 MHz, D_2O) δ (ppm): 9.31-9.24 (m, 2H), 9.01 (d, J = 6.6 Hz, 2H), 8.66-8.59 (m, 2H), 8.52 (d, J = 6.6 Hz, 2H), 7.70-7.62 (m, 2H), 7.55 (d, J = 8.6 Hz, 2H), 4.45 (s, 3H), 2.77 (t, J = 7.5 Hz, 2H), 2.34 (t, J = 7.3 Hz, 2H), 1.94 (p, J = 7.5 Hz, 2H) **^{13}C NMR** (125 MHz, D_2O) δ (ppm): 150.49, 149.63, 146.33, 145.25, 140.30, 130.65, 126.86, 126.72, 123.90, 48.36, 33.91, 33.50, 25.81. **MS** ESI-MS: m/z [M-2Cl]2+ calcd for $C_{21}H_{22}N_2O_2$: 167.0835, found: 167.0833

1-(p-Tolyl)-[4,4'-bipyridin]-1-ium

^{1}H NMR (400 MHz, D_2O) δ (ppm): 9.11 (d, 2H, 4 Hz), 8.72(d, 2H, 4 Hz), 8.48(d, 2H, 8Hz), 7.90(d, 2H, 4 Hz), 7.60(d, 2H, 8 Hz), 7.50(d, 2H, 8 Hz), 2.41(s, 3H **^{13}C NMR** (125 MHz, D_2O) δ (ppm): 154.21, 150.03, 144.60, 142.71, 142.38, 139.86, 130.97, 125.92, 123.63, 122.56, 20.31 **MS** ESI-MS (M^+): found 247.12; **Mp.**: 275.8 °C,

1-Phenyl-[4,4'-bipyridin]-1-ium chloride

^{1}H NMR (400 MHz, D_2O) δ (ppm):9.16(d, 2H, 8 Hz), 8.75(d, 2H, 8Hz), 8.51(d, 2H, 4 Hz), 7.93(d, 2H, 8 Hz), 7.71(m, 5H, 4 Hz) ppm; **^{13}C NMR** (125 MHz, D_2O) δ (ppm): 154.62, 150.02, 144.71, 142.40, 142.26, 131.62, 130.50, 125.94, 123.95, 122.54 ppm; **MS** ESI-MS (M^+): found 233.10; **Mp.**: 217.4 °C,

1-(2,4-Dinitrophenyl)-1'-(p-tolyl)-[4,4'-bipyridine]-1,1'-dium

A solution of 1-(p-tolyl)-[4,4'-bipyridin]-1-ium (202 mg, 0.817 mmol) and 2,4-dinitrophenyl 4-methylbenzenesulfonate (1.38 g, 4.08 mmol) were mixed in 6 mL of DMF. Small sample of a reacting mixture were taken after every 24 h, mixed with an excess of toluene, and allowing to precipitated in 2 °C, for 2 h. Then, centrifuged for 5 min at 8000 rpm, and separated precipitant was dried under vacuum. The product was dissolved in 1:1 mixture acetonitrile:water and HPLC-MS was carried out. ESI-MS (M^{2+}): found 207.4

Synthesis and characterisation of I3D2 peptide and AVI3D2 conjugate

An initial batch of the I3D2 peptide sequence was synthesised using solid-phase methodology (FMOC, tBu, MBHA resin) on an automated microwave peptide synthesizer (Liberty, CEM). Following the automated synthesis, a manual coupling step was used to fabricate the AVI3D2 conjugate material. 0.25 mmol of I3D2 labelled resin was reacted with 2 equivalence of the synthesised AV, along with 2.5 equivalence of both HCTU and DIPEA in DMF and shaken overnight. Both the crude I3D2 peptide and AVI3D2 conjugate were cleaved from the resin with a cleavage cocktail of 0.1% trifluoroacetic acid (TFA), 2.5% triisopropyl silane and 2.5% DI H_2O and left to shake for 2.5 h. Following cleavage, the crude peptides were precipitated and washed with cold diethyl ether, then left to dry under vacuum overnight.

The crude peptides were then purified by high pressure liquid chromatography (HPLC). A gradient from 5% acetonitrile 95% water to 100% acetonitrile was run, the I3D2 peptide was purified in basic conditions (0.1% ammonium hydroxide and 20 mM ammonium formate) and the AVI3D2 conjugate material in acidic conditions (0.1% TFA).

4.4 Acknowledgements

Dr. David Clarke is acknowledge for the synthesis of pentapeptide, CD as well as FTIR measurements and analysis. Dr. Tobias Mönch is acknowledge for help in conducting c-AFM. Dr. Guanglu Wu is acknowledge for his help in conducting 500 NMR CB[8] titration experiments.

Chapter 5

Summary and Outlook

The degree of control over inter-and intramolecular interactions given by both chemical synthesis of molecular building blocks and their rational supramolecular organisation plays a crucial role in the development of new functional molecules and materials. This PhD thesis describes the design, synthesis and characterisation of new families of π- extended viologen-based molecules and their supramolecular interactions with CB[7] and CB[8] macrocycles.

Chapter 2 focuses on the synthesis and characterisation of structure and physicochemical properties of aromatic and heteroaromatic extended methyl viologens (EV[X]MVs, where [X]= phenylene [Ph], naphthalene [Np], pyrene [Pyr], chrysene [CH], thiophene [Th] and dithiophene [DTh]) as well as their supramolecular complexes formed upon encapsulation within CB[7] and CB[8] macrocycles. NMR and ITC experiments on the assembly process of the EV[X]MVs with CB[7] and CB[8] showed that extended methyl viologens exhibit different binding modes depending on type of bridging unit [X] and the applied macrocycle. EV[X]MVs with X= [Np], [$Pyr_{1,6}$], [$Pyr_{2,7}$] and [CH], bound with CB[8] in 1:1 manner (EV[X]MV:CB[8]), while [Ph] and [Th] extensions were found to bind with CB[8] in 1:2 manner (EV[X]MV:$CB[8]_2$). The latter systems led to the unique charge accumulative properties, which were expressed by four different redox processes observed in CV experiments. Such behaviour of the supramolecular systems suggests the formation of a through-space mixed-valence structures, which redox properties are dependent on the controllable redox states of the particular molecule and as a consequence the different manner of complexation within the CB[8] macrocycle. In contrast, all of the studied EV[X]MVs bound with CB[7] in 1:1 manner.

Steady-state UV – Vis and photoluminescence (PL) spectroscopy of EV[X]MVs showed that modification of the bridging unit allows for the tunability of their optical properties both in their free form as well as complex with CB[7] and CB[8]. For example, encapsulation

of these molecules within the cavity of macrocycles led to the enhancement of the PL quantum yield of the resultant complexes. The family of presented EV[X]MV molecules is characterised by excitation wavelength maximum in the range of 317-452 nm and emission maximum from 372 to 545 nm with Stokes shifts as high as 219 nm. Such properties along with high quantum yields up to 90% make EV[X]MVs and their complexes with CB[n] macrocycles highly attractive for the use as fluorophores and labelling dyes.

Controlled formation of homo- and heteroquaternary dimeric complexes of extended aryl viologens and CB[8] is described in Chapter 3. In this part of work, a new family of extended aryl viologens (EV[X]R) is designed and synthesised through a modular strategy enabling the incorporation of a wide range of chromophores through generic synthetic coupling approaches. EV[X]Rs consist of both optically tunable π-bridging units between charged pyridiniums ([X]= [Ph], [Np], [Pyr], [CH], [Th], [DTh]), and optically tunable molecular recognition units (R= phenyl moiety, functionalised with electron donating or electron withdrawing groups). The interactions of EV[X]Rs with CB[7] and CB[8] macrocycles were investigated. The EV[X]R with electron donating R substitution showed 2:2 type host-guest complexation with CB[8], whereas electron withdrawing functionalisation resulted in 1:1 binding mode. These results demonstrated, that on account of the unique property of CB[8] to bind two guest simultaneously and the rational selection of aromatic substitution of pyridine in EV[X]Rs, the formation of quaternary dimeric complexes was achieved. ITC and NMR experiments performed for the CB[7] encapsulation of extended aryl viologens, showed formation of 2:1 host guest complexes.

Subsequently, the effect of encapsulation on the EV[X]R spectroscopic properties was investigated. Steady-state UV – Vis and PL spectroscopy, PL quantum yield, lifetime measurements as well as time-resolved spectroscopy were used to characterise the EV[X]R molecules as well as their corresponding complexes with CB[7] and CB[8]. With the possibility of tailoring the bridging unit in the EV[X]Rs molecules, the tunability of their optical properties was achieved. This new family of dyes based on EV[X]R exhibited an excitation wavelengths ranging from 343 nm up to 478 nm and emission wavelengths in the range of 420-611 nm. Upon mixing with CB[8], the difference of at least 20 nm in excitation wavelength was observed when comparing the unbound monomeric species to the CB[8]-based dimeric complex. This property is highly desirable for both biological labelling and fluorescence “turn-on-and-off” sensitive imaging probes.

To gain more insights into the dynamics of the excited states of the homoquaternary complexes, transient absorption spectroscopy was performed for selected EV[X]R and CB[8] systems. The effect of CB[8] on the extended lifetime of the triplet state for thiophene-based molecules was confirmed. The classical signatures of excimer-like structures were identify

for EV[Th]Me and EV[DTh]Me 2:2 complexes with CB[8]. These composites formed triplet state excimers which are stabilised by CT interaction. The EV[Ph]Me molecules upon mixing with CB[8] were considered to form a singlet excimer stabilised by CT and excition resonance, which was indicated by its transient absorption spectrum features. However, an explicit evidence could not be obtained to fully support this hypothesis. Similarly, the excimeric state could not be verified for the EV[Np]Me based complexes with CB[8].

In the final part of Chapter 3, the possibility of a pair-selective encapsulation of differently R-substituted extended aryl viologens inside the CB[8] cavity was explored. Here, the CB[8] macrocycle was used as a supramolecular 'glue' for two structurally different EV[Np]R and EV[Np]R' guests (where R and R' are electron donating functionalised phenyl moieties). The control over the statistical mixture based on size complementarity was achieved for heteroquaternary 2:2 complex of EV[Np]NMe_2 and EV[Np]H molecules. The studies on modulation of the absorption properties of formed mixed complexes were described.

Presented work on homo and heteroquaternary complexes is crucial for the fine-tuning of the optical properties of these emissive complexes. Insight and understanding of interchromophore interactions through molecular design can generate discrete dimeric structures with specific optical properties, such as aggregation induced emission, excimer-like excited state, and singlet fission.

In Chapter 4, the challenges of asymmetric N-aryl functionalisation of viologens are discussed. Here, the synthetic approach towards asymmetric not-extended aryl viologen (AV) and extended aryl viologen (EV[X]RR' (where [X]= naphthalene bridging unit and R= phenyl group functionalised with Me, OMe, NO_2, EtCOOH) is presented. Zincke reaction is a standard reaction used for aromatic functionalisation of pyridnes. In the case of viologens *i.e.* bipyridines, single activation of a first pyridine substantially changes the reactivity of the non-functionalised second pyridine. In Chapter 4, the systematic research on synthetic approach to overcome the low reactivity of asymmetric aryl viologens *via* the extension of the bridging unit between two pyridines is presented. Here, it was demonstrated that asymmetric extended aryl-aryl' viologens can be successfully synthesised for naphthalene extension, with EDG and EWG aromatic groups in N-position of bipyridine. The interactions with CB[8] and CB[7] as well as optical properties of asymmetric EV[Np](OMe)(EtCOOH) were studied. It was demonstrated that by changing the pH of the solution the type and dynamics of this molecule complexation with CB[8] as well as the optical properties can be controlled.

The potential application of the asymmetric viologens (AV) was explored. The presence of anchoring group (*i.e.* carboxylate moiety) in the structure of AV, provides the opportunity for conjugation to structures such as polymers or peptides. This approach, enables for doping those materials with functionalities of viologens such as redox activity, conductivity, optical

responsiveness and supramolecular assembly. The asymmetric aryl viologen functionalised with carboxylate group was connected to a pentapeptide. The resultant peptide-viologen hybrid exhibited high propensity to self-assembly forming nanofibers of substantial higher conductivity in comparison to that of the peptide alone. Further studies on conductive nanofibers could involve asymmetric extended aryl viologens given their higher electron densities and advanced control over their excitation and emission wavelengths, improvement of the fiber's optoelectronic properties can be achieved.

In summary, the presented research provides new comprehensive insights into design and synthesis of a variety of viologen derivatives, their supramolecular chemistry based on CB[n] complexation as well as their optical properties both in free as well as complexed form. The studied molecular and supramolecular systems are of interest to develop novel materials for molecular switches and machines, light-harvesting and charged accumulative systems, self reporting systems, fluorescence labelling as well as optoelectronic and nanophotonic devices.

Bibliography

[1] J. M. Lehn. “Dynamers: Dynamic molecular and supramolecular polymers”. In: *Aust. J. Chem.* 63.4 (2010), pp. 611–623. DOI: 10.1071/CH10035.

[2] E. V. Anslyn and D. Dougherty. *Modern Physical Chemistry*. University Science Book, 2006.

[3] C. A. Hunter and J. K. M. Sanders. “The nature of pi-pi interactions”. In: *J. Am. Chem. Soc.* 112.14 (1990), pp. 5525–5534. DOI: 10.1021/ja00170a016.

[4] E. M. Cabaleiro-Lago and J. Rodríguez-Otero. “σ-σ, σ-π, and π-π Stacking Interactions between Six-Membered Cyclic Systems. Dispersion Dominates and Electrostatics Commands”. In: *ChemistrySelect* 2.18 (2017), pp. 5157–5166. DOI: 10.1002/slct.201700671.

[5] F. C. Spano. “The spectral signatures of frenkel polarons in H- And J-aggregates”. In: *Acc. Chem. Res.* 43.3 (2010), pp. 429–439. DOI: 10.1021/ar900233v.

[6] N. J. Hestand and F. C. Spano. “Expanded Theory of H- and J-Molecular Aggregates: The Effects of Vibronic Coupling and Intermolecular Charge Transfer”. In: *Chem. Rev.* 118.15 (2018), pp. 7069–7163. DOI: 10.1021/acs.chemrev.7b00581.

[7] T. Förster. “Excimers”. In: *Angew. Chemie Int. Ed. English* 8.5 (May 1969), pp. 333–343. DOI: 10.1002/anie.196903331.

[8] O. P. Dimitriev, Y. P. Piryatinski, and Y. L. Slominskii. “Excimer Emission in J-Aggregates”. In: *J. Phys. Chem. Lett.* 9.9 (2018), pp. 2138–2143. DOI: 10.1021/acs.jpclett.8b00481.

[9] K. Cai, J. Xie, D. Zhang, W. Shi, Q. Yan, and D. Zhao. “Concurrent Cooperative J-Aggregates and Anticooperative H-Aggregates”. In: *J. Am. Chem. Soc.* 140.17 (2018), pp. 5764–5773. DOI: 10.1021/jacs.8b01463.

[10] A. Furube, M. Murai, Y. Tamaki, S. Watanabe, and R. Katoh. “Effect of aggregation on the excited-state electronic structure of perylene studied by transient absorption spectroscopy”. In: *J. Phys. Chem. A* 110.20 (2006), pp. 6465–6471. DOI: 10.1021/jp060649b.

[11] Guglielmo Lanzani. *The Photophysics behind Photovoltaics and Photonics*. Wiley-VCH Verlag & Co. KGaA, 2012.

[12] J. L. Bricks, Y. L. Slominskii, I. D. Panas, and A. P. Demchenko. “Fluorescent J-aggregates of cyanine dyes: Basic research and applications review”. In: *Methods Appl. Fluoresc.* 6.1 (2018), p. 12001. DOI: 10.1088/2050-6120/aa8d0d.

[13] S. Ghosh, X. Q. Li, V. Stepanenko, and F. Würthner. "Control of H- and J-type π stacking by peripheral alkyl chains and self-sorting phenomena in perylene bisimide homo- and heteroaggregates". In: *Chem. Eur. J.* 14.36 (2008), pp. 11343–11357. DOI: 10.1002/chem.200801454.

[14] J. B. Birks. "Excimers". In: *Reports Prog. Phys.* 38.8 (1975), pp. 903–974. DOI: 10.1088/0034-4885/38/8/001.

[15] K. Kasper. "Untersuchungen über Viskositätsabhängigkeit und Löschung der Fluoreszenz des Pyrens". In: *Zeitschrift für Phys. Chemie* 12 (1957), pp. 52–67. DOI: 10.1524/zpch.1957.12.1_2.052.

[16] T. Förster and K. Kasper. "Ein Konzentrationsumschlag der Fluoreszenz." In: *Zeitschrift für Phys. Chemie* 1 (1954), pp. 275–277. DOI: 10.1524/zpch.1954.1.5_6.275.

[17] K. R. Wang, Z. B. Yang, and X. L. Li. "High excimer-state emission of perylene bisimides and recognition of latent fingerprints". In: *Chem. Eur. J.* 21.15 (2015), pp. 5680–5684. DOI: 10.1002/chem.201406447.

[18] J. J. Han, A. D. Shaller, W. Wang, and A. D. Li. "Architecturally diverse nanostructured foldamers reveal insightful photoinduced single-molecule dynamics". In: *J. Am. Chem. Soc.* 130.22 (2008), pp. 6974–6982. DOI: 10.1021/ja078302p.

[19] F. Würthner, Z. Chen, V. Dehm, and V. Stepanenko. "One-dimensional luminescent nanoaggregates of perylene bisimides". In: *Chem. Commun.* 4.11 (2006), pp. 1188–1190. DOI: 10.1039/b517020f.

[20] T. Heek, C. Fasting, C. Rest, X. Zhang, F. Würthner, and R. Haag. "Highly fluorescent water-soluble polyglycerol-dendronized perylene bisimide dyes". In: *Chem. Commun.* 46.11 (2010), pp. 1884–1886. DOI: 10.1039/b923806a.

[21] X. Zhang, Z. Chen, and F. Würthner. "Morphology control of fluorescent nanoaggregates by co-self-assembly of wedge- and dumbbell-shaped amphophilic perylene bisimides". In: *J. Am. Chem. Soc.* 129.16 (2007), pp. 4886–4887. DOI: 10.1021/ja070994u.

[22] P. F. Jones and M. Nicol. "Excimer emission of naphthalene, anthracene, and phenanthrene crystals produced by very high pressures". In: *J. Chem. Phys.* 48.12 (1968), pp. 5440–5447. DOI: 10.1063/1.1668237.

[23] B. Z. Tang. "Are Excimers Emissive?" In: *ACS web page* https://www.acs.org (May 2016).

[24] C. B. Dover, J. K. Gallaher, L. Frazer, P. C. Tapping, A. J. Petty, M. J. Crossley, J. E. Anthony, T. W. Kee, and T. W. Schmidt. "Endothermic singlet fission is hindered by excimer formation". In: *Nat. Chem.* 10.3 (2018), pp. 305–310. DOI: 10.1038/nchem.2926.

[25] J. B. Birks. "Excimers and exciplexes". In: *Nature* 214.5094 (1967), pp. 1187–1190. DOI: 10.1038/2141187a0.

[26] J. Mohanty, S. D. Choudhury, H. P. Upadhyaya, A. C. Bhasikuttan, and H. Pal. "Control of the supramolecular excimer formation of thioflavin T within a cucurbit[8]uril host: A fluorescence on/off mechanism". In: *Chem. Eur. J.* 15.21 (2009), pp. 5215–5219. DOI: 10.1002/chem.200802686.

[27] S. Gadde, E. K. Batchelor, J. P. Weiss, Y. Ling, and A. E. Kaifer. "Control of H- and J-aggregate formation via host-guest complexation using cucurbituril hosts". In: *J. Am. Chem. Soc.* 130.50 (2008), pp. 17114–17119. DOI: 10.1021/ja807197c.

[28] A. Ueno, K. Takahashi, and T. Osa. "One host-two guests complexation between γ-cyclodextrin and sodium α-naphthylacetate as shown by excimer fluorescence". In: *J. Chem. Soc. Chem. Commun.* 19 (1980), pp. 921–922. DOI: 10.1039/C39800000921.

[29] A. Ueno, F. Moriwaki, T. Osa, F. Hamada, and K. Murai. "Association, Photodimerization, and Induced-Fit Types of Host-Guest Complexation of Anthracene-Appended γ-Cyclodextrin Derivatives". In: *J. Am. Chem. Soc.* 110.13 (1988), pp. 4323–4328. DOI: 10.1021/ja00221a036.

[30] S. R. McAlpine and M. A. Garcia-Garibay. "Studies of naphthyl-substituted β-cyclodextrins. Self-aggregation and inclusion of external guests". In: *J. Am. Chem. Soc.* 120.18 (1998), pp. 4269–4275. DOI: 10.1021/ja972810p.

[31] F. Winnik. "Photophysics of Preassociated Pyrenes in Aqueous Polymer Solutions and in Other Organized Media". In: *Chem. Rev.* 93.2 (1993), pp. 587–614. DOI: 10.1021/cr00018a001.

[32] K. Hayashi, Y. Miyaoka, Y. Ohishi, T.-a. Uchida, M. Iwamura, K. Nozaki, and M. Inouye. "Observation of Circularly Polarized Luminescence of the Excimer from Two Perylene Cores in the Form of [4]Rotaxane". In: *Chem. Eur. J.* 24.55 (2018), pp. 14613–14616. DOI: 10.1002/chem.201803215.

[33] A. L. L. East and E. C. Lim. "Naphthalene dimer: Electronic states, excimers, and triplet decay". In: *J. Chem. Phys.* 113.20 (2000), pp. 8981–8994. DOI: 10.1063/1.1319345.

[34] B. Nickel and M. F. R. Prieto. "Triplet Excimer Phosphorescence from Aromatic Compounds in Liquid Solutions: A Critical Review and New Negative Results". In: *Zeitschrift fur Phys. Chemie* 150.1 (1986), pp. 31–67. DOI: 10.1524/zpch.1986.150.1.031.

[35] E. A. Chandross and C. J. Dempster. "Excimer fluorescence and dimer phosphorescence from a naphthalene sandwich pair". In: *J. Am. Chem. Soc.* 92.3 (1970), pp. 704–706. DOI: 10.1021/ja00706a050.

[36] N. N. Barashkov, T. V. Sakhno, R. N. Nurmukhametov, and O. A. Khakhel'. "Excimers of organic molecules". In: *Russ. Chem. Rev.* 62.6 (1993), pp. 539–552. DOI: 10.1070/RC1993v062n06ABEH000032.

[37] J. B. Birks, M. Gordon, and W. R. Ware. *The Exciplex*. Elsevier, 1975. DOI: 10.1016/B978-0-12-290650-3.X5001-5.

[38] S. J. Barrow, S. Kasera, M. J. Rowland, J. Del Barrio, and O. A. Scherman. "Cucurbituril-Based Molecular Recognition". In: *Chem. Rev.* 115.22 (2015), pp. 12320–12406. DOI: 10.1021/acs.chemrev.5b00341.

[39] L. Isaacs, S. K. Park, S. Liu, Y. H. Ko, N. Selvapalam, Y. Kim, H. Kim, P. Y. Zavalij, G. H. Kim, H. S. Lee, and K. Kim. "The inverted cucurbit[n]uril family". In: *J. Am. Chem. Soc.* 127.51 (2005), pp. 18000–18001. DOI: 10.1021/ja056988k.

[40] R. Behrend, E. Meyer, and F. Rusche. "I. Ueber Condensationsproducte aus Glycoluril und Formaldehyd". In: *Justus Liebigs Ann. Chem.* 339.1 (1905), pp. 1–37. DOI: 10.1002/jlac.19053390102.

[41] W. L. Mock and N. Y. Shih. “Host-Guest Binding Capacity of Cucurbituril”. In: *J. Org. Chem.* 48.20 (1983), pp. 3618–3619. DOI: 10.1021/jo00168a069.

[42] W. A. Freeman, W. L. Mock, and N. Y. Shih. “Cucurbituril”. In: *J. Am. Chem. Soc.* 103.24 (1981), pp. 7367–7368. DOI: 10.1021/ja00414a070.

[43] A. Day, A. P. Arnold, R. J. Blanch, and B. Snushall. “Controlling factors in the synthesis of cucurbituril and its homologues”. In: *J. Org. Chem.* 66.24 (2001), pp. 8094–8100. DOI: 10.1021/jo015897c.

[44] J. Kim, I. S. Jung, S. Y. Kim, E. Lee, J. K. Kang, S. Sakamoto, K. Yamaguchi, and K. Kim. “New cucurbituril homologues: Syntheses, isolation, characterization, and X-ray crystal structures of cucurbit[n]uril (n = 5, 7, and 8)”. In: *J. Am. Chem. Soc.* 122.3 (2000), pp. 540–541. DOI: 10.1021/ja993376p.

[45] E. Masson, X. Ling, R. Joseph, L. Kyeremeh-Mensah, and X. Lu. “Cucurbituril chemistry: A tale of supramolecular success”. In: *RSC Adv.* 2.4 (2012), pp. 1213–1247. DOI: 10.1039/c1ra00768h.

[46] S. Moghaddam, C. Yang, M. Rekharsky, Y. H. Ko, K. Kim, Y. Inoue, and M. K. Gilson. “New ultrahigh affinity host-guest complexes of cucurbit[7]uril with bicyclo[2.2.2]octane and adamantane guests: Thermodynamic analysis and evaluation of M2 affinity calculations”. In: *J. Am. Chem. Soc.* 133.10 (2011), pp. 3570–3581. DOI: 10.1016/j.cmi.2015.05.032.

[47] J. Lagona, J. C. Fettinger, and L. Isaacs. “Cucurbit[n]uril analogues”. In: *Org. Lett.* 5.20 (2003), pp. 3745–3747. DOI: 10.1021/ol035468w.

[48] J. W. Lee, S. Samal, N. Selvapalam, H. J. Kim, and K. Kim. “Cucurbituril homologues and derivatives: New opportunities in supramolecular chemistry”. In: *Acc. Chem. Res.* 36.8 (2003), pp. 621–630. DOI: 10.1021/ar020254k.

[49] K. A. Kellersberger, J. D. Anderson, S. M. Ward, K. E. Krakowiak, and D. V. Dearden. “Encapsulation of N2, O2, methanol, or acetonitrile by decamethylcucurbit[5]uril(NH4+)2complexes in the gas phase: Influence of the guest on "lid" tightness [14]”. In: *J. Am. Chem. Soc.* 123.45 (2001), pp. 11316–11317. DOI: 10.1021/ja017031u.

[50] H. J. Buschmann, E. Cleve, and E. Schollmeyer. “Cucurbituril as a ligand for the complexation of cations in aqueous solutions”. In: *Inorganica Chim. Acta* 193.1 (1992), pp. 93–97. DOI: 10.1016/S0020-1693(00)83800-1.

[51] H. J. Buschmann, K. Jansen, and E. Schollmeyer. “Cucurbituril as host molecule for the complexation of aliphatic alcohols, acids and nitriles in aqueous solution”. In: *Thermochim. Acta* 346.1-2 (2000), pp. 33–36. DOI: 10.1016/S0040-6031(99)00407-4.

[52] M. E. Aliaga, L. García-Río, M. Pessêgo, R. Montecinos, D. Fuentealba, I. Uribe, M. Martín-Pastor, and O. García-Beltrán. “Host-guest interaction of coumarin-derivative dyes and cucurbit[7]uril: Leading to the formation of supramolecular ternary complexes with mercuric ions”. In: *New J. Chem.* 39.4 (2015), pp. 3084–3092. DOI: 10.1039/c5nj00162e.

[53] M. Baroncini, C. Gao, V. Carboni, A. Credi, E. Previtera, M. Semeraro, M. Venturi, and S. Silvi. "Light control of stoichiometry and motion in pseudorotaxanes comprising a cucurbit[7]uril wheel and an azobenzene-bipyridinium axle". In: *Chem. Eur. J.* 20.34 (2014), pp. 10737–10744. DOI: 10.1002/chem.201402821.

[54] F. Benyettou, K. Nchimi- Nono, M. Jouiad, Y. Lalatonne, I. Milosevic, L. Motte, J. C. Olsen, N. Saleh, and A. Trabolsi. "Viologen-templated arrays of cucurbit[7]uril-modified iron-oxide nanoparticles". In: *Chem. Eur. J.* 21.12 (2015), pp. 4607–4613. DOI: 10.1002/chem.201405774.

[55] K. J. Hartlieb, A. N. Basuray, C. Ke, A. A. Sarjeant, H. P. JacquotdeRouville, T. Kikuchi, R. S. Forgan, J. W. Kurutz, and J. F. Stoddart. "Chameleonic Binding of the Dimethyldiazaperopyrenium Dication by Cucurbit[8]uril". In: *Asian J. Org. Chem.* 2.3 (2013), pp. 225–229. DOI: 10.1002/ajoc.201200187.

[56] U. Rauwald, F. Biedermann, S. Deroo, C. V. Robinson, and O. A. Scherman. "Correlating solution binding and ESI-MS stabilities by incorporating solvation effects in a confined cucurbit[8]uril system". In: *J. Phys. Chem. B* 114.26 (2010), pp. 8606–8615. DOI: 10.1021/jp102933h.

[57] E. A. Appel, F. Biedermann, U. Rauwald, S. T. Jones, J. M. Zayed, and O. A. Scherman. "Supramolecular cross-linked networks via host-guest complexation with cucurbit[8]uril". In: *J. Am. Chem. Soc.* 132.40 (2010), pp. 14251–14260. DOI: 10.1021/ja106362w.

[58] E. A. Appel, R. A. Forster, M. J. Rowland, and O. A. Scherman. "The control of cargo release from physically crosslinked hydrogels by crosslink dynamics". In: *Biomaterials* 35.37 (2014), pp. 9897–9903. DOI: 10.1016/j.biomaterials.2014.08.001.

[59] A. A. Elbashir and H. Y. Aboul-Enein. "Supramolecular Analytical Application of Cucurbit[n]urils Using Fluorescence Spectroscopy". In: *Crit. Rev. Anal. Chem.* 45.1 (2015), pp. 52–61. DOI: 10.1080/10408347.2013.876354.

[60] S. Walker, R. Oun, F. J. McInnes, and N. J. Wheate. "The potential of cucurbit[n]urils in drug delivery". In: *Isr. J. Chem.* 51.5-6 (2011), pp. 616–624. DOI: 10.1002/ijch.201100033.

[61] M. Xu, S. P. Kelley, and T. E. Glass. "A Multi-Component Sensor System for Detection of Amphiphilic Compounds". In: *Angew. Chem. Int. Ed.* 57.39 (2018), pp. 12741–12744. DOI: 10.1002/anie.201807221.

[62] C. Márquez, R. R. Hudgins, and W. M. Nau. "Mechanism of Host-Guest Complexation by Cucurbituril". In: *J. Am. Chem. Soc.* 126.18 (2004), pp. 5806–5816. DOI: 10.1021/ja0319846.

[63] E. Persch, O. Dumele, and F. Diederich. "Molecular recognition in chemical and biological systems". In: *Angew. Chem. Int. Ed.* 54.11 (2015), pp. 3290–3327. DOI: 10.1002/anie.201408487.

[64] K. I. Assaf and W. M. Nau. "Cucurbiturils: From synthesis to high-affinity binding and catalysis". In: *Chem. Soc. Rev.* 44.2 (2015), pp. 394–418. DOI: 10.1039/c4cs00273c.

[65] F. Biedermann and W. M. Nau. "Noncovalent chirality sensing ensembles for the detection and reaction monitoring of amino acids, peptides, proteins, and aromatic drugs". In: *Angew. Chem. Int. Ed.* 53.22 (2014), pp. 5694–5699. DOI: 10.1002/anie.201400718.

[66] W. M. Nau, M. Florea, and K. I. Assaf. "Deep inside cucurbiturils: Physical properties and volumes of their inner cavity determine the hydrophobic driving force for host-guest complexation". In: *Isr. J. Chem.* 51.5-6 (2011), pp. 559–577. DOI: 10.1002/ijch.201100044.

[67] F. Biedermann, M. Vendruscolo, O. A. Scherman, A. De Simone, and W. M. Nau. "Cucurbit[8]uril and blue-box: High-energy water release overwhelms electrostatic interactions". In: *J. Am. Chem. Soc.* 135.39 (2013), pp. 14879–14888. DOI: 10.1021/ja407951x.

[68] G. Wu, M. Olesinska, Y. Wu, D. Matak-Vinkovic, and O. A. Scherman. "Mining 2:2 Complexes from 1:1 Stoichiometry: Formation of Cucurbit[8]uril-Diarylviologen Quaternary Complexes Favored by Electron-Donating Substituents". In: *J. Am. Chem. Soc.* 139.8 (2017), pp. 3202–3208. DOI: 10.1021/jacs.6b13074.

[69] H. J. Kim, J. Heo, W. S. Jeon, E. Lee, J. Kim, S. Sakamoto, K. Yamaguchi, and K. Kim. "Selective inclusion of a hetero-guest pair in a molecular host: formation". In: *Angew. Chem. Int. Ed.* 40.8 (2001), pp. 1526–1529. DOI: 10.1002/1521-3773(20010417)40.

[70] B. D. Wagner, S. J. Fitzpatrick, M. A. Gill, A. I. MacRae, and N. Stojanovic. "A fluorescent host-guest complex of cucurbituril in solution: a molecular Jack O'Lantern". In: *Can. J. Chem.* 79.7 (2001), pp. 1101–1104. DOI: 10.1139/cjc-79-7-1101.

[71] A. L. Koner and W. M. Nau. "Cucurbituril encapsulation of fluorescent dyes". In: *Supramol. Chem.* 19.1-2 (2007), pp. 55–66. DOI: 10.1080/10610270600910749.

[72] B. Valeur and M. N. Berberan-Santos. *Molecular Fluorescence: Principles and Applications, Second Edition*. Wiley-VCH Verlag GmbH & Co. KGaA, 2012. DOI: 10.1002/9783527650002.

[73] J. Chan, S. C. Dodani, and C. J. Chang. "Reaction-based small-molecule fluorescent probes for chemoselective bioimaging". In: *Nat. Chem.* 4.12 (2012), pp. 973–984. DOI: 10.1038/nchem.1500.

[74] J. Qu, C. Kohl, M. Pottek, and K. Müllen. "Ionic perylenetetracarboxdiimides: Highly fluorescent and water-soluble dyes for biolabeling". In: *Angew. Chem. Int. Ed.* 43.12 (2004), pp. 1528–1531. DOI: 10.1002/anie.200353208.

[75] M. A. Tarasov, V. D. Gromov, G. D. Bogomolov, E. A. Otto, and L. S. Kuzmin. "Fabrication and characteristics of mesh band-pass filters". In: *Instruments Exp. Tech.* 52.1 (2009), pp. 74–78. DOI: 10.1021/cr200213s.

[76] R. Bryaskova, N. I. Georgiev, S. M. Dimov, R. Tzoneva, C. Detrembleur, A. M. Asiri, K. A. Alamry, and V. B. Bojinov. "Novel nanosized water soluble fluorescent micelles with embedded perylene diimide fluorophores for potential biomedical applications: Cell permeability, localization and cytotoxicity". In: *Mater. Sci. Eng. C* 51 (2015), pp. 7–15. DOI: 10.1016/j.msec.2015.02.035.

[77] M. Florea and W. M. Nau. “Strong binding of hydrocarbons to cucurbituril probed by fluorescent dye displacement: A supramolecular gas-sensing ensemble”. In: *Angew. Chem. Int. Ed.* 50.40 (2011), pp. 9338–9342. DOI: 10.1002/anie.201104119.

[78] M. Fathalla, N. L. Strutt, J. C. Barnes, C. L. Stern, C. Ke, and J. F. Stoddart. “Fluorescence enhancement of a Porphyrin-Viologen dyad by pseudorotaxane formation with cucurbit[7]uril”. In: *European J. Org. Chem.* 2014.14 (2014), pp. 2873–2877. DOI: 10.1002/ejoc.201402018.

[79] M. A. Rankin and B. D. Wagner. “Fluorescence enhancement of curcumin upon inclusion into cucurbituril”. In: *Supramol. Chem.* 16.7 (2004), pp. 513–519. DOI: 10.1080/10610270412331283583.

[80] F. Biedermann, E. Elmalem, I. Ghosh, W. M. Nau, and O. A. Scherman. “Strongly fluorescent, switchable perylene bis(diimide) host-guest complexes with cucurbit[8]uril in water”. In: *Angew. Chem. Int. Ed.* 51.31 (2012), pp. 7739–7743. DOI: 10.1002/anie.201202385.

[81] C. C. Defilippo, H. Tang, L. Ravotto, G. Bergamini, P. Salice, M. Mba, P. Ceroni, E. Galoppini, and M. Maggini. “Synthesis and electronic properties of 1,2-hemisquarimines and their encapsulation in a cucurbit[7]uril host”. In: *Chem. Eur. J.* 20.21 (2014), pp. 6412–6420. DOI: 10.1002/chem.201400039.

[82] W. M. Nau and J. Mohanty. “Taming fluorescent dyes with cucurbituril”. In: *Int. J. Photoenergy* 7.3 (2005), pp. 133–141. DOI: 10.1155/S1110662X05000206.

[83] C. Marquez, F. Huang, and W. M. Nau. “Cucurbiturils: Molecular Nanocapsules for Time-Resolved Fluorescence-Based Assays”. In: *IEEE Trans. Nanobioscience* 3.1 (Mar. 2004), pp. 39–45. DOI: 10.1109/TNB.2004.824269.

[84] F. Biedermann, I. Ross, and O. A. Scherman. “Host-guest accelerated photodimerisation of anthracene-labeled macromolecules in water”. In: *Polym. Chem.* 5.18 (2014), pp. 5375–5382. DOI: 10.1039/c4py00627e.

[85] C. P. Carvalho, Z. Domínguez, J. P. Da Silva, and U. Pischel. “A supramolecular keypad lock”. In: *Chem. Commun.* 51.13 (2015), pp. 2698–2701. DOI: 10.1039/c4cc09336d.

[86] R. N. Dsouza, U. Pischel, and W. M. Nau. “Fluorescent Dyes and Their Supramolecular Host/Guest Complexes with Macrocycles in Aqueous Solution”. In: *Chem. Rev.* 111.12 (Dec. 2011), pp. 7941–7980. DOI: 10.1021/cr200213s.

[87] M. Freitag, L. Gundlach, P. Piotrowiak, and E. Galoppini. “Fluorescence enhancement of Di-p-tolyl viologen by complexation in cucurbit[7]uril”. In: *J. Am. Chem. Soc.* 134.7 (2012), pp. 3358–3366. DOI: 10.1021/ja206833z.

[88] L. Michaelis. “The Viologen Indicators”. In: *J. Gen. Physiol.* 16.6 (1933), pp. 859–873. DOI: 10.1085/jgp.16.6.859.

[89] D. Bongard, M. Möller, S. N. Rao, D. Corr, and L. Walder. “Synthesis of non-symmetrically N,N-diaryl-substituted 4,4-bipyridinium salts with redox-tunable and titanium dioxide (TiO2)-anchoring properties”. In: *Helv. Chim. Acta* 88.12 (2005), pp. 3200–3209. DOI: 10.1002/hlca.200590257.

[90] Y. Alesanco, A. Viñuales, G. Cabañero, J. Rodriguez, and R. Tena-Zaera. "Colorless to Neutral Color Electrochromic Devices Based on Asymmetric Viologens". In: *ACS Appl. Mater. Interfaces* 8.43 (2016), pp. 29619–29627. DOI: 10.1021/acsami.6b11321.

[91] C. Reus, M. Stolar, J. Vanderkley, J. Nebauer, and T. Baumgartner. "A Convenient N-Arylation Route for Electron-Deficient Pyridines: The Case of π-Extended Electrochromic Phosphaviologens". In: *J. Am. Chem. Soc.* 137.36 (2015), pp. 11710–11717. DOI: 10.1021/jacs.5b06413.

[92] M. Freitag and E. Galoppini. "Cucurbituril complexes of viologens bound to TiO2films". In: *Langmuir* 26.11 (2010), pp. 8262–8269. DOI: 10.1021/la904671w.

[93] Y. Alesanco, A. Viñuales, J. Rodriguez, and R. Tena-Zaera. "All-in-one gel-based electrochromic devices: Strengths and recent developments". In: *Materials (Basel).* 11.3 (2018), pp. 1–27. DOI: 10.3390/ma11030414.

[94] L. Striepe and T. Baumgartner. "Viologens and Their Application as Functional Materials". In: *Chem. - A Eur. J.* 23.67 (2017), pp. 16924–16940. DOI: 10.1002/chem.201703348.

[95] R. F. Service. "Advances in flow batteries promise cheap backup power". In: *Science (80-.).* 362.6414 (2018), pp. 508–509. DOI: 10.1126/science.362.6414.508.

[96] J. Sun, Z. Liu, W. G. Liu, Y. Wu, Y. Wang, J. C. Barnes, K. R. Hermann, W. A. Goddard, M. R. Wasielewski, and J. F. Stoddart. "Mechanical-Bond-Protected, Air-Stable Radicals". In: *J. Am. Chem. Soc.* 139.36 (2017), pp. 12704–12709. DOI: 10.1021/jacs.7b06857.

[97] A. Trabolsi, N. Khashab, A. C. Fahrenbach, D. C. Friedman, M. T. Colvin, K. K. Cotí, D. Benítez, E. Tkatchouk, J. C. Olsen, M. E. Belowich, R. Carmielli, H. A. Khatib, W. A. Goddard, M. R. Wasielewski, and J. F. Stoddart. "Radically enhanced molecular recognition". In: *Nat. Chem.* 2.1 (2010), pp. 42–49. DOI: 10.1038/nchem.479.

[98] J. C. Barnes, A. C. Fahrenbach, D. Cao, S. M. Dyar, M. Frasconi, M. A. Giesener, D. Benítez, E. Tkatchouk, O. Chernyashevskyy, W. H. Shin, H. Li, S. Sampath, C. L. Stern, A. A. Sarjeant, K. J. Hartlieb, Z. Liu, R. Carmieli, Y. Y. Botros, J. W. Choi, A. M. Slawin, J. B. Ketterson, M. R. Wasielewski, W. A. Goddard, and J. F. Stoddart. "A radically configurable six-state compound". In: *Science (80-.).* 339.6118 (2013), pp. 429–433. DOI: 10.1126/science.1228429.

[99] L. J. Winters, N. G. Smith, and M. I. Cohen. "Dimerization of pyridinium salts by cyanide". In: *J. Chem. Soc. D Chem. Commun.* 11 (1970), p. 642. DOI: 10.1039/c29700000642.

[100] T. Anderson. "Ueber die Producte der trockenen Destillation thierischer Materien". In: *Justus Liebigs Ann. Chem.* 154.3 (1870), pp. 270–286. DOI: 10.1002/jlac.18701540303.

[101] S. Petit, R. Azzouz, C. Fruit, L. Bischoff, and F. Marsais. "An efficient protocol for the preparation of pyridinium and imidazolium salts based on the Mitsunobu reaction". In: *Tetrahedron Lett.* 49.22 (2008), pp. 3663–3665. DOI: 10.1016/j.tetlet.2008.03.146.

[102] T. Zincke and G. Weisspfenning. "Über Dinitrophenylisochinoliniumchlorid und dessen Umwandlungsprodukte". In: *Justus Liebigs Ann. Chem.* 396.1 (1913), pp. 103–131. DOI: 10.1002/jlac.19133960107.

[103] T. Zincke, G. Heuser, and W. Möller. “I. Ueber Dinitrophenylpyridiniumchlorid und dessen Umwandlungsproducte”. In: *Justus Liebigs Ann. Chem.* 333.2-3 (1904), pp. 296–345. DOI: 10.1002/jlac.19043330212.

[104] T. Zincke and W. Walter. “II. Ueber die Einwirkung von Brom und von Chlor auf Phenole: Substitutionsproducte, Pseudobromide und Pseudochloride. XI. Ueber die Einwirkung von Brom auf pOxydiphenylmethan”. In: *Justus Liebigs Ann. Chem.* 334.3 (1904), pp. 367–385. DOI: 10.1002/jlac.19043340305.

[105] W. C. Cheng and M. J. Kurth. “The Zincke reaction. A review”. In: *Org. Prep. Proced. Int.* 34.6 (2002), pp. 585–608. DOI: 10.1080/00304940209355784.

[106] W. W. Porter and T. P. Vaid. “Isolation and characterization of phenyl viologen as a radical cation and neutral molecule”. In: *J. Org. Chem.* 70.13 (2005), pp. 5028–5035. DOI: 10.1021/jo050328g.

[107] X. Liu, K. G. Neoh, and E. T. Kang. “Viologen-functionalized conductive surfaces: Physicochemical and electrochemical characteristics, and stability”. In: *Langmuir* 18.23 (2002), pp. 9041–9047. DOI: 10.1021/la026085u.

[108] C. L. Bird and A. T. Kuhn. “Electrochemistry of the viologens”. In: *Chem. Soc. Rev.* 10.1 (1981), p. 49. DOI: 10.1039/CS9811000049.

[109] P. M. Monk. *The Viologens Physiochemical Properties, Synthesis and Application of the Salts of 4,4’-Bipyridine*. John Wiley & Sons, 1998.

[110] T. Lu, T. M. Cotton, J. K. Hurst, and D. H. Thompson. “A voltammetric study of asymmetric viologens in an organic solvent, an aqueous solution and in vesicle systems”. In: *J. Electroanal. Chem. Interfacial Electrochem.* 246.2 (May 1988), pp. 337–347. DOI: 10.1016/0022-0728(88)80170-0.

[111] W. Zhang, Y. M. Zhang, S. H. Li, Y. L. Cui, J. Yu, and Y. Liu. “Tunable Nanosupramolecular Aggregates Mediated by Host–Guest Complexation”. In: *Angew. Chem. Int. Ed.* 55.38 (2016), pp. 11452–11456. DOI: 10.1002/anie.201605420.

[112] L. Pospíšil, M. Hromadová, N. Fanelli, M. Valášek, V. Kolivoška, and M. Gál. “Extended viologen as a source of electric oscillations”. In: *Phys. Chem. Chem. Phys.* 13.10 (2011), pp. 4365–4371. DOI: 10.1039/c0cp01810d.

[113] T. Janoschka, N. Martin, U. Martin, C. Friebe, S. Morgenstern, H. Hiller, M. D. Hager, and U. S. Schubert. “An aqueous, polymer-based redox-flow battery using non-corrosive, safe, and low-cost materials”. In: *Nature* 527 (2015), pp. 78–81. DOI: 10.1038/nature15746.

[114] P. M. Monk, D. R. Rosseinsky, and R. J. Mortimer. “Electrochromic Materials and Devices Based on Viologens”. In: *Electrochromic Mater. Devices*. Wiley-VCH, 2015, pp. 57–90. DOI: 10.1002/9783527679850.ch3.

[115] M. R. Geraskina, A. T. Buck, and A. H. Winter. “An Organic Spin Crossover Material in Water from a Covalently Linked Radical Dyad”. In: *J. Org. Chem.* 79 (2014), pp. 7723–7727.

[116] E. M. Kosower and J. L. Cotter. “Stable Free Radicals. II. The Reduction of l-Methyl-4-cyanopyridinium Ion to Methylviologen Cation Radical”. In: *J. Am. Chem. Soc.* 86.24 (1964), pp. 5524–5527. DOI: 10.1021/ja01078a026.

[117] R. Kannappan, C. Bucher, E. Saint-Aman, J. C. Moutet, A. Milet, M. Oltean, E. Métay, S. Pellet-Rostaing, M. Lemaire, and C. Chaix. "Viologen-based redox-switchable anion-binding receptors". In: *New J. Chem.* 34.7 (2010), pp. 1373–1386. DOI: 10.1039/b9nj00757a.

[118] J. B. Torrance, B. A. Scott, B. Welber, F. B. Kaufman, and P. E. Seiden. "Optical properties of the radical cation tetrathiafulvalenium (TTF+ in its mixed-valence and monovalence halide salts". In: *Phys. Rev. B* 19.2 (Jan. 1979), pp. 730–741. DOI: 10.1103/PhysRevB.19.730.

[119] M. R. Geraskina, A. S. Dutton, M. J. Juetten, S. A. Wood, and A. H. Winter. "The Viologen Cation Radical Pimer: A Case of Dispersion-Driven Bonding". In: *Angew. Chem. Int. Ed.* 56.32 (2017), pp. 9435–9439. DOI: 10.1002/anie.201704959.

[120] K. Madasamy, V. M. Shanmugam, D. Velayutham, and M. Kathiresan. "Reversible 2D Supramolecular Organic Frameworks encompassing Viologen Cation Radicals and CB[8]". In: *Sci. Rep.* 8.1 (2018), p. 1354. DOI: 10.1038/s41598-018-19739-7.

[121] W. S. Jeon, H. J. Kim, C. Lee, and K. Kim. "Control of the stoichiometry in host-guest complexation by redox chemistry of guests: Inclusion of methylviologen in cucurbit[8]uril". In: *Chem. Commun.* 8.17 (2002), pp. 1828–1829. DOI: 10.1039/b202082c.

[122] F. Tian, D. Jiao, F. Biedermann, and O. A. Scherman. "Orthogonal switching of a single supramolecular complex". In: *Nat. Commun.* 3.1 (2012), p. 1207. DOI: 10.1038/ncomms2198.

[123] A. A. T. Buck, J. T. Paletta, S. A. Khindurangala, L. Christie, and A. H. Winter. "Plots, Hill Coefficient Determination, and Cyclic Voltammogram (S14-S18) K". In: *J Am Chem Soc* 135 (2013), pp. 1–44.

[124] J. Leira-Iglesias, A. Tassoni, T. Adachi, M. Stich, and T. M. Hermans. "Oscillations, travelling fronts and patterns in a supramolecular system". In: *Nat. Nanotechnol.* 13.11 (2018), pp. 1021–1027. DOI: 10.1038/s41565-018-0270-4.

[125] Y. L. Wu, N. E. Horwitz, K. S. Chen, D. A. Gomez-Gualdron, N. S. Luu, L. Ma, T. C. Wang, M. C. Hersam, J. T. Hupp, O. K. Farha, R. Q. Snurr, and M. R. Wasielewski. "G-quadruplex organic frameworks". In: *Nat. Chem.* 9.5 (2017), pp. 466–472. DOI: 10.1038/nchem.2689. arXiv: 1308.5367.

[126] T. Eder, T. Stangl, M. Gmelch, K. Remmerssen, D. Laux, S. Höger, J. M. Lupton, and J. Vogelsang. "Switching between H- and J-type electronic coupling in single conjugated polymer aggregates". In: *Nat. Commun.* 8.1 (2017), p. 1641. DOI: 10.1038/s41467-017-01773-0.

[127] X. Zhang, S. Rehm, M. M. Safont-Sempere, and F. Würthner. "Vesicular perylene dye nanocapsules as supramolecular fluorescent pH sensor systems". In: *Nat. Chem.* 1.8 (2009), pp. 623–629. DOI: 10.1038/nchem.368.

[128] X. Gong, J. Zhou, K. J. Hartlieb, C. Miller, P. Li, O. K. Farha, J. T. Hupp, R. M. Young, M. R. Wasielewski, and J. F. Stoddart. "Toward a Charged Homo[2]catenane Employing Diazaperopyrenium Homophilic Recognition". In: *J. Am. Chem. Soc.* 140.21 (2018), pp. 6540–6544. DOI: 10.1021/jacs.8b03407.

[129] G. Li, L. Xu, W. Zhang, K. Zhou, Y. Ding, F. Liu, X. He, and G. He. "Narrow-Bandgap Chalcogenoviologens for Electrochromism and Visible-Light-Driven Hydrogen Evolution". In: *Angew. Chem. Int. Ed.* 57.18 (2018), pp. 4897–4901. DOI: 10.1002/anie.201711761.

[130] M. J. Hollamby, M. Karny, P. H. Bomans, N. A. Sommerdjik, A. Saeki, S. Seki, H. Minamikawa, I. Grillo, B. R. Pauw, P. Brown, J. Eastoe, H. Möhwald, and T. Nakanishi. "Directed assembly of optoelectronically active alkyl-π-conjugated molecules by adding n-alkanes or π-conjugated species". In: *Nat. Chem.* 6.8 (2014), pp. 690–696. DOI: 10.1038/nchem.1977.

[131] I. Hwang, A. Y. Ziganshina, Y. H. Ko, G. Yun, and K. Kim. "A new three-way supramolecular switch based on redox-controlled interconversion of hetero- and homo-guest-pair inclusion inside a host molecule". In: *Chem. Commun.* 4 (2009), pp. 416–418. DOI: 10.1039/B818889K.

[132] D. W. Zhang, J. Tian, L. Chen, L. Zhang, and Z. T. Li. "Dimerization of conjugated radical cations: An emerging non-covalent interaction for self-assembly". In: *Chem. - An Asian J.* 10.1 (2015), pp. 56–68. DOI: 10.1002/asia.201402805.

[133] M. Nanasawa, M. Miwa, M. Hirai, and T. Kuwabara. "Synthesis of viologens with extended π-conjugation and their photochromic behavior on near-IR absorption". In: *J. Org. Chem.* 65.2 (2000), pp. 593–595. DOI: 10.1021/jo990911v.

[134] A. N. Woodward, J. M. Kolesar, S. R. Hall, N. A. Saleh, D. S. Jones, and M. G. Walter. "Thiazolothiazole Fluorophores Exhibiting Strong Fluorescence and Viologen-Like Reversible Electrochromism". In: *J. Am. Chem. Soc.* 139.25 (2017), pp. 8467–8473. DOI: 10.1021/jacs.7b01005.

[135] K. Takahashi, T. Nihira, K. Akiyama, Y. Ikegami, and E. Fukuyo. "Synthesis and characterization of new conjugation-extended viologens involving a central aromatic linking group". In: *J. Chem. Soc. Chem. Commun.* 8 (1992), pp. 620–622. DOI: 10.1039/C39920000620.

[136] A. G. Evans, J. C. Evans, and M. W. Baker. "Electron Spin Resonance Study of the Dimerization Equilibrium of the Radical Cation of 1,1'-Diethyl-4,4'-bipyridylium Diiodide in Methanol". In: *J. Am. Chem. Soc.* 99.18 (1977), pp. 5882–5884. DOI: 10.1021/ja00460a006.

[137] J. A. McCune, S. Kunz, M. Olesinska, and O. A. Scherman. "DESolution of CD and CB Macrocycles". In: *Chem. Eur. J.* 23.36 (2017), pp. 8601–8604. DOI: 10.1002/chem.201701275.

[138] H.-J. Kim, W. S. Jeon, Y. H. Ko, and K. Kim. "Inclusion of methylviologen in cucurbit[7]uril". In: *Proc. Natl. Acad. Sci.* 99.8 (2002), pp. 5007–5011. DOI: 10.1073/pnas.062656699.

[139] A. B. Buades, V. Sanchez Arderiu, D. Olid-Britos, C. Viñas, R. Sillanpää, M. Haukka, X. Fontrodona, M. Paradinas, C. Ocal, and F. Teixidor. "Electron Accumulative Molecules". In: *J. Am. Chem. Soc.* 140.8 (Feb. 2018), pp. 2957–2970. DOI: 10.1021/jacs.7b12815.

[140] G. L. Rikken. "A new twist on spintronics". In: *Science (80-.).* 331.6019 (2011), pp. 864–865. DOI: 10.1126/science.1201663.

[141] C. J. Schoot, J. J. Ponjee, H. T. Van Dam, R. A. Van Doorn, and P. T. Bolwijn. "New electrochromic memory display". In: *Appl. Phys. Lett.* 23.2 (1973), pp. 64–65. DOI: 10.1063/1.1654808.

[142] A. Benniston. "Corralling positively charged molecular radicals". In: *Science (80-.).* 339.6118 (2013), pp. 404–405. DOI: 10.1126/science.1233633.

[143] W. M. Albers, G. W. Canters, and J. Reedijk. "Preparation of extended Di(4-pyridyl)thiophene oligomers". In: *Tetrahedron* 51.13 (1995), pp. 3895–3904. DOI: 10.1016/0040-4020(95)00111-K.

[144] A. C. Benniston, J. Hagon, X. He, S. Yang, and R. W. Harrington. "Spring open two-plus-two electron storage in a disulfide-strapped methyl viologen derivative". In: *Org. Lett.* 14.2 (2012), pp. 506–509. DOI: 10.1021/ol203099h.

[145] S. Durben and T. Baumgartner. "3,7-diazadibenzophosphole oxide: A phosphorus-bridged viologen analogue with significantly lowered reduction threshold". In: *Angew. Chem. Int. Ed.* 50.34 (2011), pp. 7948–7952. DOI: 10.1002/anie.201102453.

[146] M. Stolar, J. Borau-Garcia, M. Toonen, and T. Baumgartner. "Synthesis and tunability of highly electron-accepting, N-benzylated "phosphaviologens"". In: *J. Am. Chem. Soc.* 137.9 (2015), pp. 3366–3371. DOI: 10.1021/ja513258j.

[147] M. Stolar, C. Reus, and T. Baumgartner. "Xylene-Bridged Phosphaviologen Oligomers and Polymers as High-Performance Electrode-Modifiers for Li-Ion Batteries". In: *Adv. Energy Mater.* 6.20 (2016), p. 1600944. DOI: 10.1002/aenm.201600944.

[148] T. W. Greulich, E. Yamaguchi, C. Doerenkamp, M. Lübbesmeyer, C. G. Daniliuc, A. Fukazawa, H. Eckert, S. Yamaguchi, and A. Studer. "Synthesis and Physical Properties of Strained Doubly Phosphorus-Bridged Biaryls and Viologens". In: *Chem. Eur. J.* 23.25 (2017), pp. 6029–6033. DOI: 10.1002/chem.201605272.

[149] X. Zhang, E. L. Clennan, N. Arulsamy, R. Weber, and J. Weber. "Synthesis, Structure, and Photochemical Behavior of [5]Heli-viologen Isomers". In: *J. Org. Chem.* 81.13 (2016), pp. 5474–5486. DOI: 10.1021/acs.joc.6b00835.

[150] J. C. Barnes, M. Juríček, N. L. Strutt, M. Frasconi, S. Sampath, M. A. Giesener, P. L. McGrier, C. J. Bruns, C. L. Stern, A. A. Sarjeant, and J. F. Stoddart. "ExBox: A polycyclic aromatic hydrocarbon scavenger". In: *J. Am. Chem. Soc.* 135.1 (2013), pp. 183–192. DOI: 10.1021/ja307360n.

[151] M. I. El-Barghouthi, K. I. Assaf, and A. M. M. Rawashdeh. "Molecular dynamics of methyl viologen-cucurbit[n]uril complexes in aqueous solution". In: *J. Chem. Theory Comput.* 6.4 (2010), pp. 984–992. DOI: 10.1021/ct900622h.

[152] Y. Wu, J. Zhou, B. T. Phelan, C. M. Mauck, J. F. Stoddart, R. M. Young, and M. R. Wasielewski. "Probing Distance Dependent Charge-Transfer Character in Excimers of Extended Viologen Cyclophanes Using Femtosecond Vibrational Spectroscopy". In: *J. Am. Chem. Soc.* 139.40 (2017), pp. 14265–14276. DOI: 10.1021/jacs.7b08275.

[153] L. F. Fieser, M. Fieser, and S. Rajagopalan. "Absorption spectroscopy and the structures of the diosterols". In: *J. Org. Chem.* 13.6 (1948), pp. 800–806. DOI: 10.1021/jo01164a003.

[154] R. B. Woodward. "Structure and the Absorption Spectra of α,β-Unsaturated Ketones". In: *J. Am. Chem. Soc.* 63.4 (1941), pp. 1123–1126. DOI: 10.1021/ja01849a066.

[155] O. Poizat, C. Sourisseau, and J. Corset. "Vibrational and electronic study of the methyl viologen radical cation MV+. in the solid state". In: *J. Mol. Struct.* 143.C (1986), pp. 203–206. DOI: 10.1016/0022-2860(86)85238-3.

[156] E. M. Kosower and J. Hajdu. "Pyridinyl Diradical pi-Mer. Magnesium Iodide Complexes". In: *J. Am. Chem. Soc.* 93.10 (1971), pp. 2534–2535. DOI: 10.1021/ja00739a030.

[157] S. Keller, C. Vargas, H. Zhao, G. Piszczek, C. A. Brautigam, and P. Schuck. "High-Precision Isothermal Titration Calorimetry with Automated Peak-Shape Analysis". In: *Anal. Chem.* 84.11 (June 2012), pp. 5066–5073. DOI: 10.1021/ac3007522.

[158] Y. Xia, S. Chen, and X. L. Ni. "White Light Emission from Cucurbituril-Based Host-Guest Interaction in the Solid State: New Function of the Macrocyclic Host". In: *ACS Appl. Mater. Interfaces* 10.15 (2018), pp. 13048–13052. DOI: 10.1021/acsami.8b02573.

[159] J. Sturala, M. K. Etherington, A. N. Bismillah, H. F. Higginbotham, W. Trewby, J. A. Aguilar, E. H. Bromley, A. J. Avestro, A. P. Monkman, and P. R. McGonigal. "Excited-State Aromatic Interactions in the Aggregation-Induced Emission of Molecular Rotors". In: *J. Am. Chem. Soc.* 139.49 (2017), pp. 17882–17889. DOI: 10.1021/jacs.7b08570.

[160] P. Deria, J. Yu, T. Smith, and R. P. Balaraman. "Ground-State versus Excited-State Interchromophoric Interaction: Topology Dependent Excimer Contribution in Metal-Organic Framework Photophysics". In: *J. Am. Chem. Soc.* 139.16 (2017), pp. 5973–5983. DOI: 10.1021/jacs.7b02188.

[161] B. Santiago-Gonzalez, A. Monguzzi, J. M. Azpiroz, M. Prato, S. Erratico, M. Campione, R. Lorenzi, J. Pedrini, C. Santambrogio, Y. Torrente, F. De Angelis, F. Meinardi, and S. Brovelli. "Permanent excimer superstructures by supramolecular networking of metal quantum clusters". In: *Science (80-.).* 353.6299 (2016), pp. 571–575. DOI: 10.1126/science.aaf4924.

[162] X. L. Ni, S. Chen, Y. Yang, and Z. Tao. "Facile Cucurbit[8]uril-Based Supramolecular Approach to Fabricate Tunable Luminescent Materials in Aqueous Solution". In: *J. Am. Chem. Soc.* 138.19 (2016), pp. 6177–6183. DOI: 10.1021/jacs.6b01223.

[163] M. Yamashina, M. M. Sartin, Y. Sei, M. Akita, S. Takeuchi, T. Tahara, and M. Yoshizawa. "Preparation of Highly Fluorescent Host-Guest Complexes with Tunable Color upon Encapsulation". In: *J. Am. Chem. Soc.* 137.29 (2015), pp. 9266–9269. DOI: 10.1021/jacs.5b06195.

[164] N. Barooah, J. Mohanty, and A. C. Bhasikuttan. "Cucurbit[8]uril-templated H and J dimers of bichromophoric coumarin dyes: Origin of contrasting emission". In: *Chem. Commun.* 51.67 (2015), pp. 13225–13228. DOI: 10.1039/c5cc05033b.

[165] H. J. Kim, D. R. Whang, J. Gierschner, and S. Y. Park. "Highly Enhanced Fluorescence of Supramolecular Polymers Based on a Cyanostilbene Derivative and Cucurbit[8]uril in Aqueous Solution". In: *Angew. Chem. Int. Ed.* 55.51 (2016), pp. 15915–15919. DOI: 10.1002/anie.201609699.

[166] A. Ueno, I. Suzuki, and T. Osa. "Host-Guest Sensory Systems for Detecting Organic Compounds by Pyrene Excimer Fluorescence". In: *Anal. Chem.* 62.22 (1990), pp. 2461–2466. DOI: 10.1021/ac00221a010.

[167] C. Zheng, C. Zhong, C. J. Collison, and F. C. Spano. "Non-Kasha Behavior in Quadrupolar Dye Aggregates: The Red-Shifted H-Aggregate". In: *J. Phys. Chem. C* (Jan. 2019), acs.jpcc.8b11416. DOI: 10.1021/acs.jpcc.8b11416.

[168] O. Khorev, C. D. Bösch, M. Probst, and R. Häner. "Observation of the rare chrysene excimer". In: *Chem. Sci.* 5.4 (2014), pp. 1506–1512. DOI: 10.1039/c3sc53316f.

[169] R. E. Cook, B. T. Phelan, R. J. Kamire, M. B. Majewski, R. M. Young, and M. R. Wasielewski. "Excimer Formation and Symmetry-Breaking Charge Transfer in Cofacial Perylene Dimers". In: *J. Phys. Chem. A* 121.8 (2017), pp. 1607–1615. DOI: 10.1021/acs.jpca.6b12644.

[170] K. E. Brown, W. A. Salamant, L. E. Shoer, R. M. Young, and M. R. Wasielewski. "Direct observation of ultrafast excimer formation in covalent perylenediimide dimers using near-infrared transient absorption spectroscopy". In: *J. Phys. Chem. Lett.* 5.15 (2014), pp. 2588–2593. DOI: 10.1021/jz5011797.

[171] J. M. Zayed, F. Biedermann, U. Rauwald, and O. A. Scherman. "Probing cucurbit[8]uril-mediated supramolecular block copolymer assembly in water using diffusion NMR". In: *Polym. Chem.* 1.9 (2010), p. 1434. DOI: 10.1039/c0py00197j.

[172] S. Y. Jon, Y. H. Ko, S. H. Park, H.-J. Kim, and K. Kim. "A facile, stereoselective [2 + 2] photoreaction mediated by cucurbit[8]uril". In: *Chem. Commun.* 41.19 (2001), pp. 1938–1939. DOI: 10.1039/b105153a.

[173] S. Liu, C. Ruspic, P. Mukhopadhyay, S. Chakrabarti, P. Y. Zavalij, and L. Isaacs. "The Cucurbit[n]uril Family: Prime Components for Self-Sorting Systems". In: *J. Am. Chem. Soc.* 127.45 (Nov. 2005), pp. 15959–15967. DOI: 10.1021/ja055013x.

[174] F. Biedermann, W. M. Nau, and H. J. Schneider. "The Hydrophobic Effect Revisited - Studies with Supramolecular Complexes Imply High-Energy Water as a Noncovalent Driving Force". In: *Angew. Chem. Int. Ed.* 53.42 (2014), pp. 11158–11171. DOI: 10.1002/anie.201310958.

[175] R. Ye, Q. Cui, C. Yao, R. Liu, and L. Li. "Tunable fluorescence behaviors of a supramolecular system based on a fluorene derivative and cucurbit[8]uril and its application for ATP sensing". In: *Phys. Chem. Chem. Phys.* 19.46 (2017), pp. 31306–31315. DOI: 10.1039/c7cp06434a.

[176] A. C. Bhasikuttan, J. Mohanty, W. M. Nau, and H. Pal. "Efficient fluorescence enhancement and cooperative binding of an organic dye in a supra-biomolecular host-protein assembly". In: *Angew. Chem. Int. Ed.* 46.22 (2007), pp. 4120–4122. DOI: 10.1002/anie.200604757.

[177] S. Salzmann, M. Kleinschmidt, J. Tatchen, R. Weinkauf, and C. M. Marian. "Excited states of thiophene: Ring opening as deactivation mechanism". In: *Phys. Chem. Chem. Phys.* 10.3 (2008), pp. 380–392. DOI: 10.1039/b710380h.

[178] M. Son, K. H. Park, C. Shao, F. Würthner, and D. Kim. "Spectroscopic demonstration of exciton dynamics and excimer formation in a sterically controlled perylene bisimide dimer aggregate". In: *J. Phys. Chem. Lett.* 5.20 (2014), pp. 3601–3607. DOI: 10.1021/jz501953a.

[179] T. Murase, S. Horiuchi, and M. Fujita. "Naphtalene diels-alder in a self-assembled molecular flask". In: *J. Am. Chem. Soc.* 132.9 (2010), pp. 2866–2867. DOI: 10.1021/ja9107275.

[180] M. Yamashina, M. Akita, T. Hasegawa, S. Hayashi, and M. Yoshizawa. "A polyaromatic nanocapsule as a sucrose receptor in water". In: *Sci. Adv.* 3.8 (2017), pp. 2–8. DOI: 10.1126/sciadv.1701126.

[181] J. Chen and J. Rebek. "Selectivity in an encapsulated cycloaddition reaction". In: *Org. Lett.* 4.3 (2002), pp. 327–329. DOI: 10.1021/ol0168115.

[182] J. Kang and J. Rebek. "Acceleration of a Diels-Alder reaction by a self-assembled molecular capsule". In: *Nature* 385 (1997), pp. 50–52. DOI: 10.1038/385050a0.

[183] C. June and S. E. E. L. Page. "Unusual Regioselectivity and Efficient Catalysis Diels-Alder in Aqueous Molecular". In: *Science (80-.).* 312 (2006), pp. 251–254. DOI: 10.1126/science.1124985.

[184] S. H. Leenders, R. Becker, T. Kumpulainen, B. de Bruin, T. Sawada, T. Kato, M. Fujita, and J. N. Reek. "Selective Co-Encapsulation Inside an M6L4Cage". In: *Chem. - A Eur. J.* 22.43 (2016), pp. 15468–15474. DOI: 10.1002/chem.201603017.

[185] Z. Huang, K. Qin, G. Deng, G. Wu, Y. Bai, J. F. Xu, Z. Wang, Z. Yu, O. A. Scherman, and X. Zhang. "Supramolecular Chemistry of Cucurbiturils: Tuning Cooperativity with Multiple Noncovalent Interactions from Positive to Negative". In: *Langmuir* 32.47 (2016), pp. 12352–12360. DOI: 10.1021/acs.langmuir.6b01709.

[186] E. Lewinsohn and J. Gressel. "Benzyl viologen-mediated counteraction of diquat and paraquat phytotoxicities". In: *Plant Physiol.* 76.1 (1984), pp. 125–130. DOI: 10.1104/pp.76.1.125.

[187] K. C. Chen, J. Y. Wu, D. J. Liou, and S. C. J. Hwang. "Decolorization of the textile dyes by newly isolated bacterial strains". In: *J. Biotechnol.* 101.1 (2003), pp. 57–68. DOI: 10.1016/S0168-1656(02)00303-6.

[188] J. Burschka, A. Dualeh, F. Kessler, E. Baranoff, N. L. Cevey-Ha, C. Yi, M. K. Nazeeruddin, and M. Grätzel. "Tris(2-(1 H -pyrazol-1-yl)pyridine)cobalt(III) as p-type dopant for organic semiconductors and its application in highly efficient solid-state dye-sensitized solar cells". In: *J. Am. Chem. Soc.* 133.45 (2011), pp. 18042–18045. DOI: 10.1021/ja207367t.

[189] W. B. Parker. "Enzymology of purine and pyrimidine antimetabolites used in the treatment of cancer". In: *Chem. Rev.* 109.7 (2009), pp. 2880–2893. DOI: 10.1021/cr900028p.

[190] R. B. Greenwald, Y. H. Choe, J. McGuire, and C. D. Conover. "Effective drug delivery by PEGylated drug conjugates". In: *Adv. Drug Deliv. Rev.* 55.2 (2003), pp. 217–250. DOI: 10.1016/S0169-409X(02)00180-1.

[191] F. Biedermann and O. A. Scherman. "Cucurbit[8]uril mediated donor-acceptor ternary complexes: A model system for studying charge-transfer interactions". In: *J. Phys. Chem. B* 116.9 (2012), pp. 2842–2849. DOI: 10.1021/jp2110067.

[192] L. Chen, H. Willcock, C. J. Wedge, F. Hartl, H. M. Colquhoun, and B. W. Greenland. "Efficient access to conjugated 4,4-bipyridinium oligomers using the Zincke reaction: Synthesis, spectroscopic and electrochemical properties". In: *Org. Biomol. Chem.* 14.3 (2016), pp. 980–988. DOI: 10.1039/c5ob02211h.

[193] M. Kamiya, H. Sekino, T. Tsuneda, and K. Hirao. "Nonlinear optical property calculations by the long-range-corrected coupled-perturbed Kohn-Sham method". In: *J. Chem. Phys.* 122.23 (2005), p. 234111. DOI: 10.1063/1.1935514.

[194] P. R. Varanasi, A. K. Jen, J. Chandrasekhar, I. N. Namboothiri, and A. Rathna. "The important role of heteroaromatics in the design of efficient second-order nonlinear optical molecules: Theoretical investigation on push-pull heteroaromatic stilbenes". In: *J. Am. Chem. Soc.* 118.49 (1996), pp. 12443–12448. DOI: 10.1021/ja960136q.

[195] J. Luo, M. Xu, R. Li, K. W. Huang, C. Jiang, Q. Qi, W. Zeng, J. Zhang, C. Chi, P. Wang, and J. Wu. "N -annulated perylene as an efficient electron donor for porphyrin-based dyes: Enhanced light-harvesting ability and high-efficiency Co(II/III)-based dye-sensitized solar cells". In: *J. Am. Chem. Soc.* 136.1 (2014), pp. 265–272. DOI: 10.1021/ja409291g.

[196] M. Makosza. "Nucleophilic substitution of hydrogen in electron-deficient arenes, a general process of great practical value". In: *Chem. Soc. Rev.* 39.8 (2010), pp. 2855–2868. DOI: 10.1039/b822559c.

[197] A. D. CounottePotman and H. C. van der Plas. "SN(ANRORC) mechanism XX. Degenerate ring transformations in reactions of 1,2,4,5tetrazines with hydrazine". In: *J. Heterocycl. Chem.* 15.3 (1978), pp. 445–448. DOI: 10.1002/jhet.5570150316.

[198] M. N. Al-Shamary, H. A. Al-Lohedan, M. Z. Rafiquee, and Z. A. Issa. "Micellar effects on aromatic nucleophilic substitution by the ANRORC mechanism. Hydrolysis of 2-chloro-3,5-dinitropyridine". In: *J. Phys. Org. Chem.* 25.8 (2012), pp. 713–719. DOI: 10.1002/poc.2908.

[199] I. H. Um, L. R. Im, J. S. Kang, S. S. Bursey, and J. M. Dust. "Mechanistic assessment of SNAr displacement of halides from 1-Halo-2,4-dinitrobenzenes by selected primary and secondary amines: Brønsted and Mayr analyses". In: *J. Org. Chem.* 77.21 (2012), pp. 9738–9746. DOI: 10.1021/jo301862b.

[200] N. A. Senger, B. Bo, Q. Cheng, J. R. Keeffe, S. Gronert, and W. Wu. "The element effect revisited: Factors determining leaving group ability in activated nucleophilic aromatic substitution reactions". In: *J. Org. Chem.* 77.21 (2012), pp. 9535–9540. DOI: 10.1021/jo301134q.

[201] T. J. Broxton, D. M. Muir, and A. J. Parker. "Aromatic Nucleophilic Substitution Reactions of Ambident Nucleophiles. III. Reactivity of the Nitrite Ion". In: *J. Org. Chem.* 40.22 (1975), pp. 3230–3233. DOI: 10.1021/jo00910a015.

[202] H. Lettré, W. Haede, and E. Ruhbaum. "Zur Darstellung von Derivaten des Nicotinsäureamids". In: *Justus Liebigs Ann. Chem.* 579.2 (1953), pp. 123–132. DOI: 10.1002/jlac.19535790207.

[203] J. Epsztajn and A. R. Katritzky. "Amine-nitroimides:a new functional group". In: *Tetrahedron Lett.* 10.54 (1969), pp. 4739–4742. DOI: 10.1016/S0040-4039(01)88797-9.

[204] K. Tao, P. Makam, R. Aizen, and E. Gazit. "Self-assembling peptide semiconductors". In: *Science (80-.).* 358.6365 (2017). DOI: 10.1126/science.aam9756.

[205] L. Zang. "Interfacial Donor-Acceptor Engineering of Nanofiber Materials to Achieve Photoconductivity and Applications". In: *Acc. Chem. Res.* 48.10 (2015), pp. 2705–2714. DOI: 10.1021/acs.accounts.5b00176.

[206] J. W. Chung, H. Yang, B. Singh, H. Moon, B. K. An, S. Y. Lee, and S. Y. Park. "Single-crystalline organic nanowires with large mobility and strong fluorescence emission: A conductive-AFM and space-charge-limited-current study". In: *J. Mater. Chem.* 19.33 (2009), pp. 5920–5925. DOI: 10.1039/b903882e.

[207] S. Fleming and R. V. Ulijn. "Design of nanostructures based on aromatic peptide amphiphiles". In: *Chem. Soc. Rev.* 43.23 (2014), pp. 8150–8177. DOI: 10.1039/c4cs00247d.

[208] C. G. Pappas, R. Shafi, I. R. Sasselli, H. Siccardi, T. Wang, V. Narang, R. Abzalimov, N. Wijerathne, and R. V. Ulijn. "Dynamic peptide libraries for the discovery of supramolecular nanomaterials". In: *Nat. Nanotechnol.* 11.11 (2016), pp. 960–967. DOI: 10.1038/nnano.2016.169.

[209] P. W. Frederix, G. G. Scott, Y. M. Abul-Haija, D. Kalafatovic, C. G. Pappas, N. Javid, N. T. Hunt, R. V. Ulijn, and T. Tuttle. "Exploring the sequence space for (tri-)peptide self-assembly to design and discover new hydrogels". In: *Nat. Chem.* 7.1 (2015), pp. 30–37. DOI: 10.1038/nchem.2122.

[210] S. Marchesan, C. D. Easton, K. E. Styan, L. J. Waddington, F. Kushkaki, L. Goodall, K. M. McLean, J. S. Forsythe, and P. G. Hartley. "Chirality effects at each amino acid position on tripeptide self-assembly into hydrogel biomaterials". In: *Nanoscale* 6.10 (2014), pp. 5172–5180. DOI: 10.1039/c3nr06752a.

[211] C. A. E. Hauser, R. Deng, A. Mishra, Y. Loo, U. Khoe, F. Zhuang, D. W. Cheong, A. Accardo, M. B. Sullivan, C. Riekel, J. Y. Ying, and U. A. Hauser. "Natural tri- to hexapeptides self-assemble in water to amyloid -type fiber aggregates by unexpected -helical intermediate structures". In: *Proc. Natl. Acad. Sci.* 108.4 (2011), pp. 1361–1366. DOI: 10.1073/pnas.1014796108.

[212] C. Guo, Y. Luo, R. Zhou, and G. Wei. "Triphenylalanine peptides self-assemble into nanospheres and nanorods that are different from the nanovesicles and nanotubes formed by diphenylalanine peptides". In: *Nanoscale* 6.5 (2014), pp. 2800–2811. DOI: 10.1039/c3nr02505e.

[213] M. Reches and E. Gazit. "Formation of closed-cage nanostructures by self-assembly of aromatic dipeptides". In: *Nano Lett.* 4.4 (2004), pp. 581–585. DOI: 10.1021/nl035159z.

[214] J. James and A. B. Mandal. "The aggregation of Tyr-Phe dipeptide and Val-Tyr-Val tripeptide in aqueous solution and in the presence of SDS and PEO-PPO-PEO triblock copolymer: Fluorescence spectroscopic studies". In: *J. Colloid Interface Sci.* 360.2 (2011), pp. 600–605. DOI: 10.1016/j.jcis.2011.04.058.

[215] M. Reches and E. Gazit. "Casting metal nanowires within discrete self-assembled peptide nanotubes". In: *Science (80-.).* 300.5619 (2003), pp. 625–627. DOI: 10.1126/science.1082387.

[216] A. Lakshmanan, D. W. Cheong, A. Accardo, E. Di Fabrizio, C. Riekel, and C. A. E. Hauser. "Aliphatic peptides show similar self-assembly to amyloid core sequences, challenging the importance of aromatic interactions in amyloidosis". In: *Proc. Natl. Acad. Sci.* 110.2 (2013), pp. 519–524. DOI: 10.1073/pnas.1217742110.

[217] A. K. Das, P. P. Bose, M. G. Drew, and A. Banerjee. "The role of protecting groups in the formation of organogels through a nano-fibrillar network formed by self-assembling terminally protected tripeptides". In: *Tetrahedron* 63.31 (2007), pp. 7432–7442. DOI: 10.1016/j.tet.2007.05.045.

[218] C. Subbalakshmi, S. V. Manorama, and R. Nagaraj. "Self-assembly of short peptides composed of only aliphatic amino acids and a combination of aromatic and aliphatic amino acids". In: *J. Pept. Sci.* 18.5 (2012), pp. 283–292. DOI: 10.1002/psc.2395.

[219] G. L. Eakins, J. K. Gallaher, R. A. Keyzers, A. Falber, J. E. A. Webb, A. Laos, Y. Tidhar, H. Weissman, B. Rybtchinski, P. Thordarson, and J. M. Hodgkiss. "Thermodynamic factors impacting the peptide-driven self-assembly of perylene diimide nanofibers". In: *J. Phys. Chem. B* 118.29 (2014), pp. 8642–8651. DOI: 10.1021/jp504564s.

[220] G. L. Eakins, R. Pandey, J. P. Wojciechowski, H. Y. Zheng, J. E. Webb, C. Valéry, P. Thordarson, N. O. Plank, J. A. Gerrard, and J. M. Hodgkiss. "Functional Organic Semiconductors Assembled via Natural Aggregating Peptides". In: *Adv. Funct. Mater.* 25.35 (2015), pp. 5640–5649. DOI: 10.1002/adfm.201502255.

[221] J. S. Lee, I. Yoon, J. Kim, H. Ihee, B. Kim, and C. B. Park. "Self-assembly of semiconducting photoluminescent peptide nanowires in the vapor phase". In: *Angew. Chem. Int. Ed.* 50.5 (2011), pp. 1164–1167. DOI: 10.1002/anie.201003446.

[222] N. Amdursky, E. Cazit, and G. Rosenman. "Quantum confinement in self-assembled bioinspired peptide hydrogels". In: *Adv. Mater.* 22.21 (2010), pp. 2311–2315. DOI: 10.1002/adma.200904034.

[223] P. Y. Chou and G. D. Fasman. "Prediction of Protein Conformation". In: *Biochemistry* 13.2 (1974), pp. 222–245. DOI: 10.1021/bi00699a002.

[224] M. Levitt and M. Levitt. "Conformational Preferences of Amino Acids in Globular Proteins". In: *Biochemistry* 17.20 (1978), pp. 4277–4285. DOI: 10.1021/bi00613a026.

[225] D. E. Clarke, C. D. Parmenter, and O. A. Scherman. "Tunable Pentapeptide Self-Assembled β-Sheet Hydrogels". In: *Angew. Chem. Int. Ed.* 57.26 (2018), pp. 7709–7713. DOI: 10.1002/anie.201801001.

[226] A. I. Tolmachov, A. K. Zaitsev, N. Koska, and G. B. Schuster. "Counter-ion effects in cationic dyes: photophysics and photochemistry of a macrocyclic dimer of dimethylindocarbocyanine". In: *J. Photochem. Photobiol. A Chem.* 77.2-3 (1994), pp. 237–242. DOI: 10.1016/1010-6030(94)80048-0.

[227] S. Doose, H. Neuweiler, and M. Sauer. "Fluorescence quenching by photoinduced electron transfer: A reporter for conformational dynamics of macromolecules". In: *ChemPhysChem* 10.9-10 (2009), pp. 1389–1398. DOI: 10.1002/cphc.200900238.

[228] E. T. Pashuck, H. Cui, and S. I. Stupp. "Tuning Supramolecular Rigidity of Peptide Fibers through Molecular Structure". In: *J. Am. Chem. Soc.* 132.17 (2010), pp. 6041–6046. DOI: 10.1021/ja908560n.

[229] C. L. Nesloney and J. W. Kelly. "Progress towards understanding β-sheet structure". In: *Bioorganic Med. Chem.* 4.6 (1996), pp. 739–766. DOI: 10.1016/0968-0896(96)00051-X.

[230] M. C. Manning, M. Illangasekare, and R. W. Woody. “Circular dichroism studies of distorted α-helices, twisted β-sheets, and β-turns”. In: *Biophys. Chem.* 31.1-2 (1988), pp. 77–86. DOI: 10.1016/0301-4622(88)80011-5.

[231] S. E. Paramonov, H. W. Jun, and J. D. Hartgerink. “Self-assembly of peptide-amphiphile nanofibers: The roles of hydrogen bonding and amphiphilic packing”. In: *J. Am. Chem. Soc.* 128.22 (2006), pp. 7291–7298. DOI: 10.1021/ja060573x.

[232] D. M. Byler and H. Susi. “Examination of the secondary structure of proteins by deconvolved FTIR spectra”. In: *Biopolymers* 25.3 (1986), pp. 469–487. DOI: 10.1002/bip.360250307.

[233] J. Kubelka and T. A. Keiderling. “Differentiation of β-sheet-forming structures: Ab initio-based simulations of IR absorption and vibrational CD for model peptide and protein β-sheets”. In: *J. Am. Chem. Soc.* 123.48 (2001), pp. 12048–12058. DOI: 10.1021/ja0116627.

[234] A. Lampel, S. A. McPhee, H. A. Park, G. G. Scott, S. Humagain, D. R. Hekstra, B. Yoo, P. W. Frederix, T. D. Li, R. R. Abzalimov, S. G. Greenbaum, T. Tuttle, C. Hu, C. J. Bettinger, and R. V. Ulijn. “Polymeric peptide pigments with sequence-encoded properties”. In: *Science (80-.).* 356.6342 (2017), pp. 1064–1068. DOI: 10.1126/science.aal5005.

[235] L. Pospíil, F. Teplý, M. Gál, L. Adriaenssens, M. Horáek, and L. Severa. “Helquats, helical extended diquats, as fast electron transfer systems”. In: *Phys. Chem. Chem. Phys.* 12.7 (2010), pp. 1550–1556. DOI: 10.1039/b915148f.

[236] W. W. Porter, T. P. Vaid, and A. L. Rheingold. “Synthesis and characterization of a highly reducing neutral "extended viologen" and the isostructural hydrocarbon 4,4-di-n-octyl-p- quaterphenyl”. In: *J. Am. Chem. Soc.* 127.47 (2005), pp. 16559–16566. DOI: 10.1021/ja053084q.

[237] S. V. Rosokha and J. K. Kochi. “Fresh look at electron-transfer mechanisms via the donor/acceptor bindings in the critical encounter complex”. In: *Acc. Chem. Res.* 41.5 (2008), pp. 641–653. DOI: 10.1021/ar700256a.

[238] P. M. S. Monk. *The Viologens: Physicochemical Properties, Synthesis, and Application of the Salt of 4,4’-Bipyridine*. Wiley-VCH, 1998.

[239] A. T. Bockus, L. C. Smith, A. G. Grice, O. A. Ali, C. C. Young, W. Mobley, A. Leek, J. L. Roberts, B. Vinciguerra, L. Isaacs, and A. R. Urbach. “Cucurbit[7]uril-Tetramethylrhodamine Conjugate for Direct Sensing and Cellular Imaging”. In: *J. Am. Chem. Soc.* 138.50 (2016), pp. 16549–16552. DOI: 10.1021/jacs.6b11140.

Appendix A

Appendix for chapter 2

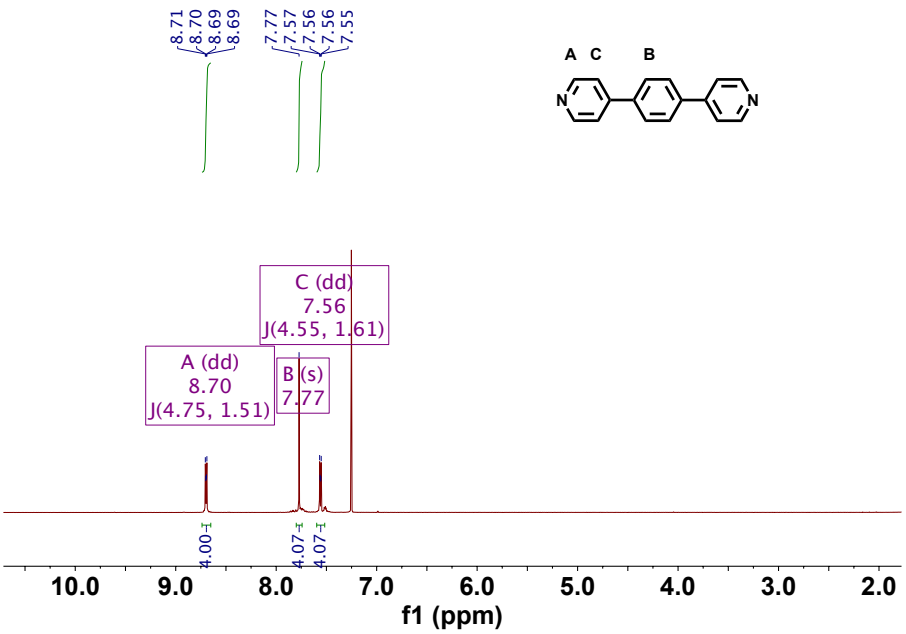

Fig. A.1 ^{1}H NMR of 1,4-di(pyridin-4-yl)benzene - EV[Ph] (500 MHz, D_2O).

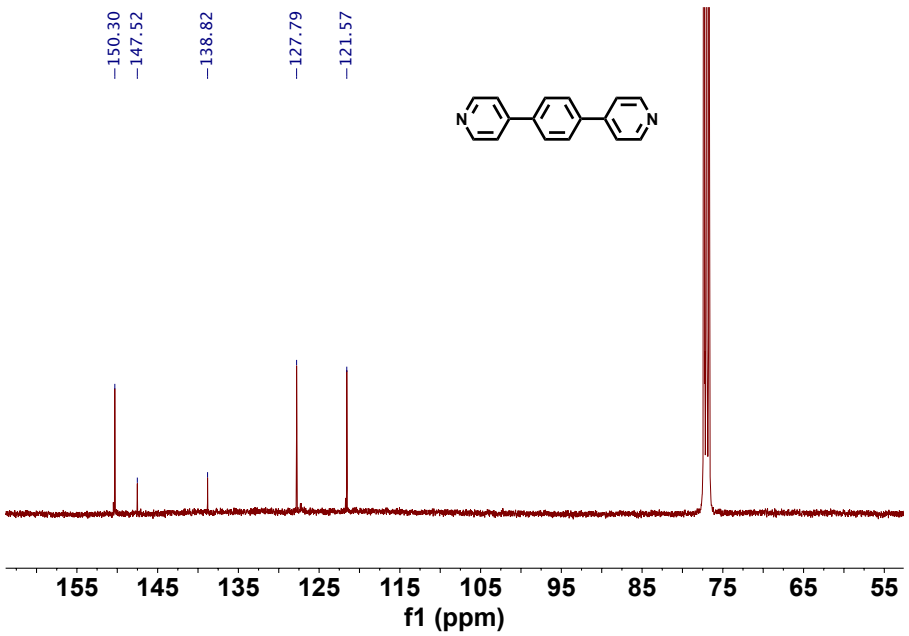

Fig. A.2 ^{13}C NMR of 1,4-di(pyridin-4-yl)benzene - EV[Ph] (126 MHz, D_2O).

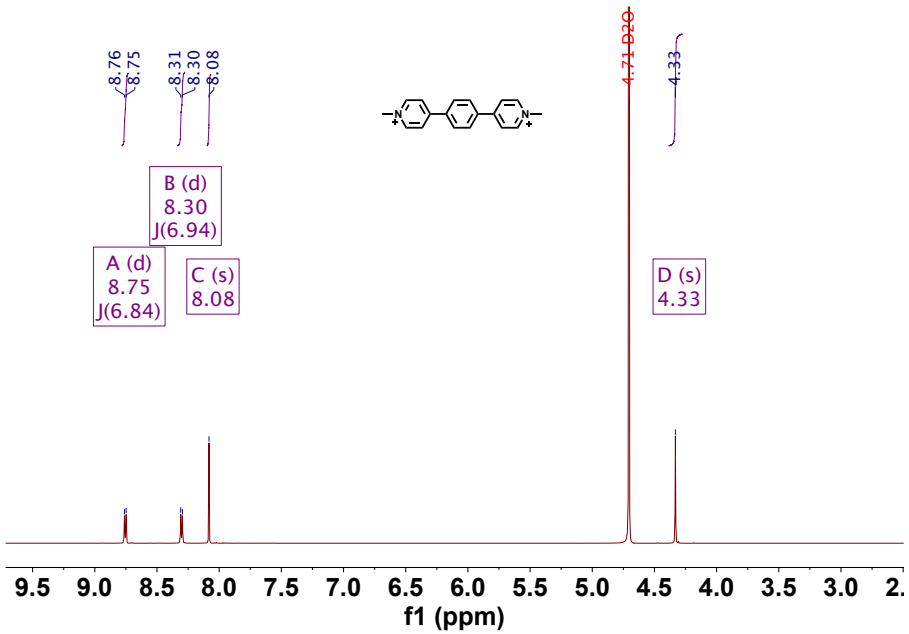

Fig. A.3 ^{1}H NMR of 4,4'-(1,4-phenylene)bis(1-methylpyridin-1-ium)iodide - EV[Ph]MV (500 MHz, D_2O).

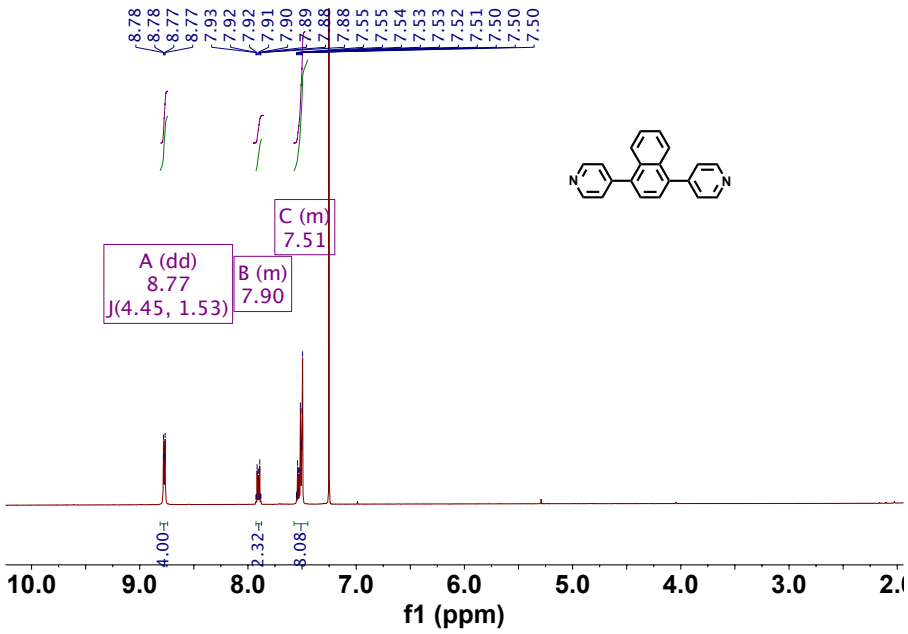

Fig. A.4 ^{1}H NMR of 1,4-di(pyridin-4-yl)naphthalene - EV[Np] (500 MHz, D_2O).

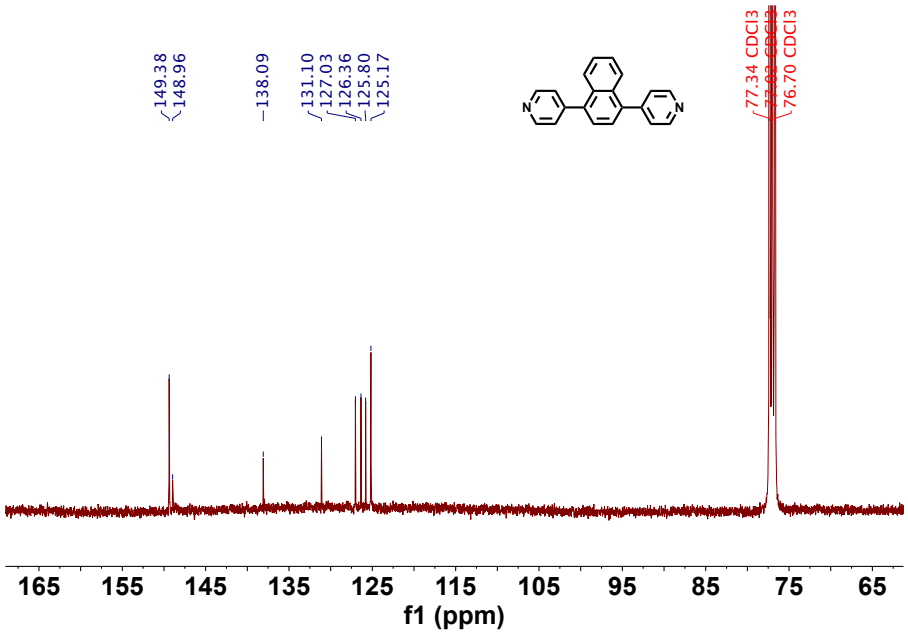

Fig. A.5 ^{13}C NMR of 1,4-di(pyridin-4-yl)naphthalene - EV[Np] (126 MHz, D_2O).

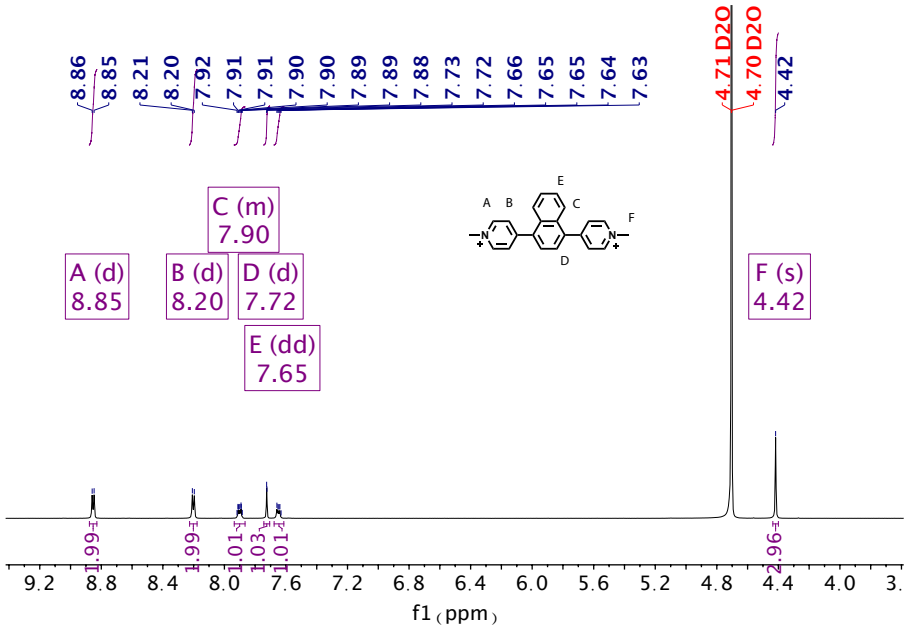

Fig. A.6 ^{1}H NMR of 4,4'-(naphthalene-1,4-diyl)bis(1-methylpyridin-1-ium)iodide - EV[Np]MV (500 MHz, D_2O).

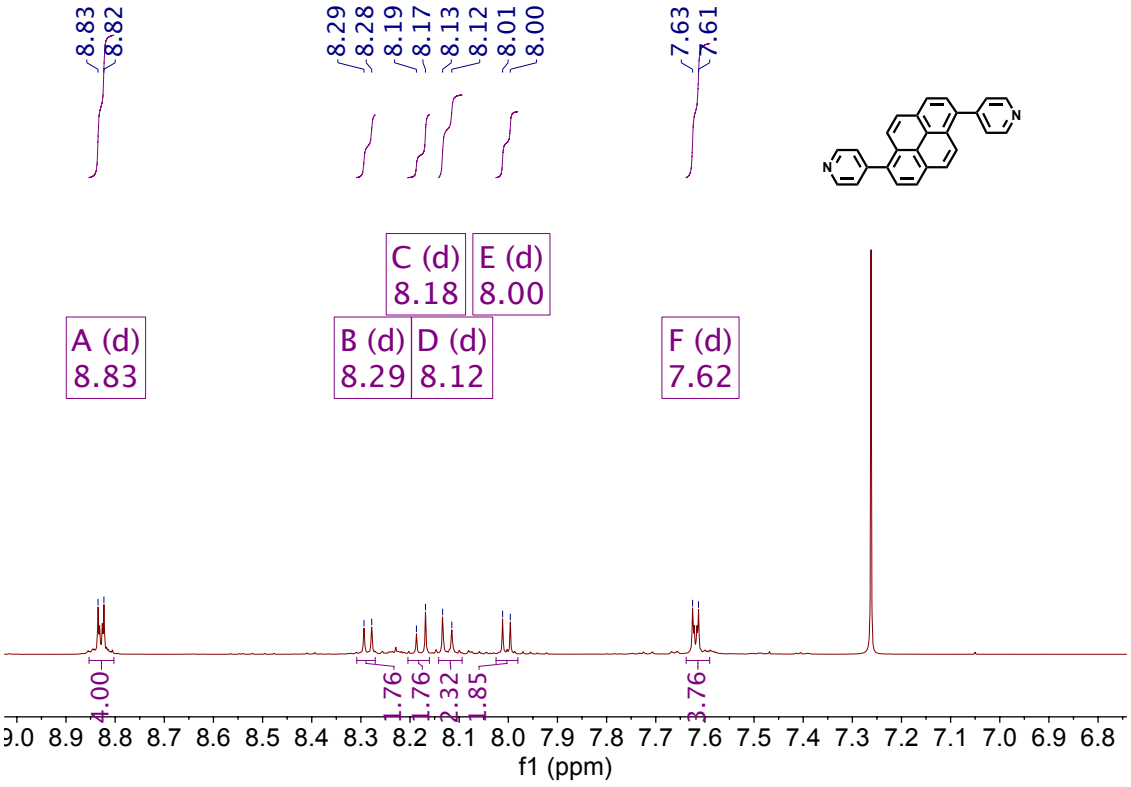

Fig. A.7 ^{1}H NMR of 1,6-di(pyridin-4-yl)pyrene - EV[$Pyr_{1,6}$] (500 MHz, D_2O).

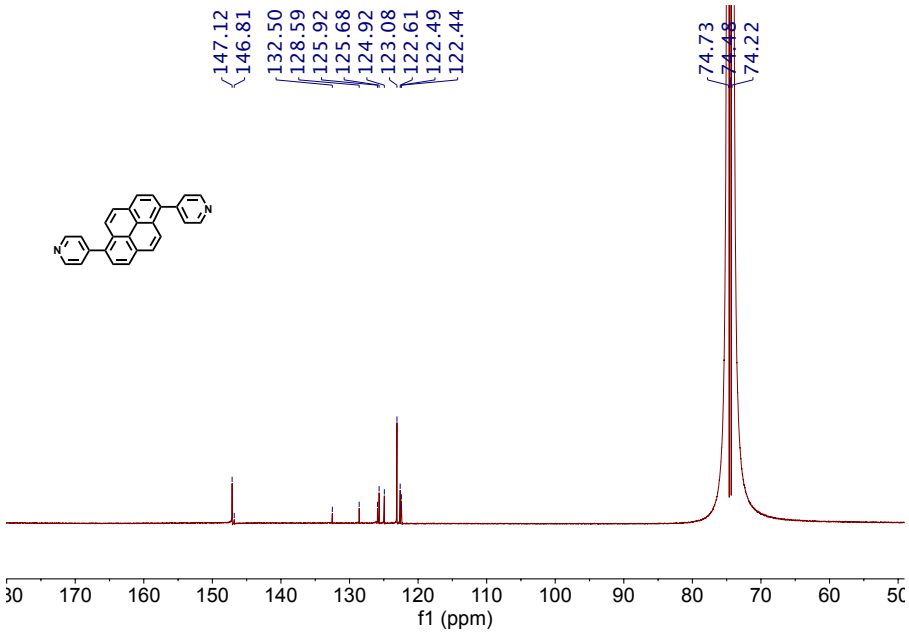

Fig. A.8 ^{13}C NMR of 1,6-di(pyridin-4-yl)pyrene - EV[$Pyr_{1,6}$] (126 MHz, D_2O).

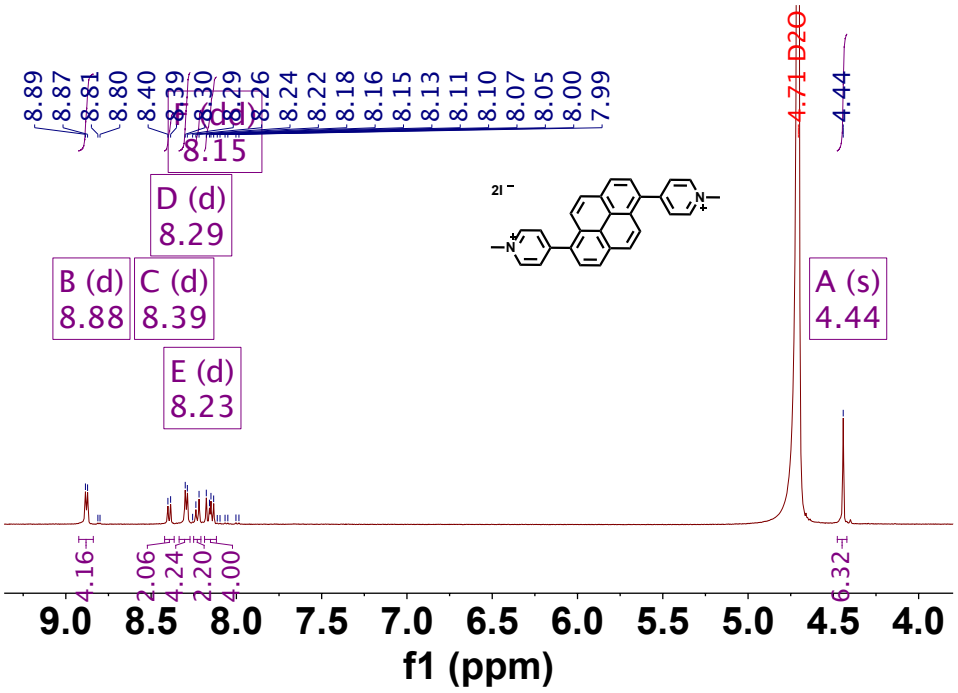

Fig. A.9 ^{1}H NMR of 4,4'-(pyrene-1,6-diyl)bis(1-methylpyridin-1-ium) - EV[$Pyr_{1,6}$]MV (500 MHz, D_2O).

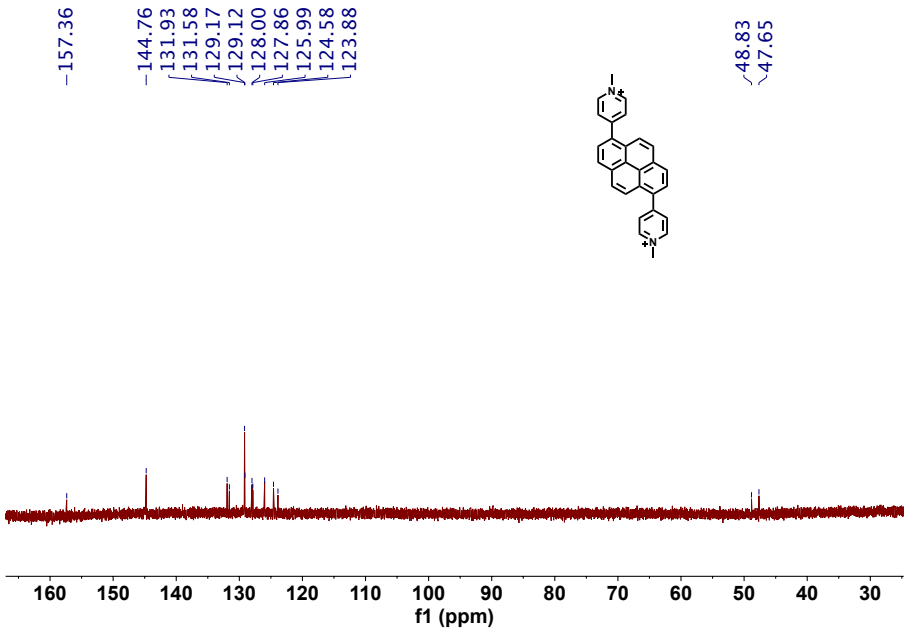

Fig. A.10 ^{13}C NMR of 4,4'-(pyrene-1,6-diyl)bis(1-methylpyridin-1-ium) - EV[$Pyr_{1,6}$]MV (126 MHz, D_2O).

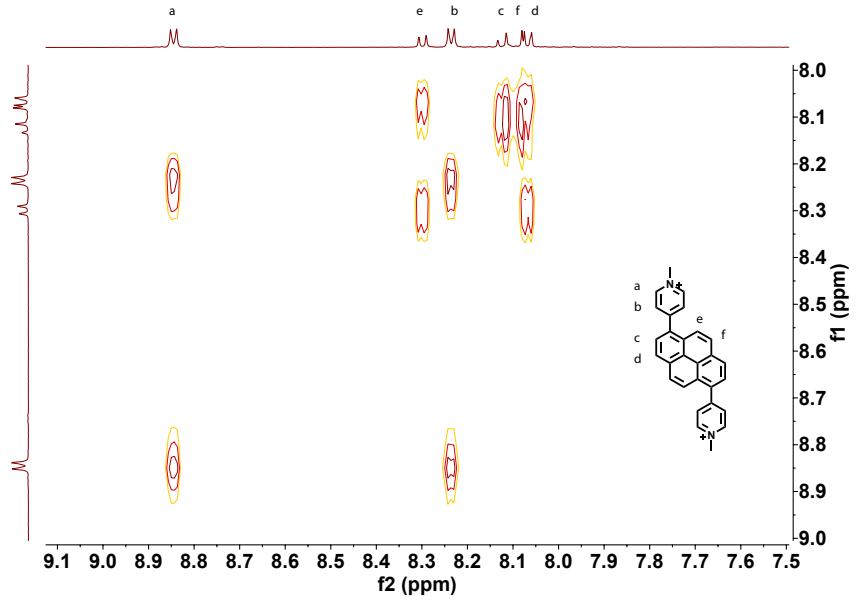

Fig. A.11 ^{1}H - ^{1}H COSY of 4,4'-(pyrene-1,6-diyl)bis(1-methylpyridin-1-ium)-EV[$Pyr_{1,6}$]MV (500 MHz, D_2O).

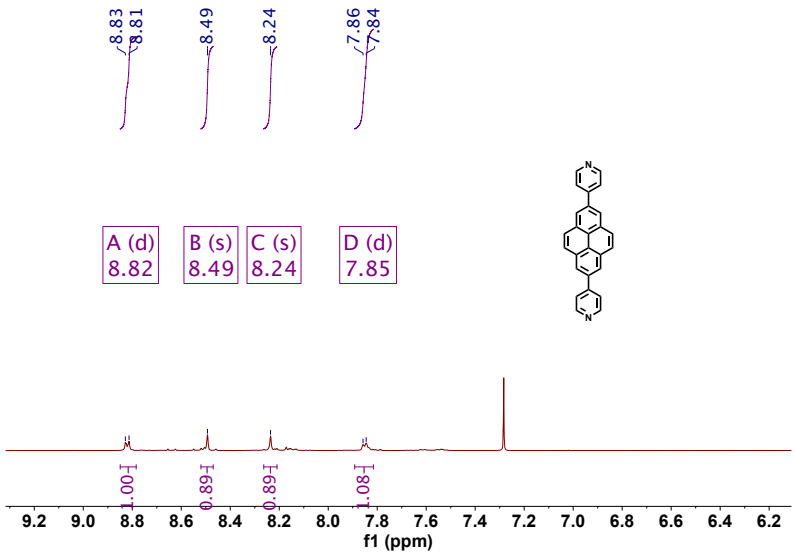

Fig. A.12 ^{1}H NMR of 2,7-di(pyridin-4-yl)pyrene - EV[$Pyr_{2,7}$] (500 MHz, D_2O).

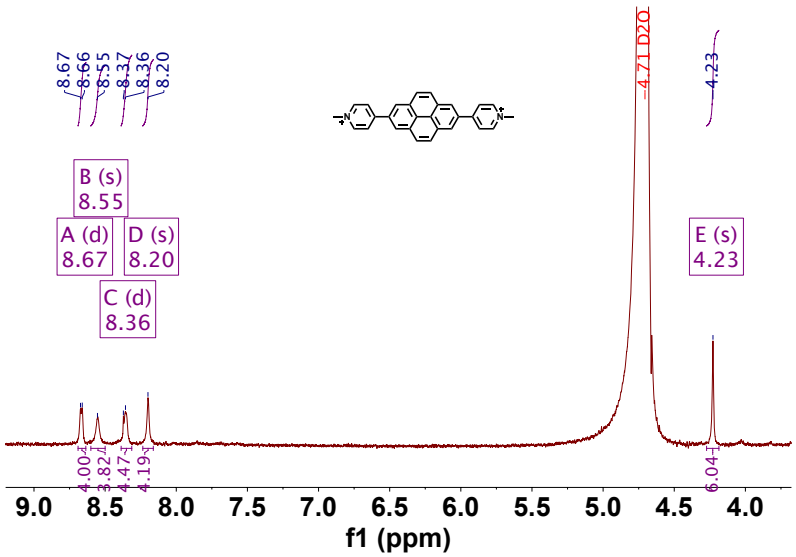

Fig. A.13 ^{1}H NMR of 4,4'-(pyrene-2,7-diyl)bis(1-methylpyridin-1-ium) iodide - EV[$Pyr_{2,7}$]MV (500 MHz, D_2O).

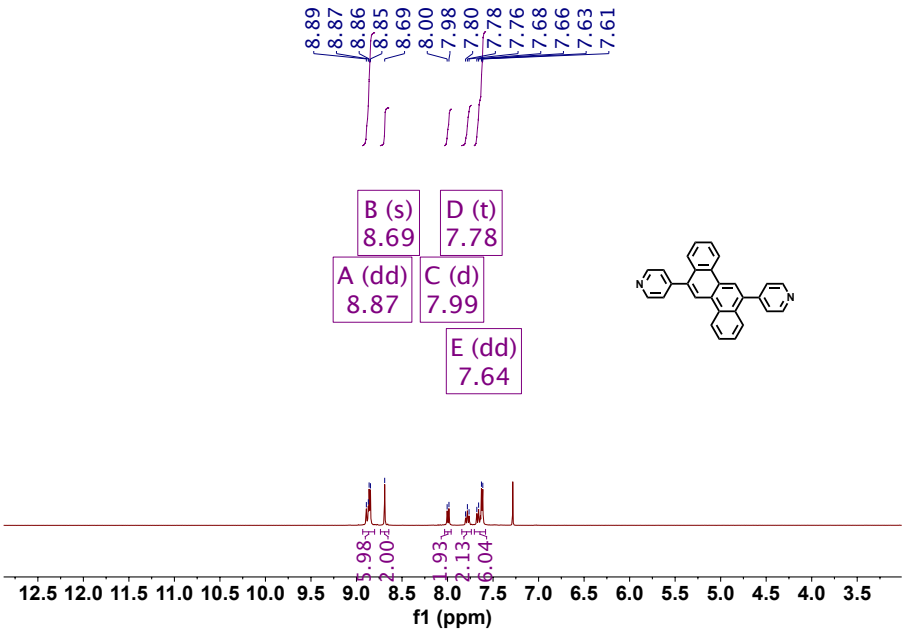

Fig. A.14 ^{1}H NMR of 6,12-di(pyridin-4-yl)chrysene - EV[CH] (500 MHz, D_2O).

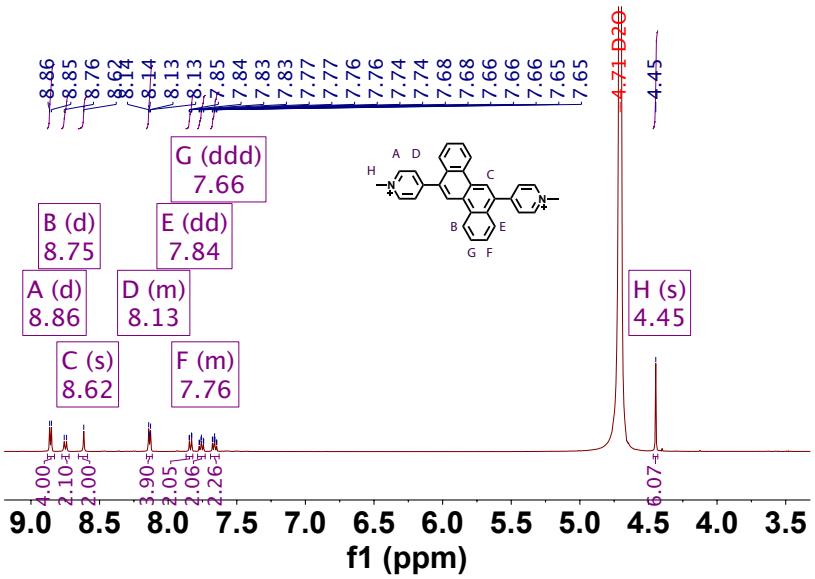

Fig. A.15 ^{1}H NMR of 4,4'-(chrysene-6,12-diyl)bis(1-methylpyridin-1-ium)iodide - EV[CH]MV (500 MHz, D_2O).

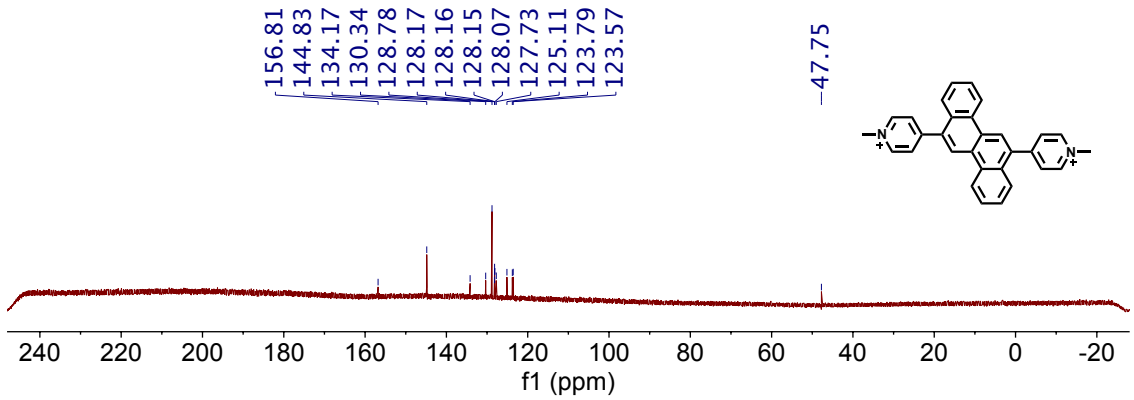

Fig. A.16 ^{13}C NMR of 4,4'-(chrysene-6,12-diyl)bis(1-methylpyridin-1-ium)iodide - EV[CH]MV (126 MHz, D_2O).

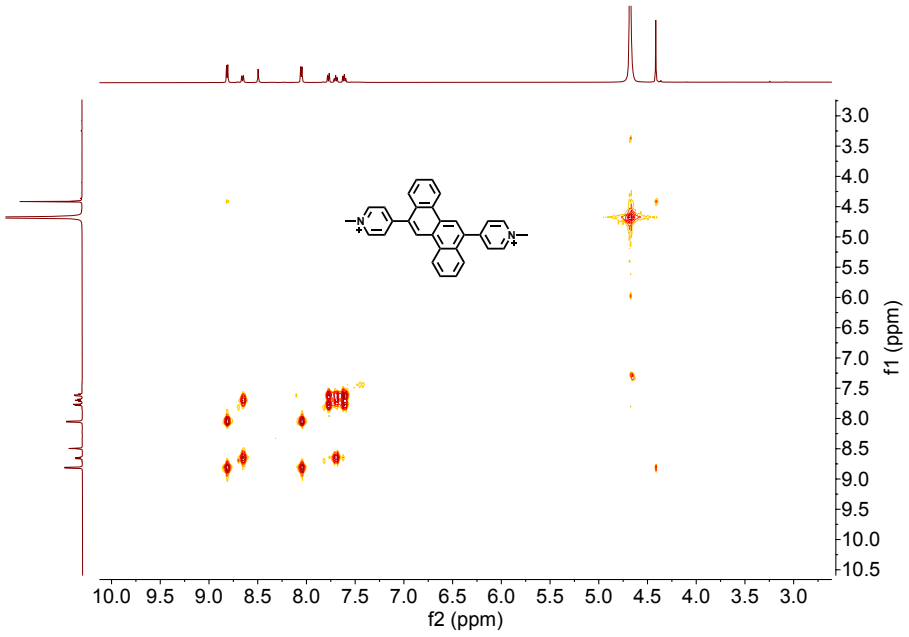

Fig. A.17 COSY NMR of 4,4'-(chrysene-6,12-diyl)bis(1-methylpyridin-1-ium)iodide - EV[CH]MV (500 MHz, D_2O).

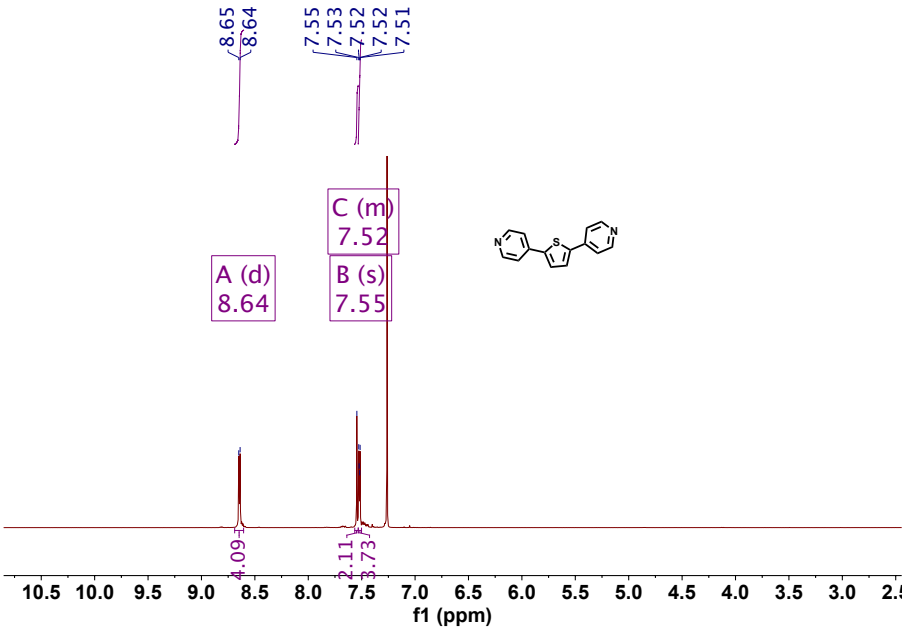

Fig. A.18 ^{1}H NMR of 2,5-di(pyridin-4-yl)thiophene - EV[Th] (500 MHz, D_2O).

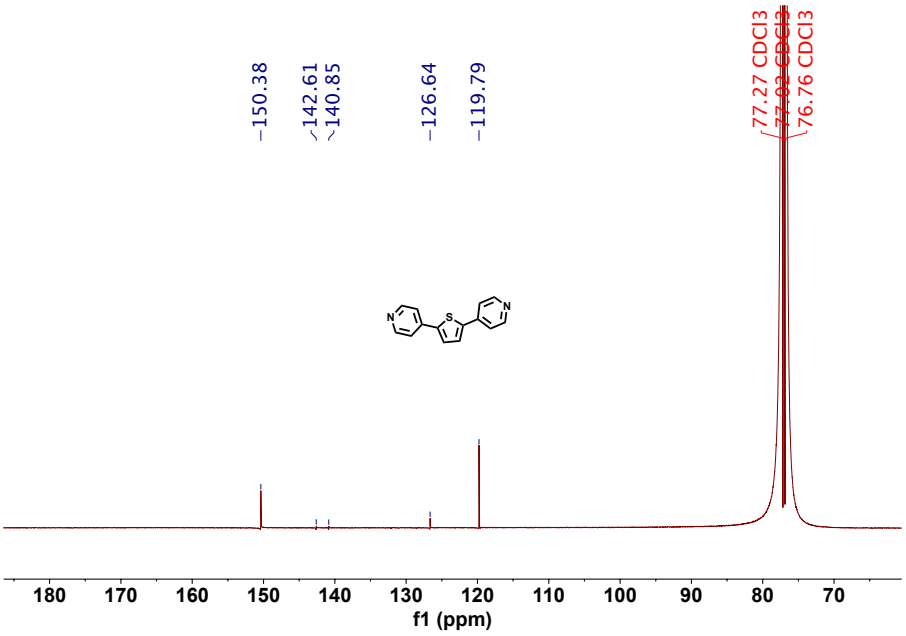

Fig. A.19 ^{13}C NMR of 2,5-di(pyridin-4-yl)thiophene - EV[Th] (126 MHz, D_2O).

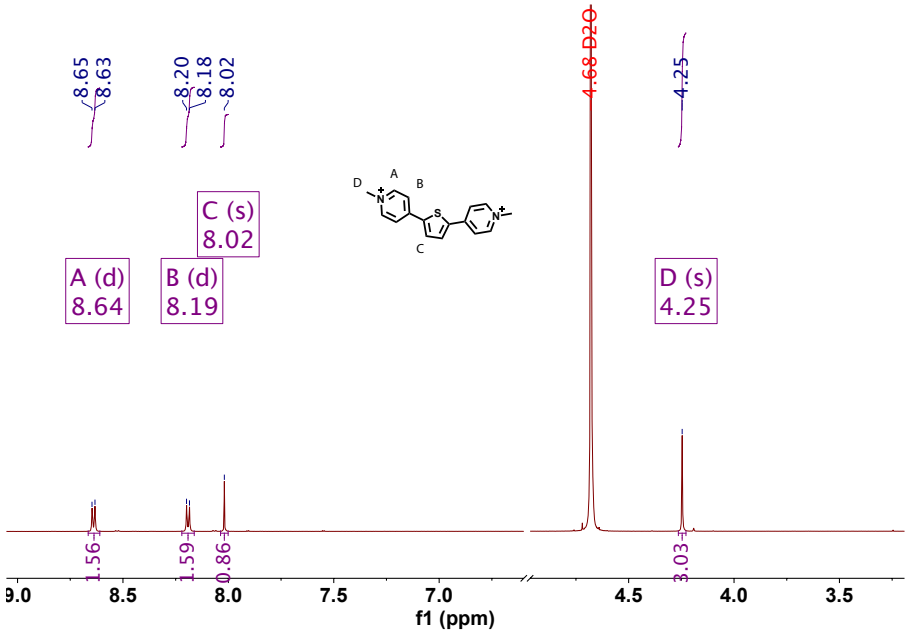

Fig. A.20 ^{1}H NMR of 4,4'-(thiophene-2,5-diyl)bis(1-methylpyridin-1-ium) iodide - EV[Th]MV (500 MHz, D_2O).

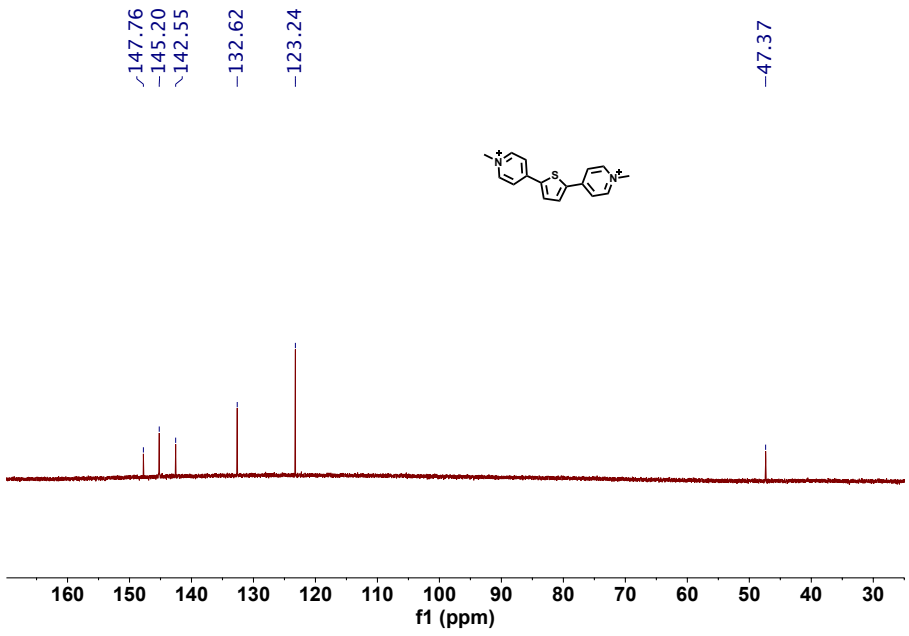

Fig. A.21 ^{13}C NMR of 4,4'-(thiophene-2,5-diyl)bis(1-methylpyridin-1-ium) iodide - EV[Th]MV (126 MHz, D_2O).

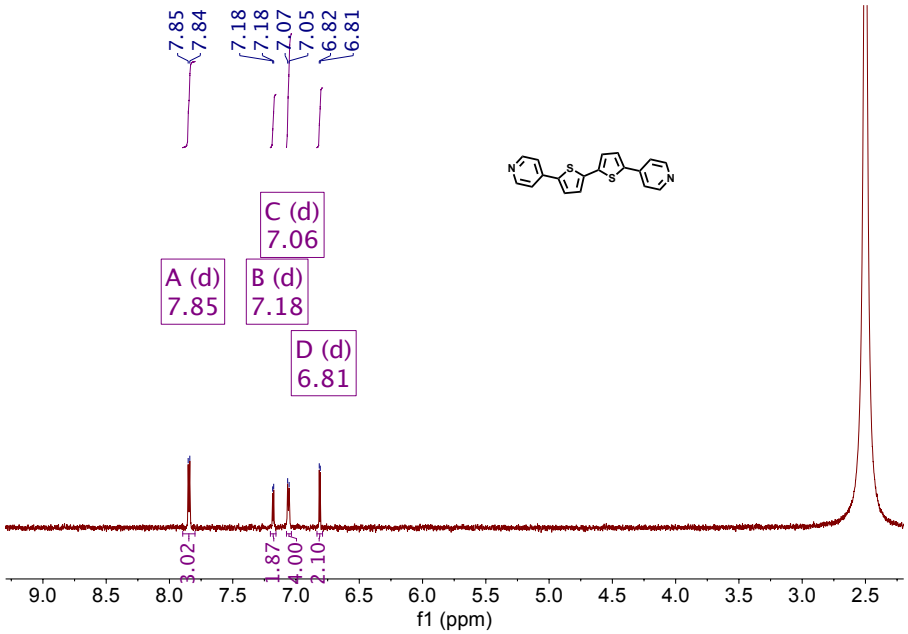

Fig. A.22 ^{1}H NMR of 5,5'-di(pyridin-4-yl)-2,2'-bithiophene - EV[DTh] (500 MHz, D_2O).

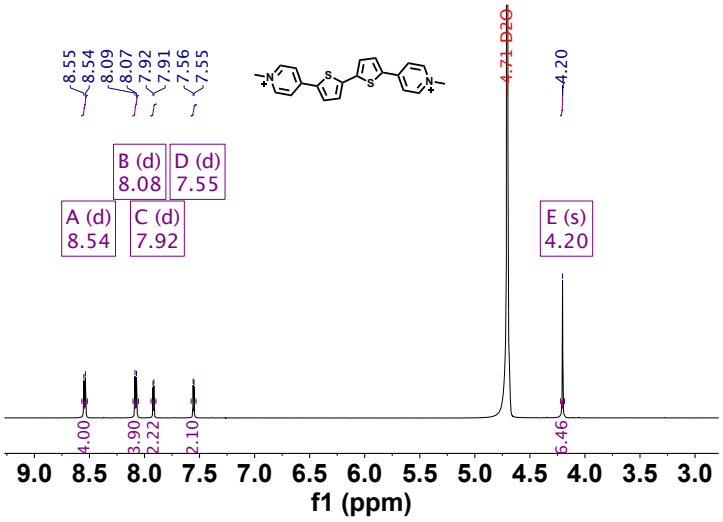

Fig. A.23 ^{1}H NMR of 4,4'-([2,2'-bithiophene]-5,5'-diyl)bis(1-methylpyridin-1-ium) - EV[DTh]MV (500 MHz, D_2O).

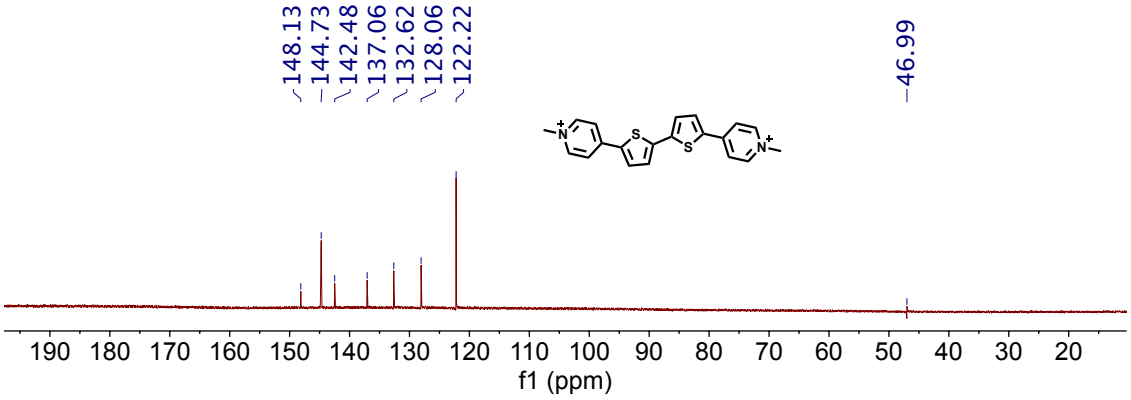

Fig. A.24 ^{13}C NMR of 4,4'-([2,2'-bithiophene]-5,5'-diyl)bis(1-methylpyridin-1-ium) - EV[DTh]MV (126 MHz, D_2O).

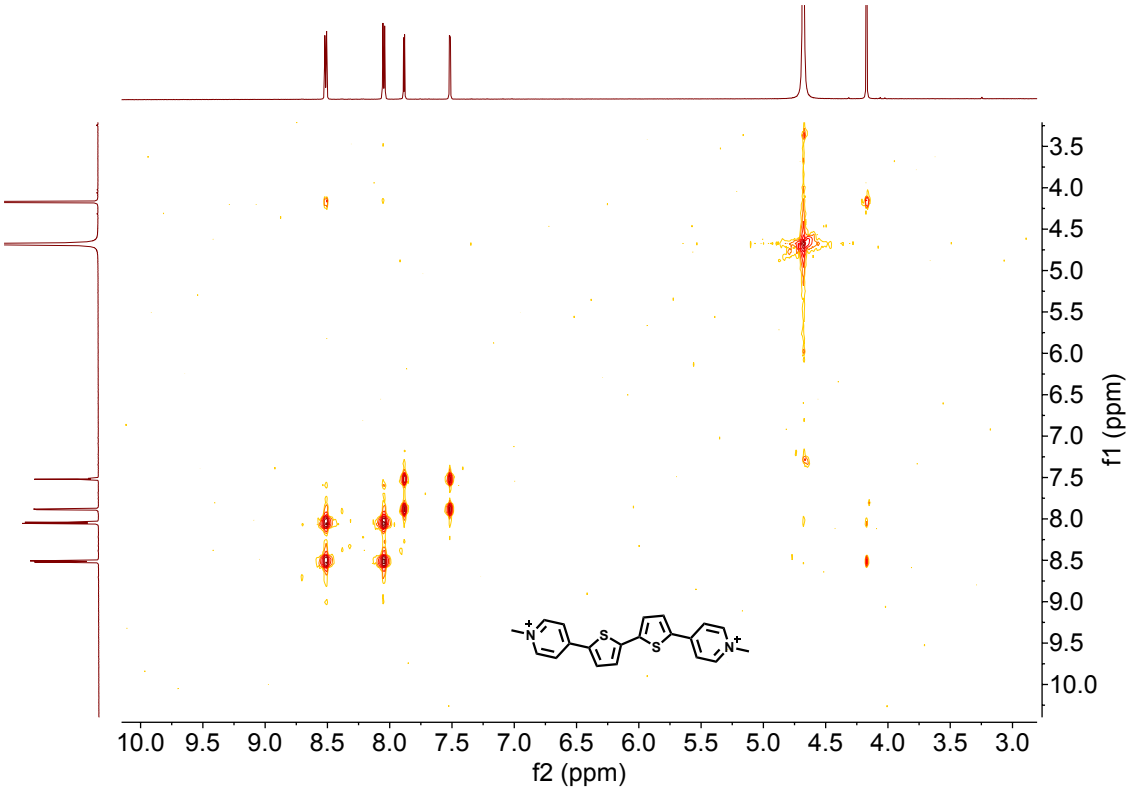

Fig. A.25 COSY NMR of 4,4'-([2,2'-bithiophene]-5,5'-diyl)bis(1-methylpyridin-1-ium) - EV[DTh]MV (500 MHz, D_2O).

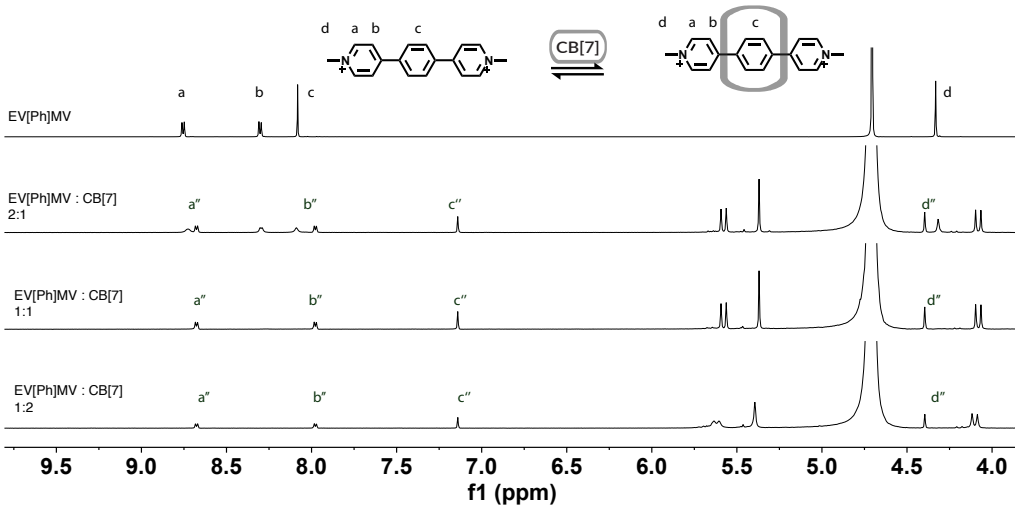

Fig. A.26 ^{1}H NMR titration of EV[Ph]MV to CB[7] (500 MHz, D_2O).

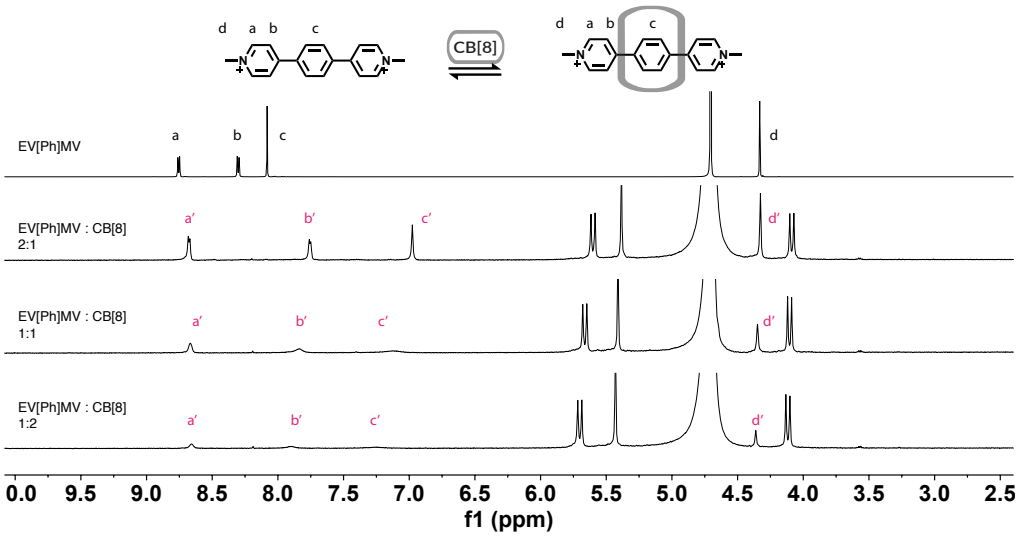

Fig. A.27 ^{1}H NMR titration of EV[Ph]MV to CB[8] (500 MHz, D_2O).

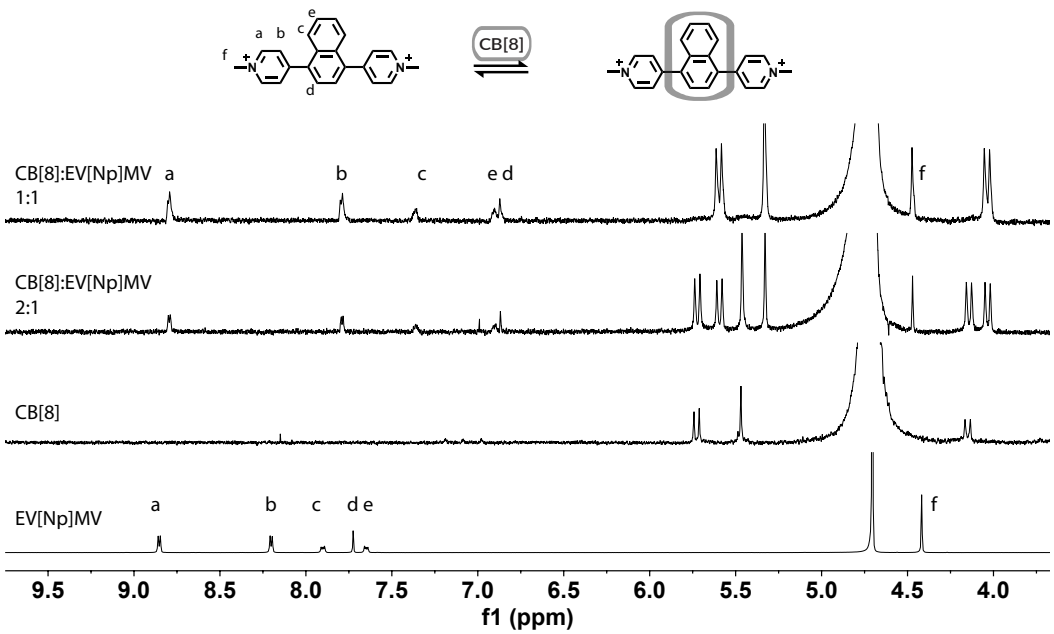

Fig. A.28 ^{1}H NMR · titrations of EV[Np]MV to CB[8] (500 MHz, D_2O).

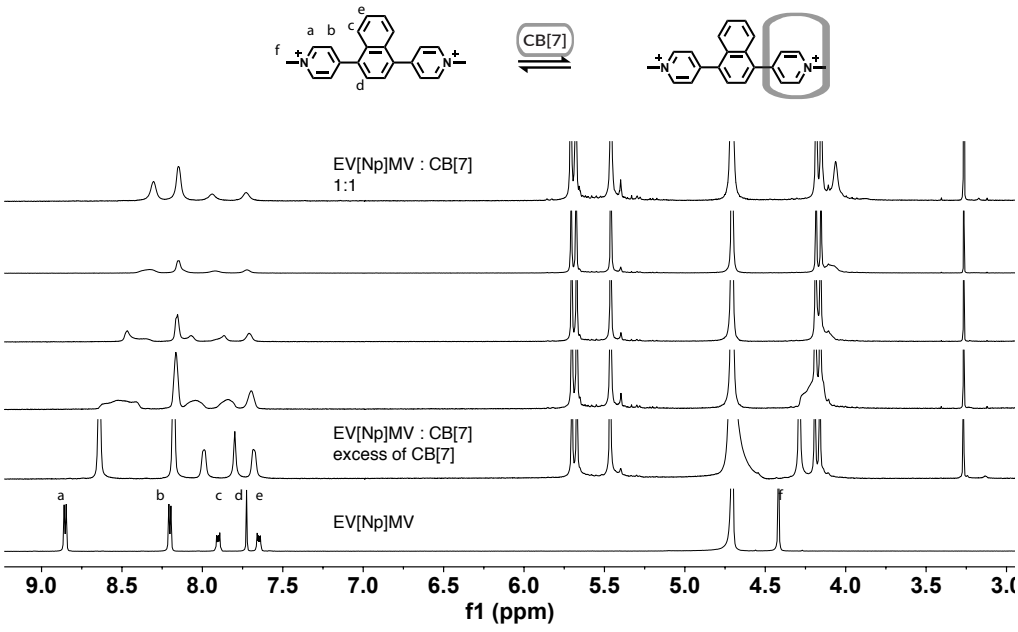

Fig. A.29 ^{1}H NMR · titrations of EV[Np]MV to CB[7] (500 MHz, D_2O).

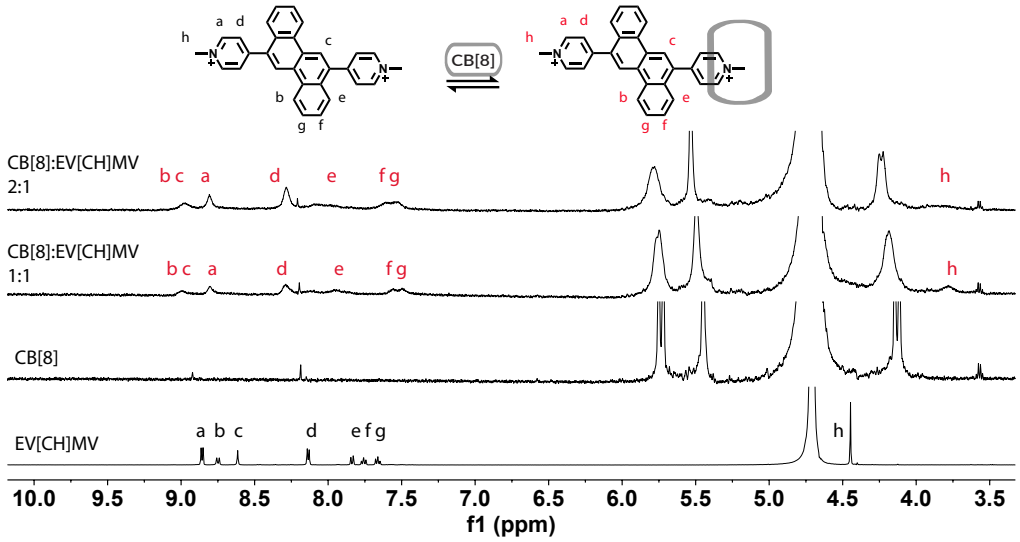

Fig. A.30 ^{1}H NMR titration of EV[CH]MV to CB[8] (500 MHz, D_2O).

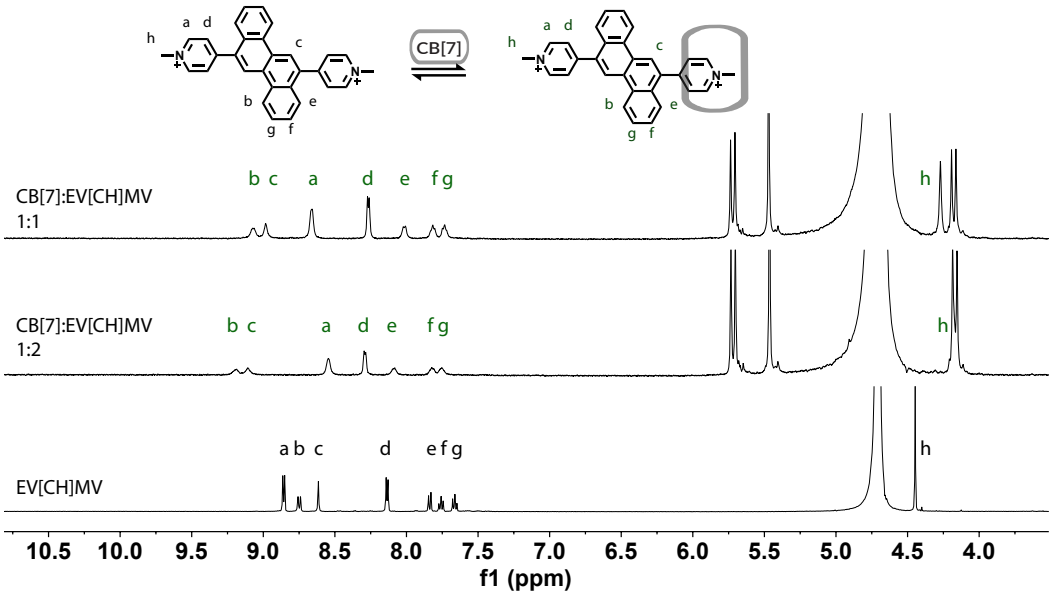

Fig. A.31 ^{1}H NMR titration of EV[CH]MV to CB[7] (500 MHz, D_2O).

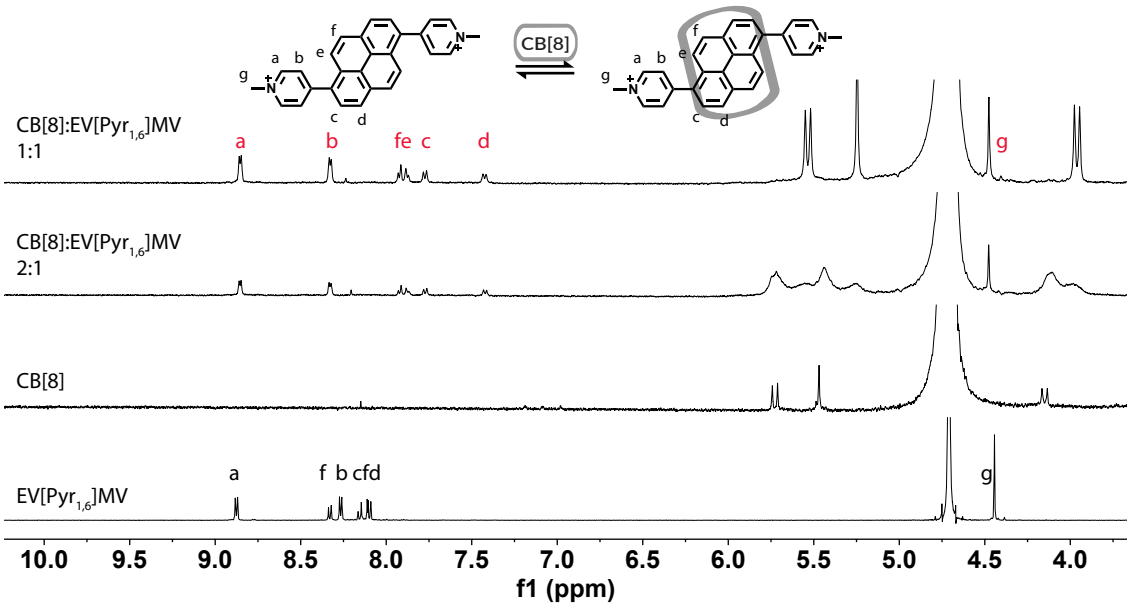

Fig. A.32 ^{1}H NMR titration of EV[CH]MV to CB[8] (500 MHz, D_2O).

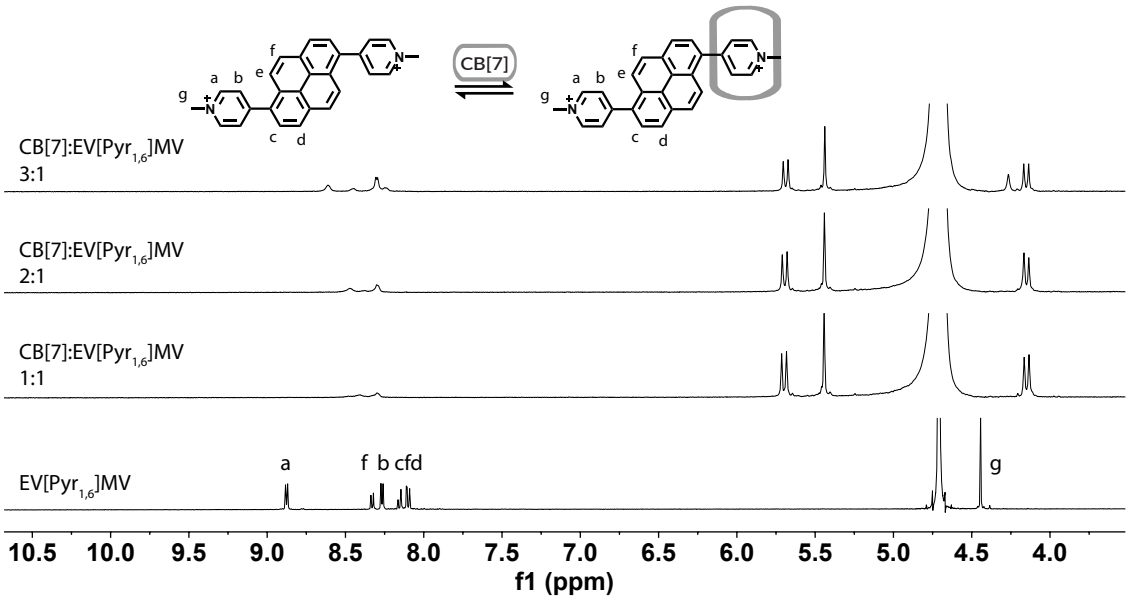

Fig. A.33 ^{1}H NMR titration of EV[CH]MV to CB[7] (500 MHz, D_2O).

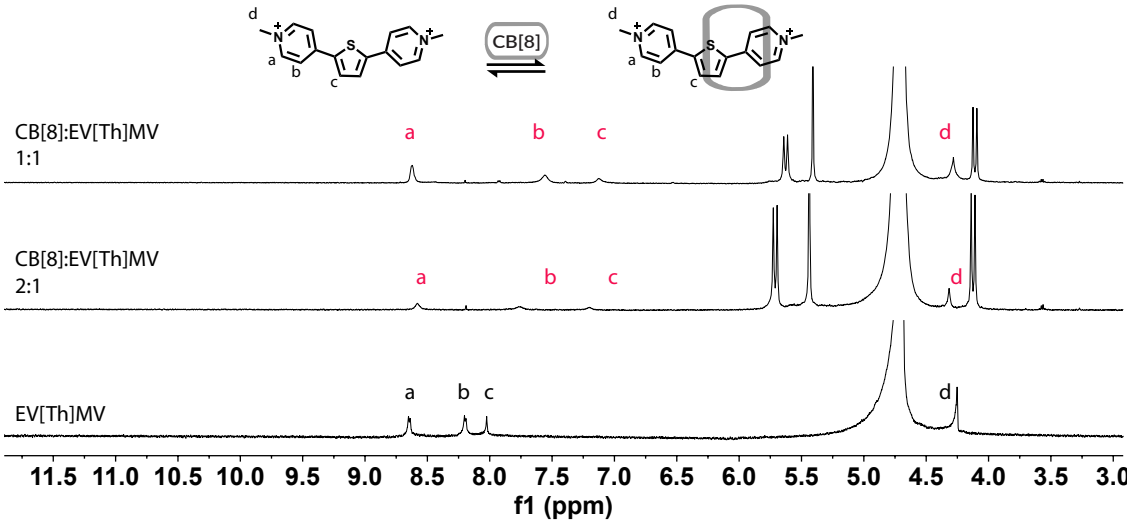

Fig. A.34 ^{1}H NMR titration of EV[Th]MV to CB[8] (500 MHz, D_2O).

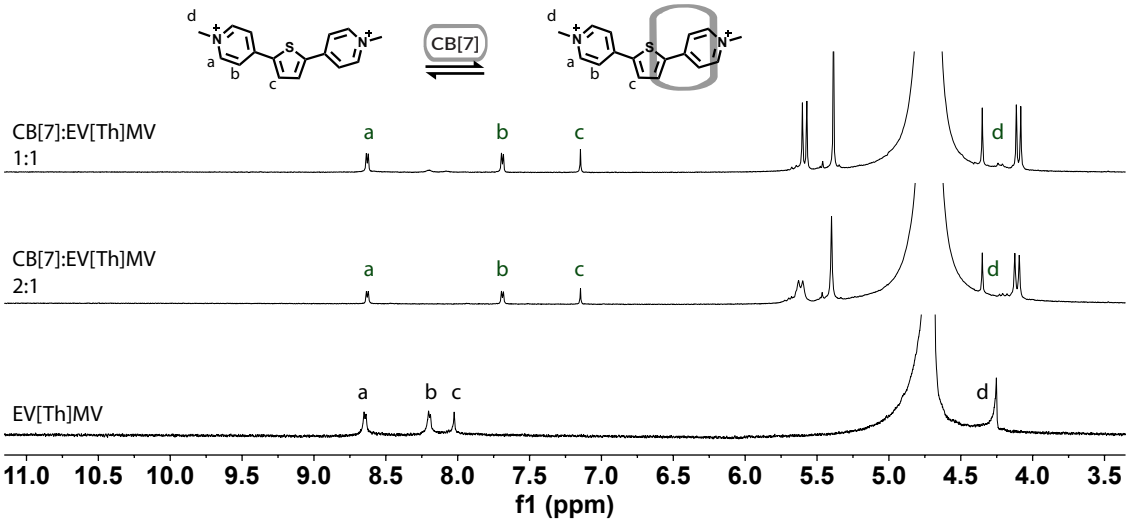

Fig. A.35 ^{1}H NMR titration of EV[Th]MV to CB[7] (500 MHz, D_2O).

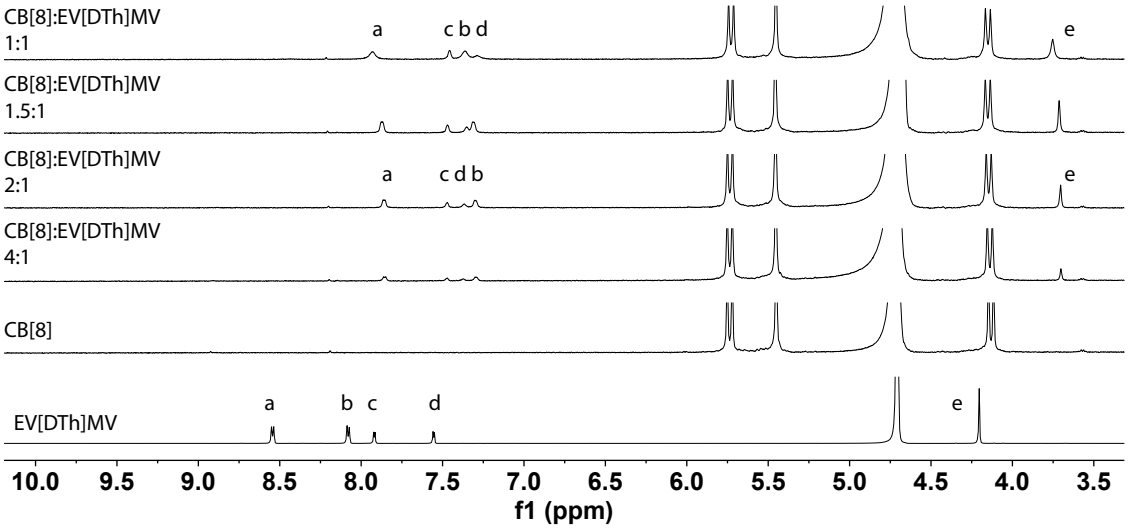

Fig. A.36 ^{1}H NMR titration of EV[DTh]MV to CB[8] (500 MHz, D_2O).

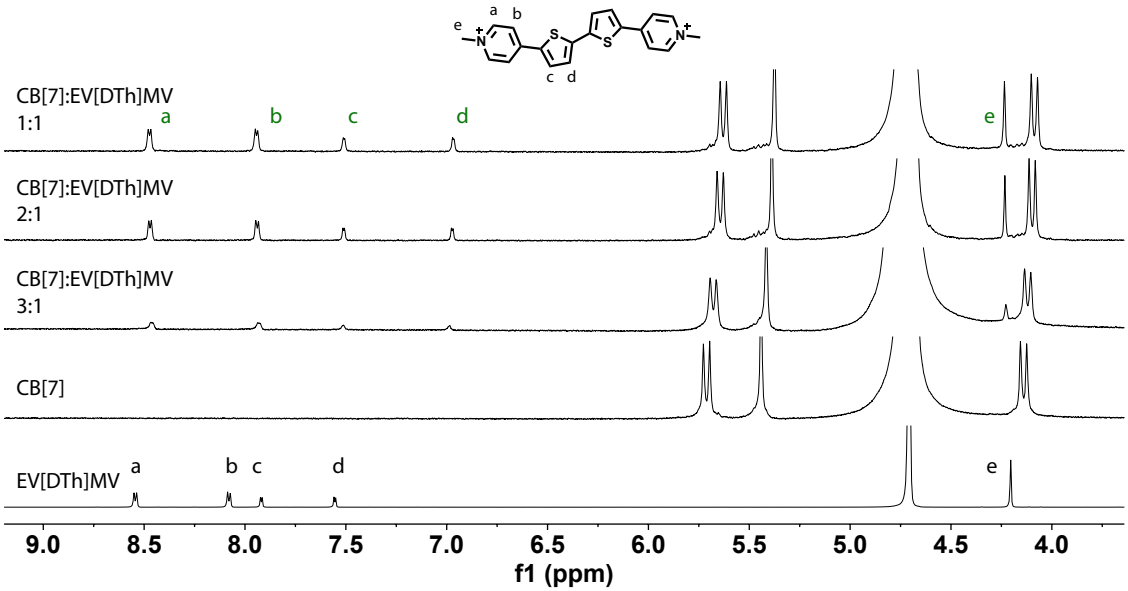

Fig. A.37 ^{1}H NMR titration of EV[DTh]MV to CB[7] (500 MHz, D_2O).

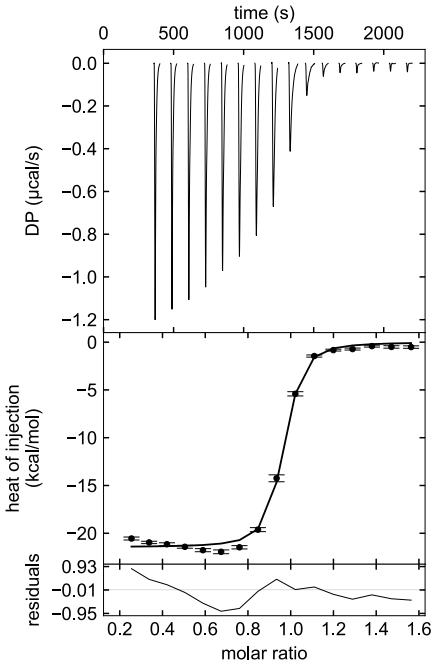

EV[Ph]MV : CB[8]
T=298.15 K

complex AB:
Kab = 2.81e^{06} M^{-1},
ΔGab = -8.797 kcal/Mol
ΔHab = -10.097 kcal/Mol
TΔSab = -1.3 kcal/Mol

complex BAB
Kbab = 3.86e^{04} M^{-2},
ΔGbab = - 6.257kcal/Mol
ΔHbab = -22.86 kcal/Mol
TΔSbab = -16.608 kcal/Mol

Fig. A.38 ITC titration of EV[Ph]MV to CB[8].

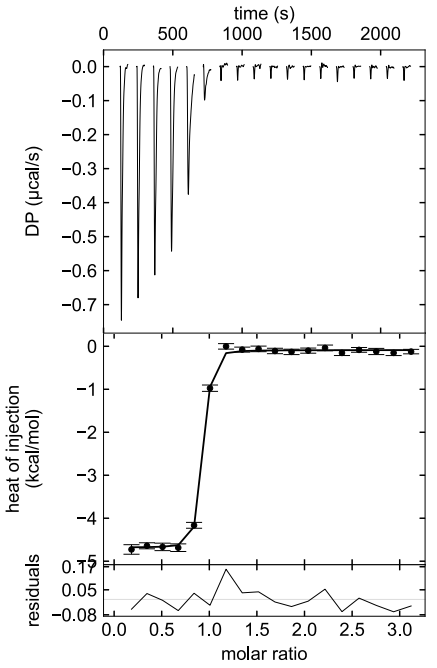

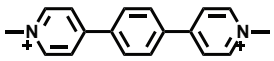

EV[Ph]MV : CB[7]
T=298.15 K

complex AB:
Kab = 5.69e^{07} M^{-1},
ΔGab = -10.392 kcal/Mol
ΔHab = -7.051 kcal/Mol
TΔSab = 3.341 kcal/Mol

Fig. A.39 ITC titration of EV[Ph]MV to CB[7].

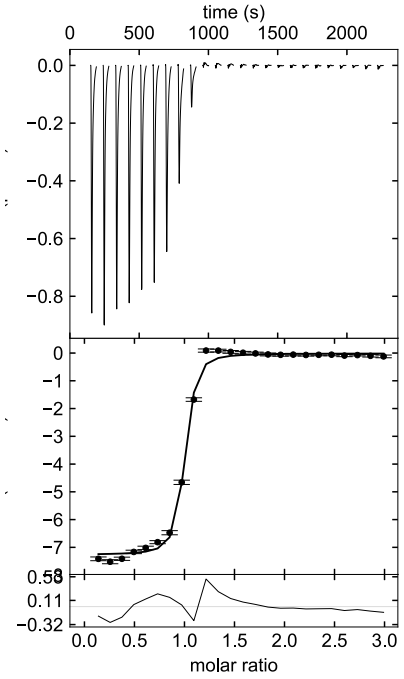

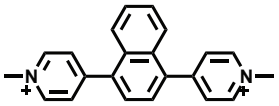

EV[Np]MV : CB[8]
T=298.15 K

complex AB:
Kab = 1.05e^{07} M^{-1},
ΔGab = -9.581 kcal/Mol
ΔHab = -9.999 kcal/Mol
TΔSab = -0.419 kcal/Mol

Fig. A.40 ITC titration of EV[Np]MV to CB[8].

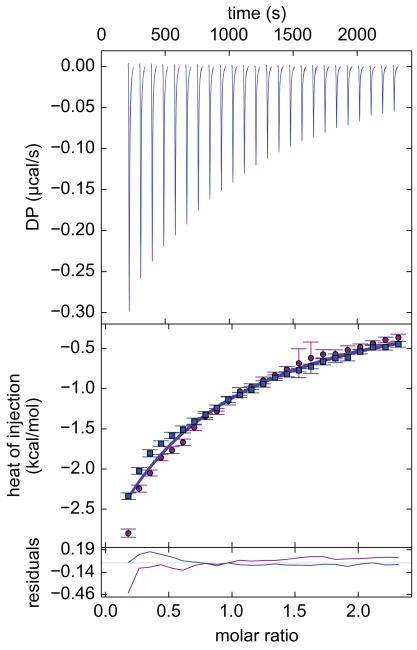

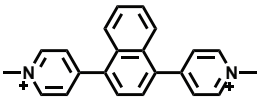

EV[Np]MV : CB[7]
T=298.15 K

A + B <=> AB
K=9.25e^{03} M^{-1}
ΔG=-5.411 kcal/Mol
ΔH=-18.918 kcal/Mol
TΔS=-13.507 kcal/Mol

Fig. A.41 ITC titration of EV[Np]MV to CB[7].

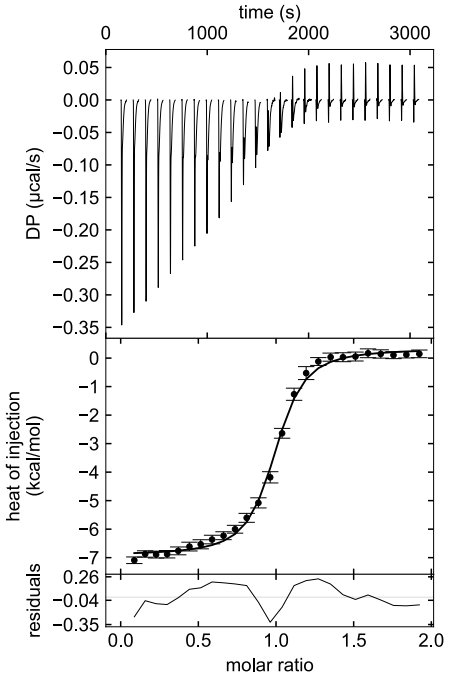

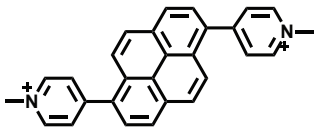

EV[Pyr$_{1,6}$]MV : CB[8]
T=298.15 K

A + B <=> AB
K=4.72e^{06} M^{-1}
ΔG=-9.104 kcal/Mol
ΔH=-22.944 kcal/Mol
TΔS=-13.84 kcal/Mol

Fig. A.42 ITC titration of EV[Pyr$_{1,6}$]MV to CB[8].

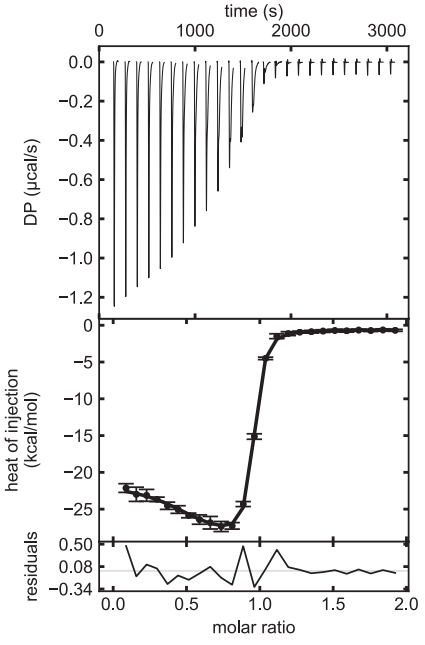

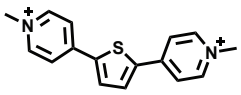

EV[Th]MV : CB[8]
T=298.15 K

complex AB:
Kab = 1.421e^{06} M^{-1},
ΔGab = -11.122 kcal/Mol
ΔHab = -21.808 kcal/Mol
TΔSab = -10.685 kcal/Mol
ΔSab = -35.839 cal/Mol*K

complex BAB
Kbab = 2.135e+15 M^-2,
ΔGbab = -20.913 kcal/Mol
ΔHbab = -6.398 kcal/Mol
TΔSbab = -7.729 kcal/Mol
ΔSbab = -25.923 cal/Mol*K

Fig. A.43 ITC titration of EV[Th]MV to CB[8].

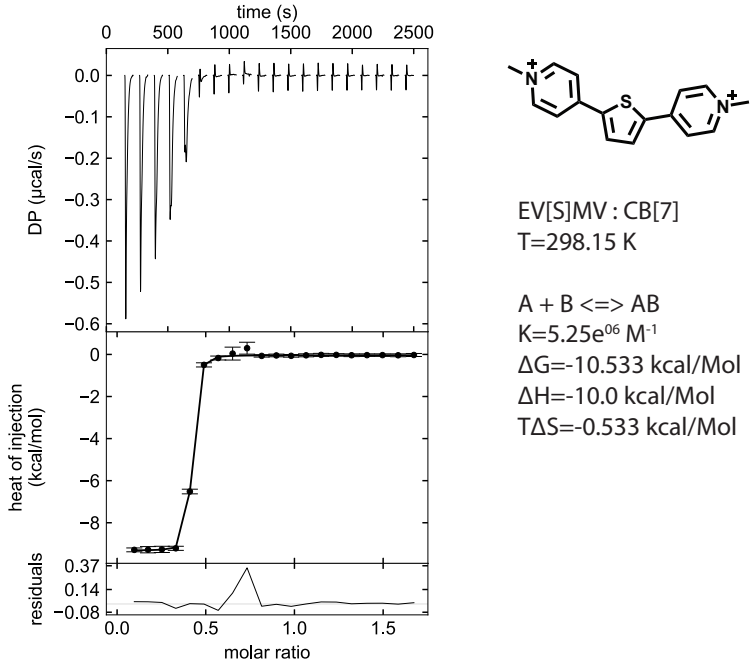

Fig. A.44 ITC titration of EV[Th]MV to CB[7].

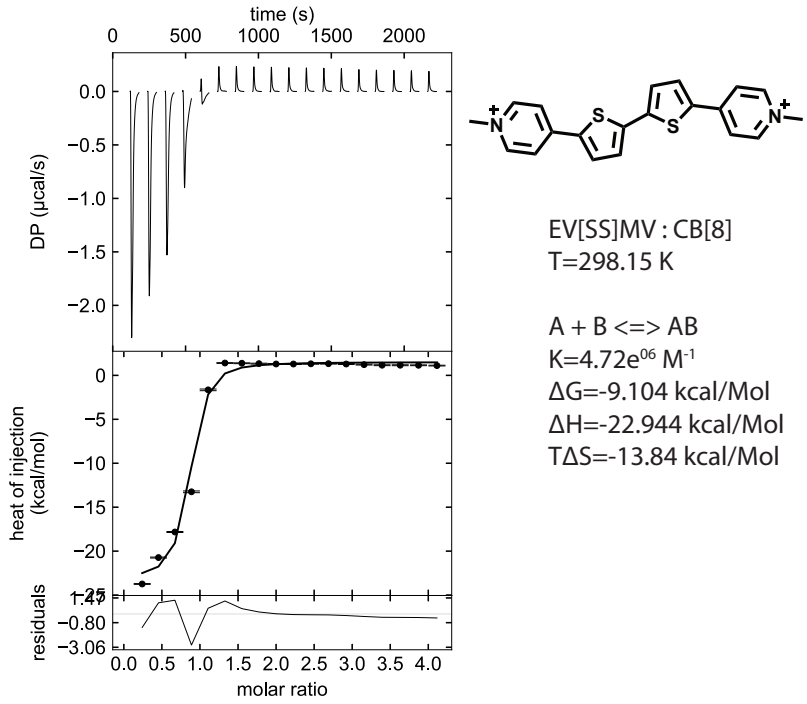

Fig. A.45 ITC titration of EV[DTh]MV to CB[8].

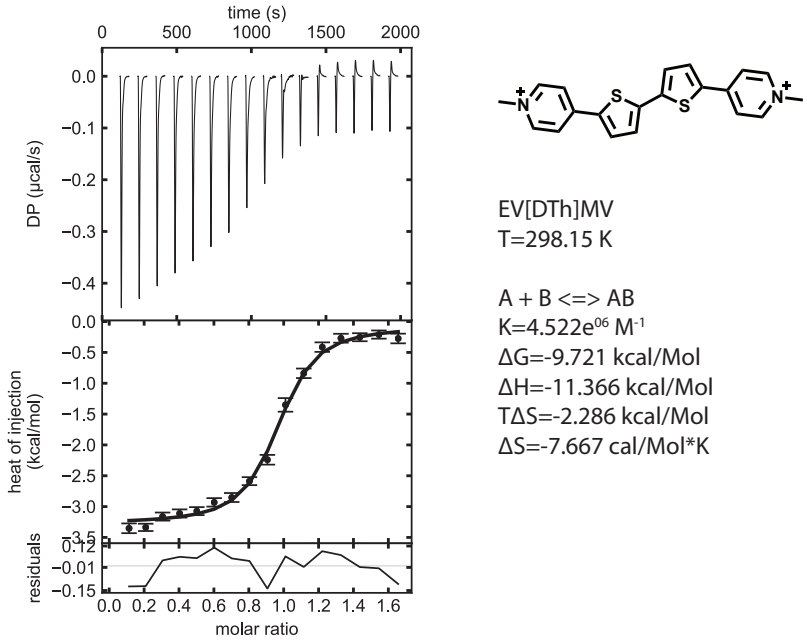

Fig. A.46 ITC titration of EV[DTh]MV to CB[7].

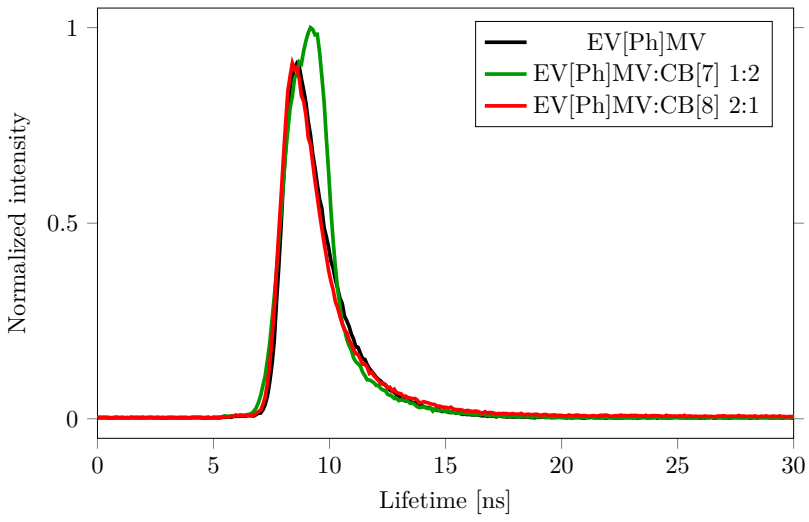

Fig. A.47 TCSPC decay profile for EV[Ph]MV, EV[Ph]MV with CB[7] and EV[Ph]MV with CB[8].

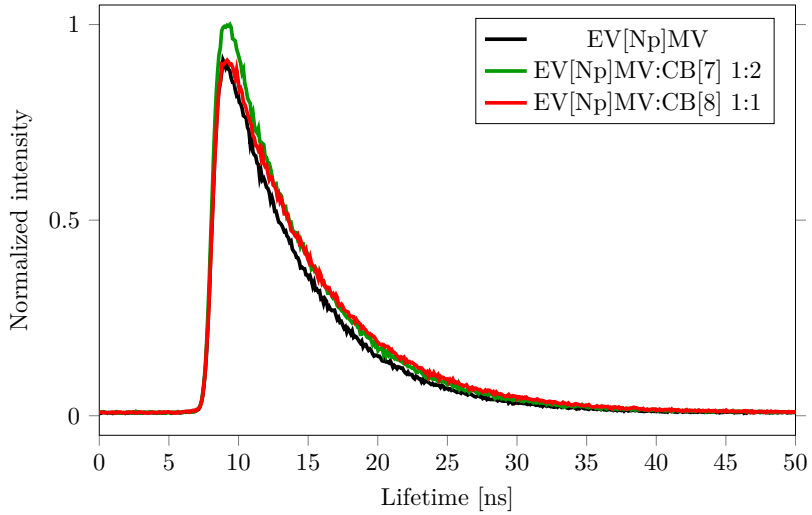

Fig. A.48 TCSPCdecay profile for EV[Np]MV, EV[Np]MV with CB[7] and EV[Np]MV with CB[8].

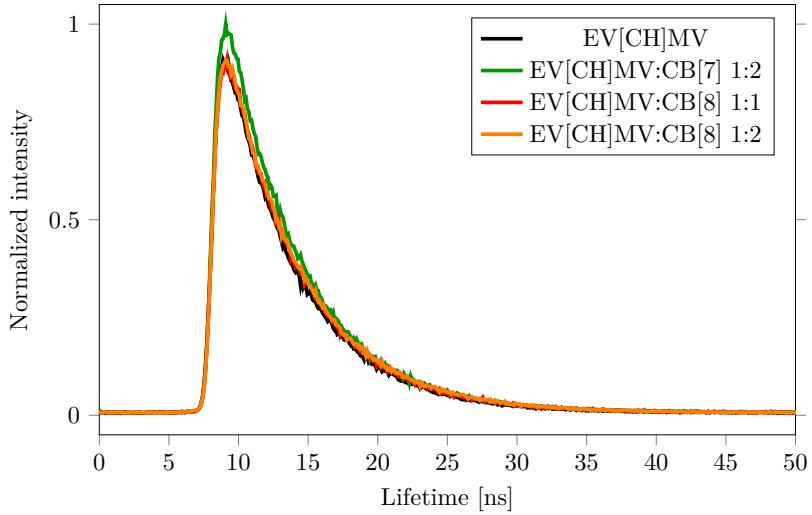

Fig. A.49 TCSPC decay profile for EV[CH]MV, EV[CH]MV with CB[7] and EV[CH]MV with CB[8].

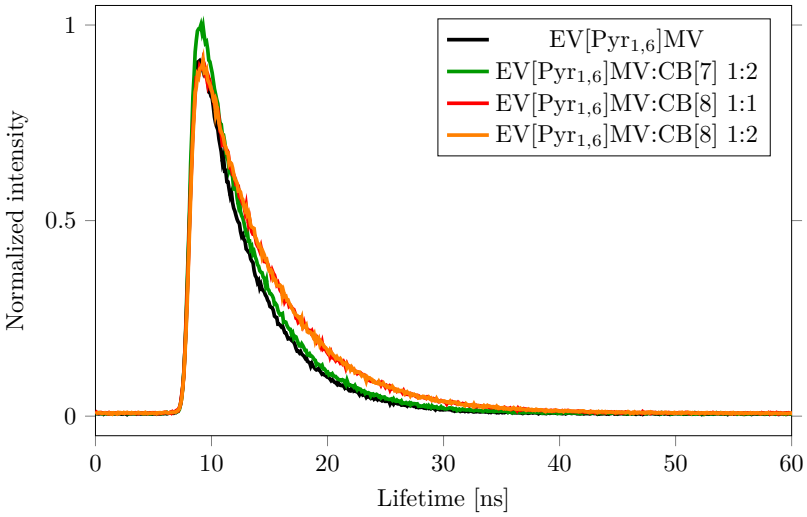

Fig. A.50 TCSPC decay profile for EV[$Pyr_{1,6}$]MV, EV[$Pyr_{1,6}$]MV with CB[7] and EV[$Pyr_{1,6}$]MV with CB[8].

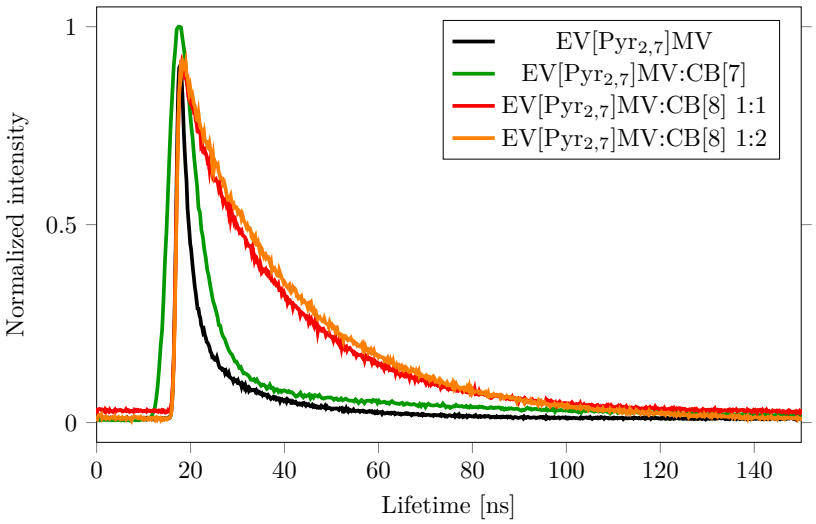

Fig. A.51 TCSPC decay profile for EV[$Pyr_{2,7}$]MV, EV[$Pyr_{2,7}$]MV with CB[7] and EV[$Pyr_{2,7}$]MV with CB[8].

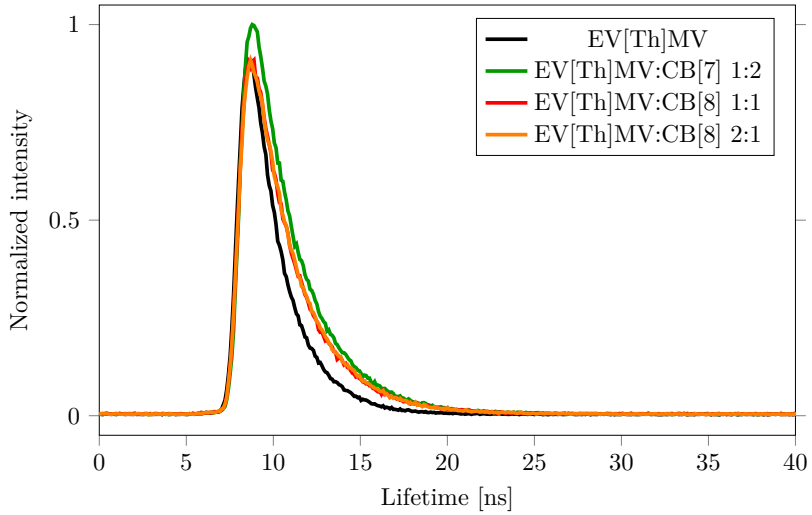

Fig. A.52 TCSPC decay profile for EV[Th]MV, EV[Th]MV with CB[7] and EV[Th]MV with CB[8].

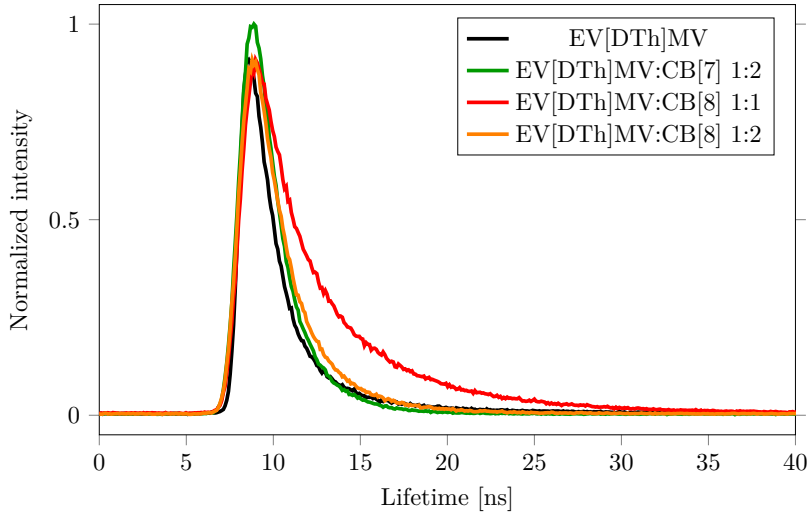

Fig. A.53 TCSPC decay profile for EV[DTh]MV, EV[DTh]MV with CB[7] and EV[DTh]MV with CB[8].

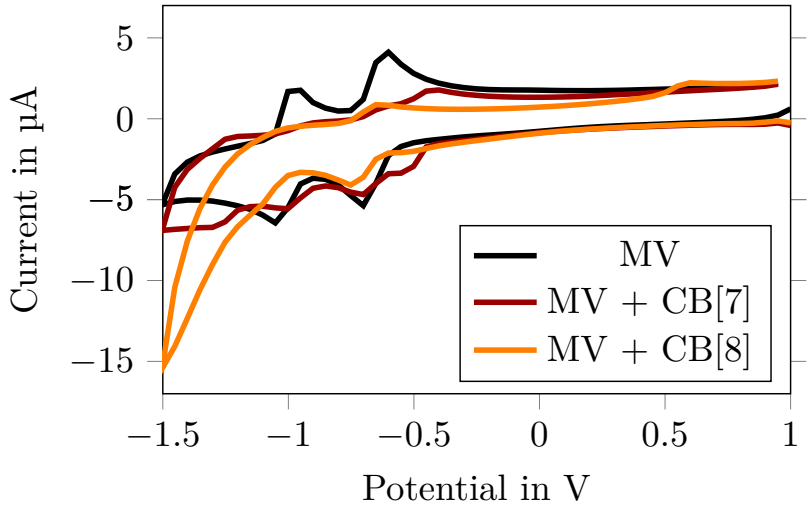

Fig. A.54 Cyclic voltammogram of 1 mM MV, MV mixed with saturated solution of CB[8], and mixed with CB[7] in 1:2 ratio at 100 mV s^{-1} in 0.1 mM KCl solution vs Ag/AgCl.

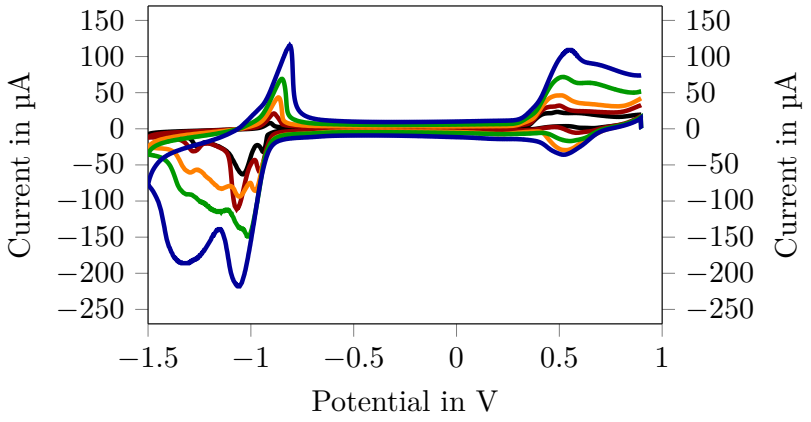

Fig. A.55 Cyclic voltammogram of 4 mM EV[Ph]MV at 25 mV s^{-1}, 50 mV s^{-1}, 100 mV s^{-1}, 200 mV s^{-1} and 400 mV s^{-1} in 0.1 mM KCl solution vs Ag/AgCl.

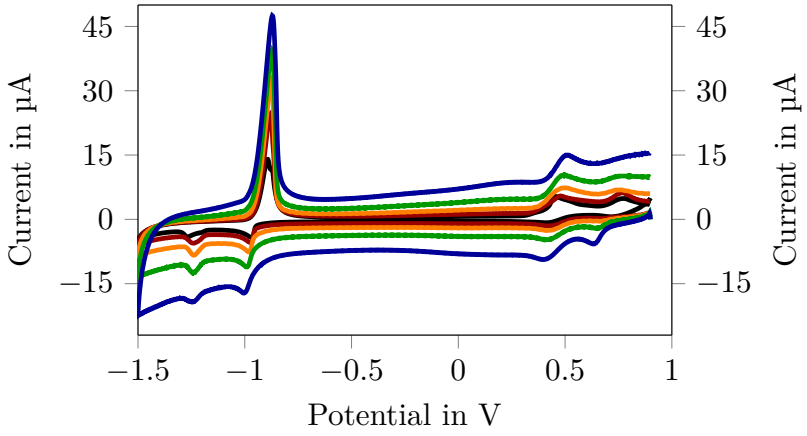

Fig. A.56 Cyclic voltammogram of 1 mM EV[Ph]MV at 25 mV s^{-1}, 50 mV s^{-1}, 100 mV s^{-1}, 200 mV s^{-1} and 400 mV s^{-1} in 0.1 mM KCl solution vs Ag/AgCl.

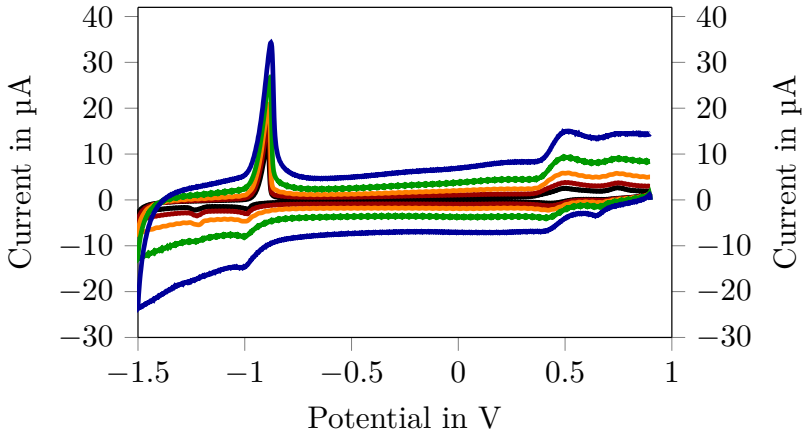

Fig. A.57 Cyclic voltammogram of 0.5 mM EV[Ph]MV at 25 mV s^{-1}, 50 mV s^{-1}, 100 mV s^{-1}, 200 mV s^{-1} and 400 mV s^{-1} in 0.1 mM KCl solution vs Ag/AgCl.

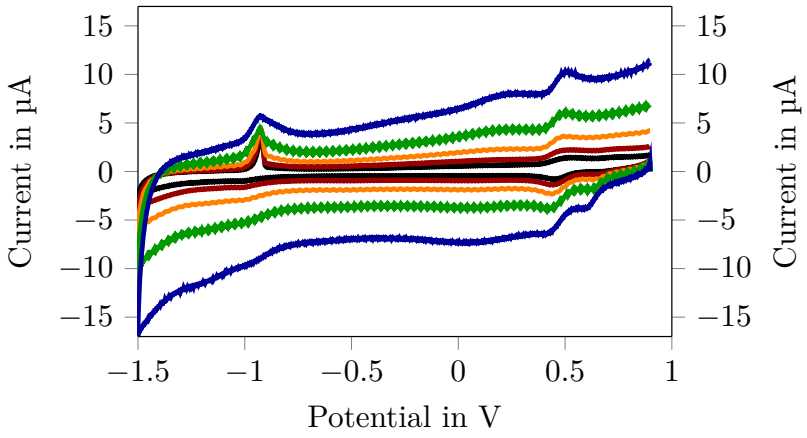

Fig. A.58 Cyclic voltammogram of 0.1 mM EV[Ph]MV at 25 mV s^{-1}, 50 mV s^{-1}, 100 mV s^{-1}, 200 mV s^{-1} and 400 mV s^{-1} in 0.1 mM KCl solution vs Ag/AgCl.

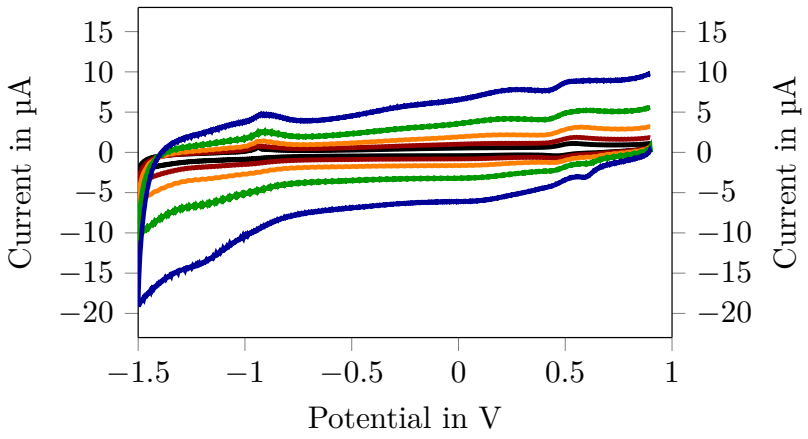

Fig. A.59 Cyclic voltammogram of 0.05 mM EV[Ph]MV at 25 mV s^{-1}, 50 mV s^{-1}, 100 mV s^{-1}, 200 mV s^{-1} and 400 mV s^{-1} in 0.1 mM KCl solution vs Ag/AgCl.

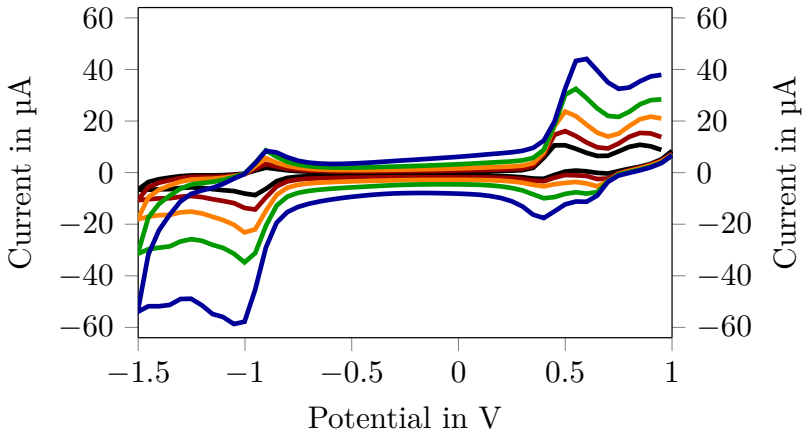

Fig. A.60 Cyclic voltammogram of 1 mM EV[Ph]MV with CB[8] at 25 mV s^{-1}, 50 mV s^{-1}, 100 mV s^{-1}, 200 mV s^{-1} and 400 mV s^{-1} in 0.1 mM KCl solution vs Ag/AgCl.

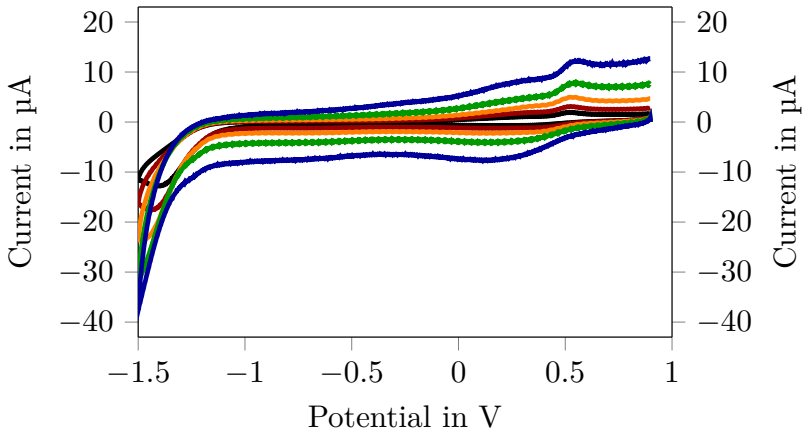

Fig. A.61 Cyclic voltammogram of 1 mM EV[Ph]MV with CB[7] at 25 mV s^{-1}, 50 mV s^{-1}, 100 mV s^{-1}, 200 mV s^{-1} and 400 mV s^{-1} in 0.1 mM KCl solution vs Ag/AgCl.

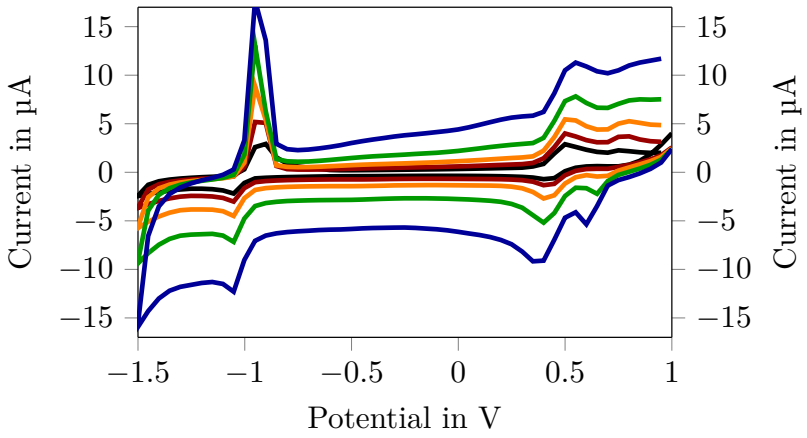

Fig. A.62 Cyclic voltammogram of 0.5 mM EV[Np]MV with CB[7] at 25 mV s^{-1}, 50 mV s^{-1}, 100 mV s^{-1}, 200 mV s^{-1} and 400 mV s^{-1} in 0.1 mM KCl solution vs Ag/AgCl.

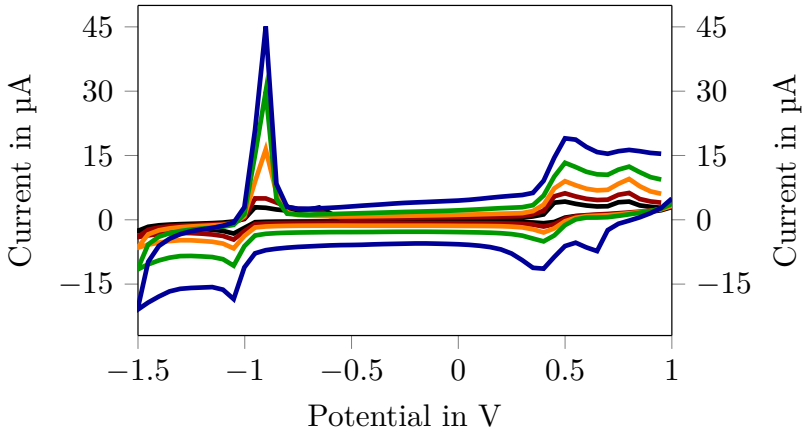

Fig. A.63 Cyclic voltammogram of 1 mM EV[Np]MV with CB[7] at 25 mV s^{-1}, 50 mV s^{-1}, 100 mV s^{-1}, 200 mV s^{-1} and 400 mV s^{-1} in 0.1 mM KCl solution vs Ag/AgCl.

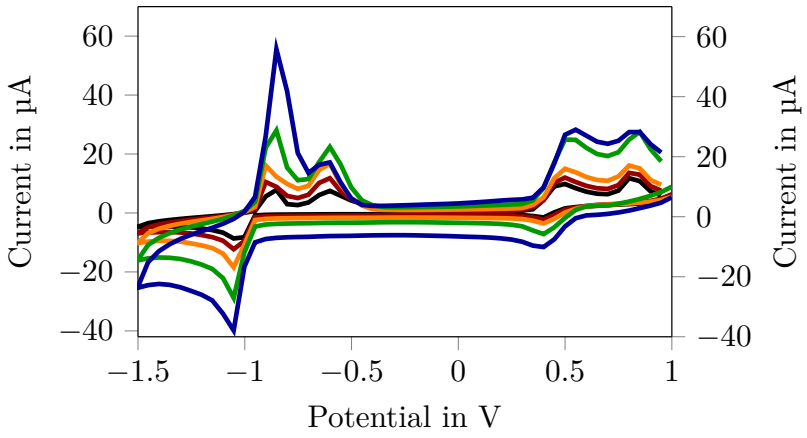

Fig. A.64 Cyclic voltammogram of 4 mM EV[Np]MV with CB[7] at 25 mV s^{-1}, 50 mV s^{-1}, 100 mV s^{-1}, 200 mV s^{-1} and 400 mV s^{-1} in 0.1 mM KCl solution vs Ag/AgCl.

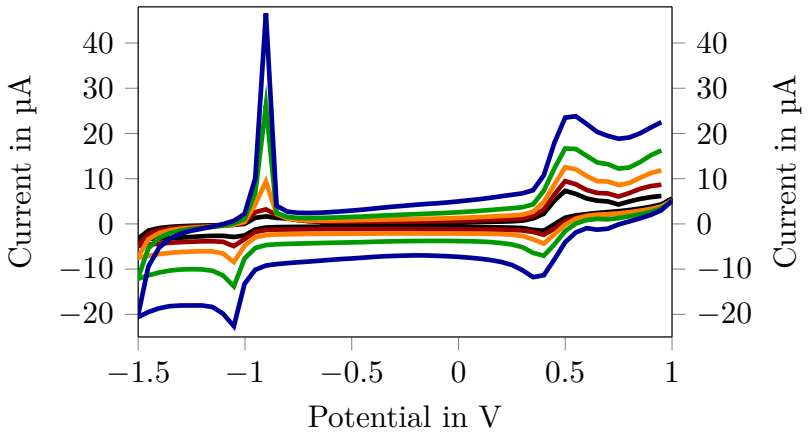

Fig. A.65 Cyclic voltammogram of 1 mM EV[Np]MV with CB[7] at 25 mV s^{-1}, 50 mV s^{-1}, 100 mV s^{-1}, 200 mV s^{-1} and 400 mV s^{-1} in 0.1 mM KCl solution vs Ag/AgCl.

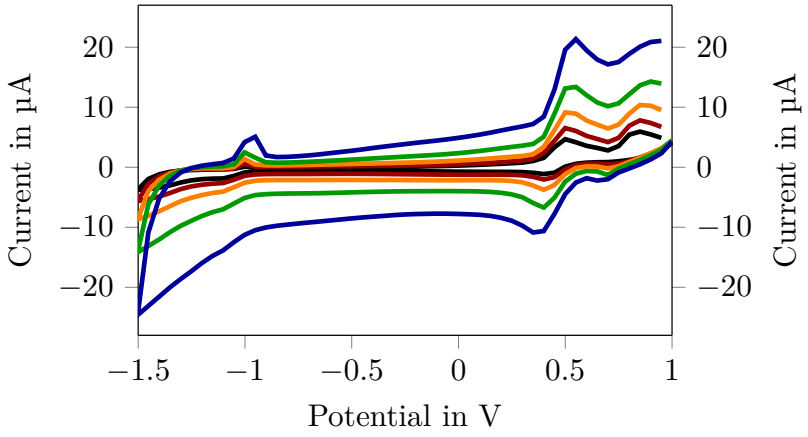

Fig. A.66 Cyclic voltammogram of 1 mM EV[Np]MV with CB[8] at 25 mV s^{-1}, 50 mV s^{-1}, 100 mV s^{-1}, 200 mV s^{-1} and 400 mV s^{-1} in 0.1 mM KCl solution vs Ag/AgCl.

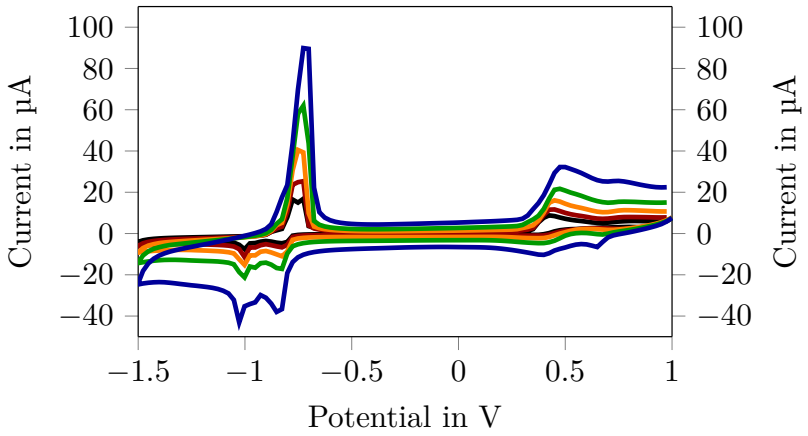

Fig. A.67 Cyclic voltammogram of 4 mM EV[Th]MV at 25 mV s^{-1}, 50 mV s^{-1}, 100 mV s^{-1}, 200 mV s^{-1} and 400 mV s^{-1} in 0.1 mM KCl solution vs Ag/AgCl.

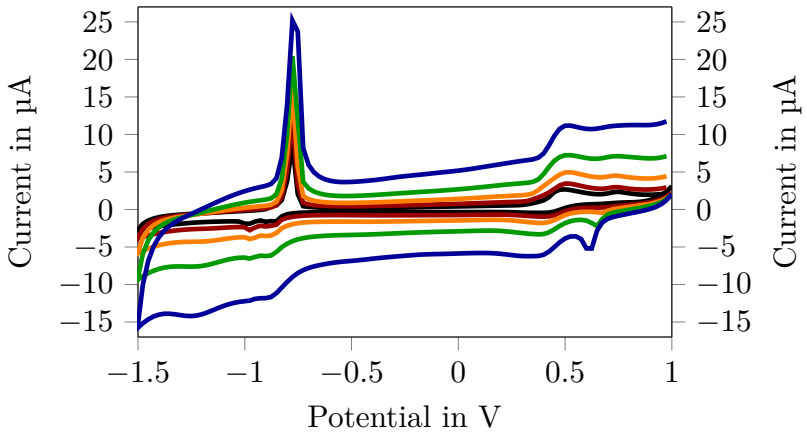

Fig. A.68 Cyclic voltammogram of 1 mM EV[Th]MV at 25 mV s^{-1}, 50 mV s^{-1}, 100 mV s^{-1}, 200 mV s^{-1} and 400 mV s^{-1} in 0.1 mM KCl solution vs Ag/AgCl.

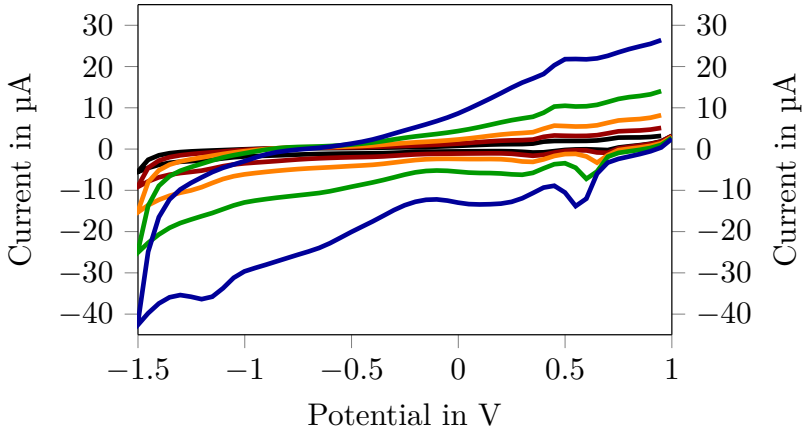

Fig. A.69 Cyclic voltammogram of 0.5 mM EV[Th]MV at 25 mV s^{-1}, 50 mV s^{-1}, 100 mV s^{-1}, 200 mV s^{-1} and 400 mV s^{-1} in 0.1 mM KCl solution vs Ag/AgCl.

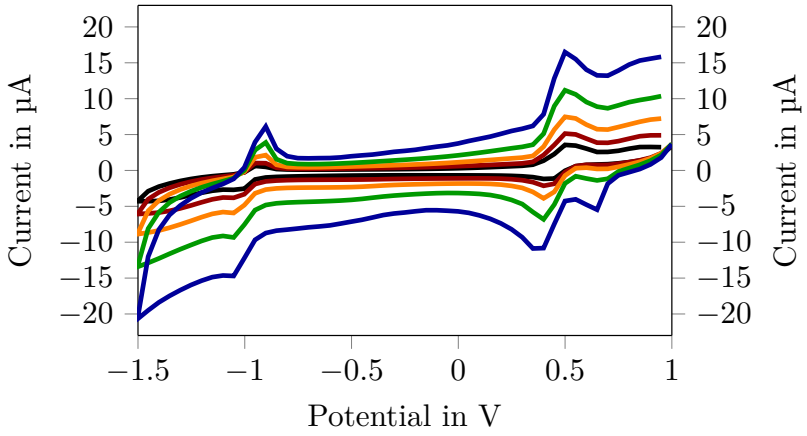

Fig. A.70 Cyclic voltammogram of 1 mM EV[Th]MV with CB[7] at 25 mV s^{-1}, 50 mV s^{-1}, 100 mV s^{-1}, 200 mV s^{-1} and 400 mV s^{-1} in 0.1 mM KCl solution vs Ag/AgCl.

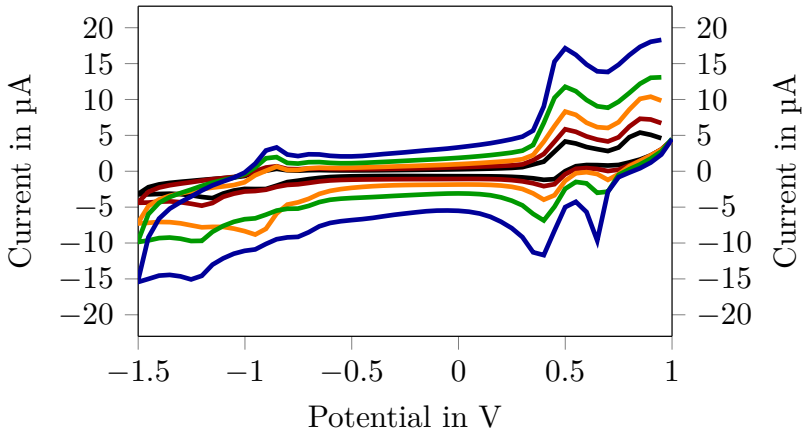

Fig. A.71 Cyclic voltammogram of 1 mM EV[Th]MV with CB[8] at 25 mV s^{-1}, 50 mV s^{-1}, 100 mV s^{-1}, 200 mV s^{-1} and 400 mV s^{-1} in 0.1 mM KCl solution vs Ag/AgCl.

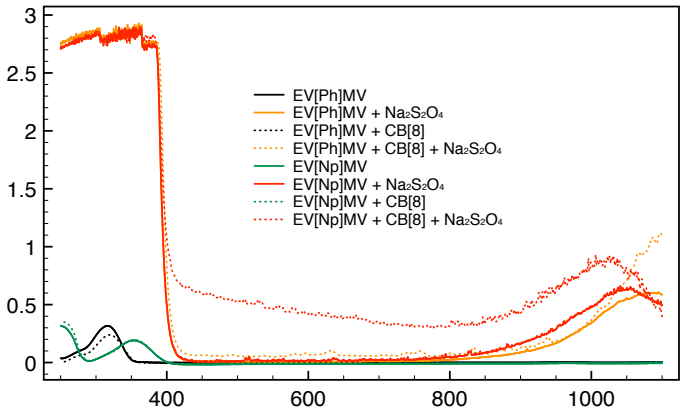

Fig. A.72 The UV – Vis of EV[Np]MV and EV[Ph]MV and their complexes with CB[8] before and after chemical reduction with sodium dithionite.

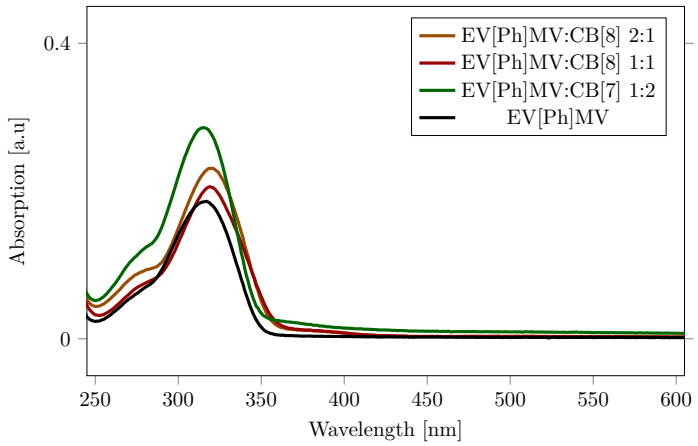

Fig. A.73 The UV – Vis of EV[Ph]MV and its complexes with CB[8] and CB[7]. All measurements were carried out at a concentration of 0.01 mM.

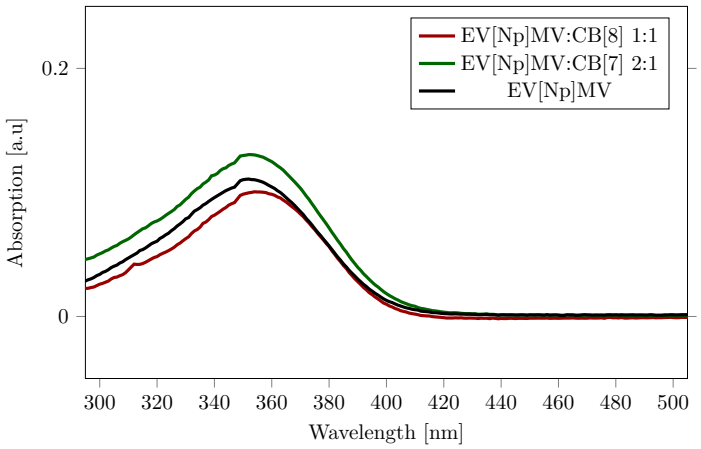

Fig. A.74 The UV – Vis of EV[Np]MV and its complexes with CB[8] and CB[7]. All measurements were carried out at a concentration of 0.01 mM.

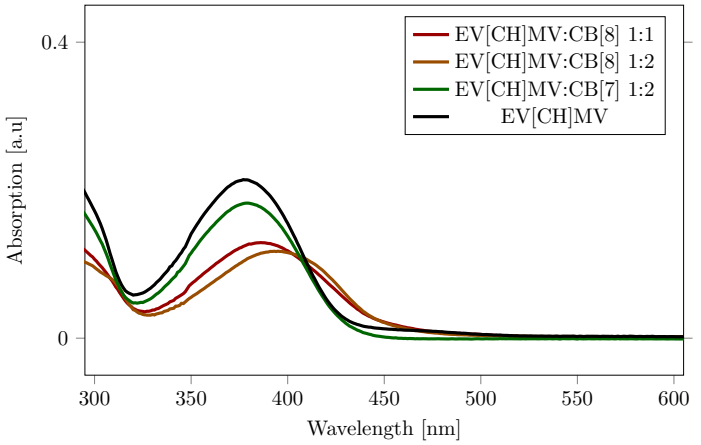

Fig. A.75 The UV – Vis of EV[CH]MV and its complexes with CB[8] and CB[7]. All measurements were carried out at a concentration of 0.01 mM.

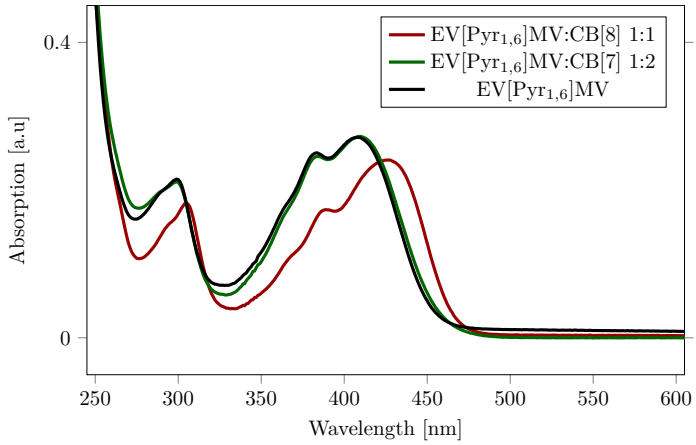

Fig. A.76 The UV – Vis of EV[$Pyr_{1,6}$]MV and its complexes with CB[8] and CB[7]. All measurements were carried out at a concentration of 0.01 mM.

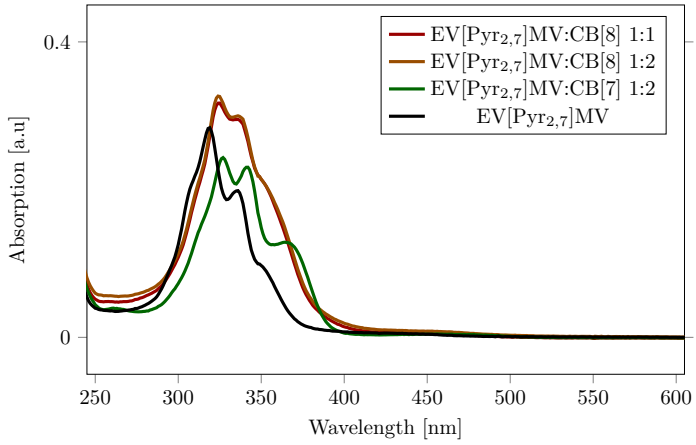

Fig. A.77 The UV – Vis of EV[$Pyr_{2,7}$]MV and its complexes with CB[8] and CB[7]. All measurements were carried out at a concentration of 0.01 mM.

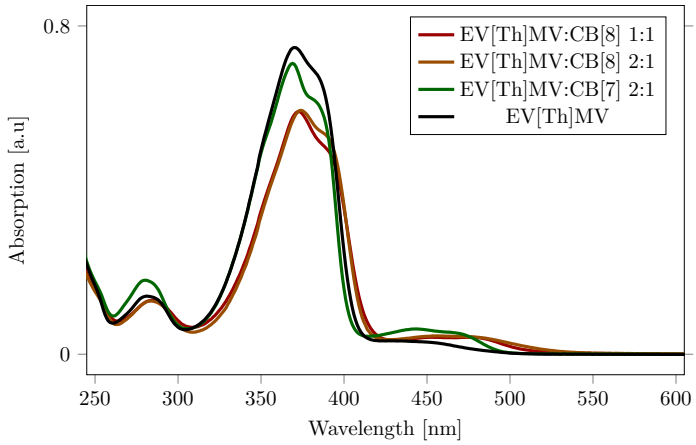

Fig. A.78 The UV – Vis of EV[Th]MV and its complexes with CB[8] and CB[7]. All measurements were carried out at a concentration of 0.01 mM.

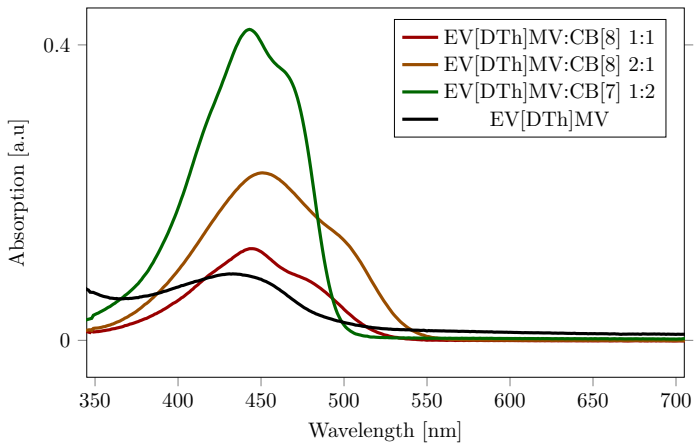

Fig. A.79 The UV – Vis of EV[DTh]MV and its complexes with CB[8] and CB[7]. All measurements were carried out at a concentration of 0.01 mM.

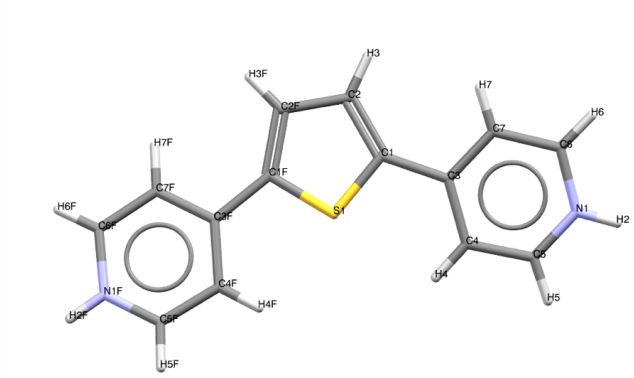

Atom1	Atom2	Atom3	Angle
C1	S1	C1F	98.7
S1	C1F	C3F	110.5

Fig. A.80 The crystallographic data of BARLEM with angles of interest.

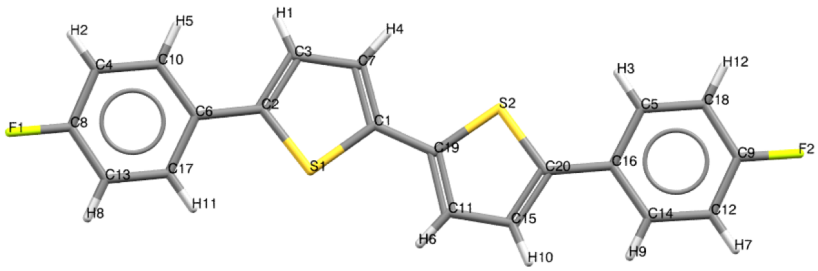

Atom1	Atom2	Atom3	Angle
C1	S1	C2	92.4(1)
S1	C2	C6	121.6(2)

Fig. A.81 The crystallographic data of COBDAA with angles of interest

Appendix B

Appendix for chapter 3

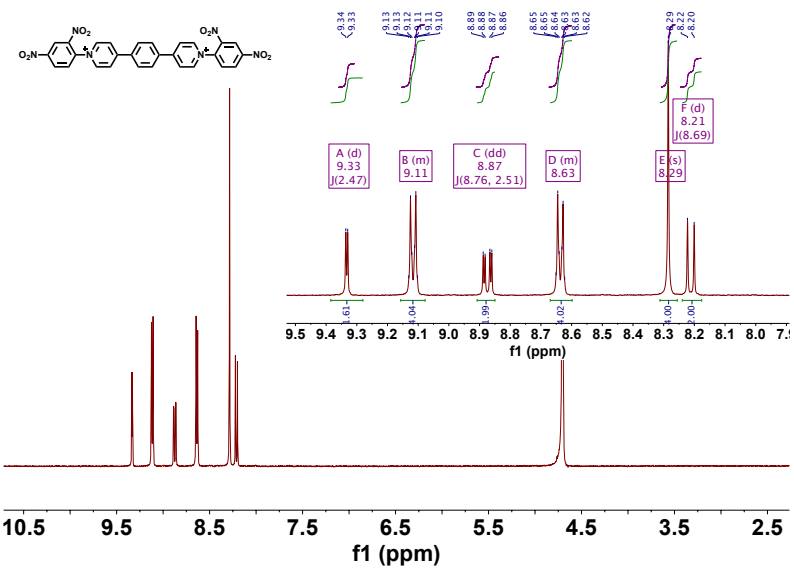

Fig. B.1 ^{1}H NMR of EV[Ph]DNB (500 MHz, D_2O).

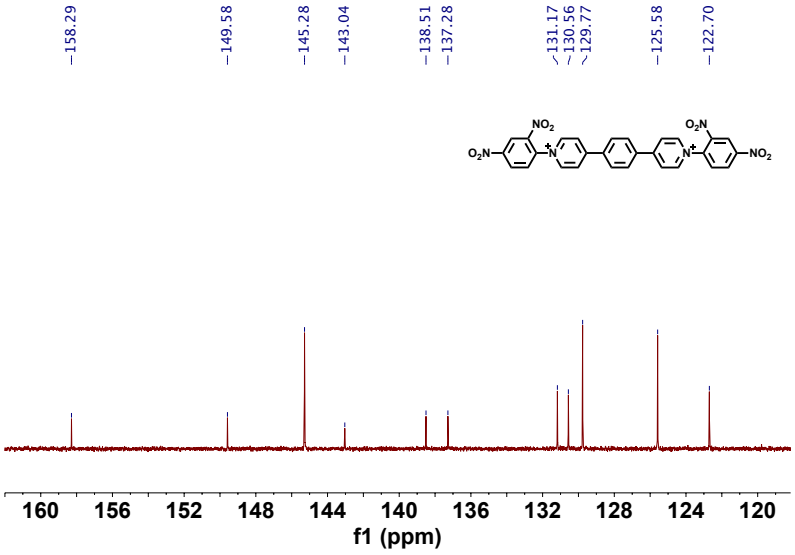

Fig. B.2 ^{13}C NMR of EV[Ph]DNB (126 MHz, D_2O).

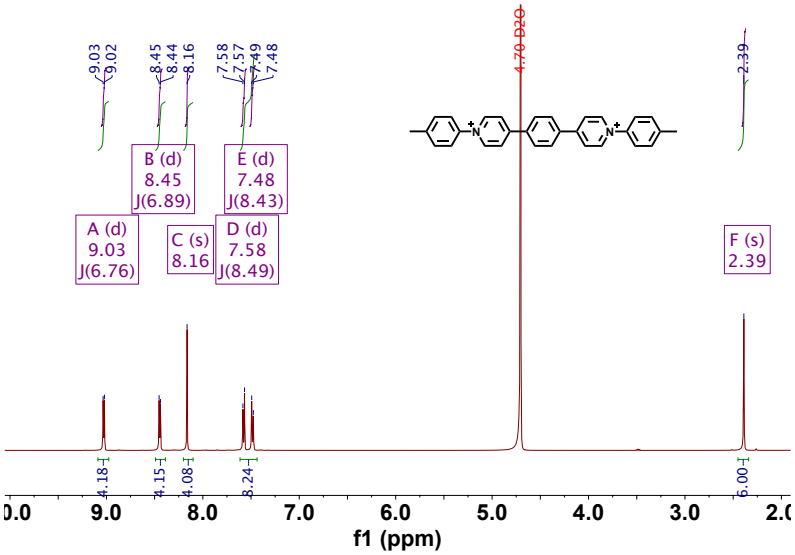

Fig. B.3 ^{1}H NMR of EV[Ph]Me (500 MHz, D_2O).

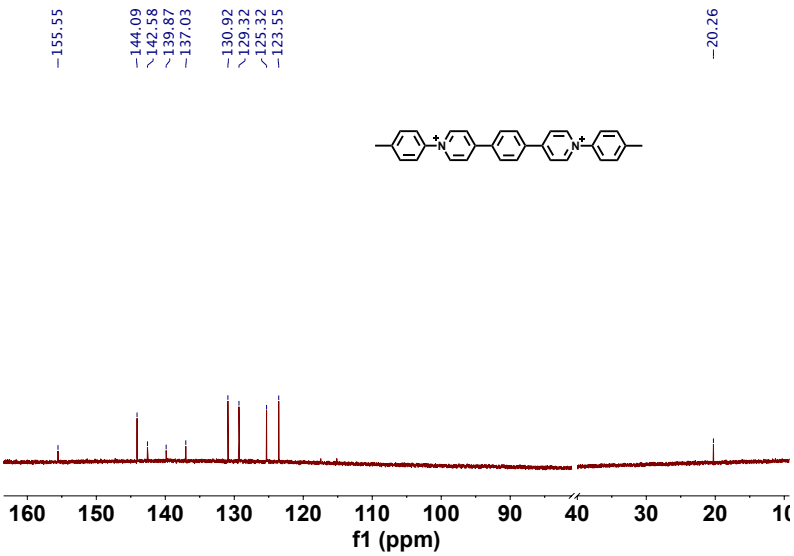

Fig. B.4 ^{13}C NMR of EV[Ph]Me (126 MHz, D_2O).

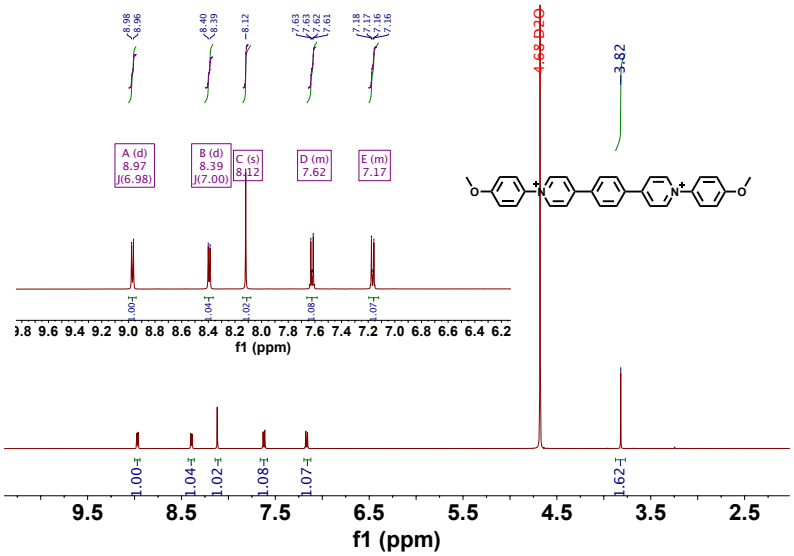

Fig. B.5 ^{1}H NMR of EV[Ph]OMe (500 MHz, D_2O).

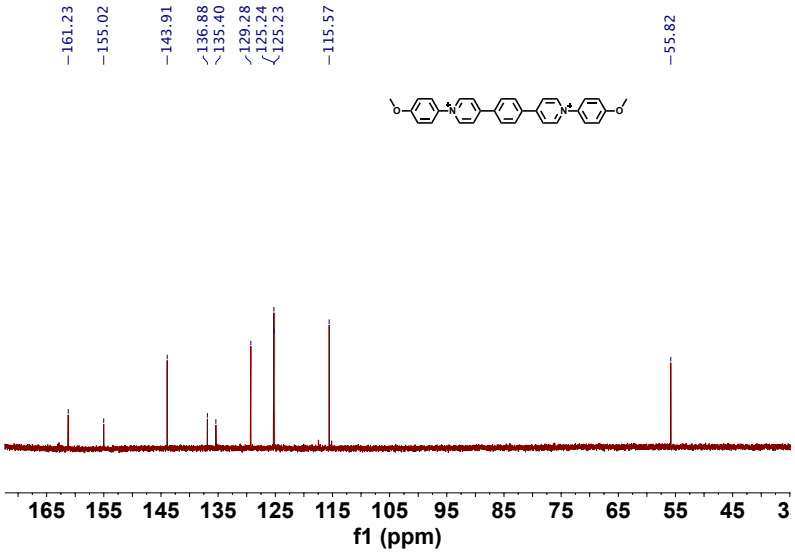

Fig. B.6 ^{13}C NMR of EV[Ph]OMe (126 MHz, D_2O).

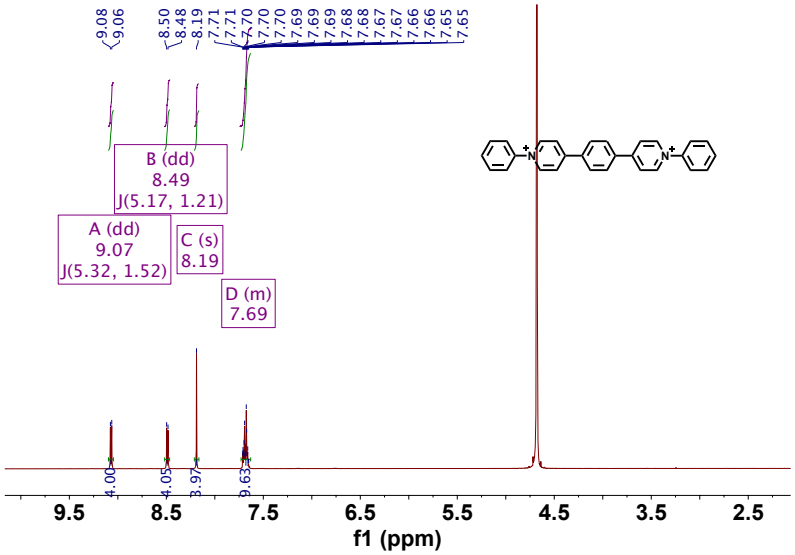

Fig. B.7 ^{1}H NMR of EV[Ph]H (500 MHz, D_2O).

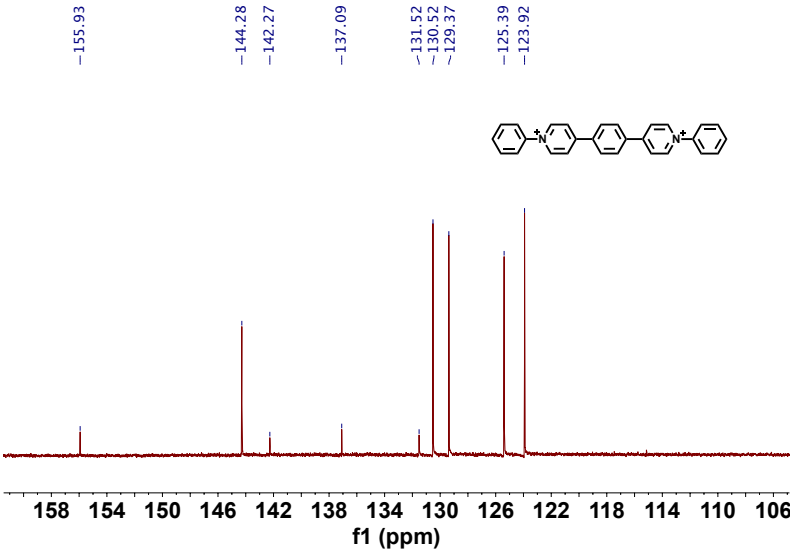

Fig. B.8 ^{13}C NMR of EV[Ph]H (126 MHz, D_2O).

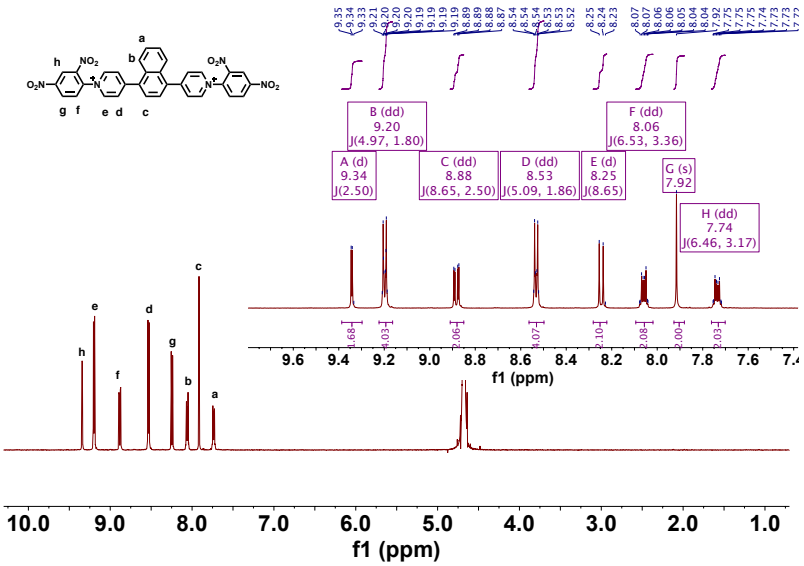

Fig. B.9 ^{1}H NMR of EV[Np]DNB (500 MHz, D_2O).

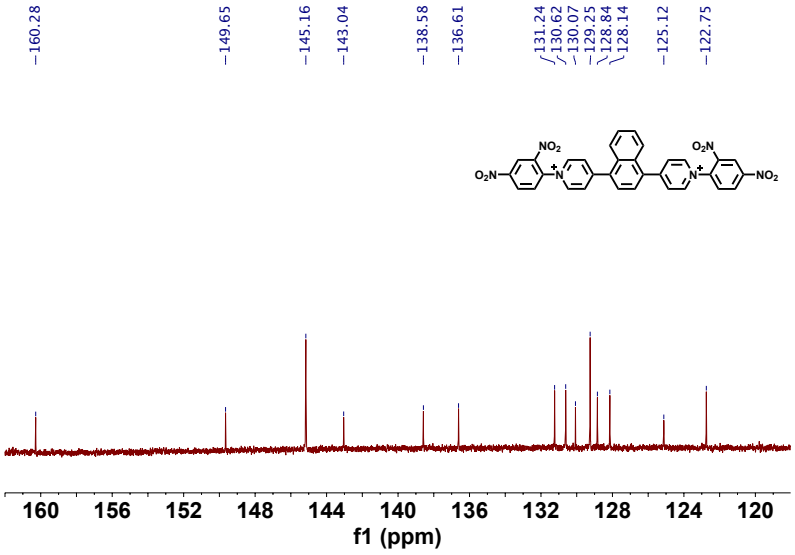

Fig. B.10 ^{13}C NMR of EV[Np]DNB (126 MHz, D_2O).

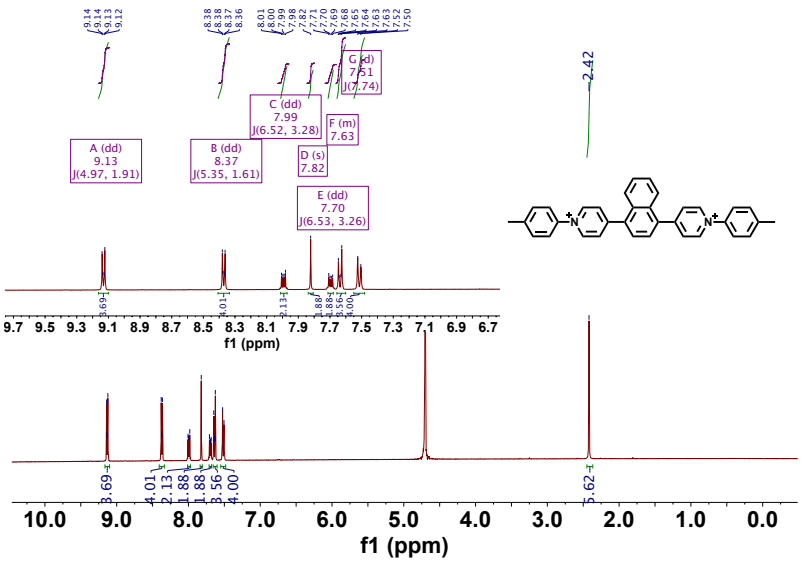

Fig. B.11 ^{1}H NMR of EV[Np]Me (500 MHz, D_2O).

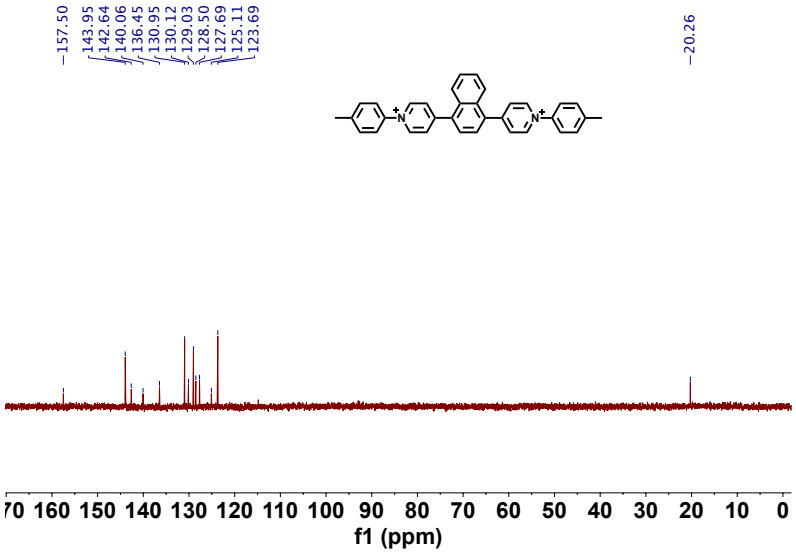

Fig. B.12 ^{13}C NMR of EV[Np]Me (126 MHz, D_2O).

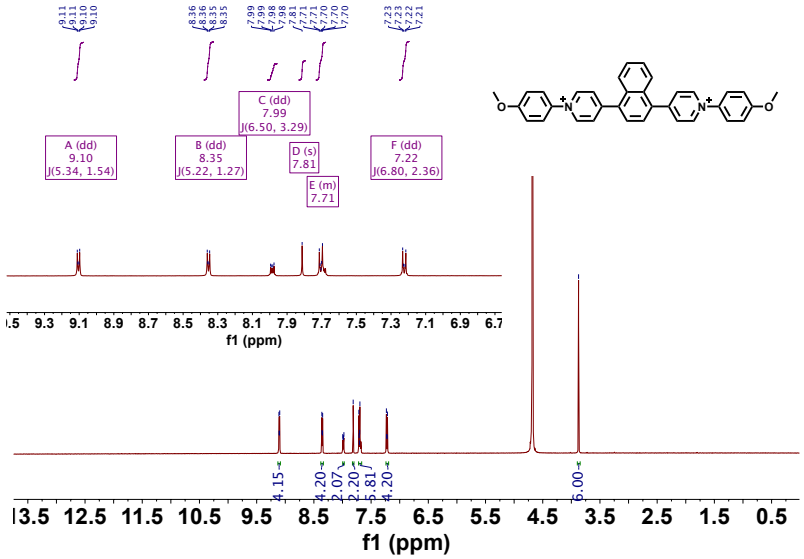

Fig. B.13 ^{1}H NMR of EV[Np]OMe (500 MHz, D_2O).

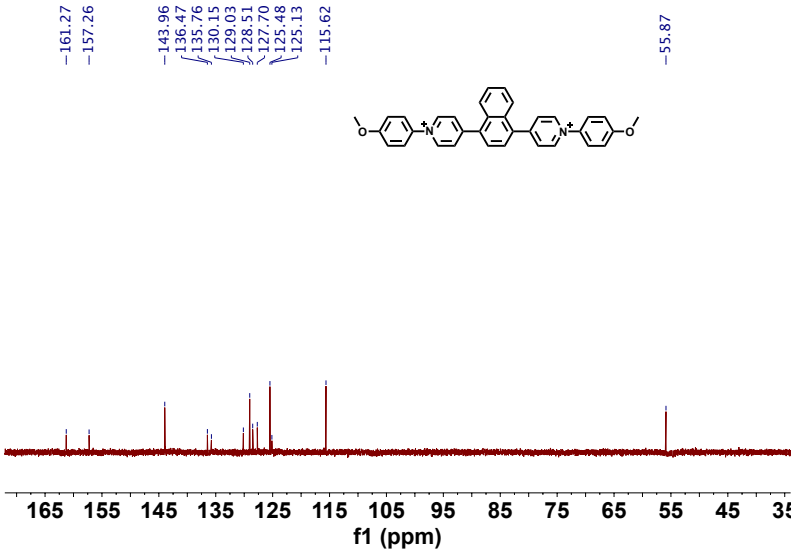

Fig. B.14 ^{13}C NMR of EV[Np]OMe (126 MHz, D_2O).

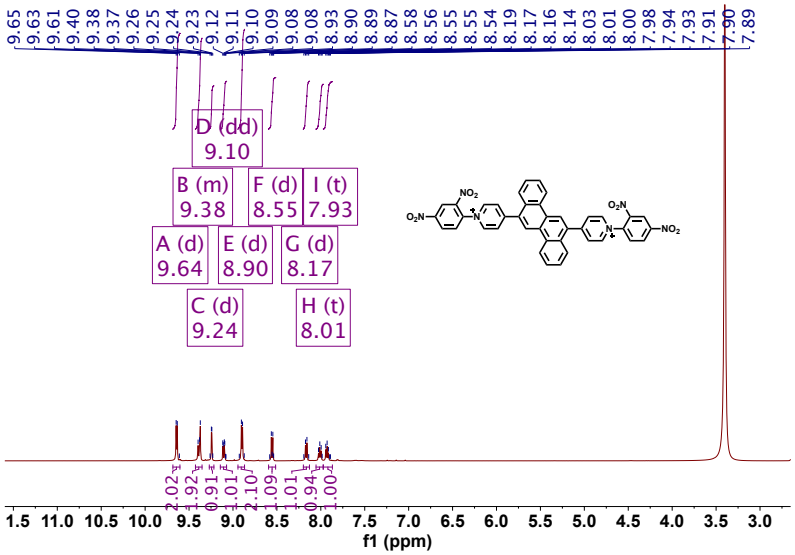

Fig. B.15 ^{1}H NMR of EV[CH]DNB (500 MHz, D_2O).

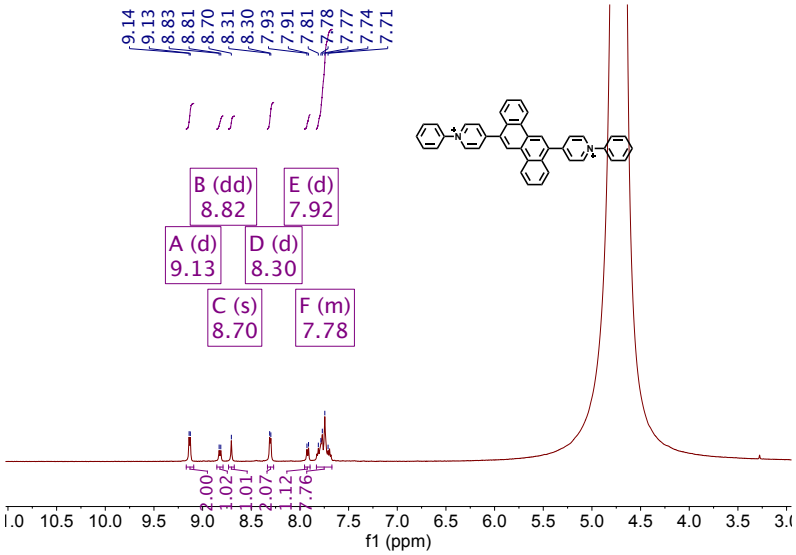

Fig. B.16 ^{1}H NMR of EV[CH]H (500 MHz, D_2O).

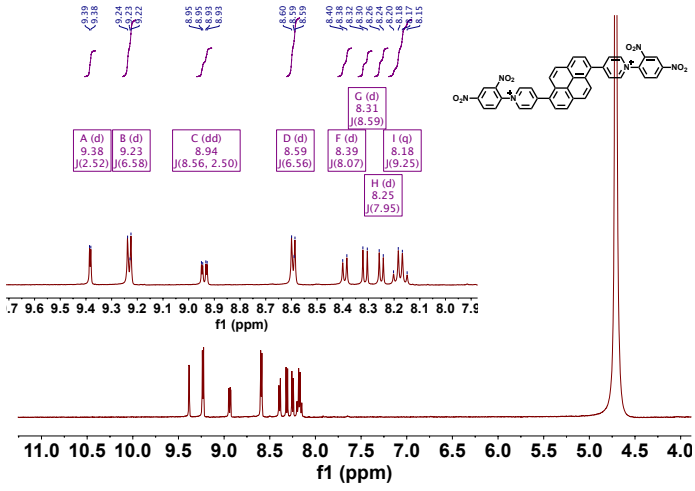

Fig. B.17 ^{1}H NMR of EV[$Pyr_{1,6}$]DNB (500 MHz, D_2O).

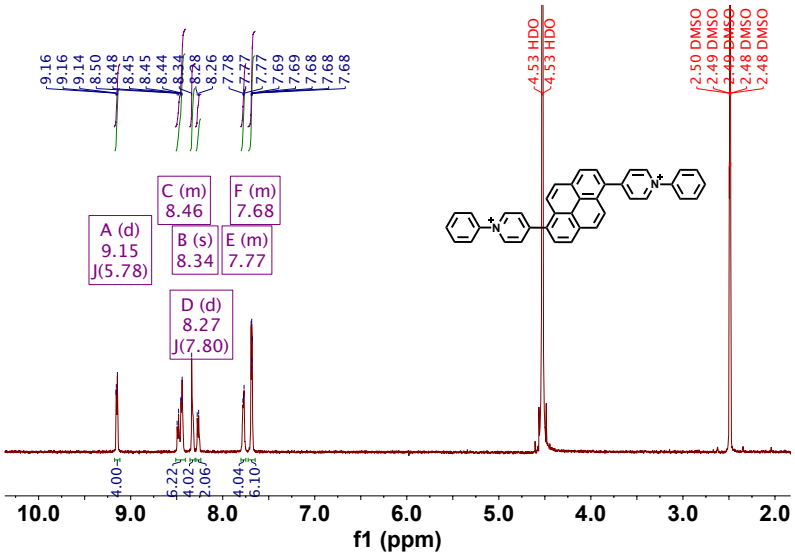

Fig. B.18 ^{1}H NMR of EV[Pyr$_{1,6}$H (500 MHz, D_2O).

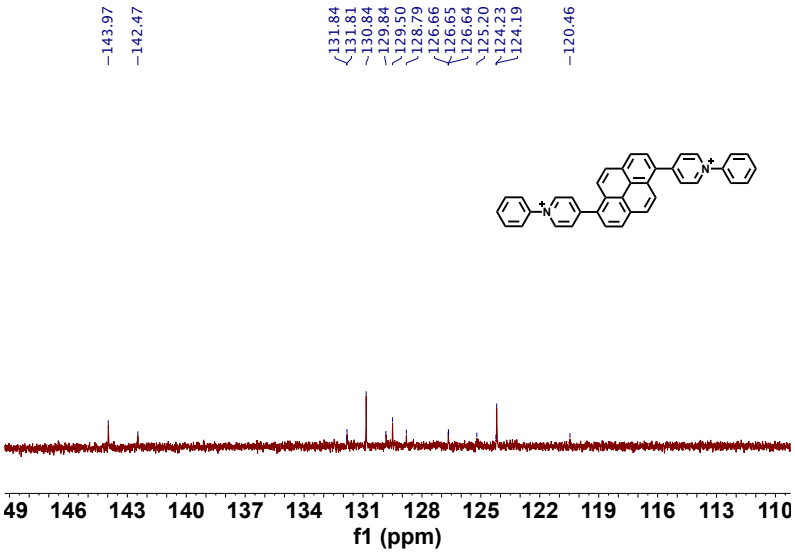

Fig. B.19 ^{13}C NMR of EV[Pyr$_{1,6}$H (126 MHz, D_2O).

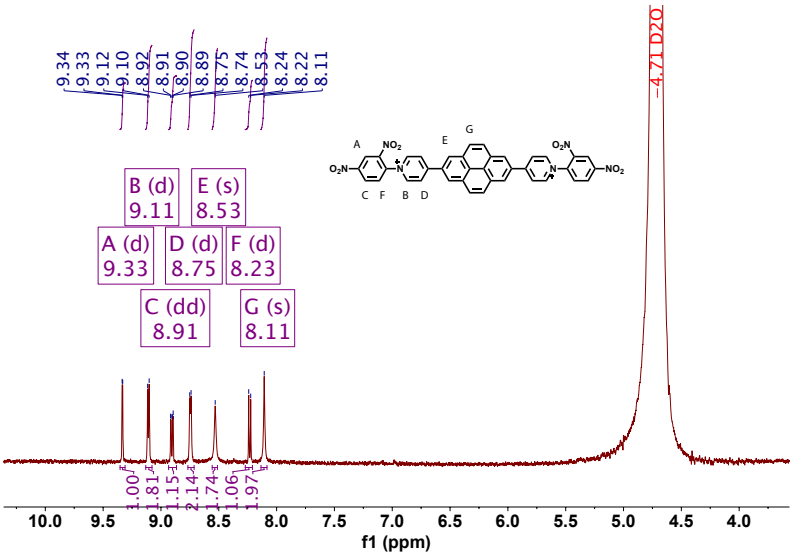

Fig. B.20 ^{1}H NMR of EV[Pyr$_{2,7}$]DNB (500 MHz, D_2O).

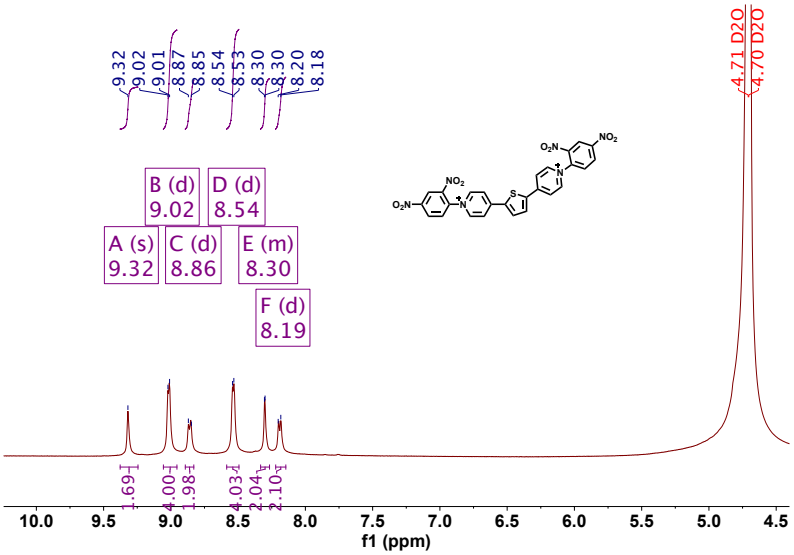

Fig. B.21 ^{1}H NMR of EV[Th]DNB (500 MHz, D_2O).

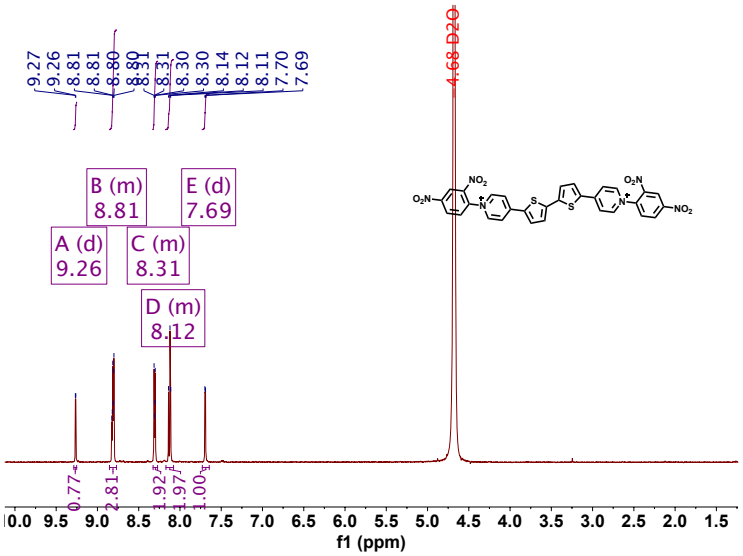

Fig. B.22 ^{1}H NMR of EV[DTh]DNB (500 MHz, D_2O).

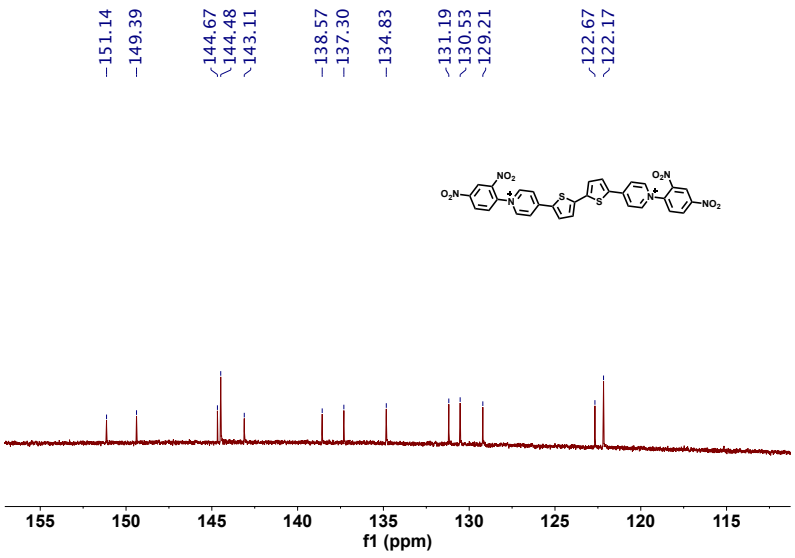

Fig. B.23 ^{13}C NMR of EV[DTh]DNB (126 MHz, D_2O).

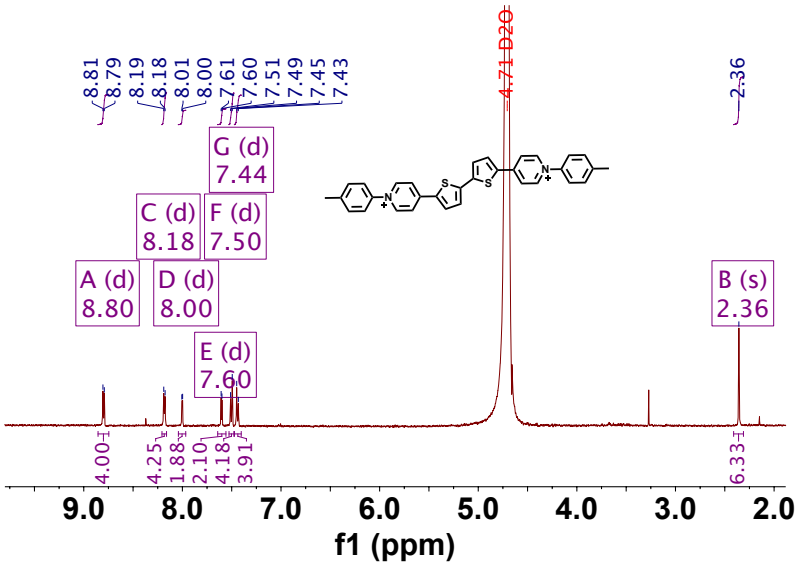

Fig. B.24 ^{1}H NMR of EV[DTh]Me (500 MHz, D_2O).

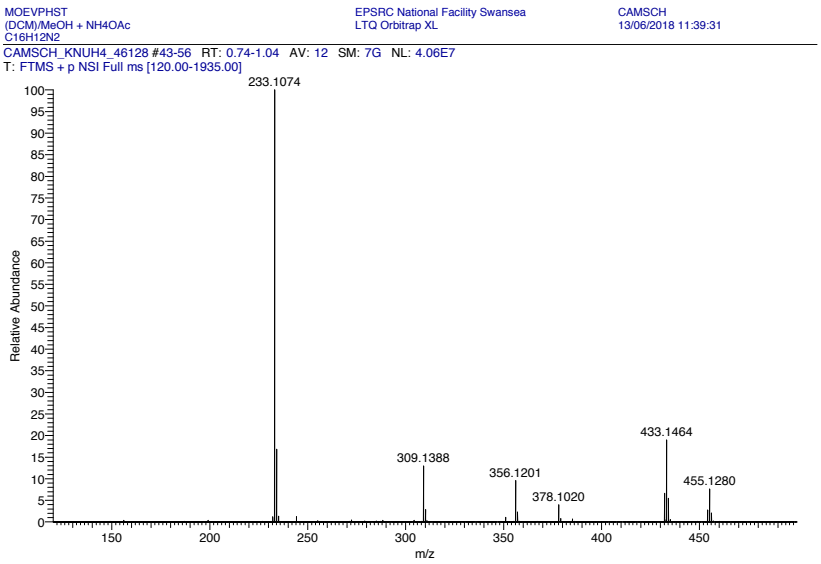

Fig. B.25 HRMS of EV[Ph]

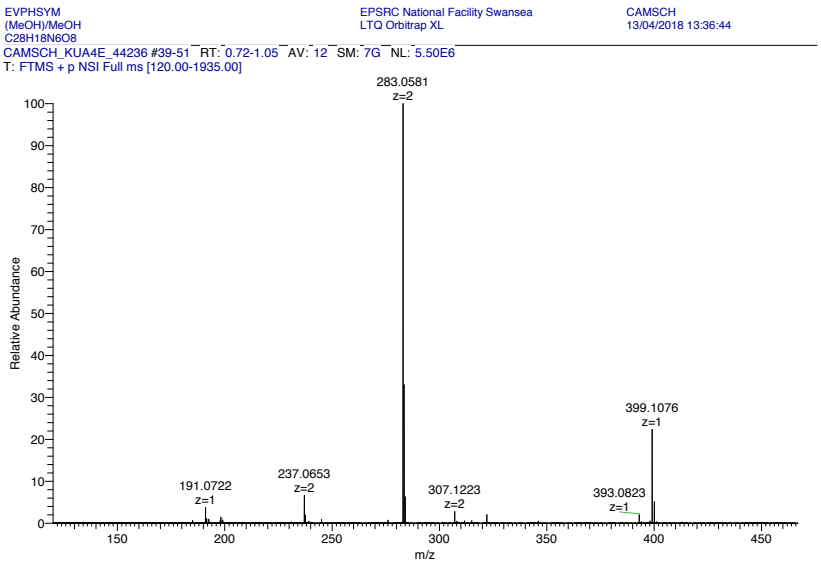

Fig. B.26 HRMS of EV[Ph]DNB

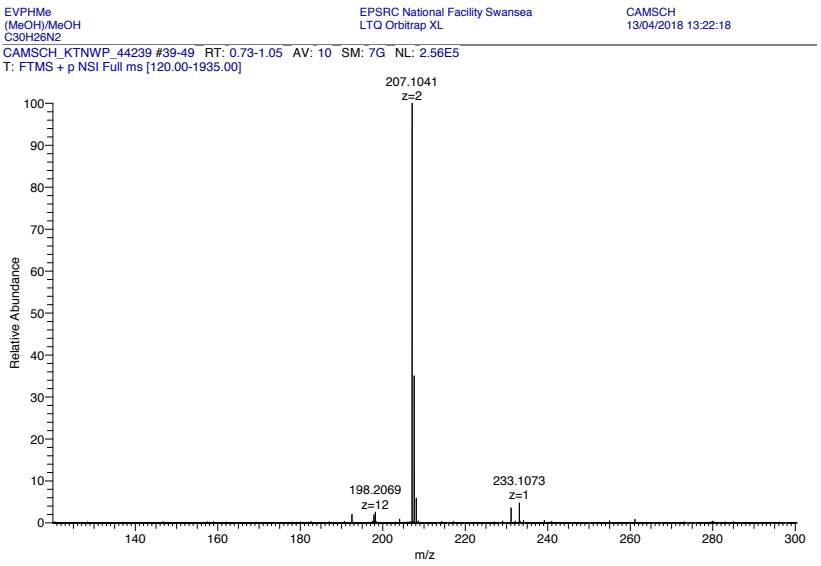

Fig. B.27 HRMS of EV[Ph]Me.

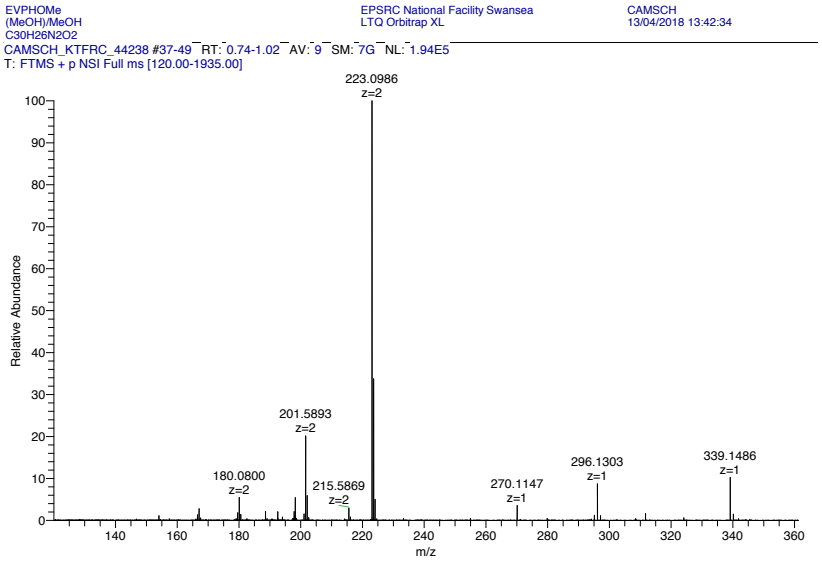

Fig. B.28 HRMS of EV[Ph]OMe

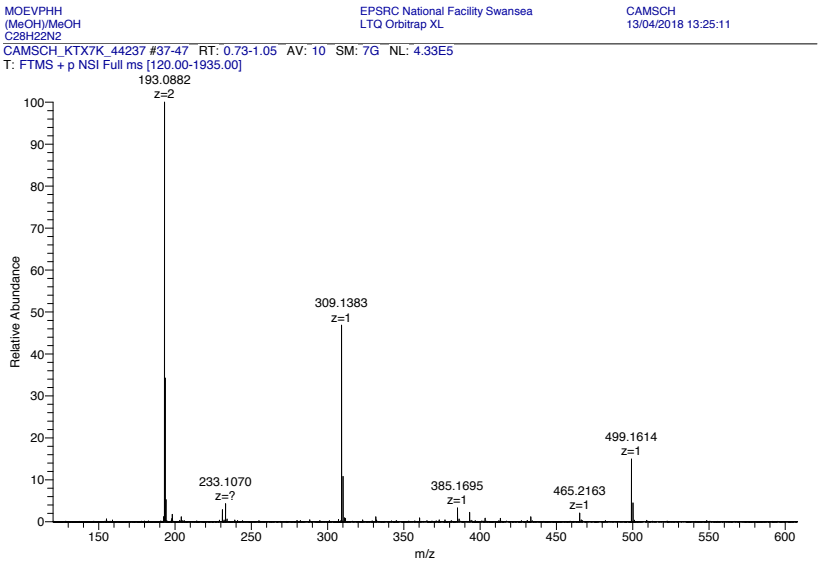

Fig. B.29 HRMS of EV[Ph]H

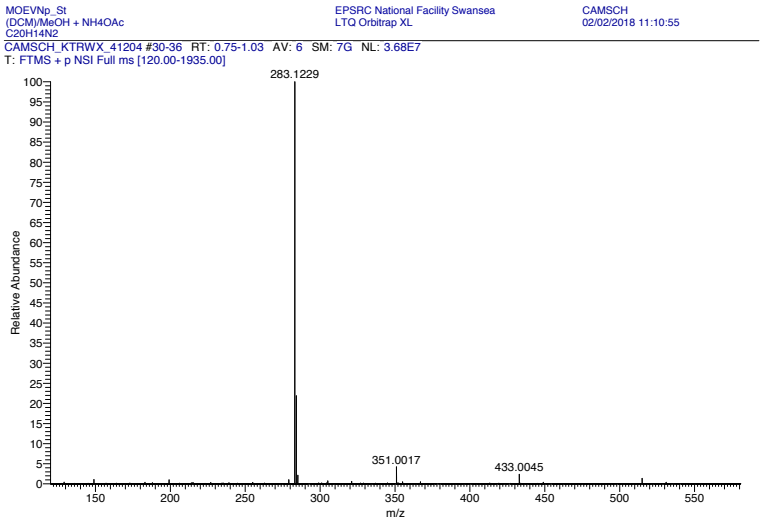

Fig. B.30 HRMS of EV[Np].

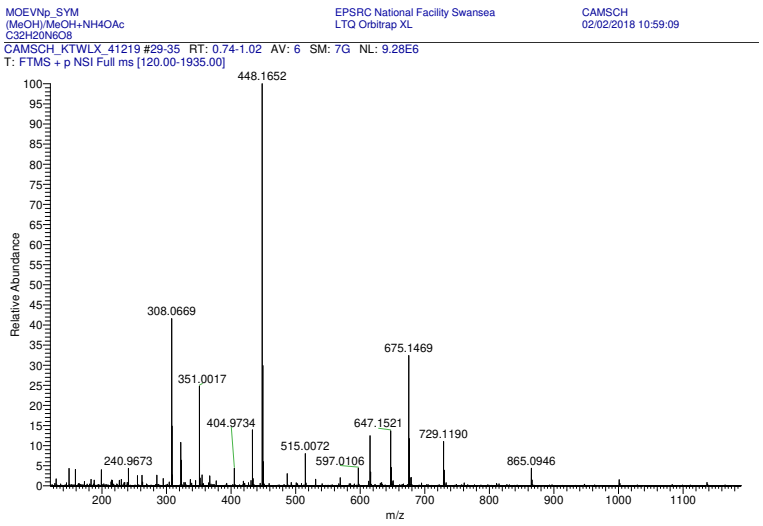

Fig. B.31 HRMS of EV[Np]DNB.

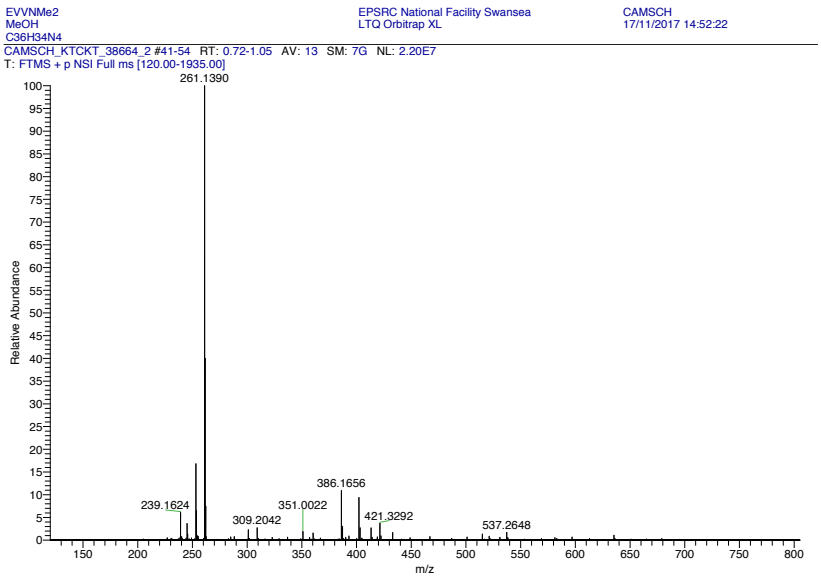

Fig. B.32 HRMS of EV[Np]Me.

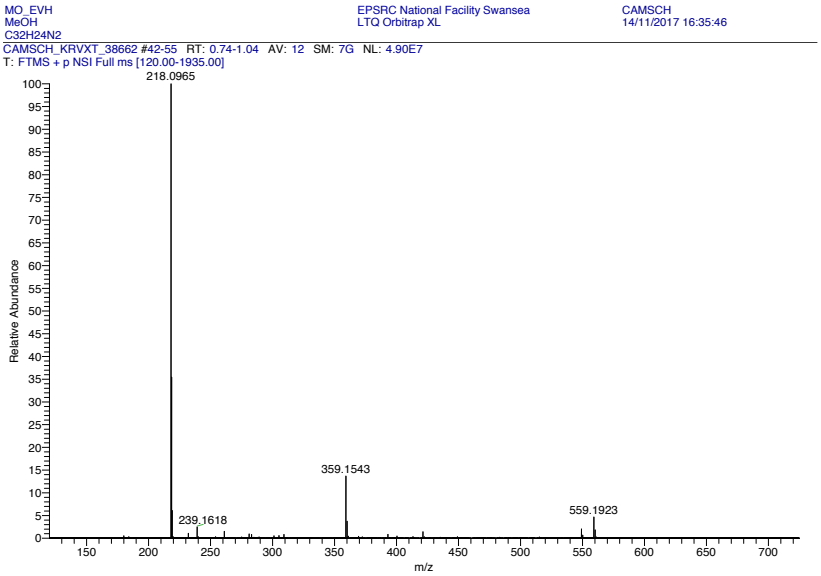

Fig. B.33 HRMS of EV[Np]H

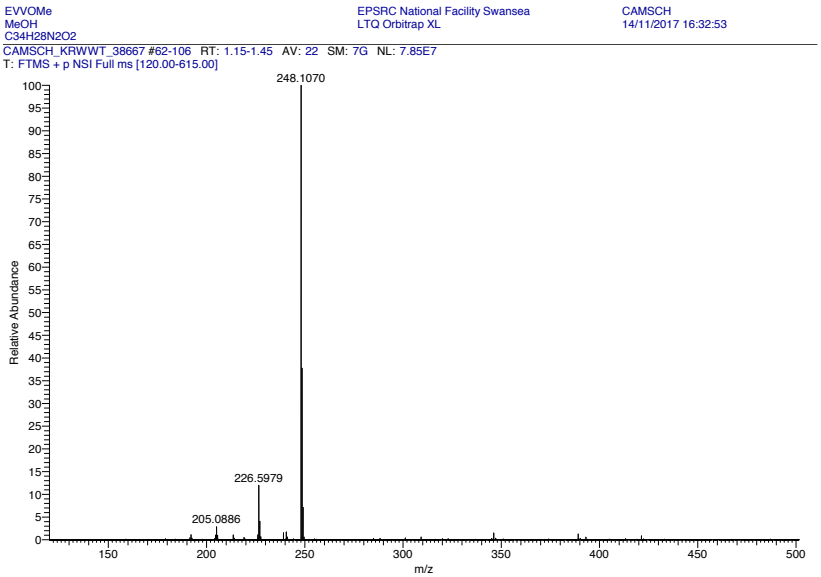

Fig. B.34 HRMS of EV[Np]OMe.

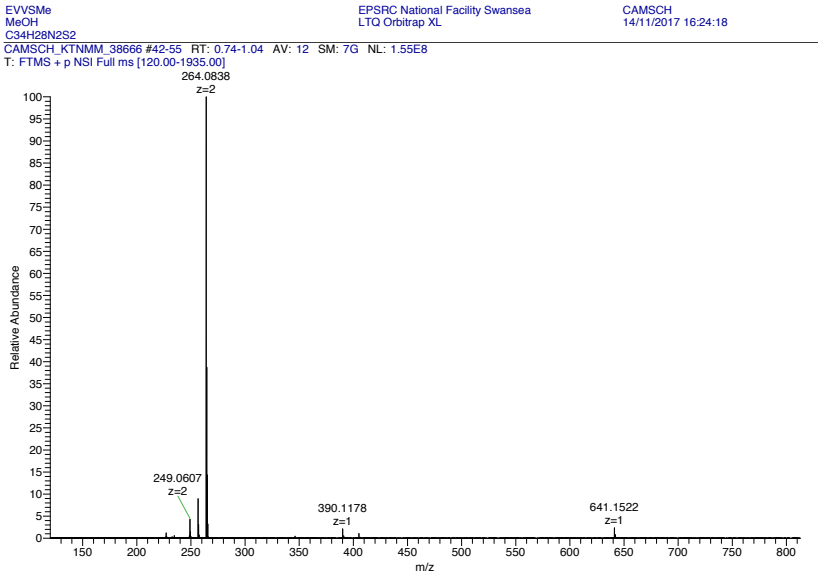

Fig. B.35 HRMS of EV[Np]SMe.

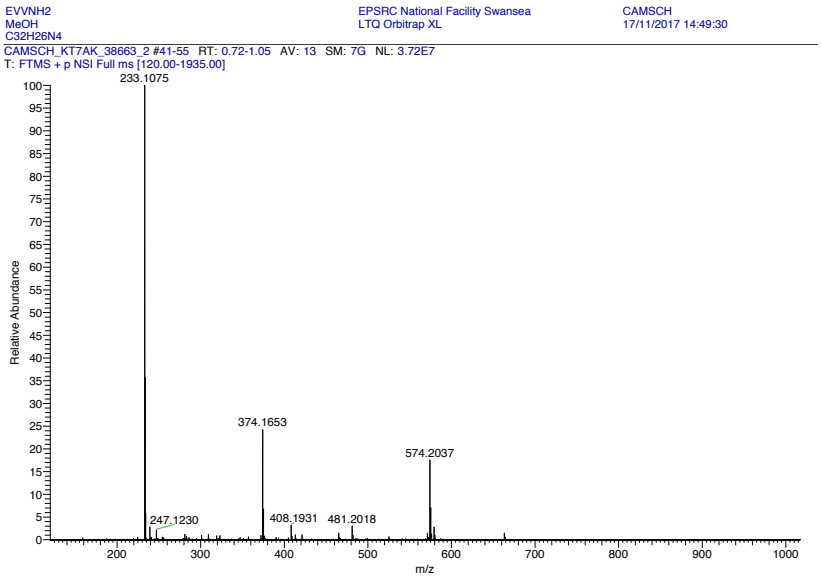

Fig. B.36 HRMS of EV[Np]NH_2.

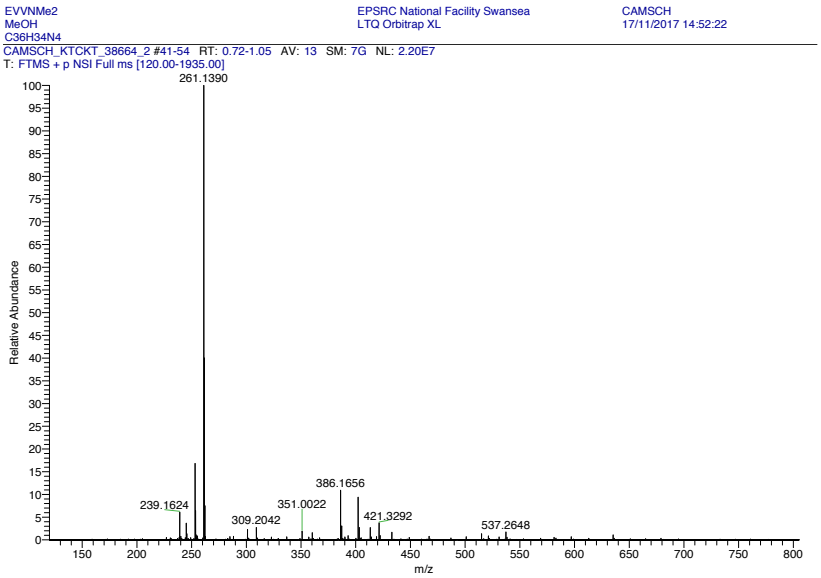

Fig. B.37 HRMS of EV[Np]NMe_2.

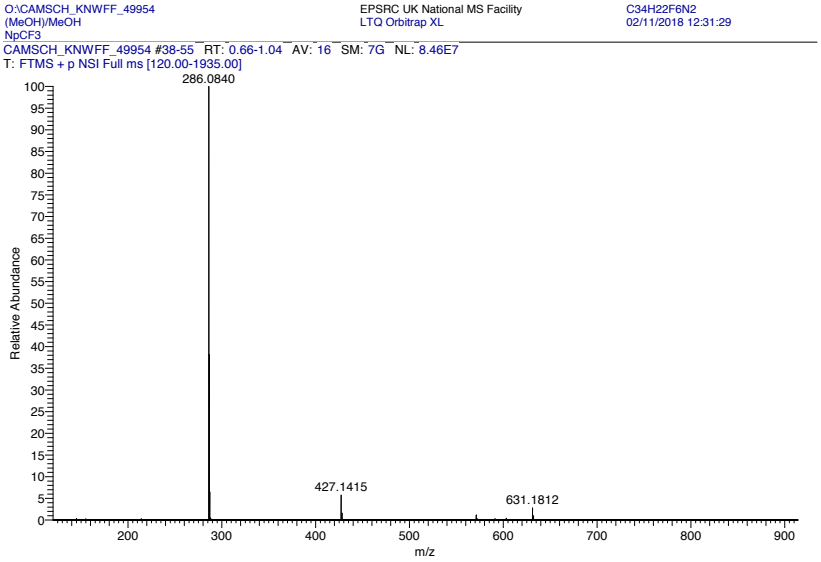

Fig. B.38 HRMS of EV[Np]CF_3.

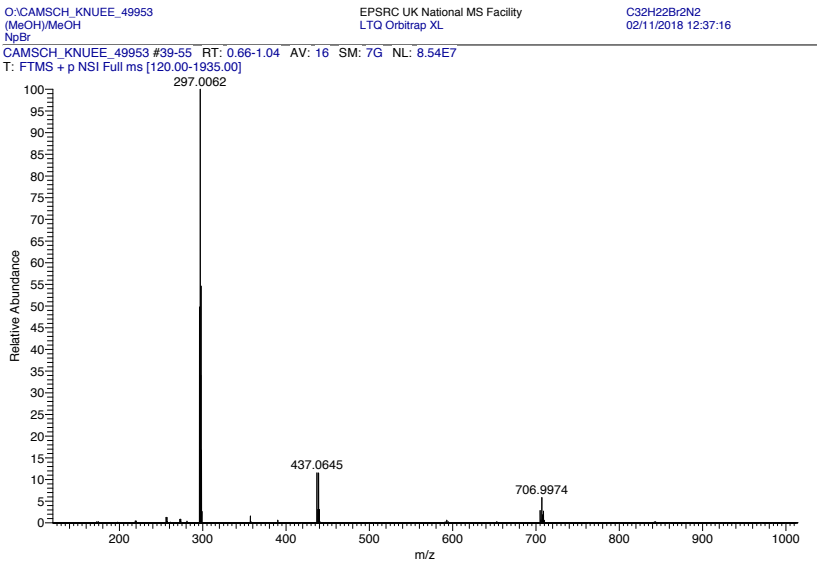

Fig. B.39 HRMS of EV[Np]Br.

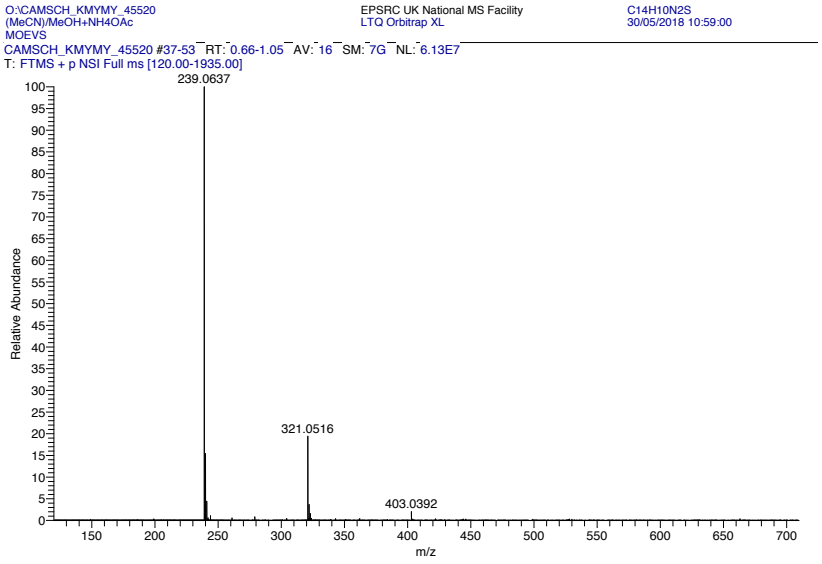

Fig. B.40 HRMS ofEV[Th].

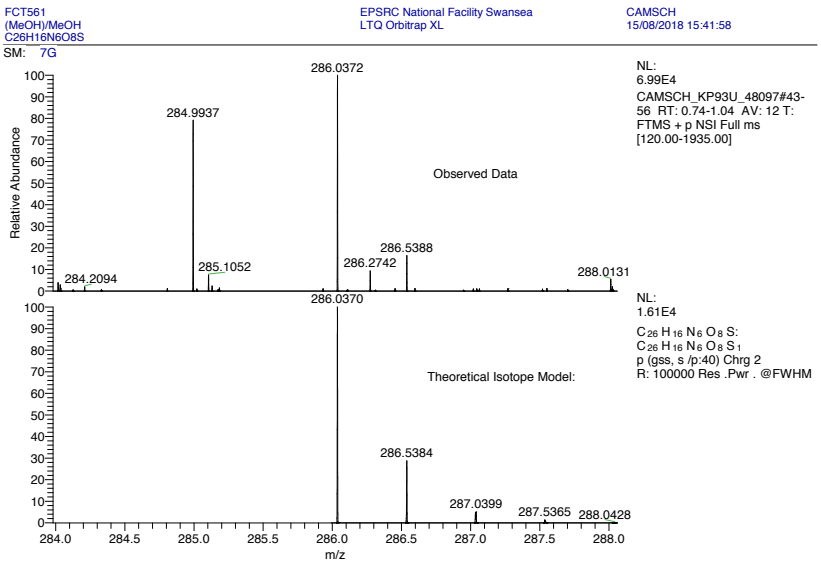

Fig. B.41 HRMS of EV[Th]DNB.

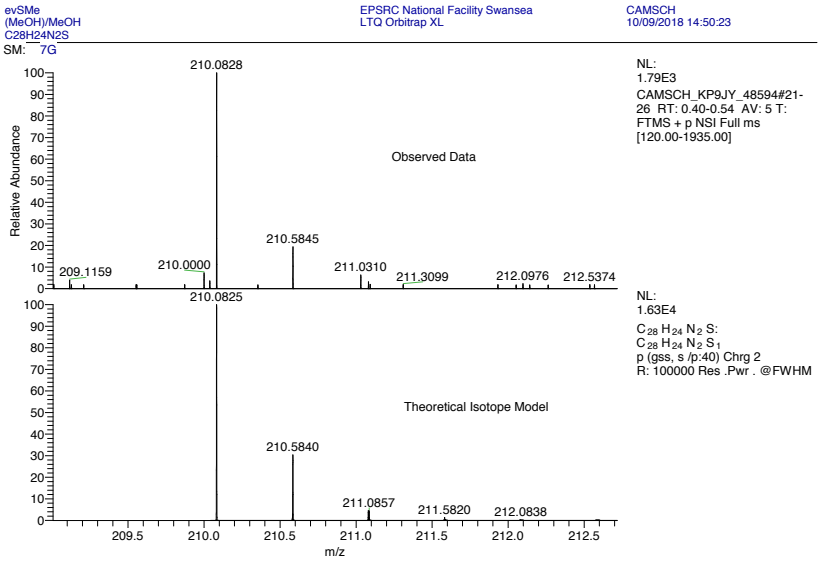

Fig. B.42 HRMS of EV[Th]Me.

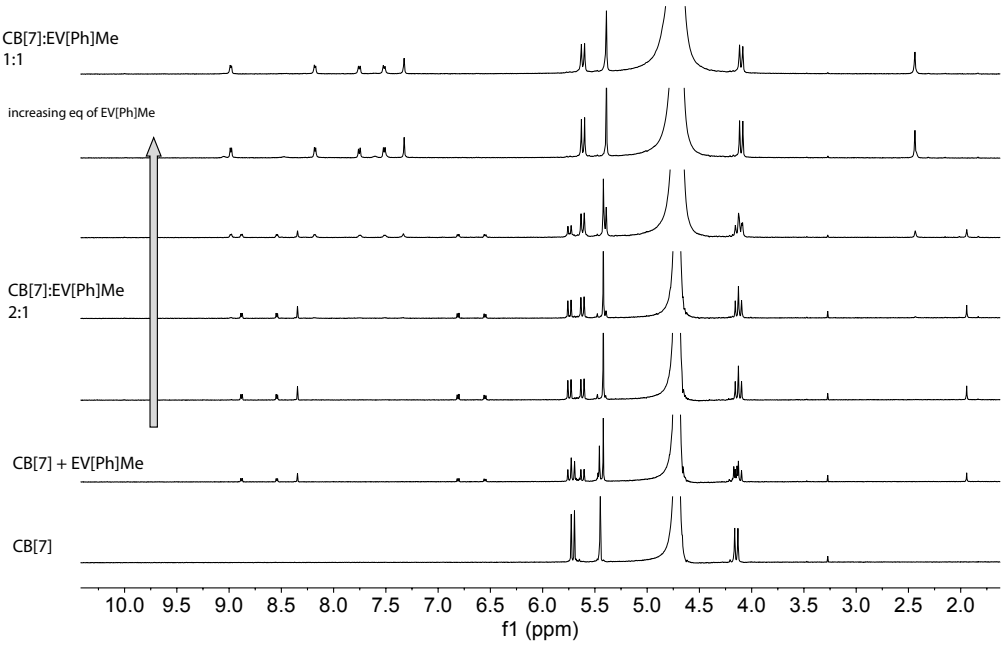

Fig. B.43 ^{1}H NMR titration of EV[Ph]Me to CB[7] (500 MHz, D_2O).

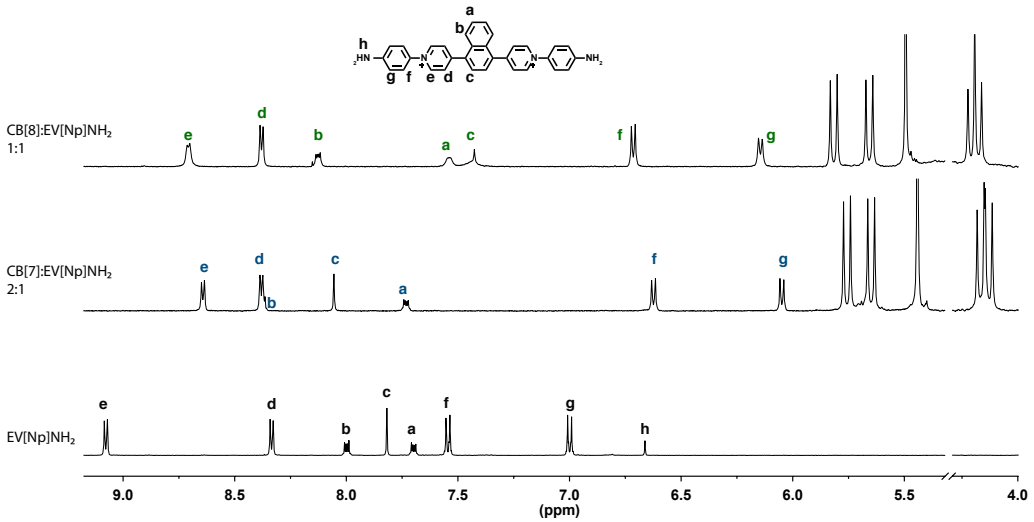

Fig. B.44 ^{1}H NMR titration of EV[Np]NH_2 to CB[8] and CB[7] (500 MHz, D_2O).

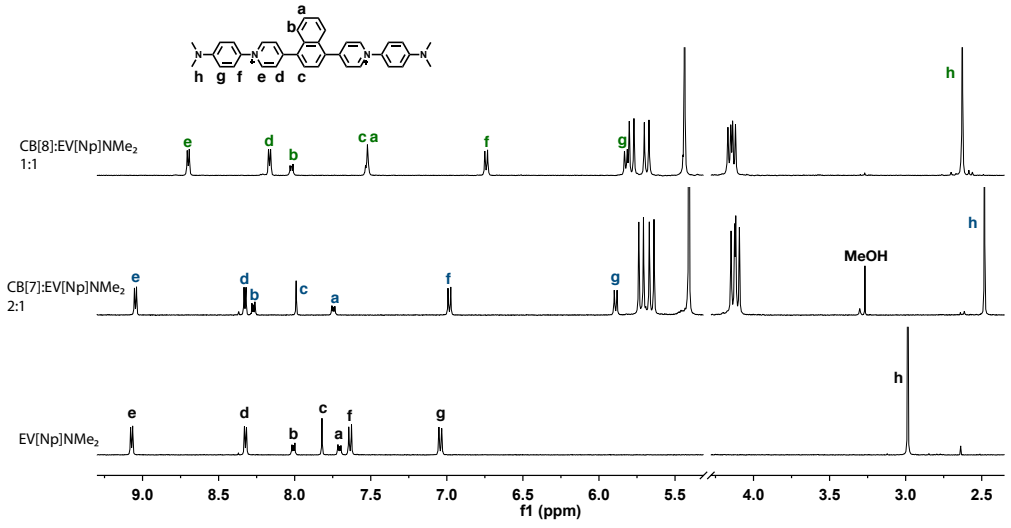

Fig. B.45 ^{1}H NMR titration of EV[Np]NMe_2 to CB[8] and CB[7] (500 MHz, D_2O).

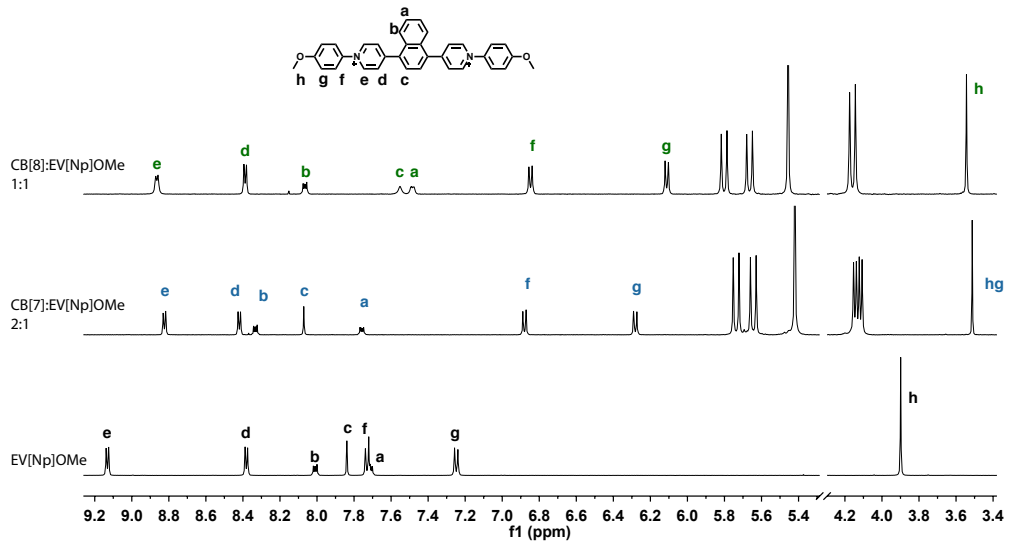

Fig. B.46 ^{1}H NMR titration of EV[Np]OMe to CB[8] and CB[7] (500 MHz, D_2O).

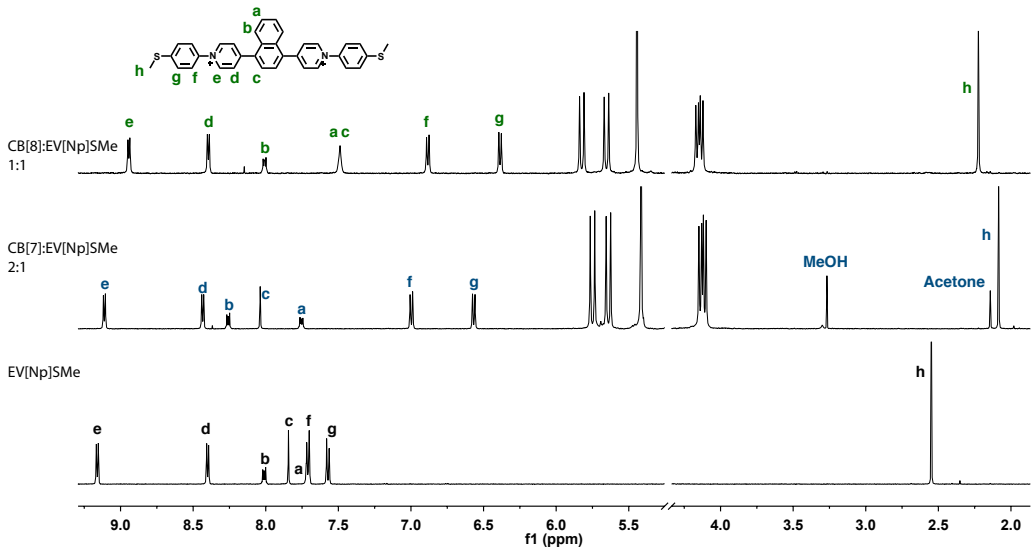

Fig. B.47 ^{1}H NMR titration of EV[Np]SMe to CB[8] and CB[7] (500 MHz, D_2O).

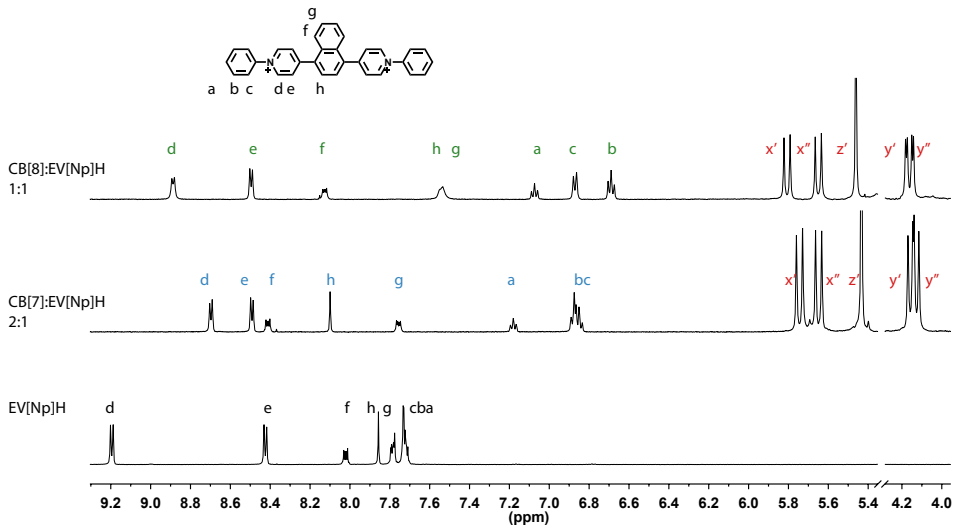

Fig. B.48 ^{1}H NMR titration of EV[Np]H to CB[8] and CB[7] (500 MHz, D_2O).

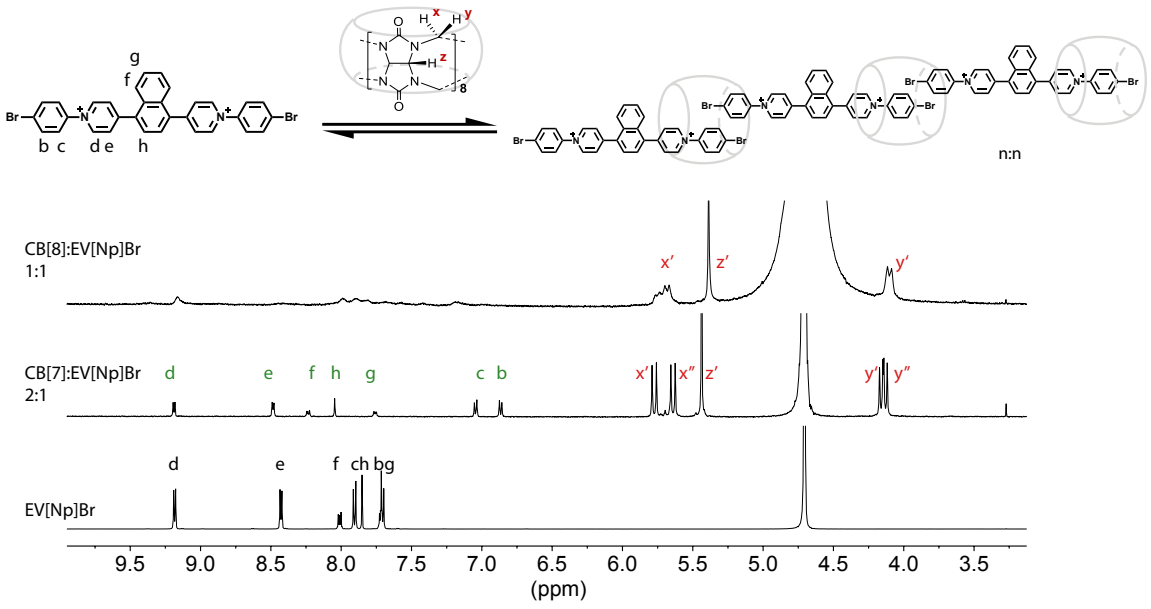

Fig. B.49 ^{1}H NMR titration of EV[Np]Br to CB[8] and CB[7] (500 MHz, D_2O).

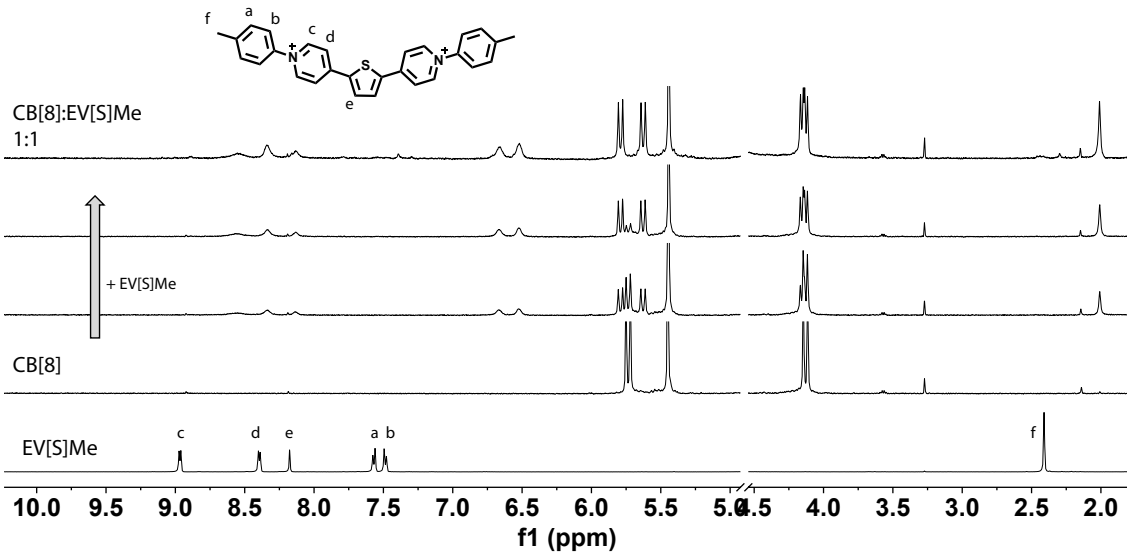

Fig. B.50 ^{1}H NMR titration of EV[Th]Me to CB[8] (500 MHz, D_2O).

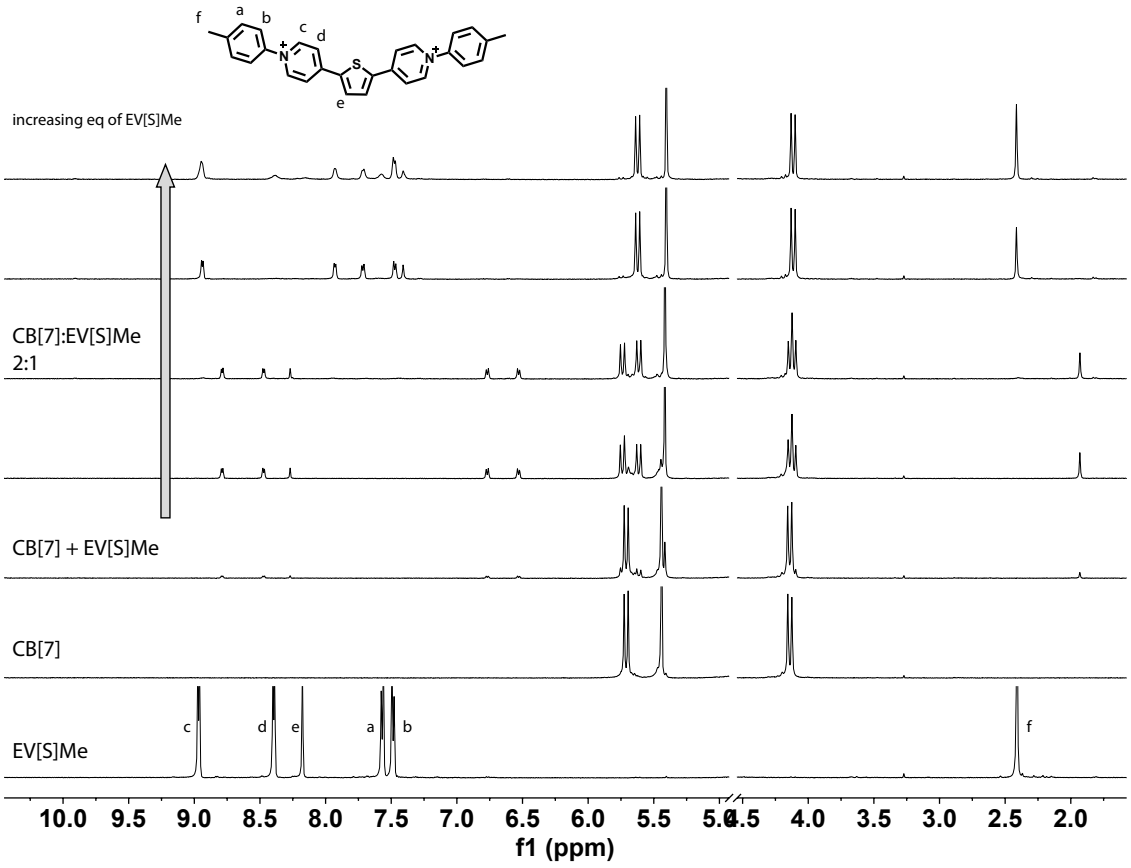

Fig. B.51 ^{1}H NMR titration of EV[Th]Me to CB[7] (500 MHz, D_2O).

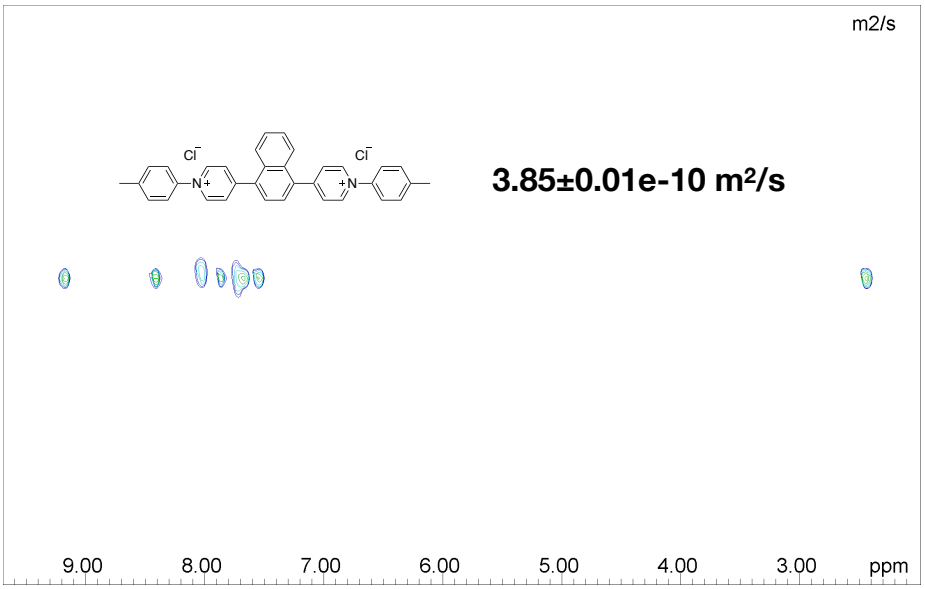

Fig. B.52 ^{1}H DOSY NMR spectrum of EV[Np]Me (500 MHz, D_2O, 298 K).

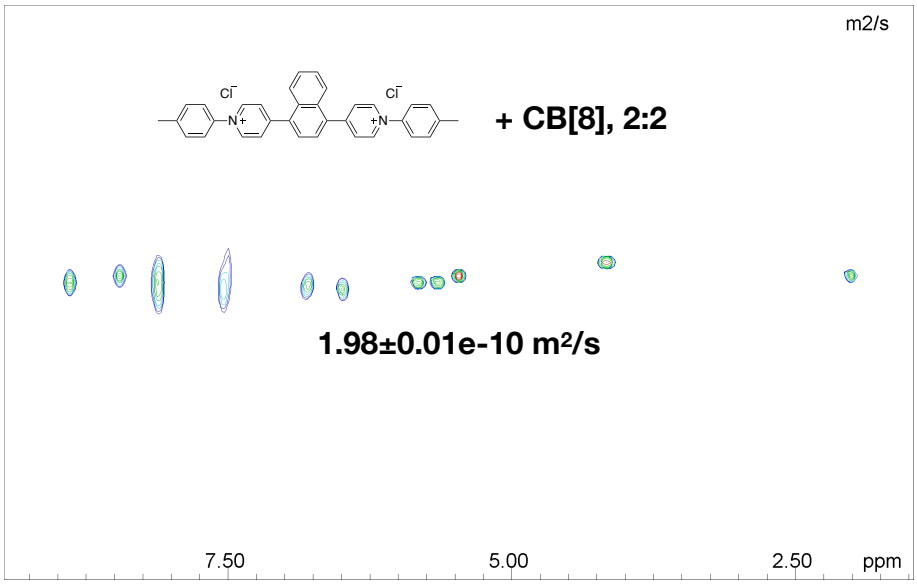

Fig. B.53 ^{1}H DOSY NMR spectrum of 2:2 complex of CB[8] and EV[Np]Me (500 MHz, D_2O, 298 K).

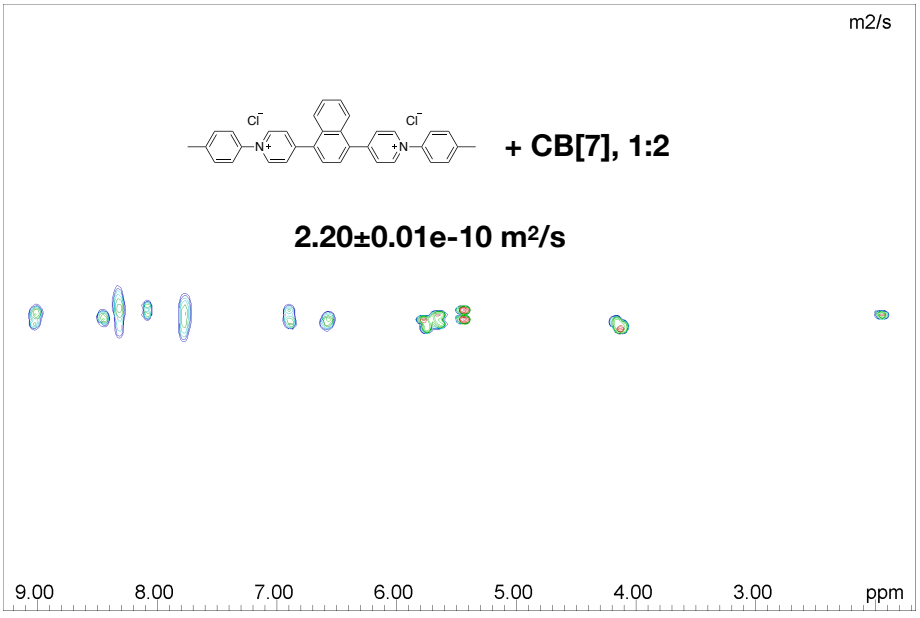

Fig. B.54 ^{1}H DOSY NMR spectrum of 2:1 complex of CB[7] and EV[Np]Me (500 MHz, D_2O, 298 K).

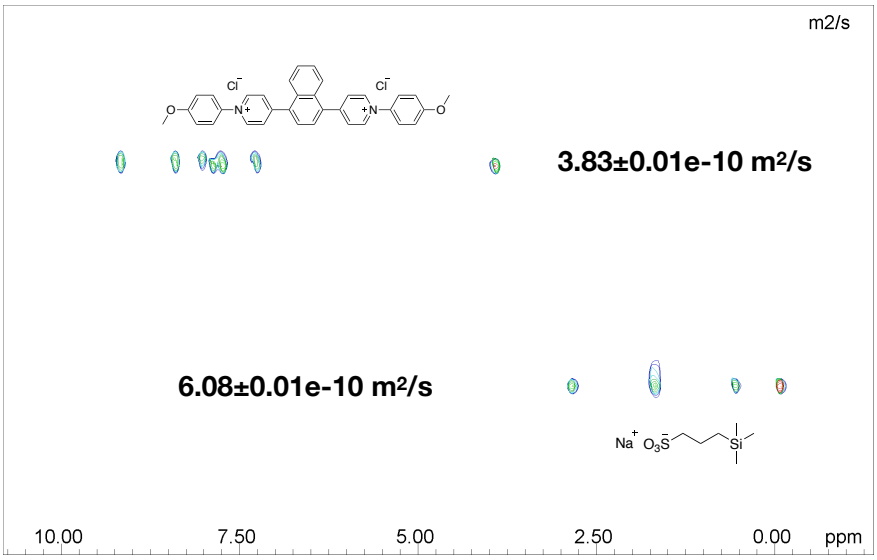

Fig. B.55 ^{1}H DOSY NMR spectrum of EV[Np]OMe (500 MHz, D_2O, 298 K).

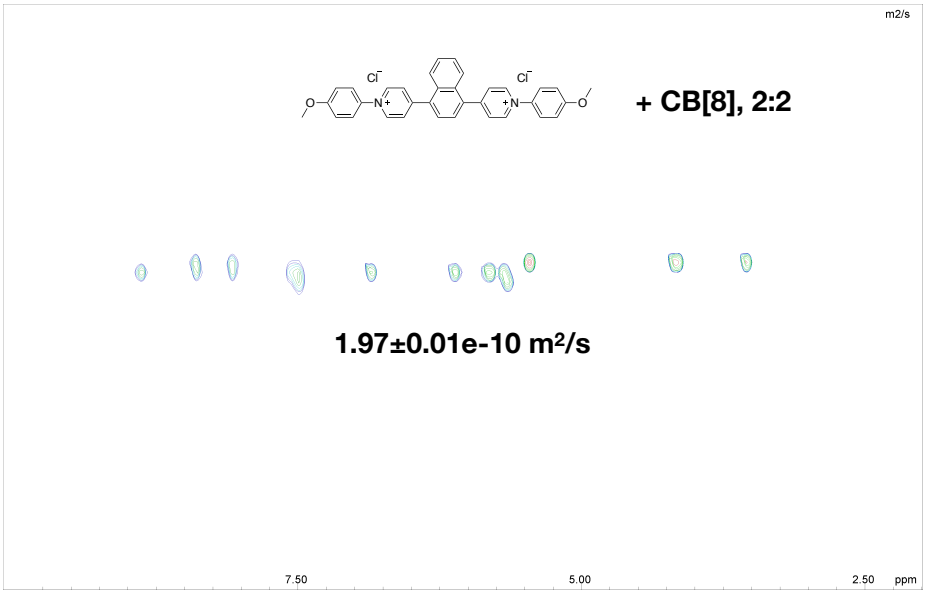

Fig. B.56 ^{1}H DOSY NMR spectrum of 2:2 complex of CB[8] and EV[Np]OMe (500 MHz, D_2O, 298 K).

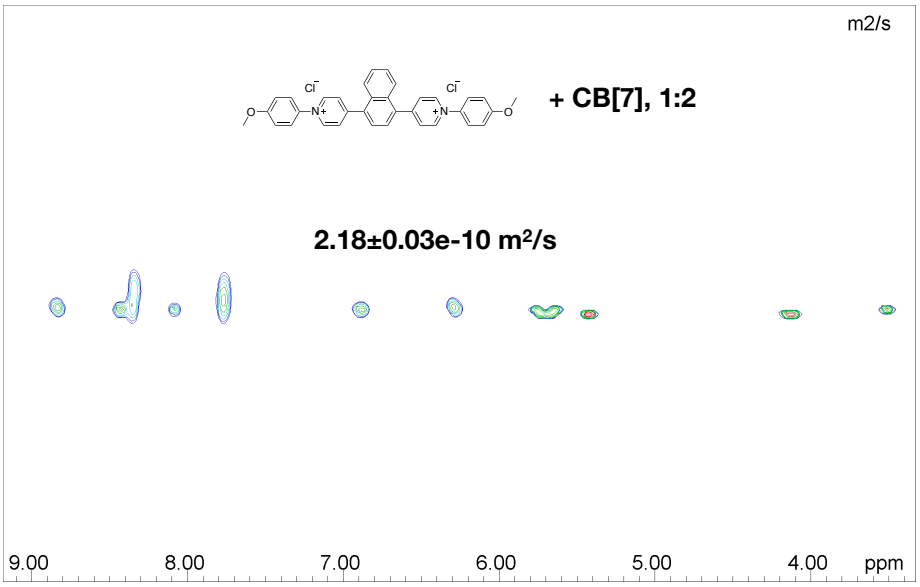

Fig. B.57 ^{1}H DOSY NMR spectrum of 2:1 complex of CB[7] and EV[Np]OMe (500 MHz, D_2O, 298 K).

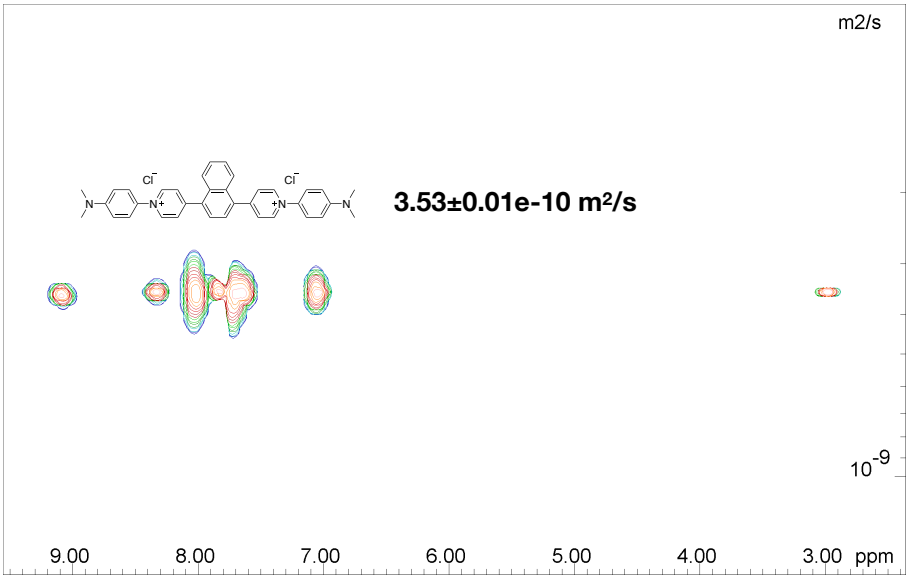

Fig. B.58 ^{1}H DOSY NMR spectrum of EV[Np]NMe_2 (500 MHz, D_2O, 298 K).

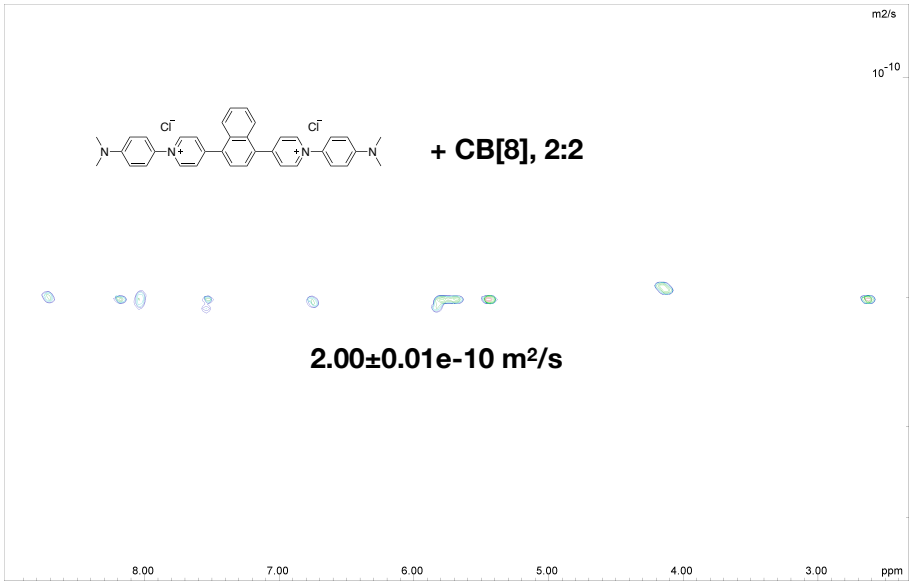

Fig. B.59 ^{1}H DOSY NMR spectrum of 2:2 complex of CB[8] and EV[Np]NMe$_2$ (500 MHz, D_2O, 298 K).

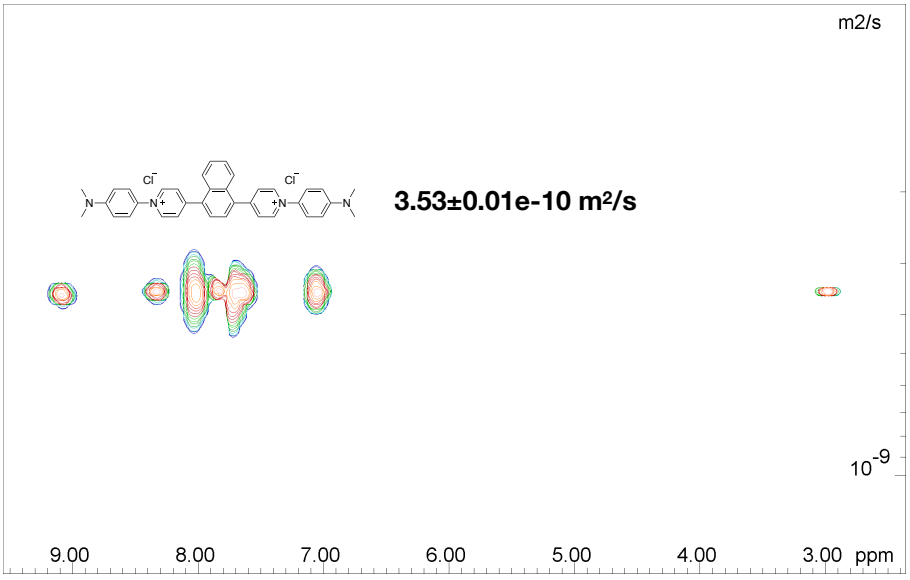

Fig. B.60 ^{1}H DOSY NMR spectrum of 2:1 complex of CB[7] and EV[Np]NMe$_2$ (500 MHz, D_2O, 298 K).

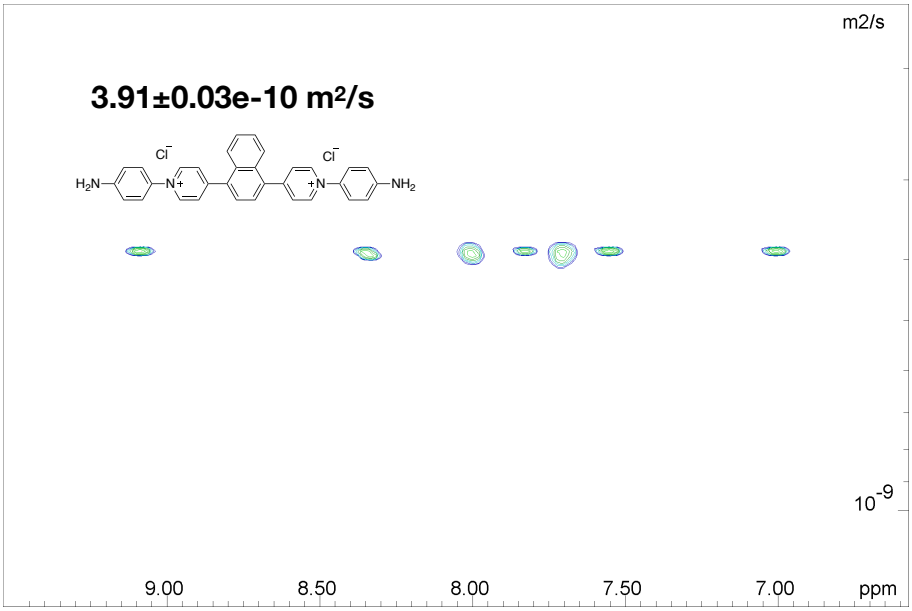

Fig. B.61 ^{1}H DOSY NMR spectrum of EV[Np]NH_2 (500 MHz, D_2O, 298 K).

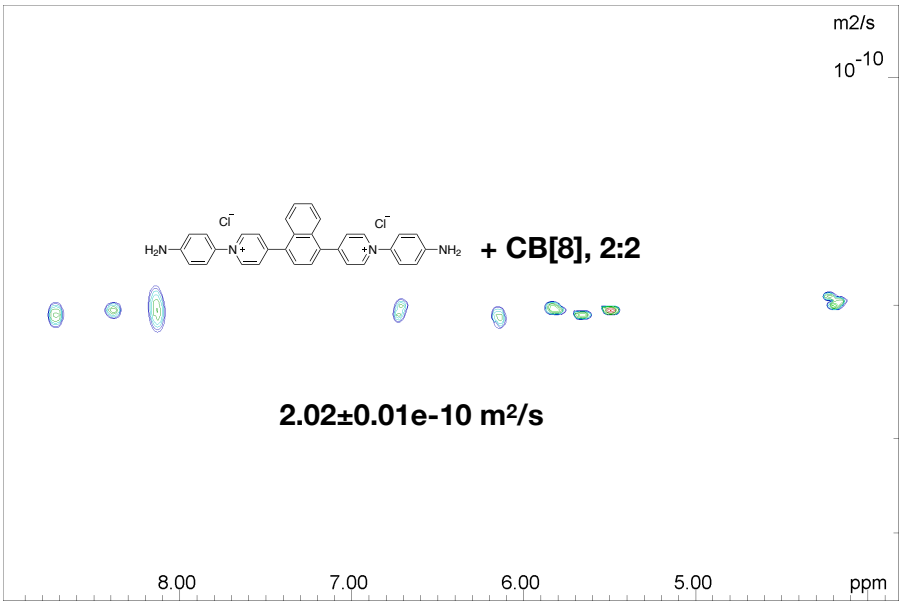

Fig. B.62 ^{1}H DOSY NMR spectrum of 2:2 complex of CB[8] and EV[Np]NH_2 (500 MHz, D_2O, 298 K).

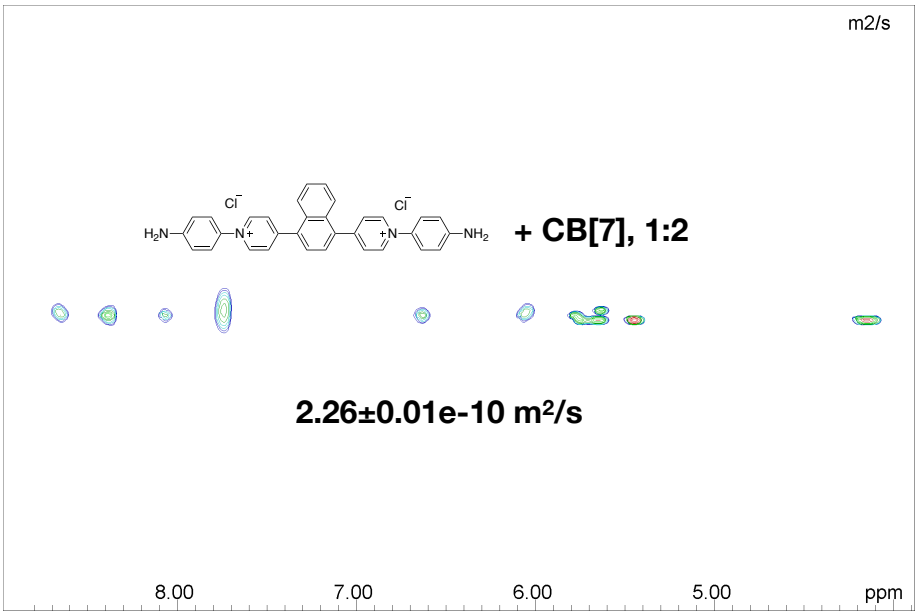

Fig. B.63 ^{1}H DOSY NMR spectrum of 2:1 complex of CB[7] and EV[Np]NH_2 (500 MHz, D_2O, 298 K).

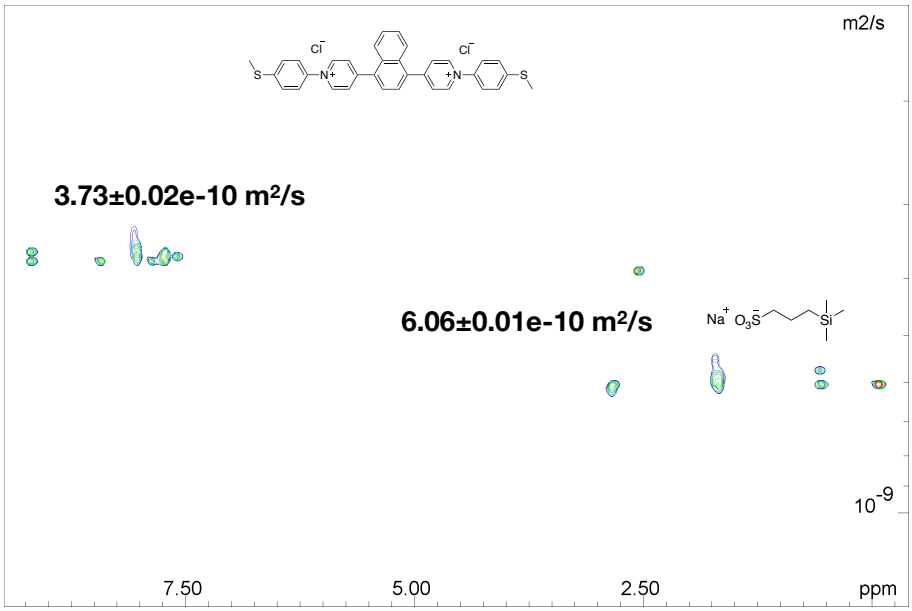

Fig. B.64 ^{1}H DOSY NMR spectrum of EV[Np]SMe (500 MHz, D_2O, 298 K).

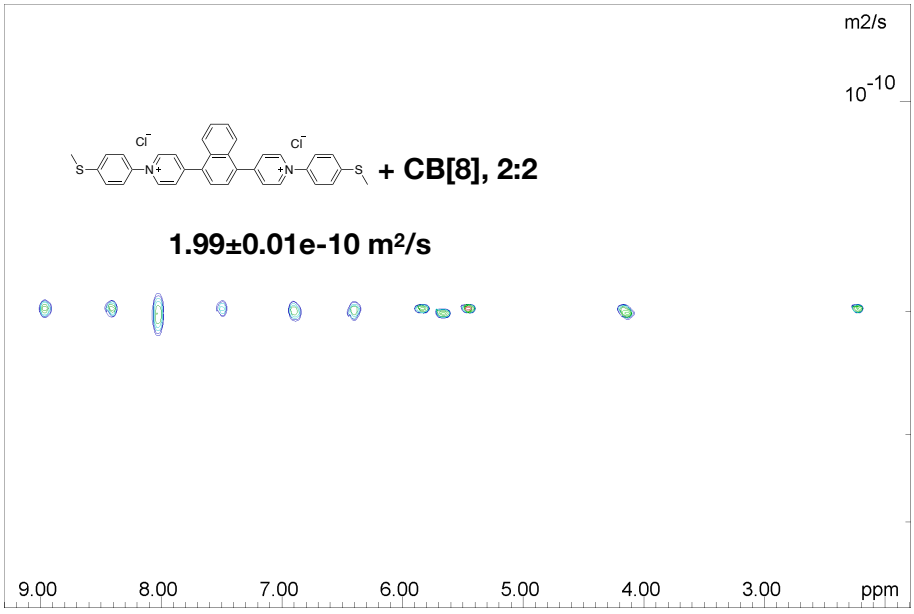

Fig. B.65 ^{1}H DOSY NMR spectrum of 2:2 complex of CB[8] and EV[Np]SMe (500 MHz, D_2O, 298 K).

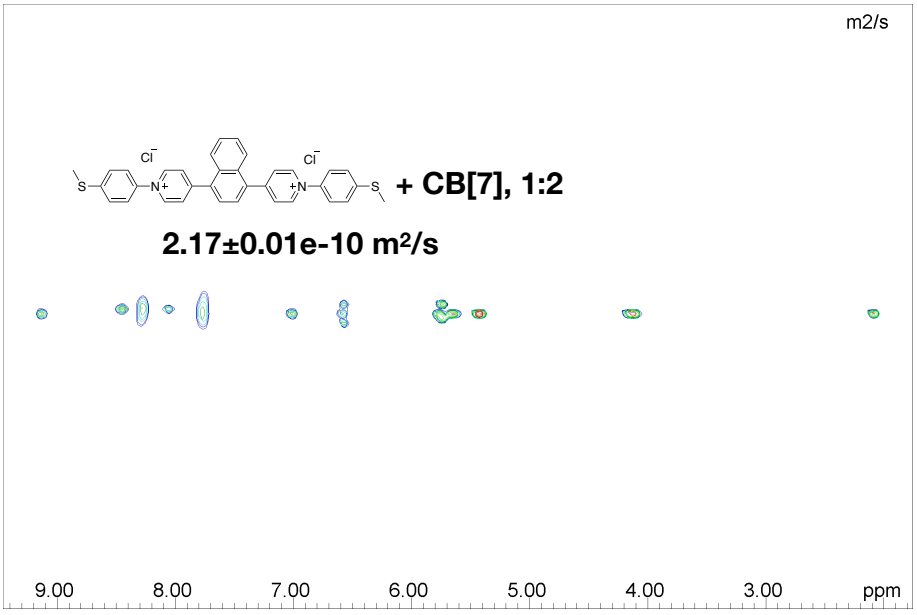

Fig. B.66 ^{1}H DOSY NMR spectrum of 2:1 complex of CB[7] and EV[Np]SMe (500 MHz, D_2O, 298 K).

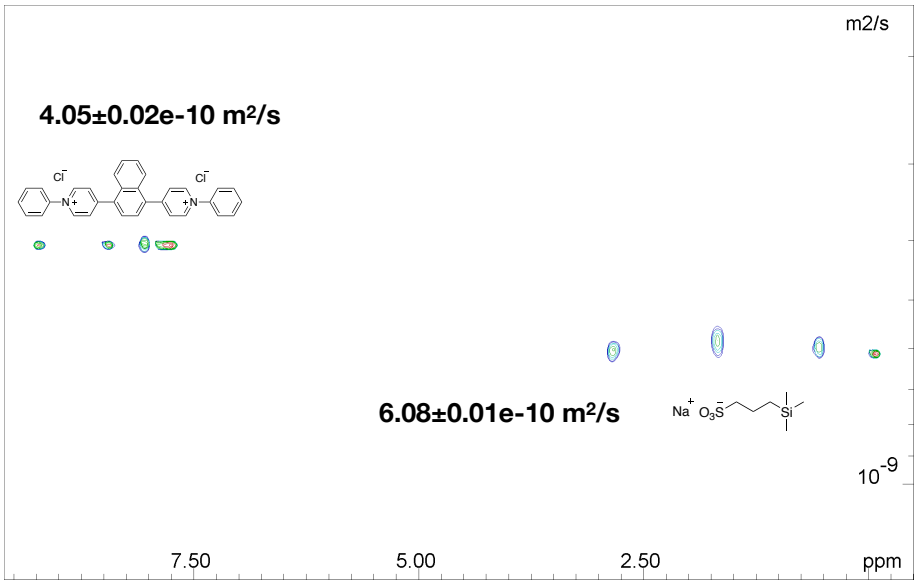

Fig. B.67 ^{1}H DOSY NMR spectrum of EV[Np]H (500 MHz, D_2O, 298 K).

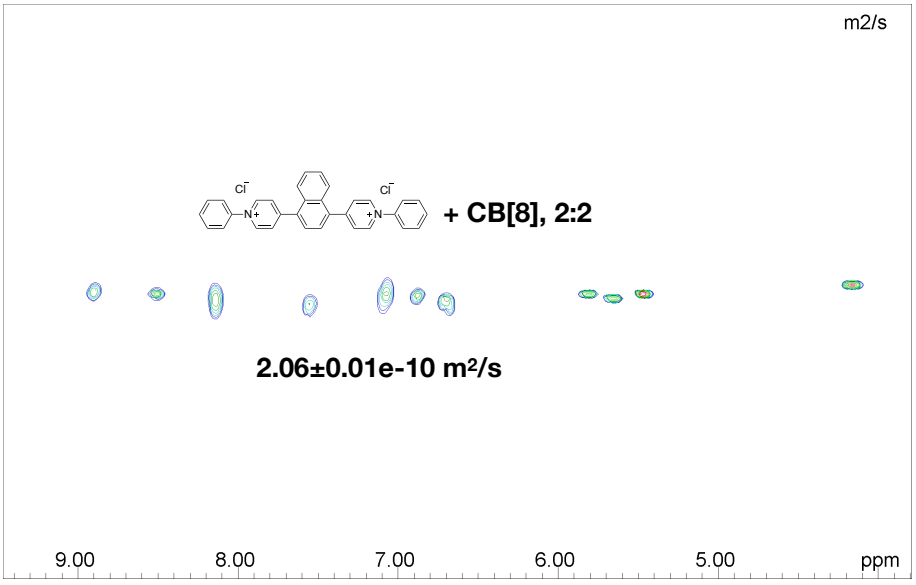

Fig. B.68 ^{1}H DOSY NMR spectrum of 2:2 complex of CB[8] and EV[Np]H (500 MHz, D_2O, 298 K).

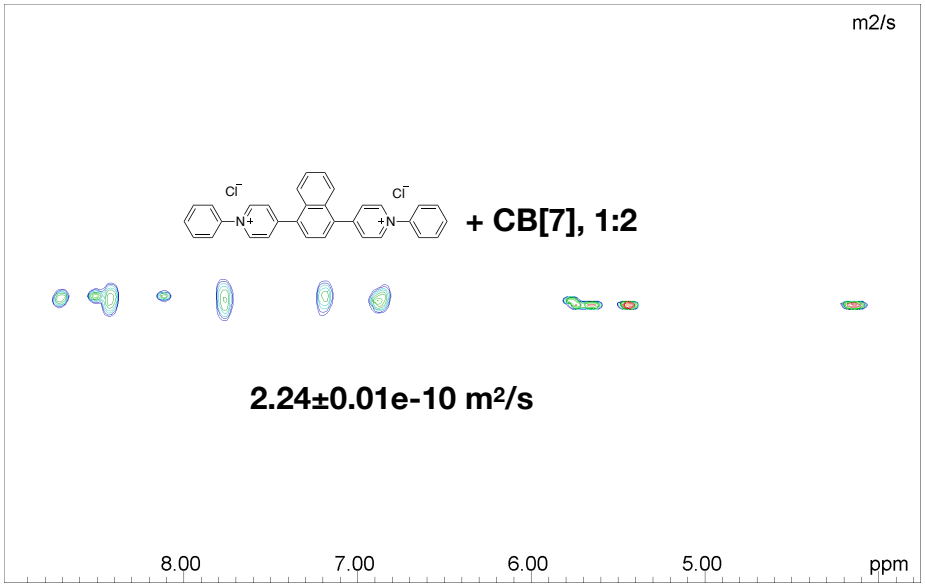

Fig. B.69 ^{1}H DOSY NMR spectrum of 2:1 complex of CB[7] and EV[Np]H (500 MHz, D_2O, 298 K).

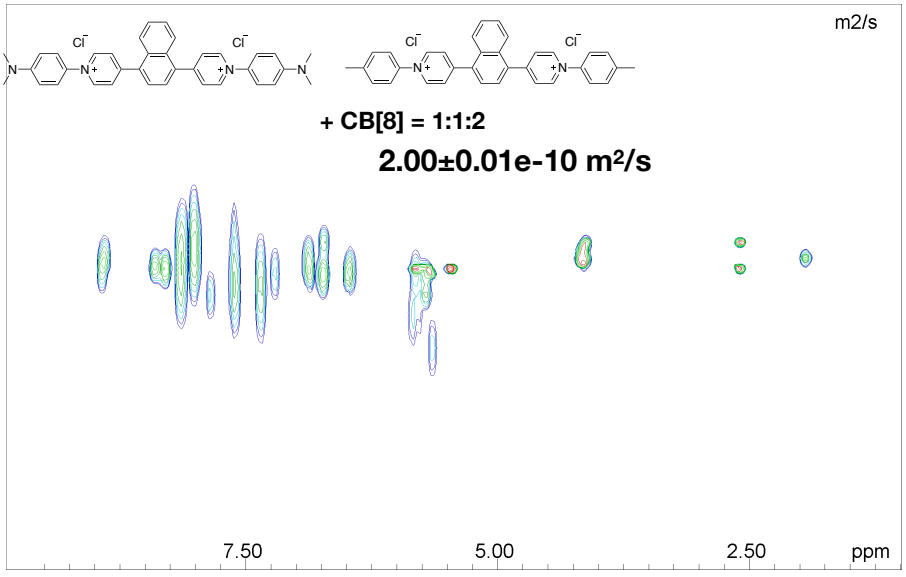

Fig. B.70 ^{1}H DOSY NMR spectrum of 2:1:1 complex of CB[8], EV[Np]NMe_2 and EV[Np]Me (500 MHz, D_2O, 298 K).

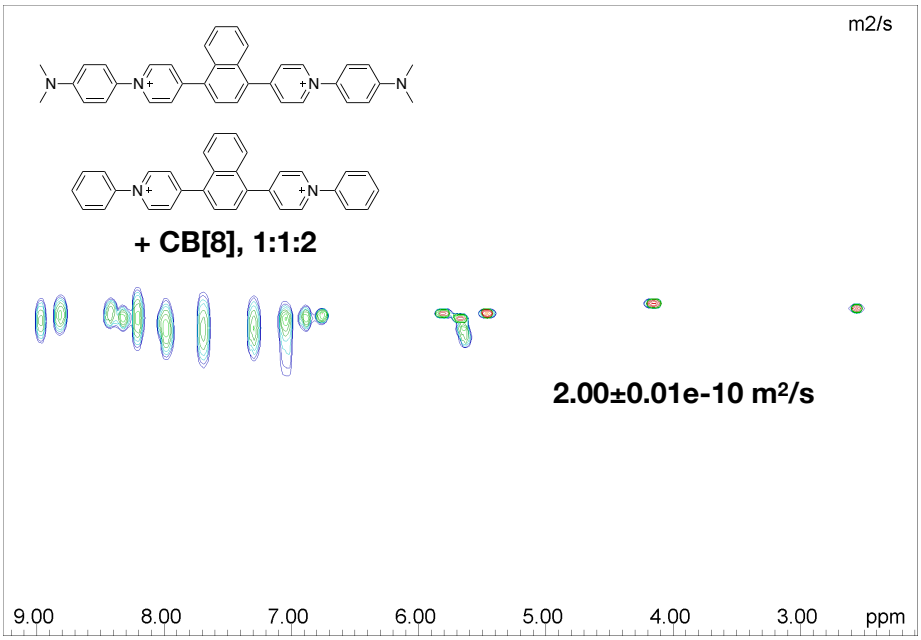

Fig. B.71 ^{1}H DOSY NMR spectrum of 2:1:1 complex of CB[8], EV[Np]NMe$_2$ and EV[Np]H (500 MHz, D_2O, 298 K).

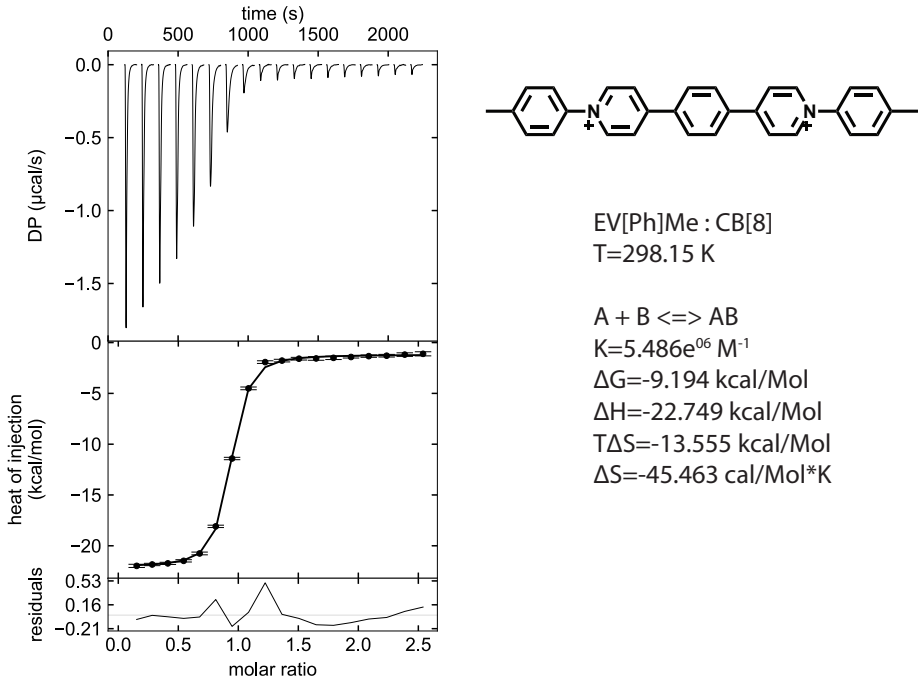

Fig. B.72 ITC titration of EV[Ph]Me to CB[8].

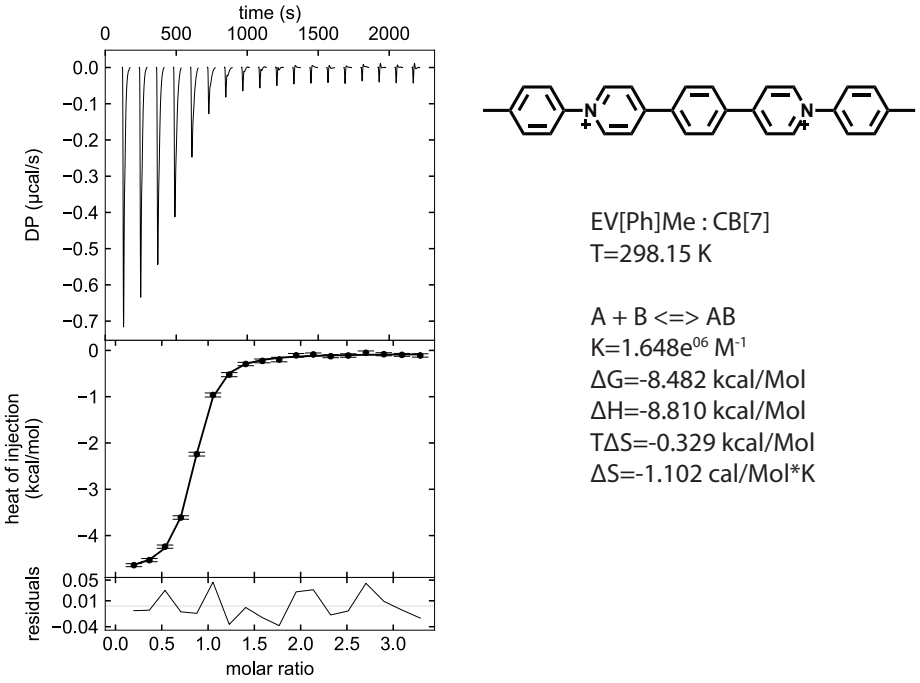

Fig. B.73 ITC titration of EV[Ph]Me to CB[7].

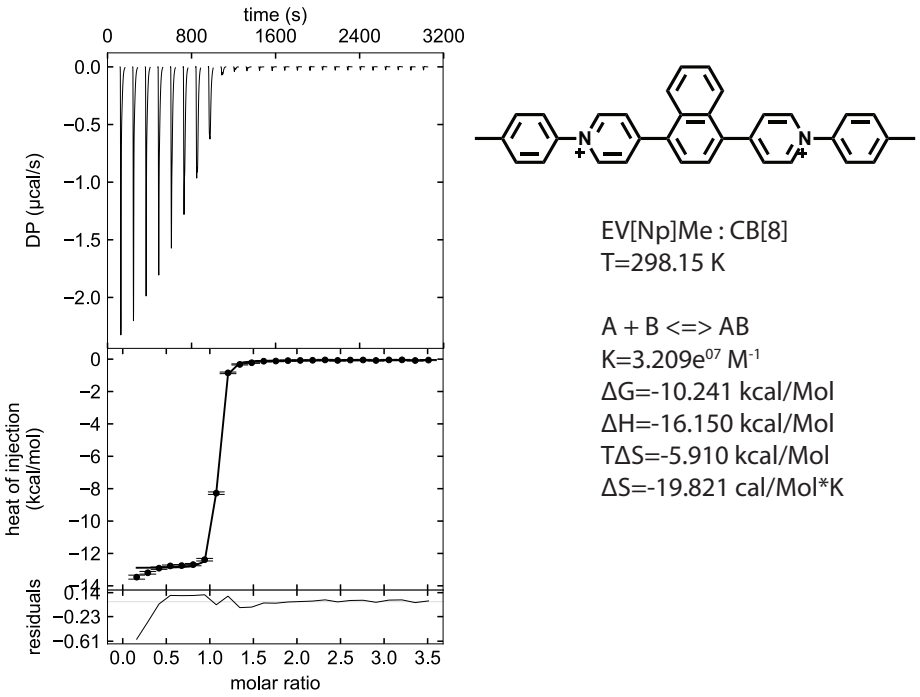

Fig. B.74 ITC titration of EV[Np]Me to CB[8].

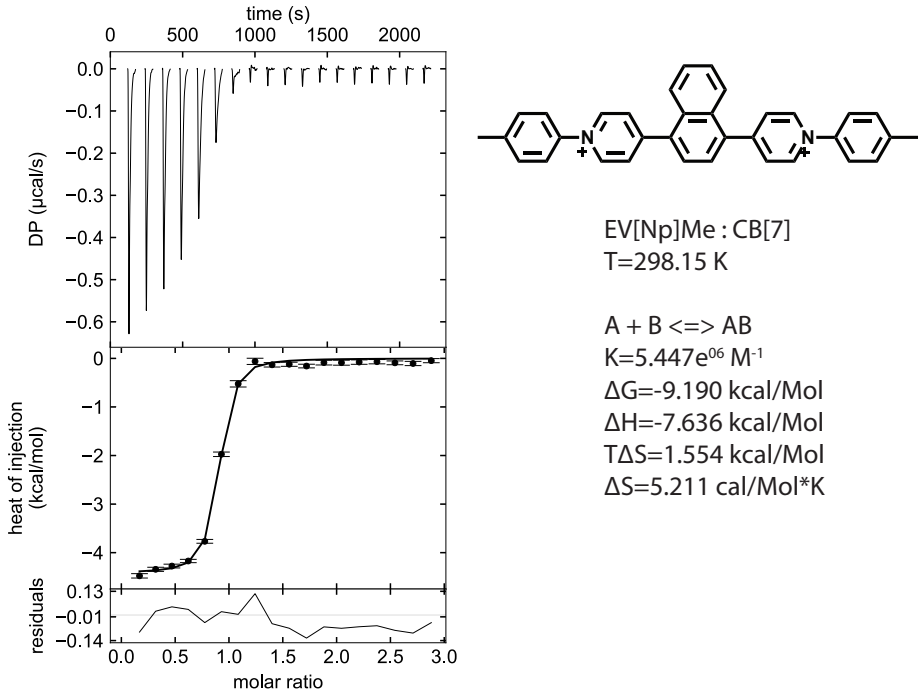

Fig. B.75 ITC titration of EV[Np]Me to CB[7].

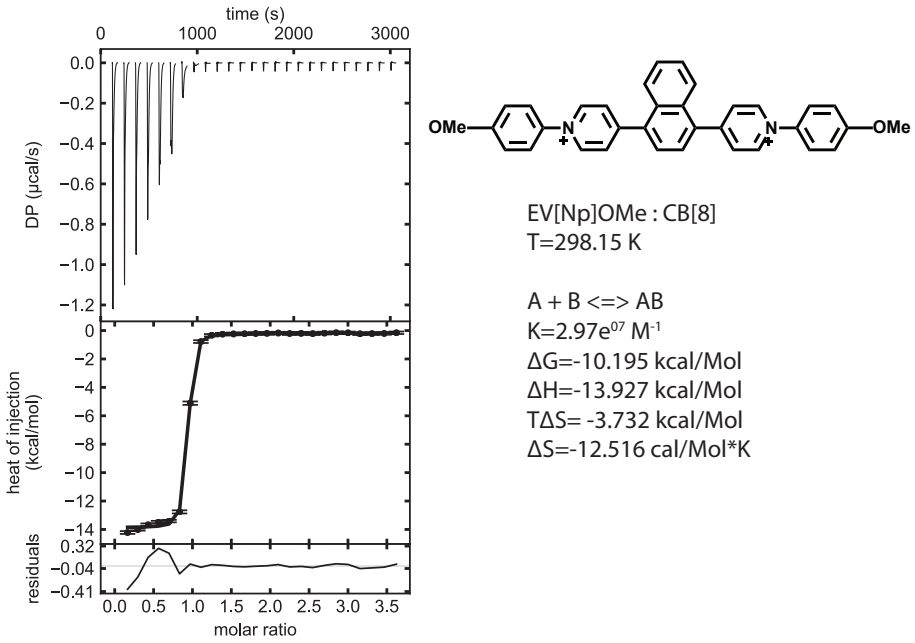

Fig. B.76 ITC titration of EV[Np]OMe to CB[8].

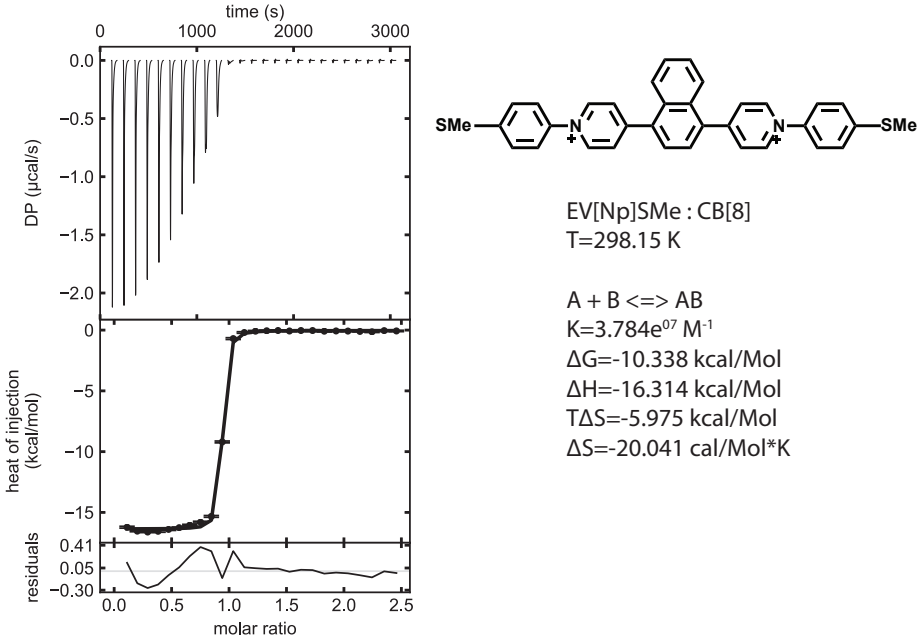

Fig. B.77 ITC titration of EV[Np]SMe to CB[8].

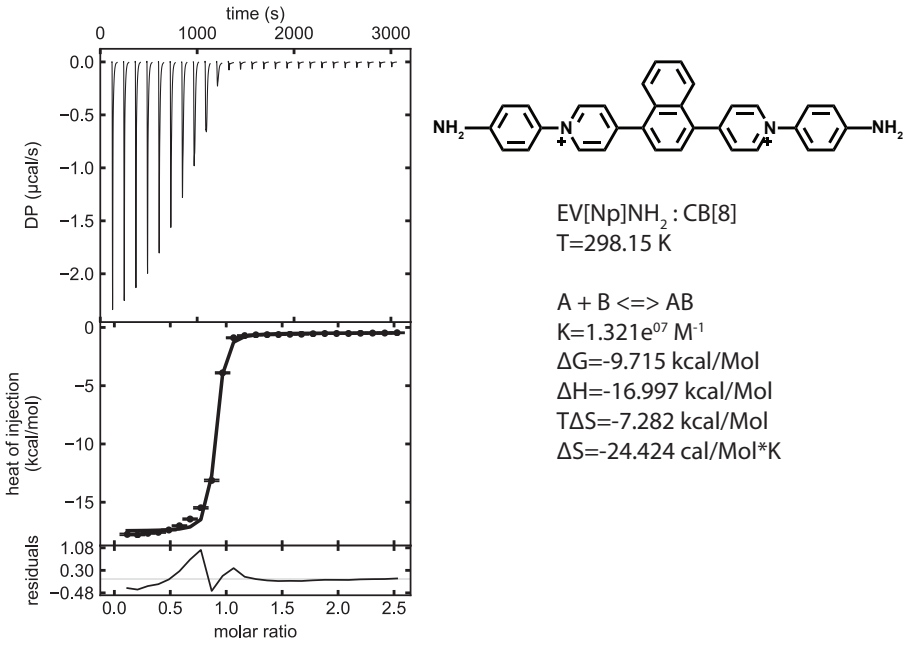

Fig. B.78 ITC titration of EV[Np]NH_2 to CB[8].

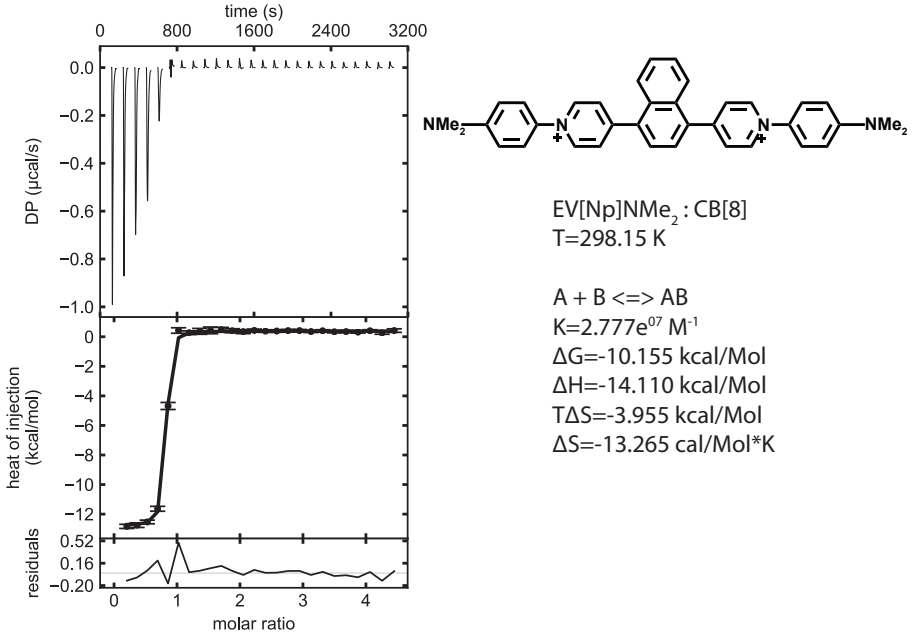

Fig. B.79 ITC titration of EV[Np]NMe_2 to CB[8].

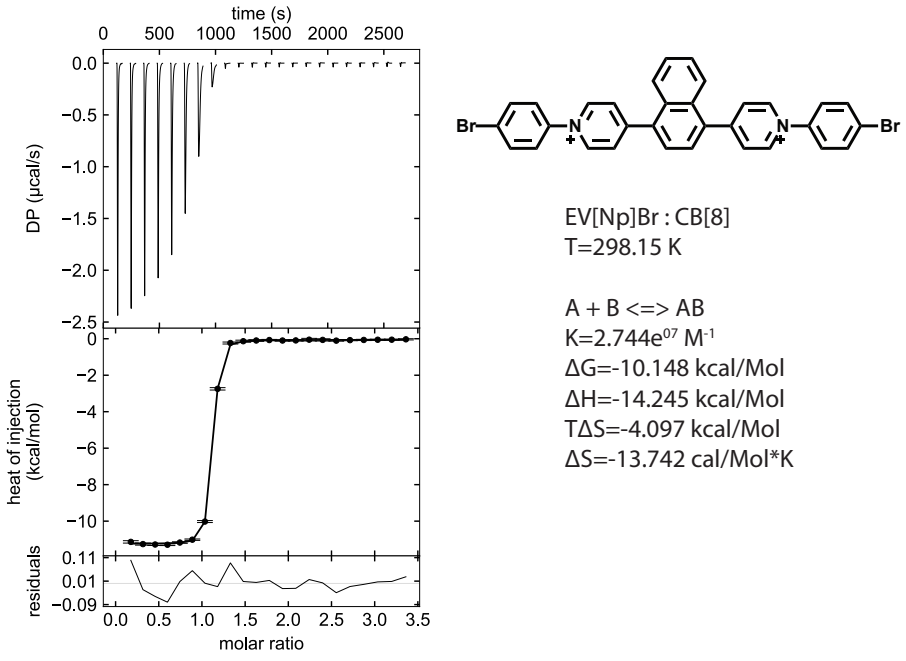

Fig. B.80 ITC titration of EV[Np]Br to CB[8].

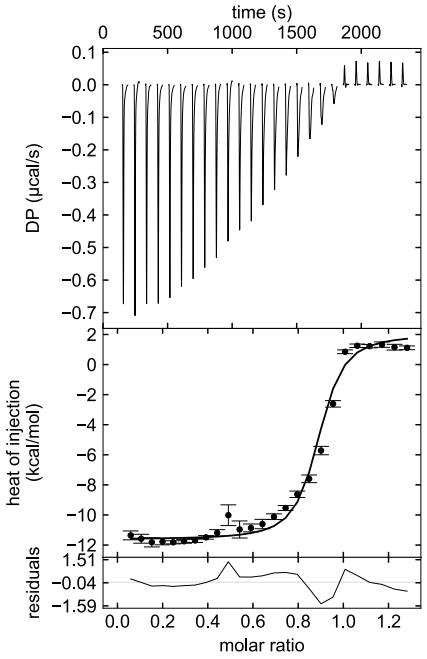

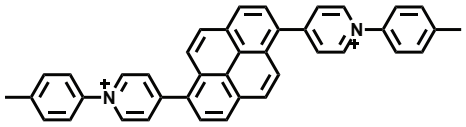

EV[Pyr$_{1,6}$]Me : CB[8]
T=298.15 K

A + B <=> AB
K=7.359e^{06} M^{-1}
ΔG=-9.368 kcal/Mol
ΔH=-15.009 kcal/Mol
TΔS=-5.641 kcal/Mol
ΔS=-18.921 cal/Mol*K

Fig. B.81 ITC titration of EV[Pyr$_{1,6}$]Me to CB[8].

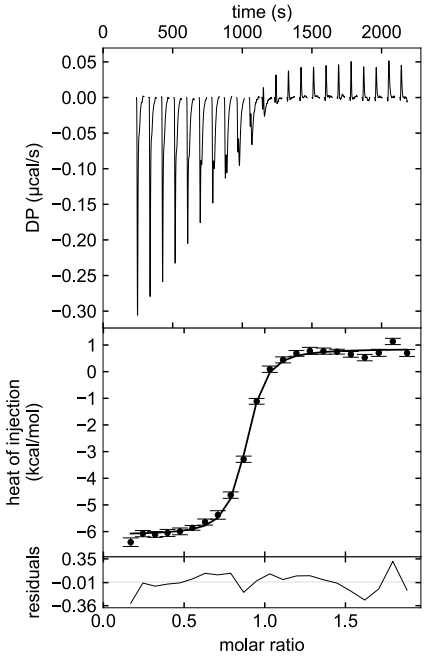

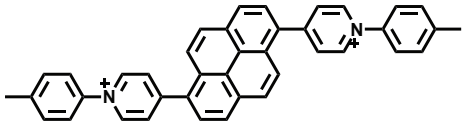

EV[Pyr$_{1,6}$]Me : CB[7]
T=298.15 K

A + B <=> AB
K=9.589e^{06} M^{-1}
ΔG=-9.525 kcal/Mol
ΔH=-8.384 kcal/Mol
TΔS=1.141 kcal/Mol
ΔS=3.826 cal/Mol*K

Fig. B.82 ITC titration of EV[Pyr$_{1,6}$]Me to CB[7].

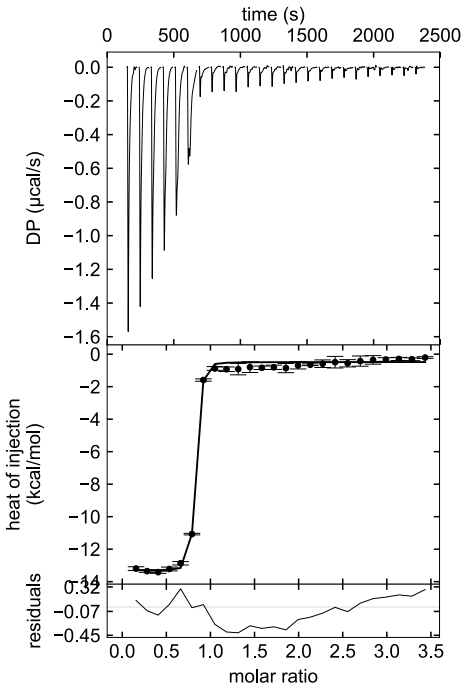

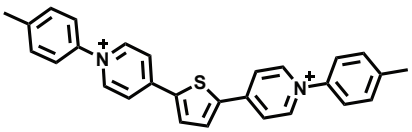

EV[S]Me : CB[8]
T=298.15 K

A + B <=> AB
K=3.780e^{07} M^{-1}
ΔG=-10.338 kcal/Mol
ΔH=-12.822 kcal/Mol
TΔS=-2.484 kcal/Mol
ΔS=-8.331 cal/Mol*K

Fig. B.83 ITC titration of EV[Th]Me to CB[8].

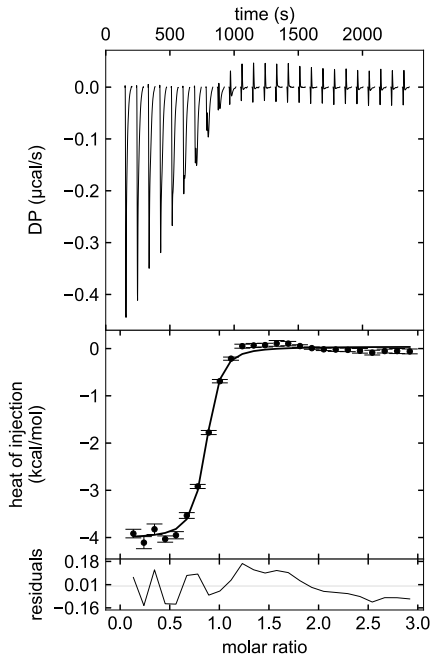

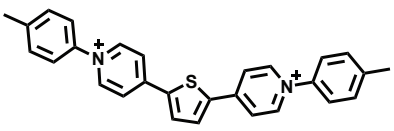

EV[S]Me : CB[7]
T=298.15 K

A + B <=> AB
K=2.719e^{06} M^{-1}
ΔG=-8.778 kcal/Mol
ΔH=-4.054 kcal/Mol
TΔS=4.724 kcal/Mol
ΔS=15.844 cal/Mol*K

Fig. B.84 ITC titration of EV[Th]Me to CB[7].

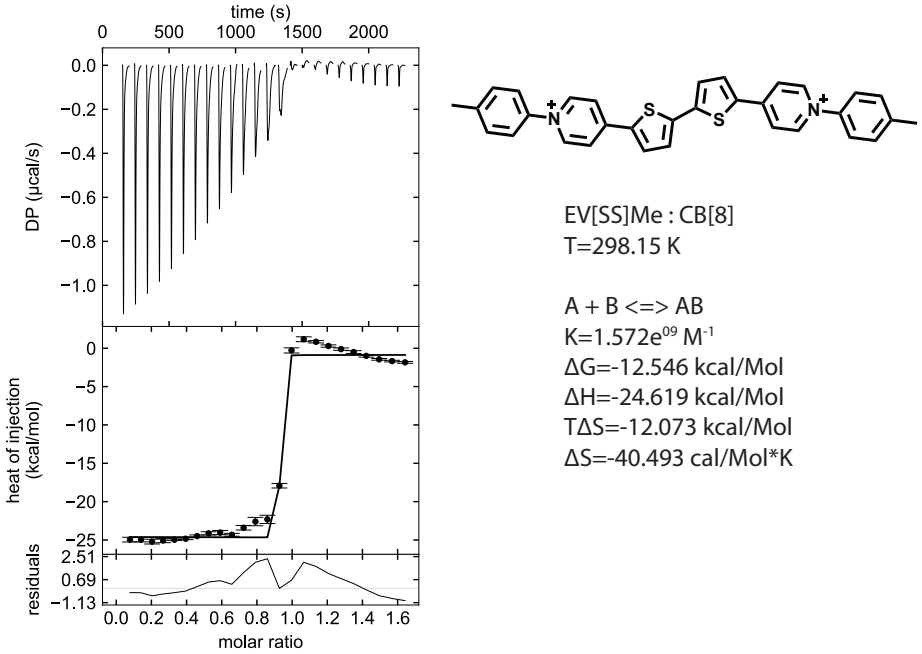

Fig. B.85 ITC titration of EV[DTh]Me to CB[8].

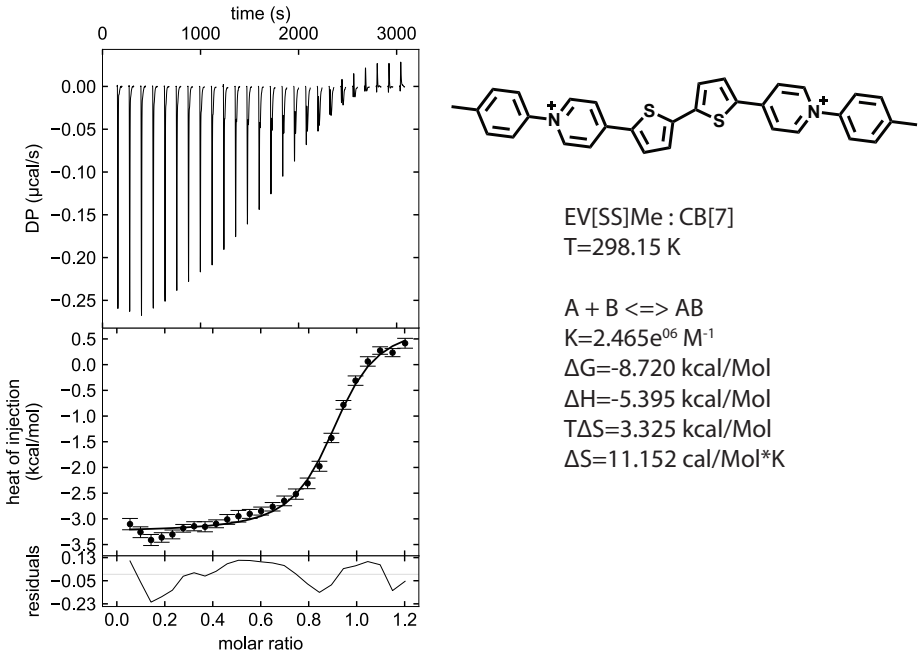

Fig. B.86 ITC titration of EV[DTh]Me to CB[7].

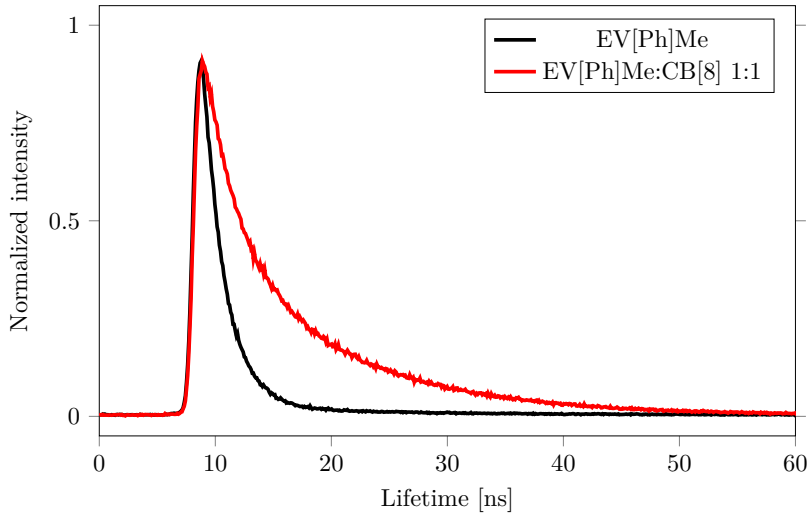

Fig. B.87 TCSPC decay profile for EV[Ph]Me and EV[Ph]Me with 1 eq of CB[8].

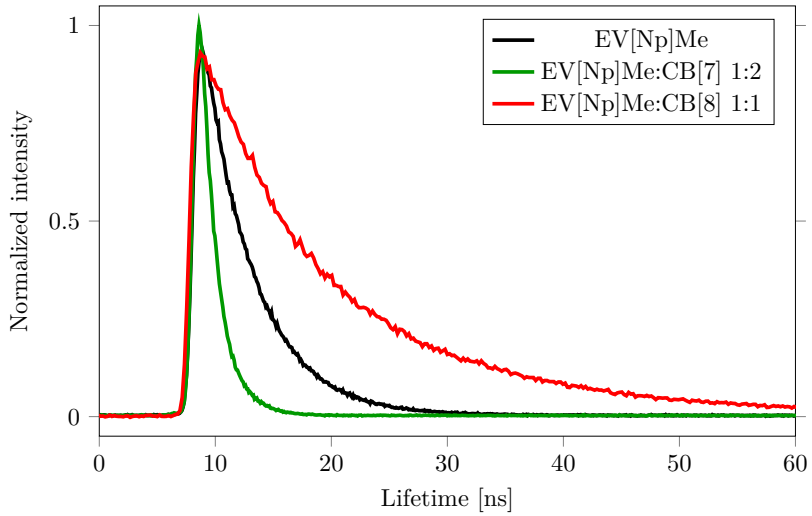

Fig. B.88 TCSPC decay profile for EV[Np]Me, EV[Np]Me with 2 eq of CB[7], and EV[Np]Me with 1 eq of CB[8].

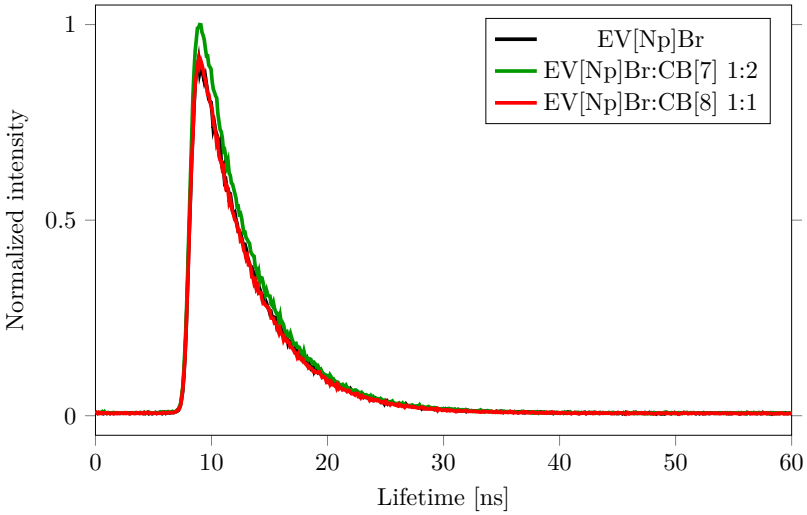

Fig. B.89 TCSPC decay profile for EV[Np]Br, EV[Np]Br with 2 eq of CB[7], and EV[Np]Br with 1 eq of CB[8].

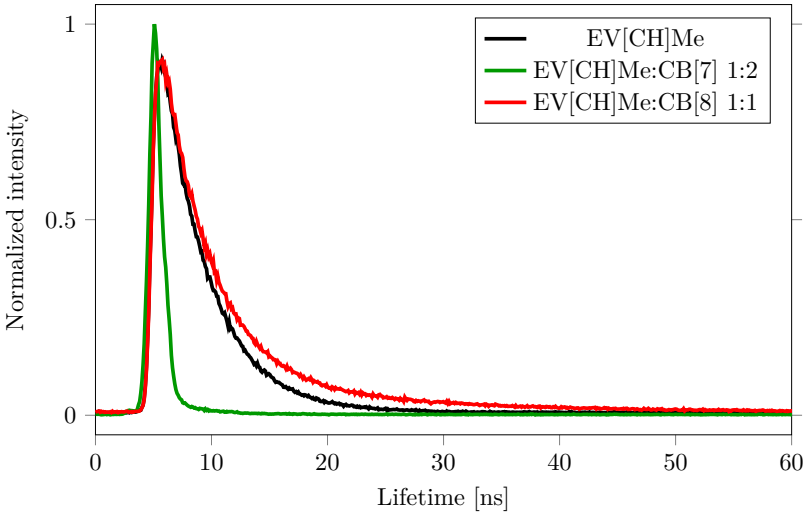

Fig. B.90 TCSPC decay profile for EV[CH]Me, EV[CH]Me with 2 eq of CB[7], and EV[CH]Me· with 1 eq of CB[8].

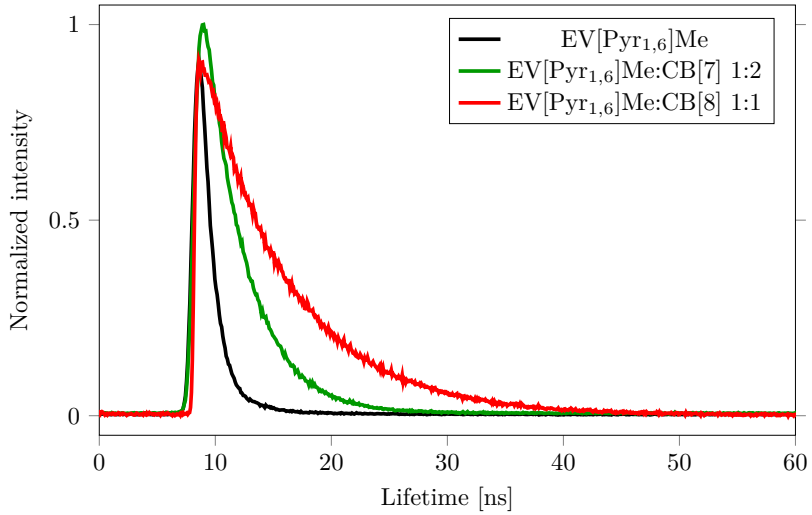

Fig. B.91 TCSPC decay profile for EV[$Pyr_{1,6}$]Me, EV[$Pyr_{1,6}$]Me with 2 eq of CB[7], and EV[$Pyr_{1,6}$]Me with 1 eq of CB[8].

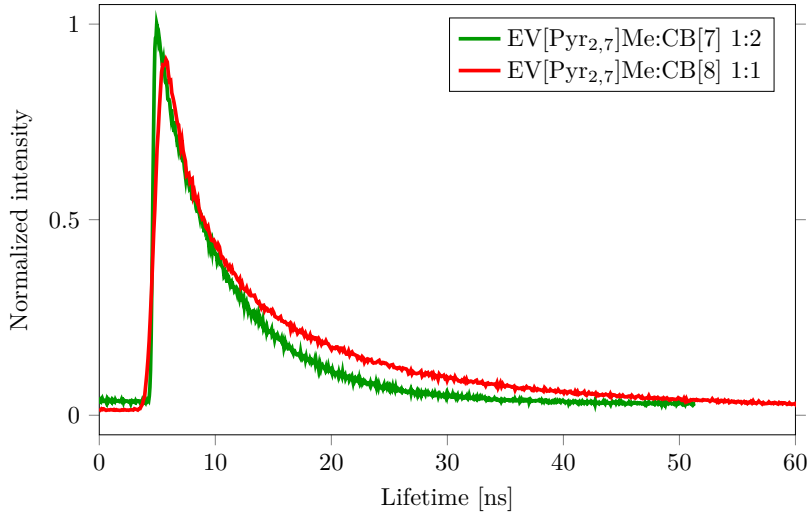

Fig. B.92 TCSPC decay profile for EV[$Pyr_{2,7}$]Me with 2 eq of CB[7], and EV[$Pyr_{2,7}$]Me with 1 eq of CB[8].

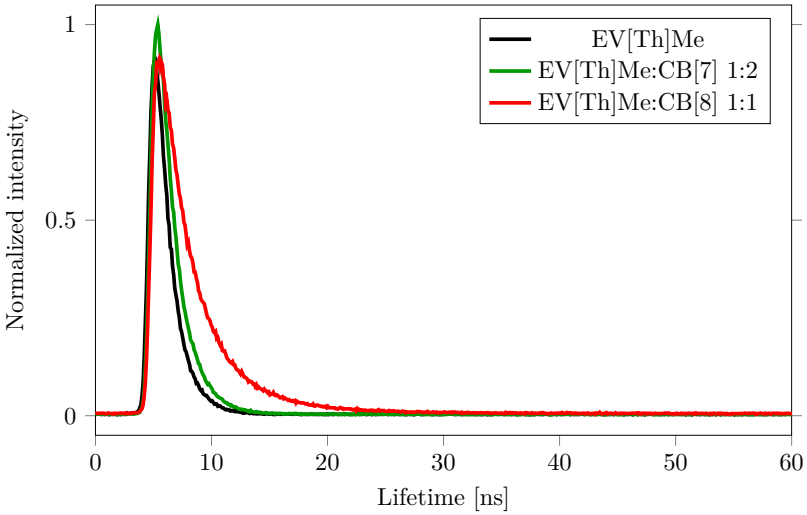

Fig. B.93 TCSPC decay profile for EV[Th]Me, EV[Th]Me with 2 eq of CB[7], and EV[Th]Me with 1 eq of CB[8].

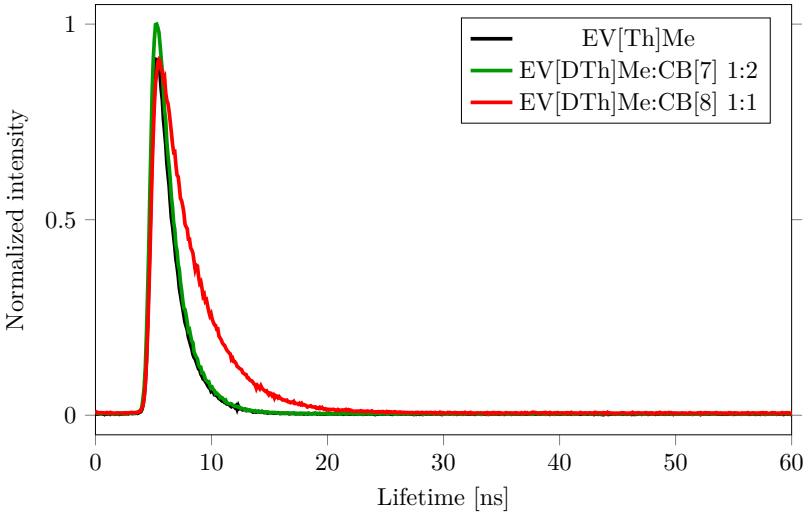

Fig. B.94 TCSPC decay profile for EV[DTh]Me, EV[DTh]Me with 2 eq of CB[7], and EV[DTh]Me with 1 eq of CB[8].

Table B.1 Steady-state spectral data of EV[X]Rs in water.

.Guest	Host	Host:Guest	λ_{abs}^{max}. (nm)	λ_{em}^{max}. (nm)	Stokes shift (nm)	Φ_{PL}.	τ_1 (ns)	τ_2 (ns)
EV[Ph]H	-	-	337	404	67	0.84	1.94	-
EV[Ph]H	CB[8]	1:1	350	428	78	0.94	1.75 (97%)	8.89 (3%)
EV[Ph]H	CB[7]	1:2	356	420	64	0.93	1.4	-
EV[Ph]OMe	-	-	348	402	54	0.01	<1	-
EV[Ph]OMe	CB[8]	1:1	374	548	174	0.31	1.14 (51%)	10.33 (49%)
EV[Ph]OMe	CB[7]	1:2	356	420	64	0.93	1.4	
EV[Np]OMe	-	-	373	483	110	0.31	1.82	-
EV[Np]OMe	CB[8]	1:1	402	516	115	0.66	6.23 (20%)	11.98 (80%)
EV[Np]H	-	-	372	485	114	0.28	4.6	-
EV[Np]H	CB[8]	1:1	396	518	125	0.76	6.62	19.01

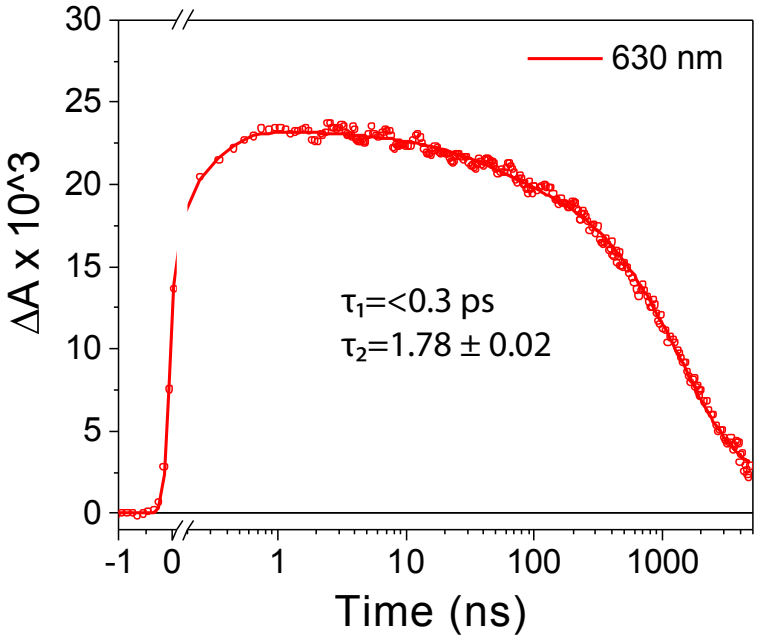

Fig. B.95 fsTA decay kinetics for EV[Ph]Me at 630 nm probe wavelength.

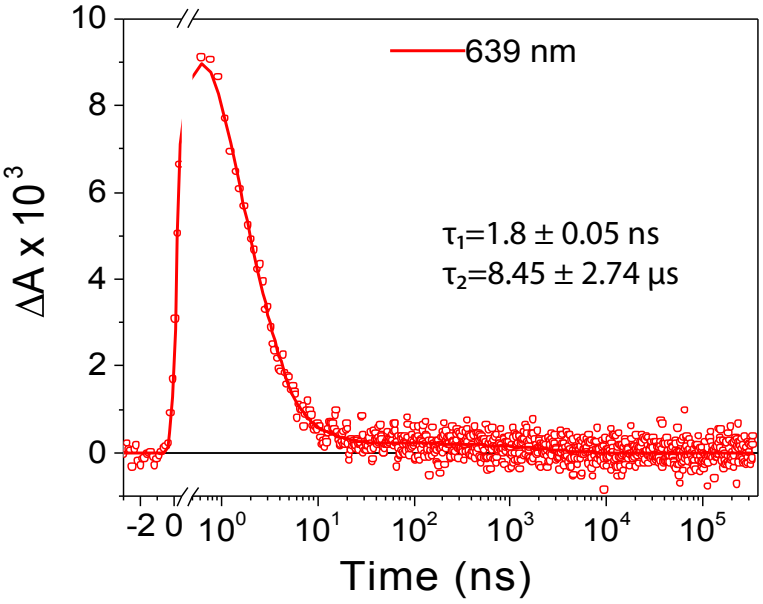

Fig. B.96 nsTA decay kinetics for EV[Ph]Me at 639 nm probe wavelength.

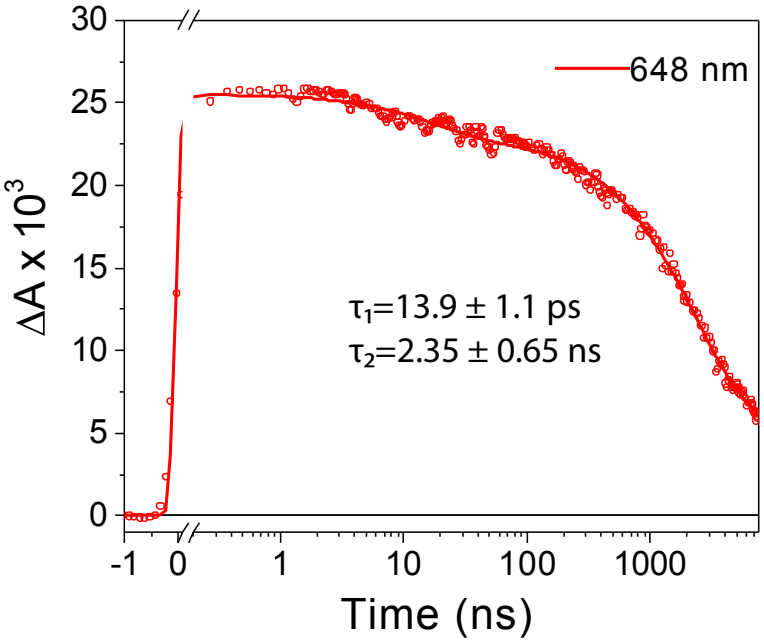

Fig. B.97 fsTA decay kinetics for EV[Ph]Me with 1 eq of CB[8] at 648 nm probe wavelength

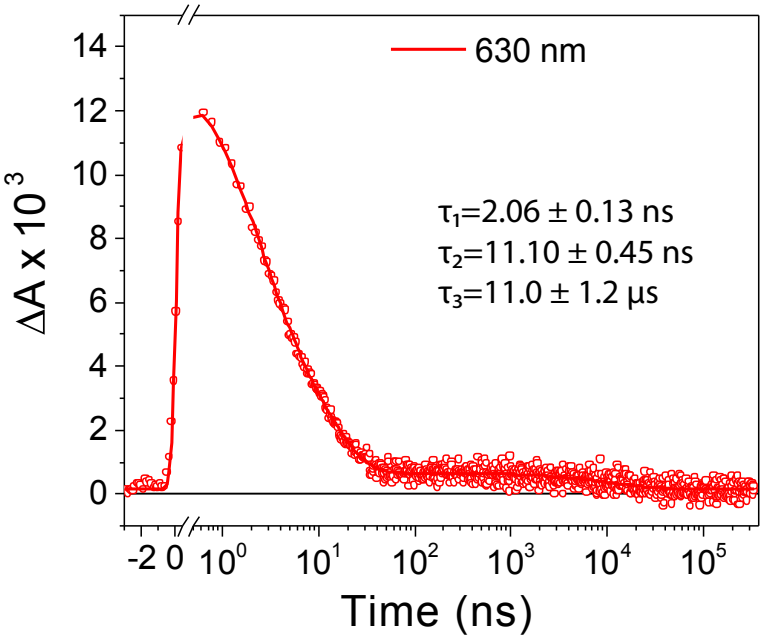

Fig. B.98 nsTA decay kinetics for EV[Ph]Me with 1 eq of CB[8] at 630 nm probe wavelength.

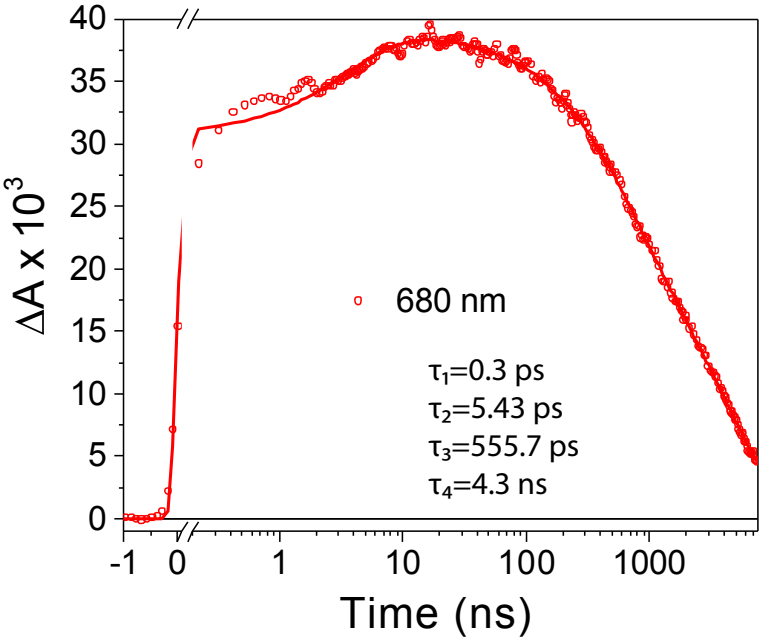

Fig. B.99 fsTA decay kinetics for EV[Np]Me at 680 nm probe wavelength.

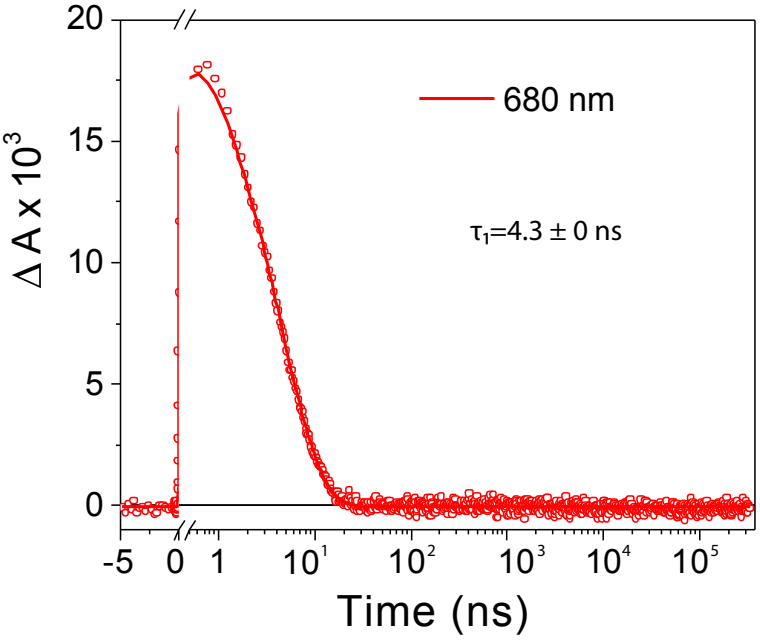

Fig. B.100 nsTa decay kinetics for EV[Np]Me at 680 nm probe wavelength.

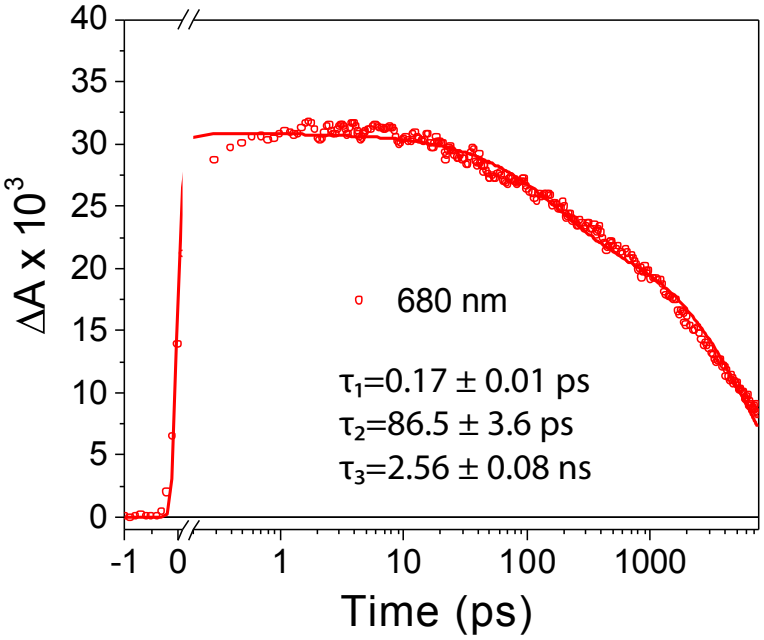

Fig. B.101 fsTA decay kinetics for EV[Np]Me with 1 eq of CB[8] at 680 nm probe wavelength.

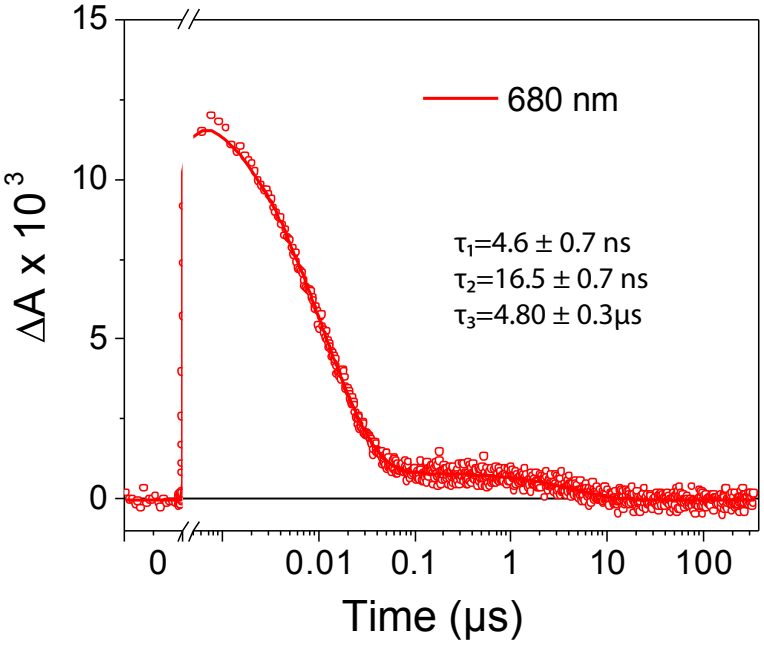

Fig. B.102 nsTA decay kinetics for EV[Np]Me with 1 eq of CB[8] at 680 nm probe wavelength.

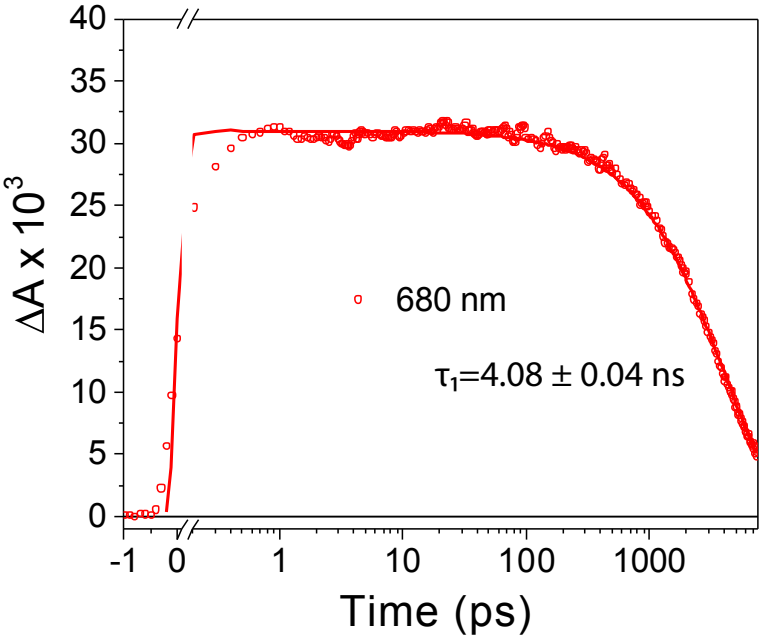

Fig. B.103 fsTA decay kinetics for EV[Np]Me with CB[7] at 680 nm probe wavelength.

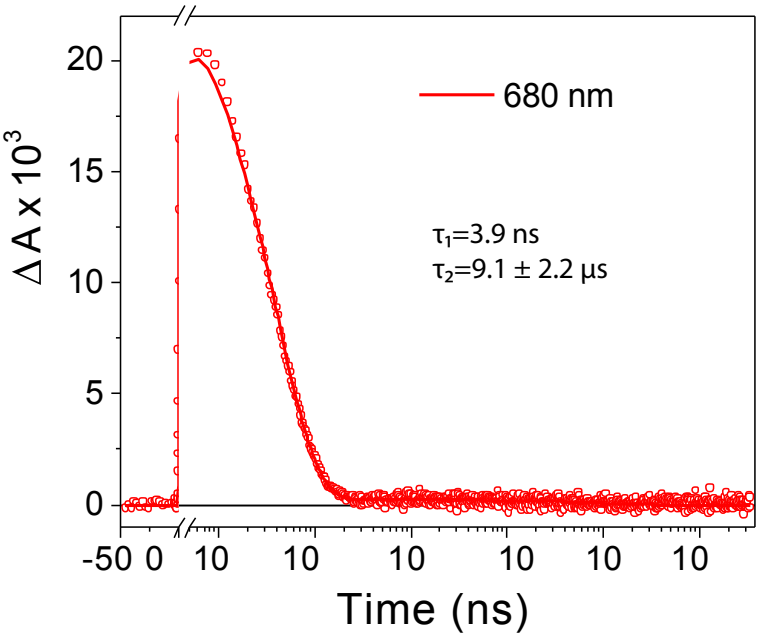

Fig. B.104 nsTA decay kinetics for EV[Np]Me with CB[7] at 680 nm probe wavelength.

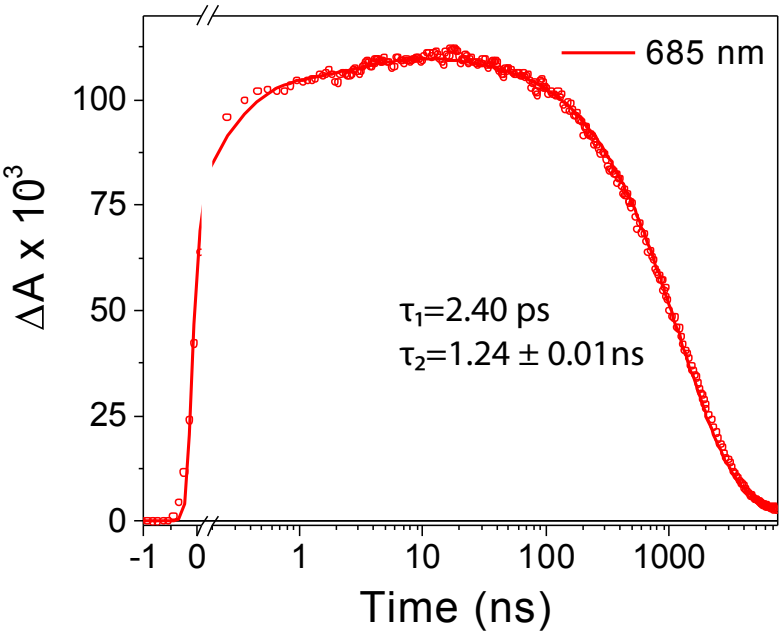

Fig. B.105 fsTA decay kinetics for EV[Th]Me at 685 nm probe wavelength.

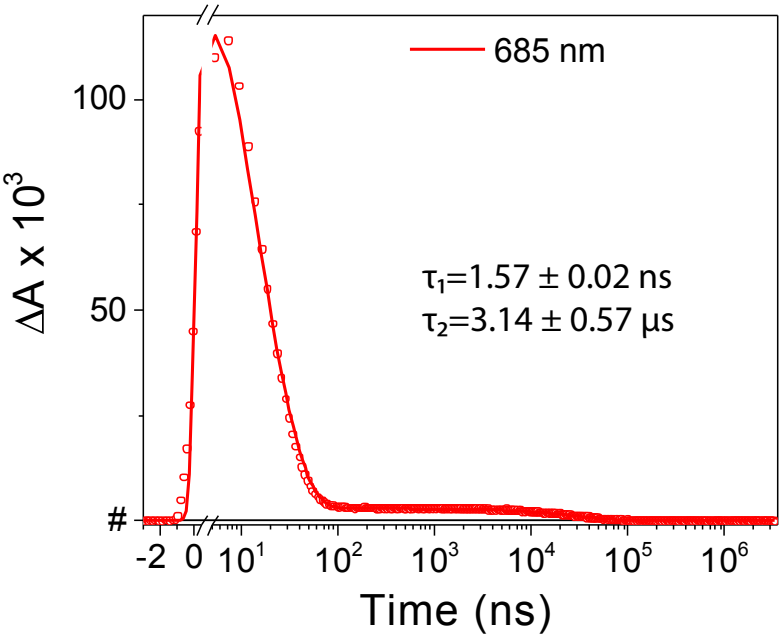

Fig. B.106 nsTA decay kinetics for EV[Th]Me at 685 nm probe wavelength.

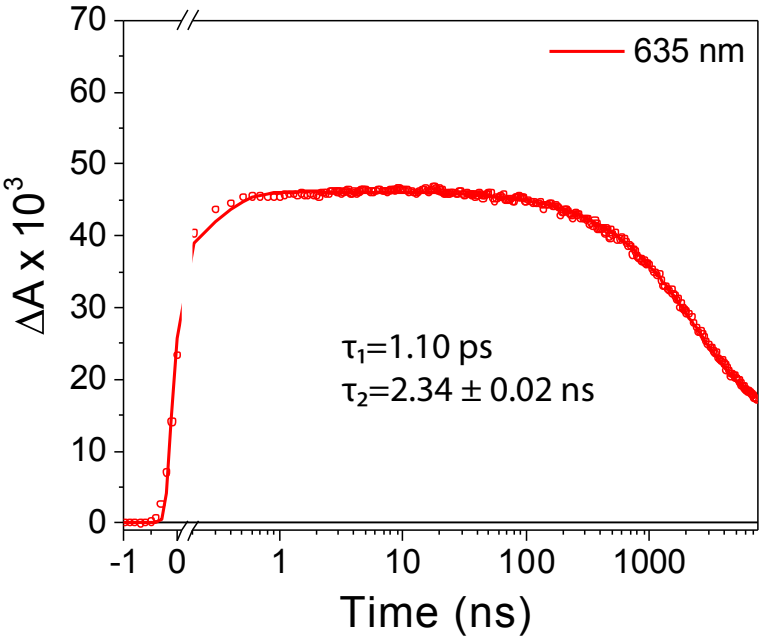

Fig. B.107 fsTA decay kinetics for EV[Th]Me with 1 eq of CB[8] at 635 nm probe wavelength.

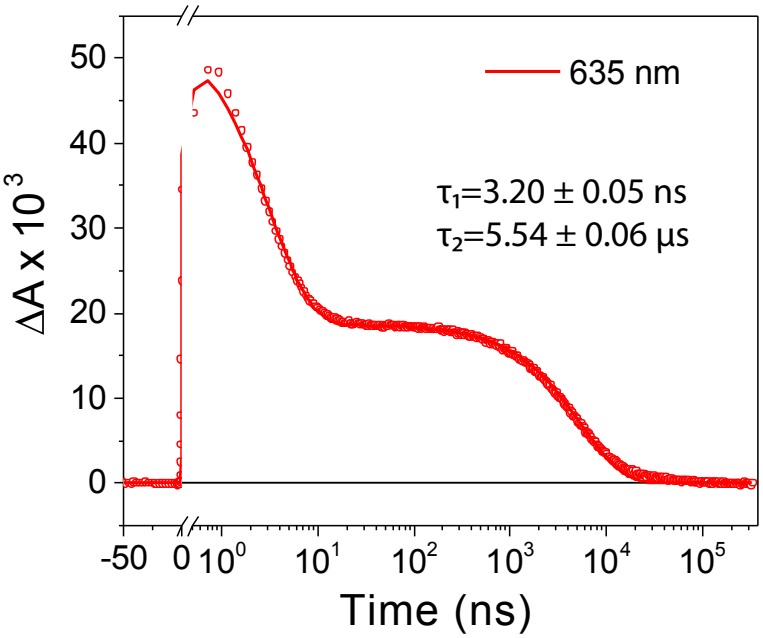

Fig. B.108 nsTA decay kinetics for EV[Th]Me with 1 eq of CB[8] at 635 nm probe wavelength.

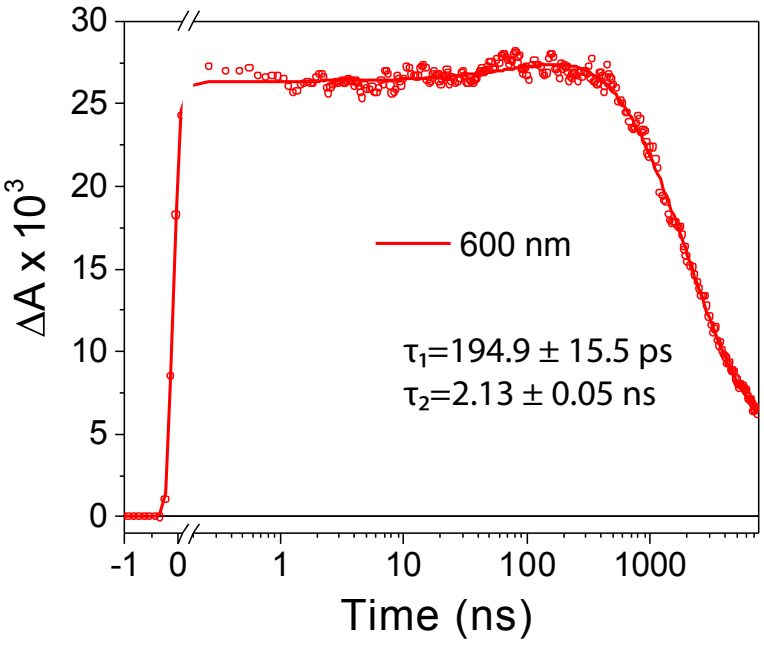

Fig. B.109 fsTA decay kinetics for EV[DTh]Me at 600 nm probe wavelength.

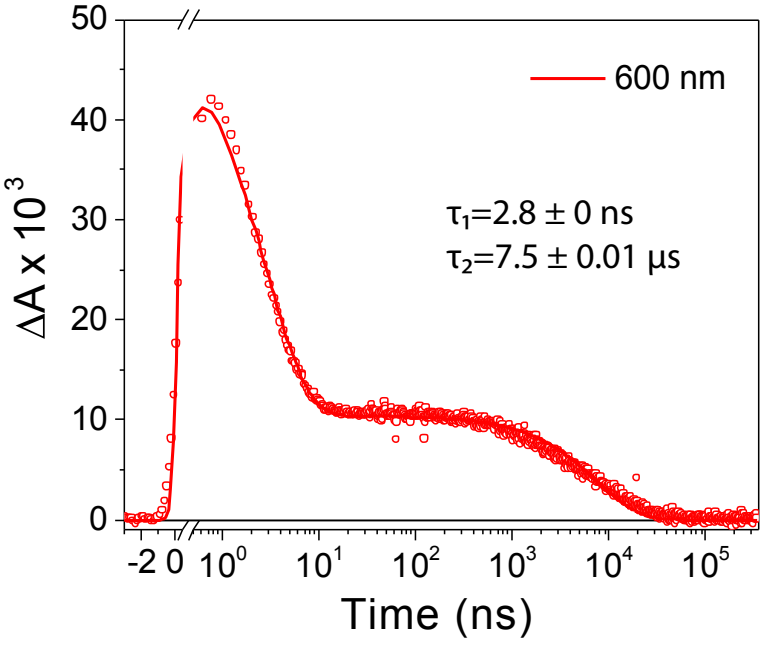

Fig. B.110 nsTA decay kinetics for EV[DTh]Me at 600 nm probe wavelength.

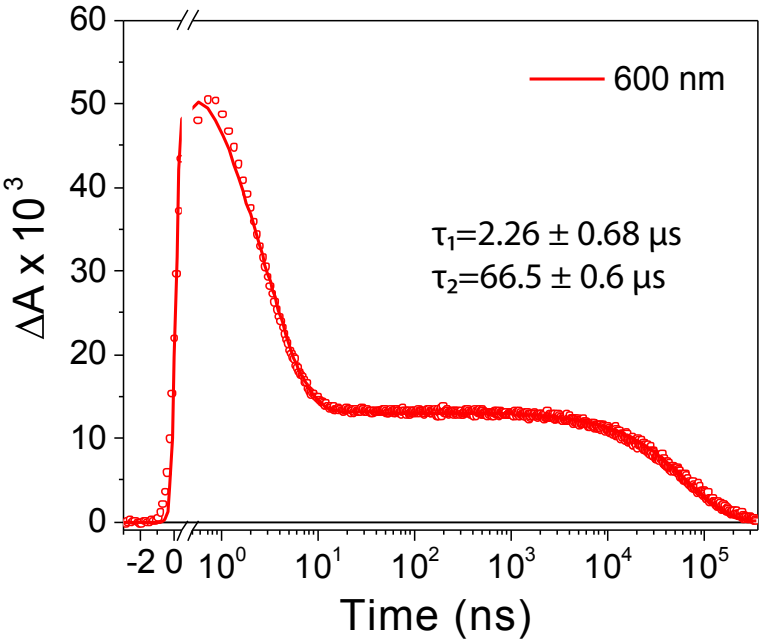

Fig. B.111 nsTA decay kinetics for EV[DTh]Me at 600 nm probe wavelength, measured in air free conditions.

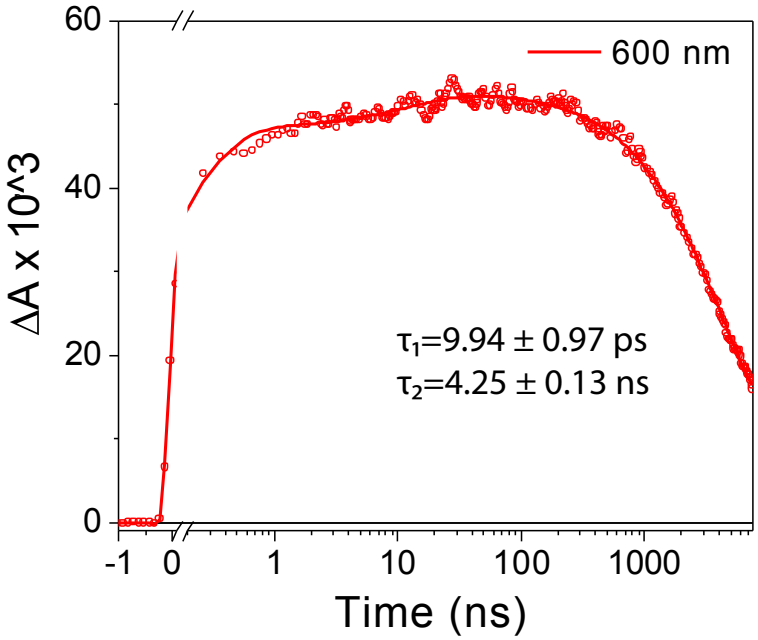

Fig. B.112 fsTA decay kinetics for EV[DTh]Me with 1 eq of CB[8] at 600 nm probe wavelength.

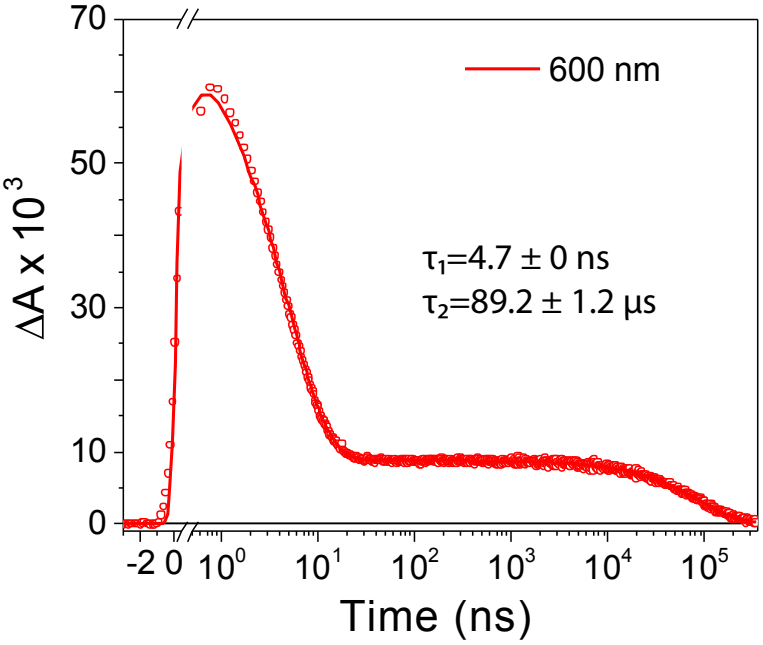

Fig. B.113 nsTA decay kinetics for EV[DTh]Me with 1 eq of CB[8] at 600 nm probe wavelength.

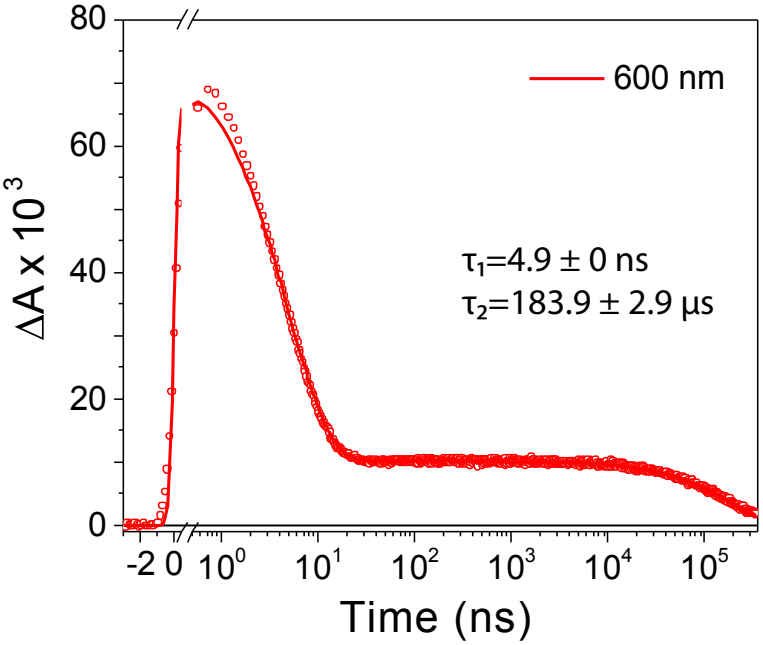

Fig. B.114 nsTA decay kinetics for EV[DTh]Me with 1 eq of CB[8] at 600 nm probe wavelength, measured in air free conditions.

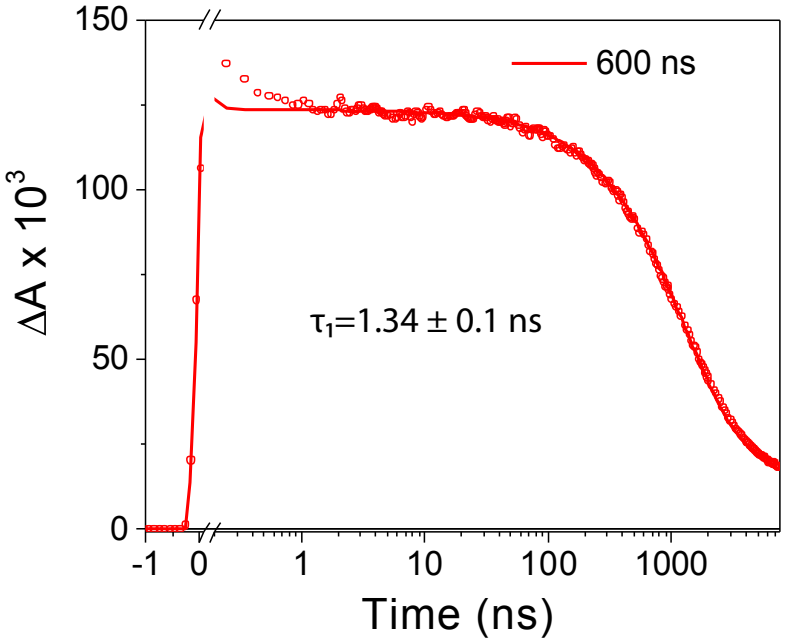

Fig. B.115 fsTA decay kinetics for EV[DTh]Me with 2 eq of CB[7] at 600 nm probe wavelength.

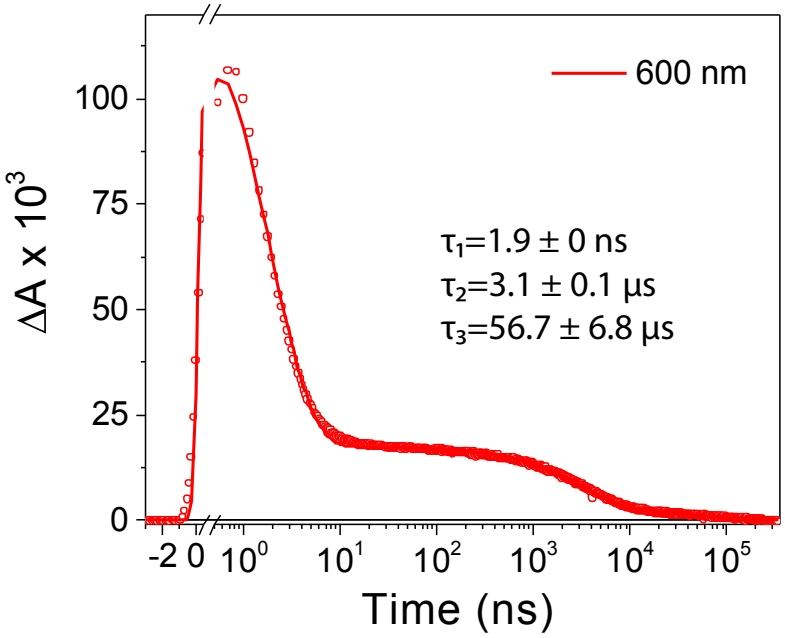

Fig. B.116 nsTA decay kinetics for EV[DTh]Me with 2 eq of CB[7] at 600 nm probe wavelength.

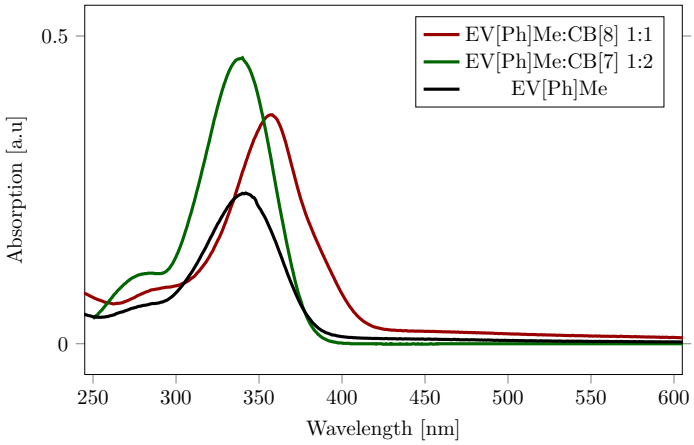

Fig. B.117 The UV – Vis of EV[Ph]Me and its complexes with CB[8] and CB[7]. All measurements were carried out at a concentration of 0.01 mM.

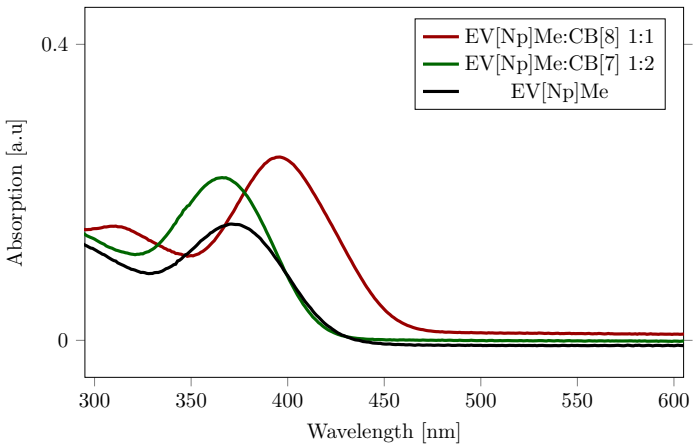

Fig. B.118 The UV – Vis of EV[Np]Me and its complexes with CB[8] and CB[7]. All measurements were carried out at a concentration of 0.01 mM.

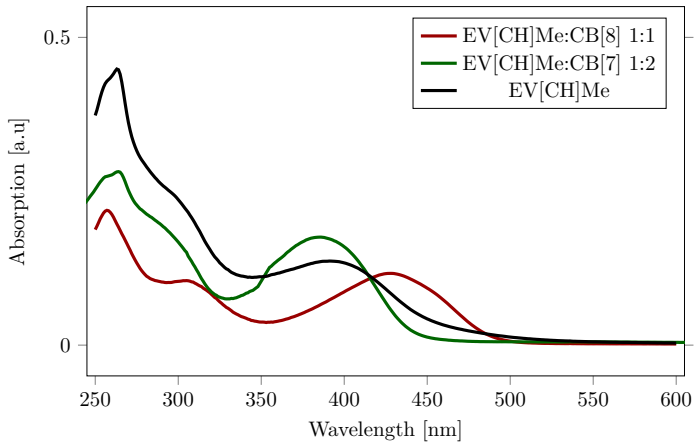

Fig. B.119 The UV – Vis of EV[CH]Me and its complexes with CB[8] and CB[7]. All measurements were carried out at a concentration of 0.01 mM.

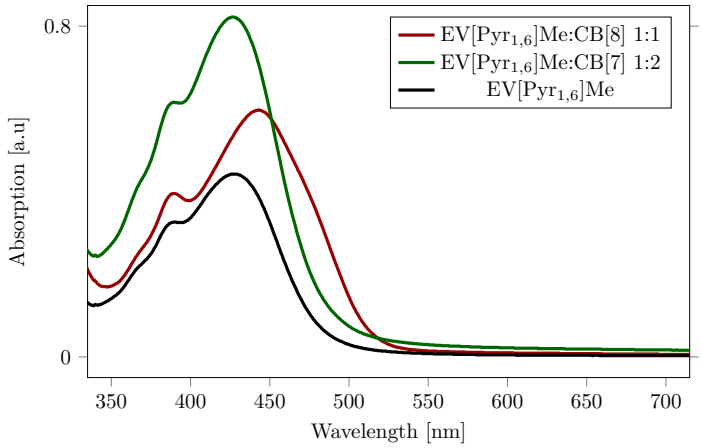

Fig. B.120 The UV – Vis of EV[$Pyr_{1,6}$]Me and its complexes with CB[8] and CB[7]. All measurements were carried out at a concentration of 0.01 mM.

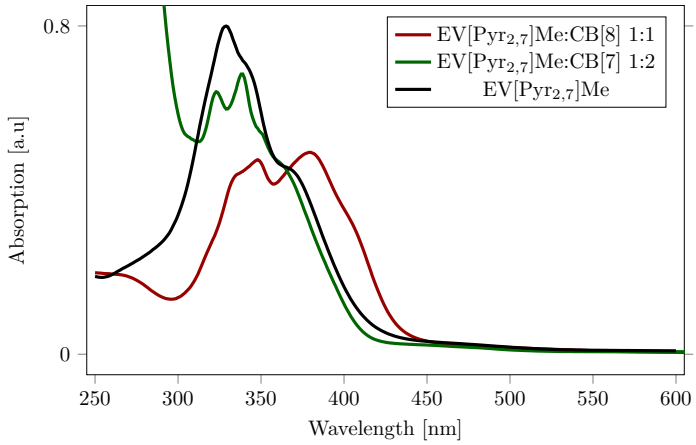

Fig. B.121 The UV – Vis of EV[$Pyr_{2,7}$]Me and its complexes with CB[8] and CB[7]. All measurements were carried out at a concentration of 0.01 mM.

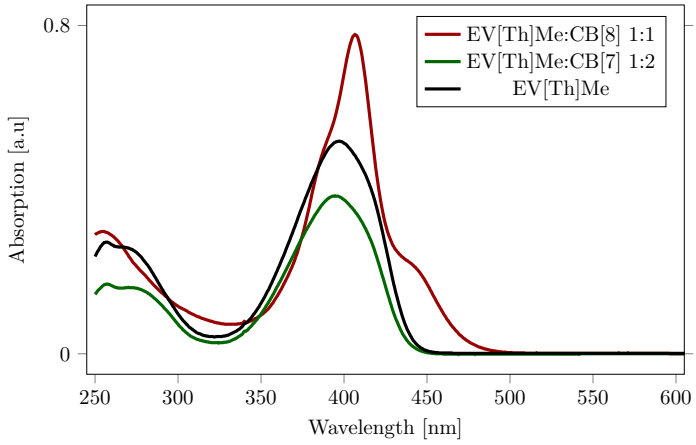

Fig. B.122 The UV – Vis of EV[Th]Me and its complexes with CB[8] and CB[7]. All measurements were carried out at a concentration of 0.01 mM.

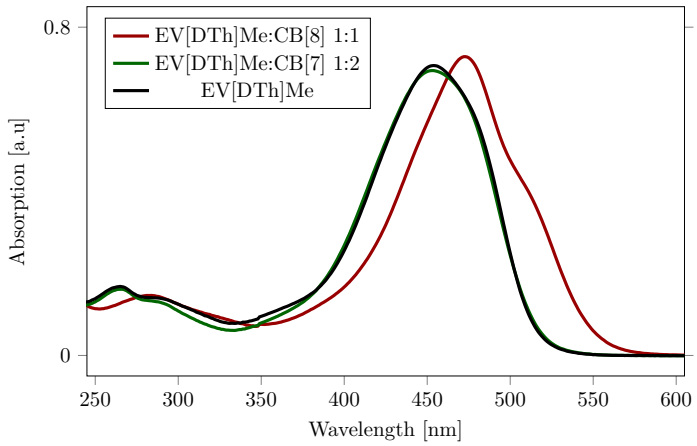

Fig. B.123 The UV – Vis of EV[DTh]Me and its complexes with CB[8] and CB[7]. All measurements were carried out at a concentration of 0.01 mM.

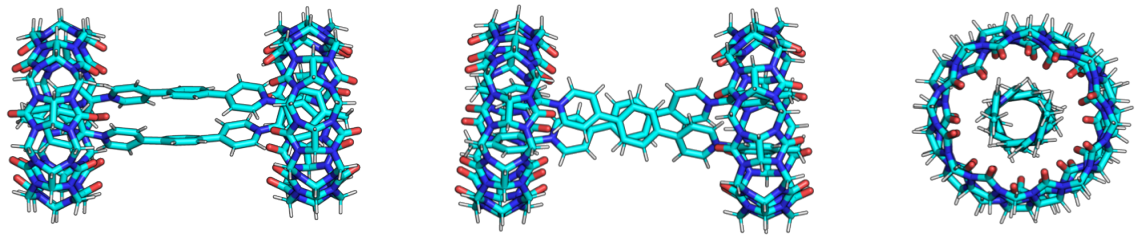

Fig. B.124 Optimised geometry of EV[Ph]Me:CB[8] complex

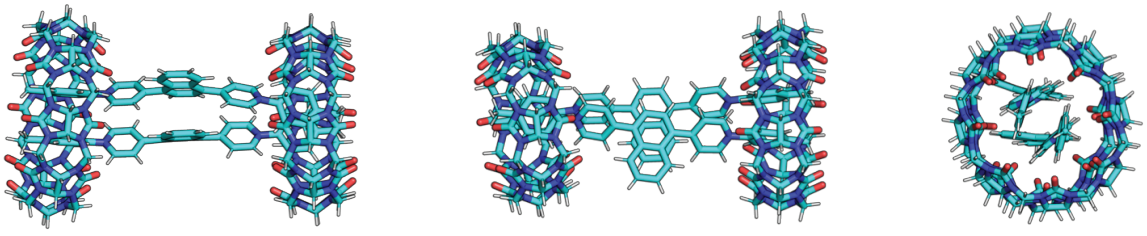

Fig. B.125 Optimised geometry of EV[Np]Me:CB[8] complex

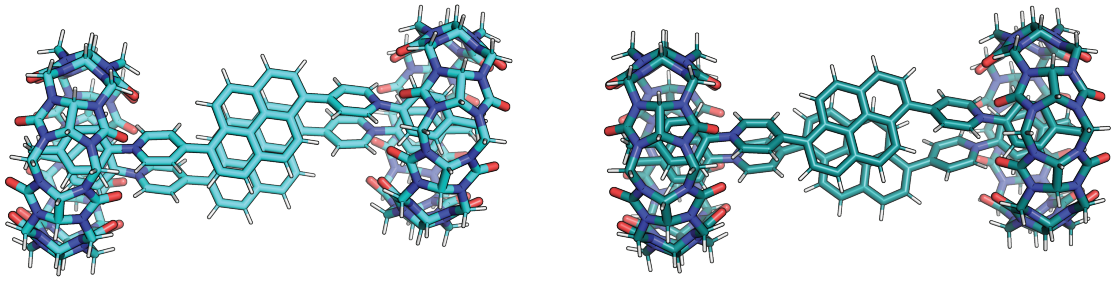

Fig. B.126 Optimised geometry of EV[$Pyr_{1,6}$]Me:CB[8] complex

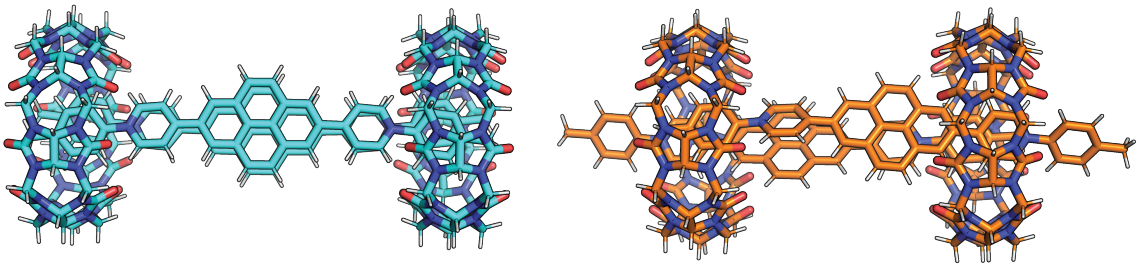

Fig. B.127 Optimised geometry of EV[$Pyr_{2,7}$]Me:CB[8] complex

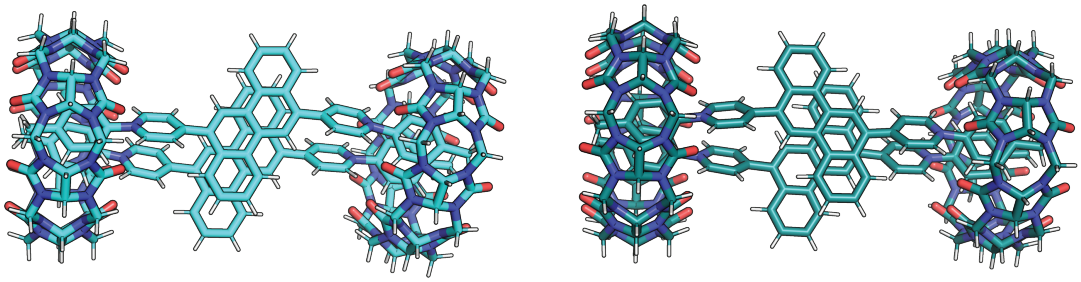

Fig. B.128 Optimised geometry of EV[CH]Me:CB[8] complex

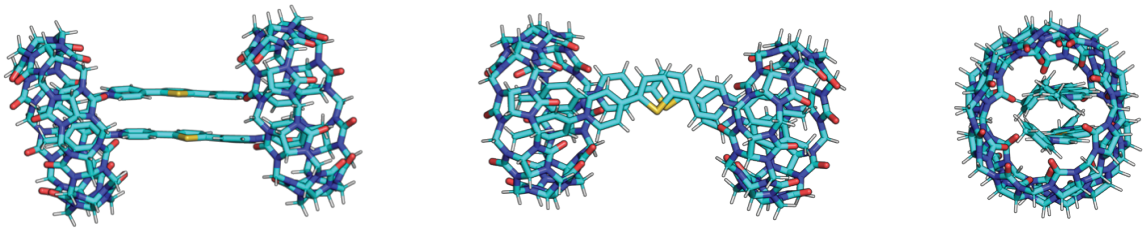

Fig. B.129 Optimised geometry of EV[Th]Me:CB[8] complex

Table B.2 Geometric parameters for 2:2 complexes of EV[Ph]Me, EV[Np]Me and EV[Th]Me with CB[8].

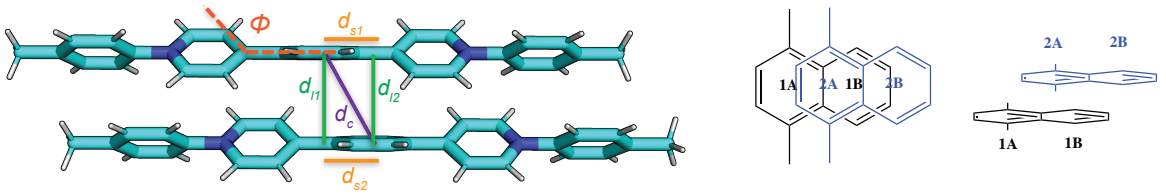

.Complex	$d_c(A)$**	α (°)	d_{l1} (A)	d_{l2} (A)	d_s1 (A)	d_s2 (A)	ϕ (°)
EV[Ph]Me: CB[8]	3.38	174.6	3.2979	3.3159	0.7432	0.6582	29.98
EV[Np]Me: CB[8] (1A-2A)*	3.84	166.3	2.9806	3.4451	2.4244	1.701	44.6
EV[Np]Me: CB[8] (1B-2A)*	3.4124	171.17	3.4121	3.3773	0.0458	0.488	
EV[Np]Me: CB[8] (1B-2B)*	3.3128	166.44	3.3159	3.8599	2.7577	1.9238	
EV[Th]Me: CB[8]	3.46	174.9	3.2427	3.2454	1.1991	1.1917	5.7

d_c - Distance between centroids of aromatic rings; α- angle between planes, α =180° for parallel orientation; d_l- distance between planes formed by central rings; d_{s1} and d_{s2} - intercentroid shifts; ϕ - average of four angles between pyridinium motif and the central ring. *There are two other $\pi - \pi$ interaction points that can be found between the central rings in the case of EV[Np]Me **We have considered a cut-off of 4 in the distance between centroids to include the interaction.

Appendix C

Appendix for chapter 4

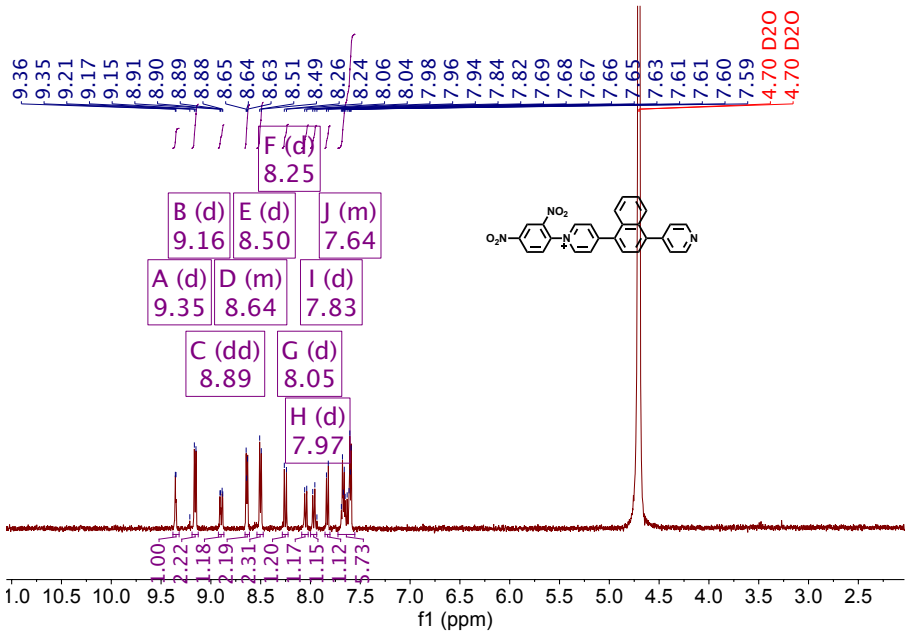

Fig. C.1 ^{1}H NMR of EV[Np]DNB (500 MHz, D_2O)

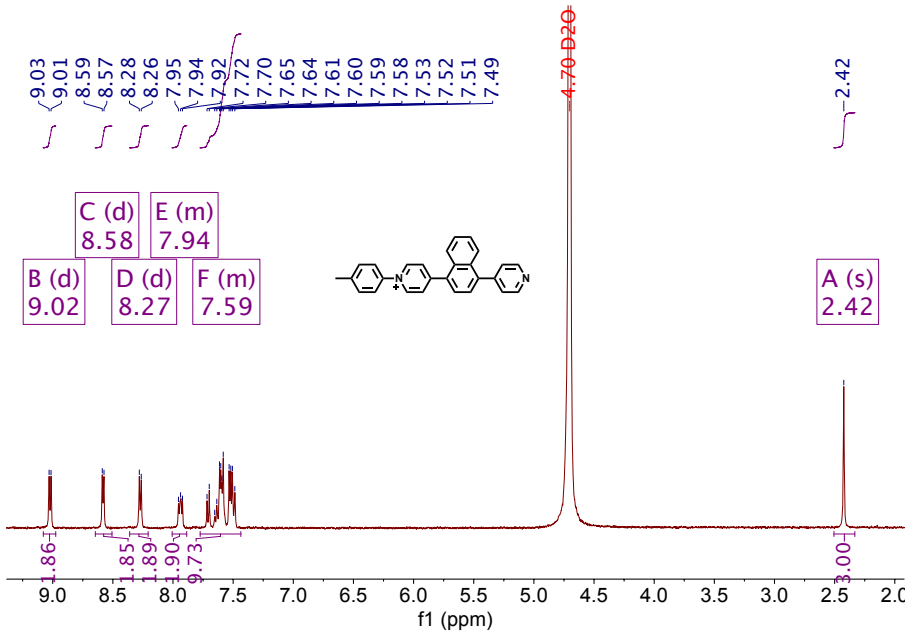

Fig. C.2 ^{1}H NMR of EV[Np]Me$_{asym}$ (500 MHz, D_2O)

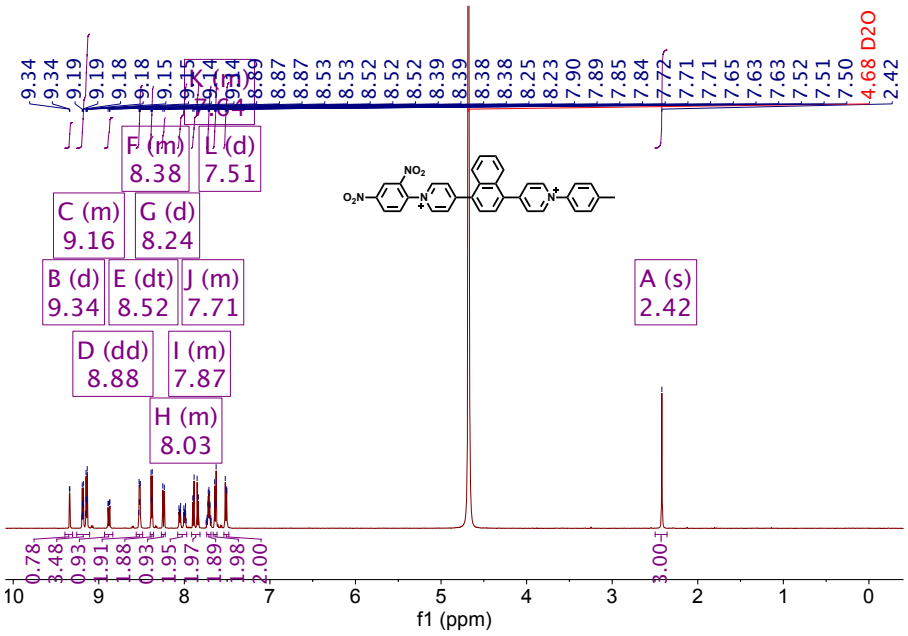

Fig. C.3 ^{1}H NMR of EV[Np]MeDNB (500 MHz, D_2O)

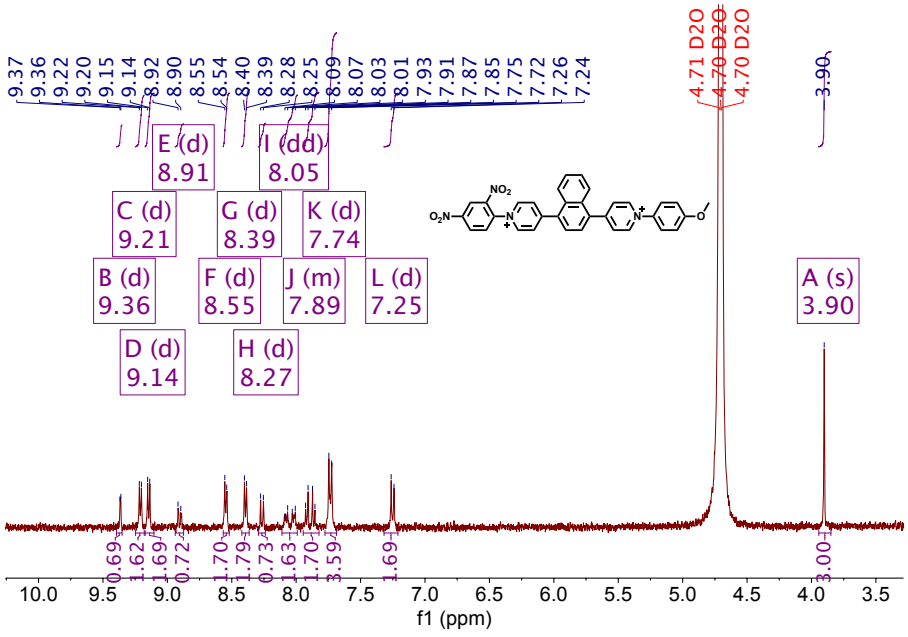

Fig. C.4 ^{1}H NMR of EV[Np]OMeDNB (500 MHz, D_2O)

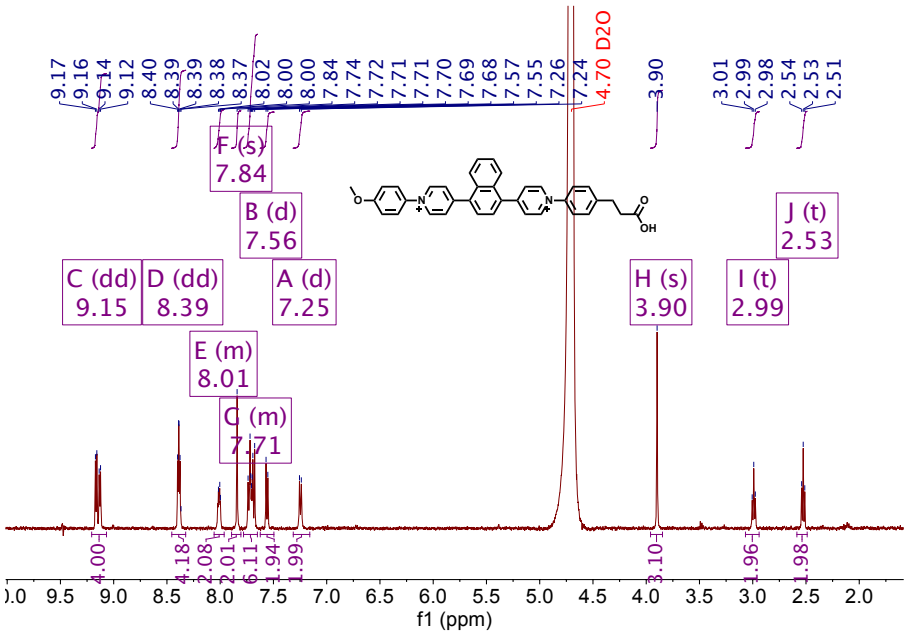

Fig. C.5 ^{1}H NMR of EV[Np]OMeEtCOOH (500 MHz, D_2O)

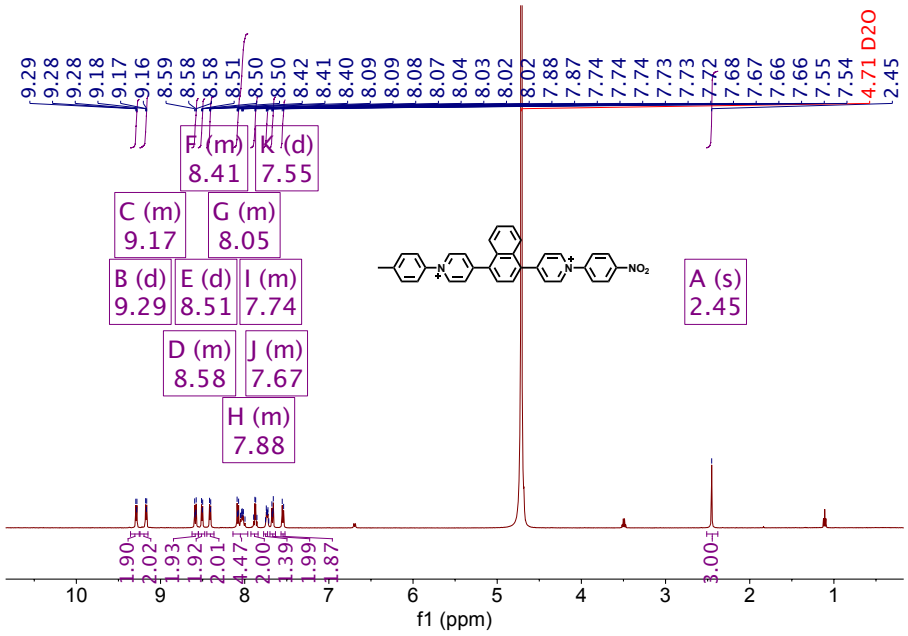

Fig. C.6 ^{1}H NMR of EV[Np]MeNO_2 (500 MHz, D_2O)

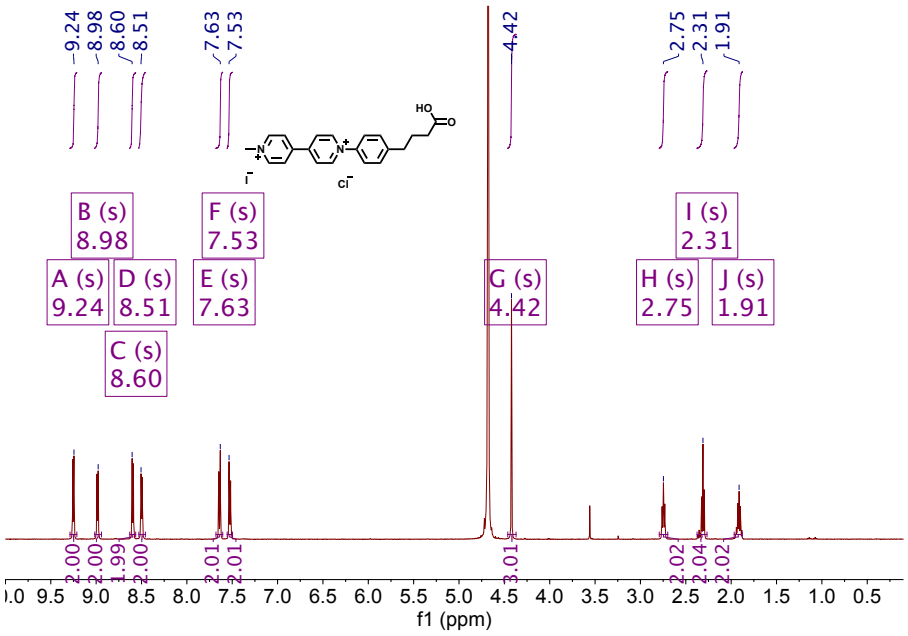

Fig. C.7 ^{1}H NMR of AV (500 MHz, D_2O)

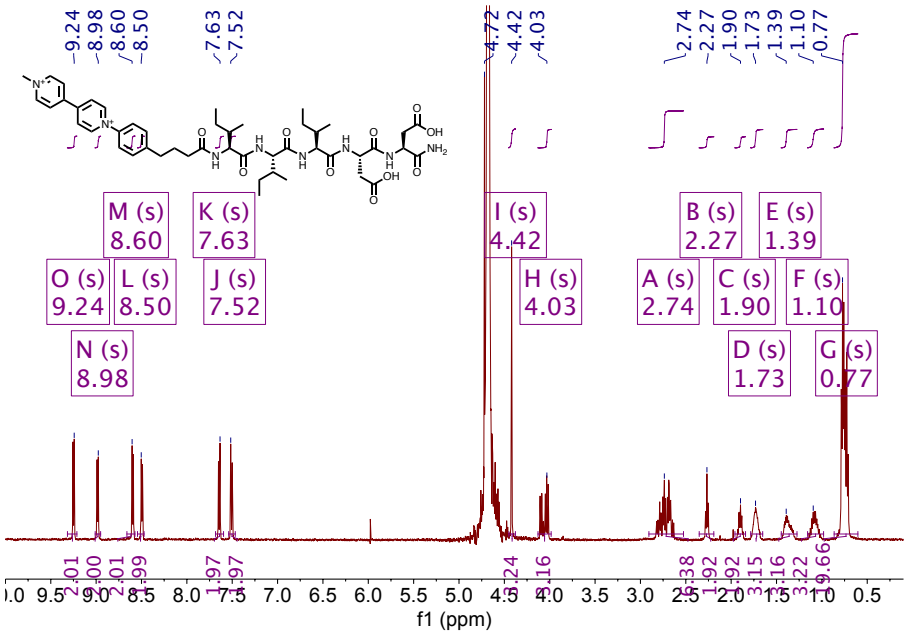

Fig. C.8 ^{1}H NMR of AVI3D2 (500 MHz, D_2O/K_2CO_3)

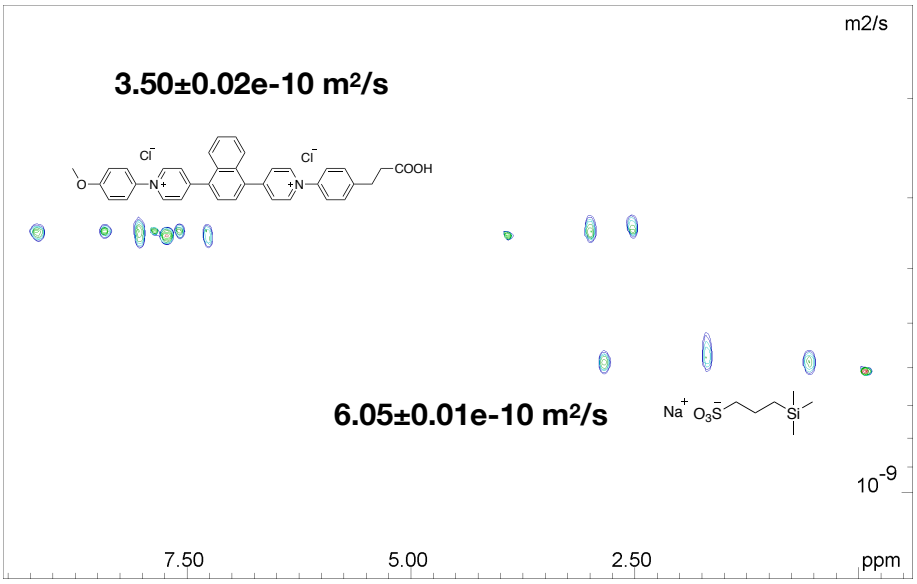

Fig. C.9 ^{1}H DOSY NMR spectrum of EV[Np]OMEtTCOOH (500 MHz, D_2O, 298 K).

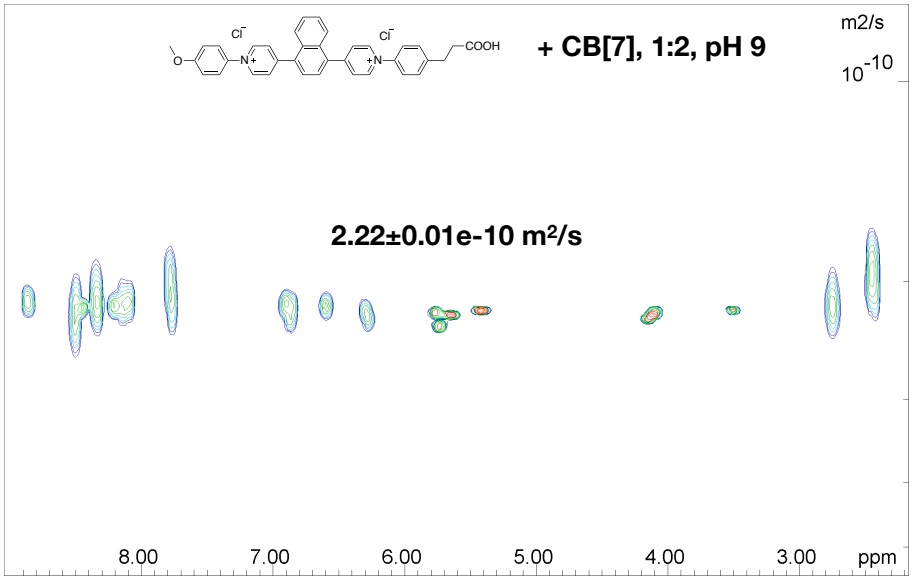

Fig. C.10 ^{1}H DOSY NMR spectrum of 2:1 complex of CB[7] and EV[Np]OMeEtCOOH (500 MHz, D_2O, 298 K).

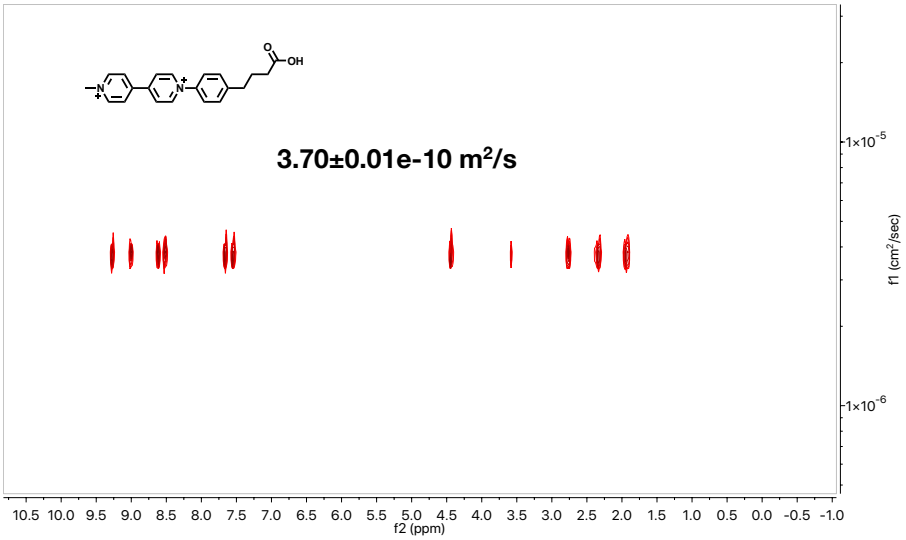

Fig. C.11 ^{1}H DOSY NMR spectrum of AV (500 MHz, D_2O, 298 K).

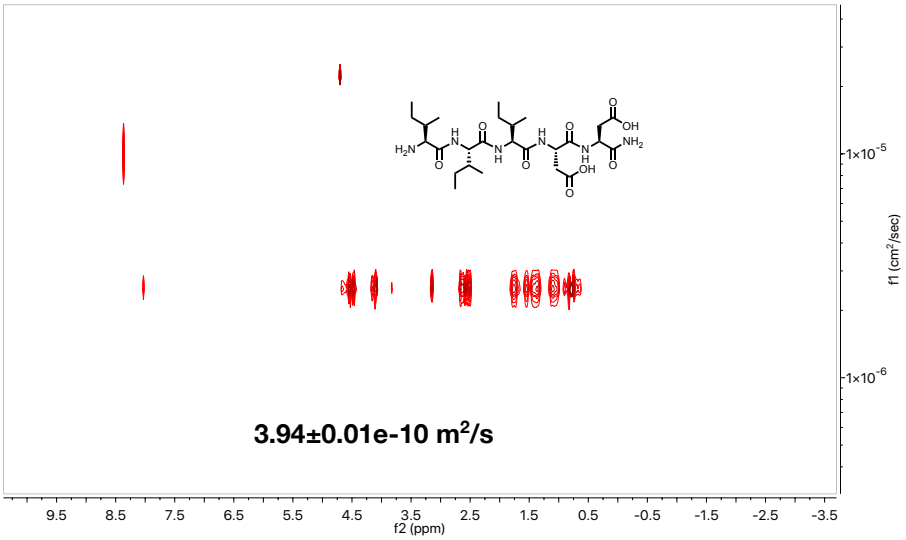

Fig. C.12 ^{1}H DOSY NMR spectrum of I3D2 peptide (500 MHz, D_2O, K_2CO_3, 298 K).

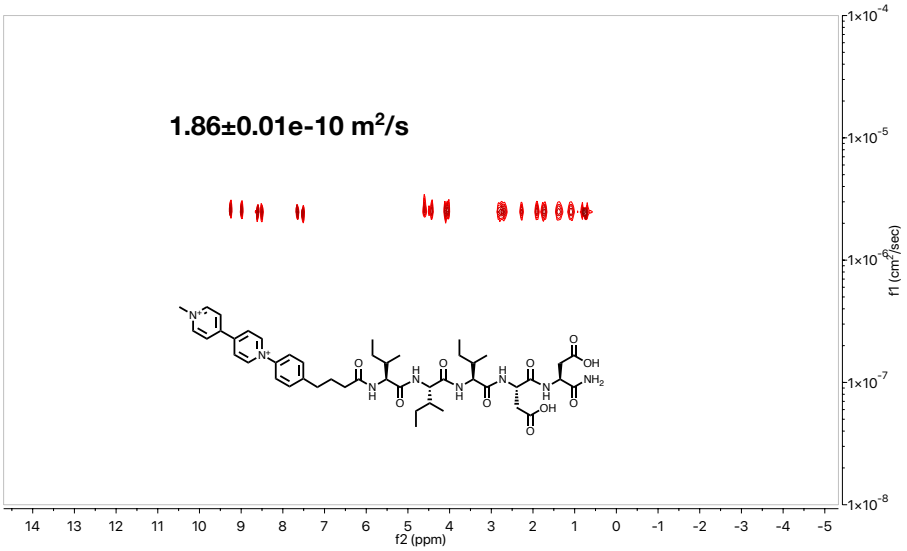

Fig. C.13 ^{1}H DOSY NMR spectrum of AVI3D2 peptide (500 MHz, D_2O, 298 K).

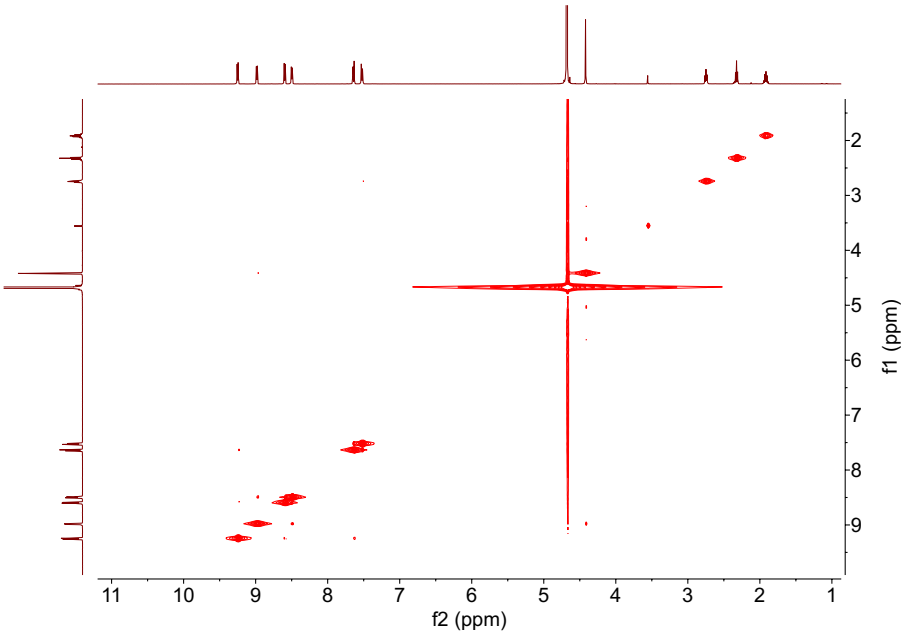

Fig. C.14 1H-1H NOESY NMR of AV at 8 mM and pD 7.4, 500 MHz, D_2O, 298 K).

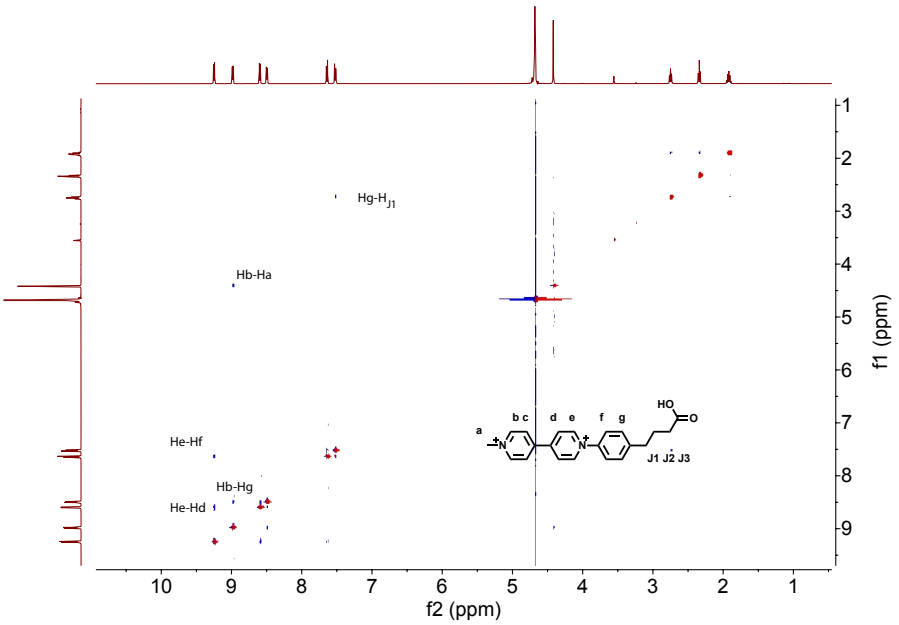

Fig. C.15 1H-1H NOESY NMR of AV at 8 mM and pD 4.0 (500 MHz, D_2O, 298 K).

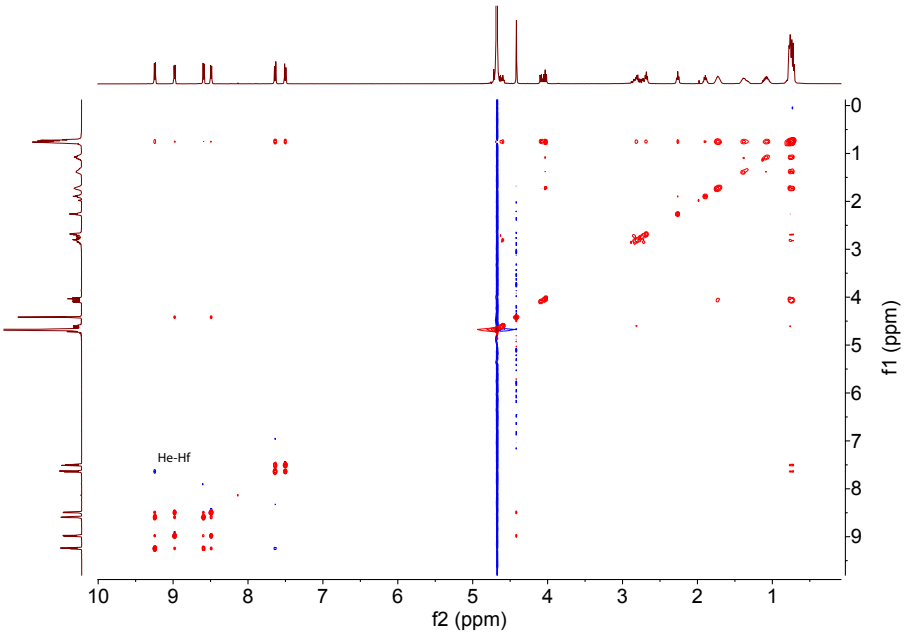

Fig. C.16 1H-1H NOESY NMR of AVI3D2 at 8 mM and pD 7.4 (500 MHz, D_2O, 298 K).

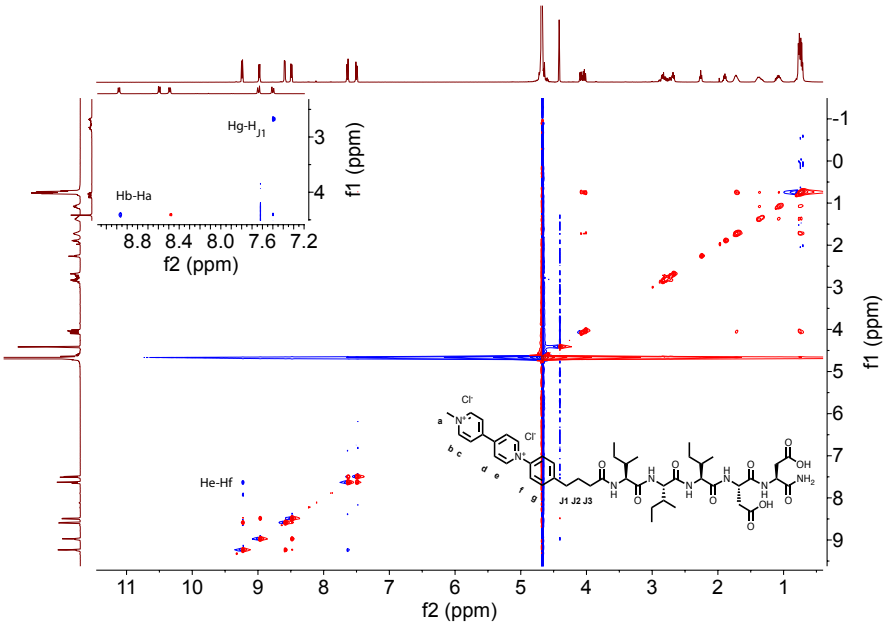

Fig. C.17 1H-1H NOESY NMR of AVI3D2 at 8 mM and pD 4.0 (500 MHz, D_2O, 298 K).

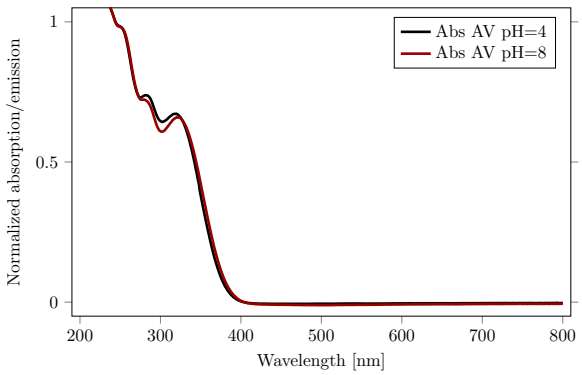

Fig. C.18 Normalised absorption spectra of AV at different pH. Measurement was done at 0.1mM.

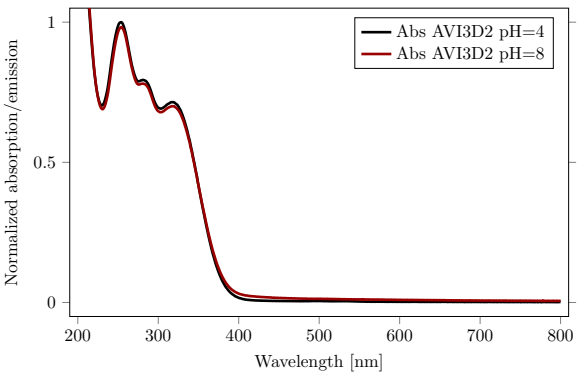

Fig. C.19 Normalised absorption spectra of AVI3D2 at different pH. Measurement was done at 0.1mM.

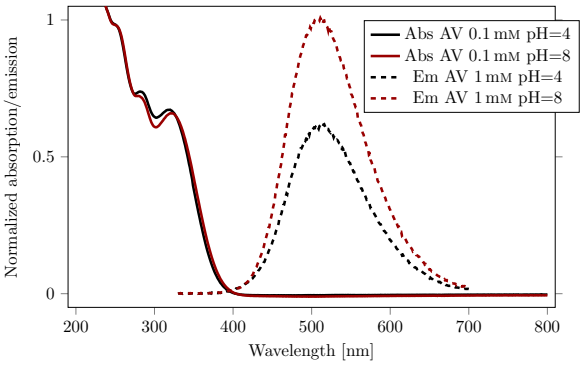

Fig. C.20 Normalised absorption and emission spectra of 1mM solution of AV at different pH after excitation at 320 nm. Absorption spectra of AV was done at 0.1mM.

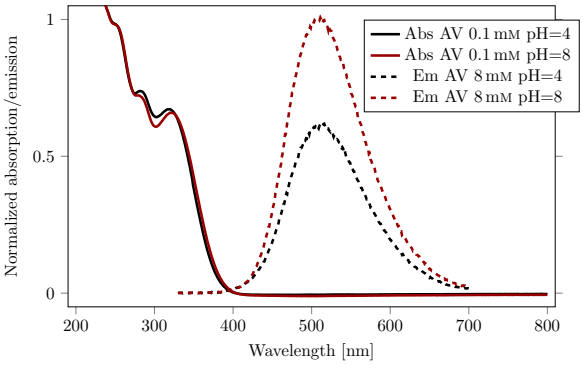

Fig. C.21 Normalised absorption and emission spectra of 8mM solution of AV at different pH after excitation at 320 nm. Absorption spectra of AV was done at 0.1mM.

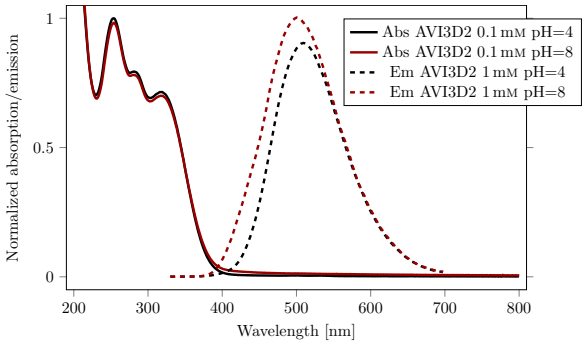

Fig. C.22 Normalised absorption and emission spectra of 1mM solution of AVI3D2 at different pH after excitation at 320 nm. Absorption spectra of AVI3D2 was done at 0.1mM.

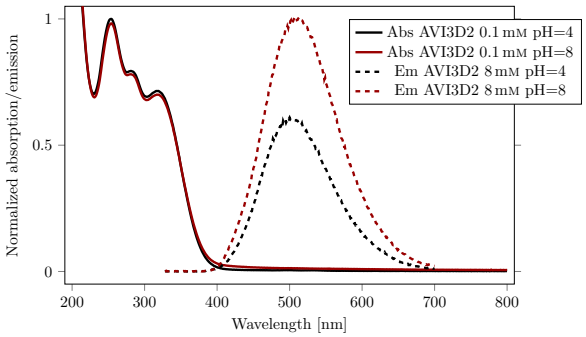

Fig. C.23 Normalised absorption and emission spectra of 8mM solution of AVI3D2 at different pH after excitation at 320 nm. Absorption spectra of AVI3D2 was done at 0.1mM.

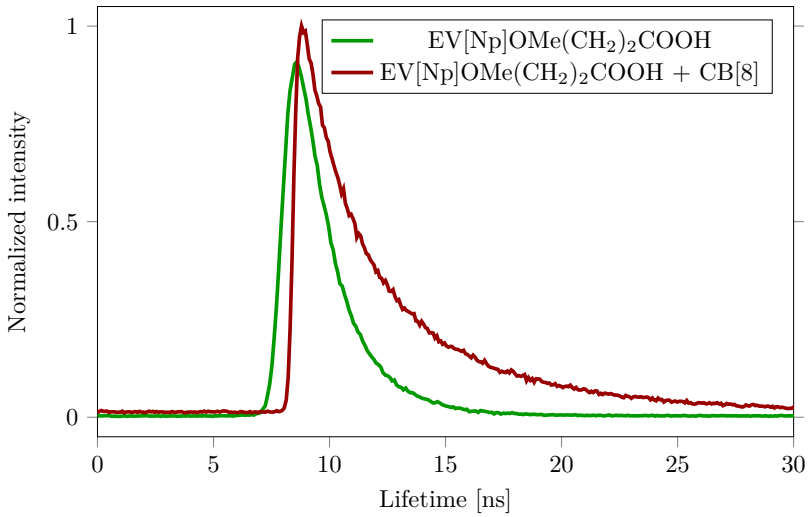

Fig. C.24 TCSPC decay profile for EV[Np](OMe)(EtCOOH) (green line) and its complexes with 1 eq of CB[8] at pH=2 (red lines). All measurements were performed at a concentration of 10 µM.

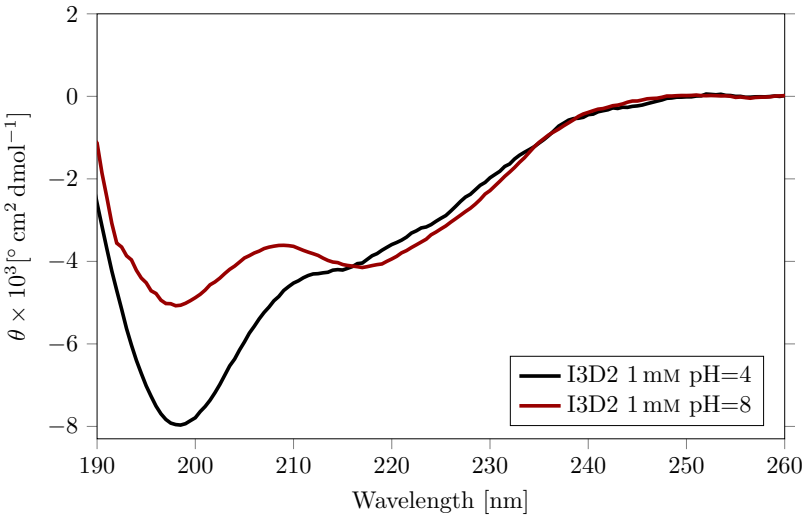

Fig. C.25 Circular Dichroism spectra of 1mM I3D2 peptide at different pH.

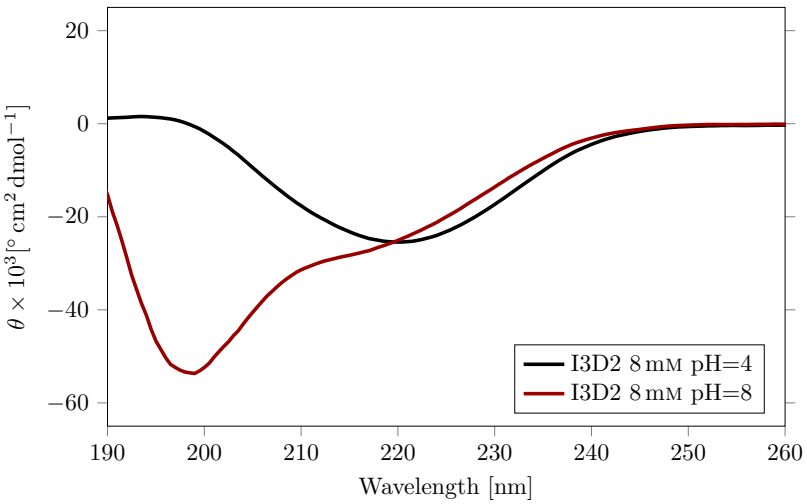

Fig. C.26 Circular Dichroism spectra of 8mM I3D2 peptide at different pH.

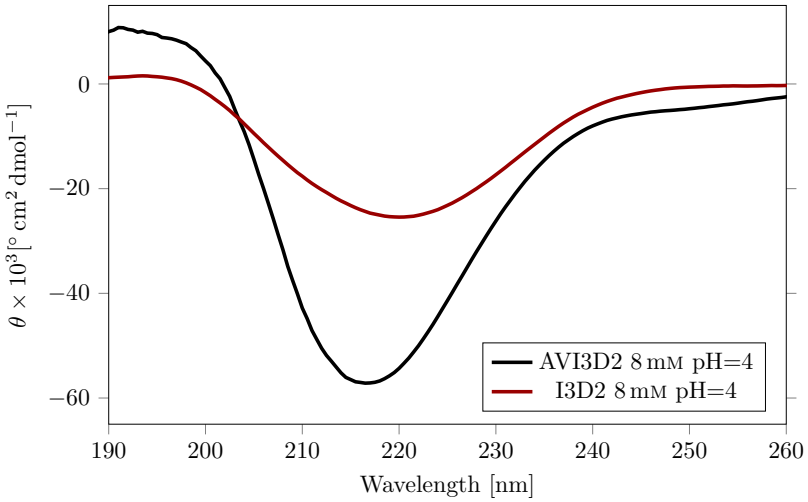

Fig. C.27 Circular Dichroism spectra of 8mM I3D2 and AVI3D2 peptide at pH4.

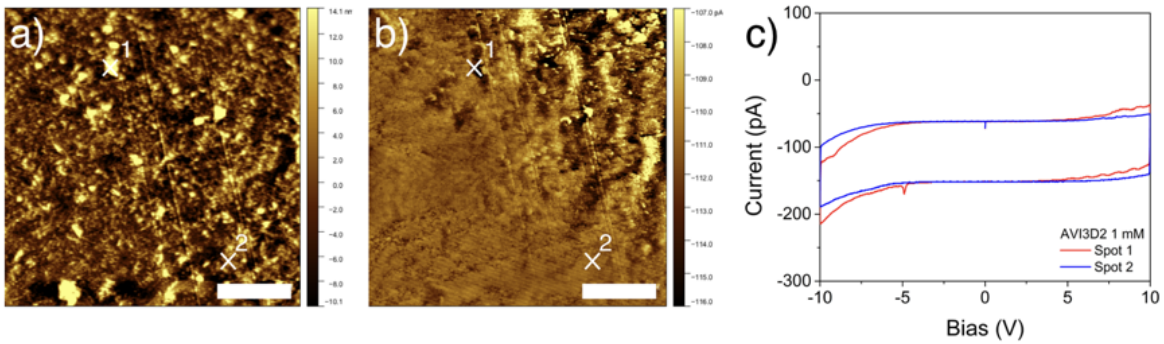

Fig. C.28 c-AFM of AVI3D2 (1 mM). a) Topography map, b) short-circuit current map and c) conductivity curves corresponding to spots 1 and 2. Scale bar on all the images is 5 µm.

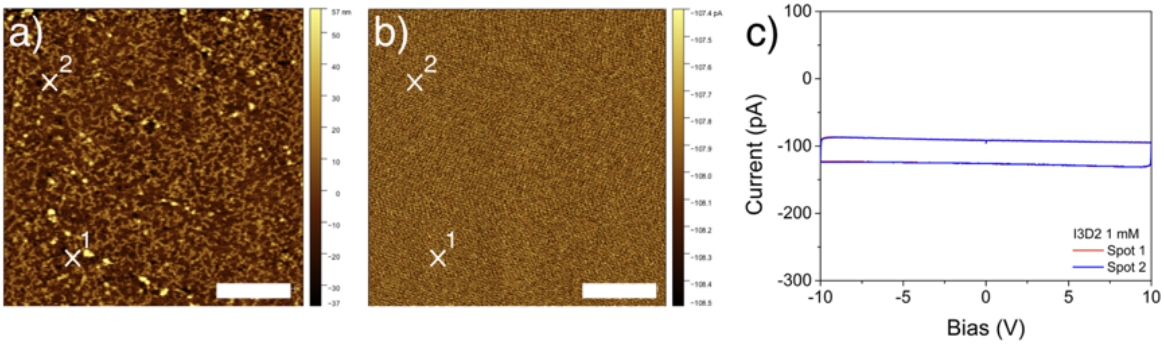

Fig. C.29 c-AFM of I3D2 (1 mM). a) Topography map, b) short-circuit current map and c) conductivity curves corresponding to spots 1 and 2. Scale bar on all the images is 5 µm